SEISMIC PERFORMANCE OF DOUBLE-CHANNEL AND DOUBLE-HSS SECTIONS, SPECIAL TRUSS MOMENT FRAME WITH BUCKLING-RESTRAINED BRACES, AND LONG SPAN SPECIAL TRUSS MOMENT FRAME

by

CHATCHAI JIANSINLAPADAMRONG

Presented to the Faculty of the Graduate School of

The University of Texas at Arlington in Partial Fulfillment

of the Requirements

for the Degree of

DOCTOR OF PHILOSOPHY

THE UNIVERSITY OF TEXAS AT ARLINGTON

December 2017

Acknowledgements

I would like to gratefully and deeply thank my supervising advisor, Dr. Shih-Ho Chao for the knowledge, guidance, support as well as his patience. My gratitude also goes to faculty and staff at the University of Texas at Arlington for their support and kindness which made my long journey seem shorter.

I take this opportunity to sincerely acknowledge the financial support from the U.S. National Science Foundation, material donation from American Institute of Steel Construction and Falcon Steel for the research project. I also greatly appreciate the help from MAST Laboratory faculty and staff for large scale testing. I would also like to extend special appreciation to former colleague at UTA, Brandon Price and Sanputt Simasathien for years of help and collaboration on the project.

I'm forever thankful for my family. Without love, understanding, and support from them, especially my parents, this milestone could not have been reached. I cannot thank Keo and Billy Baus, Justin Nguyen and Glen Ogen, who are like my family away from home, enough for their forever friendship and always being there for me.

Last but not least, I would like to thank my friends and colleague for their support and friendship.

November 20, 2017

Abstract

SEISMIC PERFORMANCE OF DOUBLE-CHANNEL AND DOUBLE-HSS SECTIONS, SPECIAL TRUSS MOMENT FRAME WITH BUCKLING-RESTRAINED BRACES, AND LONG SPAN SPECIAL TRUSS MOMENT FRAME

Chatchai Jiansinlapadamrong, PhD

The University of Texas at Arlington, 2017

Supervising Professor: Shih-Ho Chao

Until recently, all special truss moment frame (STMF) experimental research was done on only double angle STMFs. In order to satisfy the code seismic drift limitation, especially for mid-rise and tall multistory buildings, a large column section is needed, when double angle sections are used. However, heavy chord members can be used in this instance. Due to configuration of STMFs, the chord members in the special segment of an STMF experience higher rotational demand than the story drift. As a result, there is a need to verify large rotational capacity of other heavy steel shapes. Recent analytical investigation and experimental investigation at component level showed that double channel sections could be used in STMFs. However, to maintain large rotational capacity of double channel sections, lateral support was needed near plastic hinge region to prevent lateral torsional buckling (LTB).

This research investigated ways to maintain double channel rotational capacity without having to provide lateral support and viability of using double HSS sections which are not susceptible to LTB in STMFs. A new connection detail was tested and the results

showed that lateral torsional buckling was eliminated. Results on double HSS sections showed that it could maintain strength at very high rotation.

Other than verifying large rotational capacity of double channel and double HSS sections, this research also introduced incorporating buckling-restrained braces to provide additional stiffness and strength to full scale STMF subassemblage test.

Moreover, the possibility of extending span the length of STMFs to 90 ft was explored. When a span length of STMF is very long, its stiffness could be compromise. In addition, induced axial force due to gravity loading could be significant. The effect of axial load on ductility of double channel sections was studied. Seismic performance of 90 ft span STMFs was evaluated and design recommendation are proposed.

Table of Contents

List of Illustrations

List of Tables

Chapter 1

Introduction

1.1 Overview

There are several types of steel seismic resisting systems such as moment-resisting frames, concentrically braced frames, eccentrically braced frames, buckling-restrained braced frames, special truss moment frames, and steel plate shear walls. Each system has its advantages and disadvantages. Moreover, there are several structural steel shapes available. Different shapes are more commonly used than the others in different seismic resisting systems, i.e., wide flange shapes are used as beams and columns in moment-resisting frames or double angle sections are used as truss elements. However, the use of different shapes that are not common could deem some benefit. This chapter will present background, benefit, and shortcoming of special truss moment frames (STMFs). The objectives of the research and outline of the dissertation are also included.

1.2 Special Truss Moment Frames (STMFs)

1.2.1 Backgrounds on STMFs

Special truss moment frames (STMFs) were developed in the 1990s at the University of Michigan. At the time, open web framing systems had gained popularity because they were more economical than conventional solid web girders. Moreover, open web allowed mechanical and electrical ducts to pass through without having to add ceiling height. However, 1985 Mexico City earthquake revealed complex damages to the system including buckling of columns and truss girders. STMFs were developed such that inelastic behavior was contained within the middle segment of the truss girder called special segment (SS). SS is a ductile segment that dissipates earthquake energy while

the other members outside of the special segment, including truss members, columns, and girder-to-column connections are designed to remain elastic. American Institute of Steel Construction has adopted STMFs in Seismic Provisions for Structural Steel Building since 1997. Currently two configurations of SS are recognized by AISC. Figure 1-1(a) shows STMF with SS without any web members. This SS is called Vierendeel panel. When STMF of this type is subjected to lateral forces, the induced shear force in the middle of the SS is resisted by the chord members through formations of plastic hinges. The maximum expected vertical shear strength of the special segment, V_{ne}, is reached when the chord members in the special segment is fully yielded and strain-hardened. The other configuration comprises of X-diagonal and vertical web members in the SS as shown in Figure 1-1(b). In addition to the chord members, X-diagonal web members also contribute in maximum expected vertical shear strength of the SS through yielding and buckling. The vertical web members are used to carried unbalance forces and generally very small. Their contribution in maximum expected shear strength is negligible. The current maximum expected shear strength, V_{ne}, is shown in Eq. 1-1.

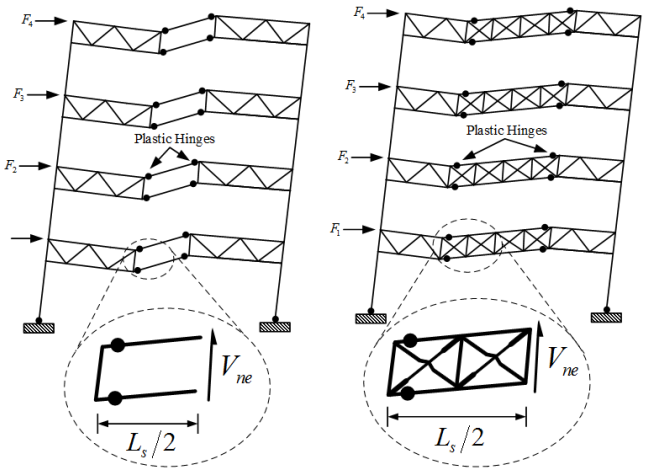

(a) (b)

Figure 1-1 (a) STMF without diagonal web member and (b) STMF with diagonal web members (Note that gravity loading is not shown here)

$$V_{ne} = \frac{3.60 R_y M_{nc}}{L_s} + 0.036 EI\left(\frac{L}{L_s^3}\right) + R_y\left(P_{nt} + 0.3P_{nc}\right)\sin\alpha \qquad [1\text{-}1]$$

where

E = modulus of elasticity of a chord member of the special segment

I = moment of inertia of a chord member of the special segment

L_s = length of the special segment

M_{nc} = nominal flexural strength of a chord member of the special segment

P_{nt} = nominal tensile strength of a diagonal member of the special segment

P_{nc} = nominal compressive strength of a diagonal member of the special segment

R_y = ratio of the expected yield stress to the specified minimum yield stress

1.2.2 Benefits and Limitations of STMFs

In general, a truss moment frame provides higher lateral stiffness with relatively less weight as compared to moment-frame systems with solid beams (SEAOC

Seismology Committee, 2008). This enables STMFs to accommodate a relatively large opening between columns or uninterrupted span up to 65 ft (AISC, 2016). Steel braced frames, while having high lateral stiffness, lack ability to provide large uninterrupted span. Steel moment resisting frames, although being able to provide open space, become very flexible and require large size sections to control their drifts when a long-span is used. As a consequence, moment resisting frames are impractical when a span exceeds approximately 40 ft (Hamburger and Malley, 2016). Moreover, yielding mechanism of STMFs which occurs through 4 plastic hinges forming at the ends of the chord members and buckling and yielding of diagonal web members in the SS provide higher structural redundancy than other systems. In conclusion, advantages of STMFs are:

1. Higher elastic stiffness than moment resisting frames.
2. Truss girders can be economically used over longer spans.
3. Open-webs can accommodate mechanical and electrical ductwork.
4. High structural redundancy.

Double curvature of the chord members in the SS occurs when STMF is subjected to lateral loading. Because the SS is shorter than the span length, rotational demand of the chord members is much larger than story drift angle. The deformed shape of an STMF is shown in Figure 1-2. Relationship between the story drift ratio and plastic rotation of the chord members are approximately estimated by Eq. 1-2 (Goel and Chao, 2008a).

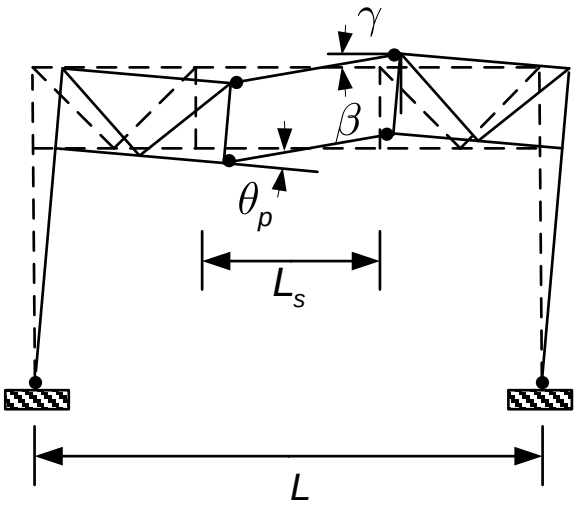

Figure 1-2 Deformed shape of an STMF

$$\theta_p = \gamma + \beta \approx \frac{L}{L_S} \times (story\ drift) - 0.015(rad) \qquad [1\text{-}2]$$

Table 1-1 shows plastic rotation of the chord member corresponding to story drift angle of an STMF with the ratio of the span length, L, to the length of SS, L_s, of 3.75. Notice that at story drift angle of 0.02 rad, the rotational demand of the chord member becomes 0.06 rad. This is larger than 0.04 rad required of flexural members used in special moment frames (SMFs).

Table 1-1 Relation between story drift angle and plastic rotation of chord members of a typical STMF

Story Drift Angle (rad)	Plastic Rotation, θ_p (rad)
0.005	0.00
0.0075	0.01
0.01	0.02
0.0125	0.03
0.015	0.04
0.0175	0.05
0.02	0.06
0.0225	0.07
0.025	0.08
0.0275	0.09
0.03	0.10

Most experimental research done in the past were on STMF made of double angle sections (Itani and Goel, 1991; Goel and Itani, 1994b; Basha and Goel, 1994). In order to satisfy the code seismic drift limitation, especially for mid-rise and tall multistory buildings, a large column section is needed, when double angle sections are used. However, heavy chord members can be used in this instance (SEAOC Seismology Committee, 2008). As a result, there is a need to verify large rotational capacity of other heavy steel shapes. Recent analytical investigation (Chao and Goel, 2006) and experimental investigation at component level (Para-Montesinos et al, 2006) showed that double channel sections could be used in STMFs. However, to maintain large rotational capacity of double channel sections, lateral support was needed near plastic hinge region.

Frequently, large openings are demanded by architectural requirements. This leads to the elimination of the X-diagonals and an STMF with multiple Vierendeel panels separated by intermediate vertical members in the SS. In current practice, intermediate

vertical members could be rather heavy. Their contribution to elastic stiffness and ultimate strength of an STMF were studied by Chao and Goel (2008) but not yet incorporated in AISC Seismic Provisions due to lack of experimental results. It is recommended to keep contribution in strength of STMF by intermediate vertical members to 50% of that of the chord members (Chao and Goel, 2008). Compared to STMFs, buckling-restrained braced frames (BRBFs) can provide much higher strength and stiffness.

Minimum axial forces in the chord members of STMFs occur in the middle zone, while the maximum axial forces occur near the ends of the truss (SEAOC Seismology Committee, 2008). As a result, maximum expected shear strength equation (Eq. 1-1) was derived based on zero axial force in the chord members in the SS. However, when span length of an STMF is longer than 65 ft, gravity loading may induce axial forces in the middle of the truss. There have been extensive studies on combined bending and axial effect on wide flange columns. However, the results might not be applicable to double channel sections. The presence of axial force makes current STMF design procedure invalid. In addition some key dimensional requirements for STMFs that could limit the use of STMFs as long span structures are as follows according to the current AISC Seismic Provisions for Structural Steel Buildings (AISC, 2016):

- Span length between columns not to exceed 65 ft.
- Overall depth of the truss not to exceed 6 ft.
- Length of the SS, L_s, shall be between 0.1 and 0.5 times the truss span length, L.
- Length-to-depth ratio, L/D of any panel in the special segment shall neither exceed 1.5 nor be less than 0.67. The upper bound length-to-depth ratio is to

control the lateral stiffness of the truss while the lower bound length-to-depth ratio is to limit the rotational demand of the chord members in the SS.

1.3 Research Objectives

This research aimed to investigate ways to enhance seismic performance of STMFs in both strength and stiffness. One way to increase STMFs strength and stiffness is to use heavy shapes such as double channel, wide flange, or double HSS sections. Due to high rotational demand of the chord members in the SS, cyclic loading behavior of heavy shapes needs to be studied. Another way is to incorporate new element in the SS such as buckling-restrained braces which provide similar strength in both tension and compression, resulting in stable ductile hysteresis responses. Moreover, the possibility of extending span the length of STMFs to 90 ft was explored. The primary objectives of this research project were the following:

1. To investigate the viability of a proposed new connection details used to eliminate lateral torsional buckling in double channel sections.
2. To investigate the viability of utilizing double HSS as flexural members and STMFs elements.
3. To explore utilizing of buckling-restrained braces in the SS of STMF to enhance strength and stiffness.
4. To investigate effect of axial loading on rotational capacity of double channel sections.
5. To evaluate the possibility of using STMFs as long span structures and propose design recommendations.

1.4 Dissertation Outline

Chapter 2 presents a review of previous research on STMFs, double channel and HSS flexural members, effect of axial load on rotational capacity, buckling-restrained brace frames and isolated buckling-restrained brace.

Chapter 3 presents a comprehensive review of the experimental program of double channel and double HSS component tests.

Chapter 4 describes the individual test results for each double channel and double HSS specimens.

Chapter 5 experimental program and test results of full scale STMF with BRBs are presented.

Chapter 6 presents analytical investigation including analytical study of effect of axial force on rotational capacity of double channel sections which led to design recommendation and analysis of long span STMFs.

Chapter 7 of this dissertation summarizes the results from this research study. Significant findings from the research program are reviewed, design recommendations are presented, and recommendations for further research are provided.

Chapter 2

Literature Review

2.1 Introduction

When subjected to lateral loading, special truss moment frames (STMFs) dissipate energy through chord members, X-diagonal web members, and intermediate vertical members in the middle part of the truss girder called special segments. STMFs provide higher lateral stiffness than moment frames but still less than braces frames. In order to increase strength and stiffness of STMFs for high seismic areas, heavy sections could be used. However, these heavy sections need to be able to sustain large rotational demand. The length of STMFs is limited to 65 ft based on previous research. In order to investigate the possibility of utilizing heavy sections, to implement buckling restrained braces in STMFs, and to extend limitation on span length of STMFs, past research on several aspects related to this research were reviewed.

2.2 Previous Research on STMFs

The devastating damages due to Mexico City earthquake in 1985 revealed poor performance of conventional open web frame (Hanson and Martin, 1987). To better understand its seismic behavior and performance, Itani and Goel (1991) of the University of Michigan, analytically and experimentally investigated seismic behavior and performance of an open web truss moment frame for a four story building. The frame was designed as an ordinary moment resisting frame (OMRF) in accordance with the requirements of the 1988 Uniform Building Code (UBC) (ICBO, 1988). Three full scale subassemblage of half joist and column under severe cyclic deformation test were conducted. Test results showed that the conventional open-web truss moment framing system performance was greatly influenced by the web members. Buckling of a diagonal web member produced a large strength and stiffness drop. Analytical studies confirmed

that this type of truss moment frame system became very flexible after buckling of the web members causing large story drifts (Goel and Itani, 1994a).

A new concept and design procedure of open web frame to limit inelastic activity to predetermined members that were able to sustain large deformations was developed. The predetermined members were X-diagonals located in the middle part of the truss girder. Vertical web members were added to carry unbalanced force when diagonal web members yielded and buckled. These panels were designed for the specified forces and members outside were design according to ultimate capacity of the middle panels. After buckling and yielding of the X-diagonals, vertical shear was resisted by flexural deformation of the chord members and plastic hinges formed at the ends of the chord members in the predetermined ductile panel. Figure 2-1 shows hysteretic response of conventional open web frame compared to that of the modified open web frame system. Analytical study showed that the modified web framing systems were more economical and stiffer than solid framing systems when designed as special moment resisting space frames.

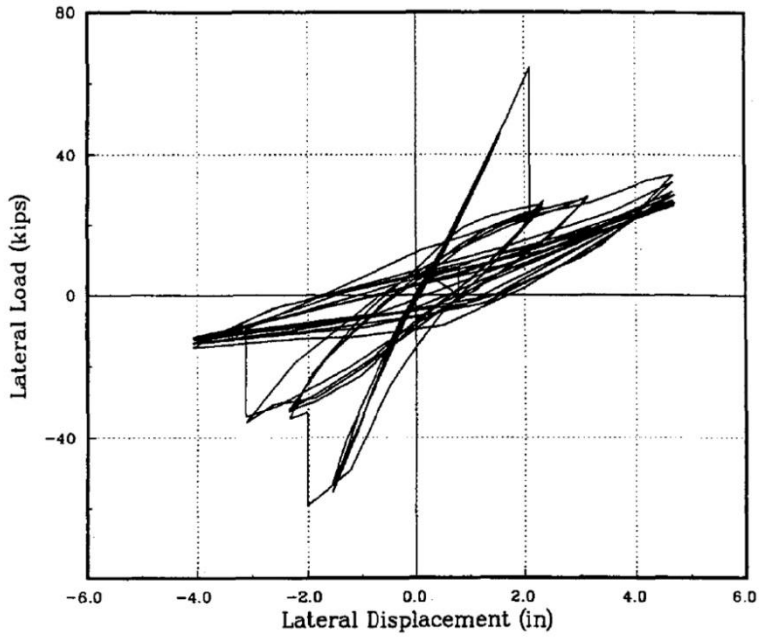

(a)

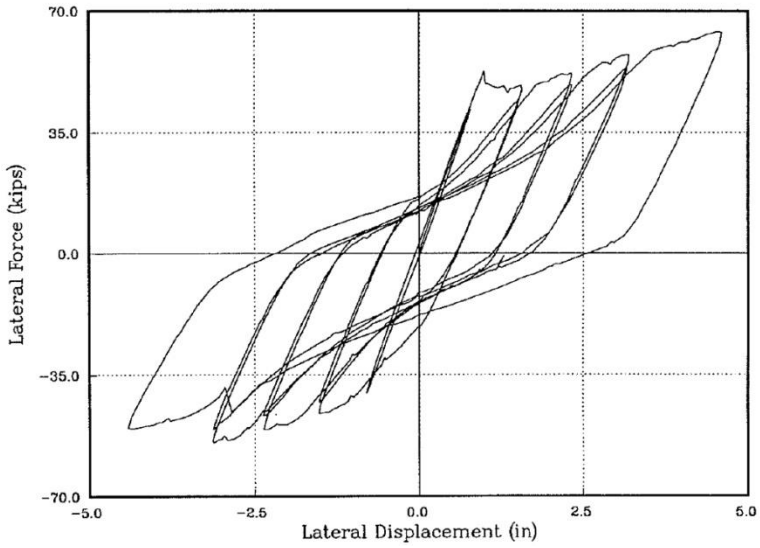

(b)

Figure 2-1 Hysteresis responses of testes specimens (Goal and Itani, 1994a; 1994b): (a) conventional open web frame; (b) modified open web frame Subassemblage 1

Basha and Goel (1994) studied a double angle STMF configuration without web members, i.e. Vierendeel configuration, in the special (ductile) segment (SS). This configuration allowed greater flexibility and architectural freedom due to more open space in the truss girder. When subjected to lateral forces, the induced vertical shear in the middle special segment was resisted solely by the chord members. This STMF dissipated energy through inelastic flexural deformations of the plastic hinges formed at the end of the chord members in the SS. Experimental results of Subassemblage 1 showed full hysteresis response without pinching or degradation up to 3% story drift (Figure 2-2). Experimental and analytical studies also suggested that truss action was not valid in the vicinity of the Vierendeel panel and consequently members adjacent to the SS must be treated as beam-column elements.

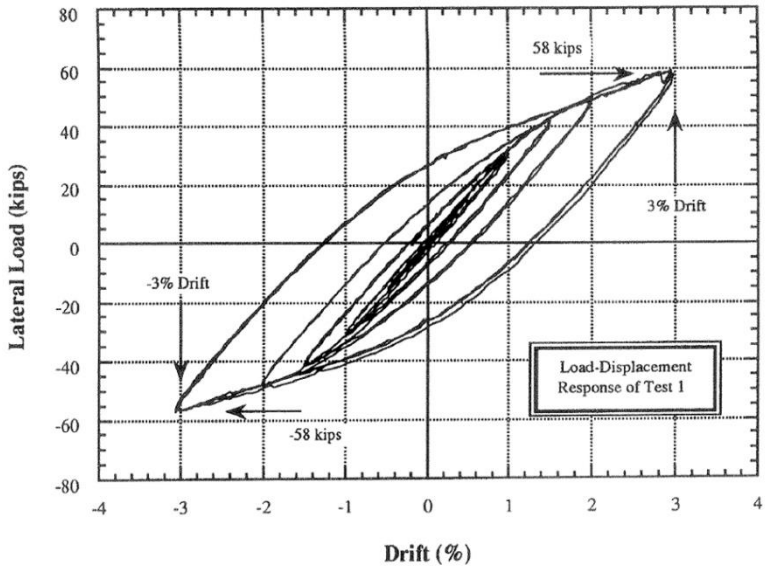

Figure 2-2 Hysteresis responses of Subassemblage 1 (Basha and Goel, 1994)

Subsequent work by Basha and Goel (1995, 1996) and led to an STMF design concept and procedure of STMF which was recognized in seismic building codes and

specifications and codes in the late 1990s (ICBO, 1997; AISC, 1997). This concept and procedure are still applicable nowadays. When subjected to gravity and lateral loadings according to applicable load combination specified by building code, required vertical shear is developed in the middle section of STMF. Ductile members (chord and X-diagonal web members) in the SS are designed so that when fully buckled, yielded and strain hardened, they are able to develop shear strength to withstand such required vertical shear. Once the members in the special segments are designed, truss members outside of the special segments including truss-to-column connections and columns are designed to remain elastic for forces generated by the fully buckled, yielded, and strain-hardened members in the special segment including applicable gravity and lateral loadings.

Basha and Goel (1995, 1996) proposed an equation to determine shear strength of an STMF according to the properties of the members in the SS which was adopted by AISC (AISC 1997) as follows:

$$V_{ne} = \frac{3.75 R_y M_{nc}}{L_s} + 0.075 EI \left(\frac{L - L_s}{L_s^3} \right) + R_y \left(P_{nt} + 0.3 P_{nc} \right) \sin\alpha \qquad [2\text{-}1]$$

where

E = modulus of elasticity of a chord member of the special segment

I = moment of inertia of a chord member of the special segment

L_s = length of the special segment

M_{nc} = nominal flexural strength of a chord member of the special segment

P_{nt} = nominal tensile strength of a diagonal member of the special segment

P_{nt} = nominal tensile strength of a diagonal member of the special segment

P_{nc} = nominal compressive strength of a diagonal member of the special segment

R_y = ratio of the expected yield stress to the specified minimum yield stress

This equation was derived based on two assumptions: 1) the maximum expected developed moments of the chord members occur at 3% story drift and 2) the strain-hardening ratio of the chord member is 10%, which is the ratio of the post-yield stiffness to the elastic stiffness in the moment-rotation relationship of the members. The V_{ne} equation was unchanged in the subsequent two AISC Seismic Provisions (AISC, 2002; 2005).

Chao and Goel (2006) proposed a new Vne equation (Eq. 2-2) which takes into account the contribution of intermediate vertical members in STMF with a multiple Vierendeel panel special segment, i.e. there are no X-diagonal members. The equation was derived based on experimental component test results conducted on heavy shapes (double channel sections) (Parra-Montesinos et.al, 2006). The first two terms are contribution from the chord members while the other is from intermediate vertical members. The equation maintain the two assumptions used in Eq. 2-1. The elastic moment at the ends of the chord members of the SS was previously assumed to result from vertical translation only, i.e., the effect of end rotation is neglected. This assumption led to overestimation of the elastic stiffness of the chord members. By considering the effect of end rotation, the coefficients of the first two terms are slightly less than those of Eq. 2-1.

$$V_{ne} = \frac{3.60 R_y M_{nc}}{L_s} + 0.036 E I_c \frac{L}{L_s^3} + \frac{m}{2}\left(\frac{3.60 R_y M_{nv}}{L_s} + 0.036 E I_v \frac{L}{L_s^3} \right) \qquad [2\text{-}2]$$

Though AISC (AISC 2010, 2016) did not adopt the equation due to lack of experimental on STMF with multiple Vierendeel panels, it adopted an equation where contribution of the chord members and X-diagonal web members are included (Eq. 1-1)

Simasathien (2016) tested full scale subassemblage of STMFs made of double channel sections with single Vierendeel panel SS and three multiple Vierendeel panel SS. STMF with single Vierendeel panel was stable up to 3% story drift before losing strength. STMF with multiple Vierendeel panel exhibited higher elastic stiffness and ultimate lateral strength than STMF with single Vierendeel panel. However, it started losing strength at 1.5% story drift when intermediate vertical members failed and hysteresis response followed that of STMF without intermediate vertical members. To avoid sudden drop of strength in this type of STMF, the contribution of the intermediate vertical member to V_{ne} was suggested not to exceed 50% of the total V_{ne}.

2.3 Previous Research on Flexural Members

2.3.1 Double-Channel Flexural Member

Flexural behavior of double channel built-up members under reverse cyclic bending was studied by Parra-Montesino et.al (2016). The results from six cantilever double channel specimens suggested that the current lateral bracing required by AISC LRFD provisions was not adequate to prevent lateral-torsional buckling (LTB) of the sections. Stitches spacing for built up chord members in the SS was proposed and adopted by AISC (AISC 2010, 2016) as shown in Eq. 2-3 to prevent LTB of individual member. Moreover, lateral bracing in the region adjacent to the plastic hinge is required in order to prevent LTB of the built-up member and ensure 0.06 rad total plastic rotation. To achieve total plastic rotation of larger than 0.06 rad, the connection need a combination of lateral bracing in the plastic hinge region, a reinforced gusset plate connection, and a trapezoid-shaped web cutout detail as shown in Figure 2-3.

$$L_{pd} = \frac{0.04Er_y}{F_y} \quad [2\text{-}3]$$

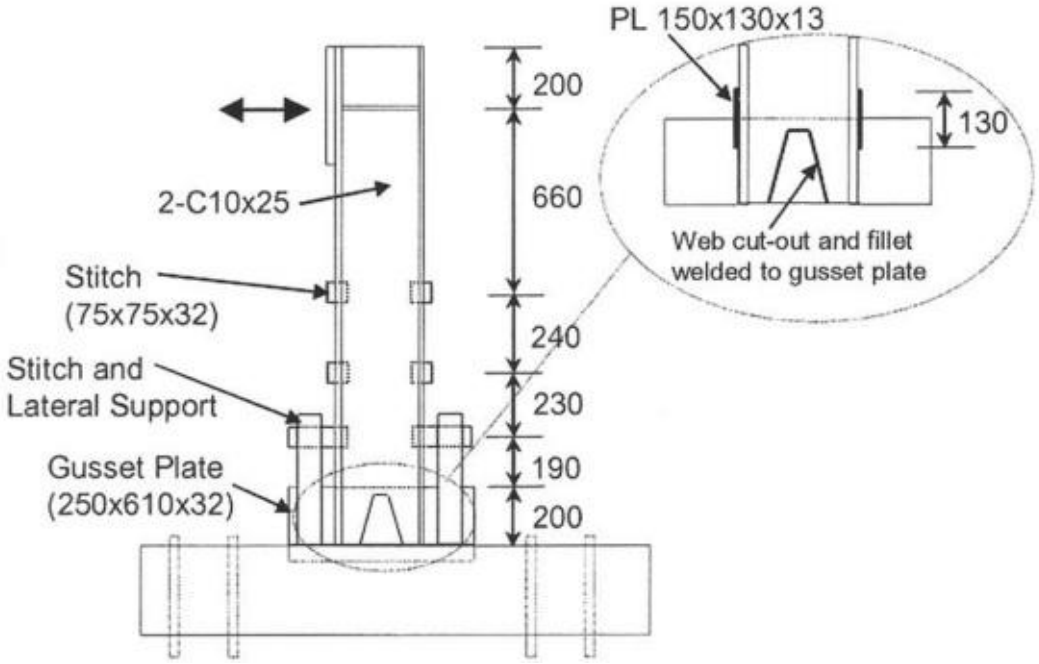

Figure 2-3 Connection details of Specimen 6 (Parra-Montesinos et al, 2006)

2.3.2 Hollow Structural Section (HSS) Flexural Member

Limited understanding of HSS cyclic flexural behavior prevents its application as seismic resisting elements. According to Bresscia et al. (2009), it is safe to assume that collapse occurs when the cumulative plastic ductility in one direction is greater than that available under monotonic conditions. However, this approach is very conservative because their monotonic test of HSS only absorbed 18% of the corresponding energy dissipated under cyclic condition prior to collapse.

Fadden and McCormick (2012a) tested 11 HSS members under pure bending ranging from HSS8×4×1/4 to HSS12×6×1/4. They found that maximum moments occurred between 0.017 rad and 0.035 rad. The sections with 3/8 in. thickness tend to

show higher normalized maximum moment and higher rotations at maximum moment than the 1/4 in. thick specimens. They also suggested b/t ratios below 25 and h/t ratios below 40 for HSS to maintain 90% of maximum moment at beam rotations of 0.04 rad. Moreover, connections have been the limiting factor of the HSS design because reinforcing the connections of HSS assemblies often is not optionally available (Packer et al. 2010).

With double-HSS sections, two HSS are simply welded to a center gusset plates in the same manner as double-angle or double-channel joint connection. This should eliminate the need to strengthen the HSS connection. The use of double HSS also doubles bending capacity of HSS without changing width-thickness and depth-thickness ratios which, in turns, provides more readily available options for seismic compact sections to choose from. Also, when a double-HSS is used, compared to a single-HSS with similar moment capacity, the width-thickness ratio can generally be lowered than that of a single-HSS with similar moment capacity, which considerably increases the compactness under bending thereby delaying flange buckling. Due to the fact that narrower tube sections would be more practical to use in a double-HSS configuration, the requirements for b/t ratios would be easy to adhere to.

Another possible controlling factor of plastic capacity of steel members is lateral-torsional buckling (LTB). Even though, very long rectangular HSS bent about strong axis are subjected to lateral-torsional buckling, however; in normal cases, beam deflection will control (AISC 2016b). Hence, there should be no need for lateral bracing when double-HSS is used.

2.3.3 Effect of Flange Local Buckling, Web Local Buckling, and Lateral Torsional Buckling on Flexural Ductility

According to AISC Seismic Provisions for Structural Steel Buildings (AISC 341, 2016), beam-to-column moment connections in special moment frames (SMF) must maintain a beam flexural strength at the face of the column of at least $0.8M_p$ at an interstory drift angle of 0.04 rad. Note that rotational demand of the chord members in an STMF is even higher than that. This requirement is to prevent a large strength degradation, which can increase rotational demand from *P*-Δ effects, and the likelihood of structural collapse (AISC 341, 2016). The controlling factors of the inelastic rotational capacity and ductility of steel members are local instabilities of the beams including flange local buckling (FLB), web local buckling (WLB), and lateral-torsional buckling (LTB). FLB and WLB are influenced by the width-to-thickness ratio of the beam flanges ($b_f/2t_f$) and web (h/t_w), respectively, while LTB is governed by the lateral slenderness of the beam, L_b/r_y, where L_b is the unbraced length from the beam end to the first lateral support and r_y is the weak axis radius of gyration. To achieve sufficient inelastic rotational capacity for seismic applications, the three buckling modes can be delayed when the slenderness ratio for the three instabilities is within code specified limits. AISC 341 (2016) prescribes limitations on compactness ratios to delay FLB and WLB. AISC 341 (2016) also prescribes spacing between lateral supports and the lateral bracing of beam flanges adjacent to the plastic hinge locations to delay or prevent LTB. However; AISC 341 (2016) and AISC Prequalified Connections for Special and Intermediate Steel Moment Frames for Seismic Applications, (AISC 358, 2016) do not allow lateral bracing and attachment in the plastic hinge region (or the protected zone) which is the area where LTB typically occurs.

Extensive studies on the effect of the three buckling modes on wide-flange beam's rotation capacity have been carried out, especially after the 1994 Northridge earthquake in the north-central San Fernando Valley region of Los Angeles, California and the 1995 Great Hanshin earthquake in Kobe, Japan. An experimental testing conducted by Yu et al. (2000) using AISC's standard loading protocol for beam-to-column moment connections showed that adding lateral bracing near the protected zone reduces the WLB and LTB amplitudes as well as the strength degradation rate, thereby increasing plastic rotational capacity of wide-flange reduced beam sections (RBS) from 0.03 to 0.04 rad. Uang and Fan (2001) statistically evaluated the performance of 55 full-scale RBS moment connection specimens. Either when treating WLB, FLB, or LTB mode as an independent limit state or considering interaction between them, regression analyses showed that the slenderness ratio of WLB had the most influence on plastic rotation and strength degradation while that of LTB had the least impact. Studies on reinforced connections by Kim et al. (2002) also concluded that the location of lateral supports (or L_b) did not substantially affect the hysteretic response of the test connections. However, in prior tests (Uang and Fan, 2001; Kim et al., 2002), the lateral supports were placed either far away from or at the end of the plastic hinge, rather than at the center of the plastic hinge where the lateral twisting typically occurs. This is mainly due to the prohibition specified by the AISC Seismic Provisions (AISC 341, 2016) which does not allow any attachment located within the plastic hinge region. The maximum beam rotations (interstory drift angle) ranged between 0.03 and 0.04 rad in these tests. It is also noticed from these tests that the plastic zones are typically narrow, accompanied by the large amplitude of FLB and WLB. The interaction of these instabilities occurring at the same locations could have prevented the steel from developing a longer plastic hinge length. On the other hand, Nakashima et al. (2003) studied the interaction between LTB,

FLB, and WLB in beams subjected to large cyclic loading. The study showed that for beams with intermediate thick-to-thin flanges and a thick web, LTB expedited FLB and WLB, which in turn accelerated out-of-plane deformation and resulted in strength degradation. As for beams with thick flanges and a thin web, WLB occurred first but did not have accelerated out-of-plane deformations; thus, the beam rotation capacity was relatively independent of the lateral unbraced length. An investigation conducted by Okazaki et al. (2006) showed that the influence of LTB on the beam rotational capacity depended on the geometry of the beams and target rotations. They found that most steel wide-flange shapes could be categorized into two groups: 1) shallow beams ($1.5 < d/b_f < 2.1$), where d is the overall depth of the beam and b_f is the width of the flange, and 2) deep beams ($2.1 < d/b_f < 2.8$). Their analyses showed that in the shallow beams, LTB was not noticed until interstory drift angle reached 0.03 rad, while in the deep beams, LTB appeared when the interstory drift angle reached 0.02 rad. In addition, the observed buckling modes followed either one of the two cases: 1) FLB preceded simultaneous occurrence of LTB and WLB, and 2) LTB and FLB occur simultaneously, followed by WLB. In no analysis did LTB occur alone.

The above literature review shows that because the external lateral supports have to be a certain distance away from the plastic hinge, LTB cannot be completely prevented. This could be the reason why prior studies observed no significant difference in the responses with different unbraced lengths, since in all cases, LTB occurred. It also shows that the plastic rotational capacity and strength degradation rate can be strongly influenced by the interaction between the three buckling modes.

2.4 Buckling-Restrained Braces Research

Buckling-restrained braces (BRBs) have gained popularity as seismic force resisting system both in new construction and rehabilitation projects. The major advantage of BRBs when used as primary lateral force resisting elements in a buckling-restrained braced frame (BRBF) is their nearly equal strength in compression and tension, which eliminates the post-buckling load imbalance inherent in the conventional braced frames found in the special concentric braced frame (SCBF) system. The hysteretic behavior of BRBF is ductile and stable due to the elimination of brace buckling.

Compared to conventional concentrically braced frames (CBFs), BRBFs are typically more flexible due to higher brace axial design stresses. Temblay et al. (2004), tested two subassemblages with BRBs. The BRB in a one subassemblage has shorter steel core than that of the other in order to increase brace axial stiffness. The results showed that both BRBs could sustain core strain deformation up to 3.5%. The BRBs properties were then used in design and analysis of prototype 3 story building to evaluate their seismic performance. The design example showed that the building with shorter core BRB members experienced smaller story drifts, but this resulted in higher strain demand of the brace cores. The analytical results demonstrated that CBF structures experienced less lateral deformations than BRBF, however; larger forces were imposed on surrounding structural elements at the lower floor.

Black et.al (2002) conducted an experiment to investigate the stability of Buckling-Restrained Unbonded Braces. The isolated braces tested were representative of the braces designed for use in two major building project s in Northern California. The results showed that these braces deliver stable and repeatable behavior. Then, the behavior of the braces was characterized at force-deformation level where the

parameters used were geometric property of the brace and the mechanical properties of the steel core.

In order to incorporate BRBs into an STMF in places of X-diagonal and vertical intermediate members to increase its strength and stiffness, the BRBs will be rather short compared to those in BRBFs. El-Bahey and Bruneau (2010) studied the use of short BRBs (pin-to-pin dimension of 24 in.) as structural fuses in columns of a prototype bridge bent. The connection at the end of the BRB in this test was a big pin instead of the traditional bolted or welded connection. The general configuration of the BRBs is shown in Figure 2-4. The isolated BRB test was performed in order to understand a more accurate behavior of the BRB. Hysteresis responses were stable and the BRBs dissipated energy more than that required by AISC Seismic Provisions.

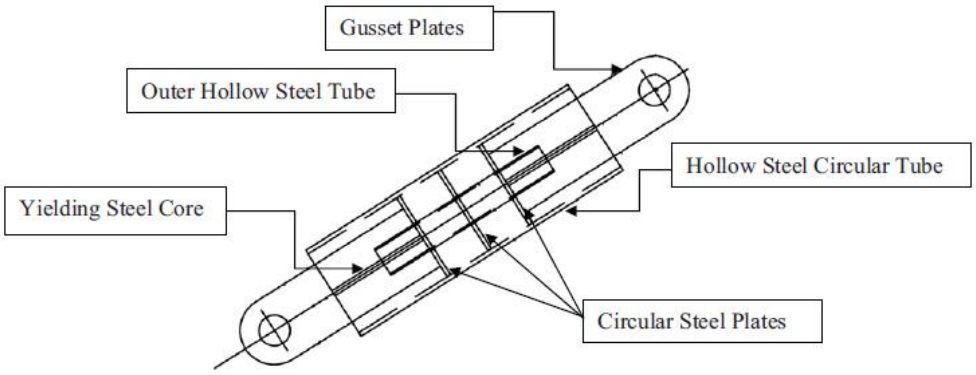

Figure 2-4 BRB Assembly Sketch (El-Bahey and Bruneau 2010)

Chapter 3

Component Test Experimental Program

3.1 Overview

The component tests comprise of the tests of flexural members (double channel and double HSS sections) and isolated buckling-restrained brace (BRB). Both double channel and double HSS both shapes represented either chord member or intermediate vertical member in the SS of prototype STMFs. One double channel specimen was tested under monotonic loading. Thirteen double channel specimens and three double HSS specimens were tested under AISC reversed cyclic displacement history. One double channel specimen was tested under Near Collapse reversed cyclic displacement history developed by the author. One isolated BRB was tested in order to understand its behavior. Two BRBs of the same properties were incorporated into a full scale STMF subassemblage test.

3.2 Flexural Members Test

3.2.1 Double Channel Specimens

Double channel specimens represented a chord member or an intermediate member of prototype STMFs. Prototype STMFs have the general configurations as full scale subassemblage STMF tests which has span length of 31.8 ft., depth of 4 ft., and special segment length of 119 in. as shown in Figure 3-1 (Simasathien, 2016). When STMF is subjected to lateral displacement, the chord members and intermediate vertical members are under double curvature with the inflection point at the middle of the middle. As a result, the component test specimens could be taken at half length of the member it represented as shown in Figures 3-2 and 3-3. The fixed end and the free end in the component test specimen represent the end join and the mid span or inflection point of the member it represents.

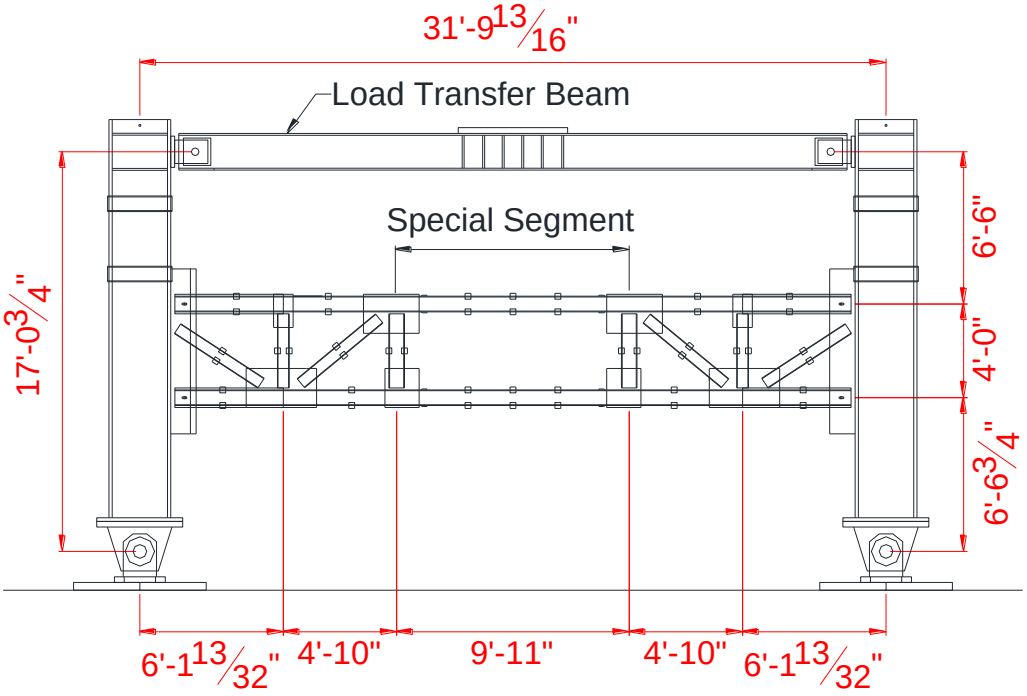

Figure 3-1 Prototype Special Truss Moment Frame Subassemblage

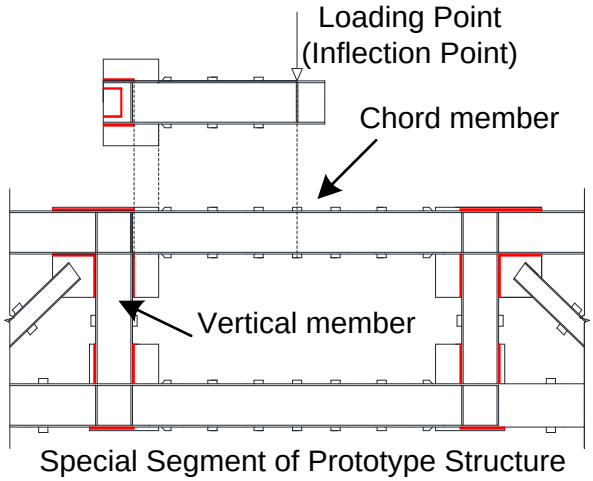

Figure 3-2 Specimen Representation of Chord Member in Special Segment of STMF

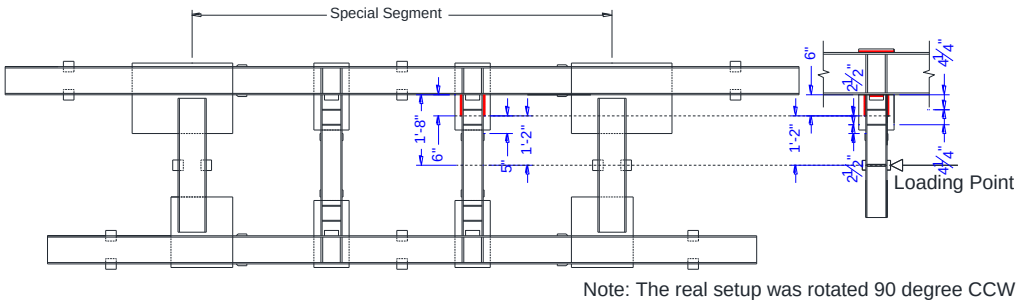

Figure 3-3 Specimen Representation of Intermediate Vertical Member in Special Segment of STMF

In special truss moment frames (STMF), the chord members in the special segment (structural fuses located in the mid-span of the truss) require a plastic rotational capacity of approximately 0.06 rad for a story drift angle of 0.02 rad (Goel and Chao, 2008; Simasathien et al., 2017). This rotational demand is much greater than that for beams in moment-resisting frames. Parra-Montesinos et al. (2006) investigated the behavior of double-channel built-up members under reversed cyclic bending. Their experimental results indicated that the lateral bracing requirement specified in the 2001 AISC-LRFD specifications could not prevent the LTB of individual members or the entire built-up member. The findings led to a minimum stitch spacing required by AISC 341 (2010, 2016). Lateral bracing in the region adjacent to the plastic hinge was required to minimize LTB and thus ensure a total member rotation of 0.06 rad.

A new connection configuration consisting of double-channel built-up components with a center gusset plate and horizontal stitches, with or without vertical web stiffeners in the plastic hinge region, was explored in this research. The purpose of the proposed configurations are: 1) to eliminate LTB and 2) to minimize the interaction between FLB and WLB. In addition, a double-channel section with flanges cut to reduce its strength was tested. This configuration resembles a wide-flange RBS. The purpose of

a double-channel RBS is to reduce its contribution in vertical shear strength when used as a chord member in the SS of an STMF, thus reducing strength demand of non-yielding members outside of STMF special segments.

In this study, a new detailing of double-channel connection, using a center gusset plate with a weld-free zone and horizontal stitches, as shown in Figure 3-4, was developed through a series of tests. The welding scheme at the connection is shown in Figure 3-5. The connection details are described as follows:

A 1 in.-thick gusset plate was first welded to the column face by a fillet weld. A fillet weld was also used to connect the two channel sections to the gusset plate and the reaction column face. Note the extended gusset plate below or above the beam (Figure 3-4), while not needed for a beam-to-column moment connection, can be used to attach other members such as a vertical or diagonal member. Part of the gusset plate on the far side from the reaction column face was not welded to the channels, forming a “weld-free zone” of the gusset plate which allows the channels to freely move. The stiff central gusset provides direct lateral support right at the plastic hinge zone without violating the AISC requirement, thus eliminating LTB. Normally, stitches are used to keep the built-up section to act as a single member by welding them in between the two channels. Test results indicated that when the double-channel member was subjected to a large rotation, the channels on the compressive side near the plastic hinge region bulged and separated from the center gusset plate (see Chapter 4). It was observed that the welds between conventional stitches and channels were not strong enough to withstand this action. As a result, horizontal stitches were used as the first pair of stitches. These stitches were placed and welded on both the top and bottom flanges. The placement of this first pair was in such a way that their edges were 1 in. away from the edge of the weld-free gusset plate. This gap proved sufficient to accommodate member rotation up to 0.10 rad. Note

that this is a final connection details developed from series of the tests. As a results, not all specimens featured this details. Table 3-1 and Figure 3-6 to Figure 3-12 show configurations and dimensional details of double channel specimens.

All the welds used in double channel specimens were SMAW fillet welds made by E70 electrodes. The horizontal weld between the specimen and the gusset plate was 1/2" in size. The welds between Gusset plate and the column and between specimen and the column were 1/2" in size. The weld in the web cutout was 1/4" in size. The welds between horizontal stitches and the channels were 1/4" for 1/4" and 3/8" thick stitches. This weld size increased to 3/8" for1/2" thick stitches. The weld between conventional stitch and channels was 3/8" in size. Finally, the weld between stiffeners and the channels was 1/4" in size.

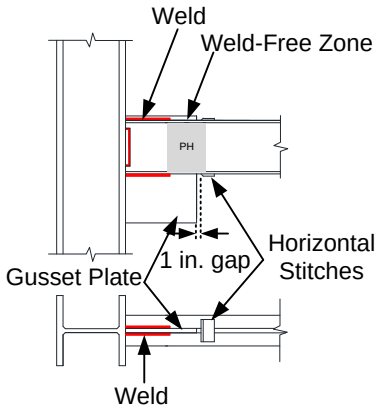

Figure 3-4 Proposed Double-Channel Connection with Self-Stabilizing Lateral Support at Plastic Hinge

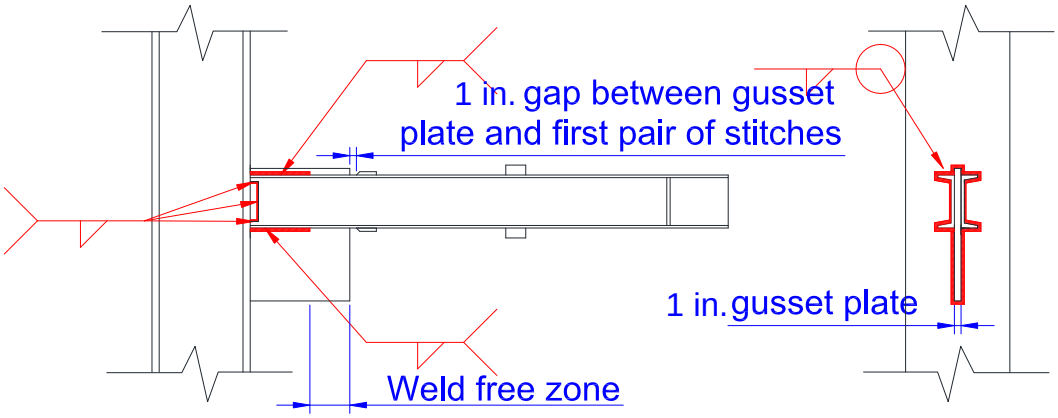

Figure 3-5 Welding Scheme at the Connection of Double Channel Component Test

Table 3-1 Dimensional Details of Double Channel Specimens

Specimen	Shape	Weld Length, A (in.)	Weld Free Length, B (in.)	L (in.)	Depth, d (in.)	Nominal Weld Length	Nominal Weld Free Length	b/t	h/t	Loading History
2C12-1[1]	2C12×20.7	8	10	55	12	0.67d	0.83d	5.87	36.3	AISC
2C12-2[1]	2C12×20.7	10	8	53	12	0.83d	0.67d	5.87	36.3	AISC
2C12-3[1]	2C12×20.7	10	8	53	12	0.83d	0.67d	5.87	36.3	AISC
2C12-4	2C12×20.7	10	8	53	12	0.83d	0.67d	5.87	36.3	AISC
2C12-5	2C12×20.7	10	8	53	12	0.83d	0.67d	5.87	36.3	AISC
2C12-6	2C12×20.7	10	6	53	12	0.83d	0.5d	5.87	36.3	AISC
2C12-7	2C12×20.7	10	6	53	12	0.83d	0.5d	5.87	36.3	AISC
2C12-8	2C12×20.7	10	6	53	12	0.83d	0.5d	5.87	36.3	AISC
2C12-9[1]	2C12×20.7	10	0	53	12	0.83d	0	5.87	36.3	AISC
2C12-10-RBS	2C12×20.7 with RBS	11	6	52	12	0.92d	0.5d	4.12	36.3	AISC
2C12-11-RBS	2C12×20.7 with RBS	11	6	52	12	0.92d	0.5d	4.12	36.3	AISC
2C12-12	2C12×20.7	10	6	53	12	0.83d	0.5d	5.87	36.3	NC
2C8-1	2C8×18.75	9	6	54	8	1.13d	0.75d	6.49	13.5	AISC
2C6-1	2C6×13	6	4	14	6	1.00d	0.67d	6.30	11.0	AISC
2C6-2	2C6×13	6	4	14	6	1.00d	0.67d	6.30	11.0	AISC

Note: [1] First pair of stitches is conventional stitches.

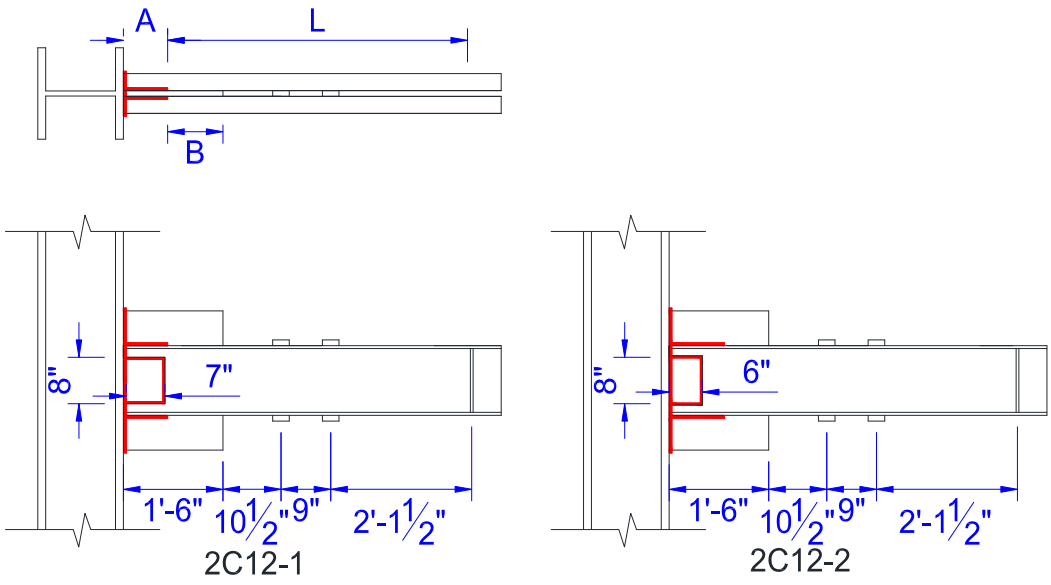

Figure 3-6 Dimensional Details of Specimens 2C12-1 and 2C12-2

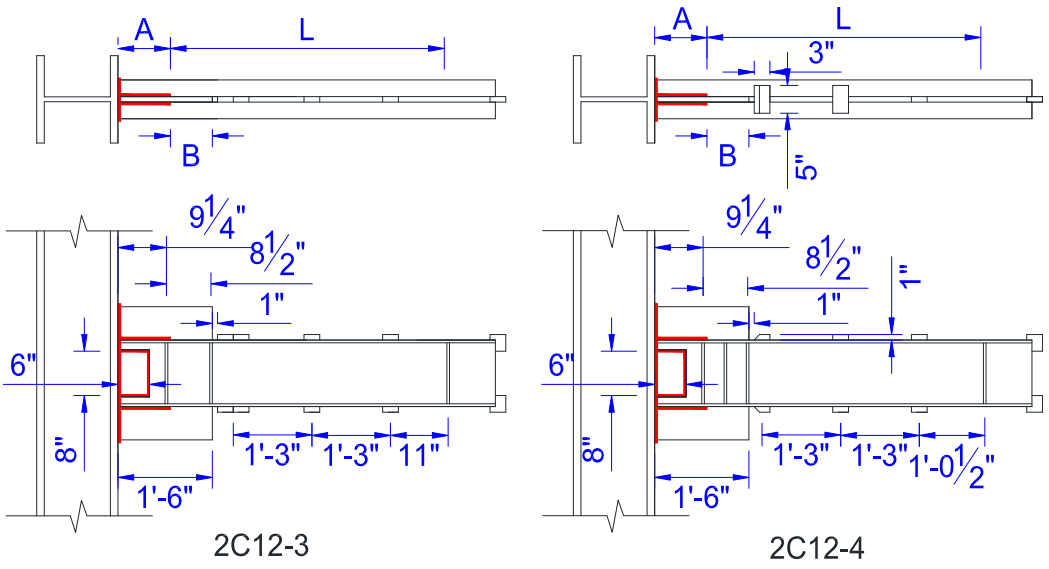

Figure 3-7 Dimensional Details of Specimens 2C12-3 and 2C12-4

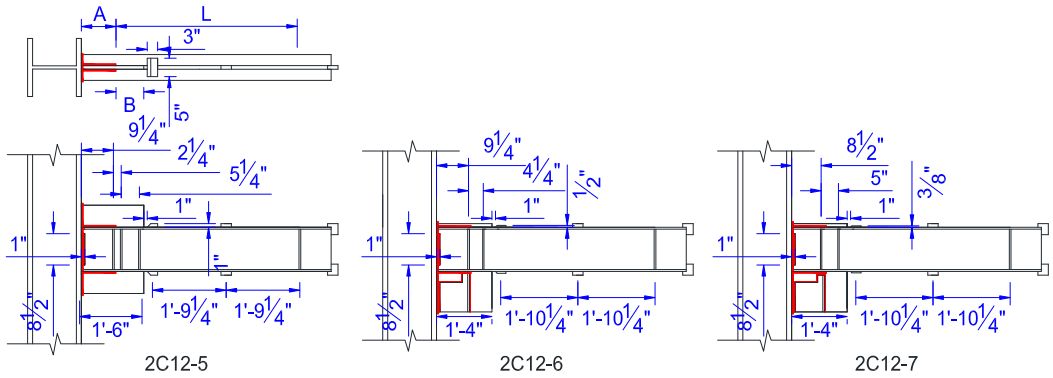

Figure 3-8 Dimensional Details of Specimens 2C12-5, 2C12-6, and 2C12-7

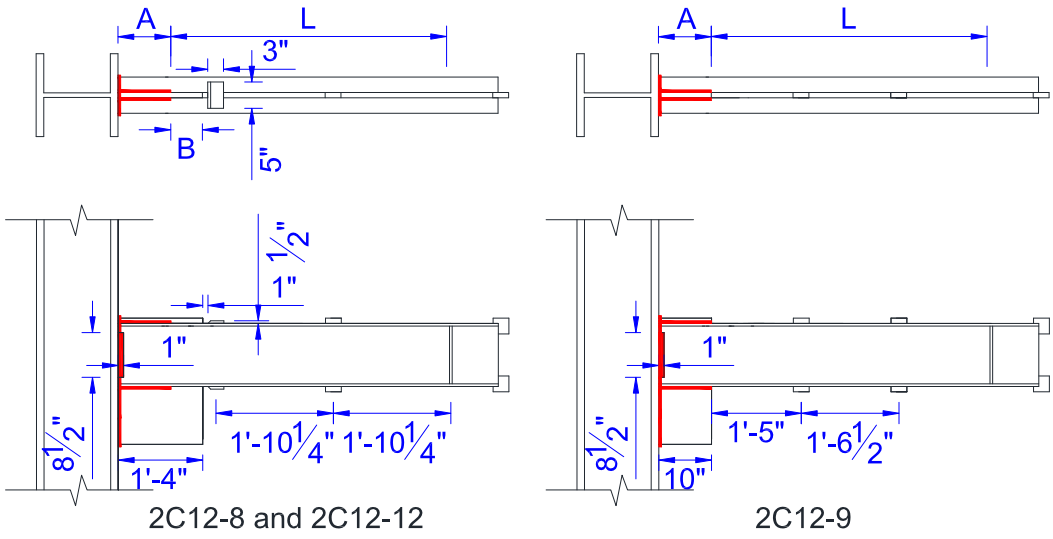

Figure 3-9 Dimensional Details of Specimens 2C12-8, 2C12-9, and 2C12-12

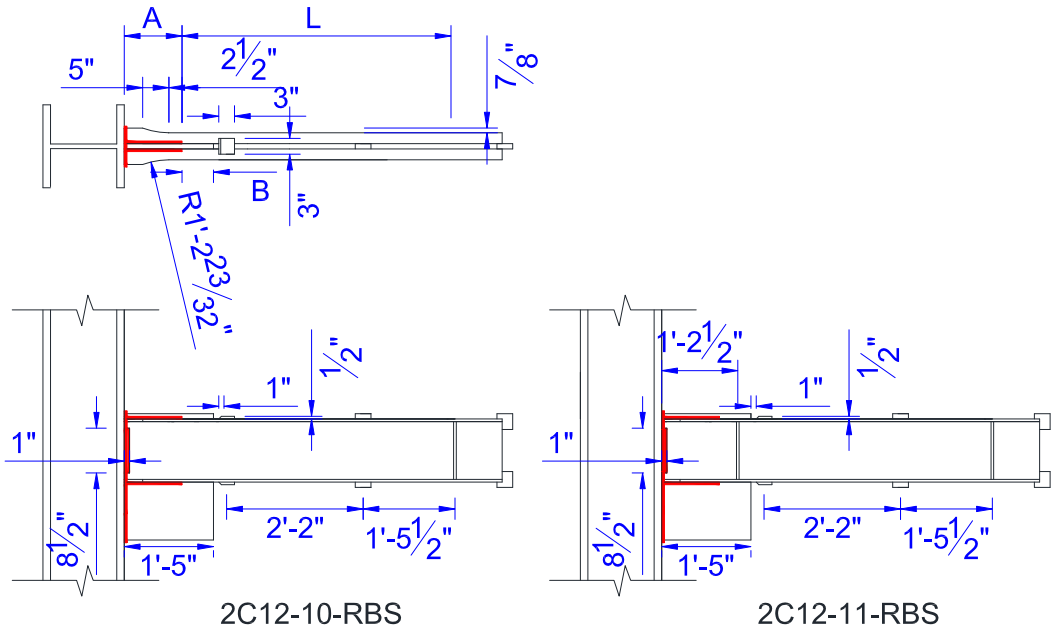

Figure 3-10 Dimensional Details of specimens 2C12-10-RBS and 2C12-11-RBS

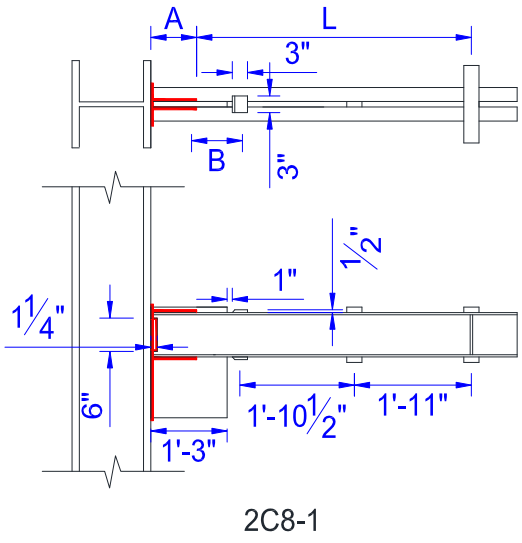

Figure 3-11 Dimensional Details of Specimen 2C8-1

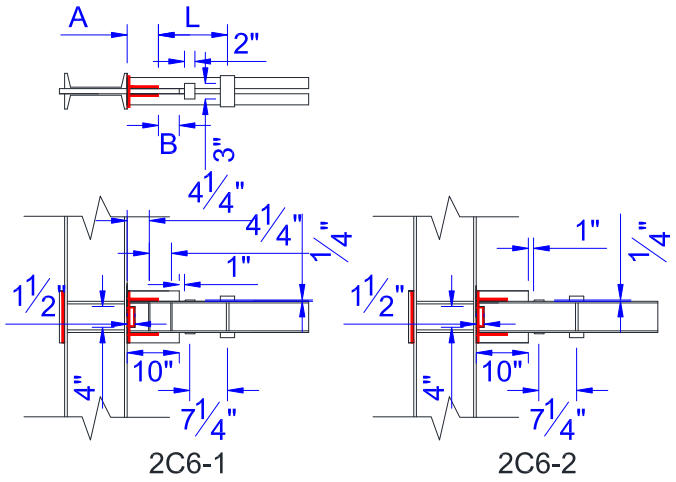

Figure 3-12 Dimensional Details of Specimens 2C6-1 and 2C6-2

3.2.2 Double HSS Specimens

Similarly to double channel specimens, three double HSS specimens represented the chord member of the STMF prototype were tested. With double-HSS sections, 2 HSS are simply welded to a center gusset plates in the same manner as double-angle or double-channel joint connection. Because LTB is not a concern in HSS sections, the connection details of double HSS do not feature extended gusset plate. Horizontal stitches can be used, however; not needed (see Chapter 4). Figure 3-13 shows welding scheme of double HSS specimen connection. Table 3-2 and Figure 3-14 show configuration and dimensional details of double HSS specimens.

All the welds used in double HSS specimens were SMAW made by E70 electrodes. The horizontal weld between the specimen and the gusset plate was bevel groove weld. Welds in other places were all fillet welds. The welds between Gusset plate and the column and between specimen and the column were 1/2" in size. The welds between all stitches and the HSS were 3/8" in size. The weld between cover plates and 2HSS-2 specimen were 1/4" in size.

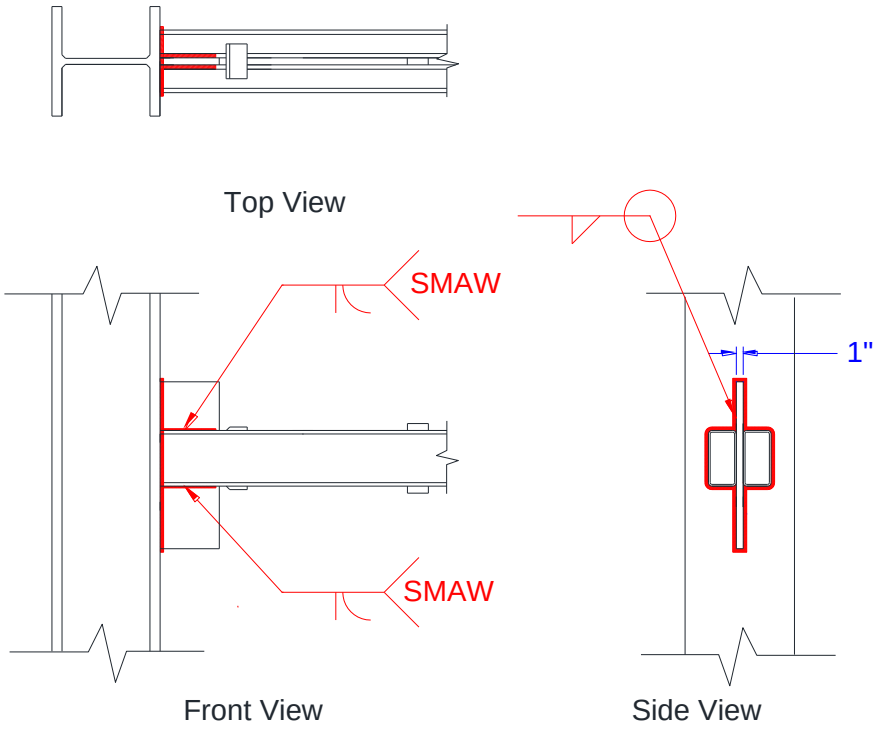

Figure 3-13 Welding Scheme at the Connection of Double HSS Component test

Table 3-2 Dimensional Details of Double HSS Specimens

Specimen	Shape	Weld Length (in.)	L (in.)	Depth, d (in.)	Nominal Weld Length	First Pair of Stitches	b/t	h/t
2HSS8-1	2HSS8×4×1/4	8	55	8	d	Horizontal	14.2	31.3
2HSS8-2	2HSS8×4×1/2	8.5	54.5	8	1.06d	Horizontal	5.6	14.2
2HSS8-3	2HSS8×4×1/2	9	54	8	1.13d	Conventional	5.6	14.2

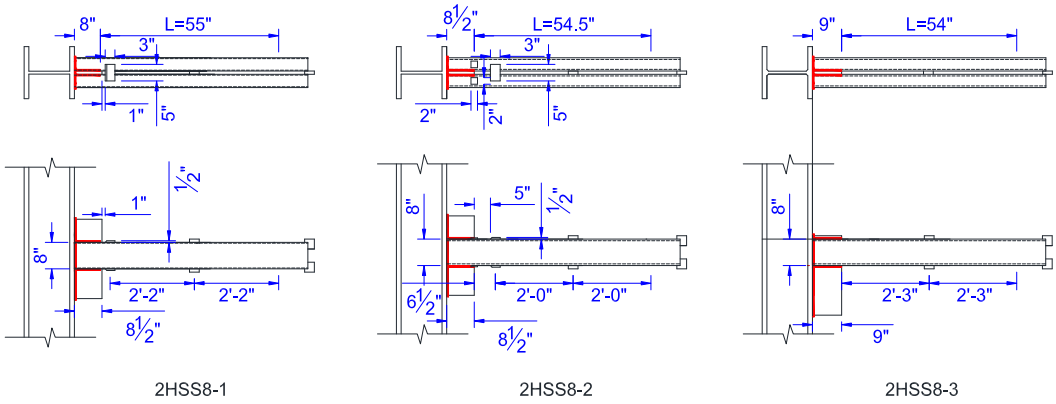

Figure 3-14 Dimensional Details of Specimens 2HSS8-1, 2HSS8-2, and 2HSS8-3

3.2.3 Test Setup

Figures 3-15 and 3-16 show the overall picture of experiment test setup. The test specimen was cantilevered from a reaction column (W14×193) that was connected to a reaction frame and a reaction floor. The reaction frame consisted of two W33×354 columns and a W33×354 beam. A 100 kip hydraulic actuator was used to apply the displacements at the tip of the specimen. A bracing frame was used to laterally support the swivel head of the actuator in order to eliminate any torque resulted from the applied load.

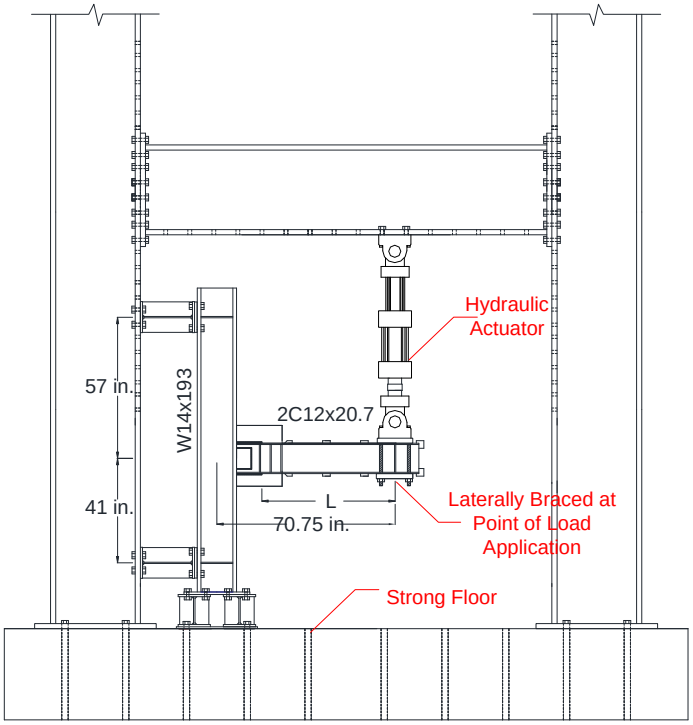

Figure 3-15 Test Setup Drawing without Lateral Bracing

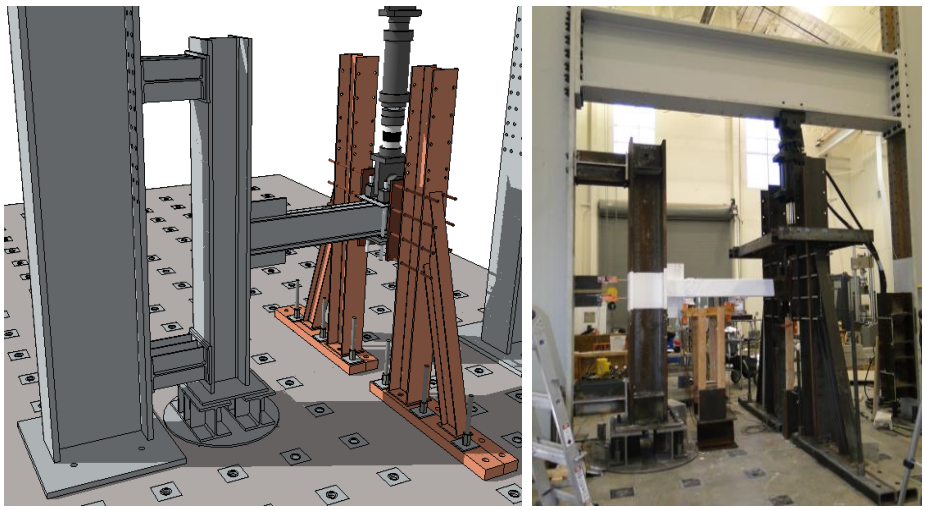

(a) (b)

Figure 3-16 (a) 3-D Test Setup Drawing and (b) Picture of Test Setup

3.2.4 Instrumentations

Test data was collected via StrainSmart Data Acquisition System. The applied force and vertical tip displacement were measured by a load cell and a displacement sensor of the hydraulic actuator MTS Series 201. Load capacity of the actuator is 100 kips and displacement limit is +/- 12.5 cm. Other instruments used in the tests are

3.2.4.1 Linear Variable Displacement Transducers (LVDTs)

Seven LVDTs were used to measure various displacement of interest. General locations of each LVDT can be seen in Figure 3-17. LVDTs 1 and 2 were located at the end of the horizontal weld connecting the specimen to the gusset plate. This location ideally was the plastic hinge. One LVDT was used to measure vertical displacement of each channel. LVDTs 3 and 4 were located underneath the channels further away from the plastic hinge region to measure vertical displacement of each channel. LVDTs 5 and 6 were used to measure rotation of the reaction column. They were mounted horizontally at the level of the top and bottom flanges of a specimen to measure horizontal displacements. LVDT 7 were mounted to the floor and used to measure uplift of the reaction column base. The exact locations of LVDTs for each specimen can be found in sensor locations in Appendix D.

The measurements from the instruments were used to determine total member rotation as:

$$Member\ \ rotation = \frac{Displacement\ -\ LVDT\ 7}{L_1} - \frac{LVDT\ \ 5\ -\ LVDT\ 6}{h} \qquad [3\text{-}1]$$

When the specimen was consider as a beam in a moment frame system, the story drift angle was the same member drift. This angle should be calculated using the distance from the middle of the column panel zone to the loading point (inflection point). As a result, moment frame member drift becomes:

$$Moment\ frame\ story\ drift = \frac{Displacement\ -\ LVDT\ 7}{L_2} - \frac{LVDT\ 5\ -\ LVDT\ 6}{h} \qquad [3\text{-}2]$$

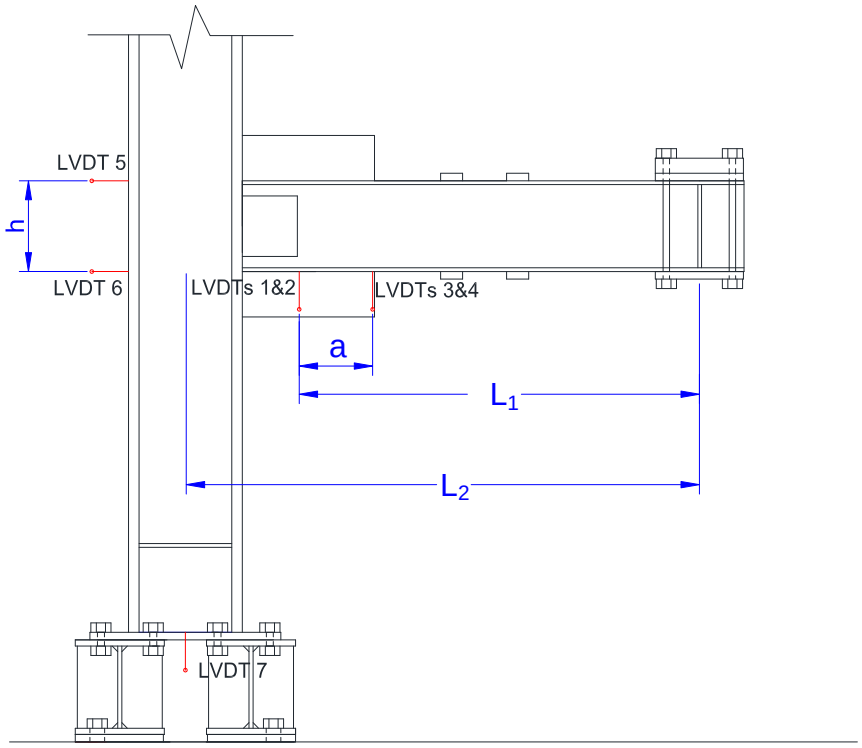

Figure 3-17 General Location of Linear Variable Displacement Transducers (LVDTs)

3.2.4.2 Strain Gauges

Uniaxial strain gauges were place on both flanges and webs of the specimens in to determine uniaxial strain at various locations. In some instance, strain gauges were place at the column panel zone and horizontal stitches as well. Drawings showing the locations of strain gauges for each specimen can be found in Appendix D.

3.2.5 Loading Histories

3.2.5.1 AISC Loading History of 2C12×20.7

The AISC loading history for beam-to-column moment connections is designated by numbers of cycles vs. story drift angle. To conform to the standard, a prototype one-bay

one-story STMF with the configuration as shown in Figure 3-1 was selected. The top and bottom of the columns were pinned connection, representing inflection points at columns' mid height in subsequent stories while the beam at the top is a loading beam in the STMF full-scale experiments. Nonlinear push-over analysis was carried out on the prototype STMF with the same chord members as the component test specimen (2C12×20.7) to obtain a relationship between STMF story drift angle and member plastic rotation. A monotonic test of specimen 2C12-1 was done to acquire member elastic rotation. Finally, a relationship between total (elastic plus plastic) rotation of the member and STMF story drift angle was obtained. The total member rotations were then converted into displacements at each corresponding story drift angle according to the AISC loading history. The details on construction of the AISC Loading History of 2C12×20.7 can be found in Appendix A. The loading history is shown in Figure 3-18 and Table 3-3. Due to the limitation of the actuator's stroke, the specimens could only be pushed a displacement corresponding to STMF story drift angle of 0.028 rad. Since this limited maximum story drift angle was less than the AISC requirement at the story drift angle of 0.03 rad, two cycles of 0.024 rad which was a midpoint between 0.02 and 0.028 rad were added, from specimen 2C12-4 onward, for stringency. Note that the "member rotation" was calculated by using the vertical displacement and the distance from end of welds to the loading point while the "moment frame story drift angle" was calculated by using vertical displacement and the distance from center of the column panel zone to the loading point. Figure 3-18 shows that when considered as a moment frame, the moment frame story drift is much larger than AISC loading history required for moment connection.

3.2.5.2 AISC Loading Histories of 2C12×20.7 with Reduced Beam Section (RBS) and 2C8×18.75

Similar to that of 2C12×20.7, the loading history of 2C8×18.75 *was* constructed by finding the relationship between story drift angle and member rotation. A non-linear push-over analysis of a prototype STMF structure that had 2C8×18.75 as special segment chord members was performed to obtain the relationship between STMF story drift angles and chord member plastic rotations. The total member rotations were then determined and converted to the needed vertical displacements used in the reverse cyclic test. It should be noted that the moment arm measured from the loading point to the end of the weld line of the connection of these specimens, i.e., *L* in Figure 3-11 and Table 3-1, was slightly different from that of 2C12×20.7 specimens. This length depended on how long the weld line at the end of the chord members was. The loading cycles at 0.024 rad story drift angle were also replaced by loading cycles at the 0.025 rad story drift angle. On next cycles, the specimens were pushed to the actual limit of the actuator displacement stroke of 4.92 in. For simplicity, 2C12×20.7 with RBS used the same relationship between the story drift angle and the total member rotation to construct a displacement history for the test. Loading history for both 2C12×20.7 with RBS and 2C8×18.75 are very close to that of 2C12×20.7 so the plots are not shown here. However, the displacements at each STMF story drift angle are shown in Table 3-3.

3.2.5.3 AISC Loading History of 2C6×13

A smaller double-channel of 2C6×13 was intended to be used as intermediate vertical members in special segment of a prototype STMF with multiple Vierendeel panels as shown in Figure 3-3. Development of the loading history (Figure 3-19) was similar to those of 2C12×20.7 and 2C12×20.7 with RBS specimens. However, intermediate members experience much greater rotations than the chord members in a special segment do at the same story drift angle. Standard AISC loading history starts from 0.00375 rad story drift angle which corresponds to 0.011 rad member rotation. This

member rotation is close to the first yielding rotation. As a result, the first three cycles of 0.005 rad member rotation were added at the beginning to represent elastic loading cycles.

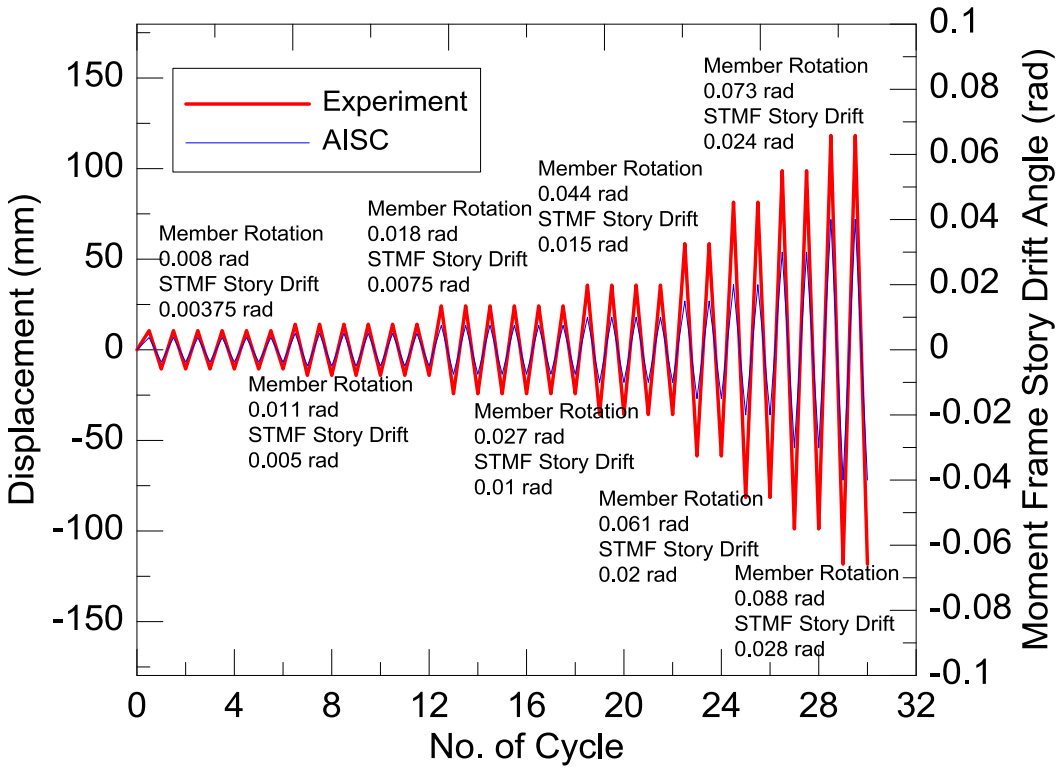

Figure 3-18 Loading History of 2C12-2 to 2C12-9

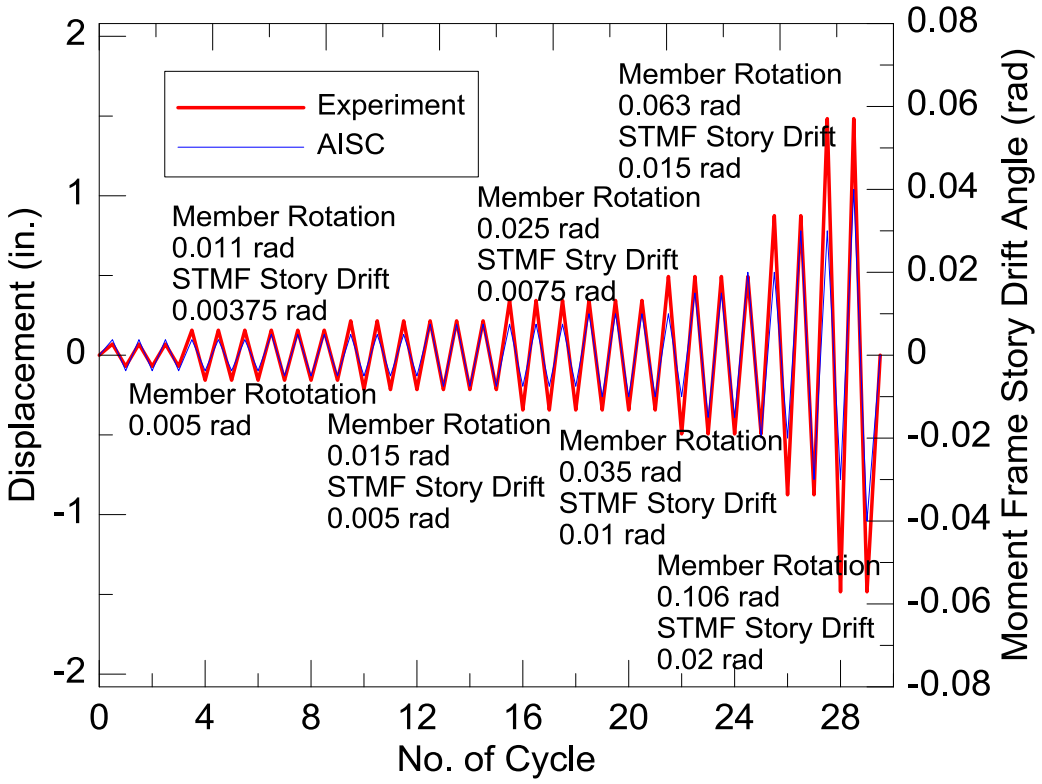

Figure 3-19 Loading History of 2C6-1 to 2C6-2

Table 3-3 Loading History of Double Channel Specimens according to AISC Seismic Provisions

AISC Loading History		2C12×20.7		2C12×20.7 with RBS		2C8×18.75		2C6×13	
Number of Cycles	Story Drift Angle (rad)	Member Rotation (rad)	Displacement (in.)	Member Rotation (rad)	Displacement (in.)	Member Rotation (rad)	Displacement (in.)	Member Rotation (rad)	Displacement (in.)
6	0.00375	0.008	0.416	0.005	0.260	0.007	0.373	0.008	0.416
6	0.005	0.011	0.555	0.009	0.479	0.009	0.498	0.011	0.555
6	0.0075	0.018	0.954	0.015	0.795	0.015	0.826	0.018	0.954
6	0.01	0.027	1.405	0.022	1.128	0.022	1.171	0.027	1.405
4	0.015	0.044	2.306	0.036	1.876	0.036	1.948	0.044	2.306
4	0.02	0.061	3.207	0.054	2.792	0.054	2.903	0.061	3.207
2	0.024	0.073	3.891	0.071	3.714	0.071	3.857		
2	0.028	0.088	4.565[1]	0.095	4.917 [2]	0.091	4.917 [2]		

Note: [1] Early specimens were pushed to 4.565 in. However, later specimens were pushed to the stroke limit at 4.92 in.
[2] Specimens were pushed to the stroke limit

3.2.5.4 AISC Loading History of 2HSS8×4×1/4 and 2HSS8×4×1/2

For simplicity and stringency double HSS specimens were tested under the same displacement history as 2C12×20.7 specimens. Due to slight difference in moment arm or the distance from the end of the horizontal weld to the loading point, member rotations of each specimen slightly differed. Table 3-4 shows loading history of 2HSS8-1 as an example. As story drift angles are those of 2C12×20.7, the numbers are merely an approximation.

Table 3-4 Loading History of Specimen 2HSS-1 according to AISC Seismic Provisions

AISC Loading History		2HSS-1	
Number of Cycles	Story Drift Angle (rad)	Member Rotation (rad)	Displacement (in.)
6	0.00375	0.008	0.416
6	0.005	0.010	0.555
6	0.0075	0.017	0.954
6	0.01	0.026	1.405
4	0.015	0.042	2.306
4	0.02	0.058	3.207
2	0.024	0.071	3.891
2	0.028	0.083	4.565

3.2.5.5 Near Collapse Loading History of 2C12×20.7

Specimen 2C12-12 was tested under Near Collapse (NC) loading history to investigate the performance of double channel section subjected to Maximum Considered Earthquake (MCE). Dimension and connection details of specimen 2C12-12 are identical to specimen 2C12-8 which was tested under AISC loading history for comparison.

Thus far, there has been no standardized Near Collapse loading history for any structural steel shape and element. Proposed NC loading protocol are shown in Figure 3-20 compared to loading protocol for specimen 2C12-8 according to AISC Seismic

Provisions. Table 3-5 shows displacements corresponding to member rotations of NC loading history. Details on how it was developed for double channel section could be found in Appendix A.

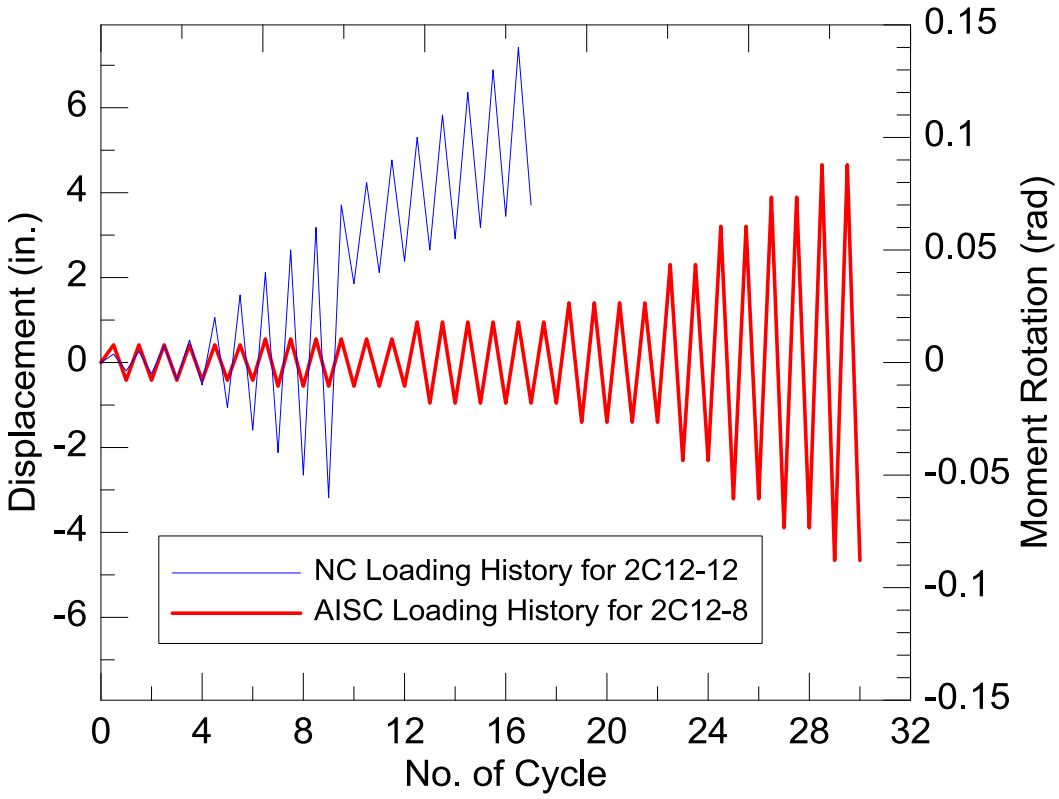

Figure 3-20 Near Collapse Loading Protocol Compared to AISC Loading Protocol

Table 3-5 Near Collapse Loading History

NC Loading History		2HSS-1
Number of Cycles	Member Rotation[1] (rad)	Displacement[1] (in.)
1	0.00375	0.199
1	0.005	0.265
1	0.0075	0.398
1	0.01	0.530
1	0.02	1.060
1	0.03	1.590
1	0.04	2.120
1	0.05	2.650
1	0.06	3.180
1	0.07 (0.035)	3.710 (1.855)
1	0.08 (0.04)	4.240 (2.120)
1	0.09 (0.045)	4.770 (2.385)
1	0.10 (0.05)	5.300 (2.650)
1	0.11 (0.055)	5.830 (2.915)
1	0.012 (0.06)	6.360 (3.180)
1	0.013 (0.065)	6.890 (3.445)
1	0.014 (0.07)	7.420 (3.710)

Note: [1] the value in parentheses denotes the member rotation and displacement on the reverse excursion.

3.3 Isolated Buckling-Restrained Brace Test

Two short buckling-restrained braced were be used in a full scale STMF subassemblage. In order to be able to properly design members outside of the special segment of the STMF, ultimate strength of the BRB had to be verified. Moreover, understanding cyclic behavior of the BRB would attribute to understanding of the behavior and performance of the full scale STMF subassemblage.

3.3.1 Buckling-Restrained Brace Specimen

Short buckling-restrained braced (BRB) specimen shown in Figure 3-21 was tested under uniaxial loading. The BRB was custom made to fit into special segment of the full scale STMF subassemblage. This BRB utilized pinned connections rather than

commonly used bolted connection on each end. The length center-to center between the two pinned ends was 43 in. The steel core length was 15.22 in. The core area was 0.941×5/8 in.^{2}. Yield strength of the core was 42.5 ksi. Two eye bars on each end of the BRB were 1 in. apart to accommodate 1 in. thick plate used in full scale subassemblage STMF. Casing was made of 3 ksi mortar filled in HSS6×6×3/16.

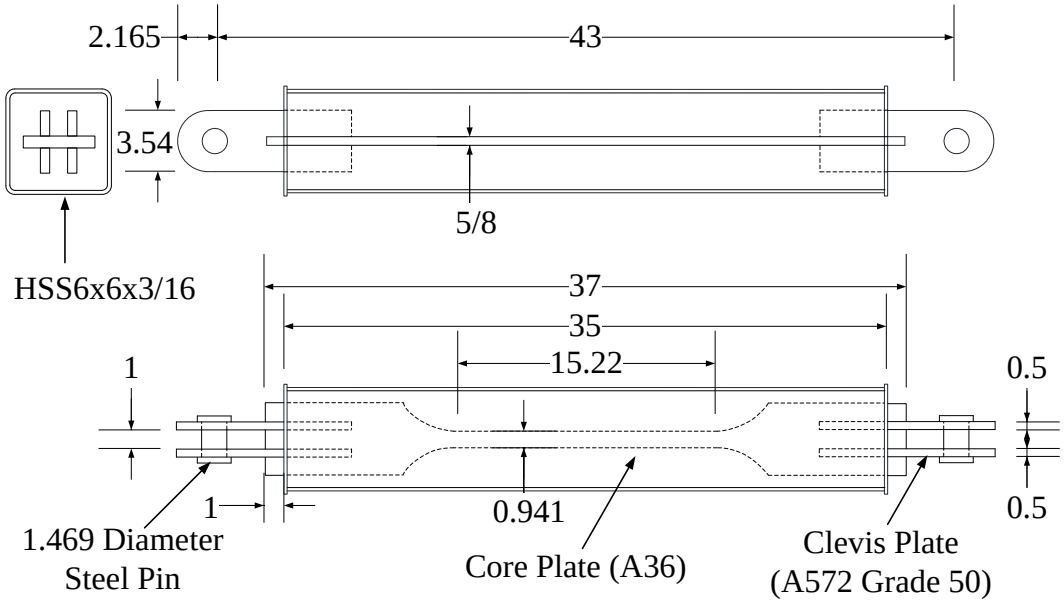

Figure 3-21 Short Buckling-Restrain Brace

3.3.2 Test Setup

The uniaxial test was done horizontally where there were two concrete reaction blocks secured to the reaction floor. The actuator was connected to one reaction block and a link beam. The specimen was connected to the other reaction block and the link beam. To prevent rotation of the swivel head of the actuator, the link beam was braced as shown in Figure 3-22.

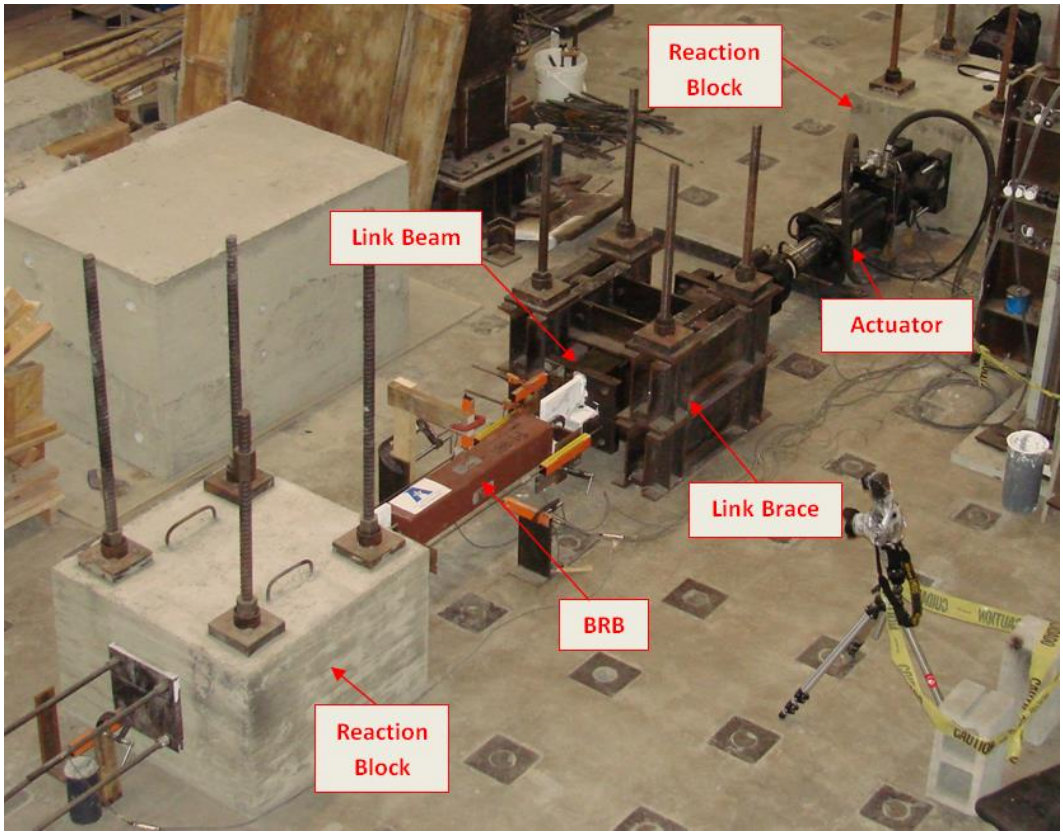

Figure 3-22 Overall Test Setup

3.3.3 Instrumentation

Test data was collected via StrainSmart Data Acquisition System. The applied force axial force was measured by a load cell of the hydraulic actuator MTS Series 201. Load capacity of the actuator is 100 kips and displacement limit is +/- 12.5 cm. Elongation of the BRB was done by linear displacement variable transducers. The development elongation measurement scheme can be found in Appendix B.

3.3.3.1 Linear Variable Displacement Transducers (LVDTs)

Seven LVDTs were used to measure various displacement of interest. Figures 3-23 through 3-25 show the locations of the LVDTs. LVDTs 1 and 2 were connected to the

two end clevis plates each side of the BRB (Figure 3-23). The elongation of the BRB was calculated from the average of these two readings. LVDTs 5 and 6 were place at the middle of the BRB orthogonally in order to measure out of plane movement. LVDT 7 was measuring the displacement of the link beam as a backup. LVDTs 3 and 4 were used to measure movement of the reaction block at each end of the test setup.

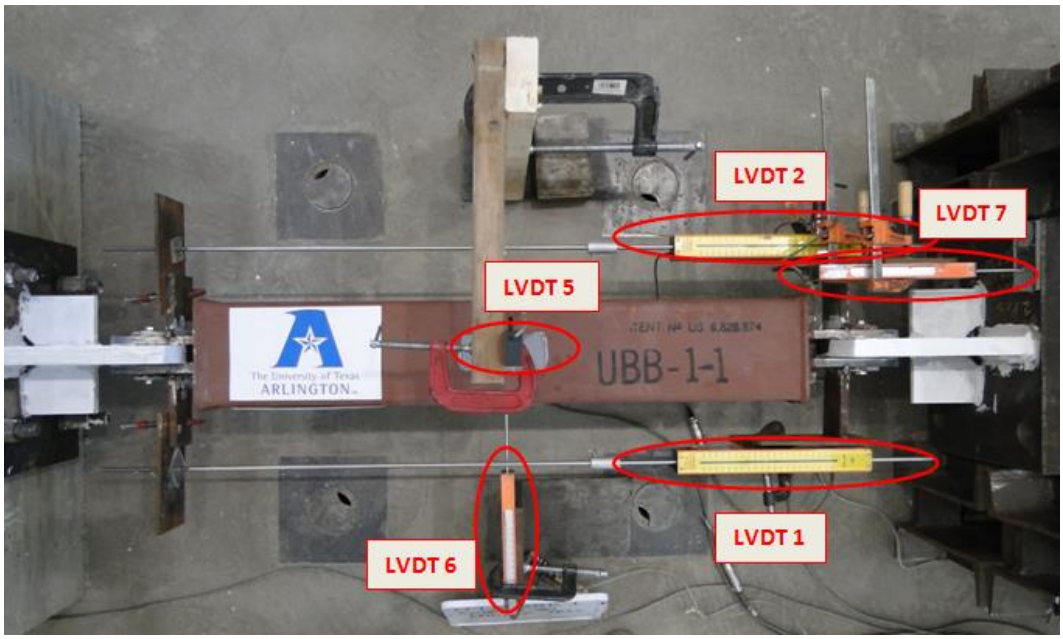

Figure 3-23 Top View of BRB with Instrumentation

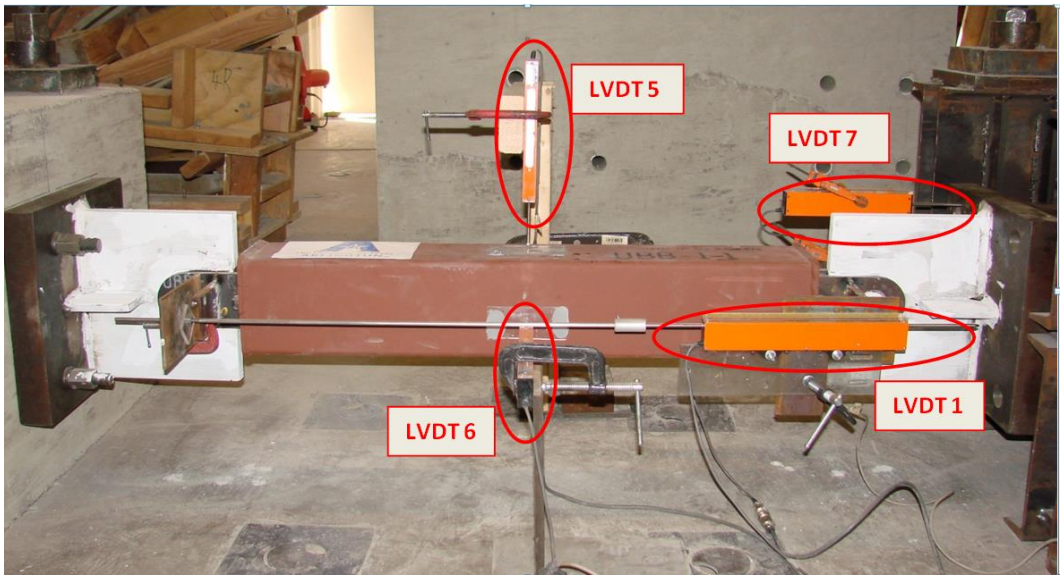

Figure 3-24 Side View of BRB with Instrumentation

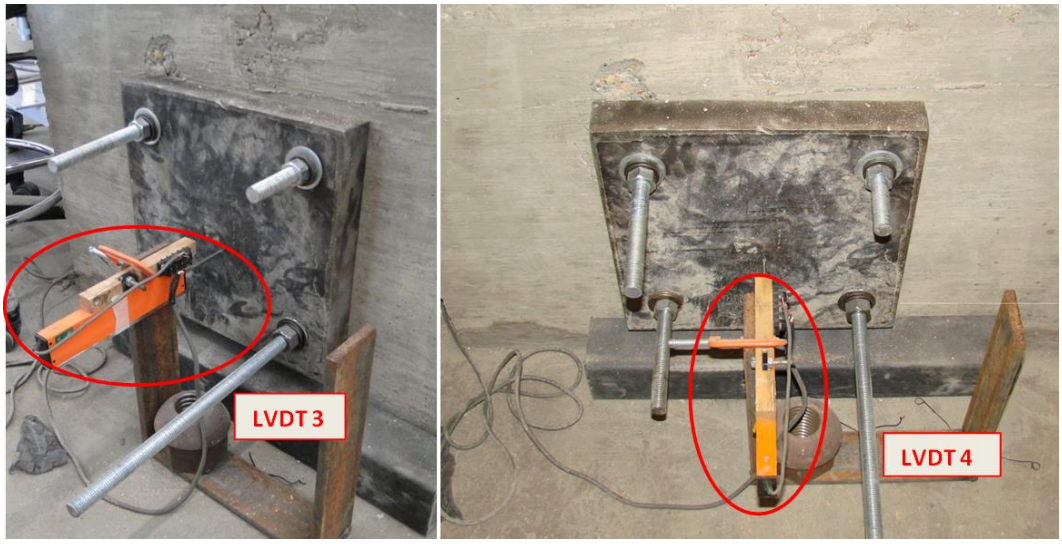

Figure 3-25 Instrumentation at the Ends of Concrete Reaction Blocks

3.3.4 Loading History

Before the test, a loading protocol was developed from a nonlinear analysis result. The pushover analysis of the full scale special truss moment frame (STMF)

incorporating with BRBs was done by program Perform-3D to find relationship between STFM story drift and elongation of the BRBs. The loading protocol is shown in Figure 3-26 and Table 3-5. The details on how it was developed could be found in Appendix B.

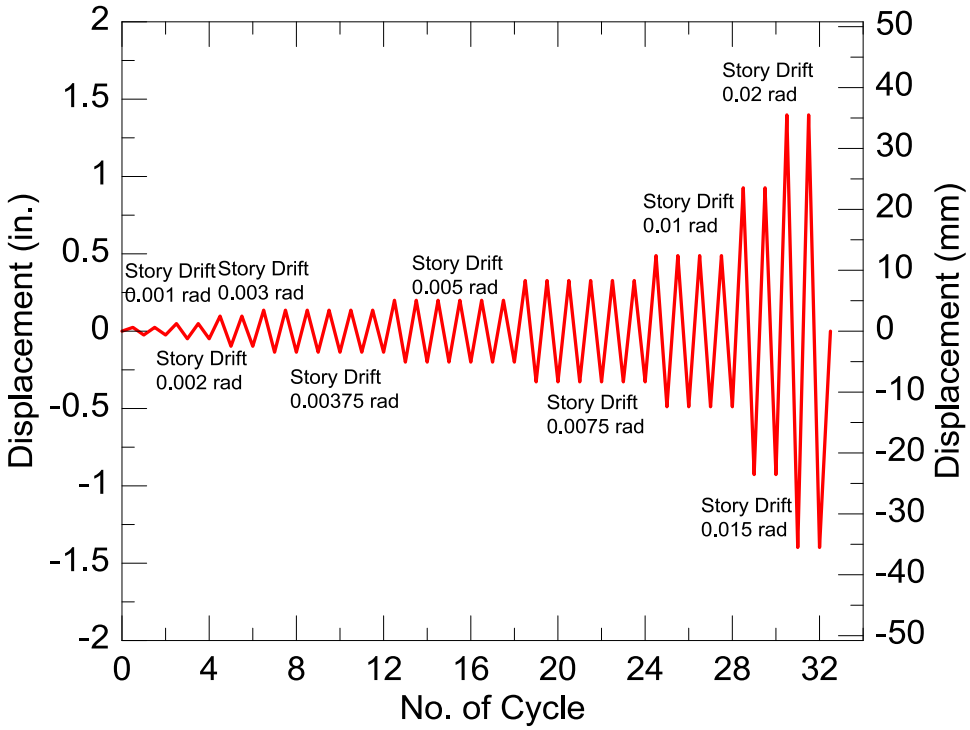

Figure 3-26 Loading History for Isolated BRB test

Table 3-6 Loading History for Isolated BRB Test

AISC Loading History		BRB
Number of Cycles	STMF Story Drift (rad)	Displacement (in.)
2	0.001[1]	0.025
2	0.002[1]	0.049
2	0.003[1]	0.098
6	0.00375	0.136
6	0.005	0.200
6	0.0075	0.328
4	0.01	0.489
2	0.015	0.927
2	0.02	1.398

Note: [1] two additional elastic drift levels and one inelastic drift level

Chapter 4

Component Test Results

4.1 Overview

The component tests results of fourteen double channel and there double HSS tests are presented. For double channel tests, the test results were separated into those tested under AISC loading history and Near Collapse (NC) loading history. For both double channel and double HSS tests under AISC loading history, rotational capacity of the specimens were presenting and discussed in terms of member rotations. Moreover, they were also considered as a beam element in a moment frame and compared to AISC rotational capacity requirement for highly ductile members of a moment frame.

Uniaxial cyclic test of the isolated buckling restrained brace is also reported.

4.2 Hysteretic Behavior of Double Channel Specimens under AISC Loading History

4.2.1 Specimens 2C12-1, 2C12-2, and 2C12-3

Specimen 2C12-1 was tested monotonically in order to acquire elastic rotation. The elastic rotation was found to be 0.012 rad and was then used to construct loading history for the flexural member test as discussed in Chapter 3 and Appendix A.

Specimen 2C12-2 was the first specimen tested under reversed cyclic loading. Unfortunately, the lateral bracing at the actuator swivel head failed before reaching the 0.02 rad STMF story drift angle (Table 4-2 and Figure 4-1), which resulted in twisting of the specimen. As a result, the test was then terminated. The first pair of stitches in this specimen was conventional stitches (3×3×1 in.) and welded 17 in. away from the end of the weld line between the gusset plate and the channels. This location of the first pair of stitches was conformed to the stitch spacing requirement in AISC Seismic Provisions (2010, 2016). Even though lateral torsional buckling occurred due to insufficient strength of lateral bracing at the loading point, this spacing was proved to be too far causing the

webs of the channels between these two points to show a significant bulge (Figure 4-2). As a result, the first pair of stitches was moved to be 1 in. away from the edge of the weld-free gusset plate in specimen 2C12-3. To prevent the web bulging of the channels, a second pair of conventional stitches was placed right next to the first pair (Figure 4-3). Moreover, two web stiffeners were introduced on each channel. The first web stiffener was welded to each channel near the end of the weld between the channels and the gusset plate—where large flange buckling amplitude was observed in specimen 2C12-2. The second web stiffener on each channel was placed at the same location where the weld-free zone gusset plate ends, intending to reduce web bulging. The hysteretic behavior of specimen 2C12-3 was stable up to 0.061 rad member rotation, as shown in Figure 4-1, with a slight loss of strength due to the pronounced flange local buckling, web local buckling, bulging and fracture of the weld between the channel and the first pair of stitches. At 0.087 rad member rotation, the strength of the specimen rapidly degraded due to the fracture of a bottom flange of a channel as well as complete separation of the channel from both pair of stitches; however, LTB was not observed.

4.2.2 Specimen 2C12-4

In specimen 2C12-3, the weld between the channels and the first two pairs of stitches fractured when the flange and web of the channels in the plastic hinge zone significantly bulged outward. As a result, the orientation of the stitches at this particular location and the second pair of stitches were modified to be horizontal as shown in Figure 4-4. As mentioned earlier, the gap distance between end of the gusset plate and the horizontal stiffener was 1 in. which was able to accommodate an approximately 0.10 rad member rotation. In addition, one more stiffener was added on each channel web in the middle between the locations of the stiffeners in Specimen 2C12-3 in order to reduce bulging and local buckling of the webs. This resulted in three pairs of stiffeners near the

plastic hinge zone at the interval of 4.25 in. center-to-center. It can be seen in Figure 4-1 that the specimen had steady hysteretic behavior with no strength degradation up to 0.061 rad member rotation. Minor flange buckling occurred at 0.044 rad member rotation, and fracture started at the end of the welds between the gusset plate and the channels; however, they did not cause strength degradation. Gradual strength loss was observed starting at 0.073 rad member rotation due to crack propagation in the welds as well as the increase in amplitude of flange and web local buckling. Figure 4-4 (a) shows that WLB and FLB were separated, and their interaction was minimized by the stiffeners. A fracture eventually occurred at the bottom flange and web of one of the channels in the panel where severe web buckling had occurred. This resulted in major strength loss and the test was terminated. Figure 4-4 (b) shows that LTB did not occur.

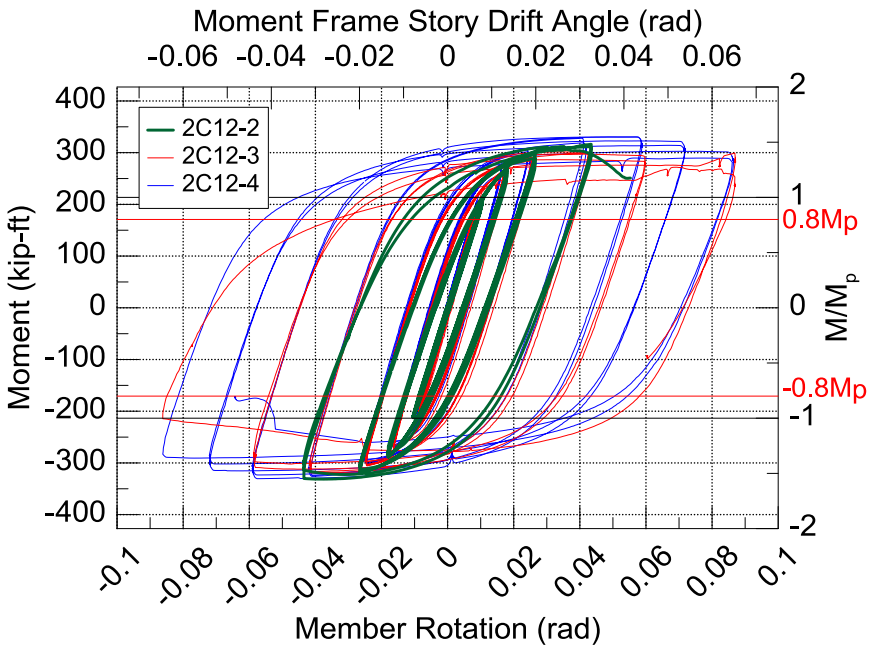

Figure 4-1 Hysteresis Behavior of Specimens 2C12-2, 2C12-3, and 2C12-4

(a) (b)

Figure 4-2 (a) Severe Flange Buckling near the End of the Weld of 2C12-2 and (b) Bulging of the Channels

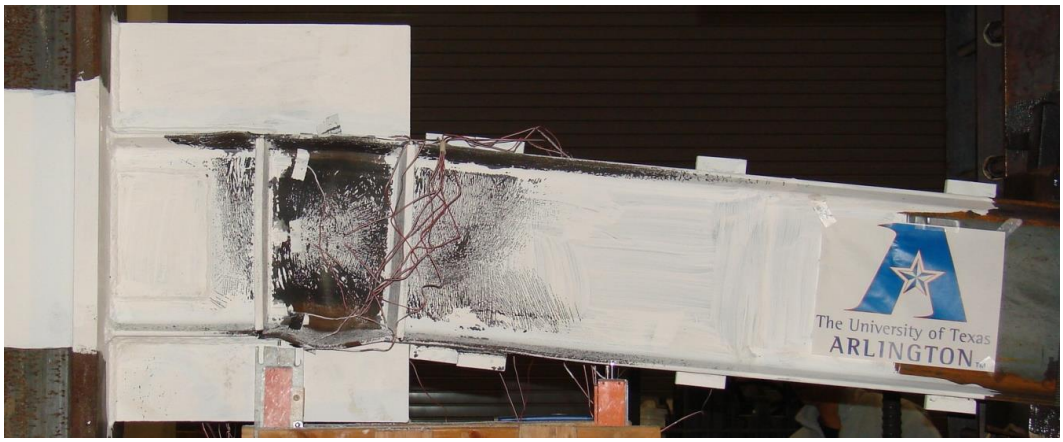

Figure 4-3 Specimen 2C12-3 at 0.028 rad STMF Story Drift

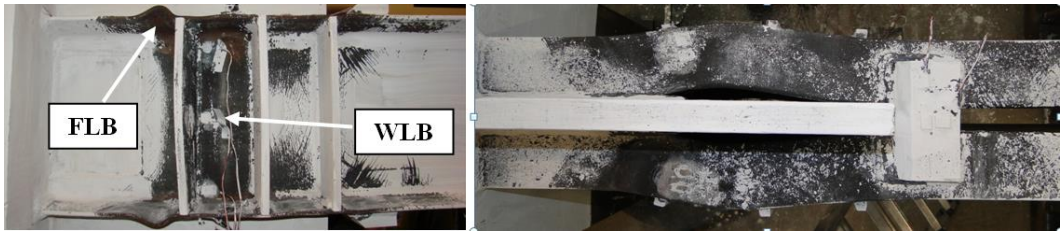

(a) (b)

Figure 4-4 (a) Yielding and local buckling of 2C310-4 and (b) horizontal stiffener effectively prevented channels from separation and centered gusset plate eliminated lateral torsional buckling

4.2.3 Specimen 2C12-5

Based on test results of specimen 2C12-4, the locations of the stiffeners were modified by moving the second pair closer to the first pair at 2.25 in. spacing, which was the location where severe web buckling was observed in specimen 2C12-4. The reason for this modification was to reduce buckling of the webs in the plastic hinge zone. Figure 4-5 shows hysteresis behavior of the specimen up to 0.042 rad member rotation when a fracture suddenly occurred at the bottom flange and in the web of one of the channels between the first and second stiffeners (Figure 4-6 (a)). It is believed that the short spacing between the first and second stiffeners resulted in high constraint against plastic flow. The highly constrained flange was under a triaxial tensile state of stress, which reduced the principal shear stress, thus fracturing at a higher ultimate stress (Barsom and Rolfe, 1999). The specimen became stronger, as evidenced by higher strength, than the previous specimen, but it was less ductile.

4.2.4 Specimen 2C12-6

In the 2C12-6 specimen, the weld-free length was reduced from 8 in. to 6 in. and the number of stitches was reduced to 2 pairs. To simulate the boundary condition of the end joint of the special segment in the prototype STMF, vertical channels were welded on

each side of the gusset plate and to the bottom flanges of the specimen as shown in Figure 4-6 (b). The first pair of stiffeners was welded on the same vertical line of the flanges of the vertical channels to simulate continuity plates. The second pair of stiffeners was placed at mid distance between the end of the welds connecting the specimen to the gusset plate and the first pair of stitches. The unrestrained distance of the flanges between the stiffeners was 4.25 in. which was the same as that of specimen 2C12-4 and 2 in. longer than that of specimen 2C12-5. However, the hysteretic behavior of this specimen, shown in Figure 4-5, turned out to be nearly identical to that of Specimen 2C12-5. In other words, the specimen only underwent reverse cyclic loading up to 0.042 rad member rotation when fracture occurred at the of the bottom flange and web (Figure 4-6 (b)). This showed that even though the restrained length of the flanges was relaxed, the plastic flow of the flange of the chord member was constrained by the stiffener and the flange of the vertical member, which in turns increased its strength but reduced its ductility.

4.2.5 Specimen 2C12-7

To minimize the constraint induced by the vertical members which were welded to the bottom flanges of the channels in the previous specimen, the vertical members were not welded to specimen 2C12-7. The first pair of stiffeners was moved 0.75 in. toward the column face to further increase the spacing between the two stiffeners to 5 in. The second pair of stiffeners was still positioned in the middle between the end of the welds and the first pair of stitches. The first crack was initiated at the end of the weld between the bottom flange and the gusset plate at 0.027 rad member rotation. Minor flange buckling was observed at this rotation level, while slight bulging of the web was noticed at 0.044 member rotation. During the cycles of 0.073 rad member rotation, strength of the specimen started to drop slightly, as shown in Figure 4-5, due to severe

local buckling, bulging, and weld crack propagation. Only slight strength loss was observed in the next two cycles of 0.087 rad member rotation, which reached the limit of the hydraulic actuator stroke. During the third positive cycle of this rotation, fracture at the top web and flange intersection occurred and the test was terminated (Figure 4-7). The performance of this specimen was slightly better than that of specimen 2C12-4 because specimen 2C12-4 fractured before completing the second cycle of the 0.087 rad member rotation. No LTB was observed throughout the test.

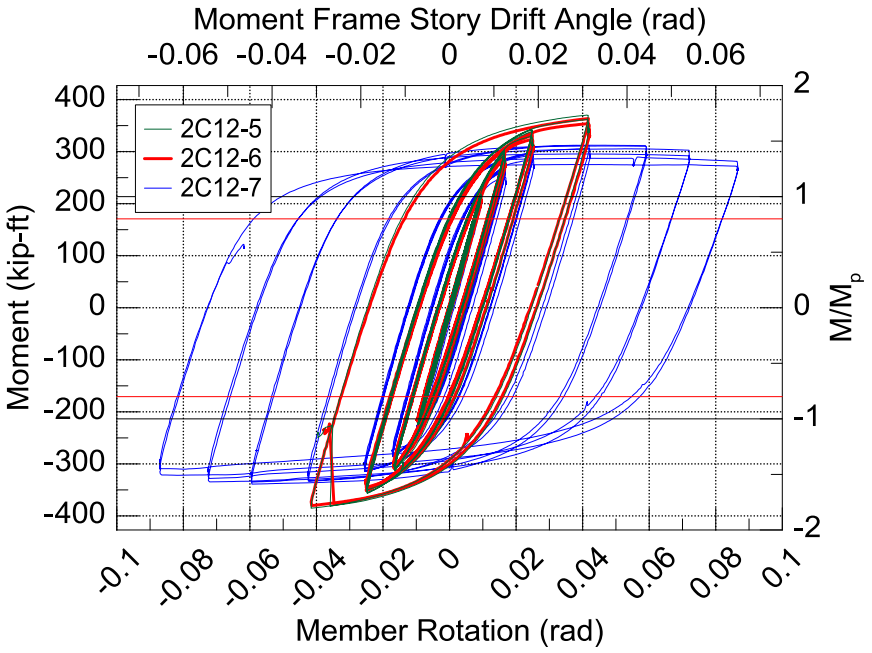

Figure 4-5 Hysteresis Behavior of Specimens 2C12-5, 2C12-6, and 2C12-7

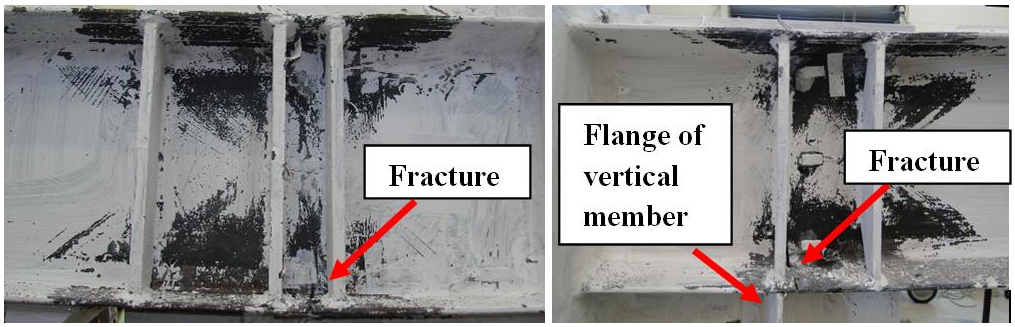

(a) (b)

Figure 4-6 Fracture in (a) specimen 2C12-5 and (b) specimen 2C12-6

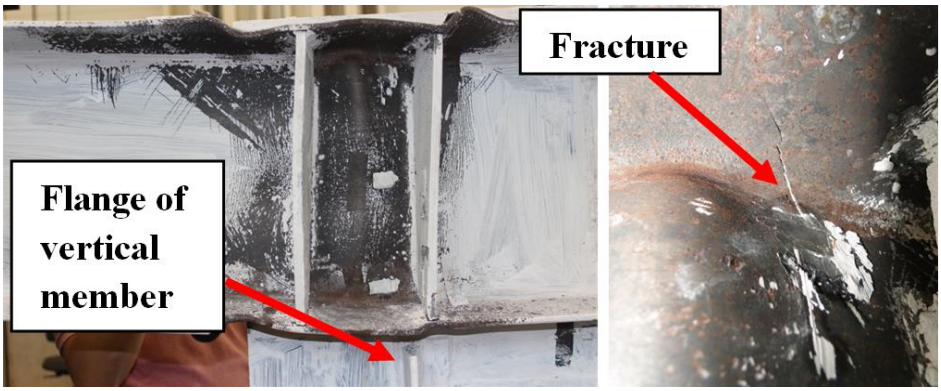

(a) (b)

Figure 4-7 (a) Local buckling and fracture in 2C12-7 at the top intersection between web and flange

4.2.6 Specimen 2C12-8 and 2C12-9

Specimen 2C12-8 and 2C12-9 were tested as baseline specimens to compare the results with the other 2C12×20.7 specimens. Specimen 2C12-8 had the same detailing as specimen 2C12-7 but without any web stiffeners. Specimen 2C12-9 had conventional detailing, which did not have an extended gusset plate or horizontal stitches. The stitch spacing followed AISC Seismic Provisions (AISC 341, 2016). Lateral support was only provided at the loading point which was 53 in. from the end of the welds.

For Specimen 2C12-8, crack initiation started at the end of the weld between the top flange of the channel and the gusset plate. A slight FLB was observed at 0.027 rad member rotation. Strength of the specimen started to drop at 0.073 rad member rotation (Figure 4-8) due to local buckling, bulging, and weld crack propagation. Loss of strength continued until the end of the test at 0.092 rad member rotation; however, the specimen still maintained strength above $0.8M_p$. The hysteretic behavior of specimen 2C12-8 was similar to that of specimen 2C12-7 except that its strain-hardening ratio was lower and strength loss was slightly faster than that of 2C12-7. The higher strength of 2C12-7 could be due to the constraint effect induced by the stiffeners. Like other specimens, the extended gusset plate performed well in preventing LTB (Figure 4-9 (a)). As shown in Figure 4-9 (b), FLB was more severe in this specimen than in specimen 2C12-7 due to lack of web stiffeners which reduced the unbraced length of the flange. Severe FLB also caused the horizontal stitches to bend more in this specimen than in the others (Figure 4-9 (a)). It was also noticed that in this specimen the line of web buckling oriented at 45 degree (Figure 4-9 (b)) while the line of web buckling oriented vertically in the other specimens.

As for specimen 2C12-9, slight FLB and LTB started at the 0.027 rad member rotation; however, they were not severe enough to cause strength degradation. Strength of the specimen peaked at a positive exertion of 0.043 rad member rotation, but started to drop at the negative excursion. As the test progressed, WLB, FLB, and especially LTB became very severe which caused rapid degradation of strength as shown in Figure 4-10. As opposed to the specimens with an extended gusset plate where the plastic hinge region extended to a greater length (in both the flange and web), the plastic hinge region was concentrated at the location where LTB occurred. Nevertheless, as shown in Figure

4-8, the strength at the moment frame story drift angle of 0.043 rad is still slightly greater than 0.8M_p.

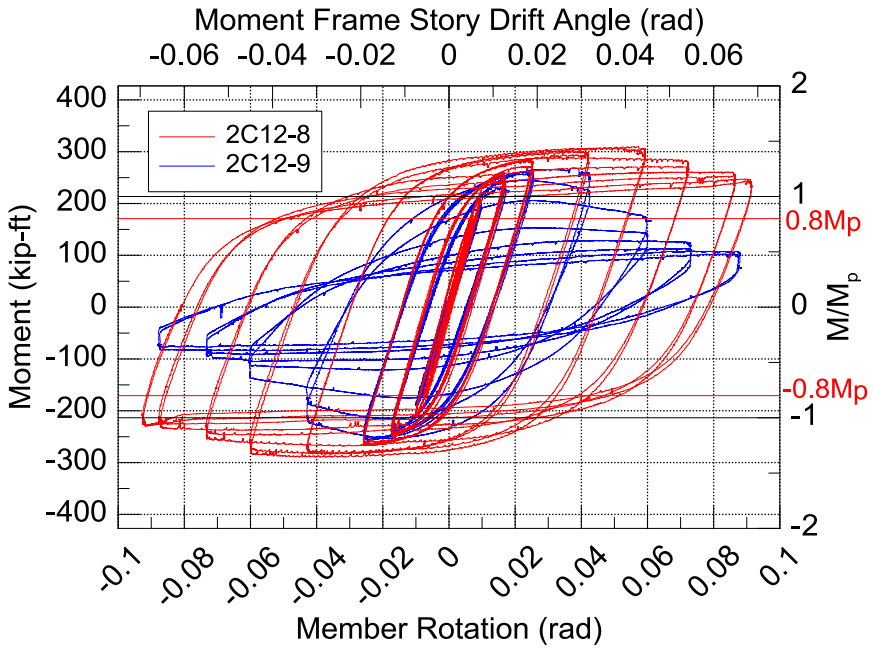

Figure 4-8 Hysteresis Behavior of Specimens 2C12-8 and 2C12-9

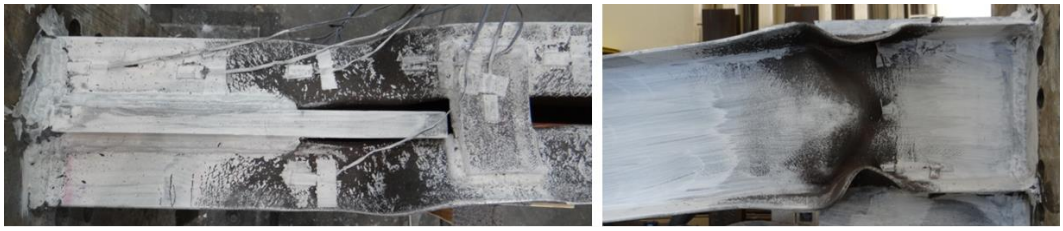

(a) (b)

Figure 4-9 (a) Top view of 2C12-8 at 0.092 member rotation and (b) severe FLB and WLB at the end of the test

(a) (b)

Figure 4-10 (a) Side view and (b) front view of 2C12-9 at 0.088 member rotation

4.2.7 Specimen 2C12-10-RBS

Specimen 2C12-10-RBS was made of double-channels 2C12×207. The width of the flanges was cut off in order to reduce the moment capacity by 20%. This was done to avoid heavy reinforcement for the non-yielding members outside of the special segment of an STMF as the same section is typically used for both the chord members (designated yielding member) in a special segment and the outside non-yielding member. The only difference in this specimen from wide-flange RBS was that, rather than a "dogbone" shape, the cut on the channel flange was made all the way from one intended plastic hinge at the end of the chord member in the special segment to the other intended plastic hinge at the other end (Figure 4-12 (a)). The weld length between the gusset plate and the channels was 11 in., while the weld-free length was 6 in. The first pair of stitches was horizontal stitches welded at 1 in. distance from the end of the gusset plate. To simplify the connection details, stiffeners were not used. The first fracture was initiated at the end of the weld between the bottom flange and the gusset plate of the channel at 0.021 rad member rotation while a slight bulging was observed at the 0.035 rad member rotation. Its strength gradually degraded starting at the 0.053 rad member rotation (Figure 4-11). The combination of crack propagation, bulging, FLB, and WLB contributed to the loss of strength (Figure 4-12 (b)). The last cycles of loading were limited by the maximum

stroke of the actuator at 4.92 in., which was equivalent to a 0.094 rad member rotation. Before reaching the first positive cycle of this displacement, the top horizontal stitch hit the gusset plate, which resulted in a slight increase of strength in the hysteresis loop as shown in Figure 4-11. The specimen maintained a strength above $0.8M_p$ for a full cycle at the moment frame story drift angle of 0.069 rad until the bottom stitch fractured (Figure 4-12 (c)) while trying to finish the second cycle of loading.

4.2.8 Specimen 2C12-11-RBS

Due to large bulging, which occurred in specimen 2C12-10-RBS, one pair of stiffeners was added in specimen 2C12-11-RBS and placed in the middle between the end of the horizontal weld connecting the channels to the gusset plate and the near end of the horizontal stitches (Figure 3-10). The spacing between the weld and stiffener, as well as the stiffener and horizontal stitch was 3.5 in. This specimen exhibited a stable behavior under cyclic loading up to a 0.036 rad member rotation (or a 0.027 moment frame story drift angle) (Figure 4-11). The narrower flange and the constraint imposed by the stiffener may have prevented plastic flow in the flanges, thereby causing premature fractures. When comparing its hysteretic behavior to that of specimen 2C12-10-RBS, as can be seen in Figure 4-11, this specimen exhibited a noticeably higher strength but much less ductility.

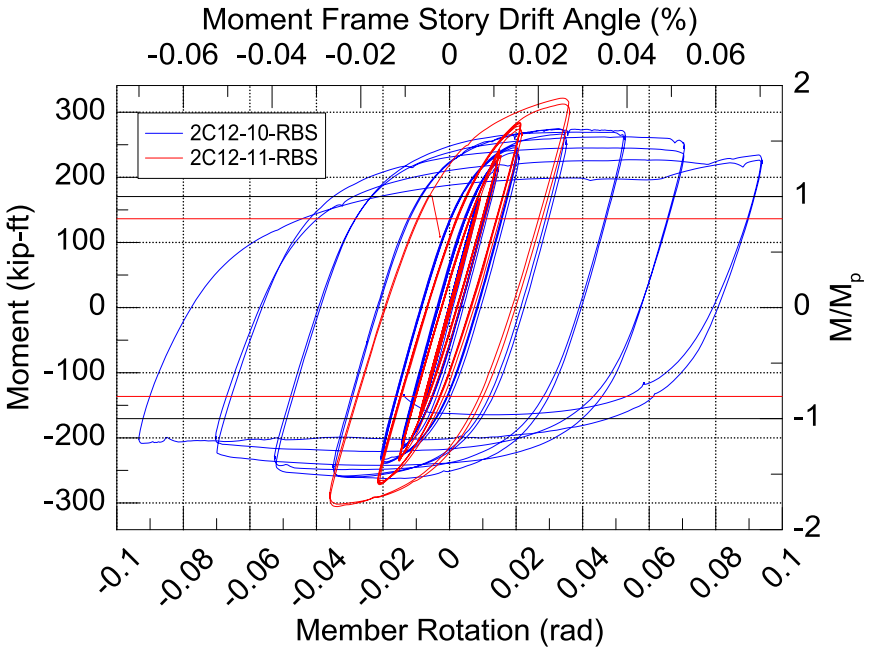

Figure 4-11 Hysteresis Behavior of Specimens 2C12-10-RBS and 2C12-11-RBS

(a) (b) (c)

Figure 4-12 (a) Reduced flange width, (b) severe web and flange local buckling in 2C12-10-RBS at 0.094 member rotation, and (c) broken horizontal stitch

4.2.9 Specimen 2C8-1

Specimen 2C8-1 has one pair of horizontal stitches welded 1 in. away from the end of the gusset plate. Since the *h/t* ratio of 2C8×18.75 is smaller than that of 2C12×20.7, large bulging was not expected. As a result, stiffeners were not used.

Hysteresis Behavior of Specimens 2C8-1 is shown in Figure 4-13. The first crack initiated at the end of the weld between the bottom flange and the gusset plate at 0.022 rad member rotation. Slight FLB and bulging was observed at 0.054 rad member rotation. At 0.071 rad member rotation, FLB was more pronounced however, the crack tip did not advance. The next cycles of loading were limited by the maximum stroke of the hydraulic actuator. As a result, the cycles of maximum displacement at 4.92 in. which is equivalent to 0.091 rad member rotation, were repeated. FLB, WLB and bulging of this specimen were not as severe as those of the 2C12×20.7 specimens due to stockier web and flange. By the end of the fourth cycle, a small fracture at the bottom flange and web intersection of one of the channels occurred which resulted in a slight drop of strength (Figure 4-13). The test was terminated when the flange and web of one of the channels fractured, as shown in Figure 4-14, during the fifth negative excursion. No LTB was observed.

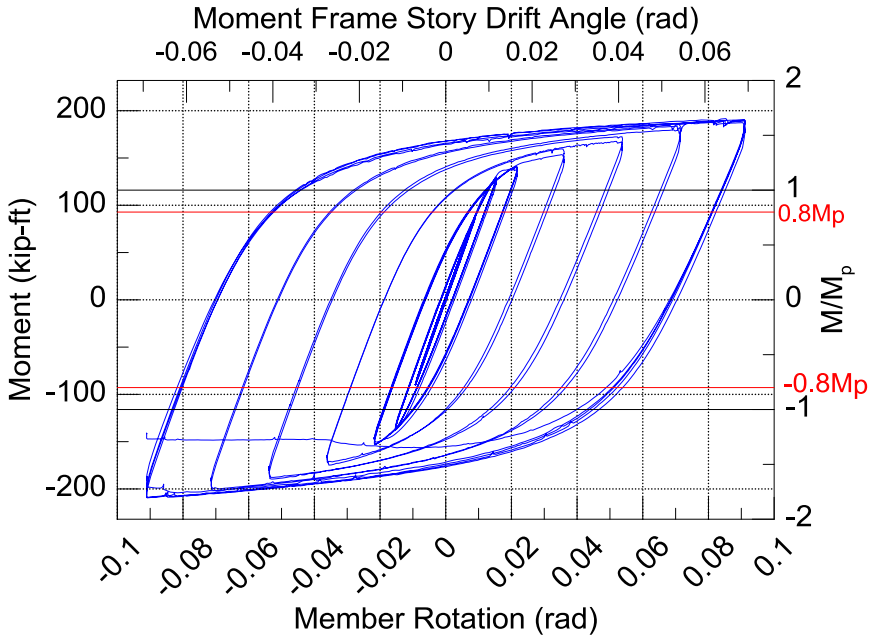

Figure 4-13 Hysteresis Behavior of Specimens 2C8-1

(a) (b)

Figure 4-14 (a) Severe flange local buckling and fracture in 2C8-1 but (b) no lateral torsional buckling

4.2.10 Specimen 2C6-1

Specimen 2C6-1 was made of double-channels 2C6×13. The test setup represented the intermediate vertical members in the special segment of a prototype STMF as shown in Figure 3-3. The weld length between the gusset plate and the channels was 6 in., while the weld-free length was 4 in. Similarly to the 2C12×20.7 specimens, one pair of horizontal stitches was used and was placed 1 in. from the end of the gusset plate. Based on the good results of the connection detailing in 2C12-7, two pairs of 0.25 in.-thick stiffeners were used. The first and second pair of stiffeners were placed at 4.25 in. and 8.5 in. from the column face, respectively. This put the second pair of stiffeners in the middle between the end of the welds and the first pair of stitches at 2.5 in. spacing. The first crack was initiated at the end of the weld between the top flange of one of the channels and the gusset plate at the 0.062 rad member drift. At this point, slight FLB and bulging were also observed. When attempting to reach a 0.106 rad member rotation, fracturing occurred and propagated at the flange and web intersection on the tension side of the channel. This location was also the end of the horizontal weld connecting the channel to the gusset plate. This resulted in strength loss as shown the hysteretic behavior in Figure 4-15. When the loading was reversed, the opposite flanges

and web fractured in the same manner, coupled with FLB, causing major strength degradation. Even though the strength of Specimen 2C6-1 dropped at the first half cycle of the 0.106 rad member rotation (or 0.057 moment frame story drift angle), it was still at 85% of the plastic moment capacity. No LTB or noticeable bulging was observed.

4.2.11 Specimen 2C6-2

Because no severe bulging was observed in 2C6-1, stiffeners were not used in this specimen. The first fracture was initiated at the end of the weld between the bottom flange and the gusset plate at 0.035 rad member rotation. Even though this happened earlier than that of specimen 2C6-1, it did not affect the strength of the specimen. Slight FLB and bulging were observed at 0.062 rad member rotation. By the end of the first positive cycle of approximately 0.106 rad member rotation, a small fracture at the flange and web intersection of the channel was noticed. Due to the force capacity limitation of the hydraulic actuator, the specimen was unable to achieve the negative cycles of -0.106 rad member rotation. As a result, the negative cycle was repeated at -0.062 rad member rotation instead. By the end of the second positive excursion of 0.106 rad member rotation, one of the channels fractured which caused a slight drop in strength. While trying to achieve the third positive excursion of 0.106 rad member rotation, the test was terminated due to large fractures of both channels on the top flanges, and webs occurred as shown in Figure 4-16. Bulging of the webs was not severe compared to that of 2C12×20.7 specimens because the *h/t* ratio of 2C6×13 is smaller and no LTB was observed. Hysteretic behavior of specimen 2C6-2 actually showed better ductility than that of 2C6-1, as shown in Figure 4-15.

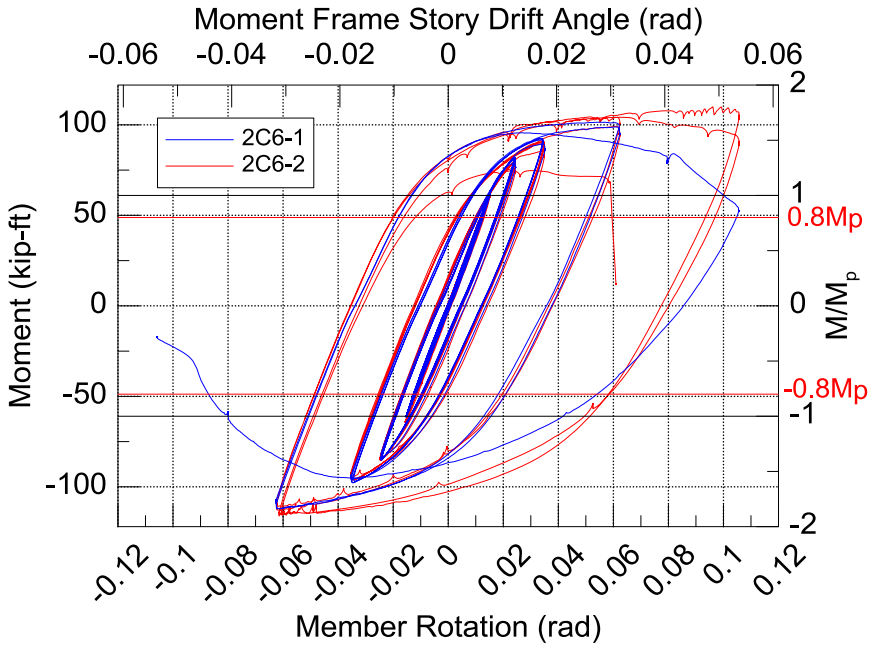

Figure 4-15 Hysteresis Behavior of Specimens 2C6-1 and 2C6-2

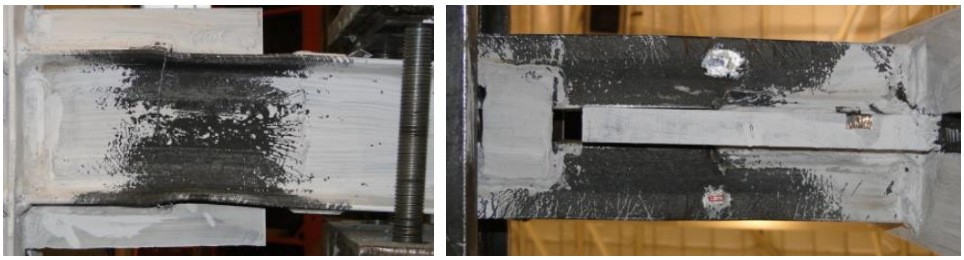

(a) (b)

Figure 4-16 (a) Fracture of 2C150-2 on top flange and web at the end of the test but (b) no lateral torsional buckling or web bulging observed

4.3 New Buckling Mode

With the new detailing scheme, the center gusset plate prevented both channels from being able to laterally displace in the same direction, hence; no global LTB of the built-up member can occur and the ductility is greatly enhanced. When looking at an

individual channel, as shown in Figure 4-17, a portion of the channel in compression (top flange and upper part of the web) between the weld end and the first pair of stitches showed lateral movement while the tension side (lower part of the specimen in Figure 17) had much smaller lateral movement. This created an out-of-plane rotation, similar to the characteristic of LTB. When the compression flanges of both channels laterally displaced in the opposite direction, the built-up member exhibited bulging as seen in Figures 4-4, 4-9, 4-12, and 4-14. The influence of bulging and its combination with web local buckling and flange local buckling on ductility of double-channel built-up members can be controlled by the location of the first stitches and the web stiffeners as described previously.

Figure 4-17 Bulging of Individual Channel

4.4 Spread of Plasticity and Maximum Member Rotation

Spread of plasticity was measured along the length of a yielded flange from the end of the weld between the center gusset plate and channels. Yielding of the flange was monitored using a series of strain gauges mounted on the flanges. Table 4-1 shows that, with the proposed connection, plastic hinges spread between 29% and 40% of the length of the specimens from the end of the weld to the loading point. Typically, this value is approximately 10% of a beam length (Bruneau et al. 2011). The longer plastic hinge length is the consequence of ever-increasing isotropic strain hardening due to delayed and minimized member instabilities.

Figure 4-18 shows all the backbone curves of the specimens that sustained more than 0.06 rad member rotation before their strength degraded to less than $0.8M_p$, along with that of specimen 2C12-9, which had conventional detailing. The new detailing effectively enhanced both the strength and ductility of double-channel built-up sections. Among specimens with special detailing, 2C12-3 exhibited earlier and faster strength degradation (especially on the negative excursion) than Specimens 2C12-4, 2C12-7, and 2C12-8, starting after approximately 0.04 rad member rotation. It had two web stiffeners in the plastic hinge region on each side of a channel. Spacing between the two web stiffeners was much larger than that of the other specimens that had web stiffeners; hence, 2C12-3 had a longer unbraced length of the flange and web, which was more susceptible to early degradation. Moreover, the failure of conventional stitches resulted in large bulging of the specimen. These factors led to greater strength degradation of the specimen. The strength degradation of Specimens 2C12-4, 2C12-7 and 2C12-8 was not obvious until after each had undergone 0.06 rad member rotation. Web stiffeners were used efficiently in Specimens 2C12-4 and 2C12-7, which helped decrease bulging and flange buckling amplitude. When web stiffeners were not used, in 2C12-8, the strength

degraded at a slightly larger degree and the strain-hardening ratio was lower than when the stiffeners were used. The final strength of these specimens in both loading directions was more than 1.2 times the nominal plastic flexural strength except for that of 2C12-3 and 2C12-8, which had a strength approximately equal to nominal plastic flexural strength. Note that final strength is defined as the strength at the last cycle right before specimens fractured, i.e. the last points on the backbone curves.

Specimen 2C12-10-RBS was able to reach a 0.094 rad member rotation, and its final strength was 1.2 times the nominal plastic flexural strength. However, when comparing the peak strength, this specimen had a slightly larger degree of strength degradation compared to the specimens with web stiffeners (2C12-4 and 2C12-7) except for specimen 2C12-3 in the negative cycle. Since the *h/t* ratio of 2C12-10-RBS is the same as the other 2C12×20.7 specimens, the strength loss was possibly due to severe WLB. This observation is in accordance with Aung and Fan (2001), who indicated that WLB affects the resistance of RBS beams most among three modes of buckling.

Specimens 2C6-2 and 2C8-1 did not show strength degradation until the fracture propagated more deeply into the flanges and webs of the specimens. Both specimens exhibited a peak and final strength more than 1.6 times the nominal plastic flexural strength. Specimen 2C6-2 reached 0.106 rad and 0.062 rad rotation capacity in positive and negative loading cycle, respectively. Specimen 2C8-1 reached 0.091 rad member rotation. It should be noted that both specimens did not have any web stiffeners; yet bulging and local buckling amplitudes were not as severe as in the other specimens. This is due to lower *h/t* and *b/t* ratios of the specimens.

Figure 4-19 shows *h/t* and *b/t* ratios of all standard and miscellaneous channel sections in AISC's Steel Construction Manual (AISC, 2017). Only a few of these sections did not meet 2016 AISC Seismic Provisions flange compactness criterion. From limited

test data in this study, it is suggested 0.5 in.-thick web stiffeners be used when the *b/t* ratio is greater than 6.49 and the *h/t* ratio is greater than 36.3 in order to achieve at least 0.06 rad member rotation while using the extended gusset plate detailing.

Table 4-1 Dimensional details and spread of yielded flange of specimens

Specimen	L (in.)	Yielded Flange Length, L_p (in.)	L_p/L
2C12-1[1]	55	NA[2]	NA
2C12-2[1]	53	NA[2]	NA
2C12-3[1]	53	NA[2]	NA
2C12-4	53	20	0.38
2C12-5	53	19	0.36
2C12-6	53	21	0.40
2C12-7	53	21	0.40
2C12-8	53	16	0.30
2C12-9	53	NA[3]	NA
2C12-10-RBS	52	16	0.31
2C12-11-RBS	52	21	0.40
2C8-1	54	15.5	0.29
2C6-1	6	4.5	0.32
2C6-2	6	4.5	0.32

Note: [1] First pair of stitches is conventional stitches.
[2] Yielding in flanges was due to severe lateral movement resulting from failure of lateral braces or conventional stitches
[3] Yielding in flanges was mainly due to the severe lateral movement as a result of LTB

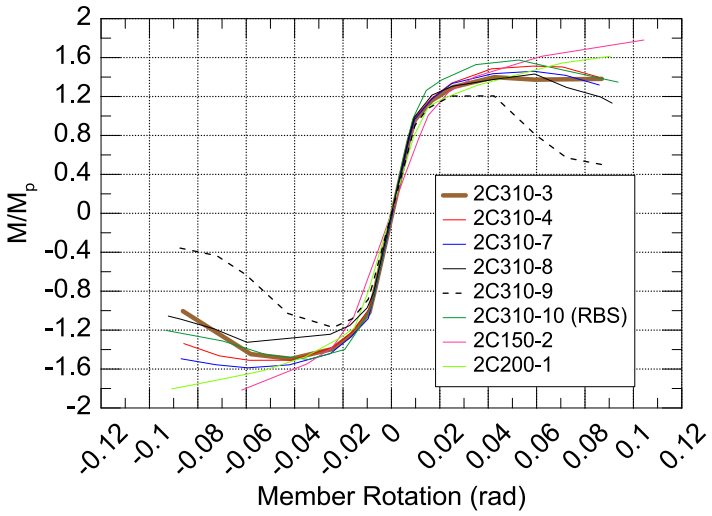

Figure 4-18 Backbone Curves

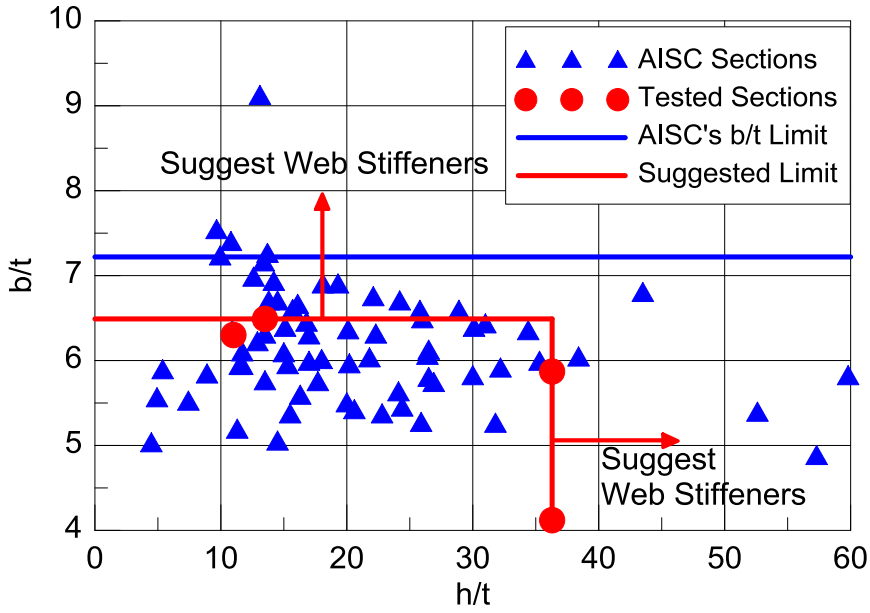

Figure 4-19 b/t and h/t ratio of American standard channels and miscellaneous channels

4.5 Effect of Axial Restraint

In isolated component tests, the specimens cantilevered from the column with reversed cyclic loading applied at the end of the members. Since swivel heads at both end of the hydraulic actuator acted as ball joints, there was nearly zero axial restraint or axial force applied to the specimens. Once the FLB and WLB occurred on the compression side of the beam, the amplitudes of this local buckling was only slightly reduced when loading was reversed. This resulted in larger bulging and local buckling amplitude as shown in Figure 4-20 (a) when Specimen 2C12-10-RBS was at a deformation corresponding to a STMF story drift ratio of 0.028 rad. In contrast, in an actual building or full-scale STMF specimen, columns and truss girders provide axial restraints against shorting of the chord members due to bulging and inelastic buckling of the web and flange. Figure 4-20 (b) shows a lesser degree of bulging and local buckling amplitudes in a full-scale STMF subassemblage test (Chapters 5 and 6) at a story drift angle of 0.028 rad. The axial deformation of the isolated component specimen due to

bulging (compression) is obvious as the gusset plate had hit the stitch; on the other hand, at the same drift ratio, the gusset plate in the full-scale STMF was still approximately 0.4 in. away from the stitch.

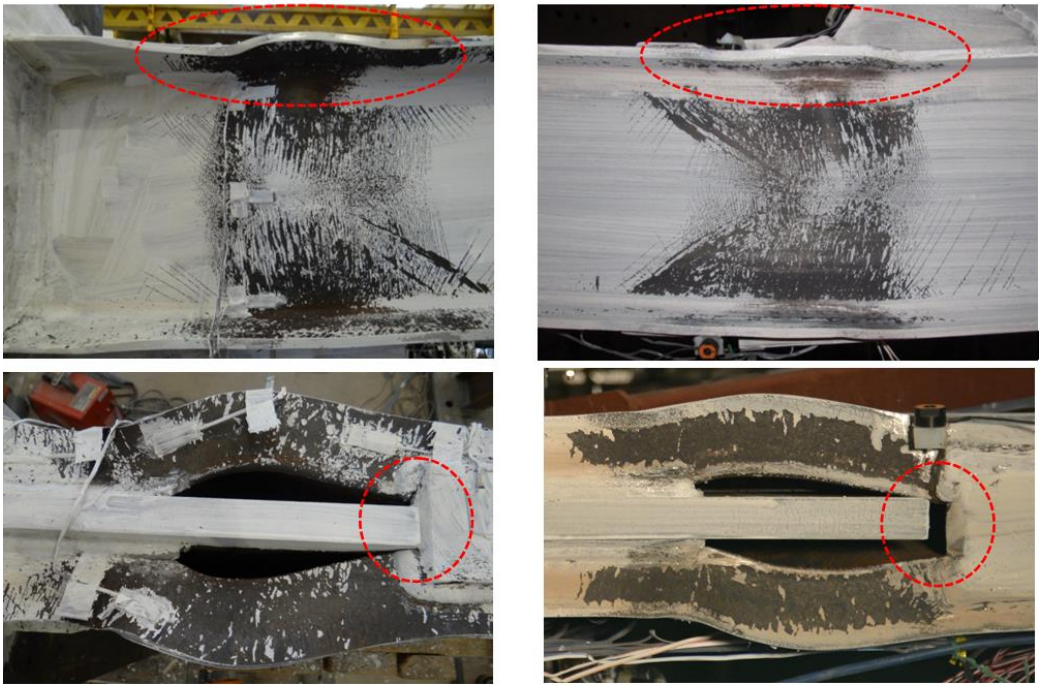

(a) (b)

Figure 4-20 (a) 2C12-10-RBS at 0.028 rad STMF story drift ratio (b) 2C12x20.7 (RBS) in full-scale STMF subassemblage test at 0.028 rad story drift angle

4.6 Proposed Double-Channel Built-Up Members as Beam-to-Column Moment Connection

According to AISC 341 (2016), qualified connections for intermediate moment frames and special moment frames require that strength degradation of a moment frame connection does not fall below 80% of the nominal plastic flexural strength before the story drift angle of 0.02 rad and 0.04 rad are achieved, respectively. Table 4-2 shows

eight specimens that qualified for special moment frame connections, while, five others qualified for intermediate moment frame connections.

Table 4-2 Achieved member rotation, STMF prototype story drift, and moment frame story drift at strength higher than 80% of nominal plastic flexural strength

Specimen	Member Rotation (rad)	Prototype STMF Story Drift Angle (rad)	Moment Frame Story Drift Angle[1] (rad)	$F_{y,actual}$ (ksi)	Overstrength Factor[2]
2C12-2[3]	0.044	0.019	0.033	50.82	1.49
2C12-3	0.087	0.028	0.065	55.39	1.31
2C12-4	0.086	0.028	0.065	55.39	1.40
2C12-5	0.042	0.015	0.031	55.39	1.60
2C12-6	0.042	0.015	0.031	55.39	1.57
2C12-7	0.087	0.028	0.065	55.39	1.38
2C12-8	0.092	0.028	0.069	55.39	1.27
2C12-9	0.043	0.015	0.032	55.39	1.12
2C12-10-RBS	0.094	0.028	0.069	55.39	1.42
2C12-11-RBS	0.036	0.015	0.027	55.39	1.66
2C8-1	0.091	0.028	0.070	51.10	1.69
2C6-1[4]	0.106	0.020	0.057	52.32	1.67
2C6-2[4]	0.106	0.020	0.057	52.32	1.75

Note: [1] Calculated by using vertical tip displacement and the distance from center of column panel zone to the loading point;
[2] Overstrength = $M_{max}/F_{y,actual} \times Z$;
[3] Test stopped due to failure of lateral bracing at loading point;
[4] For positive excursion

4.7 *Hysteretic Behavior* of Double HSS Specimens under AISC Loading History

4.7.1 Specimen 2HSS8-1

Specimen 2HSS8-1 *was* welded to a 1-in. thick gusset plate. The first pair of stitches was horizontal stitches welded at 1 in. distance away from the edge of the gusset plate. The bending capacity was determined using the moment arm from the loading point to the end of the weld. The *h/t* and *b/t* ratios are above the current limit as determined by the AISC Seismic Provisions (2016) as shown in Table 4-3. Figure 4-21 shows that this specimen reached 0.07 rad member rotation or 0.028 rad STMF story

drift before the strength dropped below 80% of nominal plastic flexural strength. The first sign of yielding was at 0.005 rad member rotation which was below 0.00375 rad STMF story drift angle observed from reading of a strain gage on the flange near the corner where the HSS was welded to the gusset plate. During cycles of 0.02 rad story drift angle the flanges of the HSSs stated to fracture as shown in Figure 4-22. It was noticed that fractures initiated from the end of the weld that connected HSSs to the gusset plate. Crack propagation due to reverse cyclic loading caused strength drop in the successive cycles. During 0.028 rad story drift cycles or 0.09 rad member rotation, cracks in the tension flanges propagated more but strength of the specimen did not drop below 80% of nominal plastic moment capacity because cracks on the compression flanges closed up and created buckling seen in Figure 4-23. At this drift level, buckling of the web on the compression half of the HSS started to be noticeable. At 0.028 rad story drift angle, fractures propagated across the entire flanges into the webs. The strength of the specimen dropped below 80% of nominal plastic moment capacity and the test was terminated. The maximum normalized strength is 1.73. However, strength slightly dropped at the first negative cycle of the same level due to fracture incurred from the positive cycle.

Table 4-3 Experimental double-HSS specimens

Section	Width-thickness ratio, *b/t*	Depth-thickness ratio, *h/t*	*b/t* and *h/t* AISC requirement	Maximum moment/nominal plastic moment ratio
2-HSS8×4×1/4	14.2	31.3	13.8	1.73
2-HSS8×4×1/2 with cover plates	5.6	14.2	13.8	1.73
2-HSS8×4×1/2	5.6	14.2	13.8	1.90

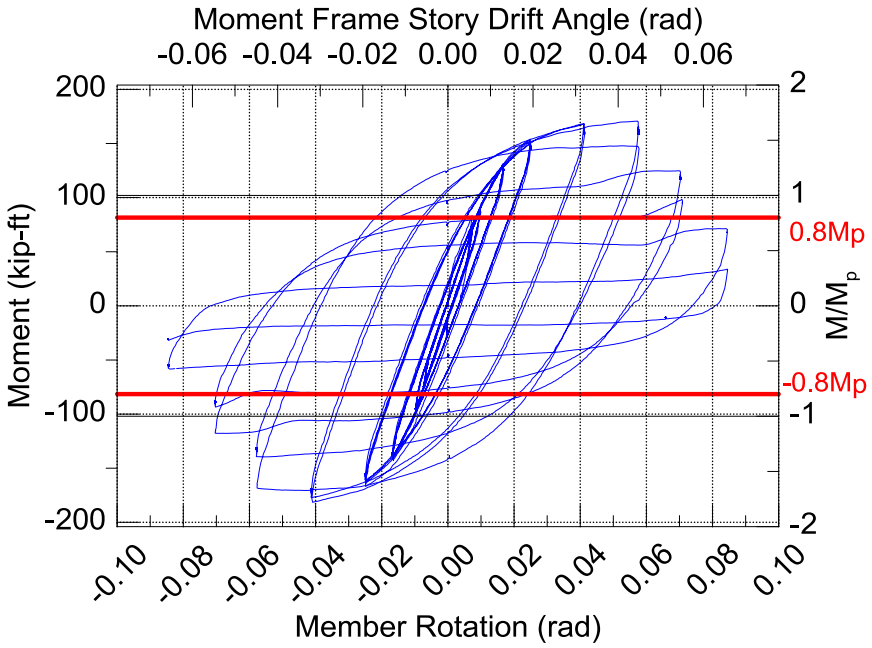

Figure 4-21 Hysteresis Behavior of Specimens 2HSS8-1

Figure 4-22 Fracture on the west flange at the end of the weld

(a) (b)

Figure 4-23 (a) Crack propagation in tension flange and (b) flange buckling in compression flange

4.7.2 Specimen 2HSS8-2

Specimen 2HSS-2 was made of 2HSS8×4×1/2 whose *h/t* is slightly above AISC requirement and *b/t* ratios is well below the requirement. In an attempt to delay fracture across the flanges at the plastic hinge, cover plates were welded on both top and bottom flanges. The horizontal stitches were also moved to 5 in. away from the gusset plate, as shown in Fig. 4-24, because there was no lateral torsional buckling observed in the previous specimen. Overall hysteretic behavior of the specimen is shown in Figure 4-25. Specimen 2HSS8-2 reached 0.084 rad member rotation or 0.028 rad story drift angle. After two cycles at 0.084 rad member rotation, the specimen did not fail. As a result, the test was continued by loading the specimen up to the maximum stroke of the hydraulic actuator at 4.92 in. or 0.09 rad member rotation which strength slightly dropped. The normalized maximum moment was 1.72. At the 1st cycle of 0.015 STMF story drift, a small crack initiated at the end of the weld between the HSS and the gusset plate. By the end of the 2nd cycle of this drift angle, it can be seen that the crack propagated into the flanges of the HSS. Facture started to propagate along the cover plate, however; web

buckling was noticeable during cycles of 0.024 rad STMF story drift angle. The test underwent on 2 more cycles of 0.028 STMF tory drift angle where the crack propagated across the flanges along the cover plate progressed, however; strength did not yet drop. Finally, the specimen was pushed to the maximum actuator stroke of 4.92 in. where the strength started to slightly drop. When the specimen reached the 1st negative cycle of this drift level, its strength noticeably degraded because the entire bottom flange of the west HSS fractured (Figure 4-26). By the 2nd cycle this drift level, crack propagated into the web of the HSSs (Figure 4-27), resulting in more loss of strength and the test was terminated at the end of the cycle.

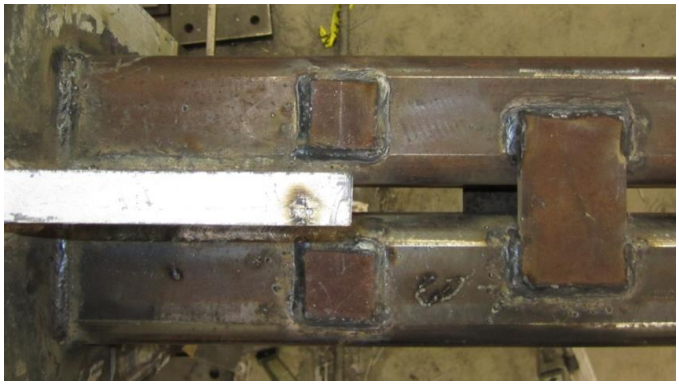

Figure 4-24 Top view of SP 5 shows cover plates and horizontal stitches.

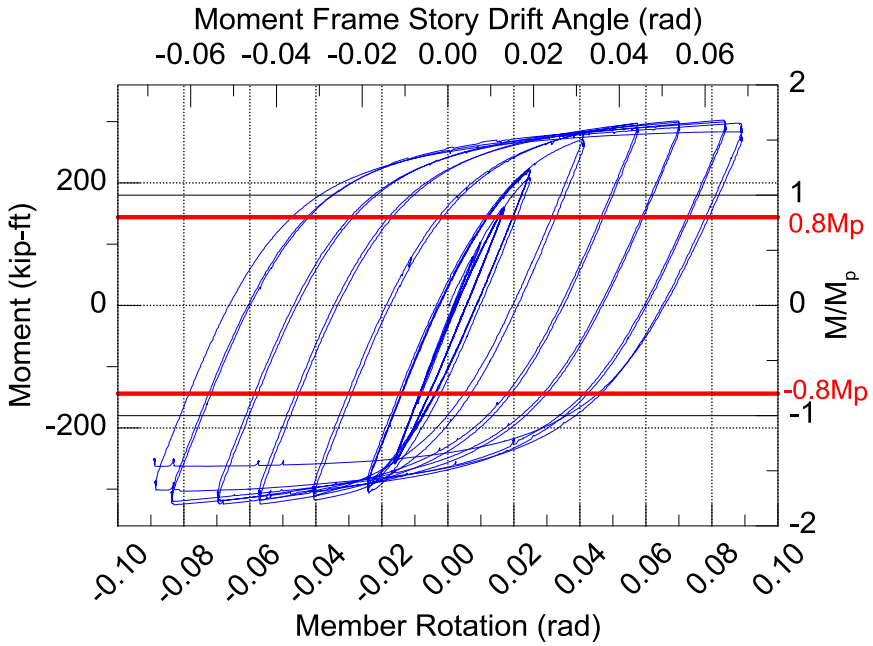

Figure 4-25 Hysteresis Behavior of Specimens 2HSS8-2

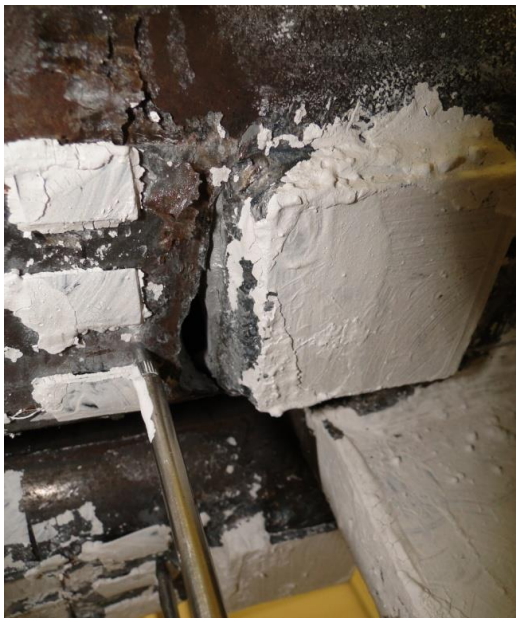

Figure 4-26 Crack Propagated across the Entire Flange at the End of the 1st Cycle of 0.09 rad Member Rotation

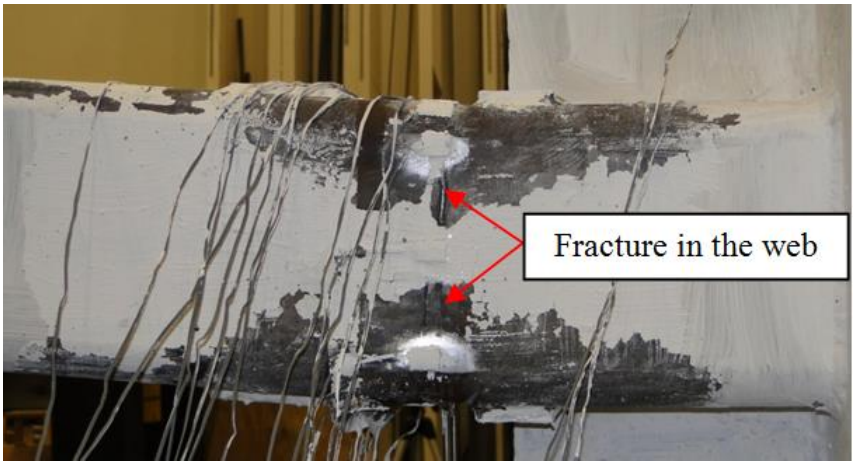

Figure 4-27 Specimen 2HSS8-2 at the End of the Test

4.7.3 Specimen 2HSS8-3

In order to determine the effect of the cover plates, specimen 2HSS8-3 was made of 2HSS 8×4×1/2 without ones. However, the first pair of stitches was removed completely due to nonexistence of lateral-torsional buckling in the previous specimens. Figure 4-28 shows hysteresis behavior of this specimen. The first sign of yielding was at 0.012 member rotation or 0.005 rad STMF story drift angle observed from reading of a strain gage on the flange near the corner of the HSS was welded to the gusset plate. This first yield happened at higher drift angle than that of 2HSS8-1 due to the thicker wall thickness. During 0.0075 rad story drift cycles, very small fractures at the weld ends were noticed but the authors believed that it did not propagate into the HSS. By 0.015 rad story drift angle, crack propagated into the HSS slightly, which was the same onset of crack propagation of 2HSS8-2. As the test continued fractures propagated a slowly leading to non-substantial strength loss in consecutive drift levels. Due to the stroke limitation of the hydraulic actuator, the final displacement of approximately 4.92 in. or 0.091 rad member rotation was achieved in the last cycles. At the end of the 1st positive cycle, yielding was more severe and fracture on the top side propagated into the flange and widened as

shown in Figure 4-29. From Figure 4-28, it can be seen that strength continued to drop from the previous cycles at this same drift level. The test continued on to finish the 3rd positive cycle when the strength of the specimen dropped to nearly 80% of its nominal plastic moment capacity. Major loss of strength was caused by necking of the corners and large fractures on both HSSs which progressed nearly across the entire flanges shown in Figure 4-30. The normalized maximum moment capacity of specimen 2HSS8-3 is 1.90 and occurred at 0.015 rad story drift angle.

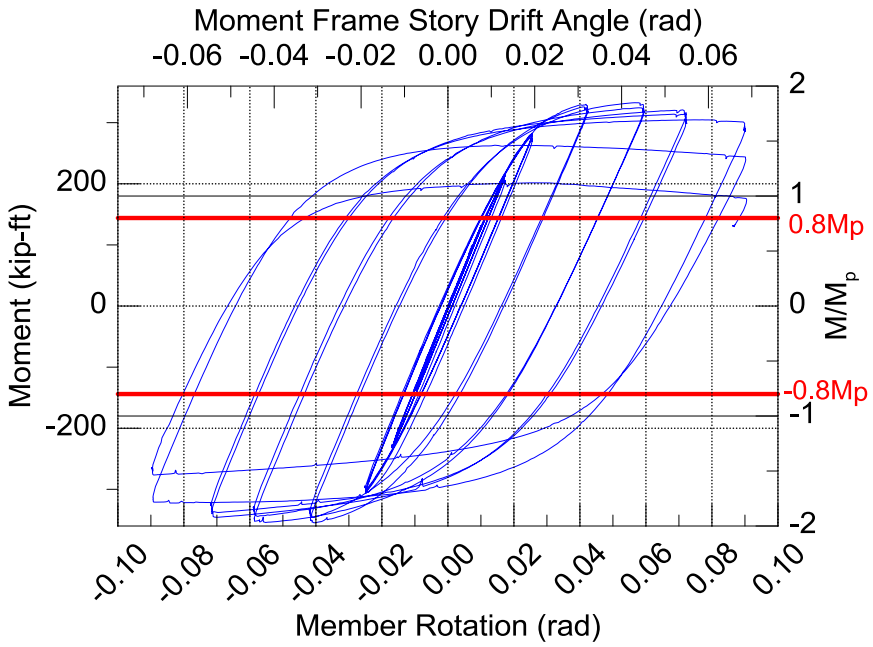

Figure 4-28 Hysteresis Behavior of Specimens 2HSS8-3

Figure 4-29 Fracture on the flange of HSS at +0.09 rad member rotation

Figure 4-30 Top view of the specimen at the end of the test

4.8 Experimental Results Comparison

4.8.1 2HSS8×4×1/4 (2HSS8-1) vs. 2HSS8×4×1/2 (2HSS8-3)

Specimens 2HSS8-1 and 2HSS8-3 have the same height and width, however; the former is ¼ in. thick while the latter is ½ in. thick. This results in much more compact flange and web of 2HSS8-3. Even though maximum strength of 2HSS8-1 occurred at 0.02 rad story drift angle while that of 2HSS8-3 occurred at 0.015 rad story drift, strength of 2HSS8-3 at 0.02 rad story drift angle only dropped by 0.5%. On the other hand, due to

much smaller wall thickness, fracture and its propagation of 2HSS8-1 were at greater and faster rate. Moreover, flange buckling and web buckling of 2HSS8-1 were more severe. As a result, strength degradation of SP 4 was more rapid.

4.8.2 2HSS8×4×1/2 with cover plates (2HSS8-2) vs. 2HSS8×4×1/2 (2HSS8-3)

2HSS8-2 and 2HSS8-3 have the same height, width, and wall thickness but 2HSS8-2 has cover plates welded on top and bottom flanges at the expected plastic hinge region (i.e. the end of the weld). Normalized maximum moment capacity of 2HSS8-2 and 2HSS8-3 were 1.72 occurred at 0.084 rad member rotation and 1.90 occurred at 0.041 rad member rotation, respectively. The reasons 2HSS8-2 had lower strength was most likely because when cracks propagated across the flanges, it had to go around the cover plates toward the section with less flexural capacity. As a result, cracks across the flanges were pushed 1.5 in. (half width of the cover plates) toward the loading point. This detour successfully delayed crack propagation across the flange but resulted in failure at the section with a slight lower moment capacity.

4.9 Proposed Double HSS Built-Up Members as Beam-to-Column Moment Connection

By assuming that double HSS component test setup represents a column and half a beam length of a bay in a moment frame. The moment arm length used to determine the story drift would have to be measured from the center of the column panel zone to the loading point. By doing so, the maximum moment frame story drift angles of 2HSS8-1, 2HSS8-2, and 2HSS8-3 before strength dropped below 80% of nominal plastic flexural strength, are 0.055 rad, 0.068 rad, and 0.068 rad respectively (Table 4-4). This means that all three specimens are qualified as highly ductile beams in a special moment frame (SMF) because they all maintained 80% of nominal plastic strength more than 0.04 rad story drift angle.

4.10 Comparison between single HSS and double HSS flexural members

Use of double HSS doubles bending capacity of HSS without changing width-thickness and depth-thickness ratios. This, in turns, provides more readily available options for seismic compact sections to choose from. Also, when a double-HSS is used, the width-thickness ratio can generally be lower than that of a single-HSS with similar moment capacity, which considerably increases the compactness under bending thereby delaying flange buckling. Due to the fact that narrower tube sections would be more practical to use in a double-HSS configuration, the requirements for *b*/*t* ratios would be easy to adhere to. Figure 4-31 shows comparison between the backbone curves of a single HSS10×8×1/4 test result done by Fadden and McCormick (2012a) and 2HSS8×4×1/4 (2HSS8-1) test result. These two members have similar nominal plastic flexural capacity of 1,293 k-in. (HSS10×8×1/4) and 1,224 k-in. (2HSS8×4×1/4) but quite different *b/t* ratios of 31.3 and 14.2, respectively. It can be seen that double HSS exhibited higher normalized flexural strength and more ductile due to higher compactness ratio.

Table 4-4 Member rotation, STMF prototype story drift, and moment frame story drift at strength higher than 80% of nominal plastic flexural strength

Specimen	Member rotation (rad)	STMF prototype story drift (%)	Moment frame story drift[1] (%)
2-HSS8×4×1/4	0.07	2.38	5.47
2-HSS8×4×1/2 with cover plates	0.09	2.88	6.84
2-HSS8×4×1/2	0.09	2.88	6.83

Note: [1] Calculated by using vertical displacement and the distance from center of column panel zone to the loading point.

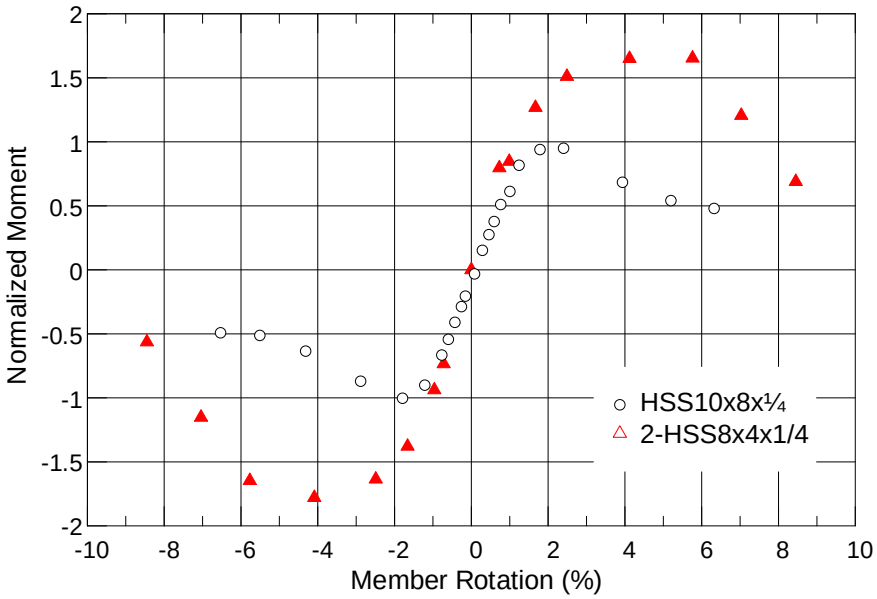

Figure 4-31 Comparison of backbone curves between single and double HSS

4.11 *Hysteretic Behavior* of Double Channel Specimens under NC Loading History

4.11.1 Specimens 2C12-12

MCE level ground motions or earthquakes with 2% probability of being exceeded in 50 years are often used for nonlinear time-history analyses to check the collapse prevention of structures. Time-history response to this type of ground motions often consists of a few excursions with larger amplitude in one direction than the other, then followed by pulse-like small cycles with a large mean deformation (Krawinkler et.al, 2000). Analytical studies carried out by Maison and Speicher (2016) on an eight-story steel-frame building and a four-story wood-frame building confirmed that time-history response of the building interstory drift under MCE ground motions was better described by single-sided cyclic and/or monotonic loading rather than fully reversed cyclic loading. As a result, the nonlinear behavior of double-channel member obtained from fully reversed symmetric loading protocol with high number of repeating cycles such as AISC loading protocol can be unrealistic to represent the time-history response of STMF

members subject to MCEs. Therefore, a more realistic loading protocol for near-collapse situation was developed and is shown in Figure 3-19. The construction of NC loading can be found in Appendix A.

Specimen 2C12-12 was tested under NC loading history. It is identical to specimen 2C12-8 which was tested under AISC loading history. The reasons 2C12-8 is chosen to be compared to because of its good performance while having the simplest connection details. Hysteretic behavior of 2C12-12 is shown in Figure 4-32. It can be seen that 2C12-12 under NC loading history can maintain its strength above 80% of nominal plastic moment up to 0.014 rad member rotation.

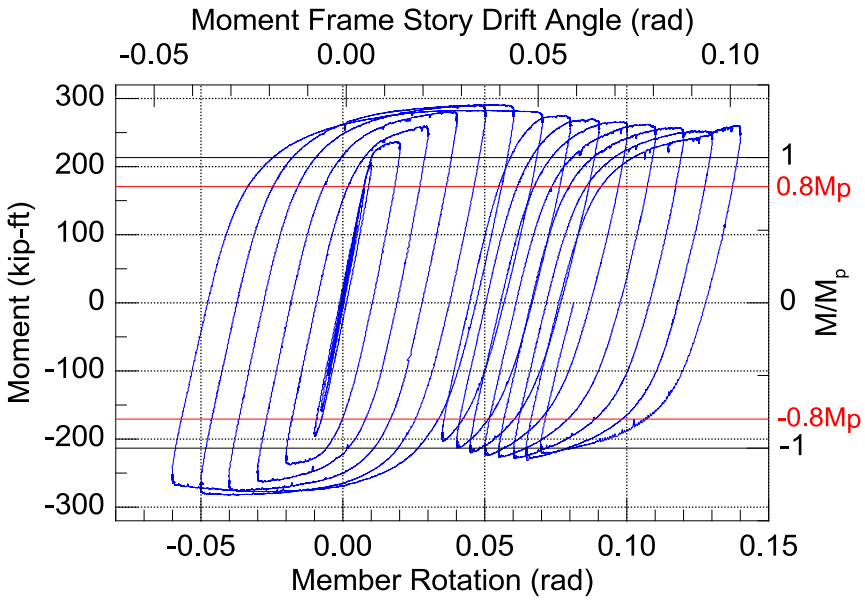

Figure 4-32 Hysteretic Behavior of 2C12-12

4.12 Isolated Buckling-Restrained Brace Test Results

4.12.1 Load vs. Elongation

Due to the very short core area embedded inside the much longer concrete-filled case in the real BRB, it seems impossible to measure the deformation of the yielding portion alone. Thus, the deformation of the BRB was measured across the approximate

length, L, of 39.5 in. This deformation of the BRB was achieved by averaging the readings from LVDTs 1 and 2. The test result showed a stable hysteretic behavior of the BRB up to 1.5% drift. The steel core of the BRB broke when it was loaded to the positive 2nd cycle of 1.5% drift. This means the BRB achieved a cumulative inelastic axial deformation of more than 200 times the yield deformation which is required by AISC 341-16. The force-displacement loops are shown in Figure 4-33 while Figures 4-34 and 4-35 show the elongation of the steel core on both ends of the BRB.

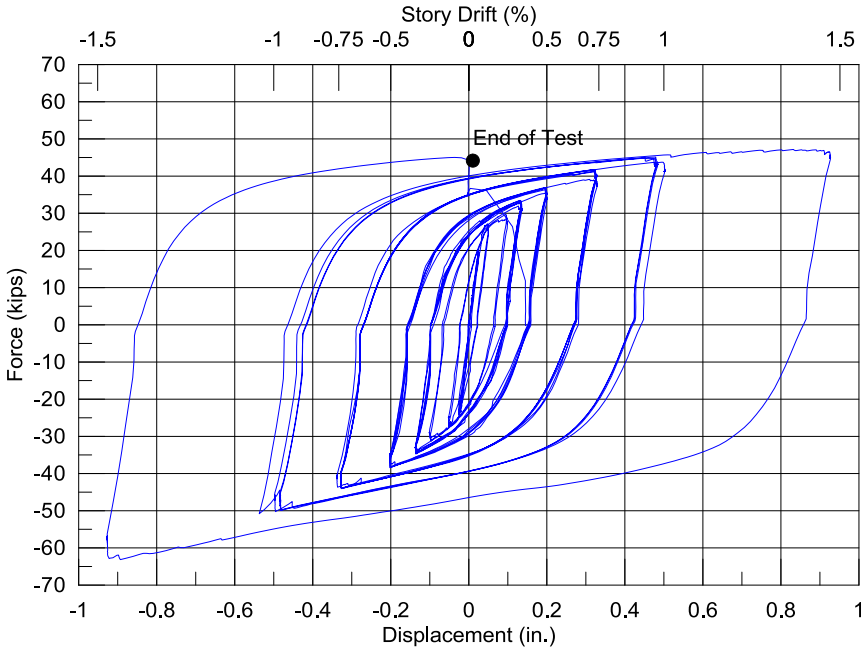

Figure 4-33 Force-Displacement Loops of BRB

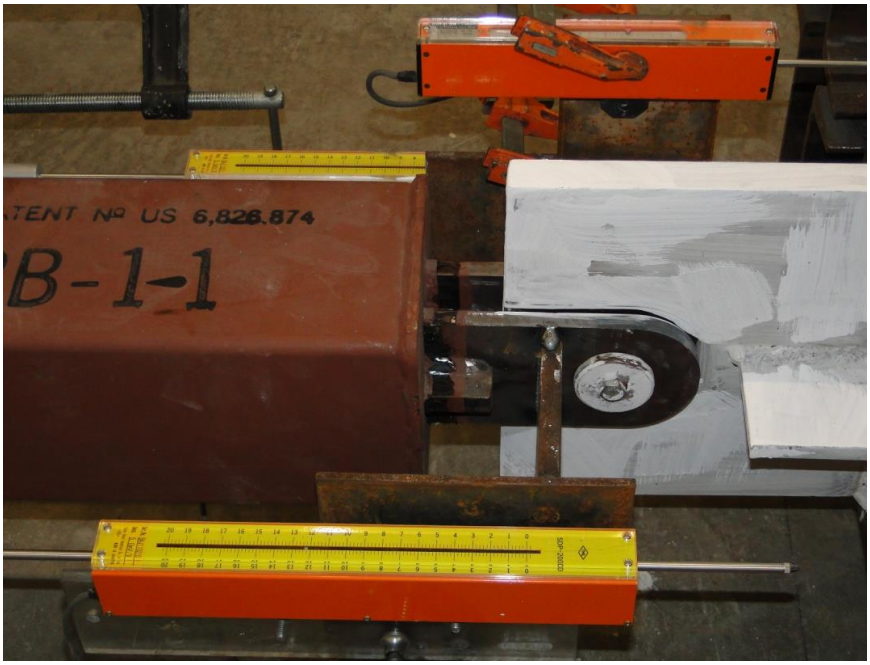

Figure 4-34 Elongation of the Steel Core on the West End

Figure 4-35 Elongation of the Steel Core on the East End

4.12.2 Stress vs. Strain

If assuming that the only yielding part is the yielding core. The elastic parts that the deformation was measured across can be divided into 4 parts (Parts 1-4) on each side of the core as shown in Figure 4-36. The information of each elastic parts and the yielding core can be seen in Table 4-5.

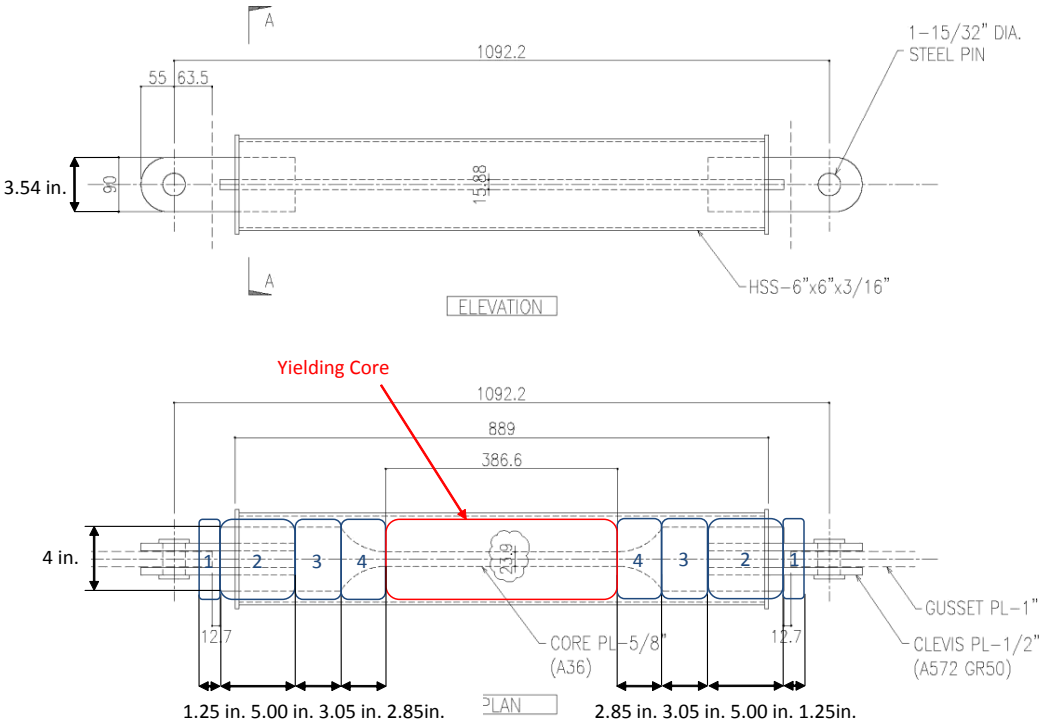

Figure 4-36 Yielding and Non-Yielding Parts across the Length that Deformation was Measured when Assuming that Yielding Core is the Only Yielding Part

Table 4-5 Information of Yielding and Non-Yielding Parts when Assuming that Yielding Core is the Only Yielding Part

Part	Description	Cross Sectional Area, A_i (in.^{2})	Length, L_i (in.)	L_i/A_iE (in./kip)
1	Clevis Plates	3.54	2.50	2.44×10^{-5}
2	Core Plate End + Clevis Plates	6.04	10.00	5.71×10^{-5}
3	Core Plate End	2.50	6.10	8.41×10^{-5}
4	Transition Zone	1.54*	5.70	1.28×10^{-4}
5	Yielding Core	0.588	15.22	-

Notes: *for simplicity, estimated by linearly average the cross sectional area.

Given a force P, the elastic deformation can be calculated as:

$$\Delta_{eny} = \sum_{i=1}^{4} \frac{PL_i}{A_i E}$$

Where $\Delta_{eny} =$ elastic deformation of non-yielding parts, in.

$P =$ Force in the brace, kips

$L_i =$ Length of each part, in.

$A_i =$ Cross sectional area of each non-yielding part, in.^{2}

$E =$ Young's modulus of elasticity, 29,000 ksi.

By deducting the elastic deformation of non-yielding parts from the total deformation, the deformation and the strain of the yielding core can be obtained as follows:

$$\Delta_{yc} = \Delta - \Delta_{eny}$$

$$\varepsilon = \frac{\Delta_{yc}}{L_5} \times 100\%$$

Where $\Delta_{yc} =$ deformation of yielding core, in.

$\Delta =$ total deformation, in.

$\varepsilon = \text{strain, \%}$

$L_5 = l\text{ength of yielding core, } 15.22 \text{ in.}$

The stress in the yielding core can also be obtained by:

$$\sigma = \frac{P}{A_5}$$

Where $A_5 = \text{cross sectional area of the yielding core, } 0.588 \text{ in.}^2$

The stress-strain curve is plotted and can be seen in Figure 4-37.

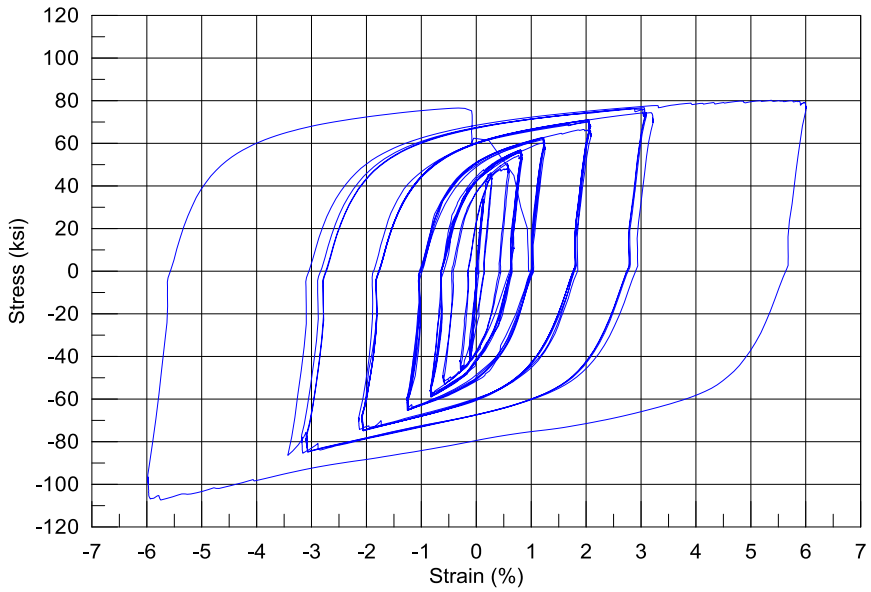

Figure 4-37 Stress vs. Strain when Assuming that Yielding Core is the Only Yielding Part

Alternatively, if assuming that the length of the yielding part proceeded past the length of the yielding core into the transition zone, the cross sectional area which the maximum force applied during the test could yield must be determined. This area is found as:

$$A_{yp} = \frac{P_{\max}}{\sigma_y}$$

where

A_{yp} = cross sectional area that the maximum force could yield, in.^{2}

$P_{\max}$ = maximum applied force, 47.2 kips.

σ_y = yield strength of the core plate, 42.5 ksi.

Thus

$$A_{yp} = \frac{47.2}{42.5}$$
$$= 1.11 \text{ in.}^2$$

Since the thickness of the yielding plate is 5/8 in., the width of the yielding plate which the maximum force could yield is found as:

$$A_{yp} = w \times \frac{5}{8}$$

where

w = width of the core plate which maximum force could yield, in.

Thus

$$1.11 = w \times \frac{5}{8}$$
$$w = 1.78 \text{ in.}$$

As a result, the length of the yielding part becomes 18.64 in. and shown in Figure 4-38. The details of the elastic parts and the yielding part for this scheme can be seen in Table 4-6. By using the information given in Table 4-6, the stress-strain could be constructed, in the same manner as Figure 4-37, and shown in Figure 4-39.

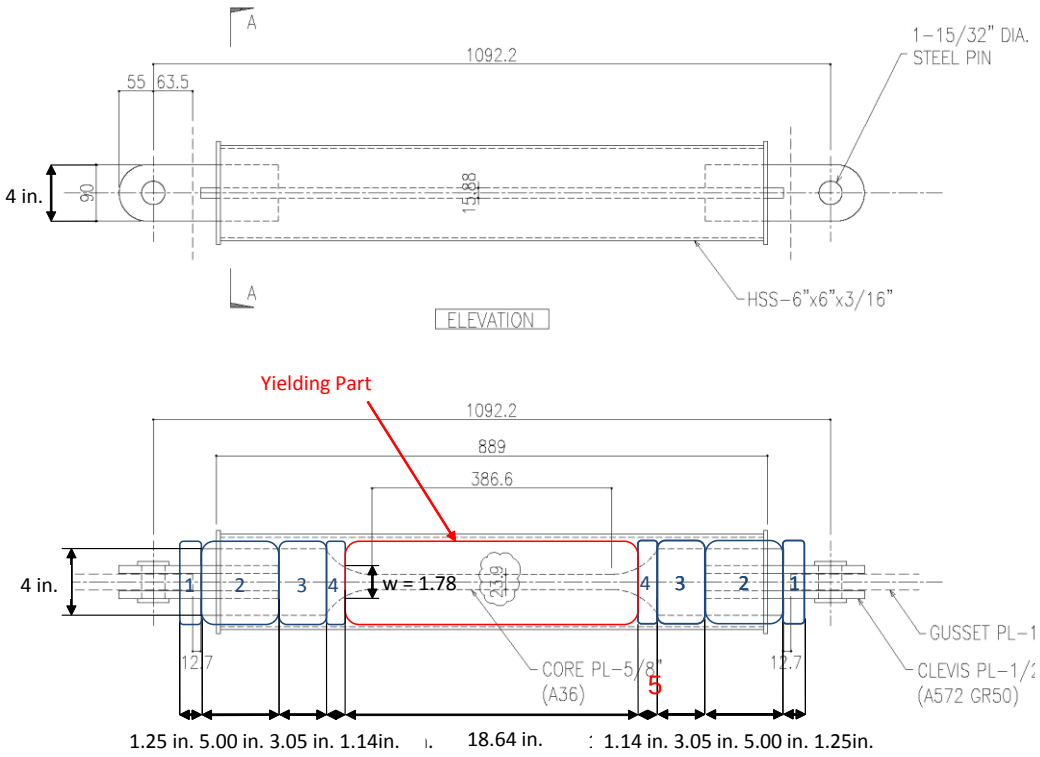

Figure 4-38 Yielding and Non-Yielding Parts across the Length that Deformation was Measured when Yielding of Transition Zone is Considered

Table 4-6 Information of Yielding and Non-Yielding Parts when Yielding of Transition Zone is Considered

Part	Description	Cross Sectional Area, A_i (in.^{2})	Length, L_i (in.)	L_i/A_iE (in./kip)
1	Clevis Plates	3.54	2.50	2.44×10^{-5}
2	Core Plate End + Clevis Plates	6.04	10.00	5.71×10^{-5}
3	Core Plate End	2.50	6.10	8.41×10^{-5}
4	Transition Zone	1.81*	2.28	1.28×10^{-4}
5	Yielding Part	0.588**	18.64	-

Notes: *for simplicity, estimated by linearly average the cross sectional area
**for simplicity, use the cross sectional area of the core

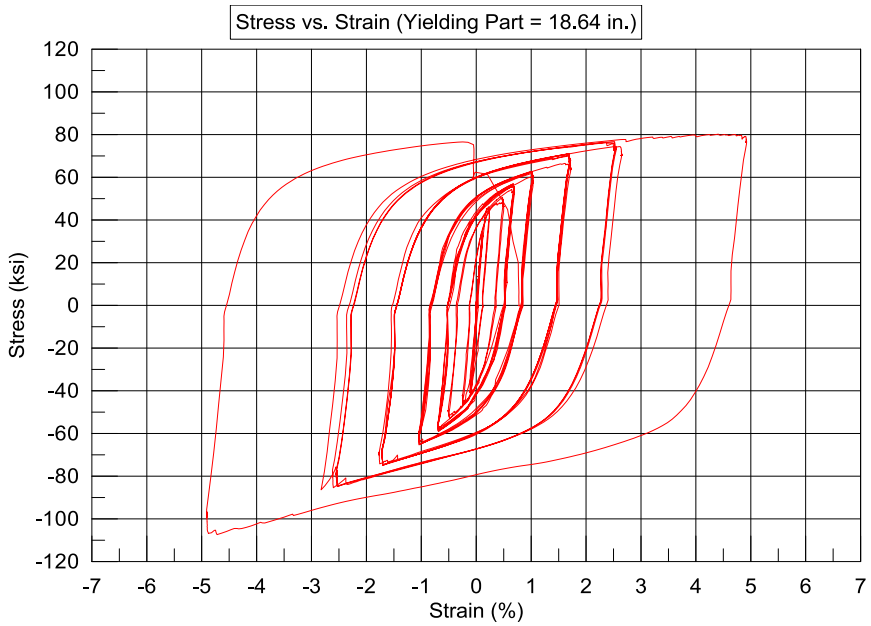

Figure 4-39 Stress vs. Strain when Yielding of Transition Zone is Considered

From Figure 4-37, the BRB underwent large strains of 6.01% in tension and -5.98% in compression respectively. When conservatively consider yielding of the transition zone, the BRB underwent strains of 4.93% in tension and -4.91% in compression as shown in Figures 4-39.

Chapter 5

Full Scale STMF with Buckling-Restrained Subassemblage Test

5.1 Overview

One of the beneficial characteristics of buckling-restrained brace which is elimination of buckling was appealing as a strength and stiffness enhancer to an STMF over conventional X-diagonal web members. Studies on component levels detailed in Chapters 3and 4 indicated that heavy sections such as double channel and double HSS could withstand as large as 0.08 to 0.09 radian of total member rotation. In the full scale STMF subassemblage test, double channel was chosen as it was proven, in chapter 4, that its strength could easily be reduced by cutting off part of the flange (2C12-10-RBS). The reason to use the double channel with reduced beam section (RBS) as chord member within the special segment (SS) is that the chord as well as other members outside of the SS need not to be heavily reinforced especially when BRBs are implemented. The BRBs selected for this hybrid system were tailored made and tested to confirm its reversed cyclic uniaxial behavior (Chapters 3 and 4). Knowing the properties of both chord members in the SS and BRBs led to the design of members outside of the SS, including the test setup components, which needed to remain elastic.

5.2 Test Specimen

The test specimen were tested at the University of Minnesota's Multi-Axial Subassemblage Testing (MAST) Laboratory represents a typical span length of STMFs. Figure 5-1shows the test setup, overall view of the specimen, test jigs, lateral bracing system, reaction wall and floor, and the cruciform-shaped loading beam at MAST laboratory called the “crosshead.” Loading was applied to the specimen through four horizontal actuators and four vertical actuators. Two of the vertical actuators are not shown in the figure for clarity. Figure 5-2 shows the elevation view of the specimen

without lateral bracing systems. The center-to-center dimension of the specimen between the two columns is 381.8125 in. (31 ft.-9-13/16 in.), while the depth of the specimen measured between center lines of top and bottom chord is 48 in. Width of the SS is 119 in. which gives length-to-depth ratio, *L/D*, of 2.5 which violated AISC dimensional requirement which states that *L/D* of any panel in the special segment shall neither exceed 1.5 nor be less than 0.67.

5.2.1 Expected Vertical Shear Strength and Base Shear

Since the maximum expected shear strength, V_{ne}, equation in AISC Seismic Provisions (AISC 2016) were not applicable to this type of STMF, it was determined by pushover analysis on program Perform 3-D. The nonlinear models of the BRBs and plastic hinges of the chord members were created from the component test results. Pushover analysis was done up to failure of the STMF and the induced maximum shear force was 164 kips. The lateral force required which was equivalent to base shear was 306 kips as shown in Table 5-1. Members outside of the SS including columns were designed to remain elastic when vertical expected shear force was reach. List of the member size according to designated name in Figure 5-3 is shown in Table 5-2.

Table 5-1 Anticipated Vertical Shear Force in Special Segments of STMF Specimens and Base Shear

Special Segment	V_{ne}, kips (AISC 341-10)[1] (Derived Equation)[2]	V_{ne}, kips (Pushover Analysis)	Base Shear, kips (Pushover Analysis)
2-C12x20.7+ RBS/BRBs	N/A	164	306

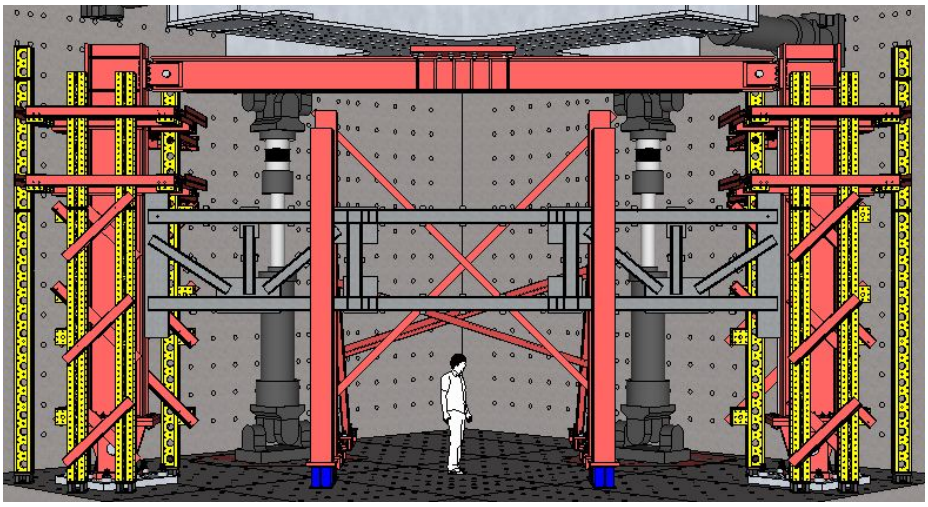

Figure 5-1 Overall Experimental Setup at MAST Laboratory

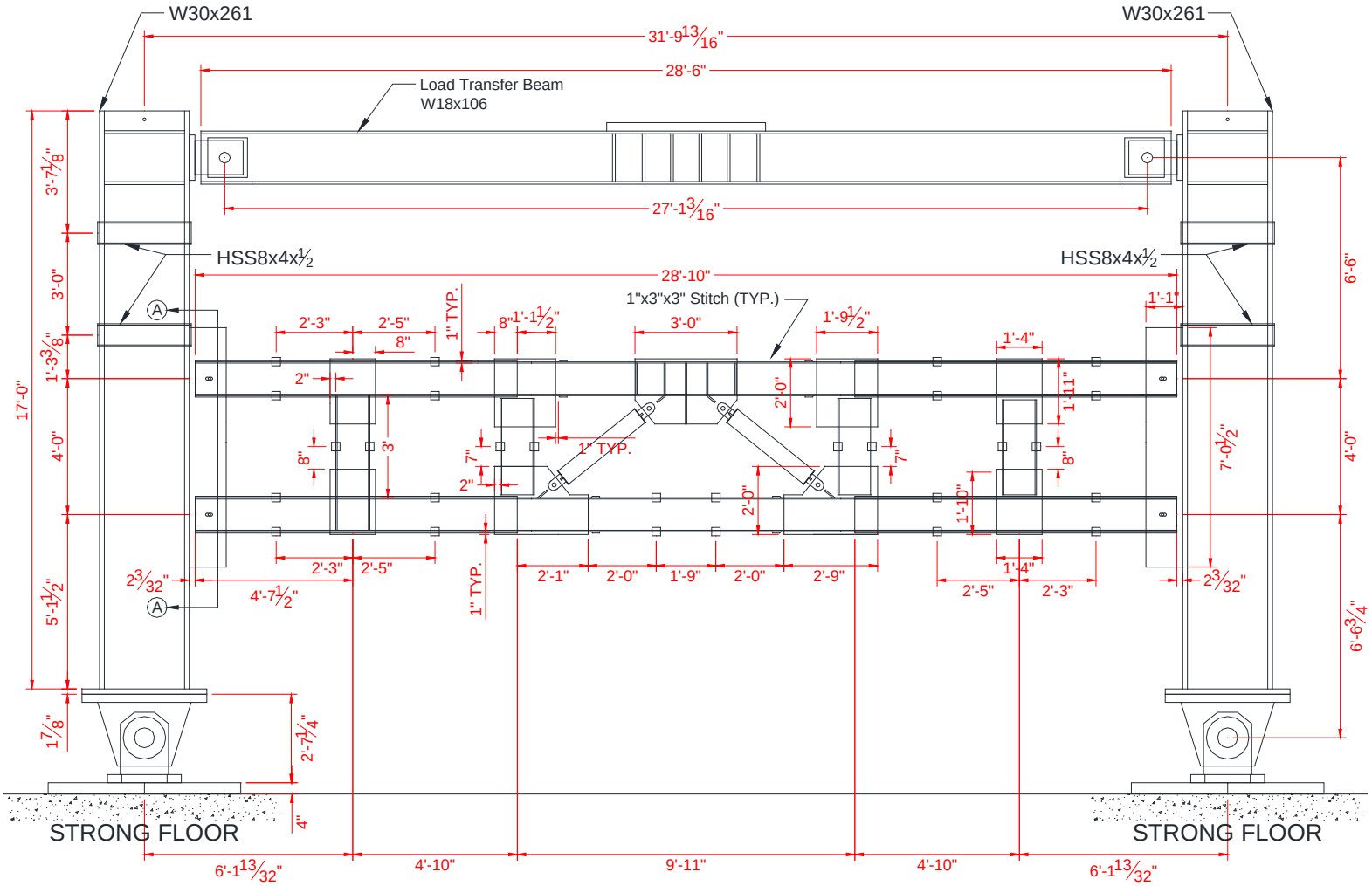

Figure 5-2 STMF Elevation without Lateral Bracing Systems

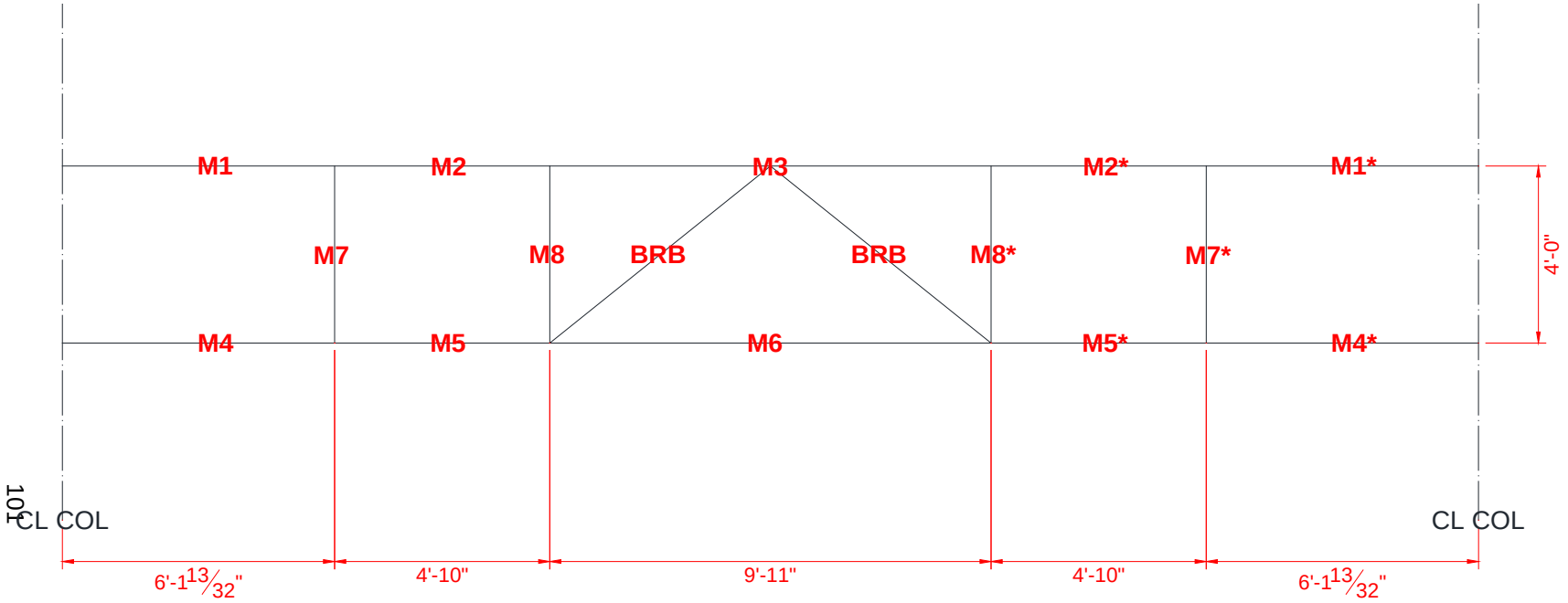

Figure 5-3 Designated Members of STMF

Table 5-2 Truss Member Sections

Member	Size
M1, M1*, M2, M2*, M4, M4*, M5, M5*	2C12×20.7 + Side Plates[1]
M3, M6	2C12×20.7-RBS
M7, M7*, M8, M8*	2C12×20.7

Note [1] side plate is 1 in. thick and 13 in. deep

5.2.2 Special Features

The connection details at various joints in the specimen had features resulting from both experimental component test and FEM analysis. These features are shown in Figures 5-4 and 5-5 and elaborated as follows:

5.2.2.1 Double Channel with Reduced Beam Section

To decrease strength demand of members outside of the SS, the width of flanges of the chord members in the SS were cut off 7/8 in which reduced flexural capacity of 2C12×20.7 sections by 20%. This is the same as 2C12-10-RBS.

5.2.2.2 Connection Details of SS End Joints

The proposed connection details featuring centered gusset plate with weld free zone and horizontal stitches were used for the joints at the end of the SS. These details followed that of component test specimen 2C12-10-RBS.

5.2.2.3 All Vierendeel Panel Truss

To accommodate large opening which is architecturally preferred, truss panels outside of the SS were all Vierendeel panels.

5.2.2.4 Boundary Condition of SS End Joints

Based on the test results of double channel specimens (specimens 2C12-7 and 2C12-8), attaching a member perpendicular to flanges of double channel flexural member near plastic hinge resulted in restraint of the flow of inelastic deformation and early fracture. As a result, the vertical members next to the SS were not welded to the flanges of the chord members.

5.2.2.5 Boundary Condition of Joints outside of the SS

For comparison purposes, the left vertical member outside of the special segment was not welded to the chord members while the right vertical member outside of the special segment was.

5.2.2.6 Lower Gusset Plates Connecting to BRBs

Gusset plates used in BRB connections were deigned according to AISC specifications. The design calculation can be found in Appendix D. At the lower joints, the gusset plates were extended horizontally to self-stabilize the bottom chord member in the SS preventing LTB. The turn of the gusset plate from 45 degrees to horizontal could be made a sharp or smooth turn. According to a finite element analysis, the sharp corner posted higher stress concentration than the smooth corner. For comparison purposes, the corners of the lower gusset plates, connecting to the BRBs, were sharp on the left connection versus smooth on the right connection.

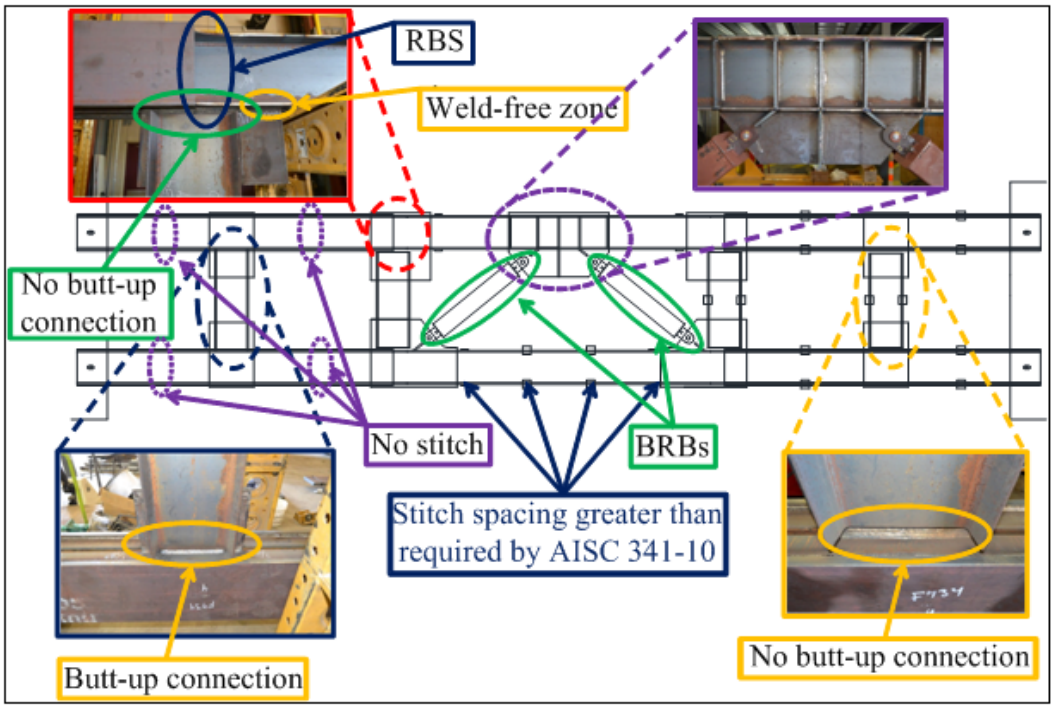

Figure 5-4 Special details of full-scale STMF with BRBs

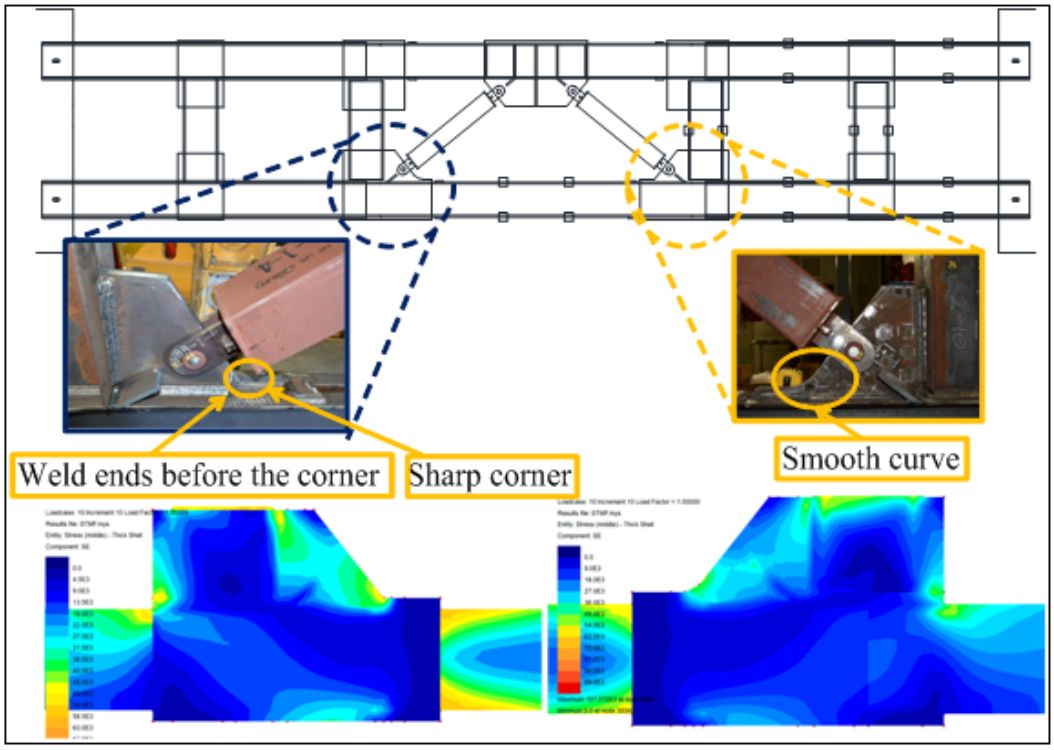

(b)

Figure 5-5 Special details of full-scale STMF with BRBs

5.3 Test Setup

The overall test setup were previously shown in Figures 5-1 and 5-2. The subassemblage specimen represented one story one bay STMF. The top and bottom of the columns were pinned connections representing inflection points at mid column height of consecutive floors. The top pinned connections were connected to a load transferred beam. The middle of the load transferred beam was connected to the crosshead that applied later force to the specimen. Stability bracing of the truss was provided, as required by AISC 341-10 through the truss bracing system shown in Figure 5-6. However, it was located slightly outside of the special segment so that it would not obstruct the movement of the specimens when local buckling initiated at the plastic

hinges at large story drift angles. Stability bracing of truss-to-column connection was also provided as per AISC 341-10 around both columns as shown in Figure 5-7.

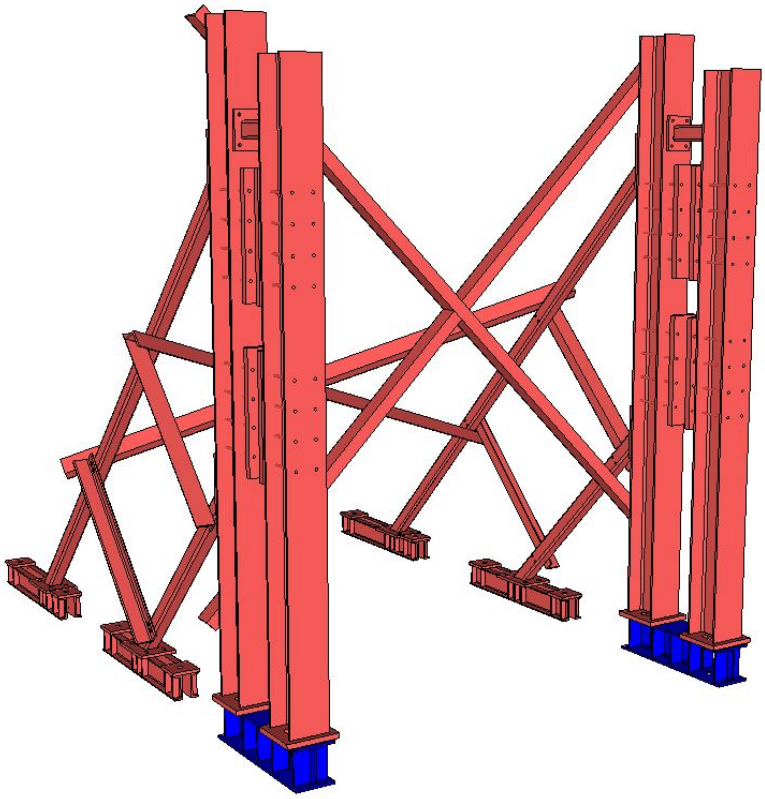

Figure 5-6 Lateral Bracing System at Ends of Special Segment

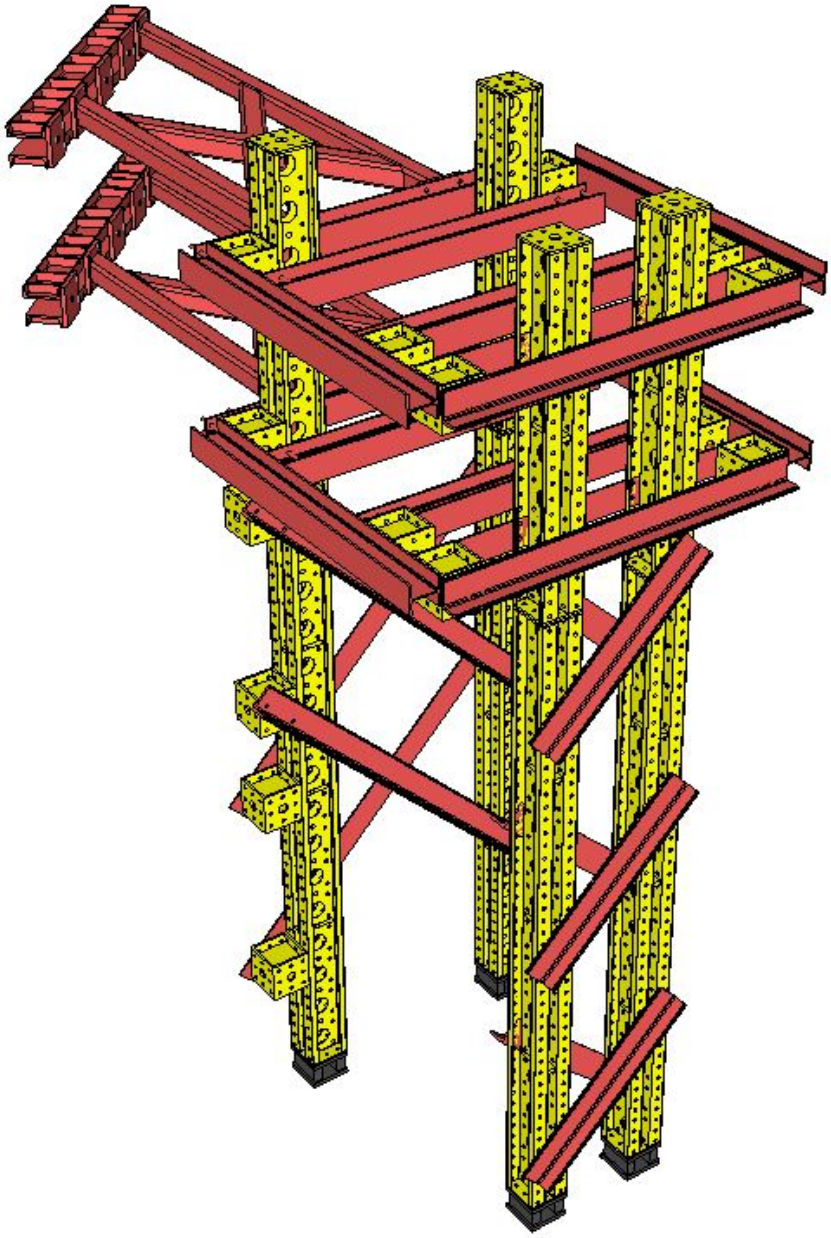

Figure 5-7 Stability Bracing System at Column

5.4 Loading History

The full-scale STMF subassemblage was cyclically loaded according to the AISC 341-16 loading sequence for prequalifying beam-to-column moment connection. Graphical representation of the loading history is shown in Figure 5-8. The displacements and number of cycles at each drift level are shown in Table 5-3.

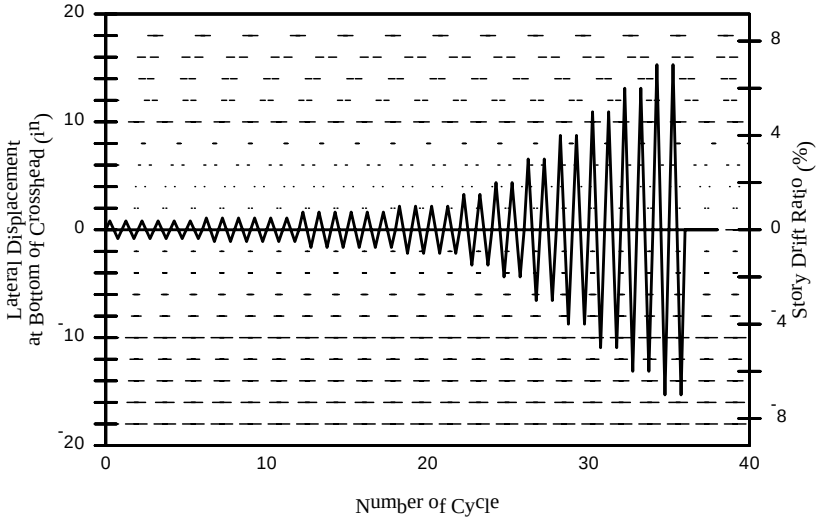

Figure 5-8. Displacement Protocol

Table 5-3 Displacement History

Load Step #	Peak Lateral Displacement (in)	Peak Drift (%), θ	Number of Cycles, n
1	0.75	0.375	6
2	1.00	0.5	6
3	1.53	0.75	6
4	2.03	1	4
5	3.03	1.5	2
6	4.03	2	2
7	6.09	3	2
8	8.13	4	2
9	10.16	5	2
10	12.19	6	2
11	14.22	7	2

5.5 Experimental Results

The hysteretic behavior is shown in Figure 5-9. It can be seen that the specimen remained elastic up to approximately 0.5% story drift ratio. The peak lateral strength of 300 kips was reached on the negative cycle at 1.5% story drift ratio as expected because the short isolated BRB achieved its maximum capacity at this story drift level according to the isolated BRB test. Stiffness and strength of the STMF slightly dropped during the second cycle of the 1.5% story drift ratio. According to the short BRB component test and pushover analysis, the BRB cores fractured due to tension force at the 1.5% story drift ratio. At the 2% story drift ratio, pinching in the hysteresis loop occurred due to the loss of stiffness caused by fracture of the BRB cores. While pushing the STMF toward 2% story drift ratio, while the tension BRB had lost its tensile strength due to the fractured core, the broken core of the compression BRB reengaged; hence, the strength started to pick up again. This created unbalanced forces at the center of the special segment. Moreover, because lateral bracing system was near the lower two gusset plates, the brace-to-vertical member connection had higher out-of-plane stiffness than the brace-to-chord member connection at the middle of top chord of the special segment. The brace-to-chord member connection started to rotate out of plane during the second cycle of the 1.5% story drift ratio. Figure 5-10 (a) and (b) show out-of-plane coordinate (z-direction) at the center of the chord members measured on both the top and bottom flanges of the top and bottom chords by using a Krypton imaging system. It can be seen that the bottom chord exhibited much less out-of-plane movement than the top chord member. The same behavior continued at 3% story drift ratio during which the strength peaked in the positive cycle at 293 kips. By 4% story drift ratio, twisting of the top chord was too large, and the bottom chord was completely broken at the right flexural plastic hinges (Figures 5-11 and 5-12) causing a quick degradation in stiffness and strength. The test was terminated after

the first cycle of the 4% story drift ratio. Figure 5-12 shows that plastic hinges occurred within the special segment. Flexural hinges formed at the ends of the chord members while shear hinge formed in the vertical members at the end of the special segment. Even though slight yielding occurred at members outside of the special segment as indicated by strain gauge readings, the yielding level was very minor and did not affect the performance of the STMF.

5.6 Comparison between STMF with BRBs and STMF with Multiple Vierendeel Panels

Simasathien et al (2016) tested full scale subassemblage of STMF with single and multiple Vierendeel panels. The results showed that intermediate vertical members effectively increased strength and elastic stiffness of the STMF. Hysteretic behavior of STMF with multiple Vierendeel panels is shown in Figure 5-13. Since intermediate vertical members experienced much higher rotational demand than the chord members, they yielded and failed first. From his test, they completely failed after 1.5% story drift ratio and hysteretic behavior of the STMF then followed the STMF with single Vierendeel Panel. He also suggested that the contribution of intermediate Vertical members should not exceed 50% of total capacity of the STMF to avoid sudden drop of strength. When compared to behavior of STMF with BRBs as shown in Figure 5-9, it can be seen that STMF with BRBs was able to maintain nearly the same peak strength up to 3% story drift ratio due to the ability to reengage of the steel core when it was under compression. Sudden drop of strength could completely be ignored in this case.

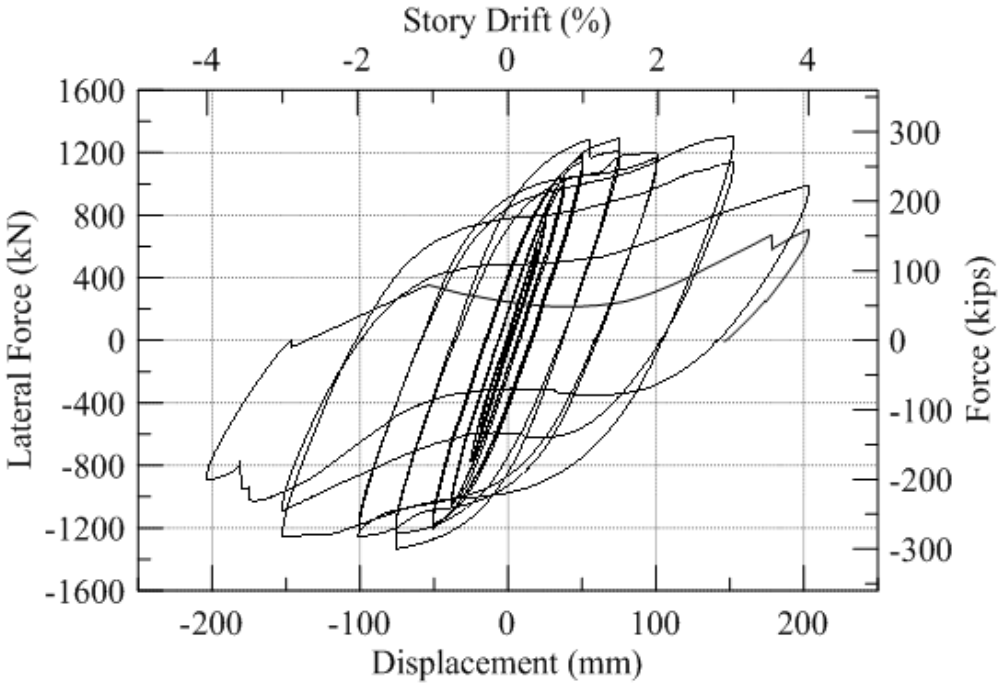

Figure 5-9 hysteretic behavior of full-scale STMF with BRBs subassemblage

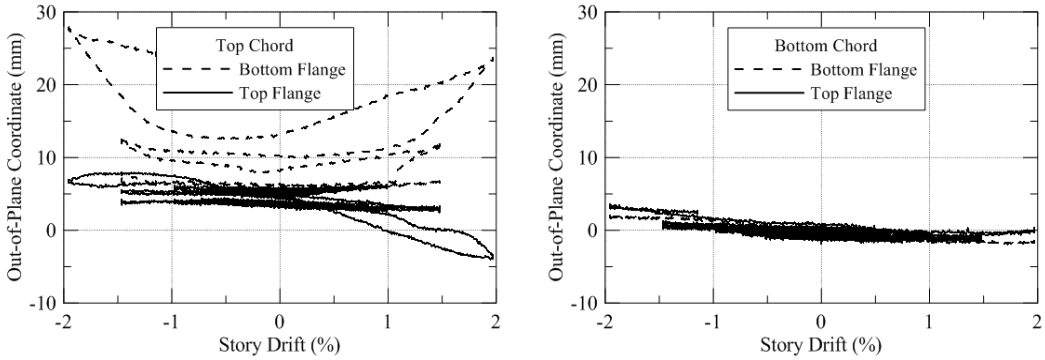

Figure 5-10 Out-of-plane coordinate of near center of the special segment of (a) top chord and (b) bottom chord

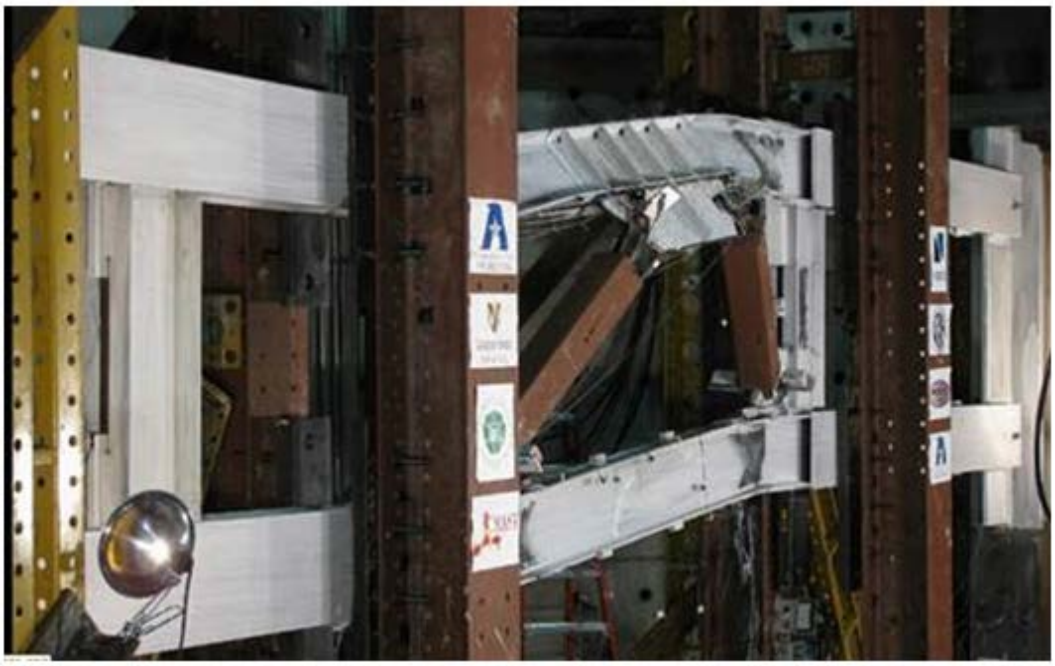

Figure 5-11 Full-scale STMF with BRBs subassemblage at the end of the test

Figure 5-12 Special Segment at the end of the test

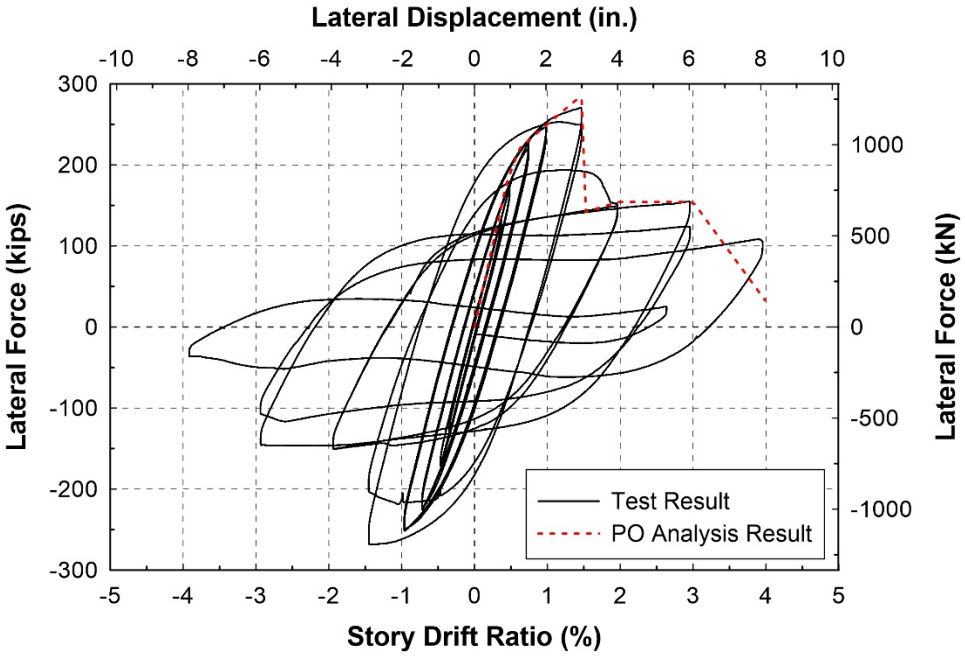

Figure 5-13 Hysteretic Behavior of STMF with multiple Vierendeel Panels

Chapter 6

Long Span Special Truss Moment Frame

6.1 Overview

The need for a very long span structure in sport and industrial venues puts steel moment frames and braced frames in a disadvantageous position. In this regard, special truss moment frames (STMFs) can accommodate large span by utilizing truss girders to provide high lateral stiffness. However, current AISC Seismic Provisions for Structural Steel Buildings (AISC 341-16) do not allow STMF's span and truss depth more than 65 ft and 6 ft, respectively. These limitations were based on experimental and analytical research in the 1990s. Moreover, when the STMF is very long, axial forces induced by the gravity load could post ductility reduction of the chord members in the special segment. An analytical study on seismic behavior of long-span STMFs with double-channel truss members, a span length of 90 ft, and a truss depth of 10 ft are presented here. Plastic hinge models of double-channel sections considering the effect of axial forces were also proposed and used in nonlinear time-history (NTH) analyses of the STMF under 20 design basis earthquakes (DBEs). The hysteresis behavior of double-channel sections under near-collapse earthquakes was studied by an experimental test of a specimen under a proposed near-collapse loading protocol. The study of the effect of axial forces on hysteretic behavior under near collapse loading protocol led to plastic hinge models used in NTH analyses under 20 maximum considered earthquakes (MCEs). A new design procedure for long-span STMFs incorporating conventional elastic design and capacity design based on pushover analysis is presented.

6.2 Prototype Structure

Figure 6-1 shows the floor plan (90 ft × 90 ft) of a one-story building structure where two 90 ft-long STMFs are used for the seismic force resisting system along the E-W direction. Three STMFs with different layouts of the SS are investigated (Figure 6- 2):

STMF-1 has one Vierendeel panel within 30 ft-long special segment. This layout provides a wide uninterrupted special segment for architectural usage.

STMF-2 has three Vierendeel panels made up by two intermediate vertical members within 30 ft-long special segment. The vertical members are typically the first one yield and can be easily replaced after a moderate earthquake (Simasathien et al., 2014). Full-scale STMF experimental testing shows that adding intermediate vertical members can considerably increase the lateral stiffness of an STMF (Simasathien et al., 2014). Chao and Goel (2008) suggested that the intermediate vertical members be treated as secondary members hence most of the truss strength and energy dissipation capacity is provided by the chord members. In addition, plastic hinges must be avoided in the chord members except at chord ends; therefore, the moment capacity of intermediate vertical members has to be limited so that the bending moment in the chord members at sections adjacent to the intermediate vertical members is less than the chord members' moment capacity when the intermediate vertical members reach their maximum capacity. Chao and Goel (2008) therefore suggested the plastic moment capacity of the intermediate vertical member, M_{pv}, be calculated as M_{pc}/m; where M_{pc} is the plastic moment capacity of the chord member and m is number of intermediate vertical members in the SS. For SS with two intermediate vertical members, $M_{pv}/M_{pc} = 0.5$. Recent full-scale STMF experiment shows that for SS designed with this moment capacity ratio, after the intermediate vertical members failed the strength of STMF specimen drastically dropped and its hysteretic behavior followed that of an STMF without intermediate

vertical members (Simasathien et al., 2014). As a result, the intermediate vertical member cannot be too strong in order to avoid a drastic drop in strength of the STMF. In this study, members sizes with M_{pv}/M_{pc} = 0.16 was selected.

STMF-3 has single Vierendeel panel within 10 ft long special segment. This configuration provides very high stiffness of the truss girder, but also causes high rotational demands to the chord members due to the short SS (Simasathien et al., 2017).

The dimensions and elevation of the three STMFs are shown in Figure 6-2. Because of the long special segments of STMF-1 and STMF-2, lateral bracing within the SS is needed to prevent premature buckling of the SS due to axial compressive forces induced by the gravity and lateral loads. The gravity load in a long-span STMF can result substantial compression in the chord members. Figure 6-1 (a) shows the floor plan for STMF-1 and STMF-2 where majority of the gravity loads are carried by the two STMFs along the E-W direction. A series of steel joist girders along the N-S direction are used to transfer the gravity loads to the two STMFs at various truss joints. Additional bracing members are also provided within the SS to reduce the unbraced length (also see Figures 6-2 (a) and (b)). Figure 6-1 (b) shows the floor plan for STMF-3 which has similar layout of steel joists girders. The joist girders near the ends of the SS also serve as bracing members for the top chord member in the SS (see Figure 6-2 (c)). Lateral bracing of the bottom chord members can be done be using steel members extending from the beams (Figure 6-1 (a)) or joist girders (Figure 6-1 (b)). Figure 6-2 (b) and Figure 6-3 shows typical details for truss-to-column connection, end joint of the SS, and intermediate vertical member-to-chord member connection within SS. These details follow the component test in Chapter 4. Detail-1 shows the simplicity of truss-to-column connection which can be done by welding truss members to a gusset plate and the gusset plate to a column flange. Detail-2 and Detail-3 show the end joint of the SS and

intermediate vertical member-to-chord connection within SS which follows the component test results of 2C6×13 specimens. In Detail-2, the vertical members at the end of the SS cannot be welded to the chord members because it will prevent plastic flow and cause the chord members to fracture early. In Detail-3, the intermediate vertical members can be welded to the chord members because plastic hinges will not form in the chord members at that location. The cutout is used to increase the weld area to provide sufficient strength.

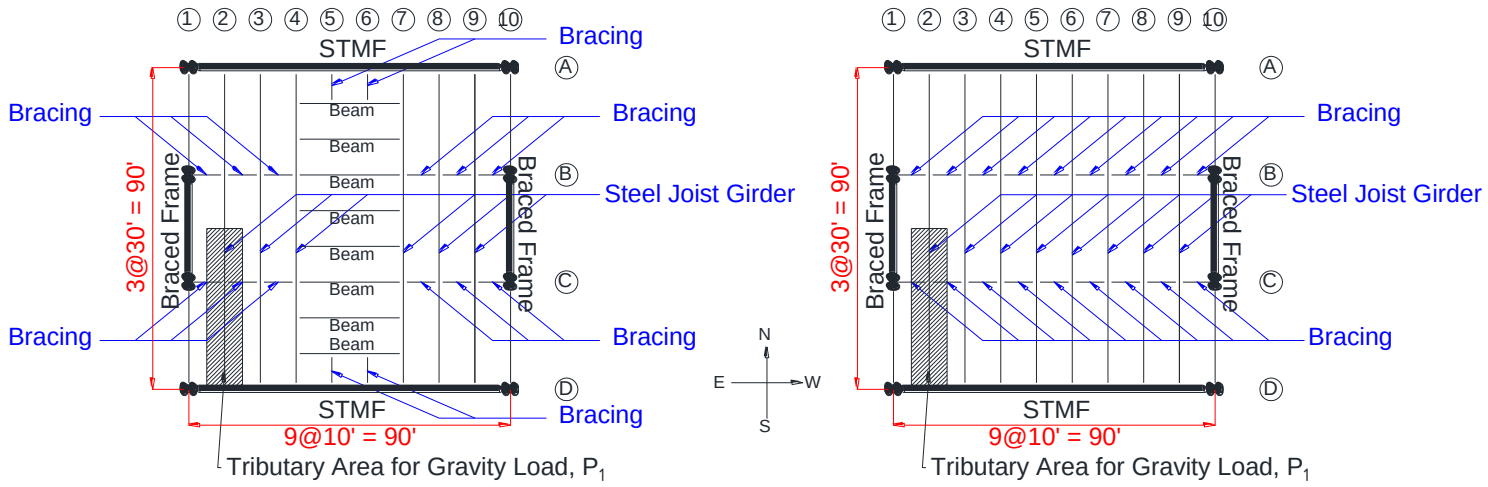

Figure 6-1 Floor plan of (a) STMF-1 and STMF-2 (b) STMF-3

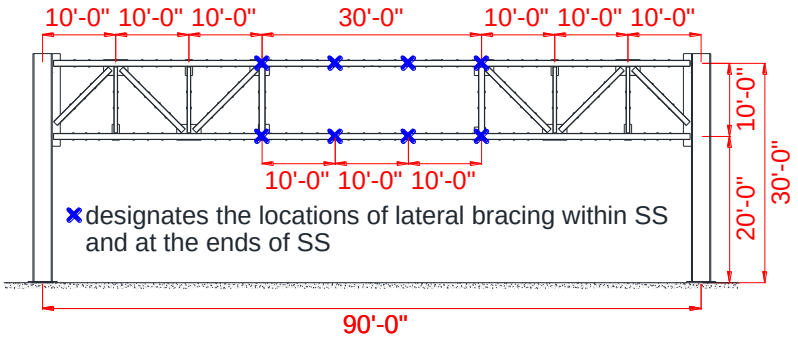

(a)

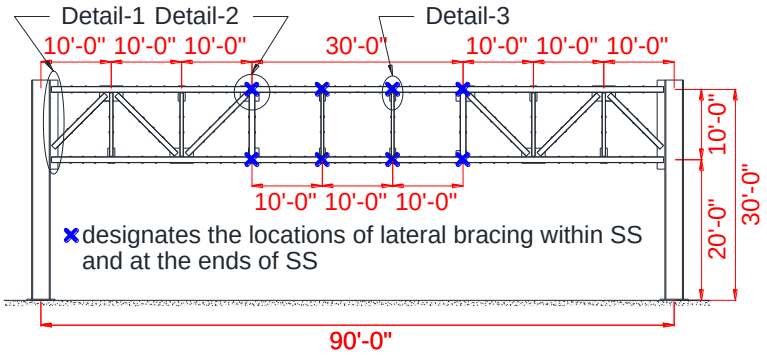

(b)

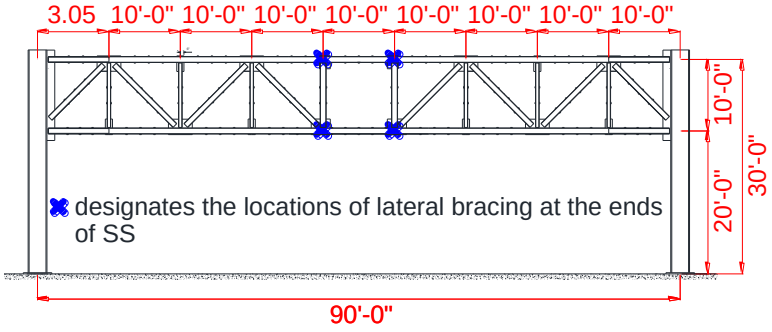

(c)

Figure 6-2 Dimensions and elevation of (a) STMF-1, (b) STMF-2, and (c) STMF-3

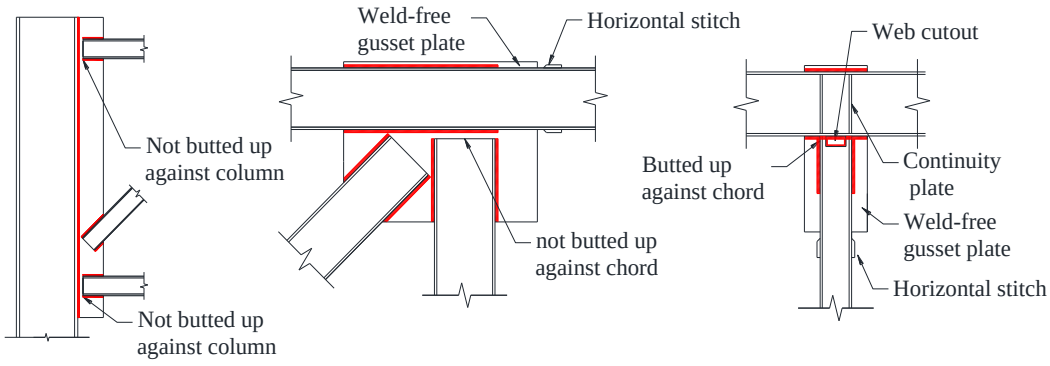

Figure 6-3 Typical details of the connections at the end of SS and intermediate vertical members. (See Figure 6-2 (b))

6.3 Effect of Axial Force on Ductility of Double Channel Flexural Members

In order to study the effect of axial force, first, a finite element analysis (FEA) of 2C12-8 which had no axial force was done in order to calibrate the model with the test result of double channel with special connection details representing chord member in the SS. Figure 6-4 shows good agreement between FEA and test results and the trilinear model was made. FEA analyses were further carried out on the 2C12×20.7 section with axial demand to capacity ratio, α, of 0.1, 0.2, and 0.3 for both compression and tension. The axial demand in this study is defined as axial load induced by gravity loading on the STMF. The axial capacity is defined as $1.1R_yF_yA$. The analyses results of axial compression cases are shown in Figures 6-5 (a), (b), and (C) along with the trilinear models. Figures 6-6 (a), (b), and (c) show the effect of axial tension on hysteresis behavior or 2C12×20.7. It is clearly seen that axial compression had higher degree of effect on ductility reduction of the double-channel section than axial tension. Moreover in both cases, ultimate moment capacity of the section also decreased when axial load increased.

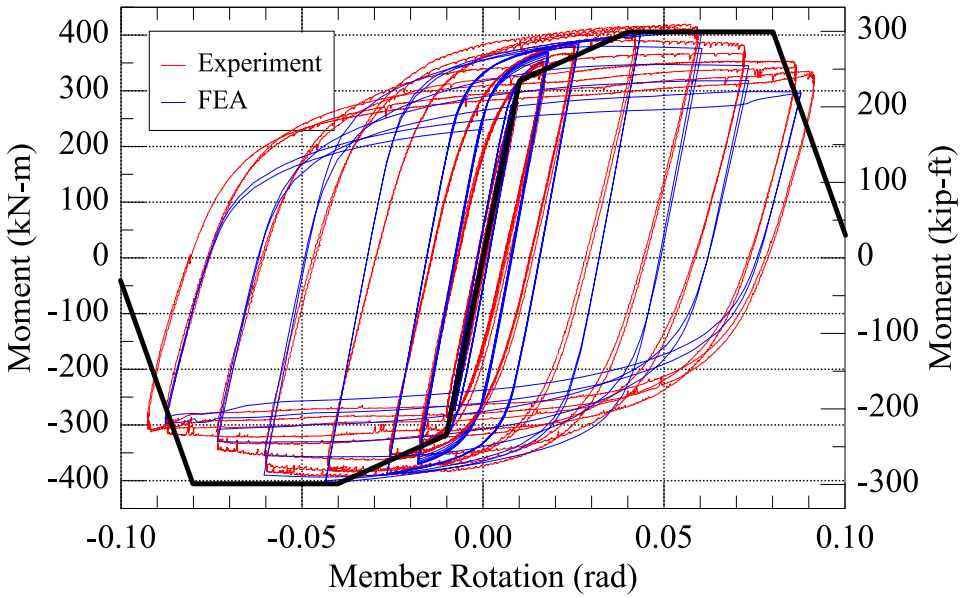

Figure 6-4 Comparison of FEA and Specimen 2C12-8 Test Results

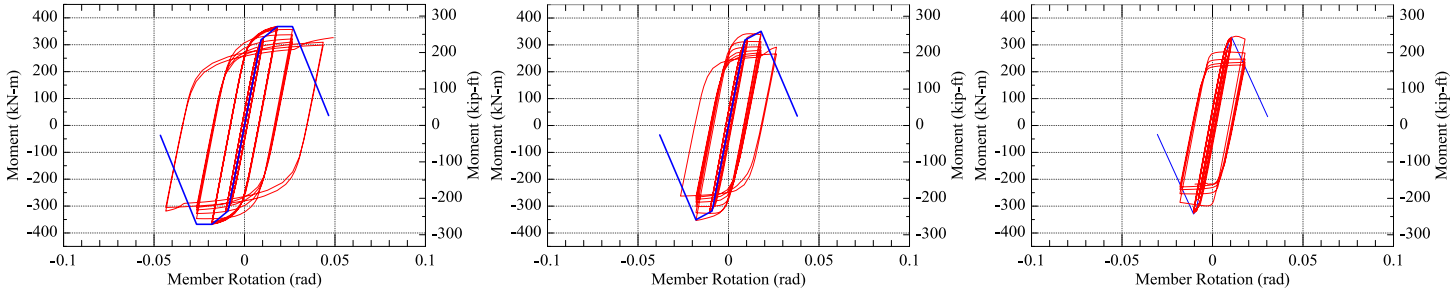

(a) (b) (c)

Figure 6-5 FEA results under AISC loading history and trilinear model of 2C12×20.7 with axial tension per capacity ratio (a) α = 0.1, (b) α = 0.2, and (c) α = 0.3

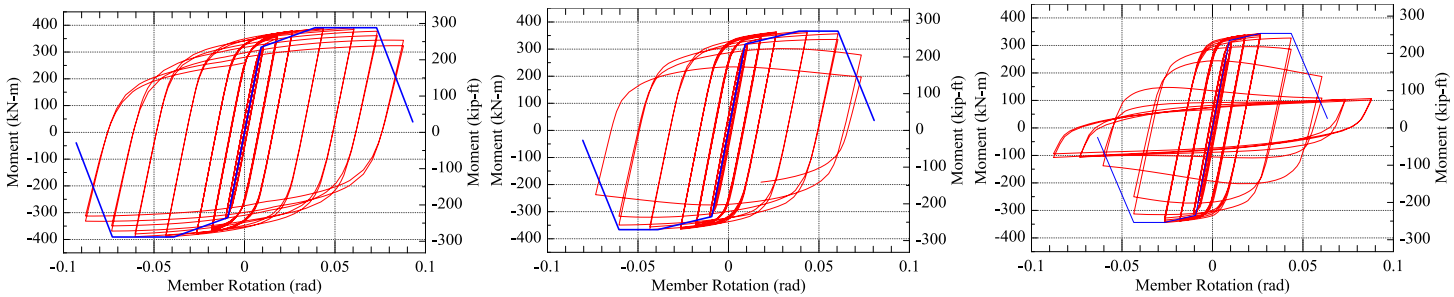

(a) (b) (c)

Figure 6-6 FEA results under AISC loading history and trilinear model of 2C12×20.7 with axial tension per capacity ratio (a) α = 0.1, (b) α = 0.2, and (c) α = 0.3

6.4 Plastic Hinge Models for Truss Members

Trilinear relationship in most commercial programs only requires plastic rotations and corresponding moments at 4 points as shown in Figure 6-7, if strength degradation is considered. These moment parameters are specified as yielding moment, M_y, ultimate moment, M_u, and residual moment, M_r. Based on component test results (Chapter 3), a generalized moment-rotation relationship for double-channel sections without axial force was suggested in Table 6-1.

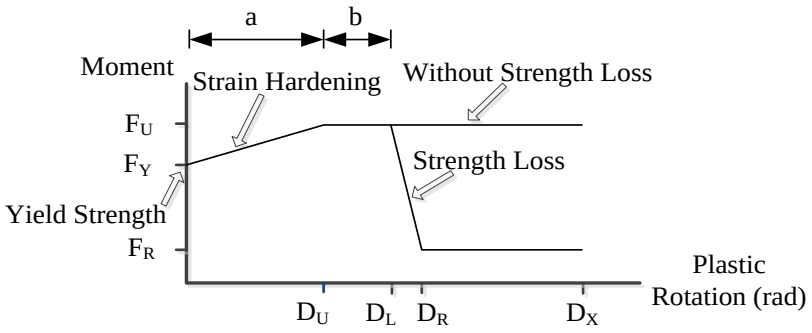

Figure 6-7 Generalized moment-plastic rotation model for plastic hinge with and without strength degradation

Table 6-1 Plastic hinge modeling parameters of double-channel sections without effect of axial force

Parameters	M_y	M_u	M_r	D_u (rad)	D_l (rad)	D_r (rad)
Recommended value	R_yF_yZ	$1.4M_y$	$0.1M_u$	0.03	0.07	0.09

. In order to generalize the plastic rotation parameters, D_u, D_l, and D_r for various axial D/C ratio, parameter *a* and *b* as shown in Figure 6-7 were determined from the trilinear models of hysteresis behavior of 2C12×20.7 in Figures 6-4, 6-5, and 6-6 for various α = 0.1, 0.2, and 0.3. Regression analyses were then carried out and the relationship between *a* and α and *b* and α are as follows (Details in Appendix C):

Axial compression case:

$a = -0.21\alpha + 0.03$ when $0 < \alpha < 0.1$ [6-1 (a)]

$= 0.009$ when $0.1 < \alpha < 0.2$ [6-1 (b)]

$= -0.08\alpha + 0.025$ when $0.2 < \alpha < 0.3$ [6-1 (c)]

$b = 1.1\alpha^2 - 0.42\alpha + 0.04$ when $0 < \alpha < 0.2$ [6-2 (a)]

$= 0$ when $0.2 < \alpha < 0.3$ [6-2 (b)]

Axial tension case:

$a = 0.03$ when $0 < \alpha < 0.2$ [6-3 (a)]

$= -0.12\alpha + 0.05$ when $0.2 < \alpha < 0.3$ [6-3 (b)]

$b = -0.08\alpha + 0.04$ when $0 < \alpha < 0.3$ [6-4]

The test result of 2C12-8 (Figure 6-4) shows that overstrength factor, β, which is defined by M_u/M_y, is 1.28 which is slightly lower than the average value from component test suggested in Table 6-1. Moreover, this ratio decreases when axial compression and tension increase. The original overstrength factor for when α are 0, 0.1, 0.2 and 0.3 were used to find a relationship between overstrength factor and α by regression analysis. Then, the result was scaled so that overstrength factor of double-channel without axial force became 1.4 to better represent general double-channel sections. The relationship between β and α becomes:

Axial compression case:

$\beta = -0.88\alpha + 1.4$ when $0 < \alpha < 0.3$ [6-4]

Axial tension case:

$\beta = -0.73\alpha + 1.4$ when $0 < \alpha < 0.3$ [6-5]

6.5 Plastic Hinge Model of Column

The studies of cyclic behavior of columns under axial loads by Newell and Uang (2008) and Zargar et.al (2014) both confirmed that ASCE-41 underestimated plastic rotational capacity of the studies columns. Nakashima and Liu (2005) performed cyclic tests on square tube columns with axial load (P) of 0, 30%, and 60% of axial yield strength (P_y). The tested columns achieved total rotation of 0.06 rad, 0.04 rad, and 0.02 rad, respectively. Experimental tests by Newell and Uang (2008) on columns with $b_f/2t_f$ and h/t_w less than 7.2 and 17.7, repectively, showed steel wide-flange columns with stocky webs under axial load, ranged from 35% to 75% of nominal axial yield strength, and double-curvature bending could achieve interstory drift capacity of 0.07-0.09 rad before strength degraded below 90% of maximum bending strength. Ozkula et.al (2017) experimentally studied the effect of axial compression on sets of W610 columns that are considered highly and moderately ductile according to AISC 341-10 (AISC, 2010). The results showed that most strong axis-bending specimens could not maintain 0.03 rad plastic rotation. In this study authors decided to use wide-flange columns with flange and web similar or less compactness ratios to those of the lightest columns tested by Newell and Uang (2008) to ensure their large rotational capacity. The plastic hinge model of the columns is shown in Table 6-2.

Table 6-2 Plastic hinge modeling parameters for yielding members with effect of axial force

Parameters	M_y	M_u	M_r	D_u (rad)	D_l (rad)	D_r (rad)
Truss Members	R_yF_yZ	βM_y	$0.1M_u$	a	D_u+b	D_l+0.02
Column	R_yF_yZ	$1.1M_y$	$0.45M_u$	0.06	0.061	0.08

Note: Parameters β, a, and b are determined from Eqs. 6-1 to 6-12

6.6 Proposed Design Procedure and Design Example

6.6.1 Design Procedure

6.6.1.1 Elastic Design

The initial elastic design of the long-span STMF is done in order to determine initial member sizes. All members in the STMF are designed, as beam-column elements, based on elastic analysis of the STMF under lateral earthquake force specified by building code and gravity loading according to standard load combinations. The load combination for gravity loading is case I (shown later) where vertical seismic load effect is included.

6.6.1.2 Design of Members Outside of SS

The design of members outside of the SS is then modified based on capacity design approach. After the structure was designed using the elastic analysis result in Step 1, a nonlinear pushover analysis is performed up to the point where chord members within the SS and intermediate vertical members, if applicable, fully strain-hardened. The load combination for gravity loading is case II (shown later) is included in this step. To simplify the design prodedure, effect of axial load was disregard in plastic hinge model of yielding truss members. In other words, the plastic hinges of the chord members in the SS and intermediate vertical members are modeled after recommended values in Table 1 or values in Table 6-2 when $\alpha = 0$. Those of non-yielding truss member could be modeled as elastic-perfectly-plastic. Plastic hinges of the column are modeled after the values in Table 2. If any member outside of the SS, except columns, yields, such member needs to be redesigned to ensure that it remains elastic. Authors suggested allowing column to yield up to 0.005 rad because it's unrealistic to completely prevent yielding in the columns. Alternatively, the members outside of the SS can also be designed according to

the expected vertical shear strength of the special segment, V_{ne}, given in the Seismic Provisions (AISC, 2016) or a proposed equation by Chao et.al (2017).

6.6.1.3 Check Axial Compressive Demand to Capacity Ratio

Due to detrimental effect of compressive axial load on rotational capacity of double-channel section in the SS shown in Figure 6-5, the ratio of axial compressive demand to axial capacity, α, of the chord member within the SS is advised to be 0.15 or lower. However, the axial compressive force should be caused by gravity load combination case II (shown later) only. This is because nonlinear time history analysis of long span STMF is done under gravity load combination case II. If α is greater than 0.15, the size of the chord members within SS should be increased and repeat steps 2.

6.6.1.4 Computer Modeling

As mentioned above, a nonlinear pushover analysis was used in capacity-design of non-yielding members outside of the SS. Moreover, seismic performances of the prototype structures were evaluated by nonlinear time-history analyses. A computer software package PERFORM-3D (CSI 2006) was used in this study. To simplify the analyses, a 2-dimensional STMF was considered to carry half of the gravity and lateral loads. Half of the seismic masses are attributed to each STMF. Loads and seismic masses at each joint were determined according to the respective tributary area. Columns were modeled as a beam-column element with a lumped plastic hinge at each end. Strain-hardening, strength loss, as well as axial force and bending moment interaction were included in the plastic hinge model. Due to sizeable gusset plates and weld connection used at each truss joints, each end of the truss members is rigid. As a result, truss members are also modeled as a beam-column element with a lumped plastic hinge at each end. End portions of the truss members which are welded to the gusset plate were modeled as elastic rigid element to represent the high rigidity of the gusset

plates. P-δ modeling is included in each member. Because all gravity loads are entirely carried by STMFs, no additional P-Δ columns were used. Rayleigh damping (combination of mass and stiffness proportional damping) of 2% was used for all modes in the nonlinear time-history analyses.

6.6.2 Design Example (STMF-1)

Lateral Load

Three prototype STMFs were designed based on American Society of Civil Engineers' Minimum Design Loads for Buildings and Other Structures (ASCE 7-10) (ASCE, 2010). The prototype structure was assumed to be a one story one bay convention hall located in San Francisco, CA. A generic site class C was used here. Detailed design parameters are summarized in Table 6-3.

Table 6-3 Design parameters for 1-story STMF convention hall from ASCE 7-10 (2010) for a San Francisco site

Parameter	ASCE 7-10	Reference
Risk Category	III	Table 1.5-1
Importance Factor	1.25	Table 1.5-2
Site Class	C	N/A
S_s	1.5 g	Fig. 22-1 and Sec.12.8.1.3
S_1	0.78g	Fig. 22-2
F_a	1.0	Table 11.4-1
F_v	1.3	Table 11.4-2
$S_{MS}= F_a S_s$	1.5g	Eq. 11.4-1
$S_{M1}= F_v S_1$	1.014g	Eq. 11.4-2
$S_{DS}=(2/3) S_{MS}$	1.0g	Eq. 11.4-3
$S_{D1}=(2/3) S_{M1}$	0.676g	Eq. 11.4-4
Seismic Design Category	E	Sec. 11.6
Building Height	9.14 m	N/A
T_L	12 s	Fig. 22-12
C_u	1.4	Table 12.8-1
T_a	0.256 s	$T_a=0.0488h_n^{0.75}$ (Eq. 12.8-7)
$T=C_u \times T_a$	0.359 s [a]	Sec. 12.8.2
Response Modification Factor, R	7	Table 12.2-1
Total Building Weight, W	502 kips	N/A
C_s=V/W (DBE)	0.179	Eqs. 12.8-2, 12.8-3, 12.8-5, 12.8-6

Note: [a] Fundamental periods for STMF-1, STMF-2, and STMF-3 are 0.428 s, 0.355 s, and 0.179 s, respectively, based on modal analysis.

Based on a dead load of 50 psf, a live load of 12 psf, and a tributary area of 90 × 90 sq.ft., the resulting seismic weight is 502.2 kips (Note: all live load is conservatively included). Since there are two STMFs sharing the design base shear, each STMF carries 44.95 kips of lateral force. As shown in Figure 6-8 (a), the design base shear was applied discretely to the top joints of the truss according to tributary ratio of masses.

Gravity Load

The gravity load at each truss joint was determined according to respective tributary area and load path. An example of the tributary area used for load P_1 is shown in Figure 6-1. Below is an example of the gravity load determination for STMF-1.

Concentrated Loads at Column and Joint:

Dead Load (DL)

$$P_{CD} = \frac{50 \times 5 \times 45}{1000} = 11.25\ kips$$

$$P_{1D} = P_{2D} = \frac{50 \times 10 \times 45}{1000} = 22.5\ kips$$

$$P_{3D} = \frac{50 \times 20 \times 45}{1000} = 45\ kips$$

Live Load (LL)

$$P_{CL} = \frac{12 \times 5 \times 45}{100} = 2.7\ kips$$

$$P_{1L} = P_{2L} = \frac{12 \times 10 \times 45}{100} = 5.4\ kips$$

$$P_{3L} = \frac{12 \times 20 \times 45}{1000} = 10.8\ kips$$

The critical load combinations were found according to ASCE 7-10 (ASCE, 2010). Case I was used in the initial elastic design while Case II was used to determine axial force to axial capacity ratio, in pushover analysis, and in nonlinear time history analyses. The design loads used in elastic design of STMF-1 is shown in Figure 6-8 (a).

Case I (for elastic design)

$$(1.2 + 0.2S_{DS})DL + 0.5LL$$

$$P_C = (1.2 + 0.2 \times 1.0)(11.25) + 0.5(2.7) = 17.1\ kips$$

$$P_1 = P_2 = (1.2 + 0.2 \times 1.0)(45) + 0.5(5.4) = 34.2\ kips$$

$$P_3 = (1.2 + 0.2 \times 1.0)(45) + 0.5(10.8) = 68.4\ kips$$

Case II (for axial force to capacity ratio check, pushover analysis, and nonlinear time history analysis)

$$1.2DL + 0.5LL$$

$$P_C = (1.2)(11.25) + 0.5(2.7) = 14.85\ kips$$

$$P_1 = P_2 = (1.2)(22.5) + 0.5(5.4) = 29.7\ kips$$

$$P_3 = (1.2)(45) + 0.5(10.8) = 59.4\ kips$$

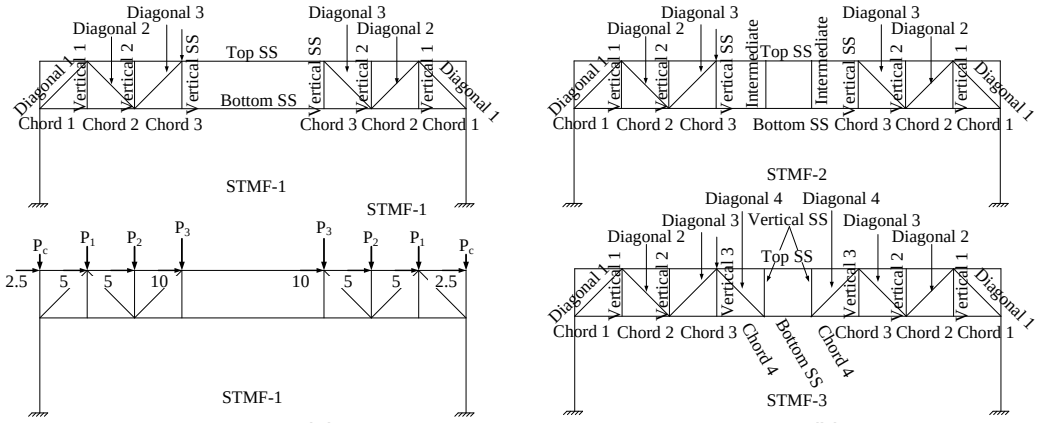

Figure 6-8 (a) Member designation and loadings of STMF-1 and (b) member designation of STMF-2 and STMF-3

Elastic Design of STMF-1

Elastic analysis of all study STMFs were performed using program RISA-3D (RISA Technologies, 2012). The initial elastic design resulted in the members shown in Table 6-4. The small design lateral force resulted in small column and truss members.

Design of Members outside of the SS of STMF-1

The final designed members of STMF-1 are shown Table 6-5. The chord member was increased in size and nonlinear pushover analysis was performed to 2.1%

story drift ratio using program Perform-3D (CSI, 2006). At this story drift ratio, all 4 plastic hinges at the end of the chord members in the SS reach $1.4M_y$ or M_u. The sizes of member outside of the SS were selected so that yielding did not occurr except for the columns. The maximum plastic rotation of the columns at 2.1% story drift ratio was 0.005 rad, as shown in Table 6-6. Figure 6-9 shows the pushover curve and Table 6-6 shows the yielding sequence of the STMF-1. The first yielding of STMF-1 occurred at the top and bottom chord in the SS at 0.89% story drift ratio. At this point, the base shear was 472 kips which was much larger than the design base shear of 45 kips. It should be noted that the left column yielded slightly later than the right column due to the effect of gravity loading.

Table 6-4 Initial elastic designed members of STMF-1, STMF-2, and STMF-3

Member	STMF-1	STMF-2	STMF-3
Column	W12×96	W12×96	W12×96
Panel Zone	W12×96	W12×96	W12×96
SS	2C12×30	2C10×30	2C10×25
Vertical SS	2C12×30	2C10×30	2C10×25
Chord 1-4 [b]	2C12×30	2C10×30	2C10×25
Diagonal 1-4 [b]	2C9×20	2C9×20	2C9×20
Vertical 1-3 [b]	2C6×13	2C6×13	2C6×13
Intermediate	-	2C5×9	-

Note: [b] STMF-1 and STMF-2 only have Chord 1-3, Diagonal 1-3, and Vertical 1-2

Table 6-5 Final designed members of STMF-1, STMF-2, and STMF-3

Member	STMF-1		STMF-2		STMF-3	
	Final Design	α	Final Design	α	Final Design	α
Column	W14×550	-	W14×605	-	W36×652	-
Panel Zone	W14×550	-	W14×605	-	W36×652	-
Top SS	2C15×50	0.14	2C15×50	0.14	2C15×50	0.13
Bottom SS	2C15×50	0.12	2C15×50	0.12	2C15×50	0.09
Vertical SS	2C15×50	-	2C15×50	-	2C15×50	-
Chord 1-2	2C15×50	-	2C15×50	-	2C15×50 + 1" thick side plates [d]	-
Chord 3-4 [c]	2C15×50	-	2C15×50	-	2C15×50	-
Diagonal 1	2C10×20		2C10×30		2MC12×35	-
Diagonal 2-4 [c]	2C9×20	-	2C10×30	-	2MC12×35	-
Vertical 1-3 [c]	2C6×13	-	2C6×13	-	2C6×13	-
Intermediate	-	-	2C130×13	-	-	-

Note: [c] STMF-1 and STMF-2 only have Chord 1-3, Diagonal 1-3 and Vertical 1-2
[d] Side plate is 11.375 in. deep and welded to the web of the member

Table 6-6 Story drift ratio at yielding and plastic rotation at 2.1% story drift ratio (fully strain-harden chord members in SS) of members of STMF-1

Yielding Sequence	Member	Story Drift Ratio when Yielding Occurs (%)	Plastic Rotation at 2.1% Story Drift Ratio (rad)
1	Top Chord in SS	0.89	0.034
1	Bottom Chord in SS	0.89	0.032
2	Right Column	1.57	0.002
3	Left Column	1.84	0.005

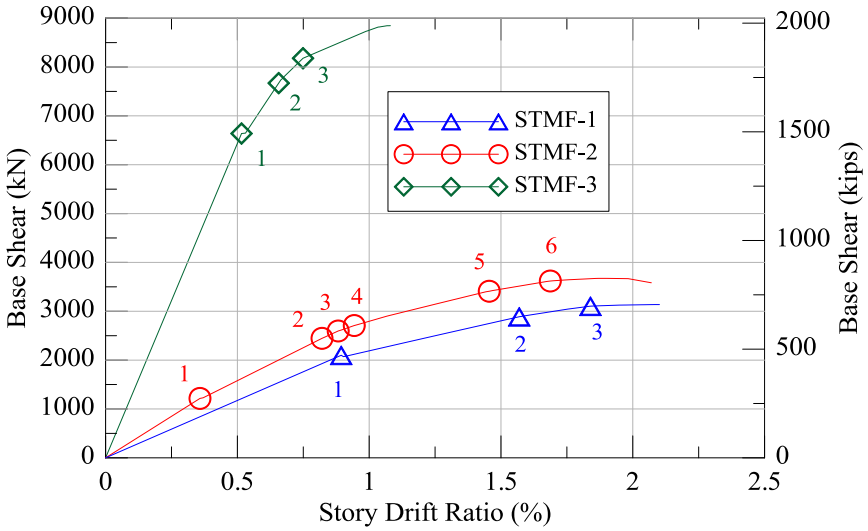

Figure 6-9 Pushover curves of STMF-1, STMF-2, and STMF-3

Design of STMF-2 and STMF-3

STMF-2 and STMF-3 were designed in the same manner of STMF-1. The elastic designed members of STMF-2 as designated in Figure 6-8 (a) are shown in Table 6-4. The designated yielding members (DYMs) in STMF-2 are the SS chord members and intermediate vertical members. Similarly to STMF-1, the final size of the chord member was increased in order to reduce α to be under 0.15. The final designed members are shown in Table 6-5. In order for the chord members to fully strain harden, STMF-2 was pushed to 2.1% story drift ratio. At this story drift, all members outside of the SS were elastic except columns which minimally yielded at 0.006 rad. The plastic rotation of yielding members and columns, at 2.1% story drift ratio, and the story drift ratio when yielding occurred are shown in Table 6-7. Figure 6-9 shows that when the first member (intermediate vertical members) of STMF-2 yields at 0.36% story drift, the base shear is 273 kips which is larger than the design base shear. It should be noted that in STMFs, intermediate vertical members generally yield before the chord member due to higher rotational demands (Simasathien, 2016).

Table 6-7 Story drift ratio at yielding and plastic rotation at 2.1% story drift ratio (fully strain-hardened chord and intermediate vertical members in SS) of members of STMF-2

Yielding Sequence	Member	Story Drift Ratio when Yielding Occurs (%)	Plastic Rotation at 2.1% Story Drift Ratio (rad)
1	Left Intermediate Vertical Member	0.36	0.090
1	Right Intermediate Vertical Member	0.36	0.088
2	Top Left Chord in SS	0.82	0.034
3	Top Right Chord in SS	0.88	0.029
3	Bottom Left Chord in SS	0.88	0.033
4	Bottom Right Chord in SS	0.94	0.028
5	Right Column	1.46	0.006
6	Left Column	1.69	0.003

Similar to STMF-1 and STMF-2, the chord member of STMF-3 was increased in size in order to keep α under 0.15. Table 6-5 shows the final design members. The chord members in the SS were fully strain-hardened when story drift was 1.1%. At this story drift, none of the members outside of the SS yielded except columns (Table 6-8). The maximum plastic rotation of the columns was 0.005 rad. First yielding occurred in the top and bottom chords in the SS at 0.52% story drift ratio and the corresponding base shear was 1492kips (Figure 6-9). The three STMFs' yield drift ratios were between that typical concentrically-braced frames (yield drift ratio approximately 0.3%) and moment frames (yield drift ratio approximately 1%). The elastic stiffness of STMF-1, STMF-2, and STMF-3 are 147 kip/in., 212 kip/in., and 804 kips/in., respectively. The results show that the SS layouts used in STMF-3 provide much higher lateral stiffness that that of STMF-1 and STMF-2.

Table 6-8 Story drift ratio at yielding and plastic rotation at 1.1% story drift ratio (fully strain-harden chord members in SS) of members of STMF-3

Yielding Sequence	Member	Story Drift Ratio when Yielding Occurs (%)	Plastic Rotation at 1.1% Story Drift Ratio (rad)
1	Top Chord in SS	0.52	0.030
1	Bottom Chord in SS	0.52	0.031
2	Right Column	0.66	0.005
3	Leftt Column	0.75	0.004

6.7 Seismic Performance Evaluation of the studied STMFs

Ground Motions

The prototype STMFs were evaluated by nonlinear time-history analyses under two suites of twenty SAC ground motions (Somerville et al., 1997) oriented in the direction of STMFs. The first suite of ground motions has a return period of 475 years (10% probability of being exceeded in 50 years) and is equivalent to design basis earthquakes (DBEs). The second suite of ground motions has a return period of 2,475 years (2% probability of being exceeded in 50 years) and is equivalent to maximum considered earthquakes (MCEs). Typically, for time-history analysis, the average response spectrum of a series of ground motions is scaled over certain period range to envelope the code-specified DBE or MCE spectrum (e.g., Maison and Speicher, 2016). The average accelerations of the 20 DBE-level and MCE-level ground motions at the design period (0.359 s, see Table 6-3) were 1.32g and 1.97g, respectively. These values are much higher than the code-specified DBE and MCE spectral accelerations of 1.0g and 1.5g (Table 6-3), respectively. In this study, however, the ground motions were not scaled down in order to obtain more conservative rotational demands of the yielding members.

6.7.1 Nonlinear Time History Analysis under Design Basis Earthquakes

The three STMFs are evaluated by nonlinear time-history analyses under twenty DBE ground motions. Plastic hinge models of the chord members in the SS, were modeled after suggested valued in Table 6-2. Gravity loading induced compression in the top chord member and tension in the bottom chord member. As a result, parameters *a, b,* and β needed for the plastic hinge model of the top chord member were obtain from Eqs. 6-1 to 6--3 while those for the bottom chord member were obtained from Eqs. 6-4 to 6-6. The average maximum story drift ratio of STMF-1, STMF-2, STMF-3 were 0.71%, 0.53%, and 0.14%, respectively (Figure -10). Table 6-9 shows the average maximum plastic rotations of DYMs. These averages were calculated based the number of ground motions that caused the yielding. Neither STMF-3 nor columns of STMF-1 and STMF-2 yielded under any DBE ground motion. Chord member in the SS of STMF-1 yielded under 3 ground motions and the average maximum plastic rotation was 0.027 rad. One ground motion caused one of the four plastic hinges which formed at the ends of the chord members in the SS to fail or reach the point where it lost strength. This resulted in plastic rotation of 0.06 rad, however; due to high redundancy of STMF, the system did not collapse. Chord members in the SS of STMF-2 only yielded under 2 ground motions and the average maximum plastic ground motion was minor. On the other hand, intermediate vertical members yielded under 17 ground motions and the average maximum plastic rotation was 0.01 rad. As a result, the proposed design procedure could safely provide seismic resistance for 90 ft long and 10 ft deep STMFs.

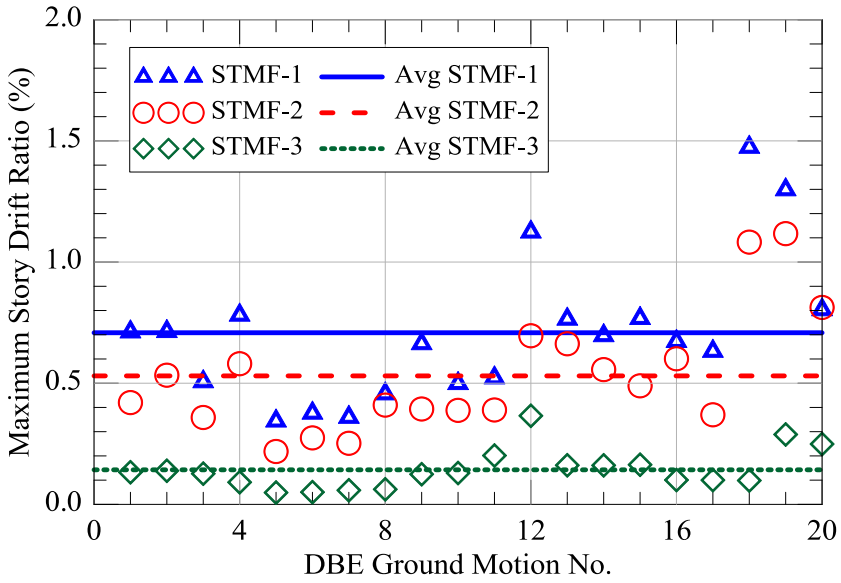

Figure 6-10 Maximum story drift ratio of STMF-1, STMF-2, and STMF-3 under 20 DBE ground motions

Table 6-9 Average maximum plastic rotations under DBEs

Member	Average Maximum Plastic Rotation (rad)			
	STMF-1	No. of DBEs	STMF-2	No. of DBEs
Chord in SS	0.027	3[e]	0.006	2
Intermediate	N/A	N/A	0.01	17

Note: [e] under one ground motion one plastic hinge failed, hence; high plastic rotation of 0.06 rad

6.7.2 Effect of Axial Force on Ductility of Double Channel Flexural Members under NC Loading History

To check collapse prevention performance level of the designed STMFs, hysteretic behavior of 2C12-12 was used. To take into account of the effect of axial load on its plastic rotation, an FEA was carried out and the model was calibrated so that the result was in good agreement with the experimental result as shown in Fig. 14a. Trilinear model is shown in blue line in this figure. The FEA model was then used to analyze

flexural behavior of 2C12×20.7 section under combined bending and various axial compression and tention. Figure 6-12 show hysteresis behavior and trilinear models of 2C12×20.7 with axial compression to axial capacity ratio of 0.1, 0.2, and 0.3 while Figure 6-13 show those of 2C12×20.7 with axial tension.

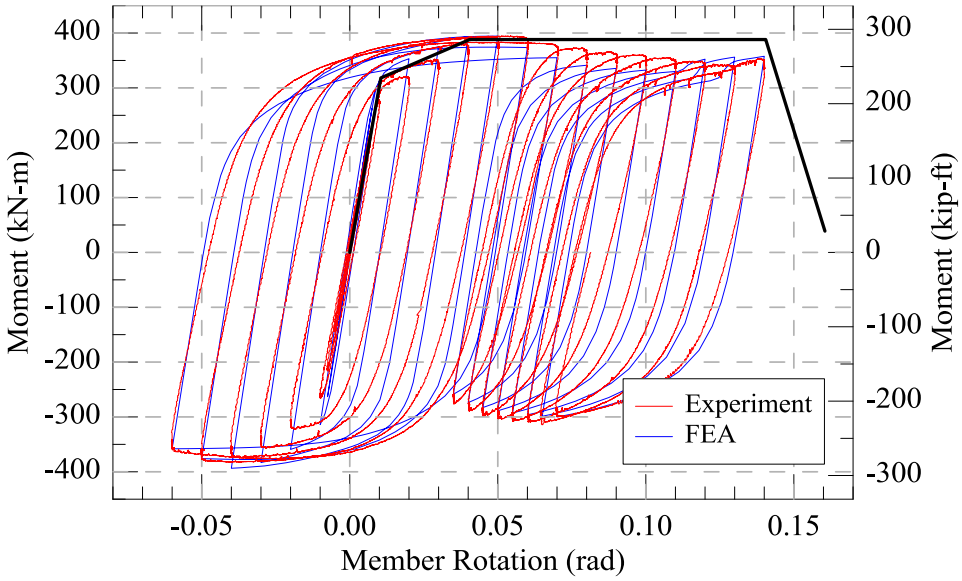

Figure 6-11 Comparison of FEA and Specimen 2C12-8 Test Results

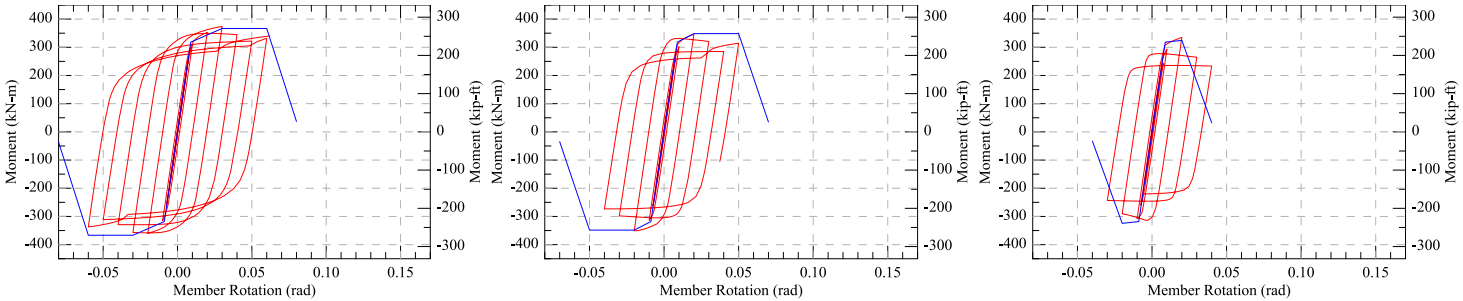

Figure 6-12 FEA results under NC loading history and trilinear model of 2C12×20.7 with axial compression when (a) α = 0.1, (b) α = 0.2, and (c) α = 0.3

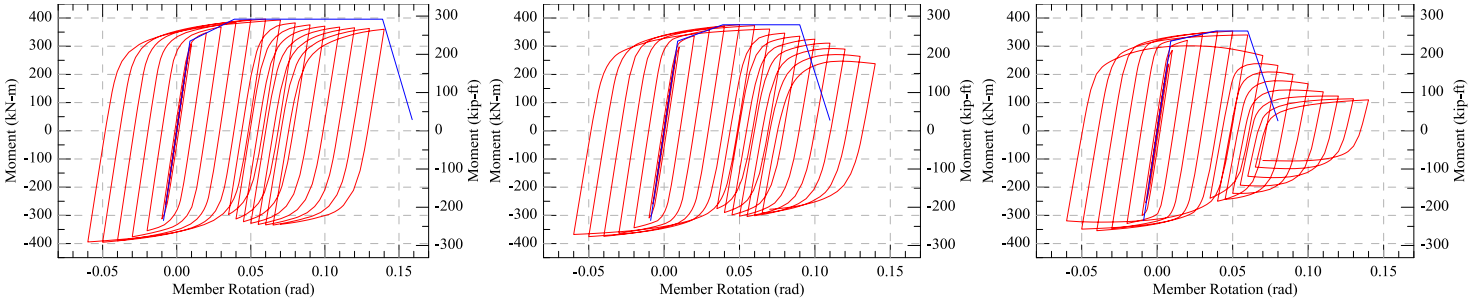

Figure 6-13 FEA results under NC loading loading history and trilinear model of 2C12×20.7 with axial tension per capacity ratio (a) α = 0.1, (b) α = 0.2, and (c) α = 0.3

Similar to the results of 2C20×20.7 under AISC loading history, the relationship between *a* and α , b and α, and β and α were determined by regression analyses as follows:

Axial compression case:

$a = -0.1\alpha + 0.03$	when $0 < \alpha < 0.2$	[6-7 (a)]
$= 0.011$	when $0.2 < \alpha < 0.3$	[6-7 (b)]
$b = -0.7\alpha + 0.1$	when $0 < \alpha < 0.1$	[6-8 (a)]
$= 0.03$	when $0.1 < \alpha < 0.2$	[6-8 (b)]
$= -0.3\alpha + 0.09$	when $0.2 < \alpha < 0.3$	[6-8 (c)]
$\beta = -0.76\alpha + 1.4$	when $0 < \alpha < 0.1$	[6-9]

Axial tension case:

$a = 0.03$	when $0 < \alpha < 0.3$	[6-10]
$b = 0.1$	when $0 < \alpha < 0.1$	[6-11 (a)]
$= -0.4\alpha + 0.14$	when $0.1 < \alpha < 0.3$	[6-11 (b)]
$\beta = 1.4$	when $0.13 < \alpha < 0.3$	[6-12 (a)]
$= -0.7\alpha + 1.4$	when $0.13 < \alpha < 0.3$	[6-12 (b)]

6.7.3 Nonlinear Time-History Analyses under Maximum Considered Earthquakes

Similar to performance evaluation under DBEs, plastic hinge models of the chord members in the SS, were modeled after suggested valued in Table 6-2. Parameters *a, b,* and β needed for the plastic hinge model of the top chord member were obtain from Eqs.6-7 to 6-9 while those for the bottom chord member were obtained from Eqs. 6-10 to 6-12. Average maximum story drift ratios of STMF-1, STMF-2, and STMF-3 were 1.11%, 0.73%, and 0.16%, respectively (Figure 6-14). Though the story drift ratios increases by

14%-56% from those of STMFs under DBEs, the analyses show that the structures are far from collapse. None of the members in STMF-3 yielded. Table 6-10 shows the average maximum plastic rotations of both DYMs and column of STMF-1 and STMF-2. Columns of STMF-1 and STMF-2 only slightly yielded under 3 and 1 MCE ground motions, respectively. The chord members in the SS of STMF-1 yielded under 17 ground motions. Average maximum plastic rotation of the chord member was 0.01 rad. This plastic rotation is exactly rotational capacity of double-channel section with α = 0.3. Among 17 ground motions, 5 ground motions caused maximum plastic rotation of the SS more than 0.01 rad and the absolute maximum plastic rotation was 0.042 rad. In order to avoid any potential collapse under any MCE ground motion, α = 0.15 was chosen as a design baseline. Average maximum plastic rotations of intermediate vertical members was 0.018 rad caused by 19 ground motions. Chord members in the SS of STMF-2 slightly yielded under 8 ground motions.

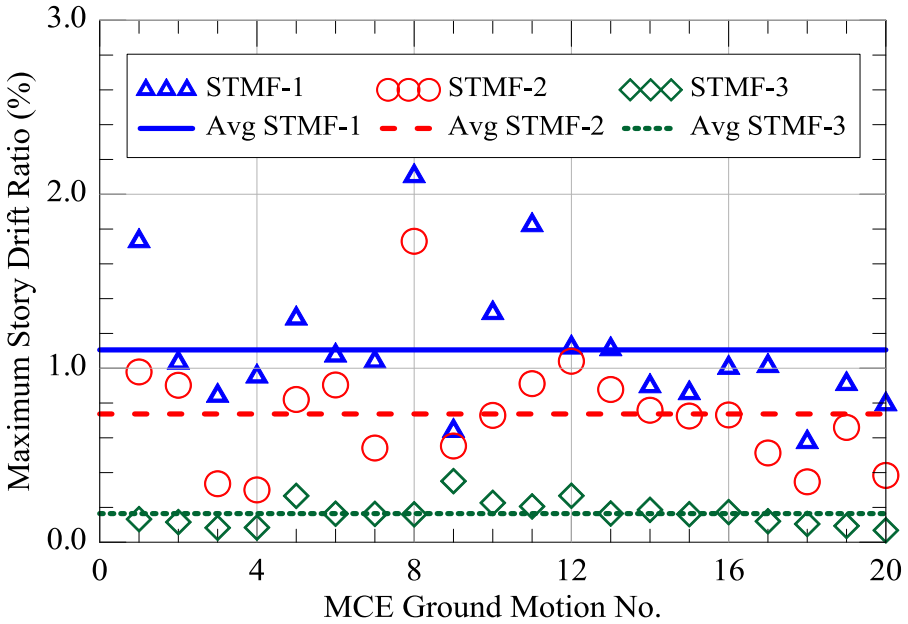

Figure 6-14 Maximum story drift ratio of STMF-1, STMF-2, and STMF-3 under 20 MCE ground motions

Table 6-10 Average maximum plastic rotations under MCEs

Member	Average Maximum Plastic Rotation (rad)			
	STMF-1	No. of MCEs	STMF-2	No. of MCEs
Column	0.004	3	0.003	1
Chord in SS	0.01	17	0.005	8
Intermediate	N/A	N/A	0.018	19

6.8 Summary

This chapter presented a design procedure, recommended plastic hinge models, and nonlinear analysis of the seismic performance for STMFs having a very long span of 90 ft, approximately 40% longer than the currently allowed span length specified in AISC Seismic Provisions. The different special segment (SS) layouts are recommended for long-span STMF by considering the overall lateral stiffness, rotational demand of the DYMs, available open space in the SS, and lateral bracing requirements. The design is done by first determining the designated yielding members, DYMs, (members within the SS) by conventional elastic design. Then non-yielding members outside of the SS are designed by using a capacity design approach when DYMs are fully strain-hardened. Plastic hinge models of the DYMs are proposed for both design and seismic performance analysis purposes. First yielding of STMF-1, STMF-2, and STMF-3 occurred at 0.89%, 0.36%, and 0.52% story drift ratio, respectively, which are between typical CBFs and moment frames. STMF-3 with single short Vierendeel special segment provides very high lateral stiffness. The average maximum story drift ratios of long-span STMFs under DBE ground motions in this study were between 0.14%-0.71% and members outside of the SS did not yield.

With the new nonlinear model of plastic hinge based on near-collapse loading protocol, the three prototype STMFs' maximum story drift ratios under MCE ground motions ranged between 0.16% and 1.11%. The members outside of SS, other than the

columns, did not yield. This suggests that the design procedure and SS layouts provide satisfactory seismic collapse prevention performance for long-span STMFs.

Chapter 7

Summary and Conclusions

The main purpose of this study is to improve seismic performance of special truss moment frame (STMF) system for high seismic activity regions. On component level, viability of double channel and double HSS shapes as designated yielding members of STMFs was investigated. A new moment connection details for double channel built-up member was proposed. Moment connection details for double HSS sections are simpler because double HSS are not susceptible to lateral torsional buckling. On subassemblage level, a hybrid system incorporating buckling-restrained braces in the special segment of a full scale STMF subassemblage were experimentally investigated. Moreover, the possibility to extend depth and length of STMFs so that they could be used as a long span structure was explored. Design procedure was proposed and the seismic performance of the designed STMFs was evaluated by nonlinear time history analysis. The effect of axial force on ductility of double channel flexural members was also considered. The followings conclusions are drawn from the entirety of this study.

1. The new detailing using the center gusset plate with a weld-free zone between 0.5d and 0.75d and horizontal stitches 1 in. away from the gusset plate could effectively prevent global LTB in double-channel members. The region in the vicinity of the column face remains essentially elastic, and the connection can be economically fabricated by using only fillet welds.

2. A new buckling mode caused by LTB of an individual channel in the opposite direction, called bulging, was observed. With right numbers and locations, ½ in. thick web stiffeners can be used to limit the bulging and local buckling thereby improving the ductility of the double-channel members. The web stiffeners can also control the

amplitudes of FLB and WLB. Nevertheless, for 2C12× 20.7 specimens, even though specimen 2C310-8 had no web stiffeners it showed stable and ductile behavior. Its ultimate strength was slightly lower and the degree of strength degradation was slightly faster than those with web stiffeners. For specimens with web stiffeners, e.g., Specimens 2C310-4 and 2C310-7, they sustained a member rotation of approximately 0.09 rad without major strength degradation.

3. If the web stiffeners were welded too close to one another near the plastic hinge, the imposed constraint on the flanges proved to hinder large plastic deformation of the flanges. This caused the strength to increase but the ductility to drastically decrease due to premature fracture. A connecting member welded to the flanges of the specimens in the plastic hinge zone could also contribute to such constraint.

4. Channels with higher h/t ratio, e.g., 2C150×19.3 and 2C200×27.9, exhibited small bulging, web local buckling, and flange local buckling without web stiffeners. These members could undergo a large member rotation of 0.09 rad without strength degradation.

5. Based on data from this study, it is recommended that web stiffeners be used in the double-channel sections only when the *b/t* ratio is greater than 6.49 and the *h/t* ratio is greater than 36.3.

6. All the double-channel specimens failed due to low-cycle fatigue fracture in the channels. Fracture of welds between channels and gusset plate is neither a brittle failure nor a major cause of strength degradation.

7. Reduced beam section (RBS) can be used in a double-channel built-up section as a chord member in a special truss moment frame to alleviate strength demand of members outside of the special segment.

8. For HSS of the same dimensions, the one with thicker wall will be less susceptible to flange and web local buckling which, in turns, slow down rate of strength degradation.

9. Width-to-thickness ratio of double HSS can generally be lowered than that of a single-HSS with similar moment capacity, which considerably increases the compactness under bending thereby delaying flange buckling. Due to the fact that narrower tube sections would be more practical to use in a double-HSS configuration, the requirements for *b*/*t* ratios would be easy to adhere to

10. Connections have been the limiting factor of the HSS design because reinforcing the connections of HSS assemblies often is not optionally available (Packer et al. 2010). With double-HSS sections, 2 HSS are simply welded to a center gusset plates in the same manner as double-angle or double-channel joint connection. Even though, very long rectangular HSS bent about strong axis are subjected to lateral-torsional buckling, however; in normal cases, beam deflection will control (AISC 2010b). Hence, there should be no need for lateral bracing when double-HSS is used.

11. HSS in general could sustain large cyclic rotation. The use of double-HSS with a simpler connection details reflect a promising alternative to wide-flange sections in seismic resisting system application.

12. BRBs could effectively increase both strength and stiffness of an STMF. Compared to STMFs with intermediate vertical member, STMF with BRB can maintain higher ductility. This is because once intermediate vertical member fail, STMF loses its

additional strength. On the other hand, steel core of BRB could reengage to provide compression strength even it already failed in tension.

13. Nonlinear time-history analyses according to MCE level ground motions indicate that the DYMs' time-history response is predominately single-sided and very different from the response based on fully reversed cyclic loading with ever-increasing displacements. A near-collapse loading protocol was developed according to analytical results. Component testing results shows that member can sustain much larger plastic rotational demands under MCE-level loading sequence. The effect of axial compression and tension on rotational ductility of double-channel section was studied. Recommended plastic hinges models of DYMs of STMFs for nonlinear analysis under both DBE and MCE level ground motions are also proposed.

14. STMFs with greater dimensions than those in current AISC Seismic Provisions (AISC, 2016) can be confidently used in high seismic area. If the axial force to axial capacity ratio is kept under 0.15, the length of STMFs can be extended from 65 ft to 90 ft, the total depth can be extended from 6 ft to 10 ft, and the length-to-depth ratio of a panel in the SS can be extended from 1.5 to 3.0, without compromising of stiffness and strength of STMFs.

Appendix A

Construction of AISC and Near Collapse Loading Histories

AISC Loading History for Component Test

Yield Rotation and Strain-Hardening Factor

Monotonic Test of 2C12x20.7

In Figure A-1, the distance between the loading point to the end of the weld line is 55 in. This distance is used to determine moment and rotation of the component test specimen 2C12-1.

The total rotation which equals to the vertical displacement at the end of the component test specimen divided by the length from the free-end to the end of the weld line is determined. The relationship of the moment and total rotation is shown in Figure A-2.

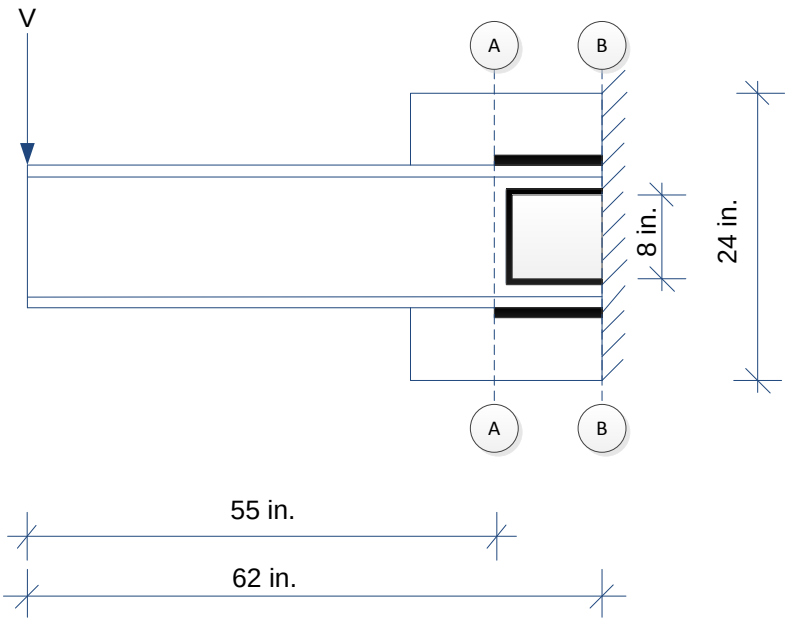

Figure A-1 Geometry of the Component Test 2C12-1

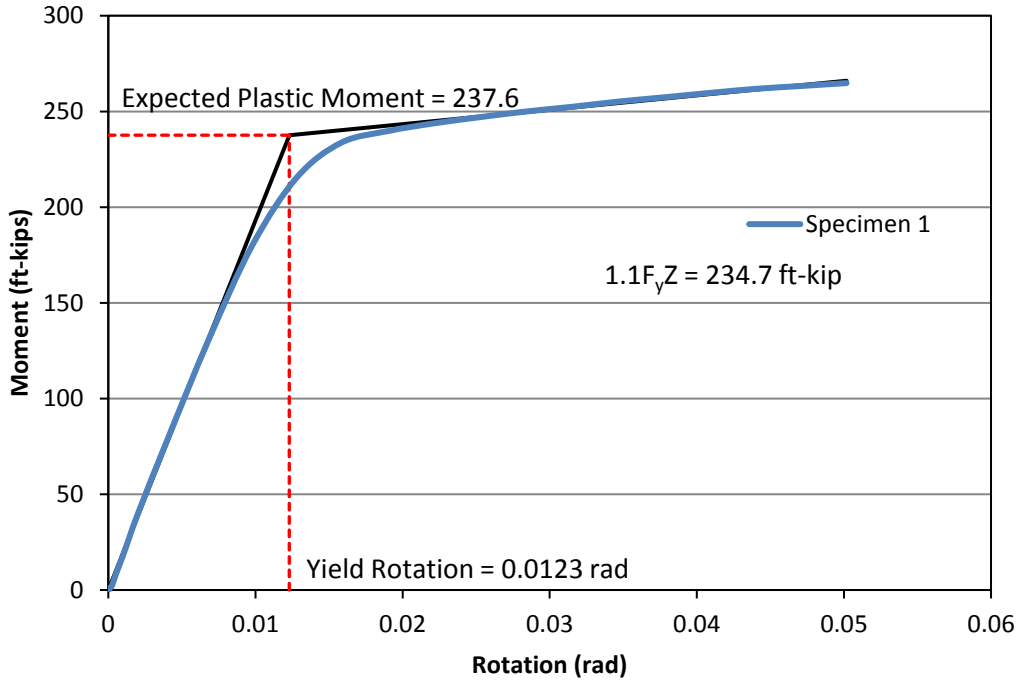

Figure A-2. Moment vs. Rotation of Monotonic Test of 2C12x20.7

Based on linear regression analysis, the elastic part of the relationship is expressed as:

$$M = 19{,}260\theta$$

The strain-hardening part of the relationship is expressed as:

$$M = 751.7\theta + 228.3$$

These two lines, then, gives yield rotation,

$$\theta_y = 0.0123$$

and corresponding expected plastic moment,

$$M_y = 237.6\ ft - kips$$

The expected plastic moment based on AISC Seismic Provision (ANSI/AISC 341-10) is given by

$$R_y M_n = 1.1 F_y Z$$

where $R_y = overstrength\ factor$

$M_n = nominal\ plastic\ moment\ capacity$

$F_y = yield\ strength\ of\ steel$

$Z = plastic\ modulus\ of\ the\ member$

For 2C12x20.7, the expected plastic moment based on AISC 341-10 is

$$R_y M_n = 1.1 F_y Z = \frac{1.1(50)(2\times 25.6)}{12} = 234.7\ ft - kips$$

It can be seen that the test result and the value according to AISC 314-10 are in reasonably good agreement.

Based on the component test result, the strain-hardening ratio,

$$\eta = \frac{751.7}{19260} = 0.039 \approx 4\%$$

From previous studies of 2C10x25 by Goel and Chao (2006), the member could undergo large plastic rotation (0.07 rad). This is assumed to be true for 2C12x20.7, hence,

$$751.7 = \frac{M_u - M_y}{0.07}$$

$$M_u = (751.7)(0.07) + 228.3 = 280.9\ ft - kips$$

$$M_u = 1.18 M_y \approx 1.2 M_y$$

Summary

From the monotonic test of 2C12x20.7 with the distance between the loading point to the end of the weld line equals to 55.0 in., the yield rotation and strain-hardening factor are approximately 0.012 rad and 1.2 respectively. The first parameter will be used

to determine total member rotation while the latter will be used in non-linear relationship modeling of the members in a modeling of plastic hinge of the prototype full scale STMF subassemblage in program Perform 3-D

Story Drift vs. Member Drift

Push-Over Analysis by Perform 3-D

In order to find relationship between the story drift and member drift, the push-over analysis of the full scaled STMF Subassemblage as shown in Figure A-3 is carried out. Figure A-4 shows the model of STMF in Perform-3D. The portion of members that are welded connecting to the gusset plates is considered as rigid end zone which has much greater stiffness than the members themselves. For simplicity the end zone is modeled using an elastic section with large stiffness. The moment of inertia of 1000 in^4 is used for every rigid endzone in the model. Figure A-5 shows the length of the end zones used in this model. The intended yielded members of the STMF can be seen in Figure B-6 below.

where SS Top = Top Chord in Special Segment

SS Bottom = Bottom Chord in Special Segment

The distance from the center of the special segment to the end of the weld line of the full scale STMF subassemblage was assumed to be 53 in. and used subsequent 2C12×20.7 component specimens. While the distance between the loading point to the end of the weld line of the component test specimen 2C12-1 was 55 in., the parameters found from the component test are believed to be a good enough approximation.

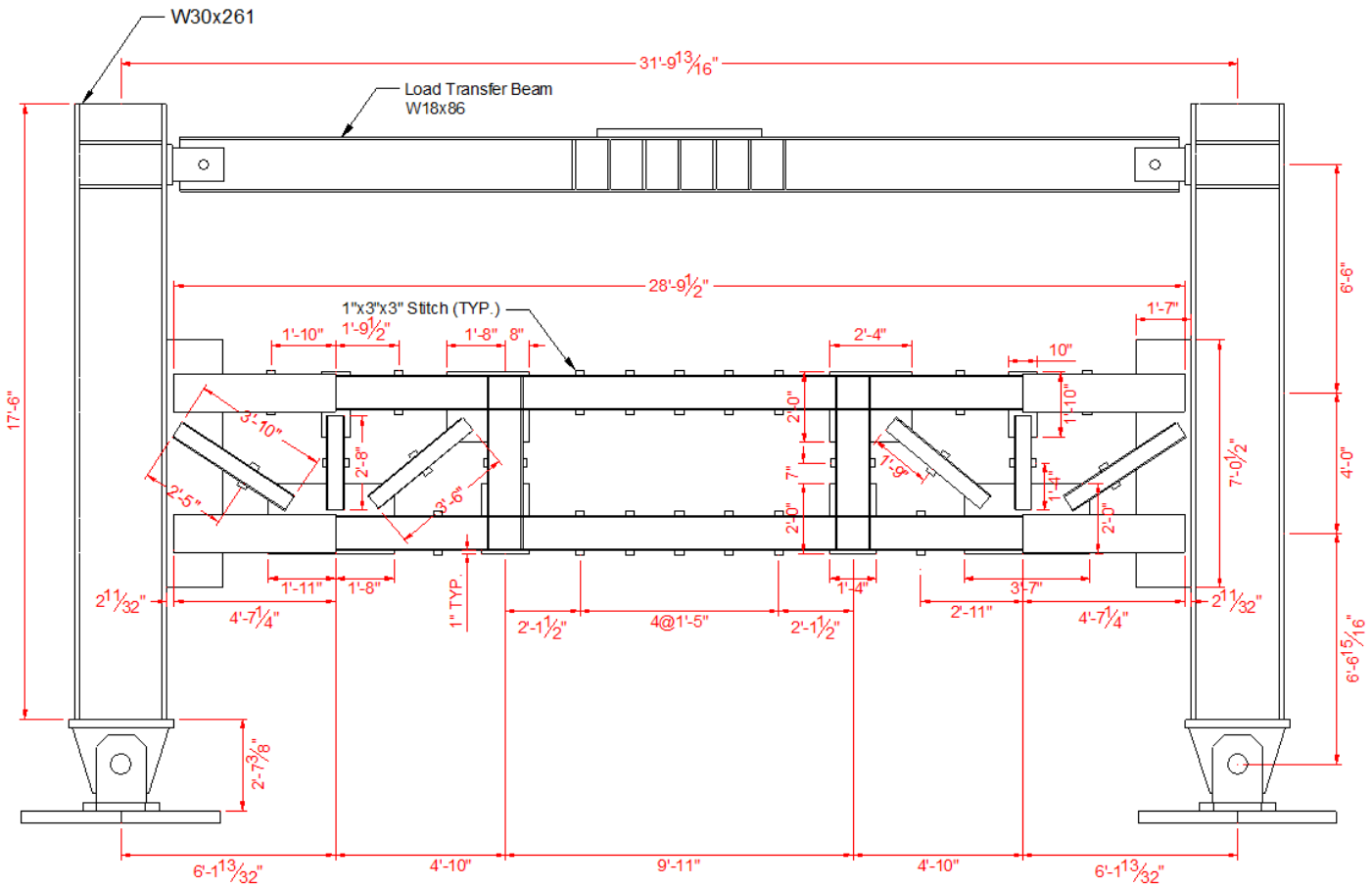

Figure A-3. Full Scaled STMF Subassemblage

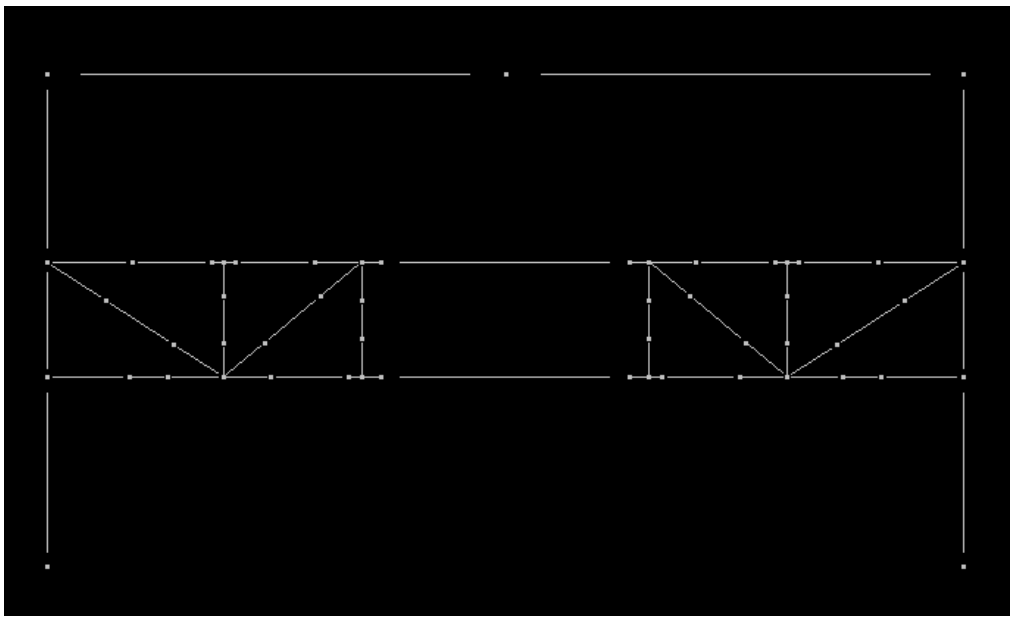

Figure A-4 Push-Over Model of STMF in Perform-3D

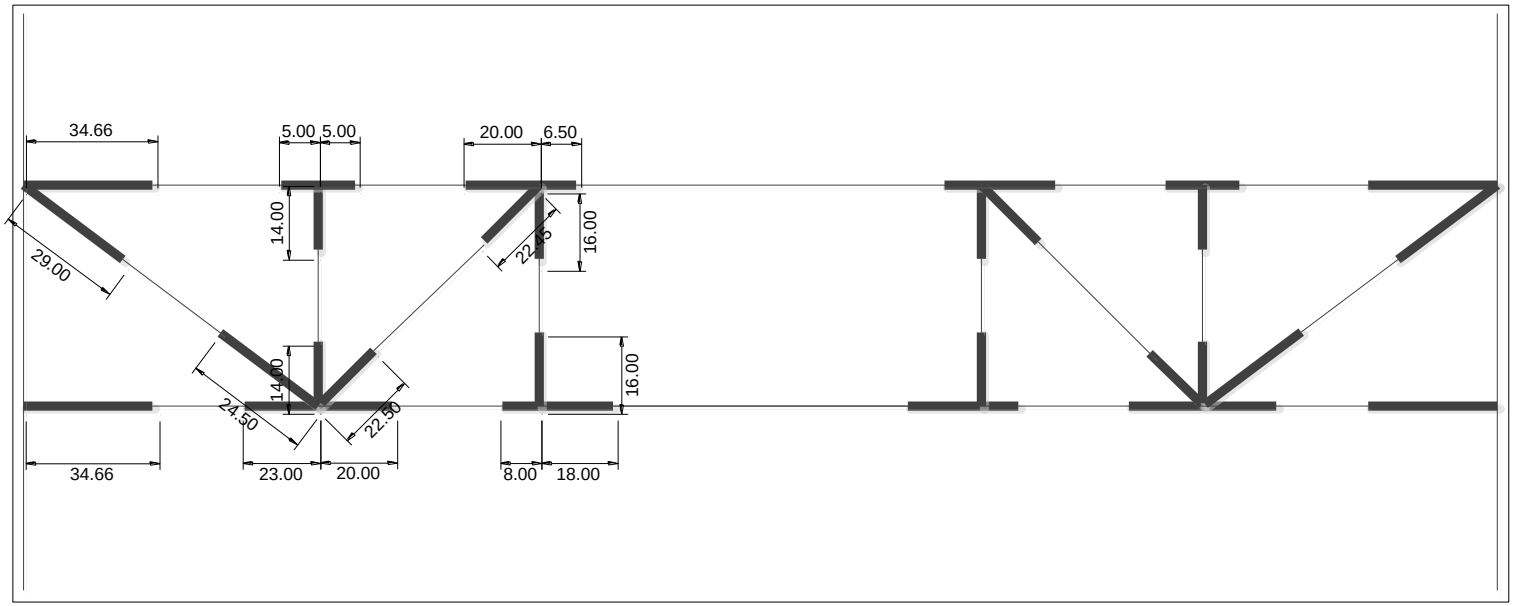

Figure A-5 Length of Rigid End Zones of STMF

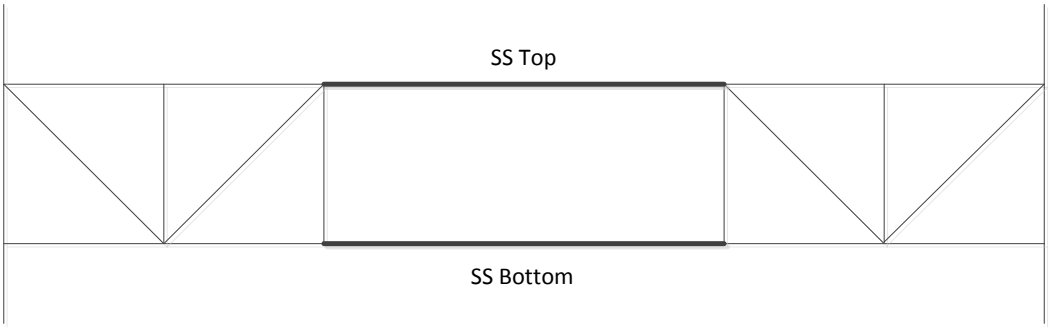

Figure A-6 Intended Yielded Members of STMF 1 and STMF with BRB

By using strain-hardening factor equals to 1.2, the tri-linear model of the chord in special segment can be shown in Figure A-7. where

$$F_Y = expected\ plastic\ moment$$

$$F_U = expected\ maximum\ moment$$

$$F_R = moment\ after\ strength\ loss$$

$$D_U = plastic\ rotation\ corresponding\ to\ F_U$$

$$D_R = plastic\ rotation\ corresponding\ to\ F_R$$

$$D_X = ultimate\ plastic\ rotation$$

As mentioned earlier that the expected plastic moment from the test and from AISC 341-10 were in good agreement, the expected plastic moment from AISC 341-10 is used in push-over analysis. The reason is that it would be simpler to make recommendation for yielding moment according to AISC 341-10.

$$F_Y = R_y F_y Z = \frac{(1.1)(50)(2\times 25.6)}{12} = 235\ ft - kips$$

$$F_U = 1.2F_Y = 1.2(188) = 282\ ft - kips$$

$$F_R is\ assumed\ to\ be\ 80\%\ of\ F_U$$

$$F_R = 0.8F_U = 0.8(282) = 226\ ft - kips$$

From previous studies of 2C10x25 under cyclic loading by Goel and Chao (2006), the member could undergo large plastic rotation (0.07 rad). As a result, parameters regarding plastic rotation are assumed to be the same as those from the studies.

$$D_U = 0.07\,rad$$

$$D_R = 0.84\,rad$$

$$D_X = 0.135\,rad$$

The interaction model between axial forces and bending moment in the reduced beam section is shown in Figure A-8.

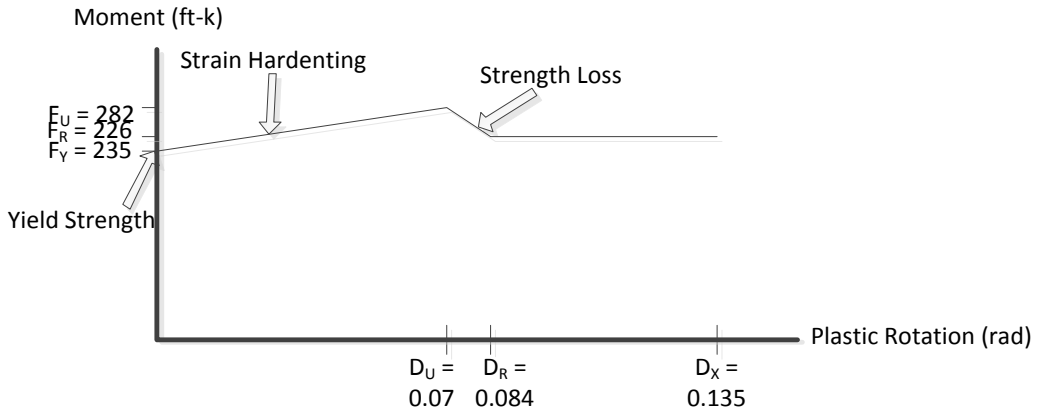

Figure A-7 The Non-Linear Model for Plastic Hinge of 2C12x20.7 when Strain-Hardening Ratio of 4% is used

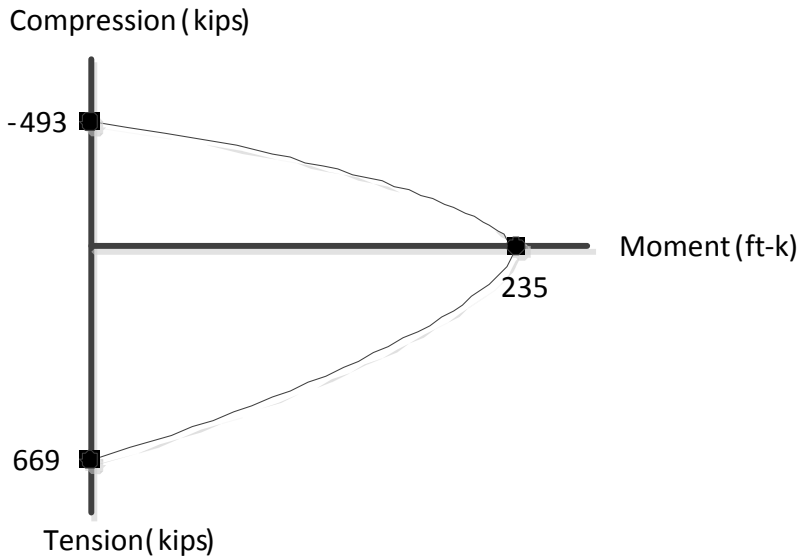

Figure A-8. Bending Moment and Axial Forces Interaction Model of Chords in Special Segment of STMF

From the push-over analysis, the relationship between story drift and plastic rotation can be found. By adding yield rotation (0.012 rad) to plastic rotation, the member drift is obtained. The relationship between story drift and member drift is shown in Figure A-9. In the same Figure, points of the story drifts according to AISC loading history are also plotted. Since the distance from point of load application to the end of the weld line in the succeeding specimen will be 53 in., the vertical displacement of the component test specimen for AISC loading protocol becomes:

$$Displacement = 53 \times Member\ Rotatoin$$

The story drift, member rotation, number of cycles, and displacement corresponding to AISC loading protocol up to 3% are shown in Table A-1

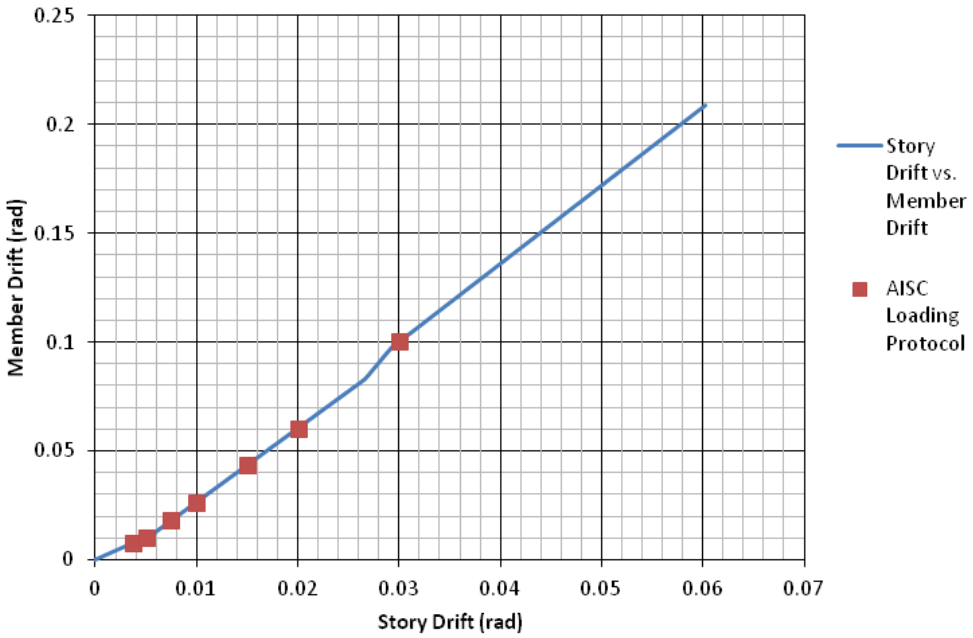

Figure A-9 Relation between Story Drift and Member Drift Corresponding to AISC Loading Protocol up to 3% Story Drift

Table A-1. Story Drift, Member Drift, Displacement, and Number of Cycles According to AISC Loading Protocol up to 3% Story Drift

Story Drift (rad)	Member Rotation (%)	Displacement (in.)	Number of Cycles
0.00375	0.79	0.416	6
0.005	1.05	0.555	6
0.0075	1.80	0.954	6
0.01	2.65	1.405	4
0.015	4.35	2.306	2
0.02	6.05	3.207	2
0.03	10.02	5.311	2

Note: Member drift is vertical displacement divided by the distance from loading point to the end of the weld line.

Due to stroke limit of the hydraulic actuator MTS Series 201 is +/- 12.5 cm, it is impossible to achieve AISC loading protocol up to 3%. Thus the last 2 cycles of the test

will be done at 2.75% story drift instead. The corresponding member drift and vertical displacement are 0.0906 and 4.656 in., respectively. Figure A-10 shows the story drifts and member rotations for the component test loading history.

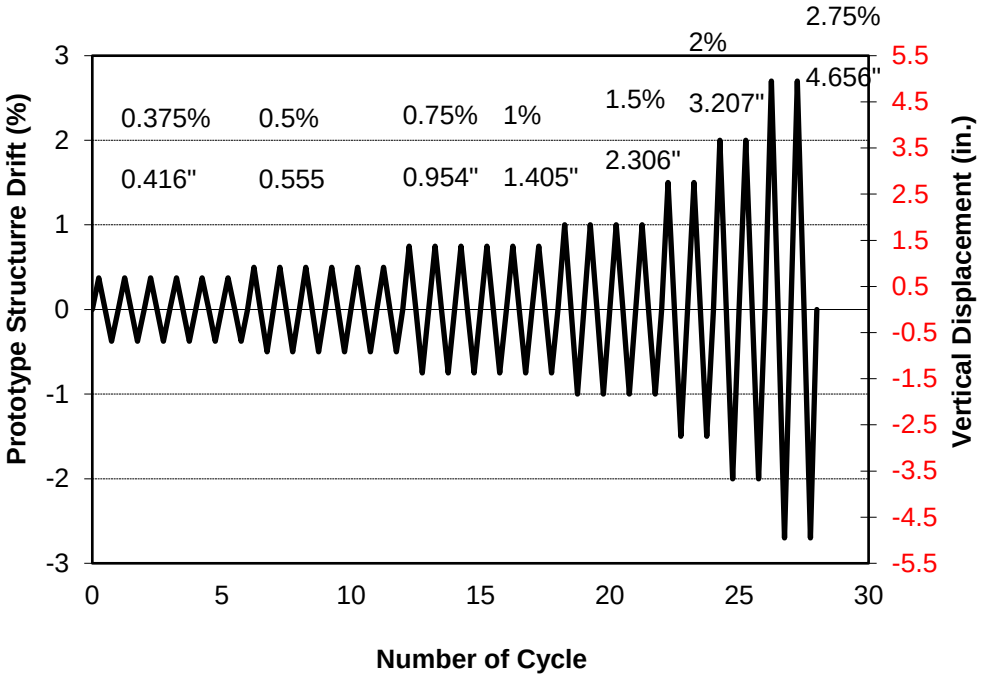

Figure A-10 Component Test AISC Loading History

Near Collapse Loading History for Component Test

Maximum Considered Earthquake

MCE level ground motions are often used for nonlinear time-history analyses to check the collapse prevention of structures. Time-history response to this type of ground motions often consists of a few excursions with larger amplitude in one direction than the other, then followed by pulse-like small cycles with a large mean deformation (Krawinkler et.al, 2000). Note that large mean deformation is the residual deformation which is the average of peaks and valleys of the last few pulse cycles. Analytical studies carried out

by Maison and Speicher (2016) on an eight-story steel-frame building and a four-story wood-frame building confirmed that time-history response of the building interstory drift under MCE ground motions was better described by single-sided cyclic and/or monotonic loading rather than fully reversed cyclic loading. As a result, the nonlinear behavior of double-channel member obtained from fully reversed symmetric loading protocol with high number of repeating cycles similar to AISC loading history can be unrealistic to represent the time-history response of STMF members subject to MCEs Therefore, a more realistic loading protocol for near-collapse situation was developed. To develop the loading protocol, the rainflow counting technique used by Krawinkler et al. (2000) was considered. They employed the first three largest excursion ranges, ($\Delta\theta_{max}$, $\Delta\theta_2$, $\Delta\theta_3$), maximum amplitude, and residual deformation to develop a loading protocol. They proposed a near-fault loading protocol using interstory drift ratio as deformation parameter. The loading protocol consists of eight cycles shown in Figure A-11. It starts with a negative excursion. The second excursion has the largest range ($\Delta\theta_{max}$) and ends at the maximum story drift ratio. The two following excursion ranges are $\Delta\theta_2$ and $\Delta\theta_3$, respectively. After that, small excursion ranges were added. The average of peaks and valley amplitudes of these pulses is used as the residual drift ratio. Finally, the last excursion stops at the maximum amplitude. In contrast to previous studies mentioned above, the deformation of interest in STMF study was plastic hinge rotation of the chord member in the SS rather than interstory drift ratio. To develop a near-collapse loading protocol for the truss members, nonlinear time history analyses of a prototype STMF shown in Figure A-12 under 20 SAC MCEs were carried out by using a plastic hinge model without considering the loss of strength (which was obtained from fully reversed cyclic testing) (Figure A-13 and Table A-2) in order to capture the rotational demand of STMF members. Figure B-14 shows a typical response of plastic rotation of the chord

member in the SS of prototype STMF under MCE ground motions. Rainflow counting technique was first used to counts numbers of excursion, three largest excursion ranges ($\Delta\theta_{max}$, $\Delta\theta_2$, and $\Delta\theta_3$), and amplitude of rotational demand of the chord member (Table A-3). The forward direction was defined as the direction that had the largest maximum rotation. The maximum three excursion ranges were approximately 0.036, 0.021, and 0.012 rad, respectively. The total number of half-cycle was approximately 8 (4 cycles). The maximum plastic rotations in forward and reverse directions were 0.03 and 0.006 rad, respectively and the residual rotation was 0.008 rad. By employing these values, a plot of loading protocol similar to that of Krawinkler is shown in Figure A-15. As can be seen, these rotational demands are much lower than that from symmetric loading protocol derived from AISC loading protocol. To be conservative, more rigorous amplitudes were selected where the maximum excursion range was 0.13 rad total rotation (roughly 0.12 rad plastic rotation). The symmetric fully reversed cycles started from one cycle each at 0.00375 rad, 0.005 rad, 0.0075 rad and 0.01 rad member rotation. Then increase the amplitude at 0.01 rad interval up to 0.06 rad which is approximately twice as large as the maximum excursion range ($\Delta\theta_{max}$). After that non-reverse cycles were added as shown in Figure A-15 and Table A-4. The non-reversed cycles progress in an ever-increasing manner.

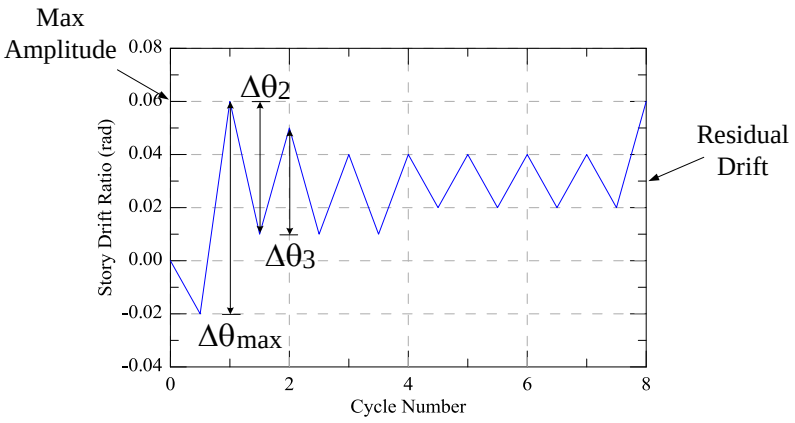

Figure A-11 Near-fault loading history (Krawinkler et al, 2000)

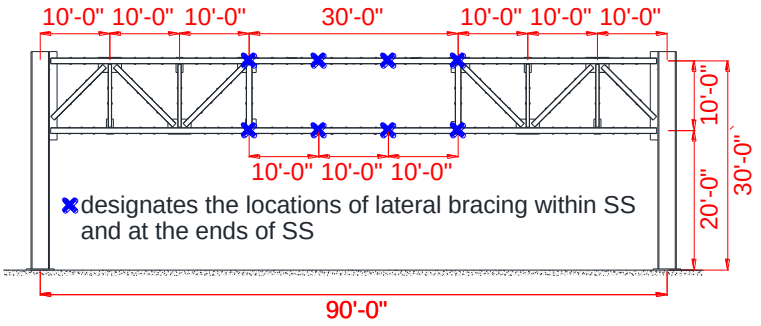

Figure A-12 Prototype STMF

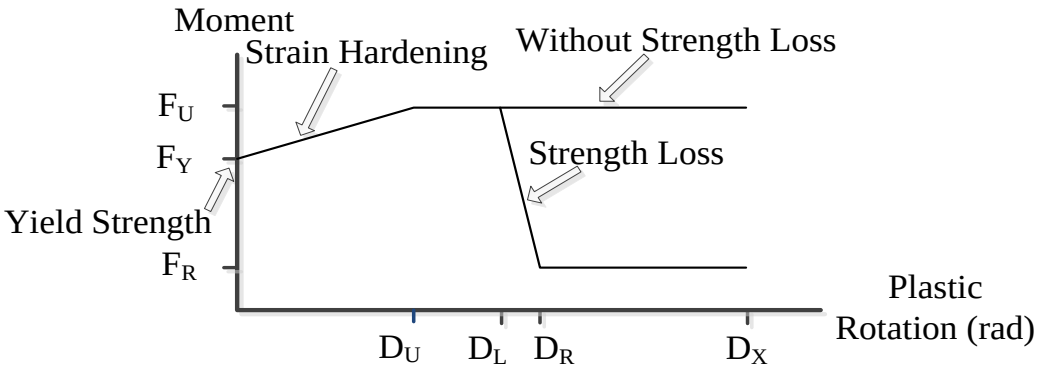

Figure A-13 Generalized moment-plastic rotation model for plastic hinge with and without strength degradation

Table A-2 Parameters for generalized plastic hinge model for analyses under MCEs

	M_Y	M_U	M_R	D_U (rad)	D_L (rad)	D_R (rad)	D_X (rad)
Intermediate Vertical Members	M_n	$1.24M_Y$	$0.1M_U$	0.048	0.128	0.138	0.15
Other Truss Members	Mn	$1.24M_Y$	$0.1M_U$	0.048	0.088	0.098	0.135

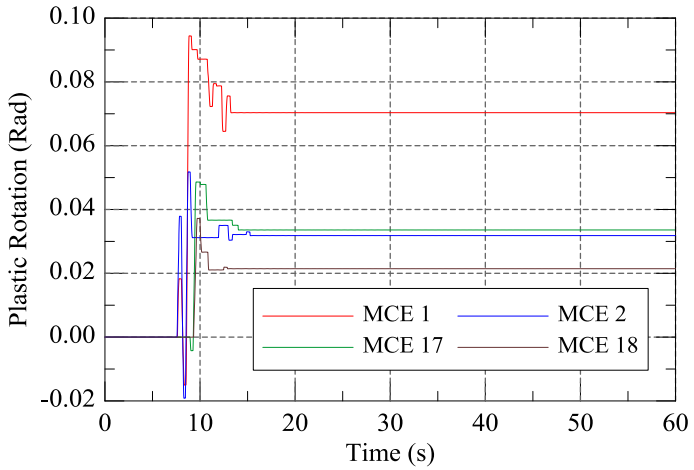

Figure A-14 Example of time-history plastic rotation of the chord member in the SS of STMF-1 under MCE ground motions.

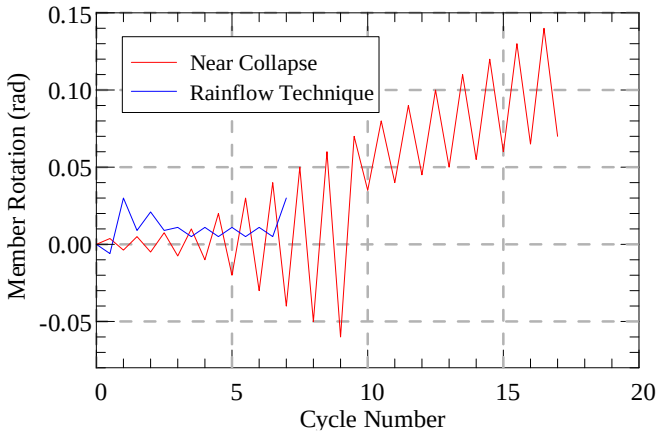

Figure A-15 Proposed near collapse loading history compared vs loading history based on rainflow counting technique

Table A-3 Rainflow cycle counting of plastic rotation of the chord member in SS of prototype STMF under MCEs

Ground Motion	$\Delta\theta_{max}$ (rad)	$\Delta\theta_2$ (rad)	$\Delta\theta_3$ (rad)	Residual Rotation (rad)	No. of Half Cycle	Max Plastic Rotation (rad)	
						Forward	Reverse
MCE 1	0.109	0.033	0.030	0.070	8	0.094	-0.015
MCE 2	0.071	0.057	0.038	0.032	8	0.052	-0.019
MCE 3	0.018	0.014	0.0087	0.005	7	0.010	-0.008
MCE 4	0.029	0.027	0.017	0.001	9	0.021	-0.008
MCE 5	0.042	0.027	0.017	0.015	4	0.042	0.000
MCE 6	0.077	0.038	0.017	0.022	5	0.060	-0.017
MCE 7	0.023	0.013	0.008	0.014	7	0.022	-0.001
MCE 8	0.034	0.028	0.014	0.008	5	0.028	-0.006
MCE 9	0.015	0.013	0.007	0.000	12	0.013	-0.003
MCE 10	0.030	0.017	0.013	0.008	11	0.016	-0.014
MCE 11	0.049	0.035	0.017	0.007	10	0.032	-0.017
MCE 12	0.071	0.031	0.016	0.046	15	0.071	0.000
MCE 13	0.026	0.021	0.007	0.001	7	0.020	-0.007
MCE 14	0.022	0.020	0.008	0.004	10	0.021	-0.001
MCE 15	0.055	0.017	0.011	0.010	6	0.039	-0.017
MCE 16	0.045	0.041	0.016	0.005	8	0.035	-0.009
MCE 17	0.053	0.015	0.004	0.034	3	0.049	-0.004
MCE 18	0.037	0.016	0.001	0.021	4	0.037	0.000
MCE 19	0.009	0.005	0.002	0.003	6	0.007	-0.002
MCE 20	0.005	0.003	0.0002	0.003	3	0.003	-0.002
median	**0.036**	**0.021**	**0.012**	**0.008**	**7**	**0.030**	**-0.006**

Table A-4 Near collapse loading protocol

Member Rotation (%)	No. of Cycle
0.375	1
0.50	1
0.75	1
1.00	1
2.00	1
3.00	1
4.00	1
5.00	1
6.00	1
7.00	0.5[a]
3.50	0.5[b]
8.00	0.5[a]
4.00	0.5[b]
9.00	0.5[a]
4.50	0.5[b]
10.00	0.5[a]
5.00	0.5[b]
See Note [c]	

Note: [a] an excursion in forward direction [b] an excursion in reverse direction
[c] continue each forward excursion at an increase of 1% member rotation from the previous forward excursion while each reverse excursion at half of the preceding forward excursion

Appendix B

Development of Instrumentation Scheme and Loading History for Isolated Buckling-Restrained Brace Test

Objective

A pair of short Buckling Restrained Braces (BRBs) as shown in Figure B-1 are to be used to enhance the performance of the Special Truss Moment Frame (STMF, see Figure B-11), as a result, its behavior was examined in order to precisely analyze and understand behavior of the STMF with BRB, as well as to formulate the basic modeling parameters.

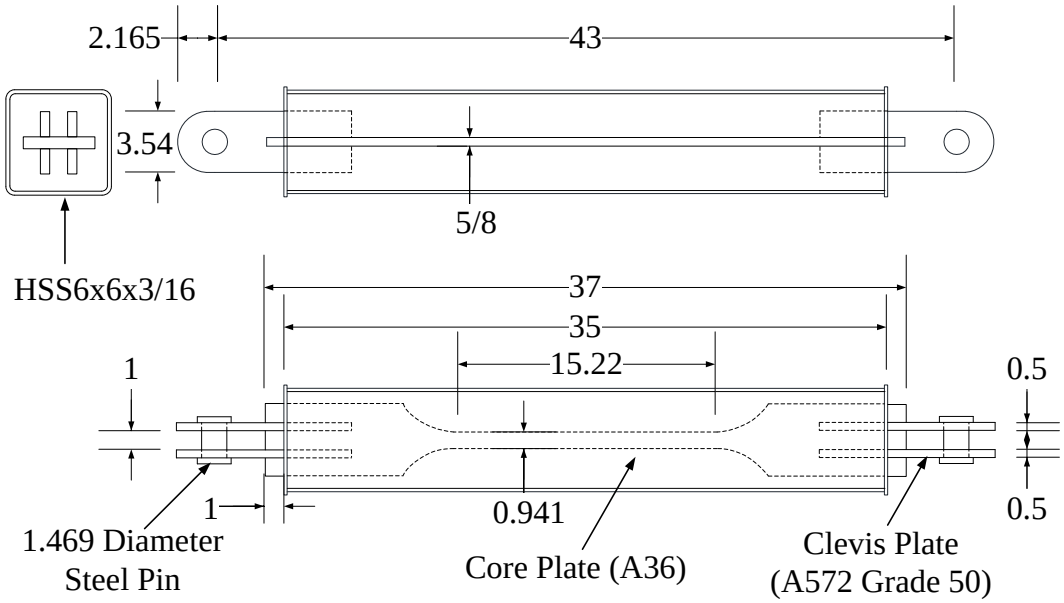

Figure B-1 General Dimensions of the Buckling Restrained Brace (BRB)

Development of the Test Setup and Instrumentation Scheme

Before the BRB was tested, a mockup specimen was made in order to verify the test setup and the instrumentation scheme. The test setup as shown in Figure B-2 for a mockup test comprises of 2 concrete blocks. One is on the specimen end, and the other is on the actuator end. Between the specimen and the actuator, there is a link beam

which is braced so that it will provide restraint to all movement (lateral and torsional) except that along the axis of a mockup.

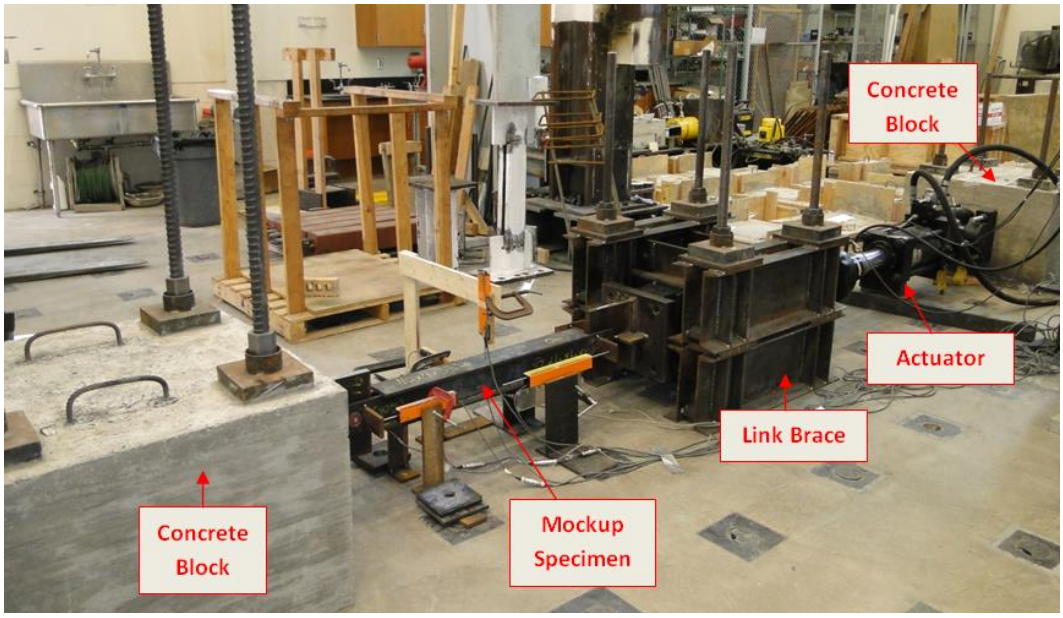

Figure B-2 Overview of the Test Setup

Due to the very short core area embedded inside the much longer concrete-filled case in the real BRB, it seems impossible to measure the deformation of the yielding portion alone. Thus, the deformation of the BRB will be measured across the approximate length, L, of 39.5 in. as shown in Figure B-3. In the first trial, the total deformation measured across the mockup was calculated by adding the deformations recorded by LVDTs 1, 2, 3, and 4 and dividing by two. Figure B-4 shows that the major portion of the mockup has a cross sectional area, A_1, of 8 in.^{2} while the 2 short ends have a cross sectional area, A_2, of 4 in.^{2}

In order to verify the test setup and instrumentation, force was exerted by the actuator to the mockup through the link beam. Estimated force in the mockup, then, was

calculated using the measured deformations, the length, L, and the cross sectional area, A_1 (i.e., $P = \varepsilon E A_1$). The relationship between the average strain, ε, and the measured deformations from the LVDTs is as follows:

$$\varepsilon = \frac{\text{average total deformation}}{L}$$
$$= \frac{\text{deformation from LVDT 1 + deformation from LVDT 2}}{2L}$$

where $\varepsilon = average\,total\,deformation, in.$

$$L = Original\,length\,of\,the\,mockup, 39.5in.$$

The reason that A_1 was used being that the length of the portions that had the area, A_2, was very short. This, in turn, had very minor contribution to the deformation of the mockup. Finally, the actual force and the calculated force were compared.

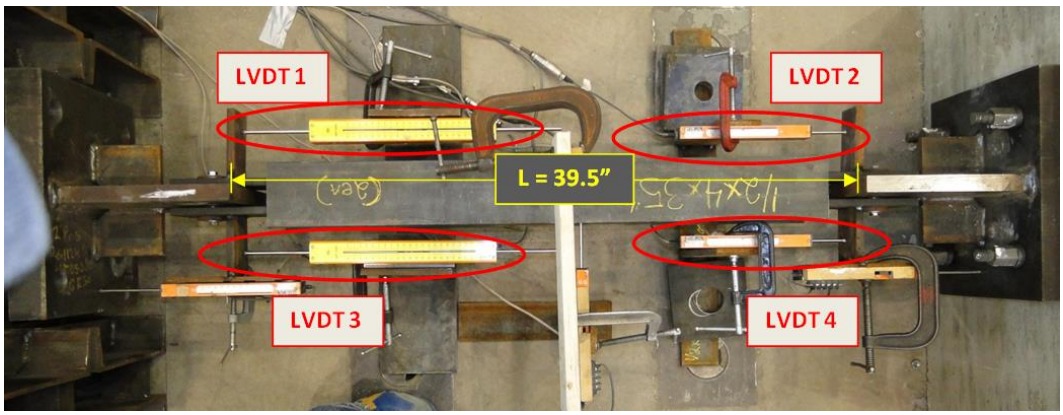

Figure B-3 Instrumentation, 1st Trial

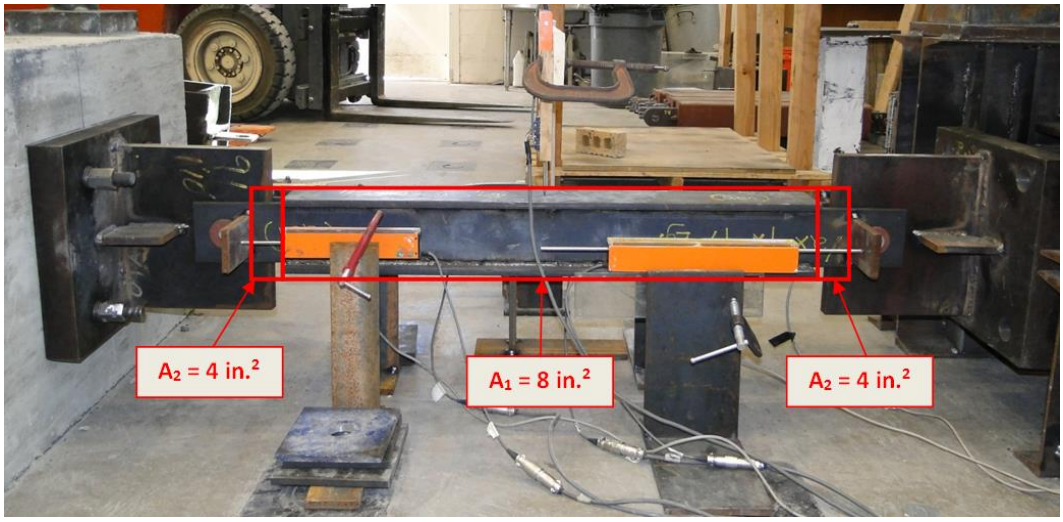

Figure B-4 Side View of the Mockup

Trial 1 Test Result

The test result showed that the estimated forces were not in good agreement with the actual forces. Examples are shown in Table B-1. One possibility was that for the given actual force, the elastic deformation of the short specimen was very small in the elastic range due to its length, thus, adding 4 readings from the LVDTs in order to calculate the force in the mockup could lead to large cumulative errors. As a result, the instrumentation needed to be adjusted.

Table B-1 Trial 1 Test Result

Actual Force (kips)	**LVDT 1 (in.)**	**LVDT 2 (in.)**	**LVDT 3 (in.)**	**LVDT 4 (in.)**	**Estimated Force (kips)**
19.3	-0.0311	-0.0260	0.026	0.0276	**10.3**
-19.9	0.0012	0.0181	-0.0106	-0.0055	**-9.4**

In order to reduce cumulative errors cause by using 4 readings to calculate force, in Trial 2, a string was used to pull the end of the LVDT to simulate a string potentiometer as shown in Figure B-5. Two strain gages were also installed on the specimen in order to compare the calculated force from the strain readings.

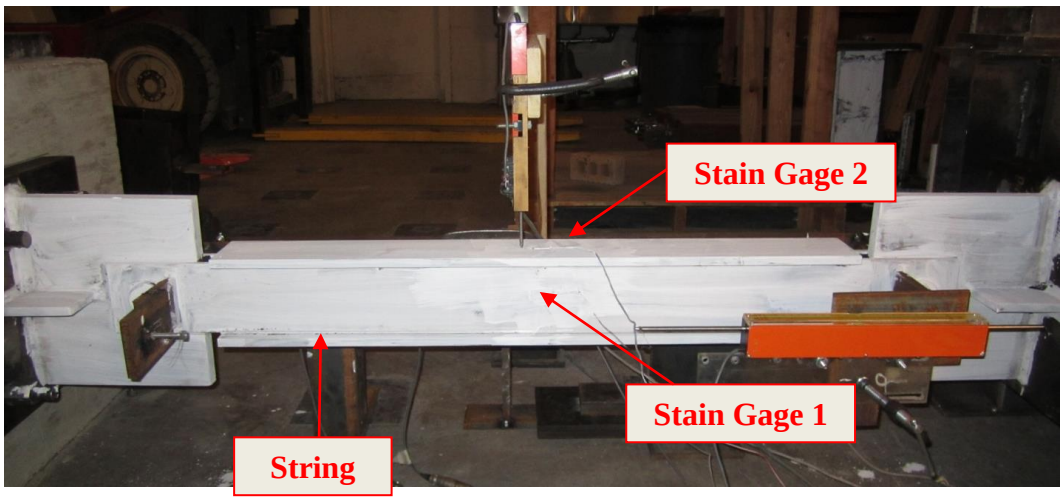

Figure B-5 Instrumentation, 2nd Trial

Trial 2 Test Result

Due to the flexibility of the string, the calculated force using the reading from the LVDT still gave a large margin of error, however; the result was not recorded. On the other hand, the forces calculated from the strain gage readings were comparable to the actual force which confirmed that the instrumentation in this trial was still flawed.

In Trial 3, in order to reduce the cumulative measurement errors, extensions to the LVDT rods were fabricated. With these extensions, two LVDT were long enough to measure the total deformation of the mockup on both sides. The total deformation measured across the mockup was calculated by averaging the deformations recorded by LVDTs 1, and 2 shown in Figure B-6. Figures B-7 to B-9 also show the connection details between the LVDTs and the specimen. Two type of strain gages, 350 Ohms and 120 Ohms were also placed on the steel plates that make up the mockup. The applied load from the actuator was recorded. The estimated force in the mockup was calculated using the elongation measured by the LVDTs and the strain readings from both strain gages. The original

length of the mockup, L, is approximately 39.5 in. and the cross sectional area, A, is approximately 8 in.[2] By using this information, three calculated forces can be found as;

$$F_{350} = \frac{\varepsilon_{350} EA}{1{,}000{,}000}$$

$$F_{120} = \frac{\varepsilon_{120} EA}{1{,}000{,}000}$$

$$F_{LVDT} = \left(\frac{\Delta_{LVDT\,1} + \Delta_{LVDT\,2}}{2}\right)\frac{EA}{L}$$

Where $F_{350} = force\ due\ to\ strain\ reading\ of\ 350\ ohms\ strain\ gage, kips$

$F_{120} = force\ due\ to\ strain\ reading\ of\ 120\ ohms\ strain\ gage, kips$

$F_{LVDT} = force\ due\ to\ average\ elongation\ reading\ of\ LVDT\ 1\ and\ LVDT\ 2, kips$

$\varepsilon_{350} = strain\ reading\ of\ 350\ ohms\ strain\ \ gage, \mu\varepsilon$

$\varepsilon_{120} = strain\ reading\ of\ 120\ ohms\ strain\ gage, \mu\varepsilon$

$\Delta_{LVDT\,1} = elongation\ reading\ of\ LVDT\ 1, in.$

$\Delta_{LVDT\,2} = elongation\ reading\ of\ LVDT\ 2, in.$

$E = Modulus\ of\ Elasticity\ of\ Steel, 29{,}000\ ksi.$

$A = cross\ sectional\ area\ of\ the\ mockup, 8\ in^2.$

$L = original\ length\ of\ the\ mockup\ where\ deformation\ is\ measured, 39.5\ in.$

The three calculated forces and the applied load by the actuator are plotted vs. the elongation as shown in Figure B-10. It can be seen that the calculated forces from the strain gages readings and the applied force by the MTS are relatively close, while the force calculated using the elongation readings deviated from the others when the mockup is in high compression. It is possible that when the mockup is in high compression, it bends so that the LVDTs readings are slightly larger than the real shortening.

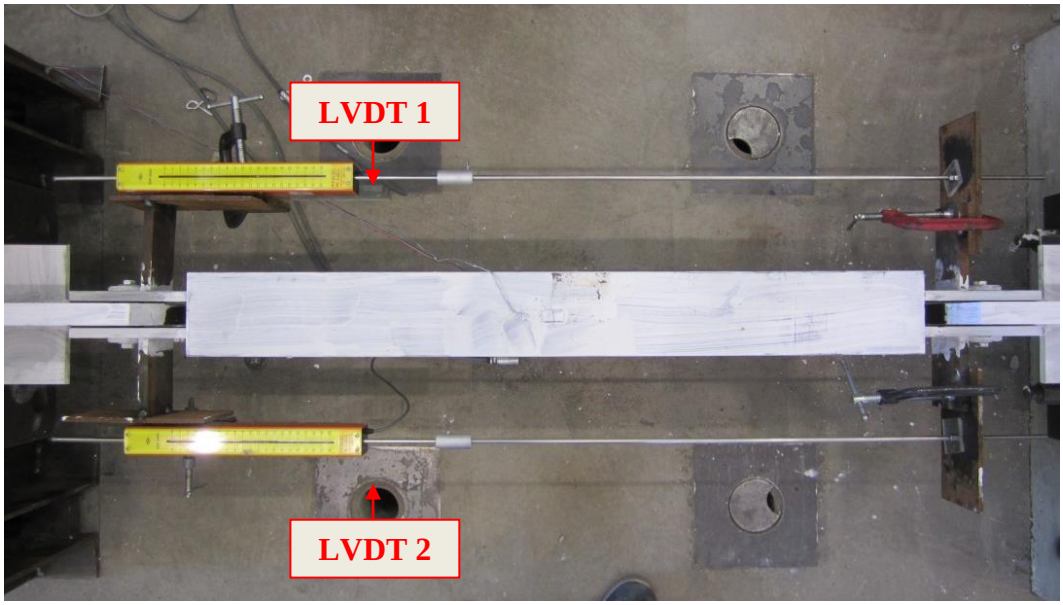

Figure B-6 Top View of the Specimen and Instrumentation, 3rd Trial

Figure B-7 Side View of the Specimen and Instrumentation

Figure B-8 Connection between LVDT and Specimen, 3rd Trial

Figure B-9 LVDT Extension Connecting to the Other End of the Specimen, 3rd Trial

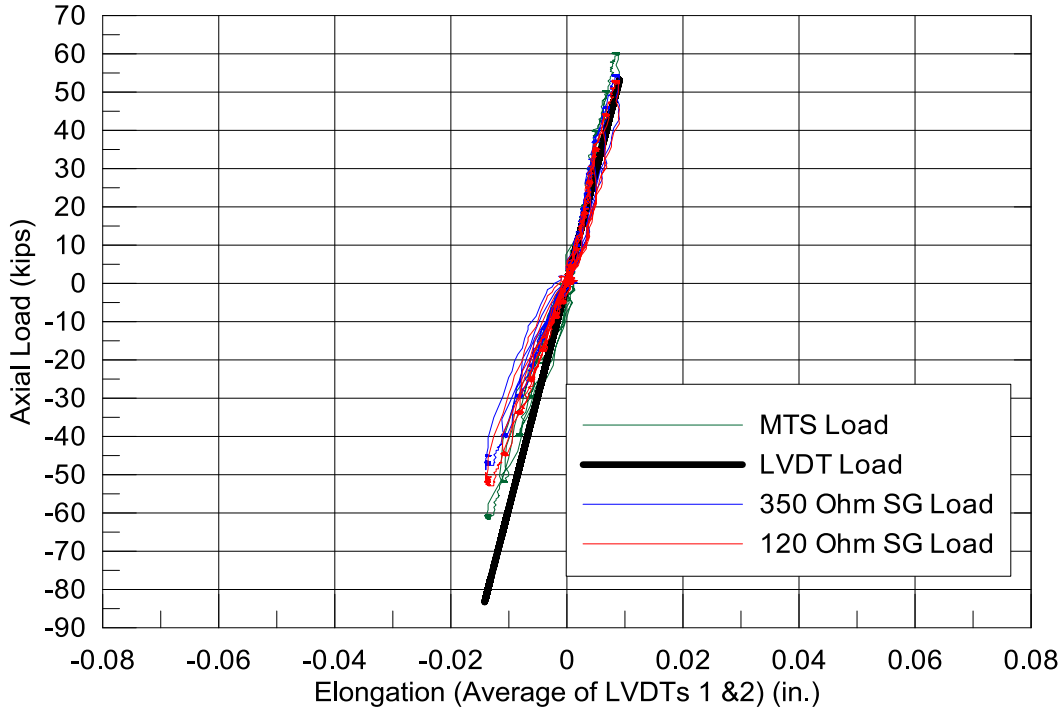

Figure B-10 Comparison between Load from MTS Load Cell and Forces Calculated from Strain Gages and LVDTs Readings

In conclusion, the test setup and instrumentation scheme in Trial 3 gave reasonably good results compared to both the actual force and the force calculated from strain gages readings. Thus it was used to test the isolated BRB specimen.

Loading Protocol

Before the test, a loading protocol was developed from a nonlinear analysis result. The pushover analysis of the prototype full scale special truss moment frame (STMF) subassemblage incorporating with BRBs was done by program Perform-3D. The general configuration of prototype full scale subassemblage test setup and the model are shown in Figures B-11 and B-12, respectively.

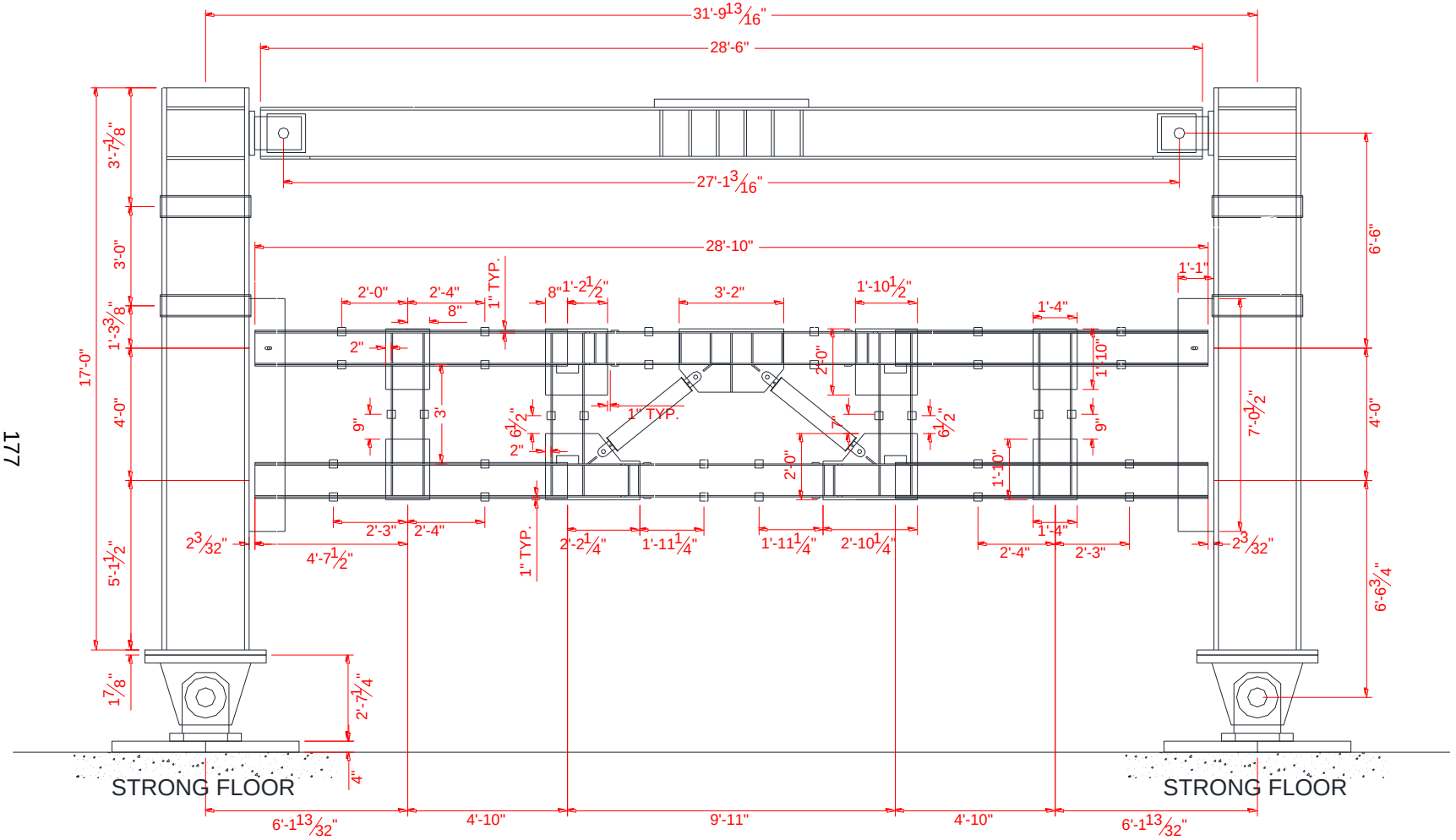

Figure B-11 Prototype Full Scale Test Setup of STMF with BRB

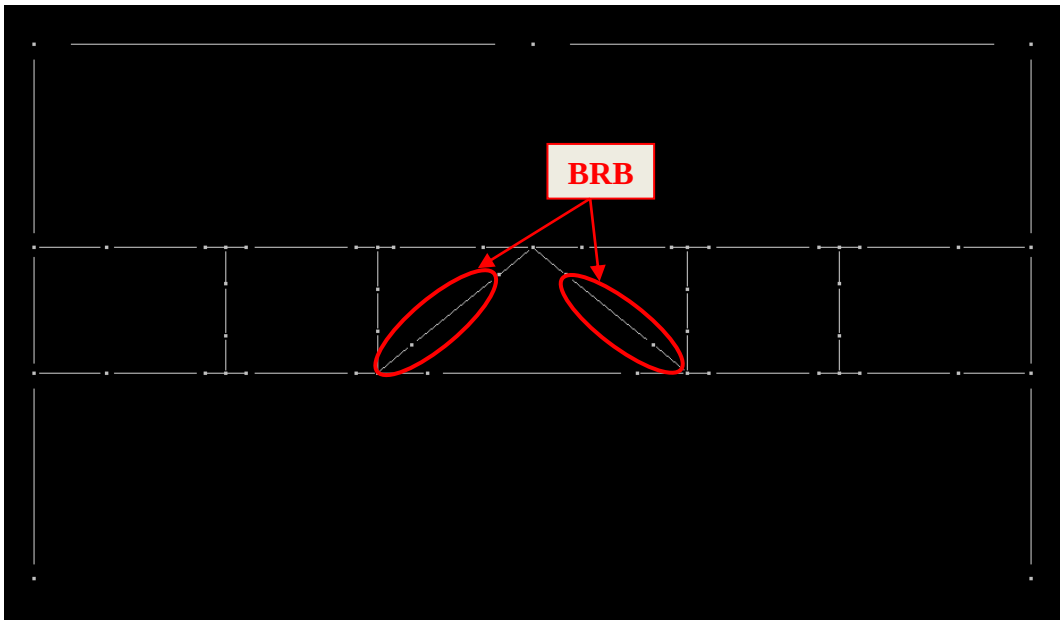

Figure B-12 STMF with BRB Model

Non-Linear Models

The nonlinear model of plastic hinge of the chord member in the special segment is shown in Figure B-13.

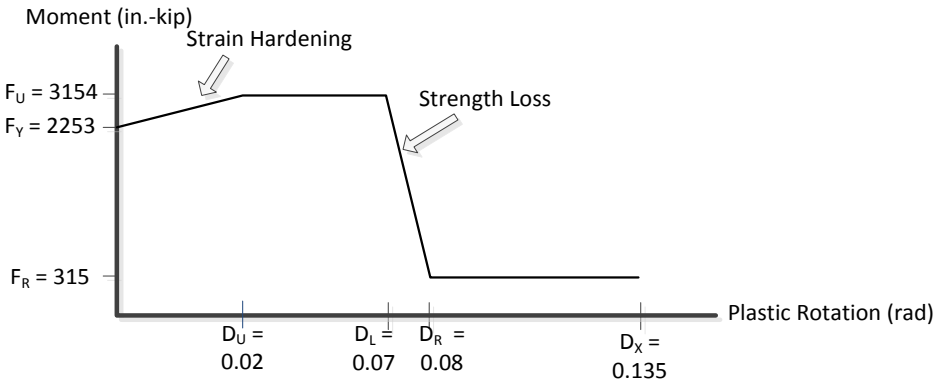

Figure B-13 Displacement vs. Strength Model of Special Segment Top Chord

where $F_Y = expected\ plastic\ moment$

$F_U = expected\ maximum\ moment$

$F_R = moment\ after\ strength\ loss$

$D_U = plastic\ rotation\ corresponding\ to\ F_U$

$D_R = plastic\ rotation\ corresponding\ to\ F_R$

$D_X = ultimate\ plastic\ rotation$

The chord member used in STMF with BRB is 2C12x20.7 with reduced beam section (RBS). The capacity of the RBS is 80% of 2C12x20.7. Material overstrength factor and strain-hardening ratio are 1.1 and 1.4, respectively. As a result,

$$F_Y = 0.8R_yF_yZ = (0.8)(1.1)(50)(2 \times 25.6) = 2{,}253\ in.-kip$$

$$F_U = 1.4F_Y = 1.4(2{,}253) = 3{,}154\ in.-kips$$

$$F_R is\ assumed\ to\ be\ 10\%\ of\ F_U$$

$$F_R = 0.1F_U = 0.1(3{,}154) = 315\ in.-kips$$

From the component test of 2C12x20.7, the members could undergo large plastic rotation (0.07 rad). As a result, parameters regarding plastic rotation are assumed to be the same as those from the studies.

$$D_U = 0.02\ rad$$

$$D_L = 0.07\ rad$$

$$D_R = 0.08\ rad$$

$$D_X = 0.135\ rad$$

The interaction model between axial forces and bending moment in the reduced beam section is shown in Figure B-14. The other members except the BRB could be modeled similarly.

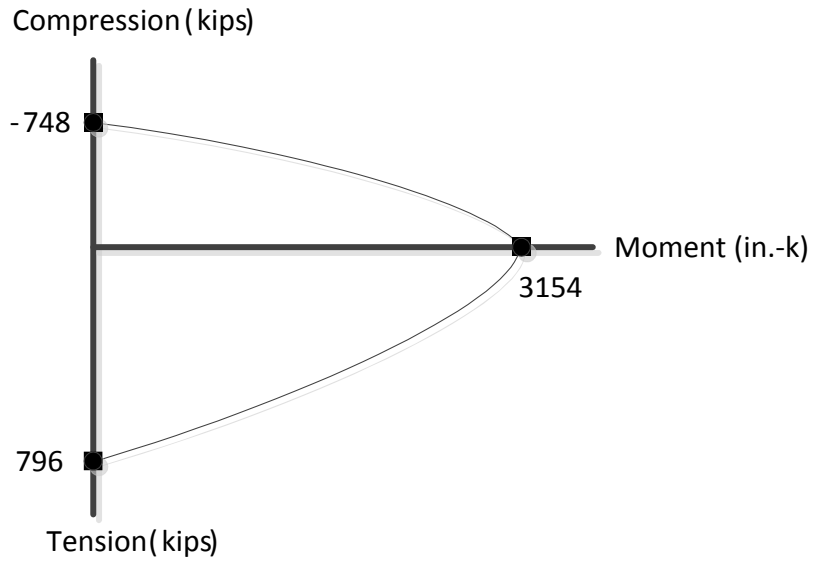

Figure B-14 Bending Moment and Axial Forces Interaction Model of Top Chord of Special Segment

The buckling restrained brace used in this analysis has the length dimensions as shown in Figure B-1 as well as the following properties:

Core:

$$A_c = 0.588\ in^2$$

$$F_y = 42.5\ ksi.$$

$$R_y = 1$$

$$Strain\ Hardening\ Ratio = 1.75$$

$$L_c = 15.22\ in.$$

Ultimate Tensile Strength:

$$F_{ut} = 1.75 R_y F_y A = (1.75)(1)(42.5)(0.588) = 43.75\ kips$$

Ultimate Compressive Strength:

Compressive strength of BRB is assumed to be 10% higher than tensile strength.

$$F_{uc} = 1.1F_{ut} = (1.1)(43.1) = 48\ kips$$

BRB Compound Element Model

The BRB compound element comprises of 3 parts:

BRB Basic Element is an inelastic behavior modeling part of the core. For convenience, kinematic and isotropic strain hardenings were not considered and this element is modeled as elastic perfectly plastic (E-P-P) as shown in Figure B-19.

$$A_c = 0.588\ in^2, F_y = 42.5\ ksi, R_y = 1, Strain\ Hardening\ Ratio = 1.75, L_c = 15.22\ in.$$

Elastic Bar Element is the linear elastic behavior part of the BRB which is estimated to have 3.77 times the area of the BRB core

$$A_e = 2.22\ in^2, E = 29{,}000\ ksi,$$

Stiff End Zone Element is accounting for the pin, and eye bars. The effective end zone area and the total length of the end zones are:

$$A_z = 5.95A_c$$

$$L = 15.84\ in.$$

The plot of the model can be seen in Figure C-15.

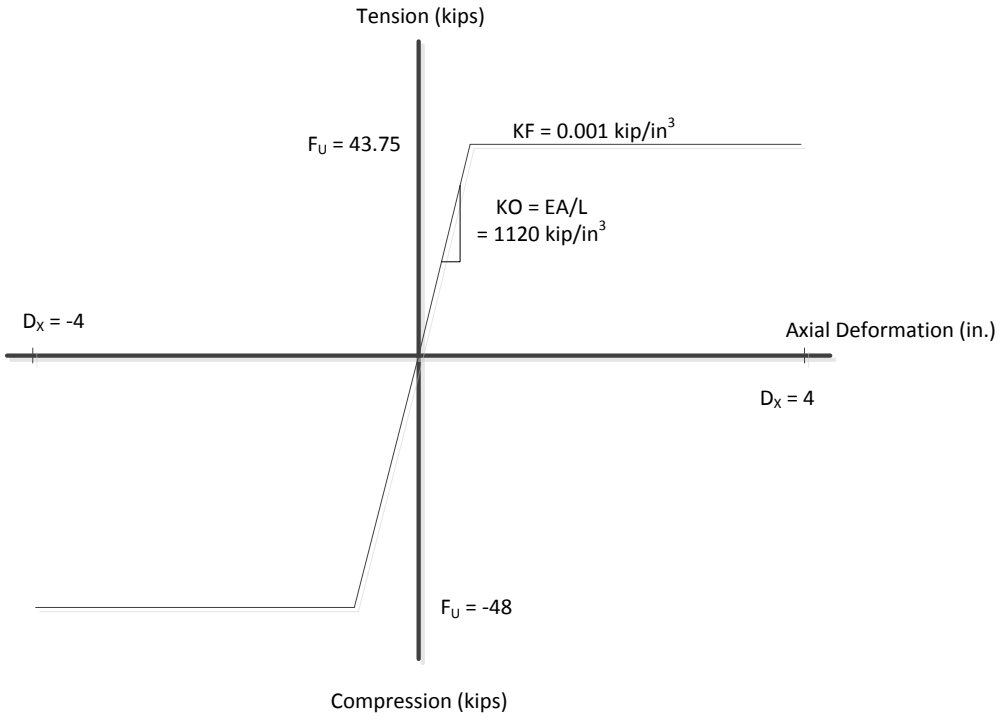

Figure B-15 Displacement vs. Strength Model of the Core of Buckling Restrained Brace (BRB)

From the pushover analysis, the relationships between prototype structure story drift vs. axial extension and contraction and were found as shown in Figures B-16 and B-17, respectively.

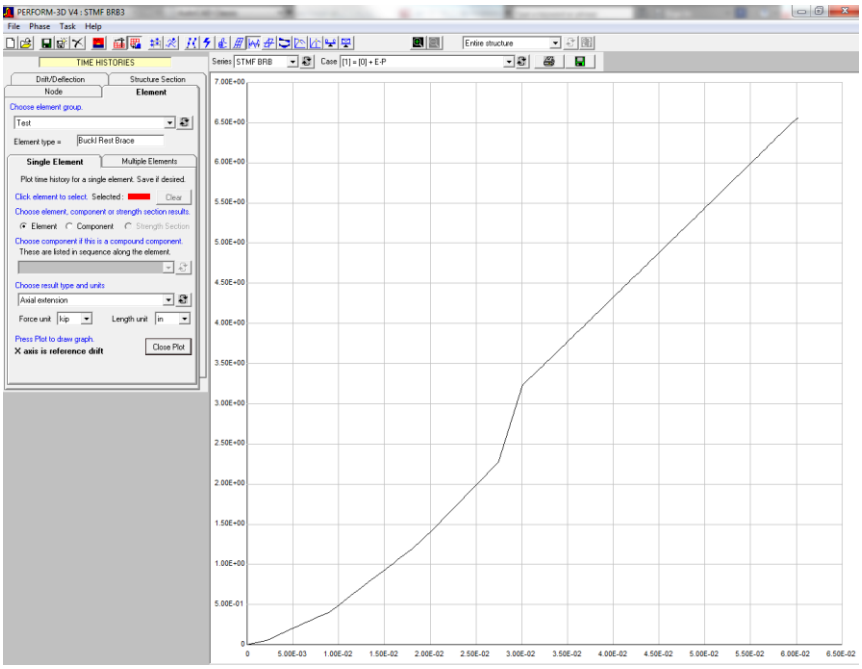

Figure B-16 Prototype Structure Story Drift vs. Axial Extension

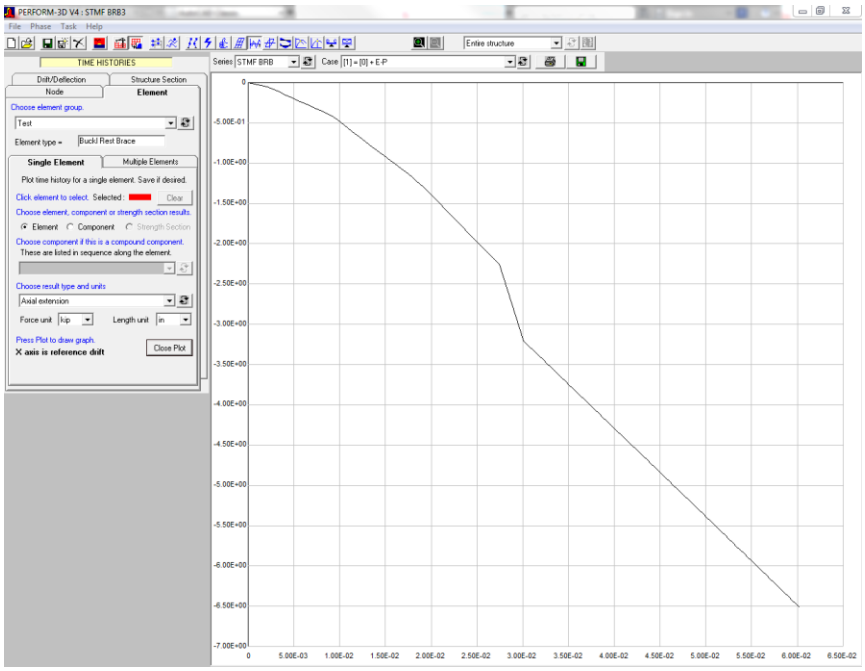

Figure B-17Prototype Structure Story Drift vs. Axial Contraction

At the same story drift, the extension and contraction were not the same due to slightly difference in tensile and compressive behaviors, the average absolute values between the two are used in loading protocol for both positive and negative cycles. By employing the Loading Sequence for Beam-to-Column Moment Connections from AISC 341-16 for the prototype STMF, with some additional elastic and inelastic cycles (at 0.1%, 0.2% and 0.3% story drifts), the loading protocol can be summarized in Table B-2 and Figure B-18.

Table B-2 Loading Protocol for BRB

Story Drift (%)	No. of Cycles	Axial Deformation		Inelastic Deformation	Cumulative Inelastic Deformation	Strain, ε (%) (Based on the core length, L, of 15.22 in.)
		Deformation, Δ_b (in.)	Δ_{bm}			
0.1	2	0.0245	0.50 Δ_{by}	0 Δ_{by}	0 Δ_{by}	0.16
0.2	2	0.0489	0.99 Δ_{by}	0 Δ_{by}	0 Δ_{by}	0.32
0.3	2	0.0975	1.97 Δ_{by}	3.88 Δ_{by}	3.88 Δ_{by}	0.64
0.375	6	0.1358	2.75 Δ_{by}	20.95 Δ_{by}	24.84 Δ_{by}	0.89
0.5	6	0.1997	4.04 Δ_{by}	36.46 Δ_{by}	61.30 Δ_{by}	1.31
0.75	6	0.3275	6.62 Δ_{by}	67.47 Δ_{by}	128.77 Δ_{by}	2.15
1	4	0.4885	9.88 Δ_{by}	71.03 Δ_{by}	199.80 Δ_{by}	3.21
1.5	2	0.9269	18.74 Δ_{by}	70.98 Δ_{by}	270.77 Δ_{by}	6.09
2	2	1.3982	28.28 Δ_{by}	109.10 Δ_{by}	323.32 Δ_{by}	9.19
3	2	3.1838	64.38 Δ_{by}	253.54 Δ_{by}	576.85 Δ_{by}	20.92

Note: The specimen will achieve 200 times the yield deformation at the end of 1% drift cycles

where Δ_b = value of deformation, in.

Δ_{bm} = value of deformation quantity, Δ_b, corresponding to the prototype structure story drift, $x\Delta_y$

Δ_{by} = value of deformation quantity, Δ_b, at first significant yield of test specimen, in.

From the push over analysis, Δ_{by} is 0.0495 in. and at 0.3% story drift, Δ_b is 0.0975 respectively. As a result, at 0.3% story drift,

$$\Delta_{bm} = \frac{0.0975}{0.0495}\Delta_{by}$$
$$= 1.97\Delta_{by}$$

When the specimen is pull or push to this deformation,

$$\text{inelastic deformation} = 1.97\Delta_{by} - \Delta_{by}$$
$$= 0.97\Delta_{by}$$

After 2 cycles at this story drift,

$$\text{inelastic deformation} = 4(0.97\Delta_{by})$$
$$= 3.88\Delta_{by}$$

Since there is no inelastic deformation in the previous cycle,

$$\text{cumulative inelastic deformation} = 0 + 3.88\Delta_{by}$$
$$= 3.88\Delta_{by}$$

Since elastic deformation in the transition zone and rigid end zone is negligible, strain in the steel core at 0.3% story drift can be found from,

$$\varepsilon = \frac{\Delta_b}{L} \times 100\%$$
$$= \frac{0.0975}{15.22} \times 100\%$$
$$= 0.64\%$$

Similar data at the other story drifts can be found in the same manner.

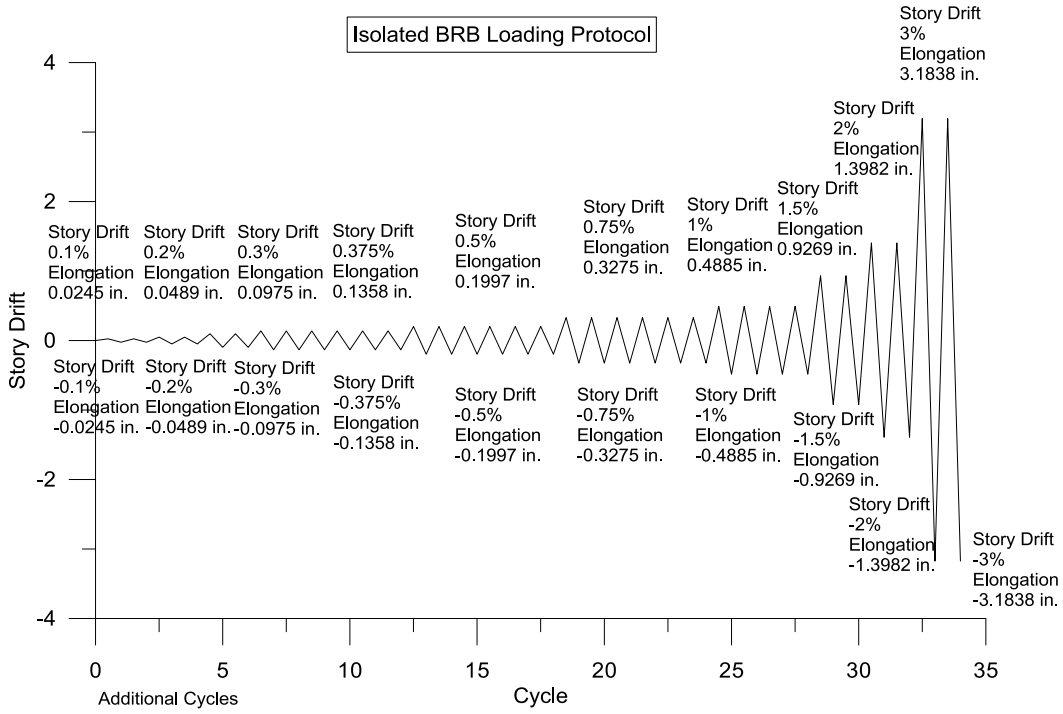

Figure B-18 Loading History for BRB

Appendix C

Plastic Hinge Modeling for Nonlinear Analysis

Plastic hinge modeling for double-channel section under combined bending and compression

In commercial nonlinear time history or pushover analysis software package, nonlinear behavior of members are modeled without elastic deformation. Generally parameters needed are shown in Figure C-1 where

M_y is yielding moment capacity,

M_u is ultimate moment capacity,

and M_r is residual moment or moment capacity after loss of strength.

D is plastic rotation corresponding to each moment capacity.

In order to create nonlinear model of double-channel flexural members when axial force exists, three parameters involving moment capacity and rotational capacity were assigned. For rotational capacity a and b are parameters of interest where

a is plastic rotation between yielding point to ultimate moment capacity,

b is plastic rotation when double-channel member maintain ultimate strength,

0.02 radian is suggested as the plastic rotation the member drop strength from M_u to M_r and is believed to be sufficiently conservative.

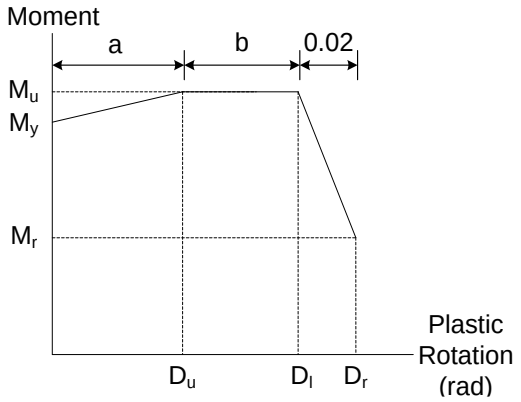

Figure C1 Generalized nonlinear model of inelastic flexural element

For moment, M_y could generally be estimate with confident as

$M_y = R_y F_y Z$

where R_y = 1.1 (AISC 341-16)

Ultimate moment can be looked at as a function of a force parameter of interest, β, times M_y:

$M_u = \beta M_y$

The objective of this study is to find relationship between the presence of axial force in double-channel flexural member and these three parameters so that one can construct a nonlinear model of a plastic hinge as shown in Figure C-1.

The presence of axial force (both tension and compression) were treated as the ratio of axial force to nominal yielding strength.

Experimental results of double-channel component tests were the case where there is no axial force in the specimen. A trilinear model as shown in Figure C1 could easily be construct from hysteresis behavior. The test results of specimen 2C12-8 was used here for the case where $\alpha = 0$. Finite element analysis was used to determine hysteretic behavior of 2C12×20.7 specimen with the same boundary condition as specimen 2C12-8 under axial load ratio of 0.1, 0.2, and 0.3 respectively. The trilinear model of all four cases (one from test result and three from FEA) were constructed as shown in Chapter 6 and the 3 parameters of interest are shown in Table C-1 when there was axial compression in the member. Note that this is the results of 2C12×20.7 under AISC loading protocol.

Table C-1 Parameters of interest

Experimental and FEA results			
Axial D/C ratio (α)	Overstrength factor (β)	Plastic rotation (a)	Plastic rotation (b)
0	1.28	0.03	0.04
0.1	1.156	0.009	0.009
0.2	1.102	0.009	0
0.3	1.035	0.001	0

The relationship between β, a, and b versus α were individually carry out. In some cases, one linear relationship well represented, however; in the others, using multiple functions yield a more accurate representation. The derivation of such relationships are shown below.

Moment Parameter

Experimental and FEA results	
Axial D/C ratio (α)	Overstrength factor (β)
0	1.28
0.1	1.156
0.2	1.102
0.3	1.035

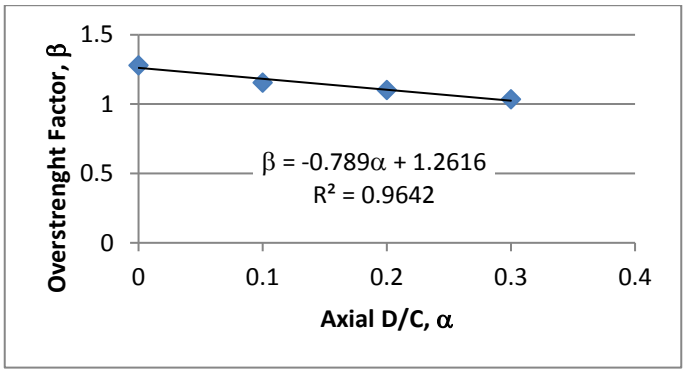

By linear regression analysis:

β = -0.79 α + 1.26

Since on average, the experimental test results suggested that average of β is 1.4 for double-channel sections when $\alpha = 0$, the above equation is scaled to;

β = -0.88 α + 1.4

Plastic Rotation Parameters

Strain hardening plastic rotation (a)

Experimental and FEA results	
Axial D/C ratio (α)	Plastic rotation (a)
0	0.03
0.1	0.009
0.2	0.009
0.3	0.001

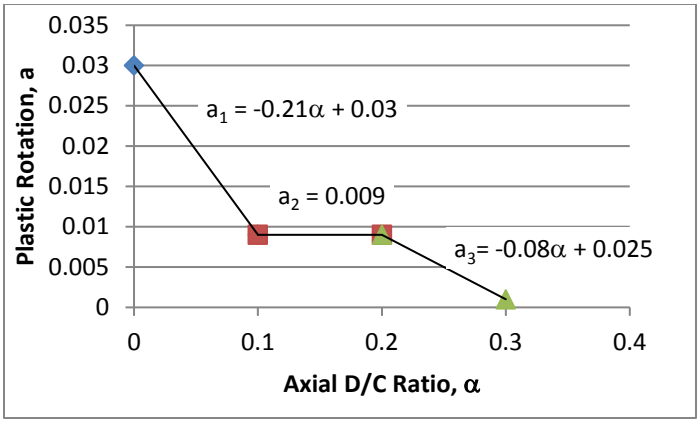

a $= -0.21\alpha + 0.03$ when $0 < \alpha < 0.1$

$= 0.009$ when $0.1 < \alpha < 0.2$

$= -0.08\alpha + 0.025$ when $0.2 < \alpha < 0.3$

Plastic rotation plateau (b)

Experimental and FEA results	
Axial D/C ratio (α)	Plastic rotation (b)
0	0.04
0.1	0.009
0.2	0
0.3	0

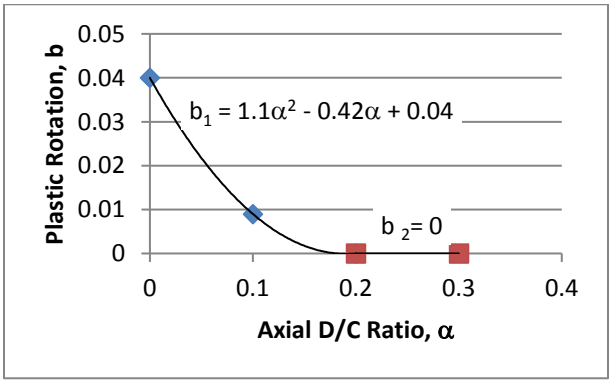

b = $1.1\alpha^2 - 0.42\alpha + 0.04$ when $0 < \alpha < 0.2$

= 0 when $0.2 < \alpha < 0.3$

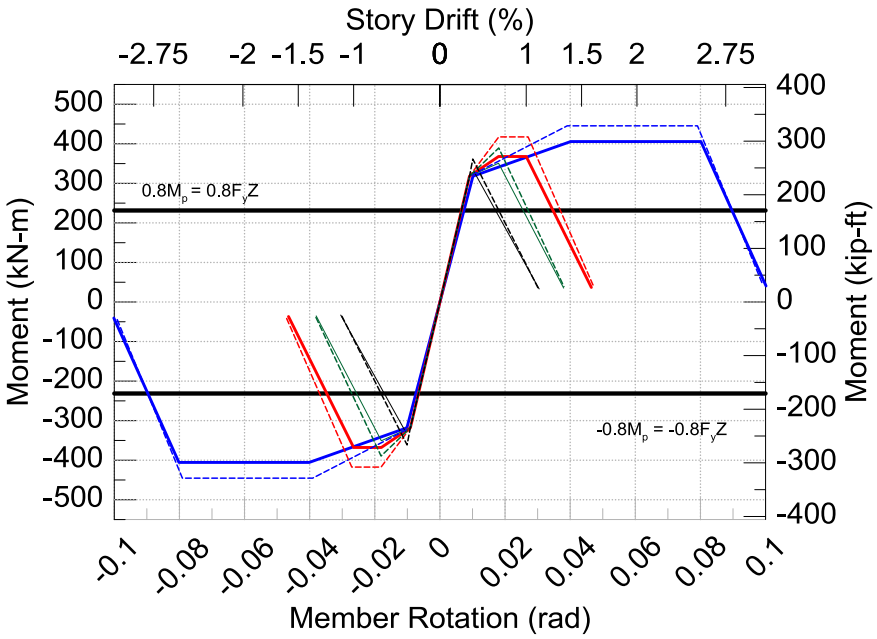

Figure C-2 Proposed Scaled Model vs Original Model for AISC Loading Protocol under combined compression and bending

Figure C-2 showed the nonlinear model of 2C12×20.7 under compression when α = 0, 0.1, 0.2, and 0.3 in solid blue, red, green, and black, respectively. These lines were actually the trilinear model constructed from the test and FEA results. When the overstrength factor, β, is scaled to 1.4 if there is no axial force in order to represent other double channel sections, the models are shown in the dotted lines.

Plastic hinge model for double channel under near collapse loading history

As previously mention that when one wants to evaluate performance of a structure at collapse prevention level, using AISC loading history might be too conservative. The next section shows regression analysis to acquire relationship between axial compression load ratio and three parameters of interest for a nonlinear model suitable for nonlinear time history analysis at collapse prevention level.

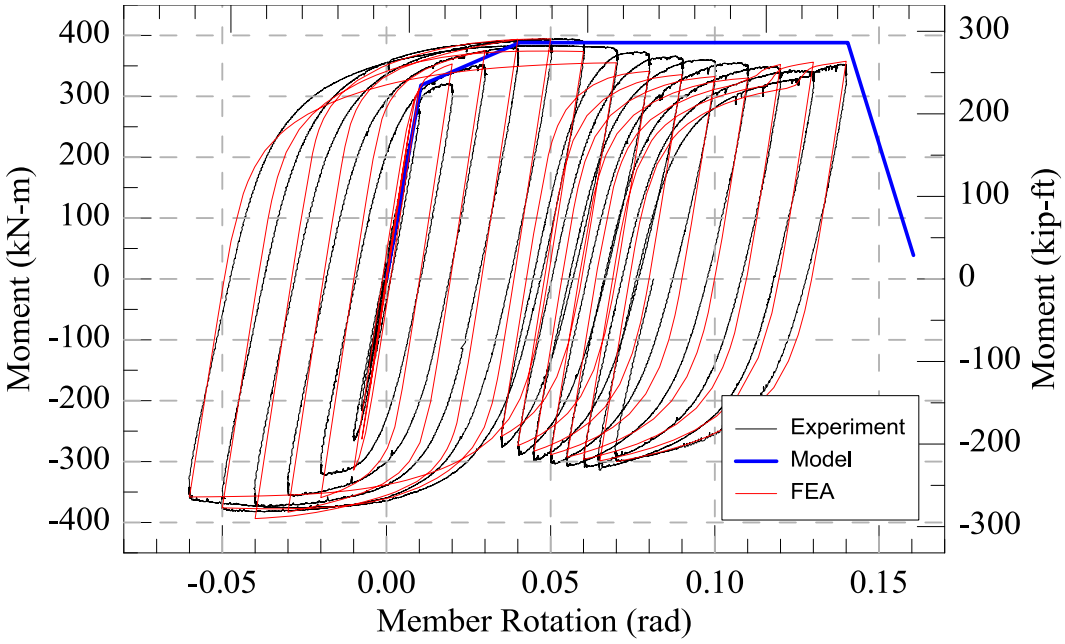

Figure C-3 FEA for near collapse loading protocol and model (no axial load)

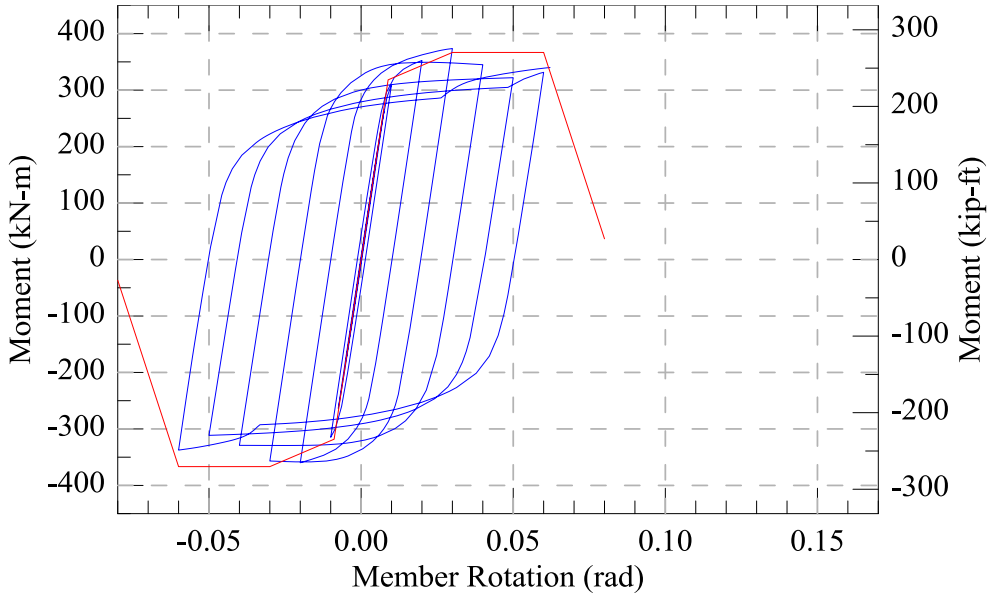

Figure C-4 FEA result and Model of 0.1 Axial D/C Ratio

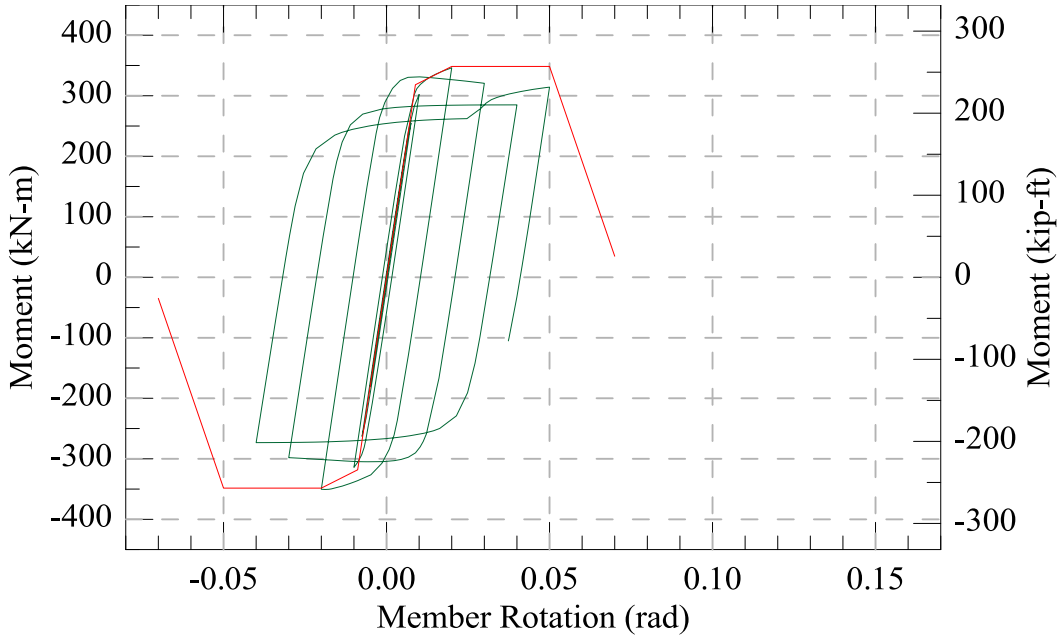

Figure C-5 FEA result and Model of 0.2 Axial D/C Ratio

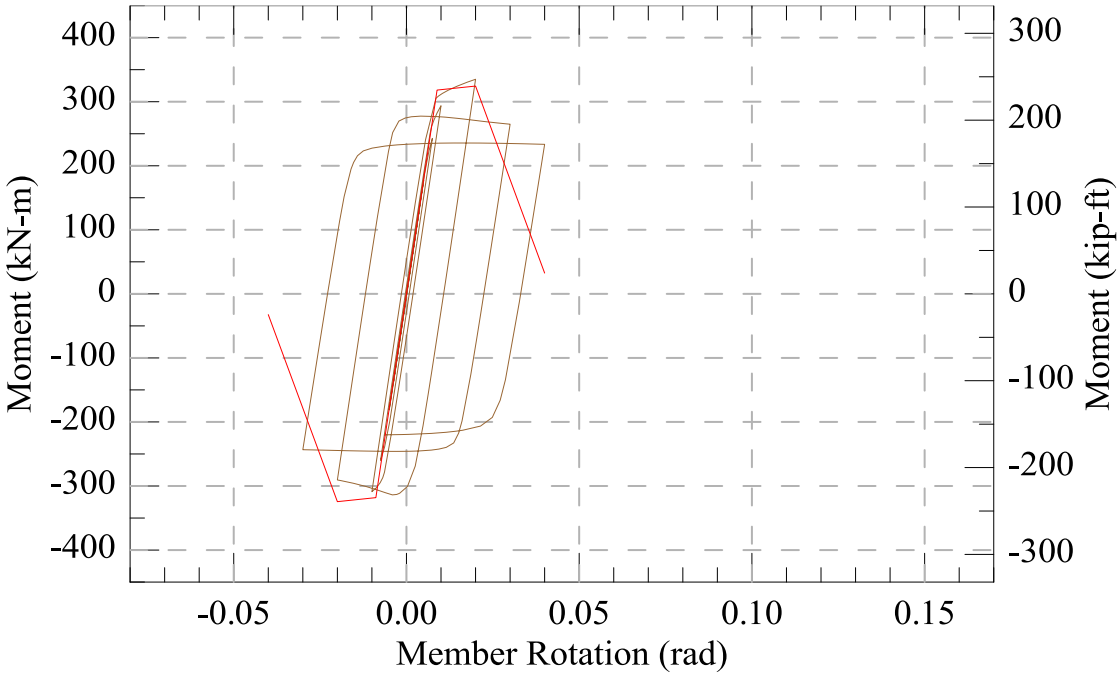

Figure C-6 FEA result and Model of 0.3 Axial D/C Ratio

Moment Parameter

Experimental and FEA results	
Axial D/C ratio (α)	Overstrength factor (β)
0	1.221
0.1	1.152
0.2	1.095
0.3	1.020

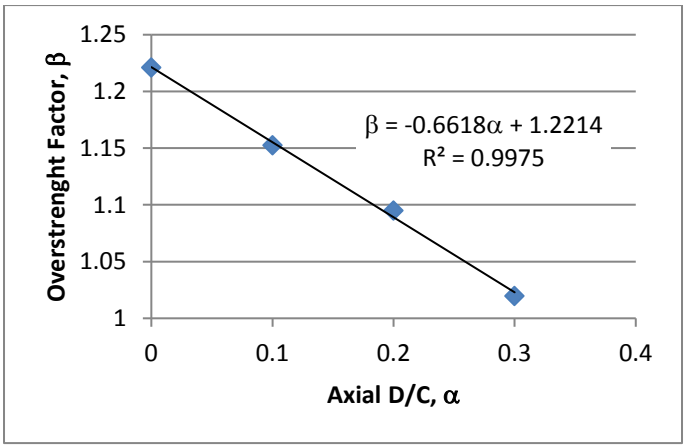

By linear regression analysis:

$\beta = -0.66\ \alpha + 1.22$

Since on average, β is 1.4 for double-channel sections, the above equation is scaled to;

$\beta = -0.76\ \alpha + 1.4$

Plastic Rotation Parameters

Strain hardening plastic rotation (a)

Experimental and FEA results	
Axial D/C ratio (α)	Plastic rotation (a)
0	0.03
0.1	0.021
0.2	0.011
0.3	0.011

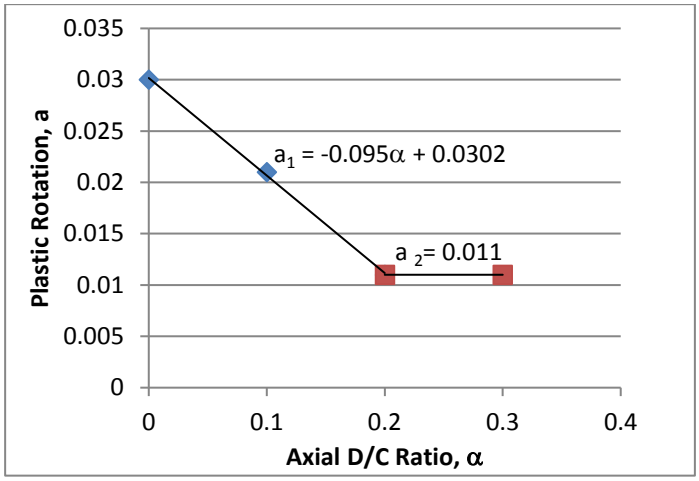

a = -0.1β + 0.03 when $0 < \alpha < 0.2$

= 0.011 when $0.2 < a\beta < 0.3$

Plastic rotation plateau (b)

Experimental and FEA results	
Axial D/C ratio (α)	Plastic rotation (b)
0	0.10
0.1	0.03
0.2	0.03
0.3	0

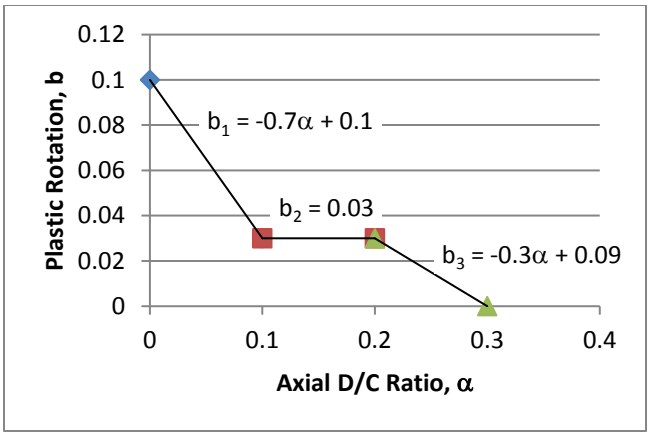

b = -0.7α + 0.1 when 0 < α < 0.1

= 0.03 when 0.1 < α < 0.2

= -0.3α + 0.09 when 0.2 < α < 0.3

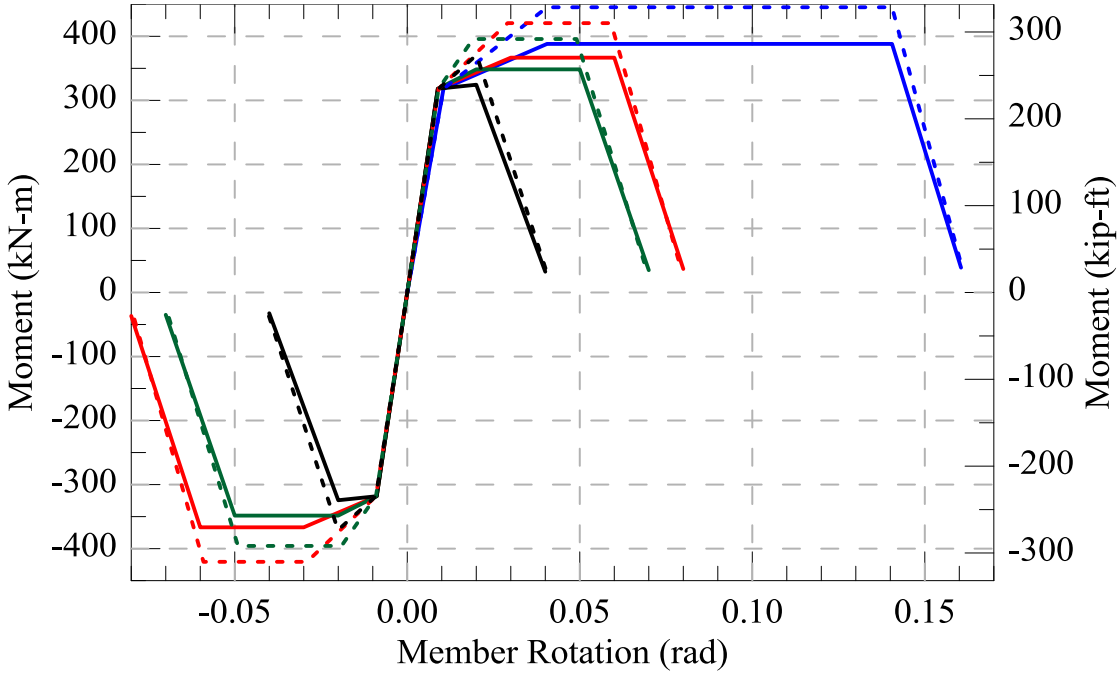

Figure C-7 Proposed Scaled Model vs Original Model for NC Loading Protocol

Combined Bending and Tension

Similar to when axial compression is present, axial tension could have an effect on ductility of flexural members as well. Below is how the modeling parameters equations were derived

Under AISC Loading History

Moment Parameter

R_y = 1.1 (AISC 341-16)

$M_y = R_y F_y Z$

$M_u = \beta M_y$

Experimental and FEA results	
Axial D/C ratio (α)	Overstrength factor (β)
0	1.28
0.1	1.229
0.2	1.152
0.3	1.081

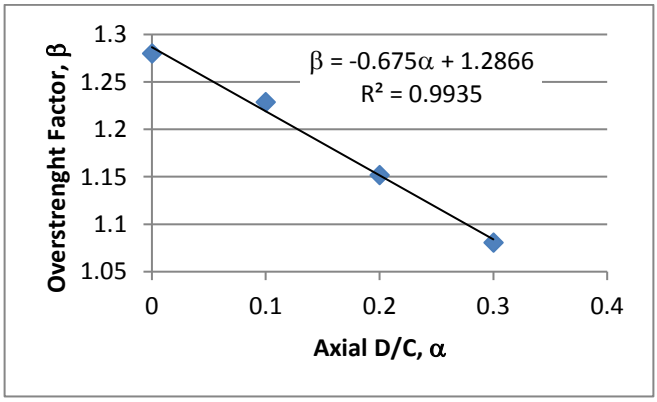

By linear regression analysis:

$\beta = -0.68\ \alpha + 1.29$

Since on average, β is 1.4 for double-channel sections, the above equation is scaled to;

$\beta = -0.73\ \alpha + 1.4$

Plastic Rotation Parameters

Strain hardening plastic rotation (a)

Experimental and FEA results	
Axial D/C ratio (α)	Plastic rotation (a)
0	0.03
0.1	0.03
0.2	0.03
0.3	0.018

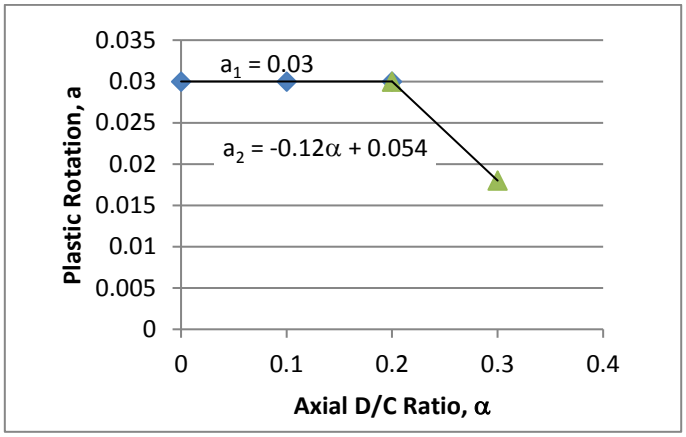

a = 0.03 when $0 < \alpha < 0.2$

= $-0.12\alpha + 0.05$ when $0.2 < \alpha < 0.3$

Plastic rotation plateau (b)

Experimental and FEA results	
Axial D/C ratio (α)	Plastic rotation (b)
0	0.04
0.1	0.009
0.2	0
0.3	0

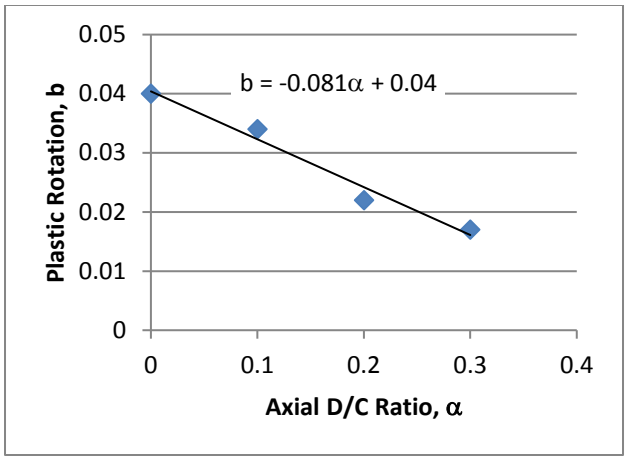

b = -0.08α +0.04 when 0 < α < 0.3

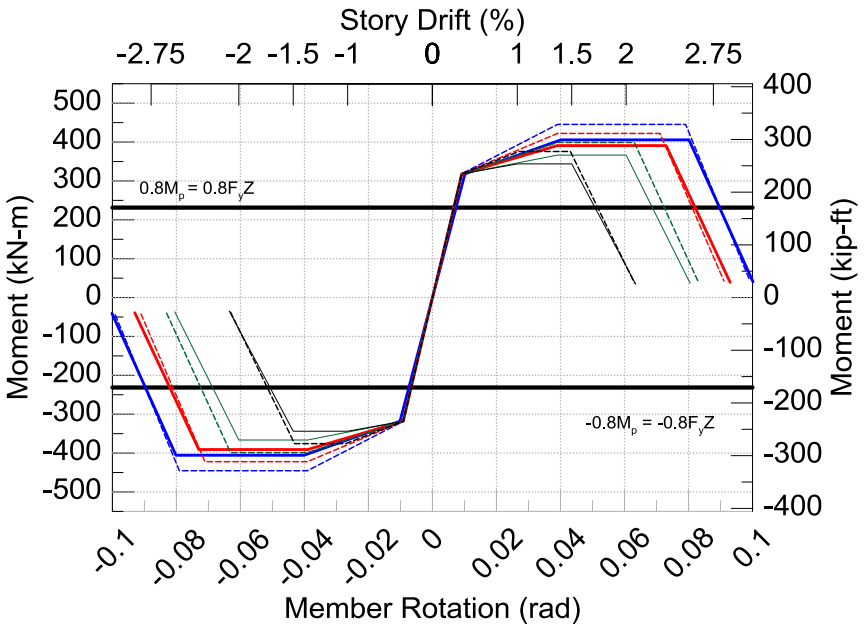

Figure C-8 Proposed Scaled Model vs Original Model for AISC Loading Protocol under combined tension and bending

Under Near Collapse Loading Protocol

Experimental and FEA results	
Axial D/C ratio (α)	Overstrength factor (β)
0	1.221
0.1	1.244
0.2	1.182
0.3	1.113

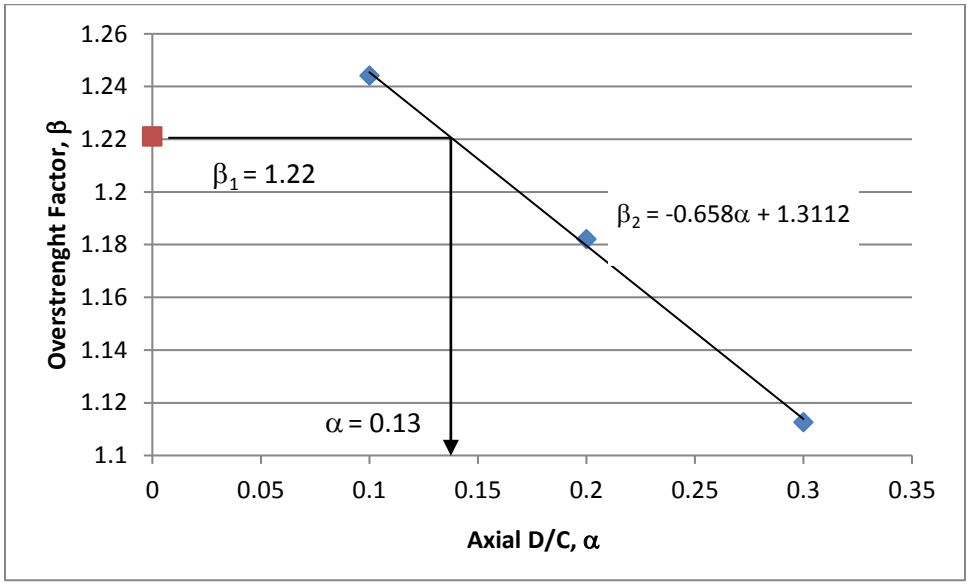

Note that overstrength factor is capped at 1.22 which is the case where there is no axial force at all to be conservative.

By linear regression analysis:

$\beta = 1.22$ when $0 < \alpha < 0.13$

$\beta = -0.66\alpha + 1.31$ when $0.13 < \alpha < 0.3$

Since on average, β is 1.4 for double-channel sections, the above equation is scaled to;

$\beta = 1.4$ when $0 < \alpha < 0.13$

$\beta = -0.7\alpha + 1.4$ when $0.13 < \alpha < 0.3$

Plastic Rotation

Strain hardening plastic rotation (a)

Experimental and FEA results	
Axial D/C ratio (α)	Plastic rotation (a)
0	0.03
0.1	0.03
0.2	0.03
0.3	0.03

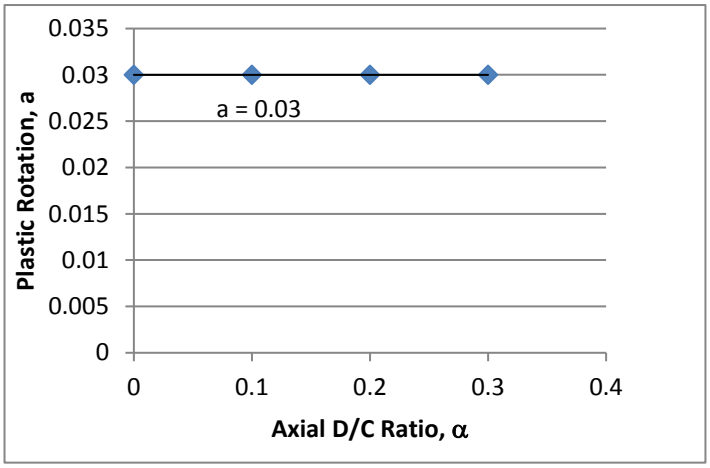

a = 0.03 when $0 < \alpha < 0.3$

Plastic rotation plateau (b)

Experimental and FEA results	
Axial D/C ratio (α)	Plastic rotation (b)
0	0.10
0.1	0.10
0.2	0.05
0.3	0.02

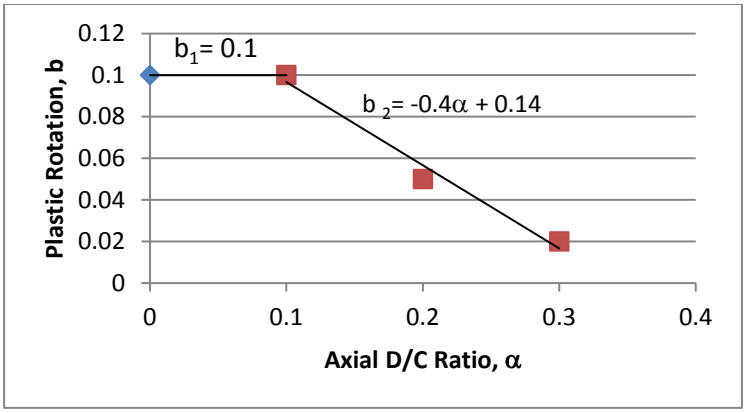

b = 0.1 when $0 < \alpha < 0.1$

= $-0.4\alpha + 0.14$ when $0.1 < \alpha < 0.3$

Appendix D

Component Test Specimen Drawings

Specimen 2C12-1

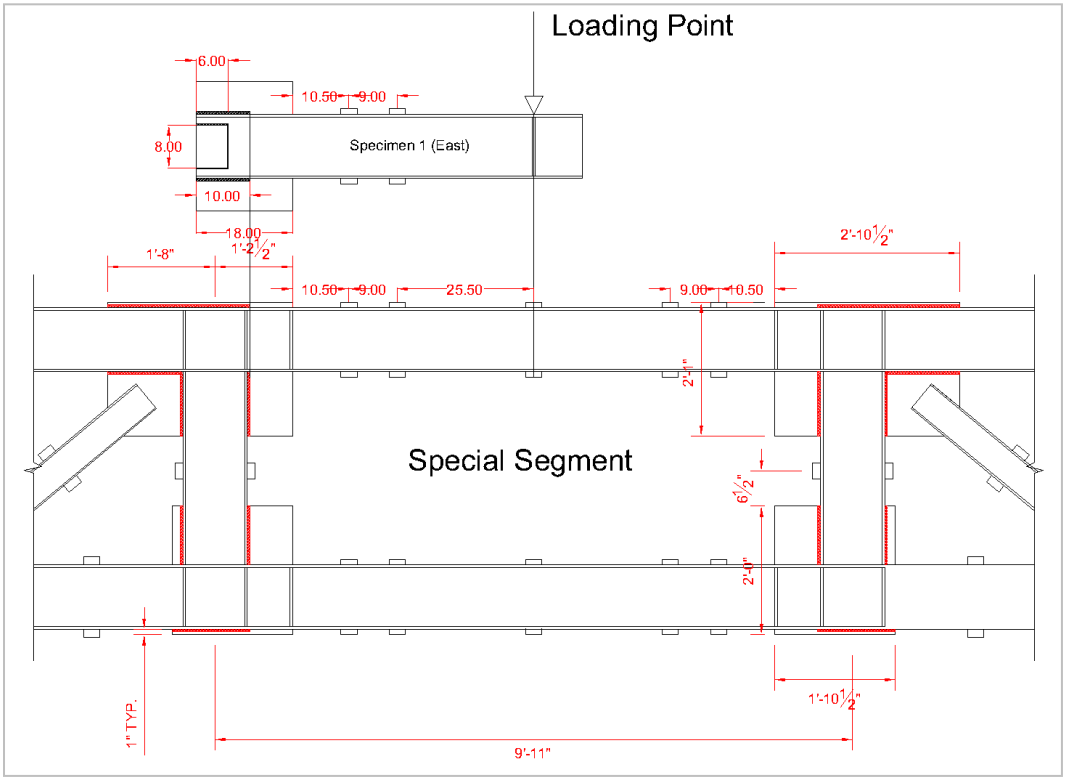

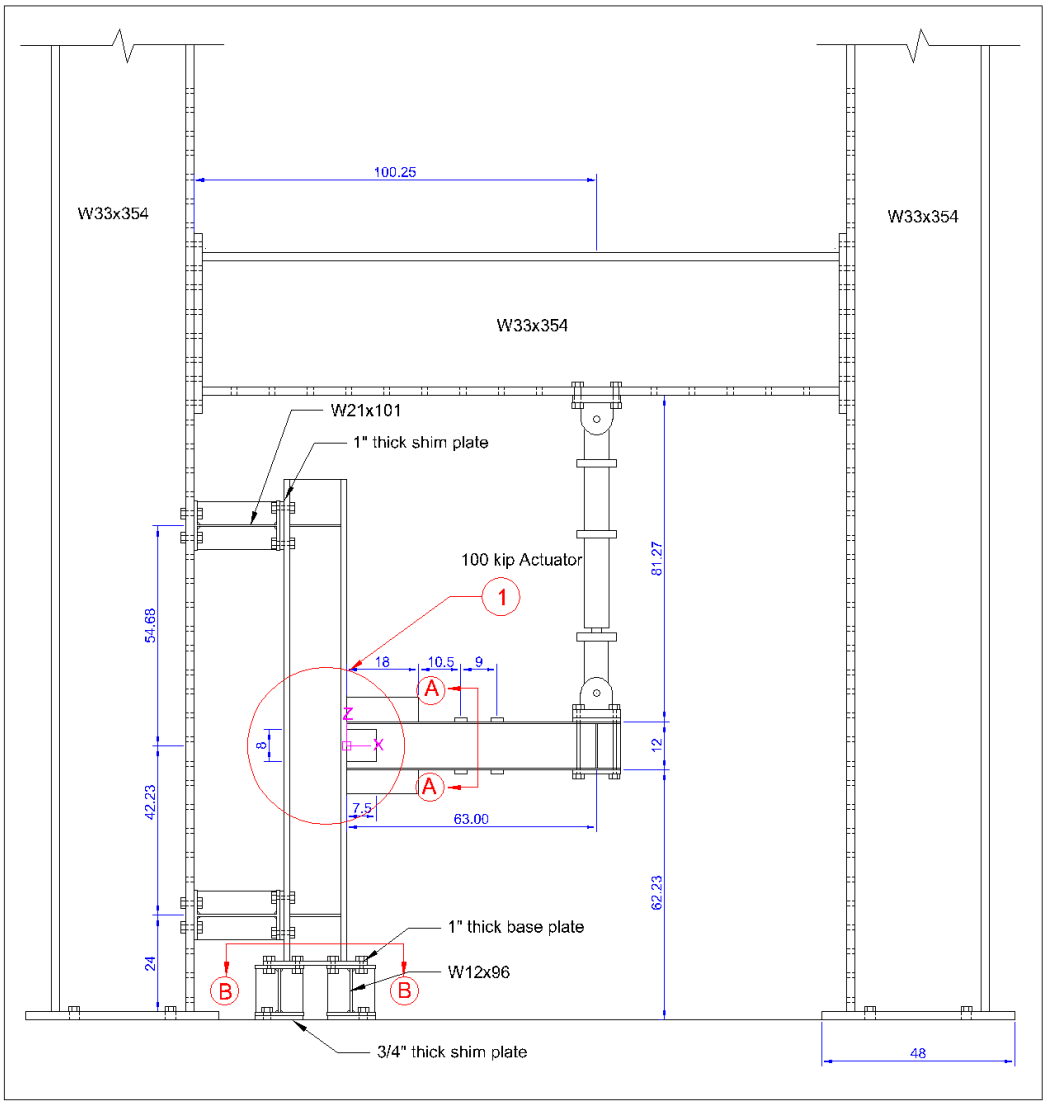
W33x354
100.25
W33x354
W33x354
W21x101
1" thick shim plate
100 kip Actuator
1
81.27
54.68
18
10.5
9
A
Z
X
8
12
A
42.23
7.5
63.00
62.23
1" thick base plate
W12x96
24
B
B
3/4" thick shim plate
48

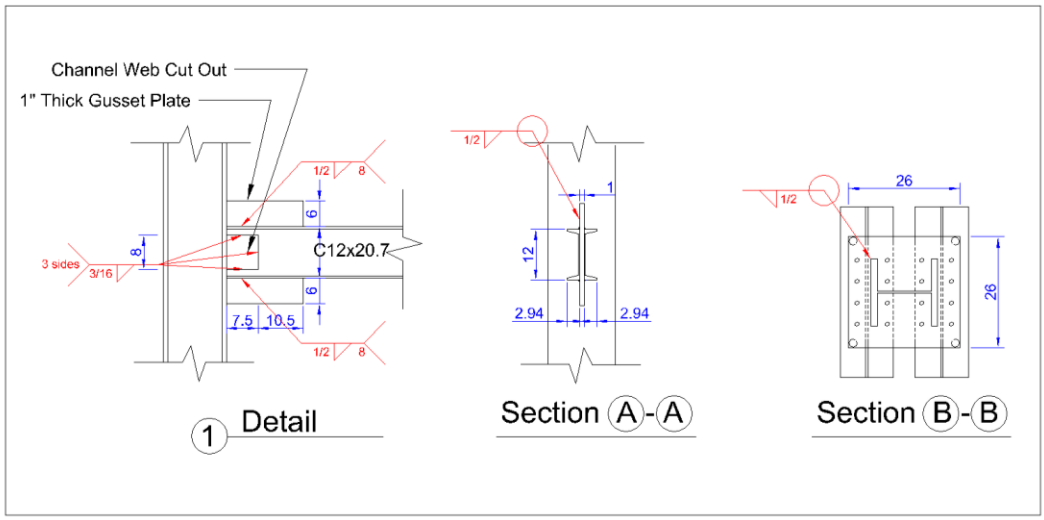
Channel Web Cut Out
1" Thick Gusset Plate
C12x20.7
3 sides
3/16
1/2
8
6
7.5
10.5
1
12
2.94
26
1 Detail
Section A-A
Section B-B

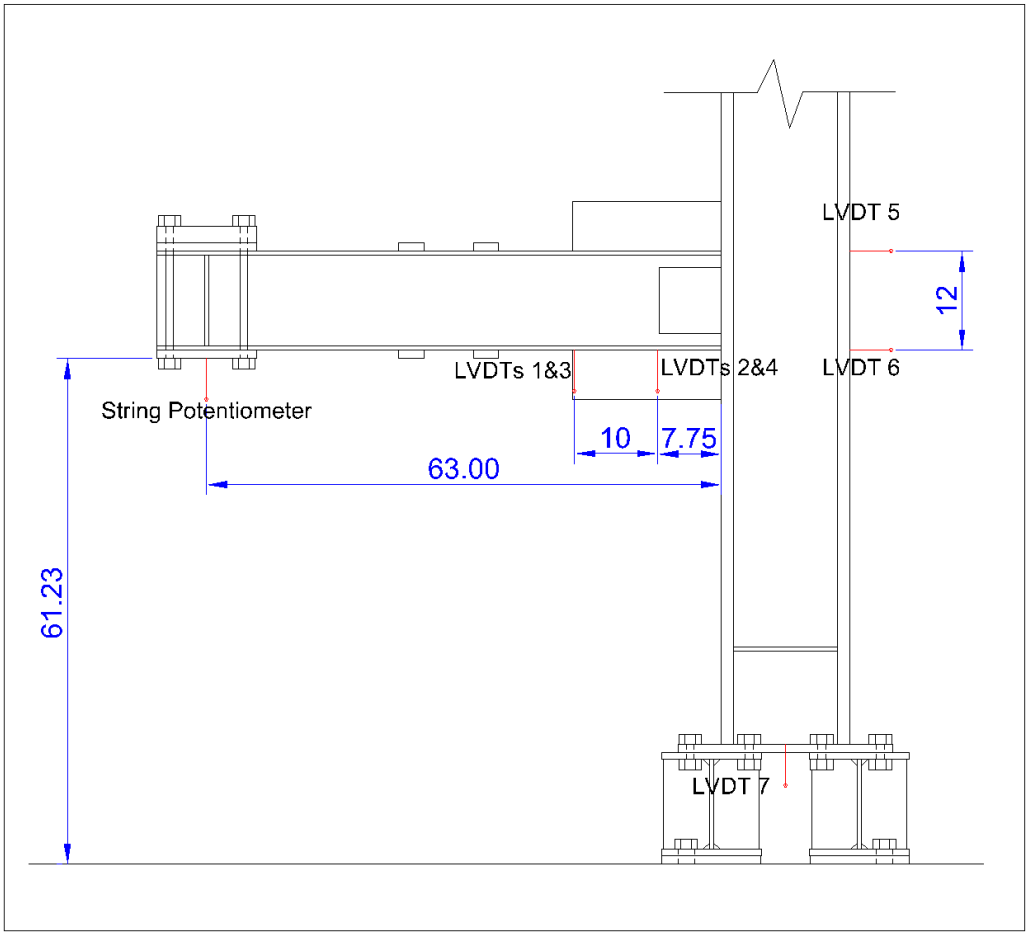
LVDT 5
12
LVDTs 1&3
LVDTs 2&4
LVDT 6
String Potentiometer
10
7.75
63.00
61.23
LVDT 7

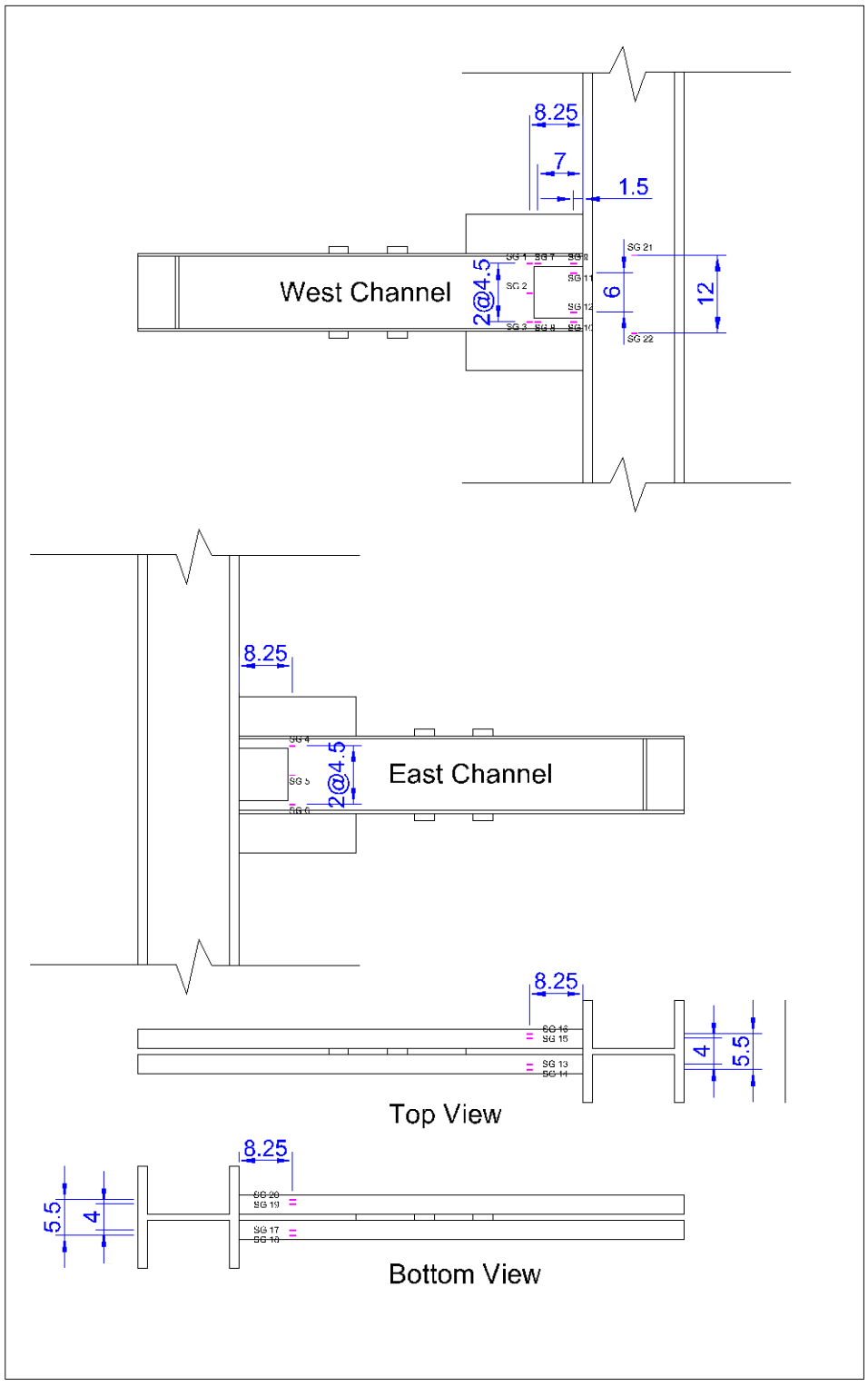
8.25
7
1.5
West Channel
2@4.5
6
12
SG 21
SG 22
8.25
East Channel
2@4.5
8.25
4
5.5
Top View
8.25
5.5
4
Bottom View

Specimen 2C12-2

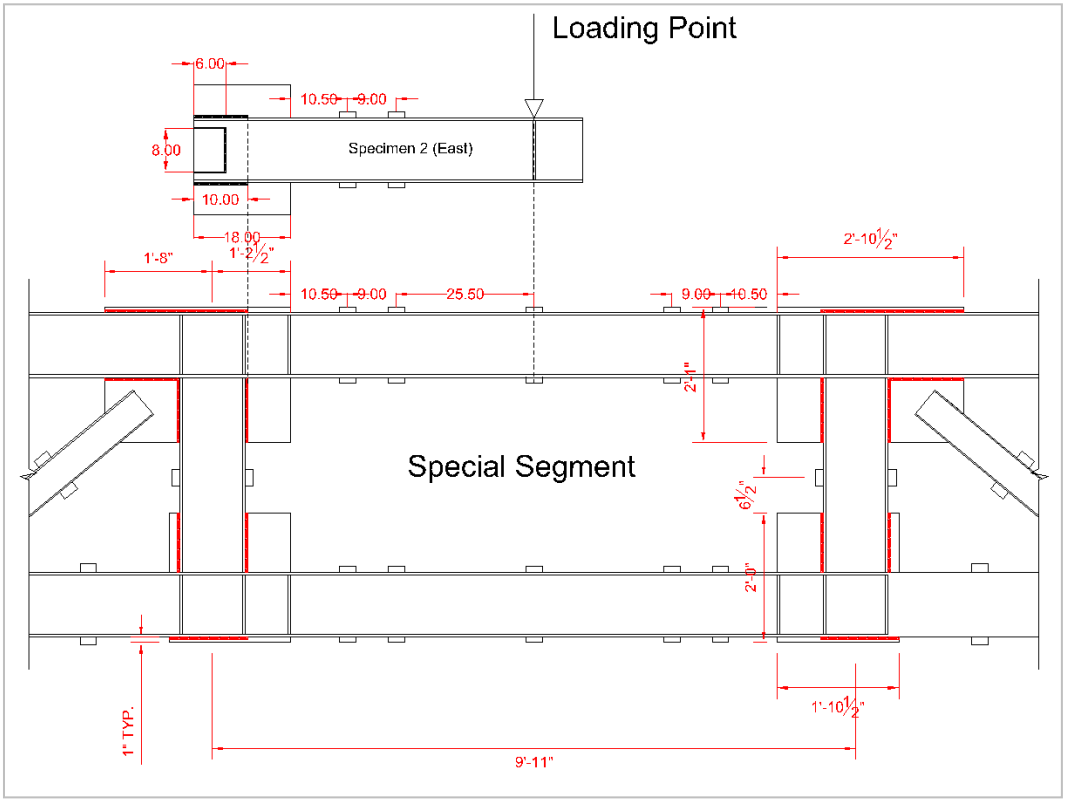

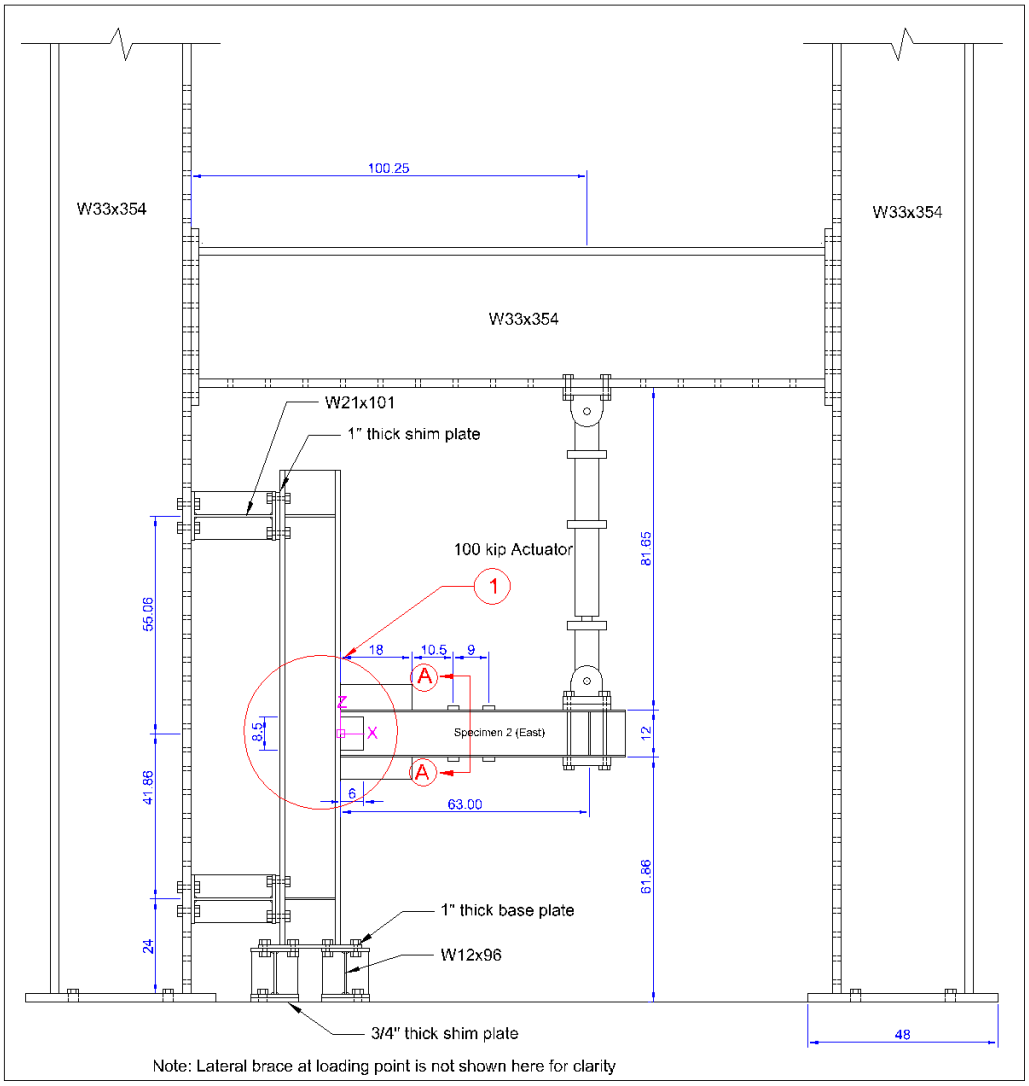
W33x354
100.25
W33x354
W33x354
W21x101
1" thick shim plate
100 kip Actuator
1
81.65
55.06
18
10.5
9
A
8.5
X
Specimen 2 (East)
12
41.86
A
6
63.00
61.86
1" thick base plate
W12x96
24
3/4" thick shim plate
48
Note: Lateral brace at loading point is not shown here for clarity

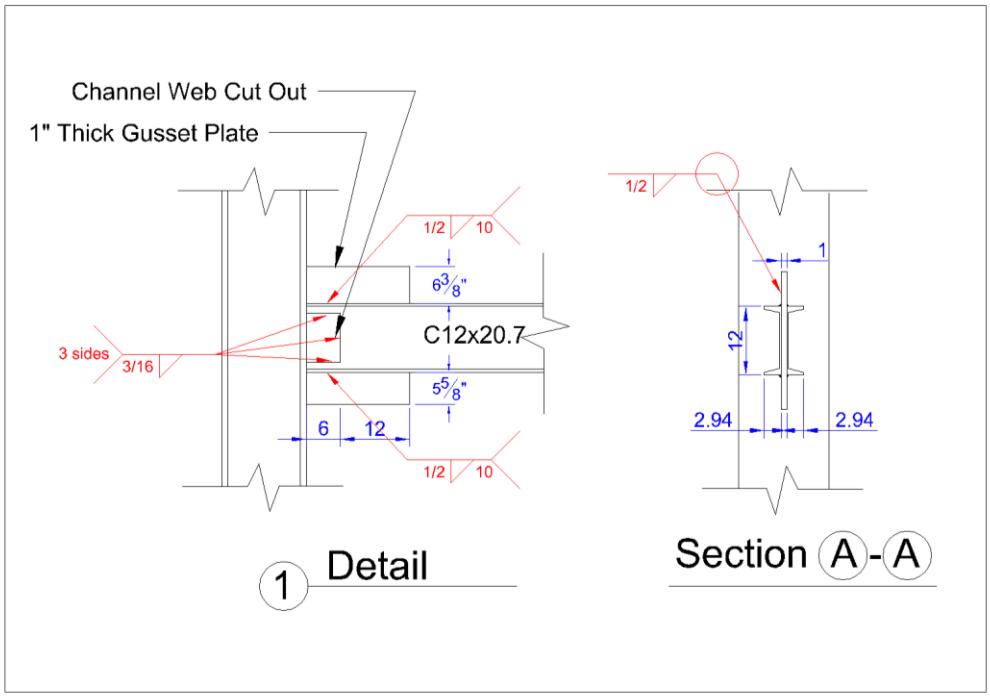
Channel Web Cut Out
1" Thick Gusset Plate
1/2
10
6 3/8"
C12x20.7
5 5/8"
3 sides
3/16
6
12
1/2
10
1/2
1
12
2.94
2.94
1 Detail
Section A-A

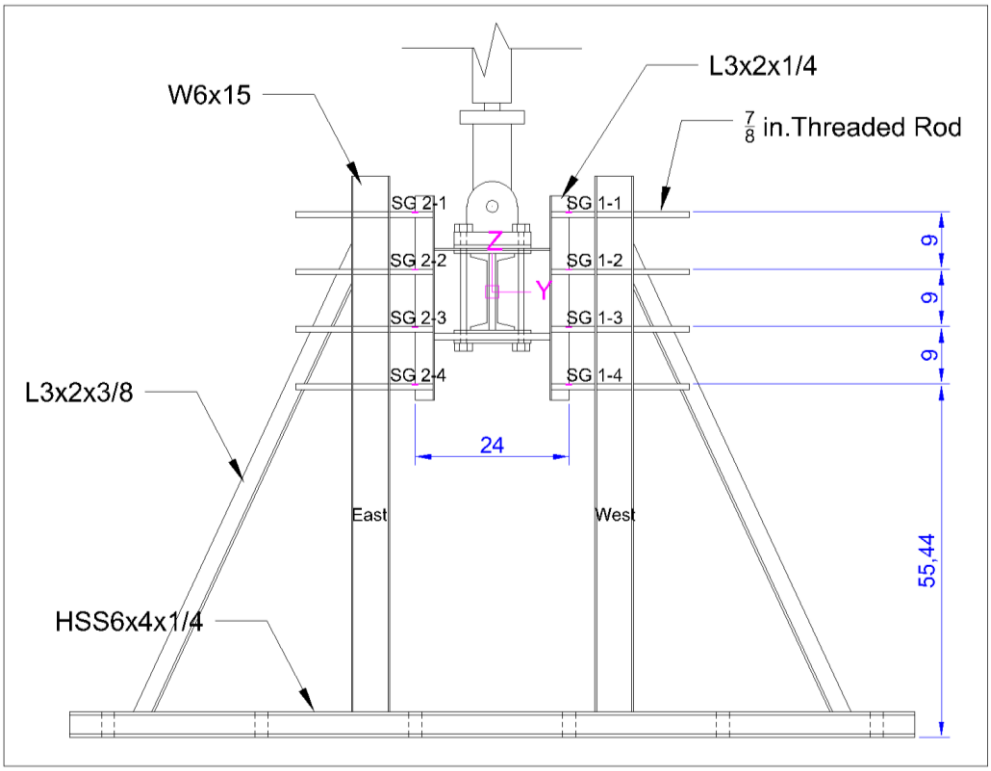
W6x15
L3x2x1/4
7/8 in.Threaded Rod
SG 2-1
SG 2-2
SG 2-3
SG 2-4
SG 1-1
SG 1-2
SG 1-3
SG 1-4
Z
Y
9
9
9
L3x2x3/8
24
East
West
55,44
HSS6x4x1/4

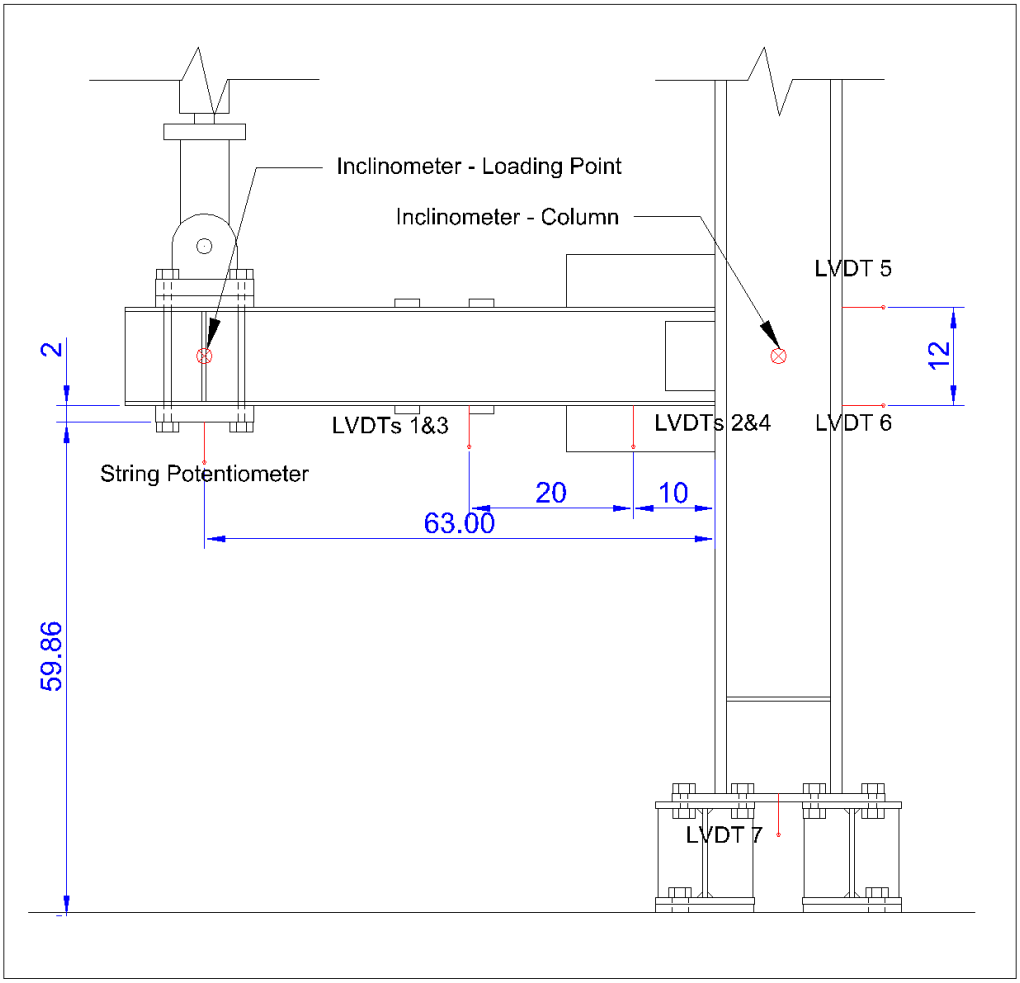
Inclinometer - Loading Point
Inclinometer - Column
LVDT 5
12
2
LVDTs 1&3
LVDTs 2&4
LVDT 6
String Potentiometer
20
10
63.00
59.86
LVDT 7

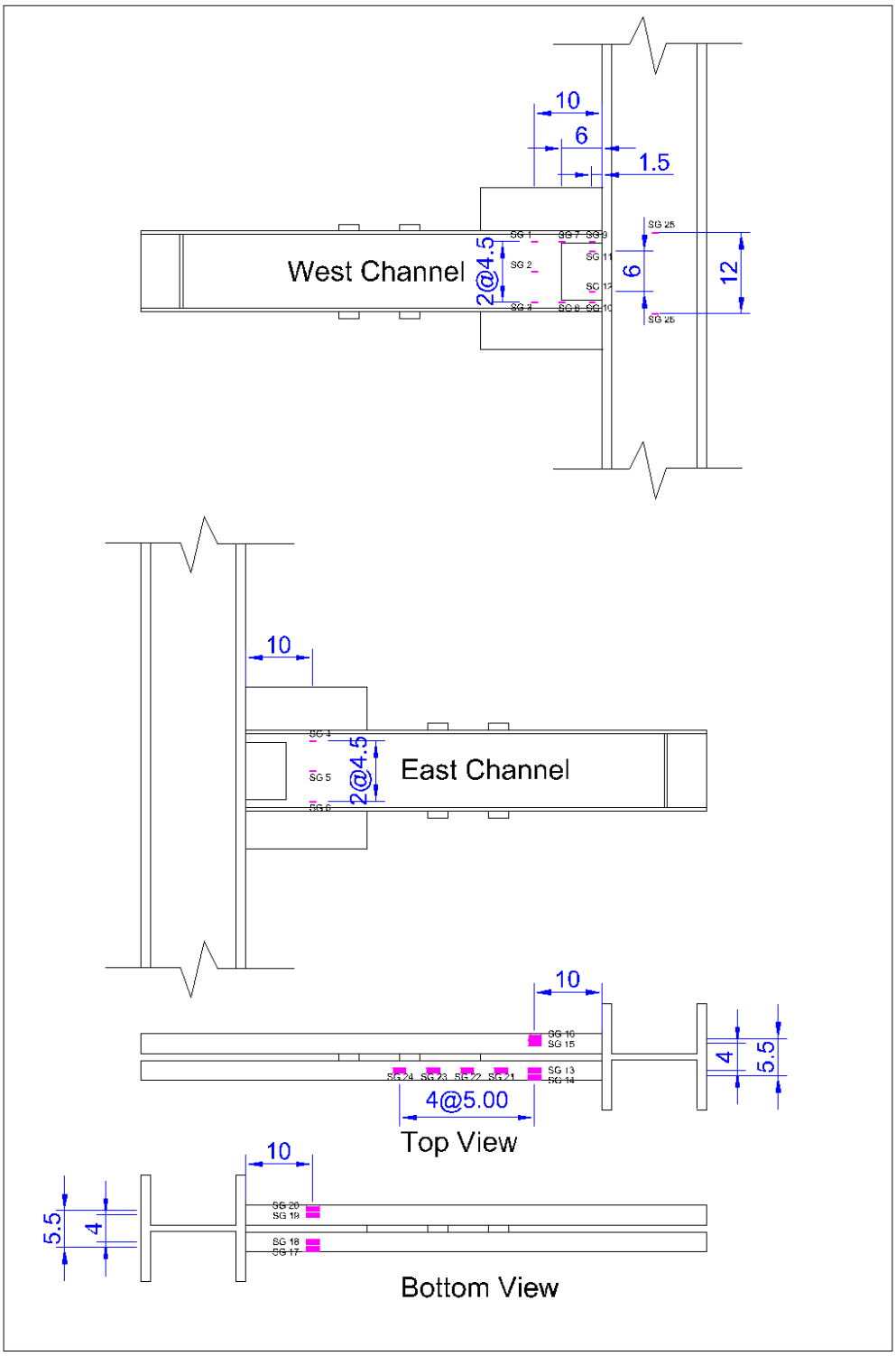
10
6
1.5
West Channel
2@4.5
6
12
10
East Channel
2@4.5
10
4
5.5
4@5.00
Top View
10
4
5.5
Bottom View

Specimen 2C12-3

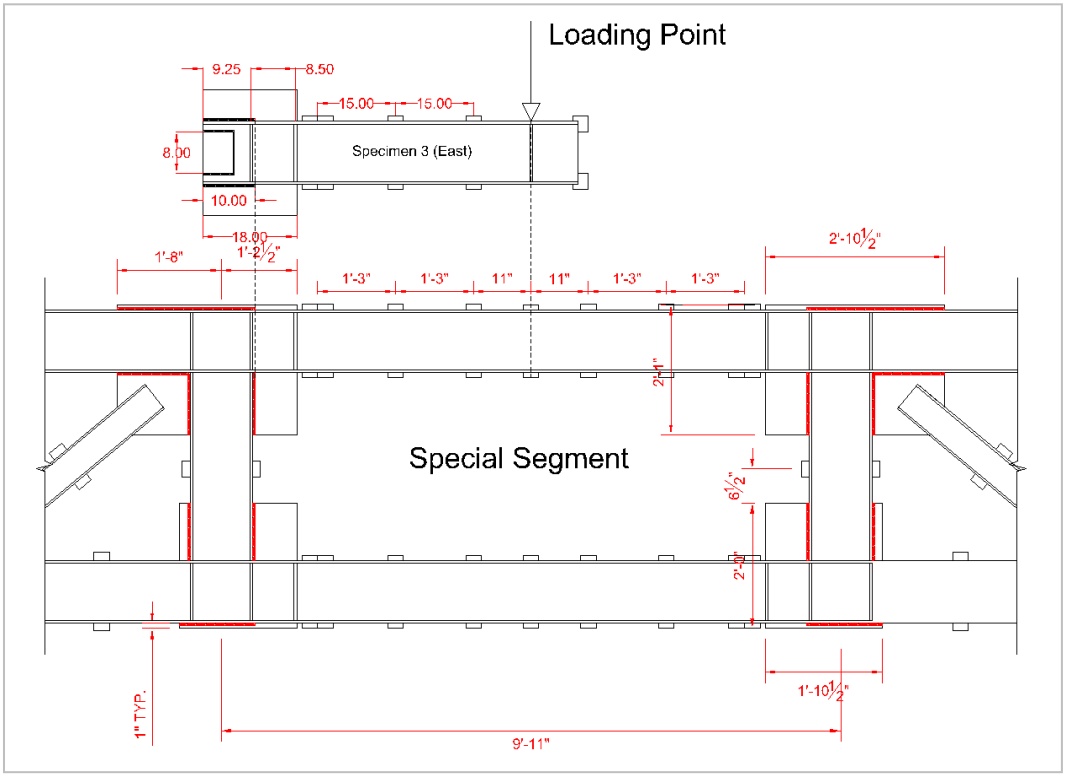

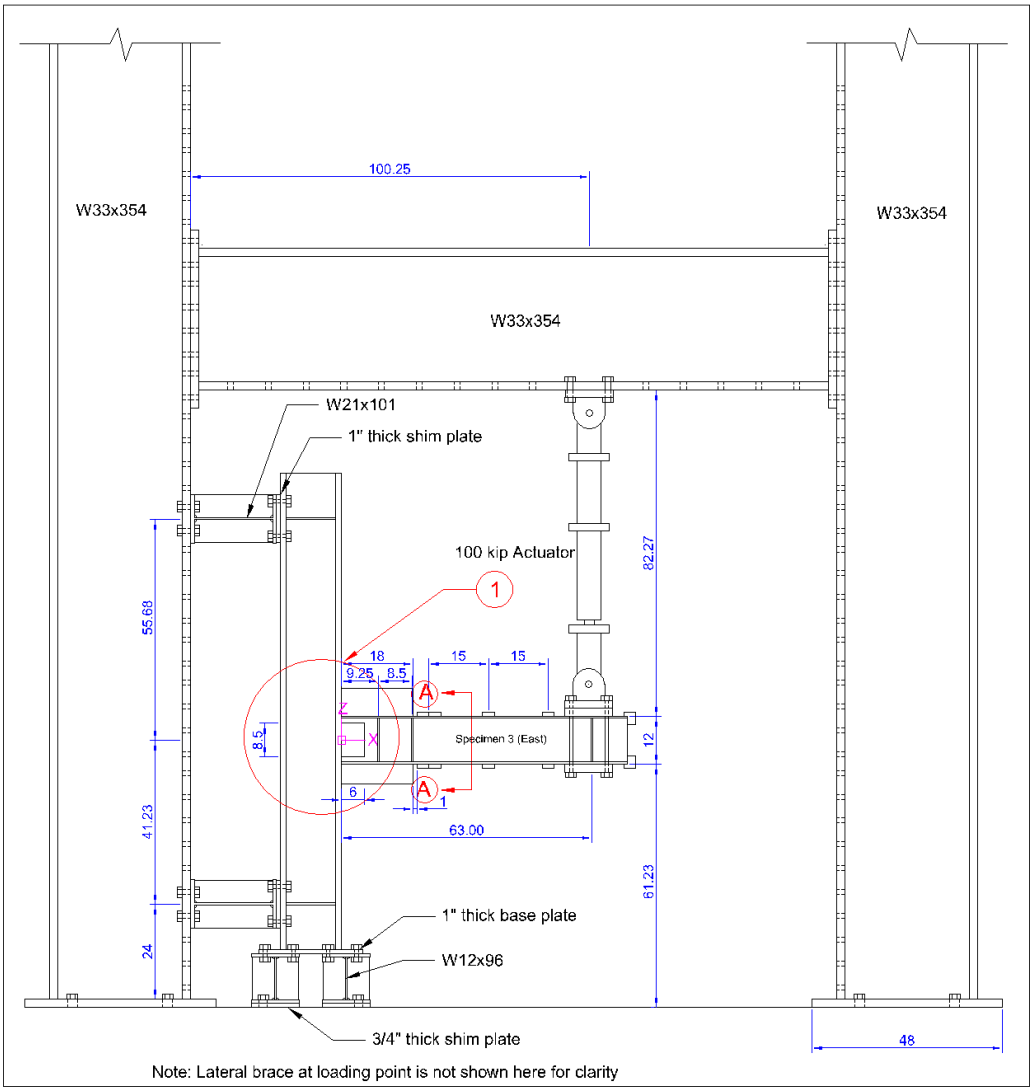
W33x354
100.25
W33x354
W33x354
W21x101
1" thick shim plate
100 kip Actuator
1
82.27
55.68
18
9.25
8.5
15
15
A
Specimen 3 (East)
12
8.5
6
1
A
63.00
41.23
61.23
1" thick base plate
W12x96
24
3/4" thick shim plate
48
Note: Lateral brace at loading point is not shown here for clarity

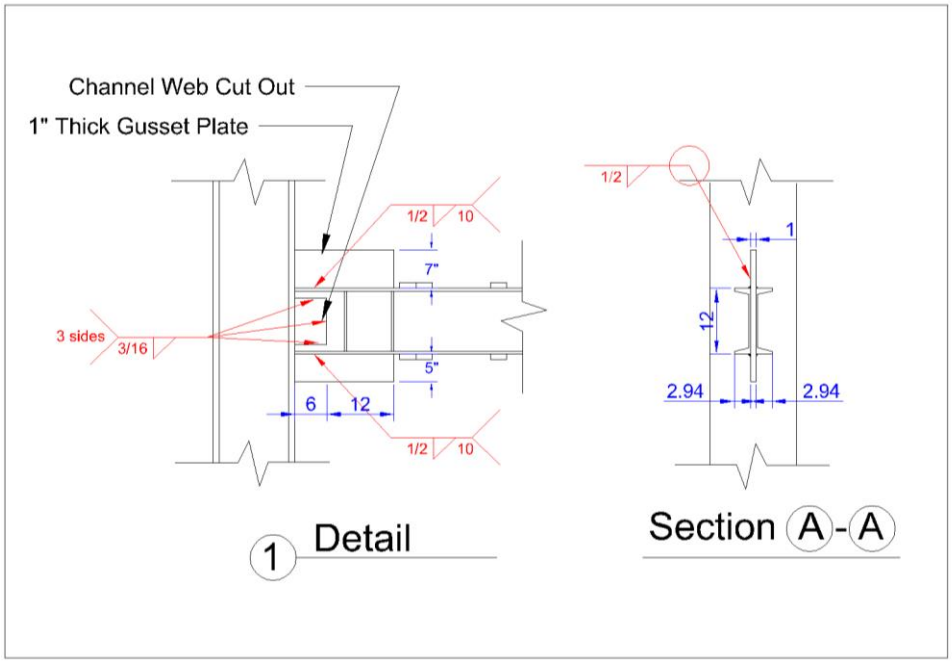
Channel Web Cut Out
1" Thick Gusset Plate
1/2
10
7"
3 sides
3/16
5"
6
12
1/2
10
1/2
1
12
2.94
2.94
1 Detail
Section A-A

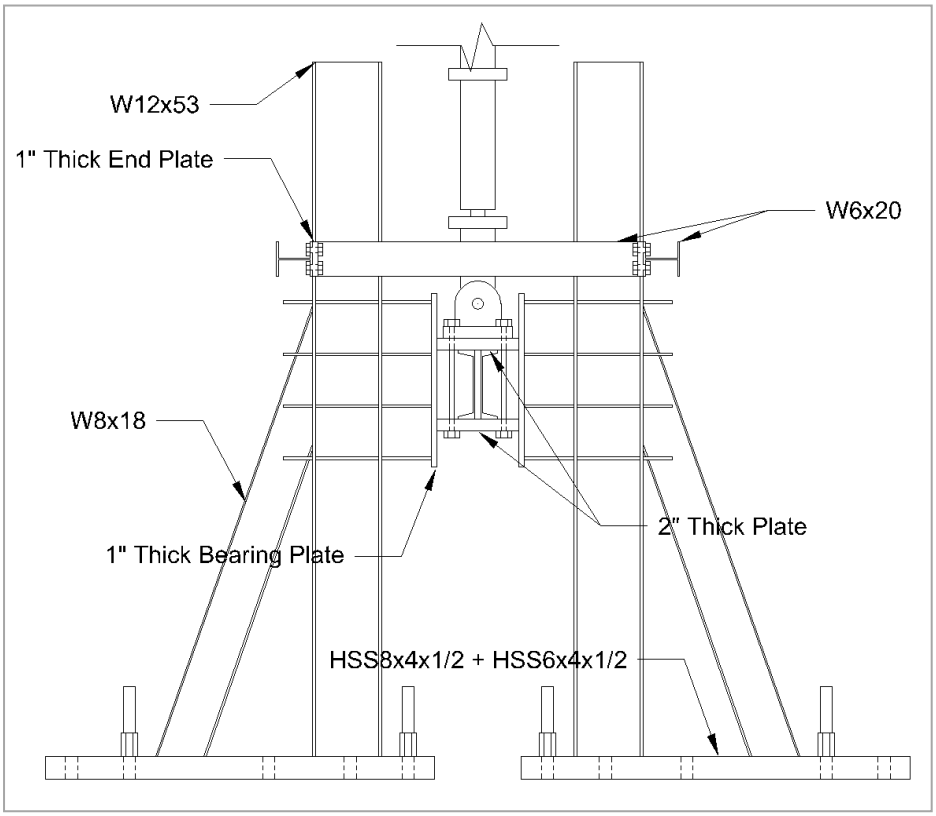
W12x53
1" Thick End Plate
W6x20
W8x18
2" Thick Plate
1" Thick Bearing Plate
HSS8x4x1/2 + HSS6x4x1/2

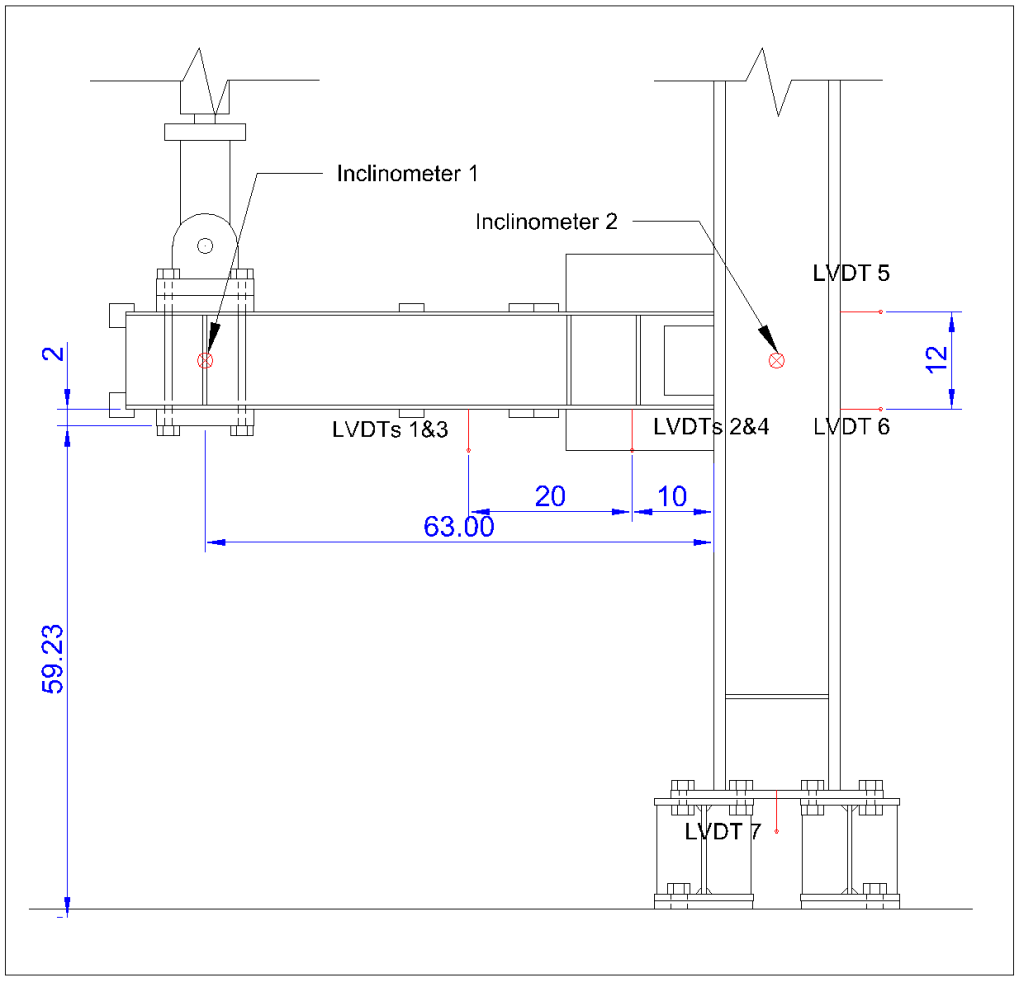
Inclinometer 1
Inclinometer 2
LVDT 5
12
2
LVDTs 1&3
LVDTs 2&4
LVDT 6
20
10
63.00
59.23
LVDT 7

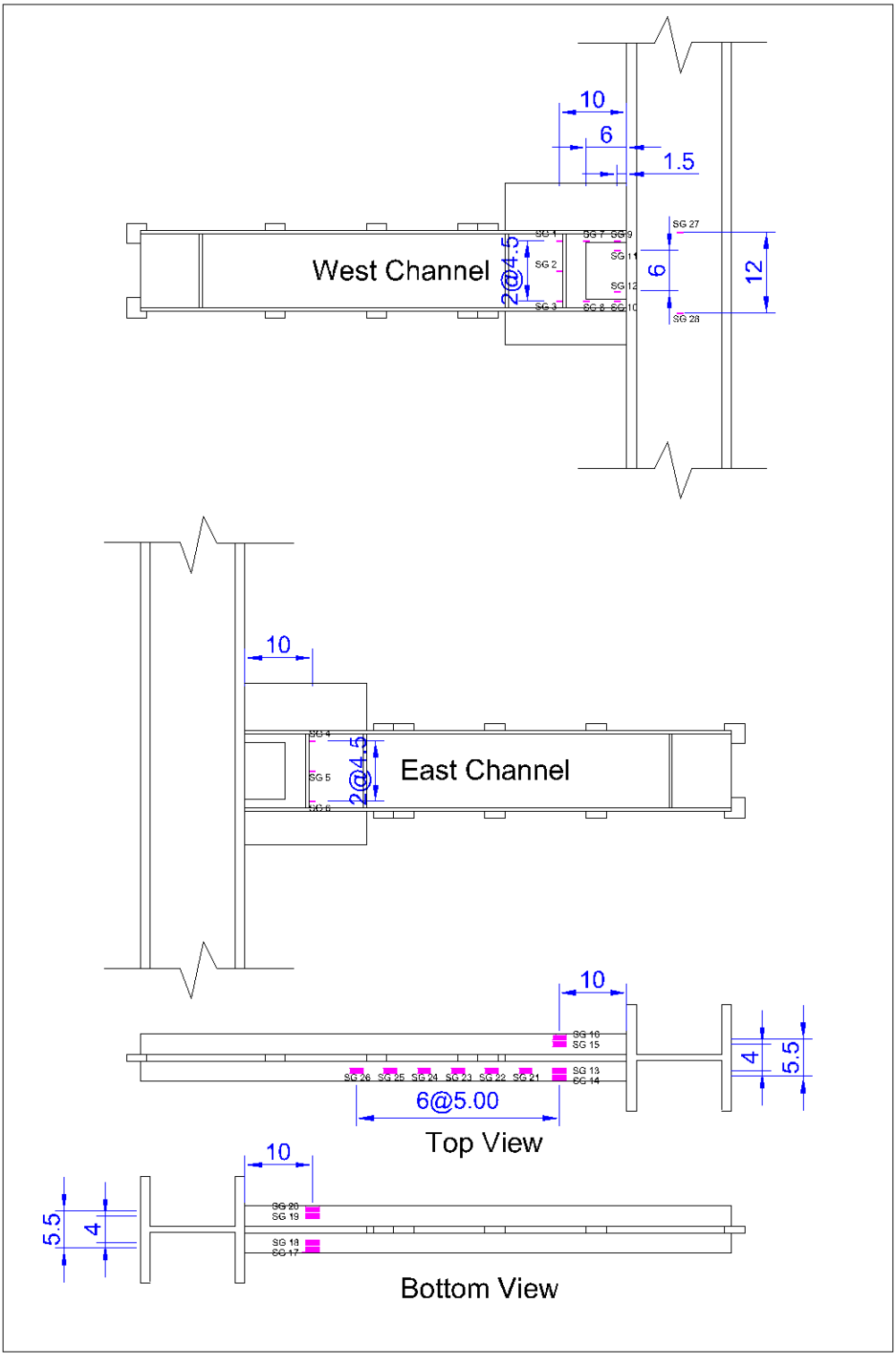
10
6
1.5
West Channel
2@4.5
6
12
10
East Channel
2@4.5
10
4
5.5
6@5.00
Top View
10
5.5
4
Bottom View

Specimen 2C12-4

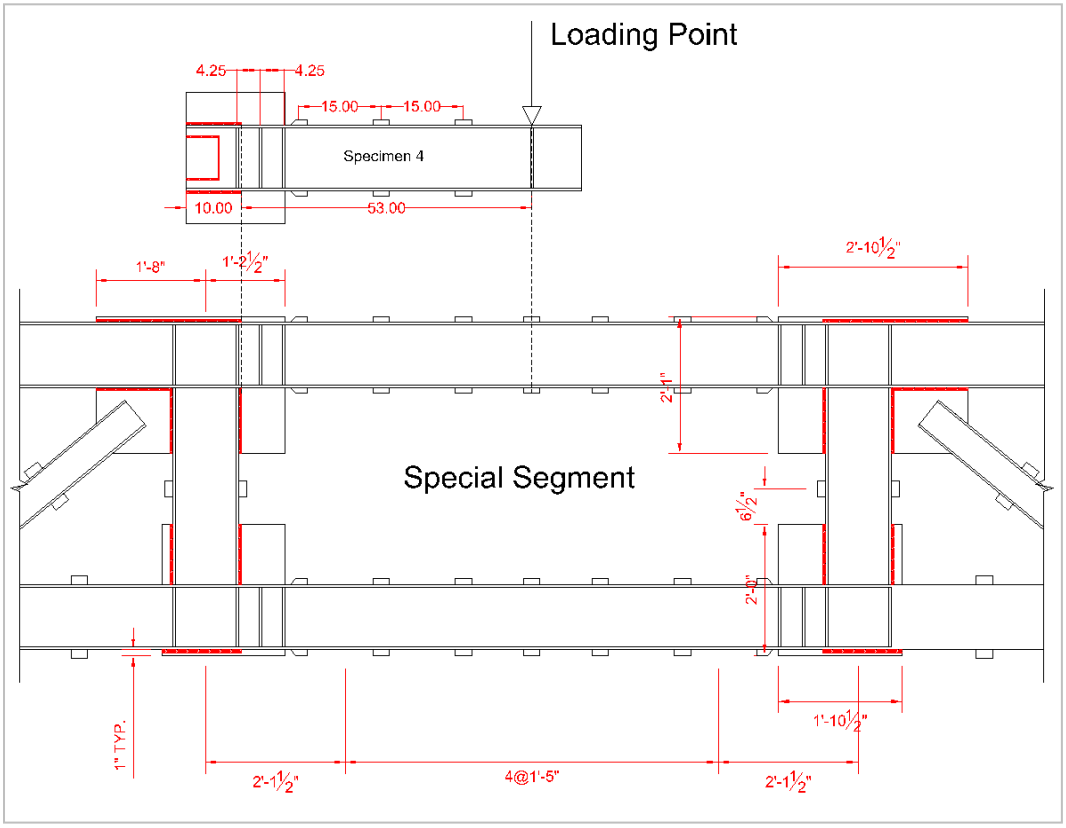

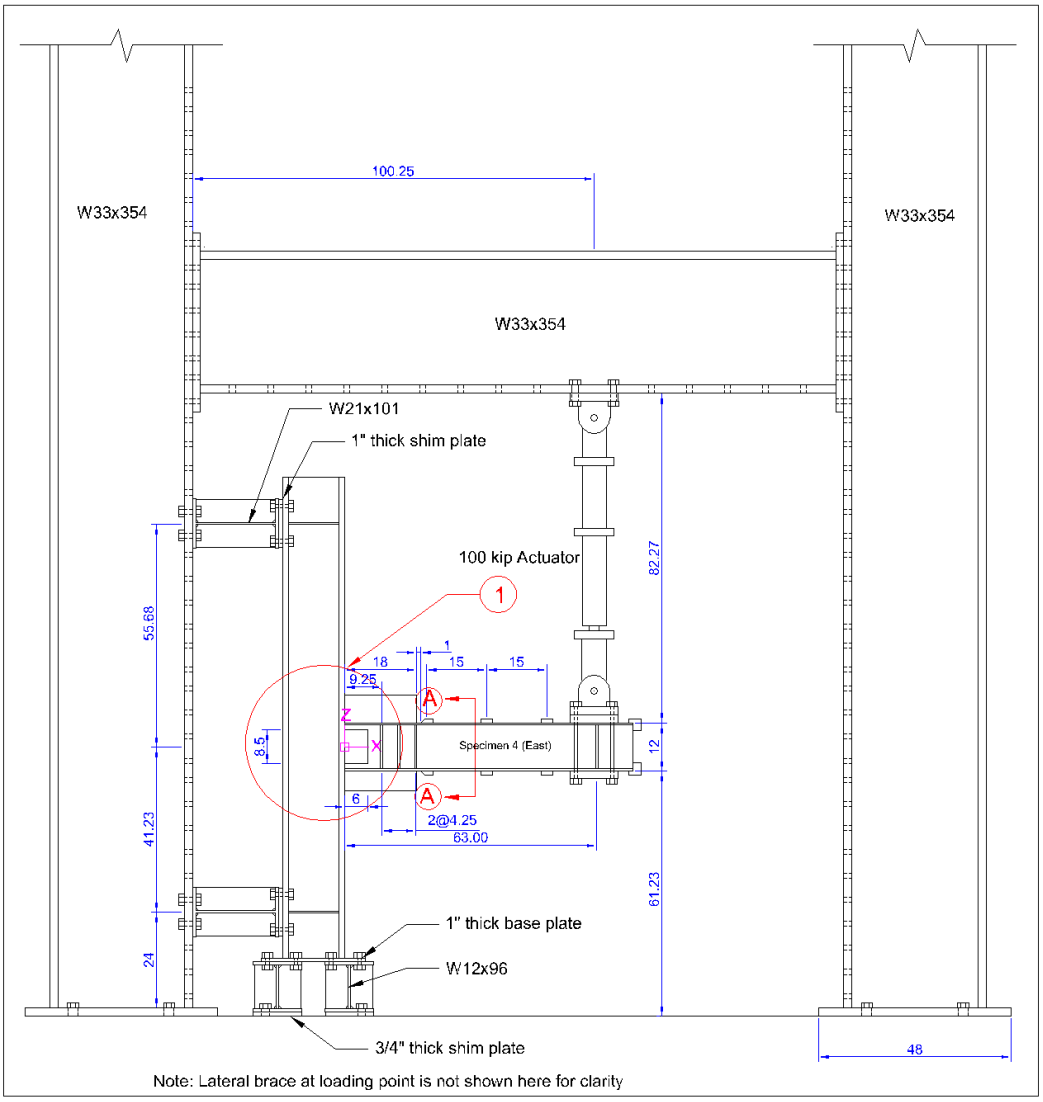
W33x354
100.25
W33x354
W33x354
W21x101
1" thick shim plate
100 kip Actuator
1
82.27
55.68
18
1
15
15
9.25
A
Z
X
8.5
Specimen 4 (East)
12
A
6
2@4.25
63.00
41.23
61.23
1" thick base plate
W12x96
24
3/4" thick shim plate
48
Note: Lateral brace at loading point is not shown here for clarity

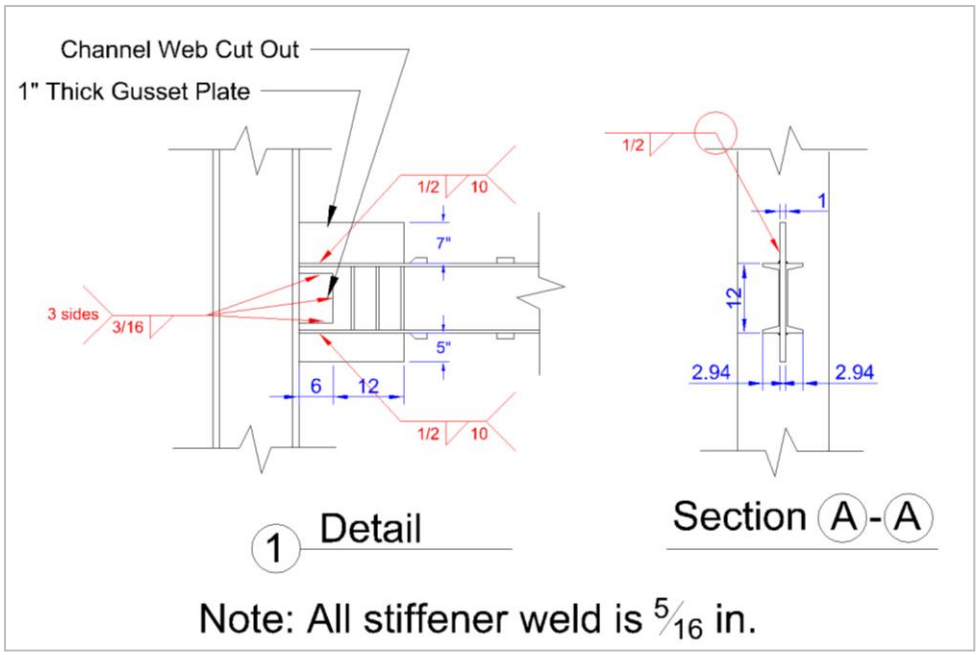
Channel Web Cut Out
1" Thick Gusset Plate
1/2
10
7"
3 sides
3/16
5"
6
12
1/2
10
1/2
1
12
2.94
2.94
1 Detail
Section A-A
Note: All stiffener weld is 5/16 in.

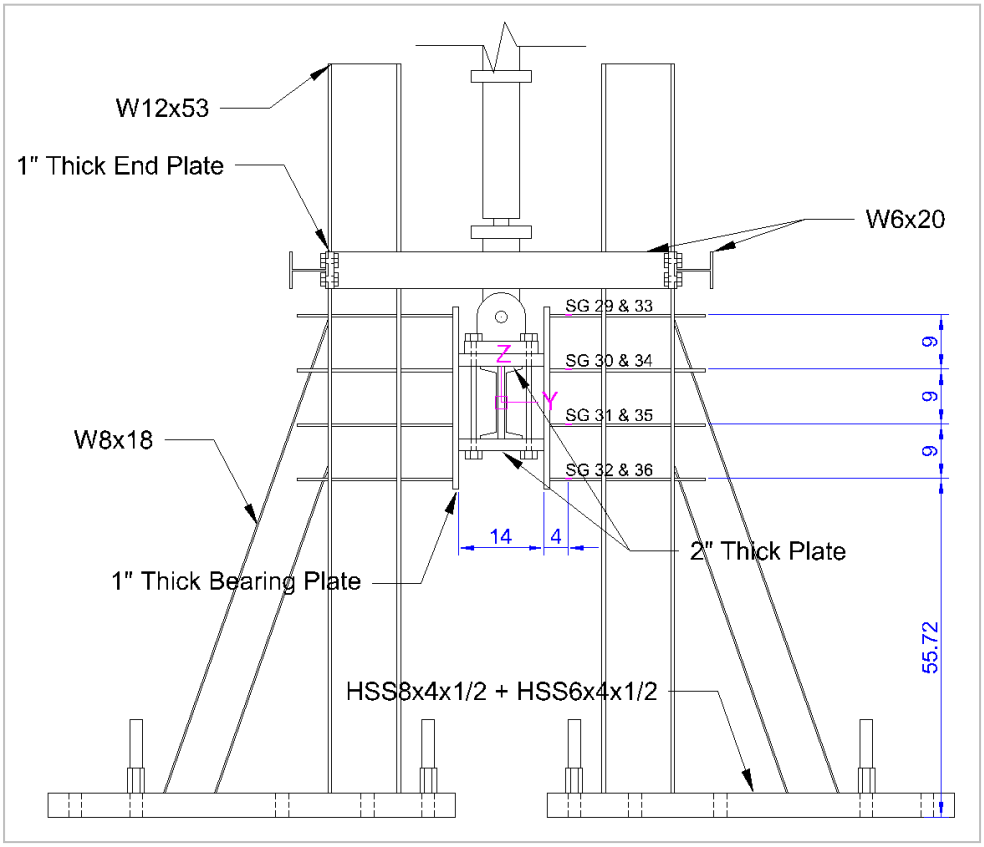
W12x53
1" Thick End Plate
W6x20
SG 29 & 33
SG 30 & 34
SG 31 & 35
SG 32 & 36
9
9
9
W8x18
14
4
2" Thick Plate
1" Thick Bearing Plate
55.72
HSS8x4x1/2 + HSS6x4x1/2

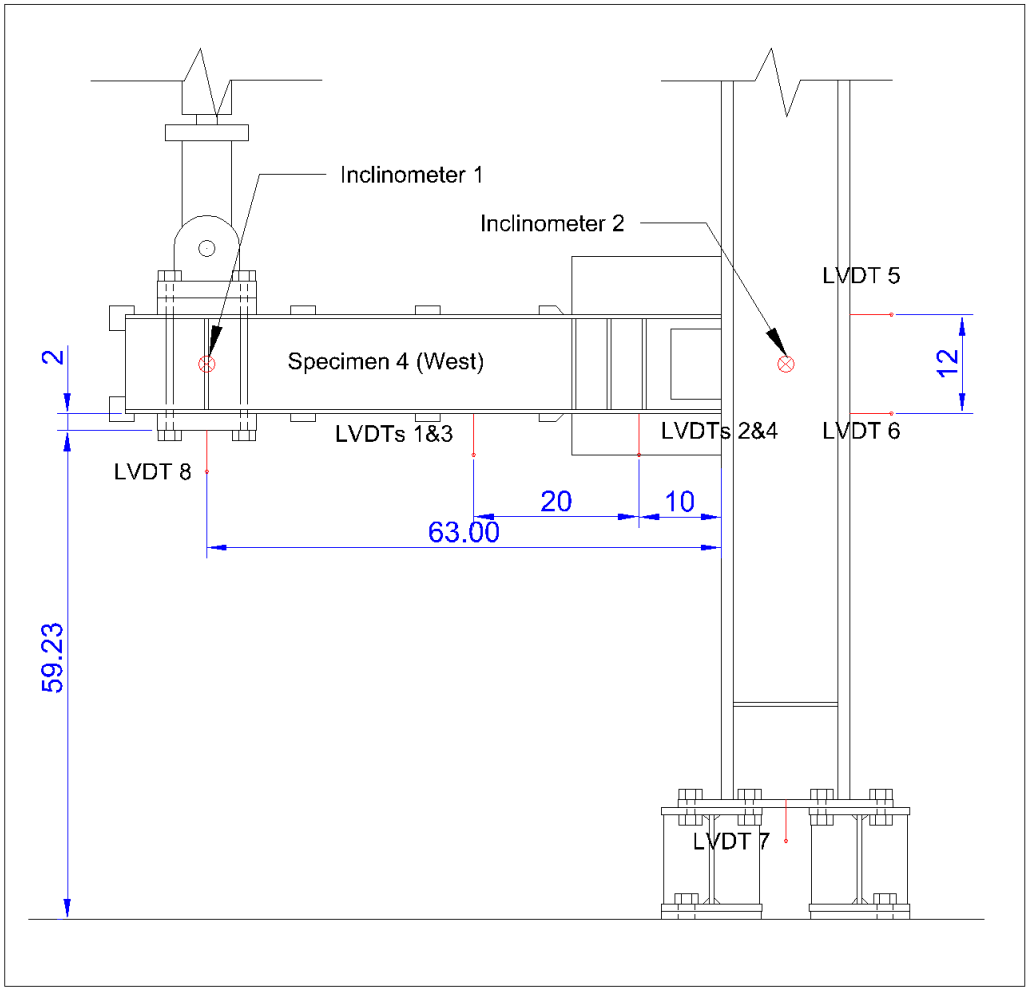
Inclinometer 1
Inclinometer 2
LVDT 5
Specimen 4 (West)
2
12
LVDTs 1&3
LVDTs 2&4
LVDT 6
LVDT 8
20
10
63.00
59.23
LVDT 7

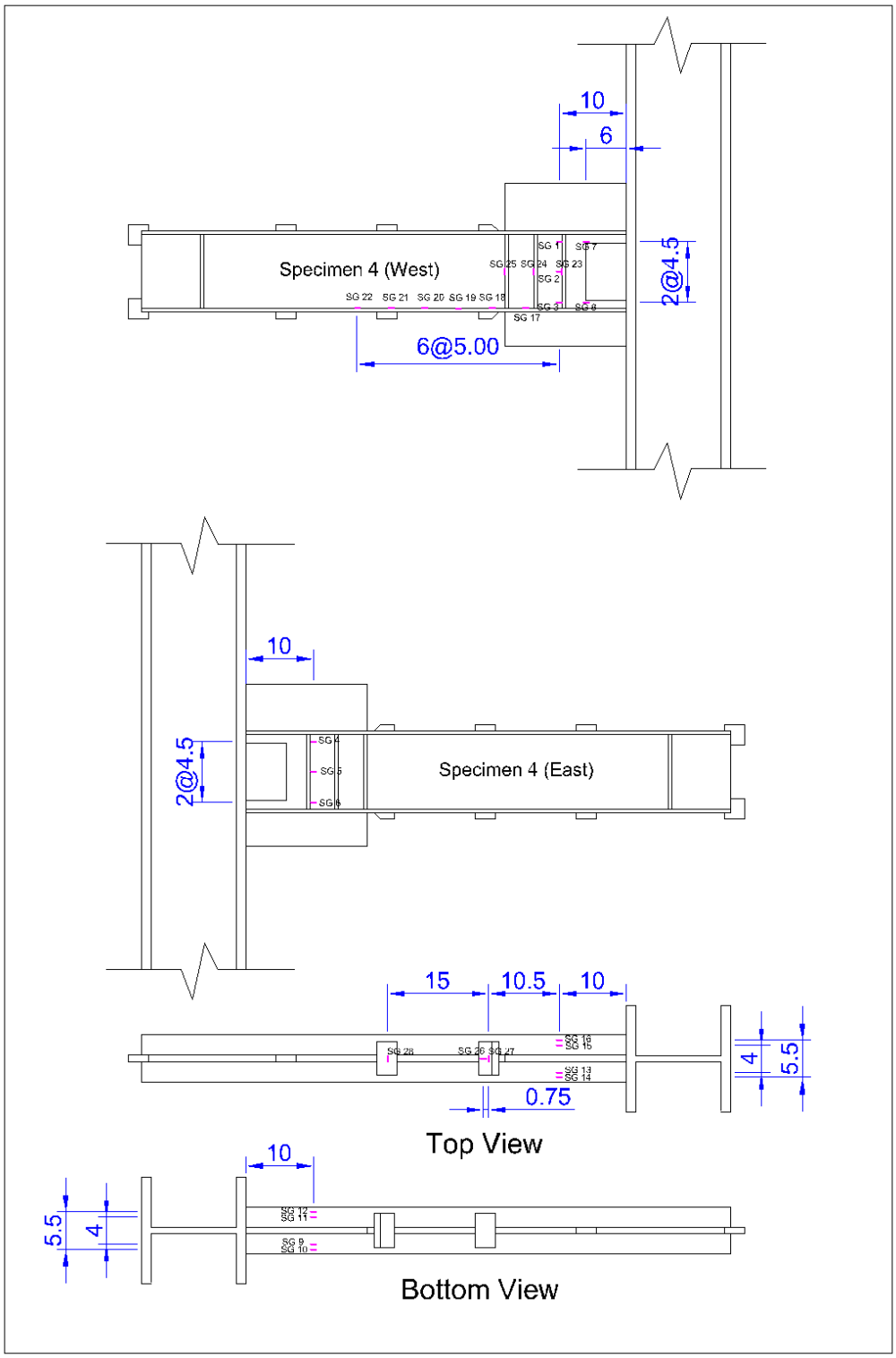
10
6
Specimen 4 (West)
SG 1
SG 7
SG 25
SG 24
SG 23
SG 2
SG 22
SG 21
SG 20
SG 19
SG 18
SG 3
SG 8
SG 17
2@4.5
6@5.00
10
2@4.5
Specimen 4 (East)
15
10.5
10
SG 28
SG 26
SG 27
SG 16
SG 15
SG 13
SG 14
4
5.5
0.75
Top View
10
5.5
4
SG 12
SG 11
SG 9
SG 10
Bottom View

Specimen 2C12-5

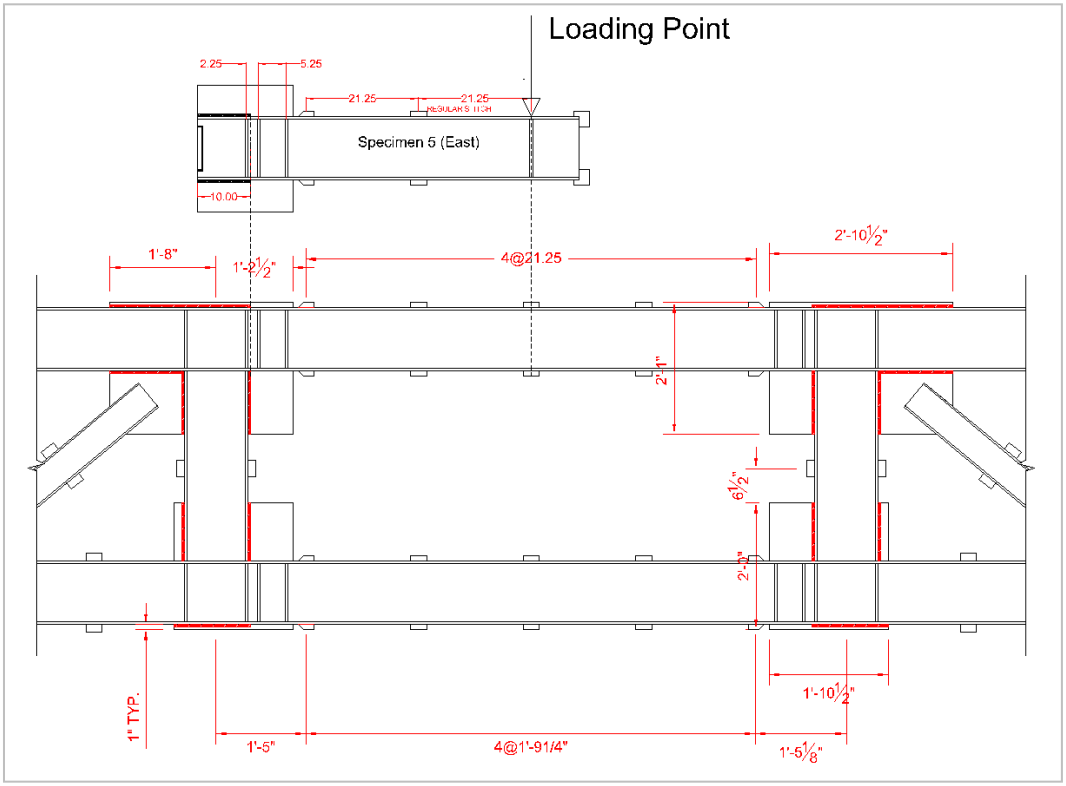

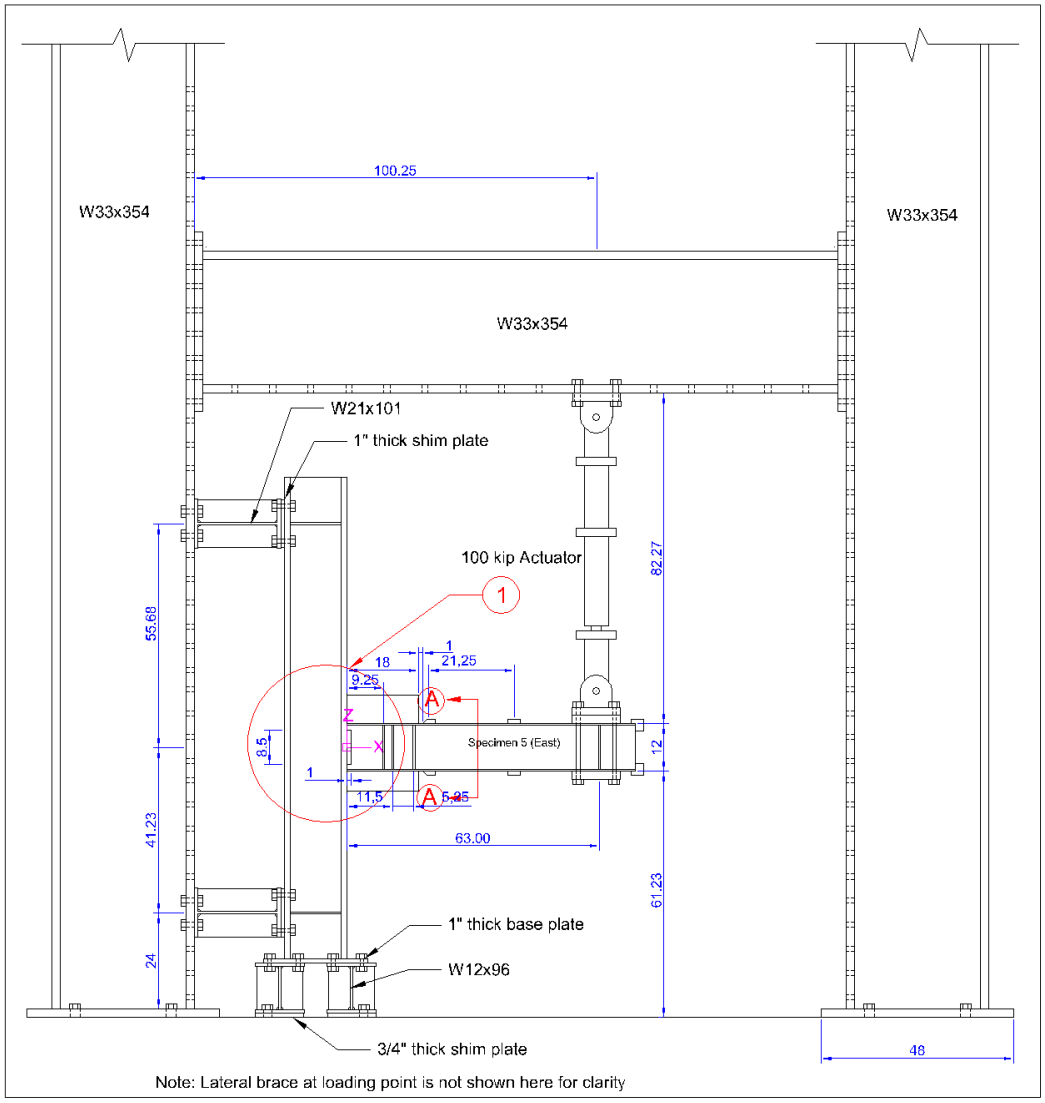
W33x354
100.25
W33x354
W33x354
W21x101
1" thick shim plate
100 kip Actuator
1
82.27
55.68
18
1
21.25
9.25
A
Z
X
8.5
Specimen 5 (East)
12
1
11.5
A
5.25
63.00
41.23
61.23
1" thick base plate
W12x96
24
3/4" thick shim plate
48
Note: Lateral brace at loading point is not shown here for clarity

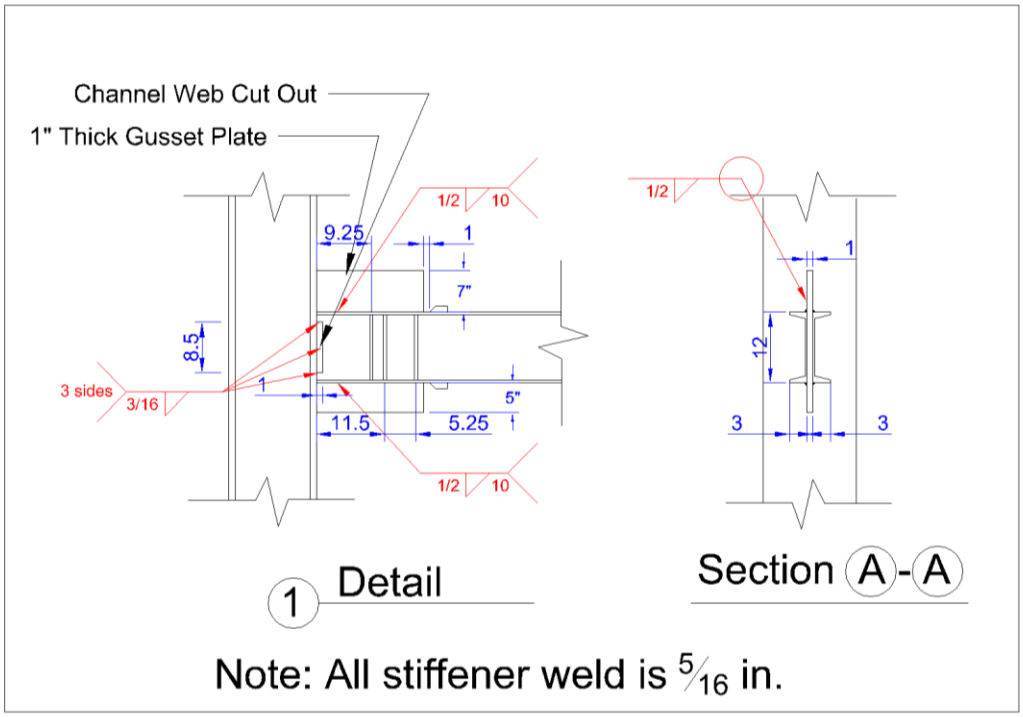
Channel Web Cut Out
1" Thick Gusset Plate
9.25
1
7"
8.5
3 sides
3/16
1
5"
11.5
5.25
1/2
10
1/2
10
1/2
1
12
3
3
1 Detail
Section A-A
Note: All stiffener weld is 5/16 in.

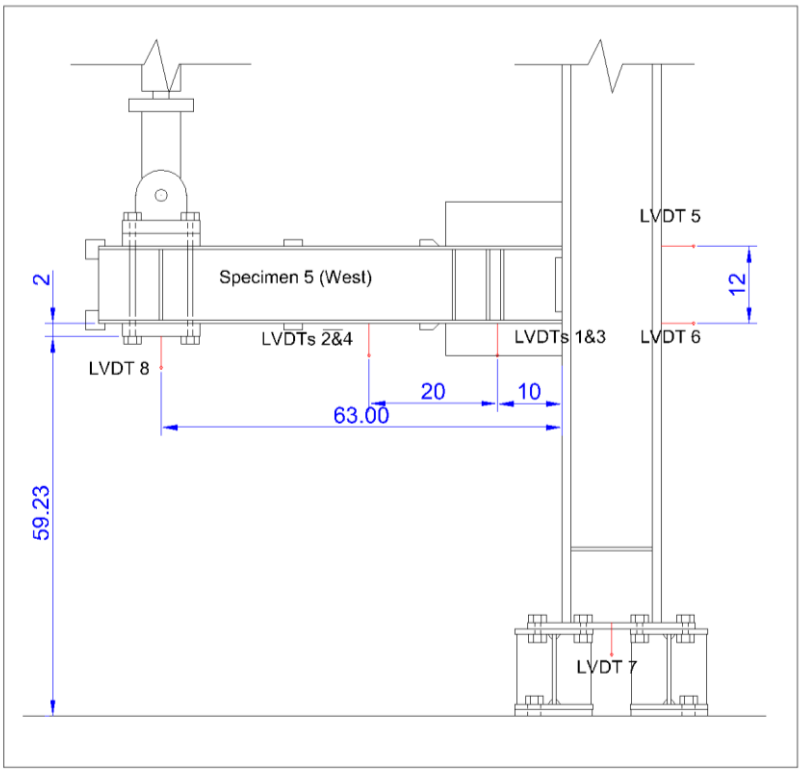
Specimen 5 (West)
LVDT 5
12
2
LVDTs 2&4
LVDTs 1&3
LVDT 6
LVDT 8
20
10
63.00
59.23
LVDT 7

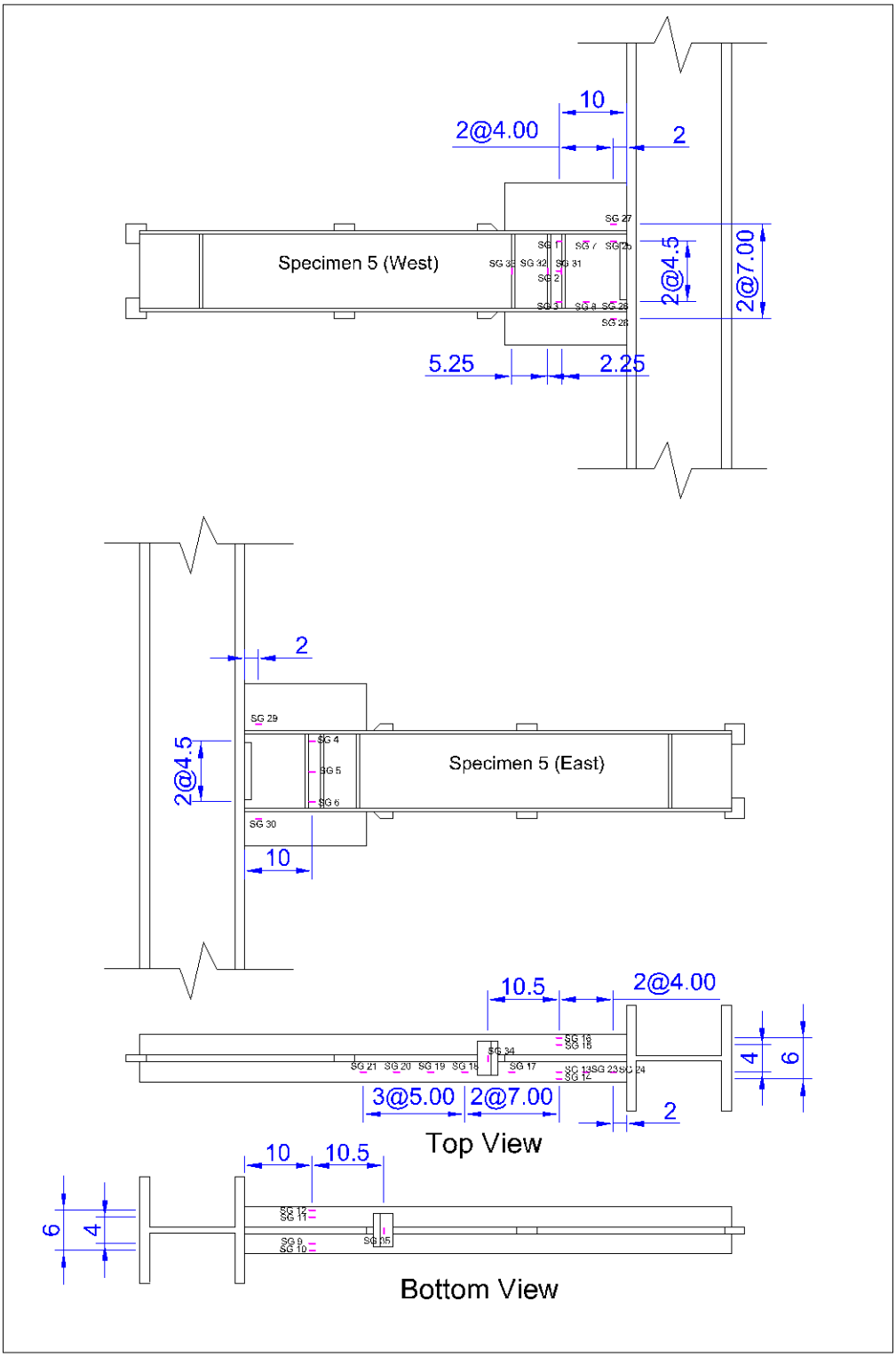
10
2@4.00
2
SG 27
Specimen 5 (West)
SG 32
SG 31
SG 2
SG 8
SG 28
SG 26
2@4.5
2@7.00
5.25
2.25
2
SG 29
SG 4
SG 5
SG 6
Specimen 5 (East)
SG 30
2@4.5
10
10.5
2@4.00
SG 34
SG 21
SG 20
SG 19
SG 18
SG 17
SG 24
4
6
3@5.00
2@7.00
2
Top View
10
10.5
SG 12
SG 11
SG 9
SG 10
SG 35
6
4
Bottom View

Specimen 2C12-6

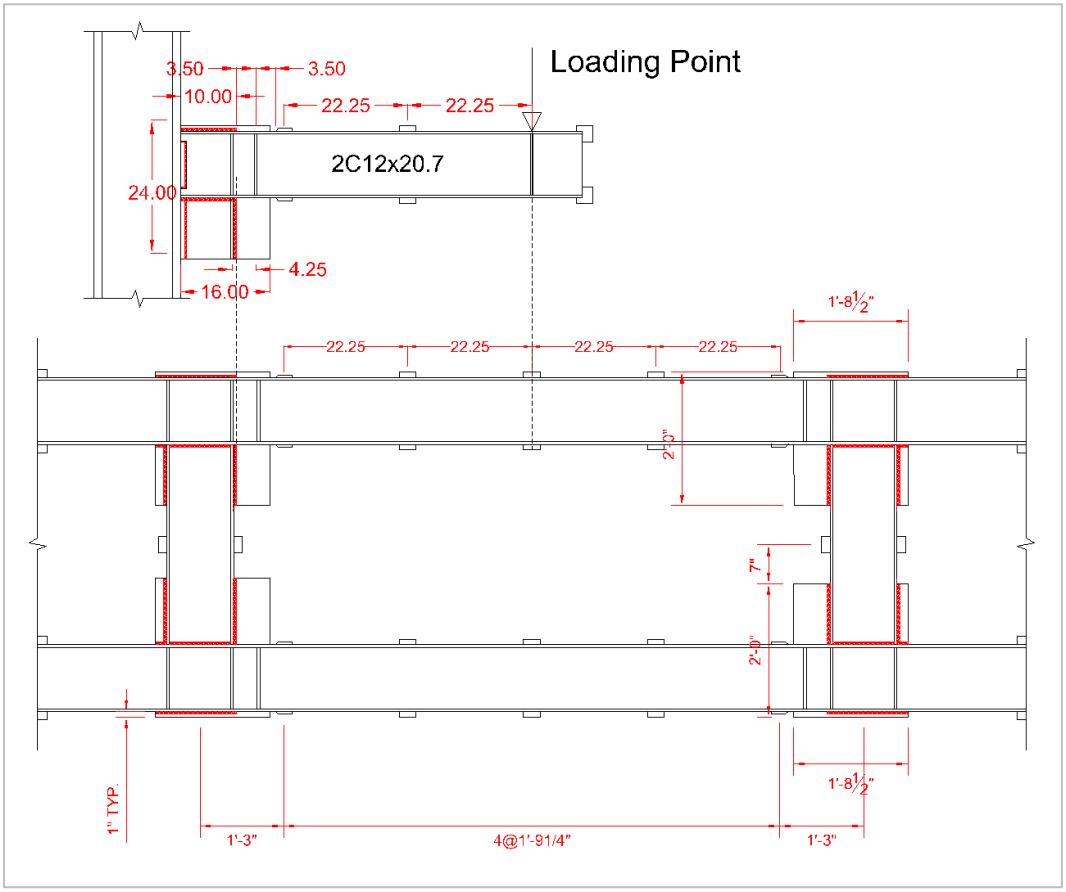

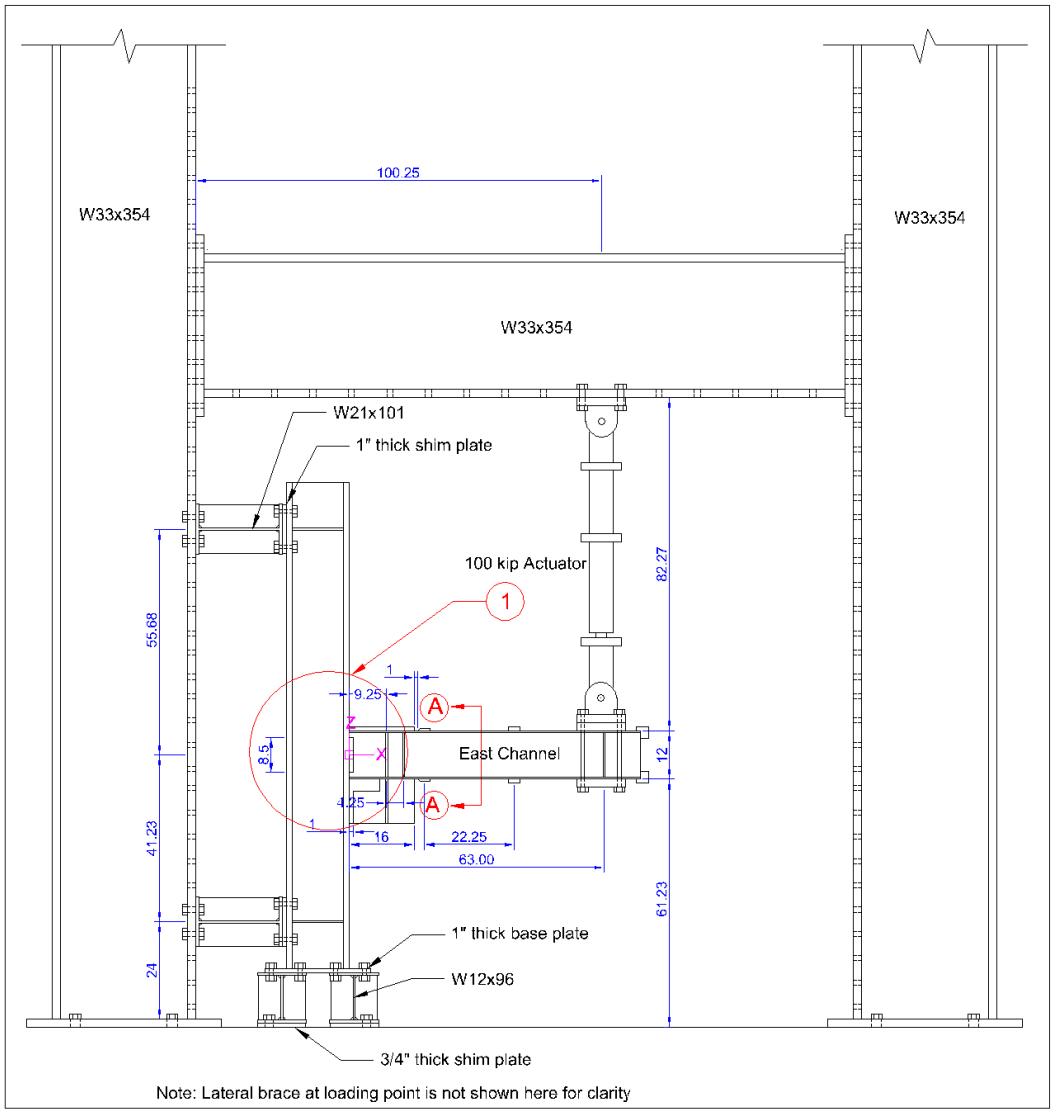
100.25
W33x354
W33x354
W33x354
W21x101
1" thick shim plate
100 kip Actuator
1
82.27
55.68
1
9.25
A
8.5
East Channel
12
4.25
A
1
16
22.25
63.00
41.23
61.23
1" thick base plate
24
W12x96
3/4" thick shim plate
Note: Lateral brace at loading point is not shown here for clarity

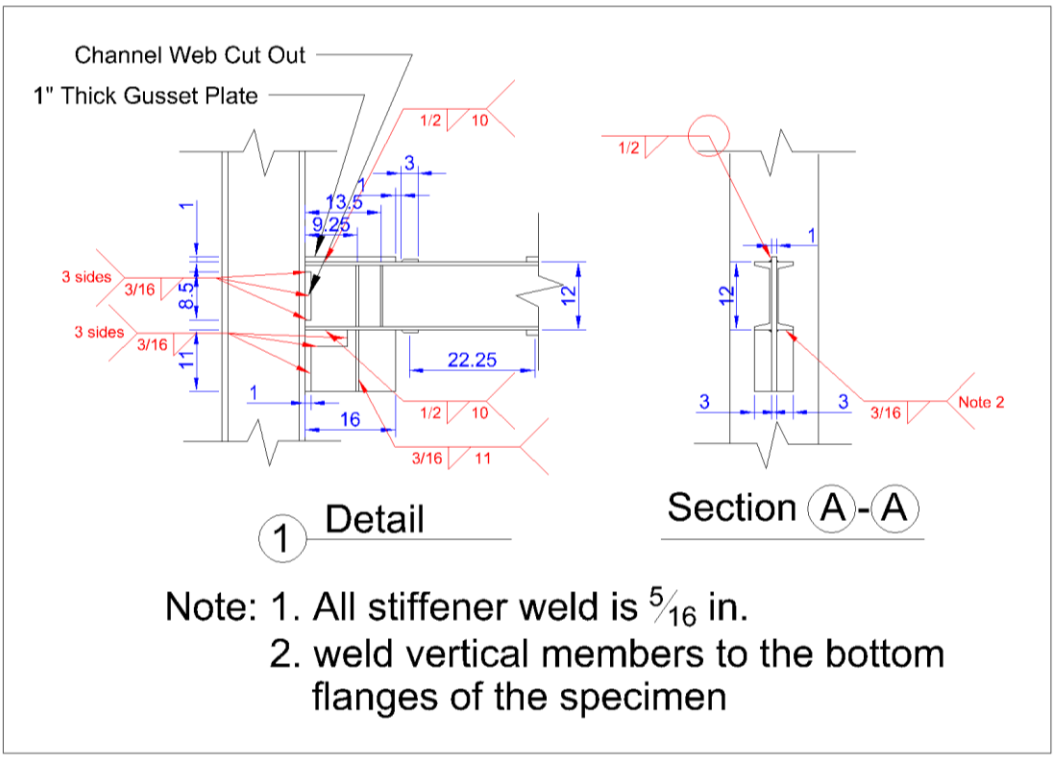
Channel Web Cut Out
1" Thick Gusset Plate
1/2
10
3
1
13.5
9.25
1
3 sides
3/16
8.5
3 sides
3/16
11
12
22.25
1
16
1/2
10
3/16
11
1/2
1
12
3
3
3/16
Note 2
1 Detail
Section A-A
Note: 1. All stiffener weld is 5/16 in.
2. weld vertical members to the bottom flanges of the specimen

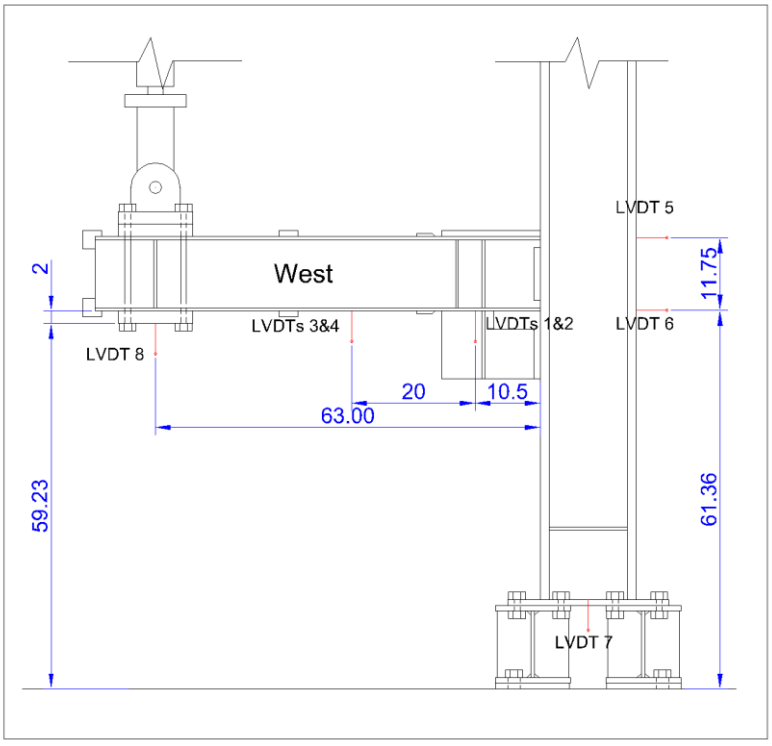
LVDT 5
11.75
West
2
LVDTs 3&4
LVDTs 1&2
LVDT 6
LVDT 8
20
10.5
63.00
59.23
61.36
LVDT 7

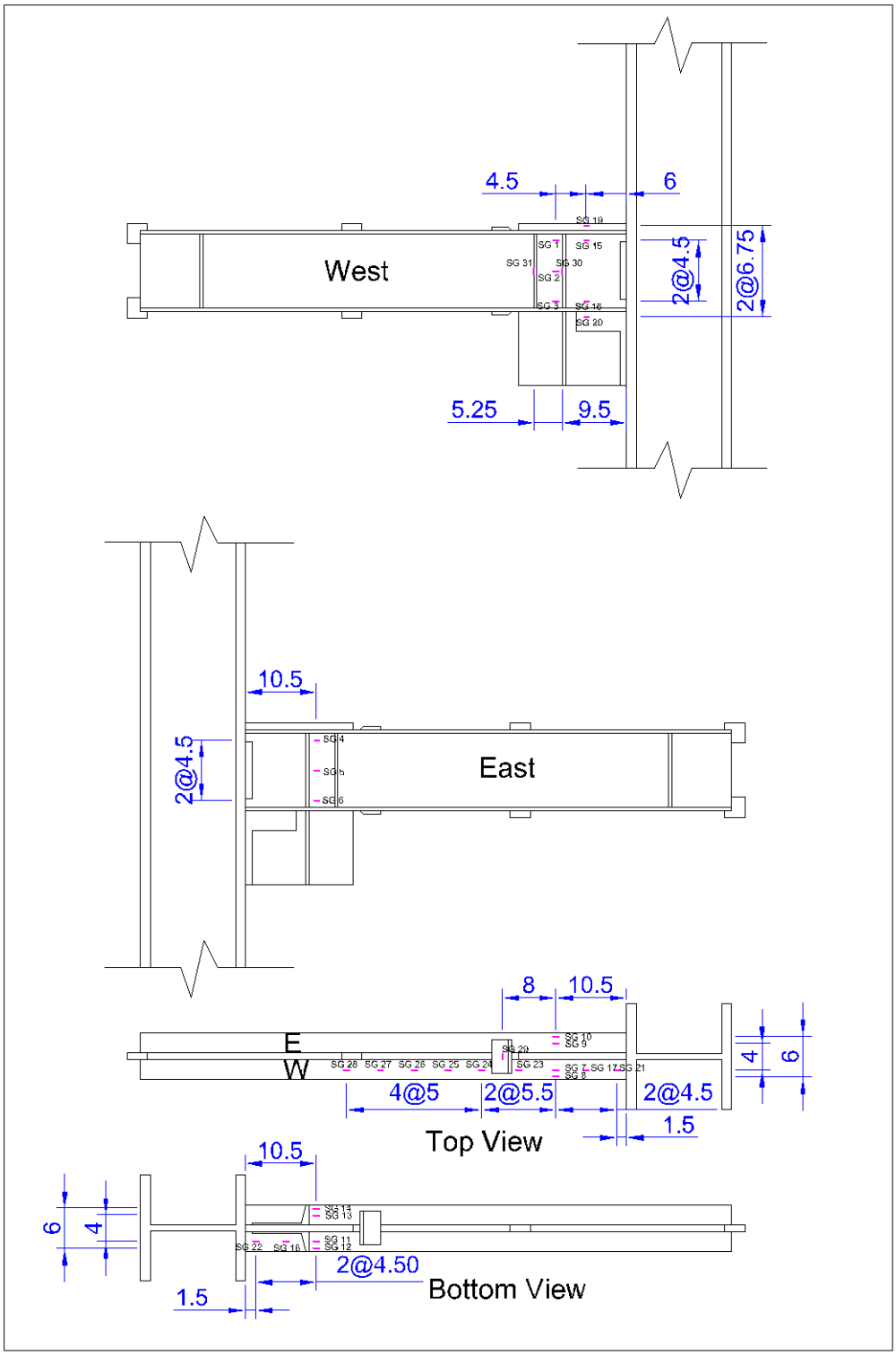
4.5
6
West
2@4.5
2@6.75
5.25
9.5
10.5
East
2@4.5
8
10.5
E
W
4
6
4@5
2@5.5
2@4.5
1.5
Top View
10.5
6
4
2@4.50
1.5
Bottom View

Specimen 2C12-7

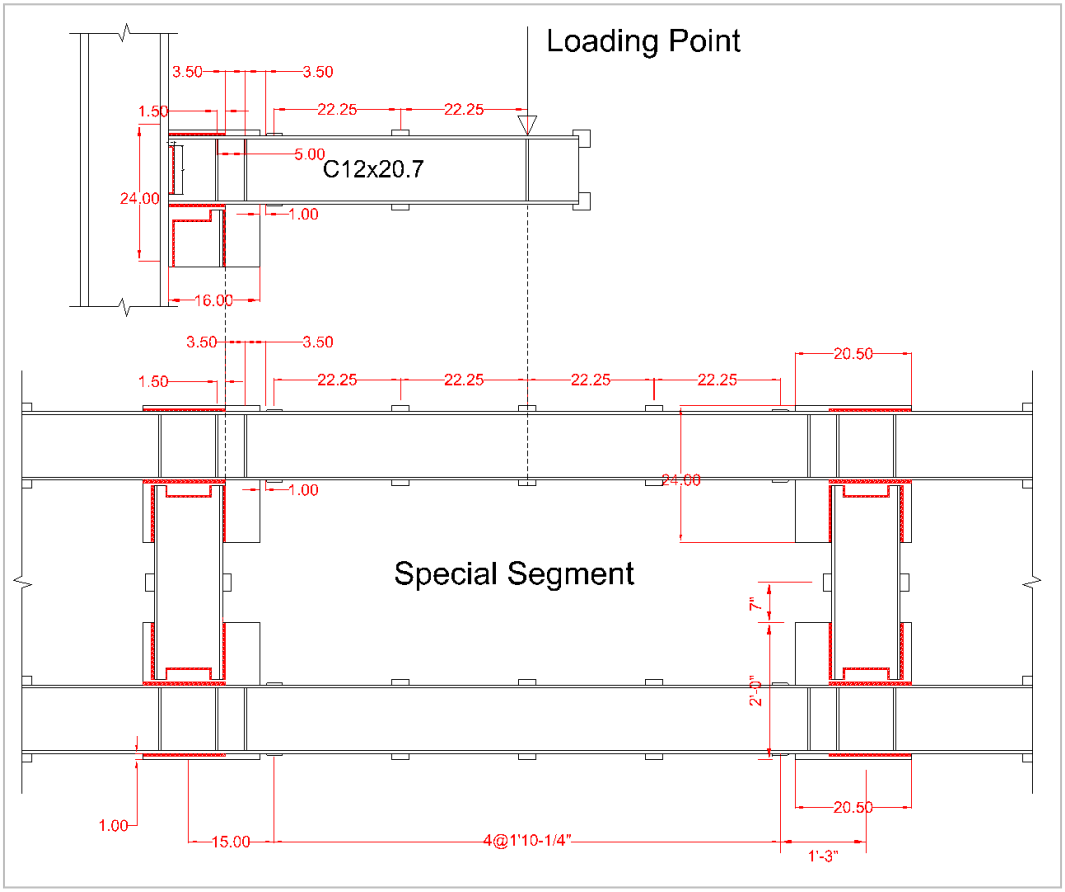

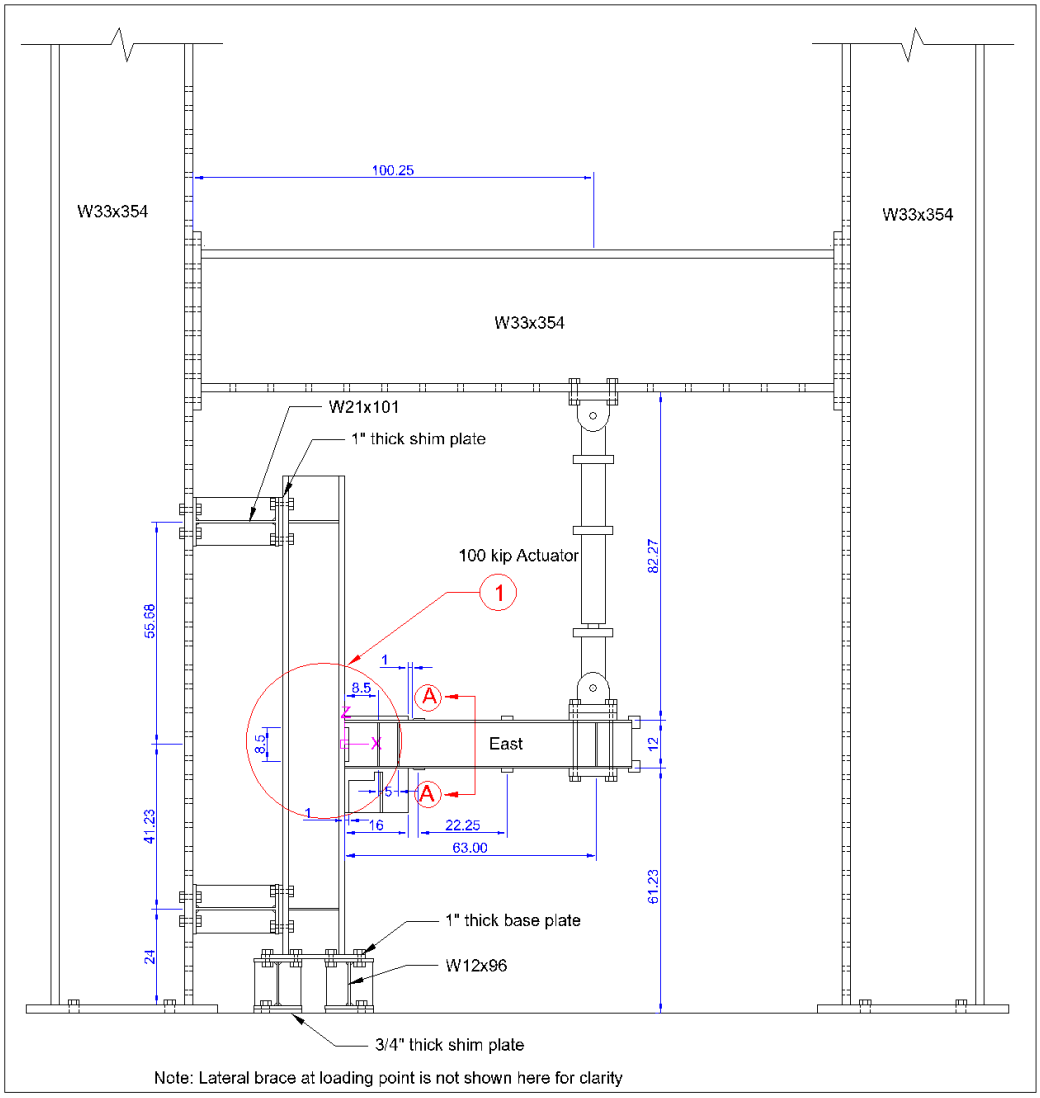
W33x354
100.25
W33x354
W33x354
W21x101
1" thick shim plate
100 kip Actuator
1
82.27
55.68
1
8.5
A
8.5
East
12
5
A
41.23
1
16
22.25
63.00
61.23
1" thick base plate
W12x96
24
3/4" thick shim plate
Note: Lateral brace at loading point is not shown here for clarity

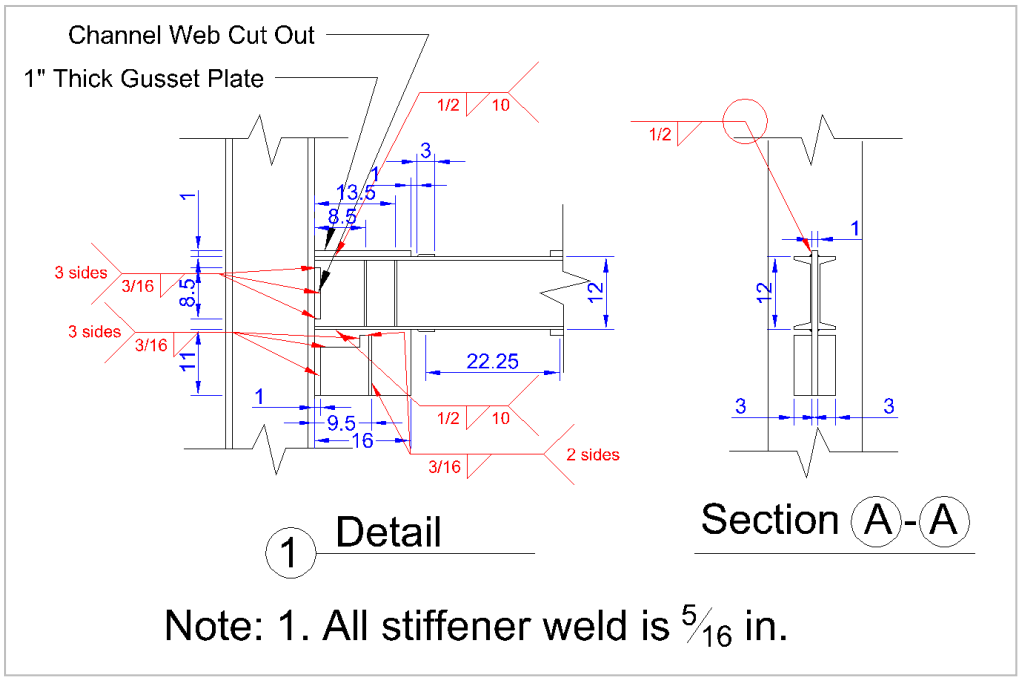
Channel Web Cut Out
1" Thick Gusset Plate
1/2
10
3
1
13.5
8.5
1
3 sides
3/16
8.5
3 sides
3/16
11
12
22.25
1
9.5
16
1/2
10
3/16
2 sides
1/2
1
12
3
3
1 Detail
Section A-A
Note: 1. All stiffener weld is 5/16 in.

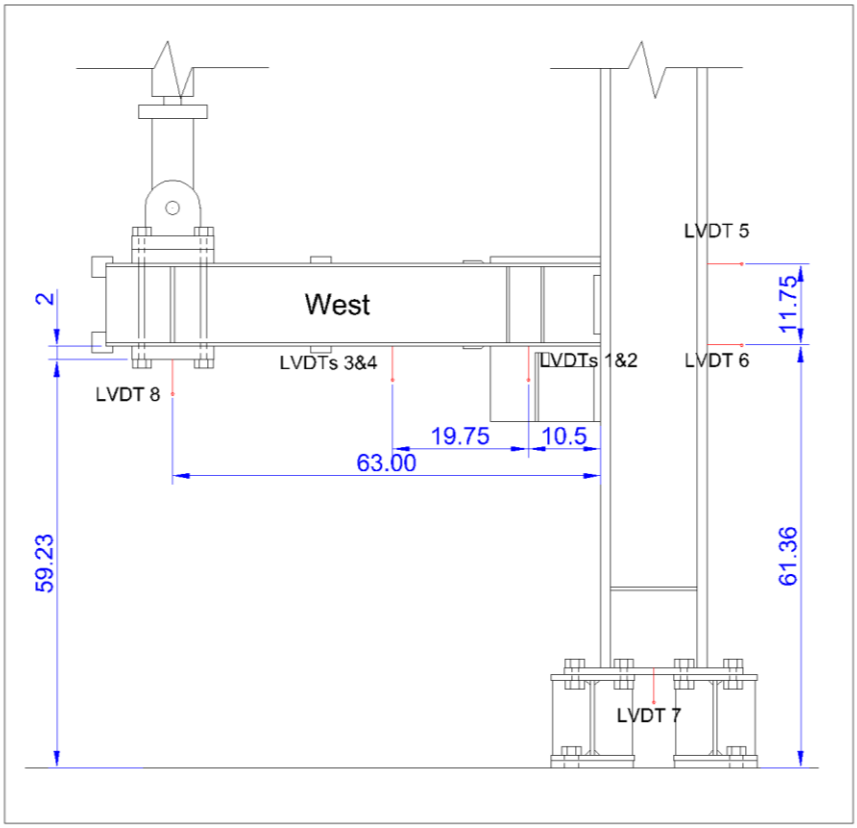
LVDT 5
11.75
West
2
LVDTs 3&4
LVDTs 1&2
LVDT 6
LVDT 8
19.75
10.5
63.00
59.23
61.36
LVDT 7

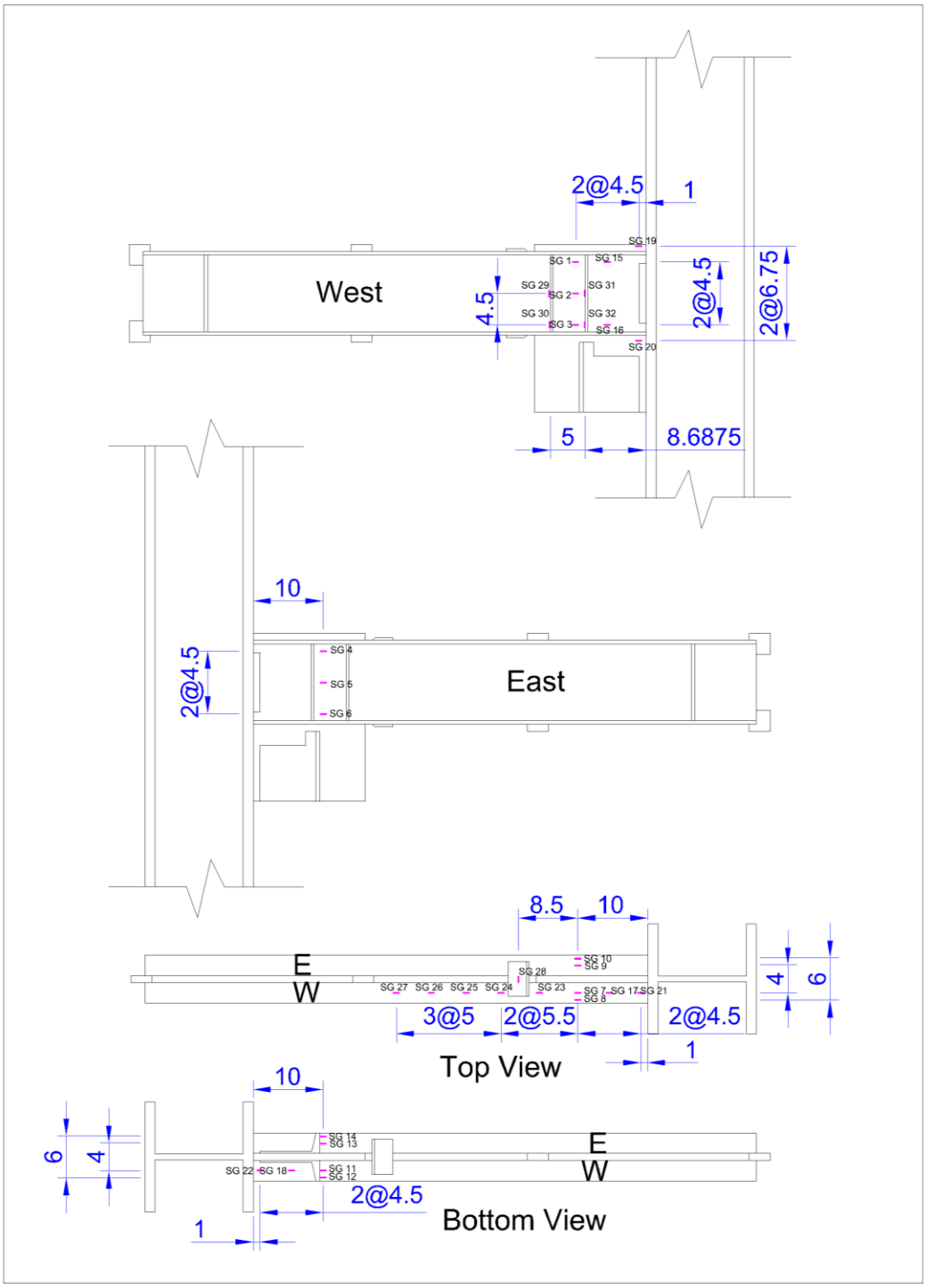
2@4.5
1
SG 19
SG 1
SG 15
West
SG 29
SG 2
SG 31
SG 30
SG 3
SG 32
SG 16
SG 20
4.5
2@4.5
2@6.75
5
8.6875
10
2@4.5
SG 4
SG 5
SG 6
East
8.5
10
E
W
SG 10
SG 9
SG 28
SG 27
SG 26
SG 25
SG 24
SG 23
SG 7
SG 17
SG 21
SG 8
4
6
3@5
2@5.5
2@4.5
1
Top View
10
6
4
SG 14
SG 13
E
W
SG 22
SG 18
SG 11
SG 12
2@4.5
1
Bottom View

Specimen 2C12-8

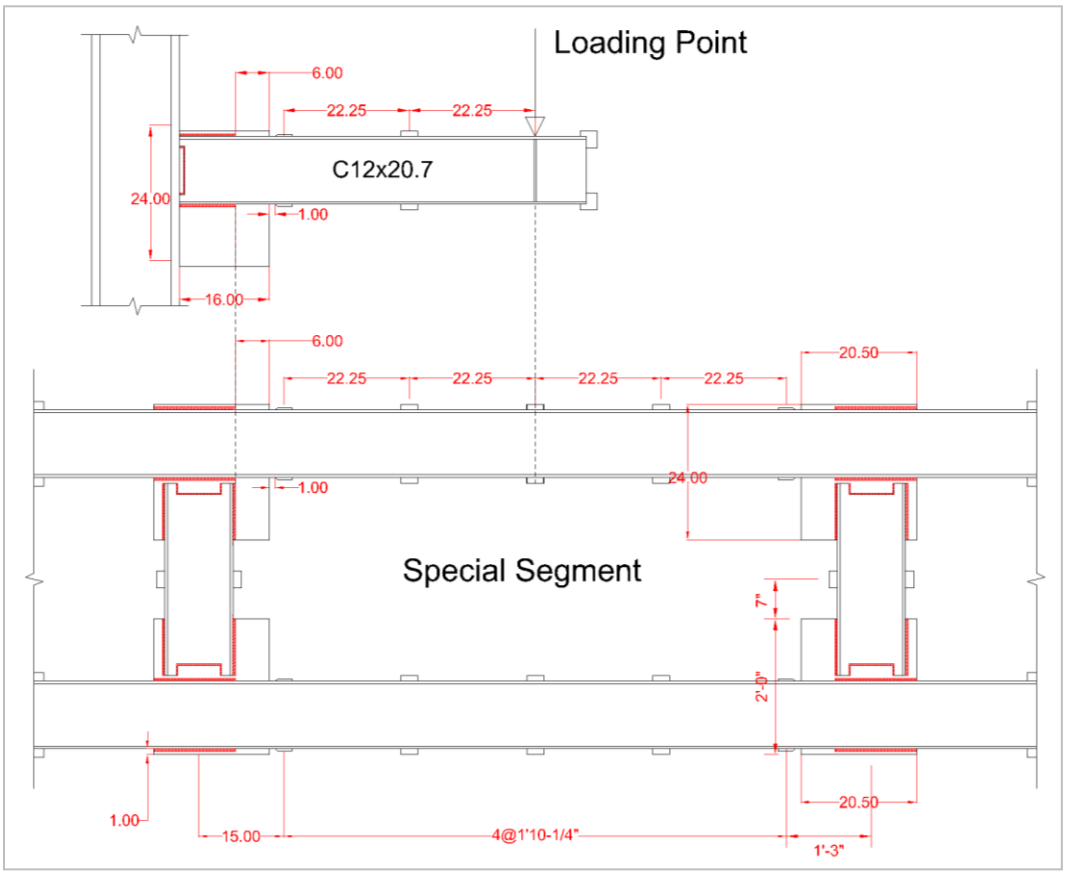

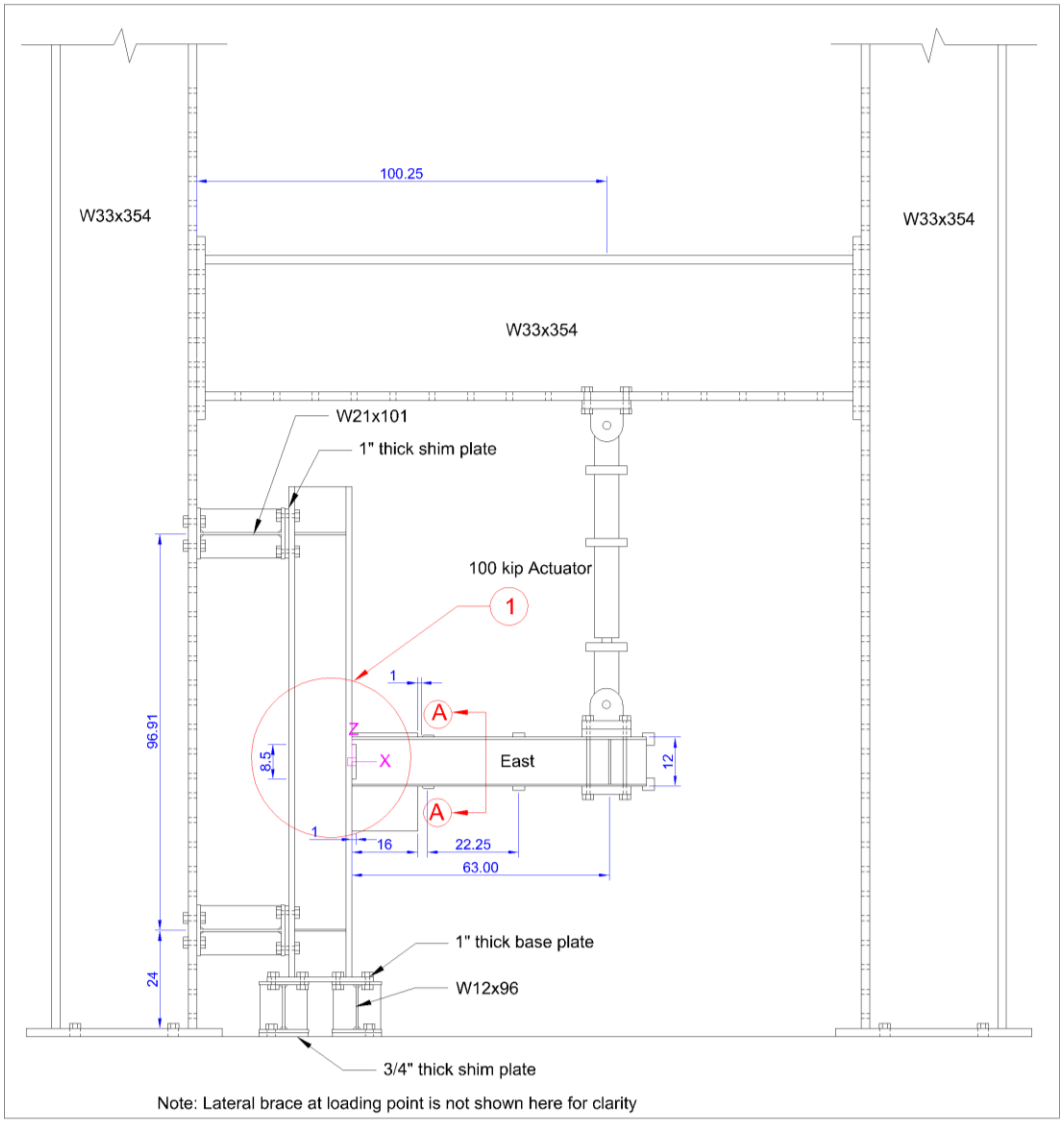
100.25
W33x354
W33x354
W33x354
W21x101
1" thick shim plate
100 kip Actuator
1
1
A
Z
X
East
12
8.5
A
1
16
22.25
63.00
96.91
24
1" thick base plate
W12x96
3/4" thick shim plate
Note: Lateral brace at loading point is not shown here for clarity

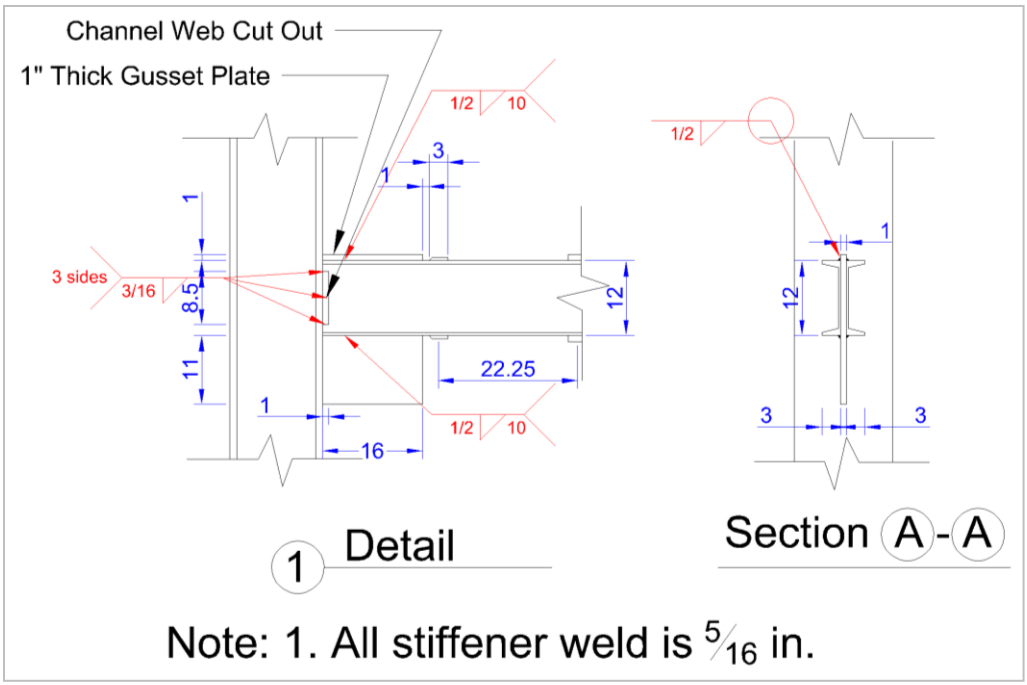
Channel Web Cut Out
1" Thick Gusset Plate
1/2
10
3
1
1
3 sides
3/16
8.5
11
12
22.25
1
16
1/2
10
1/2
1
12
3
3
1 Detail
Section A-A
Note: 1. All stiffener weld is 5/16 in.

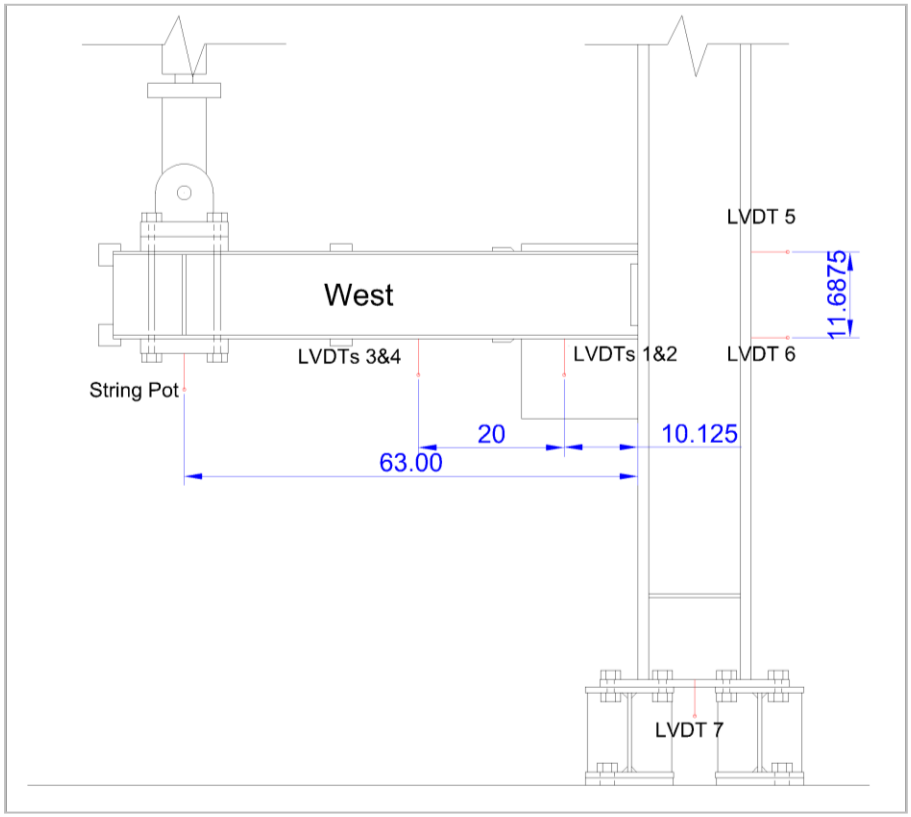
West
LVDT 5
11.6875
LVDTs 3&4
LVDTs 1&2
LVDT 6
String Pot
20
10.125
63.00
LVDT 7

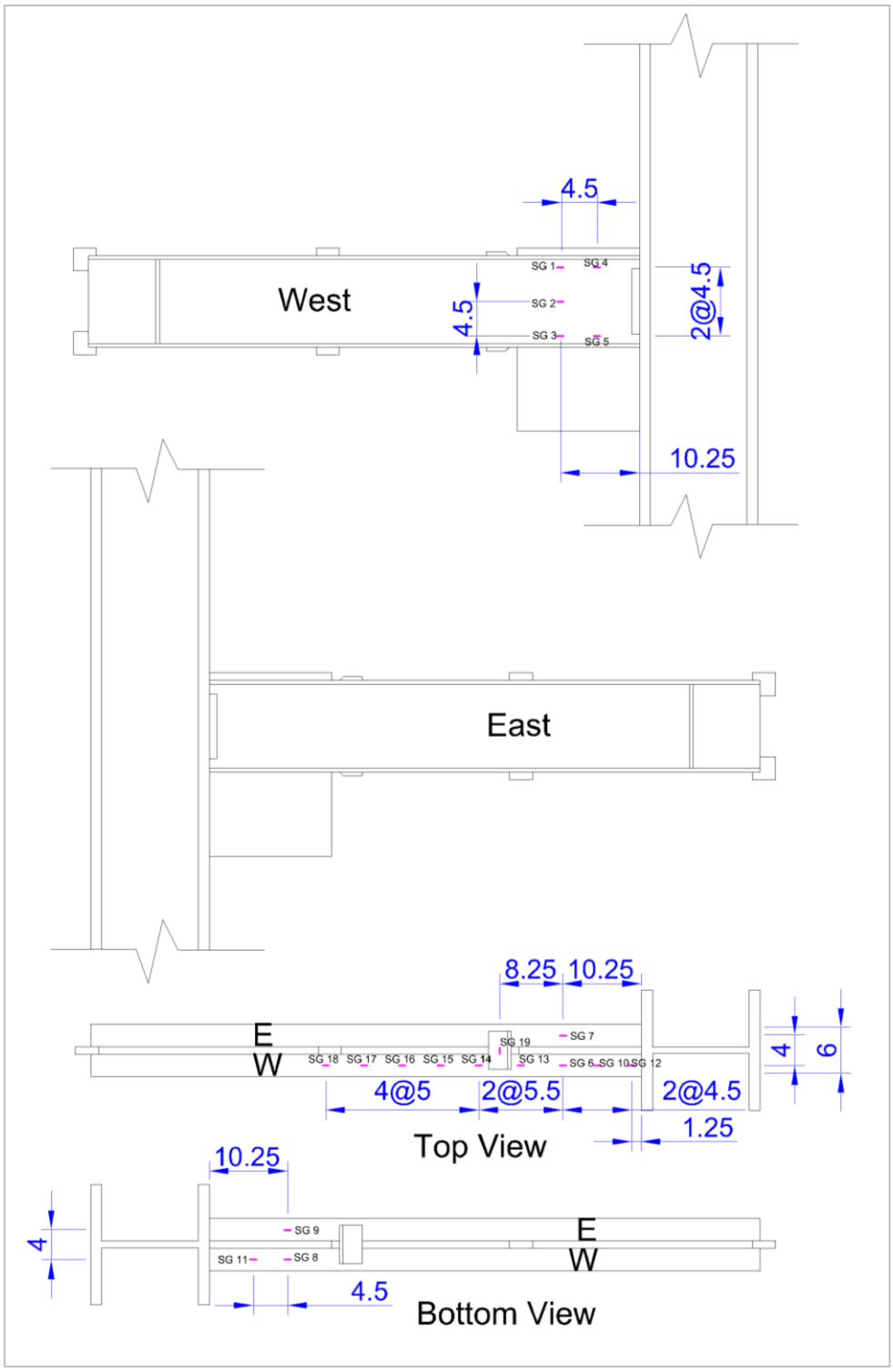
4.5
West
SG 1
SG 4
SG 2
SG 3
SG 5
4.5
2@4.5
10.25
East
8.25
10.25
E
W
SG 19
SG 7
SG 18
SG 17
SG 16
SG 15
SG 14
SG 13
SG 6
SG 10
SG 12
4@5
2@5.5
2@4.5
4
6
1.25
Top View
10.25
4
SG 9
SG 11
SG 8
E
W
4.5
Bottom View

Specimen 2C12-9

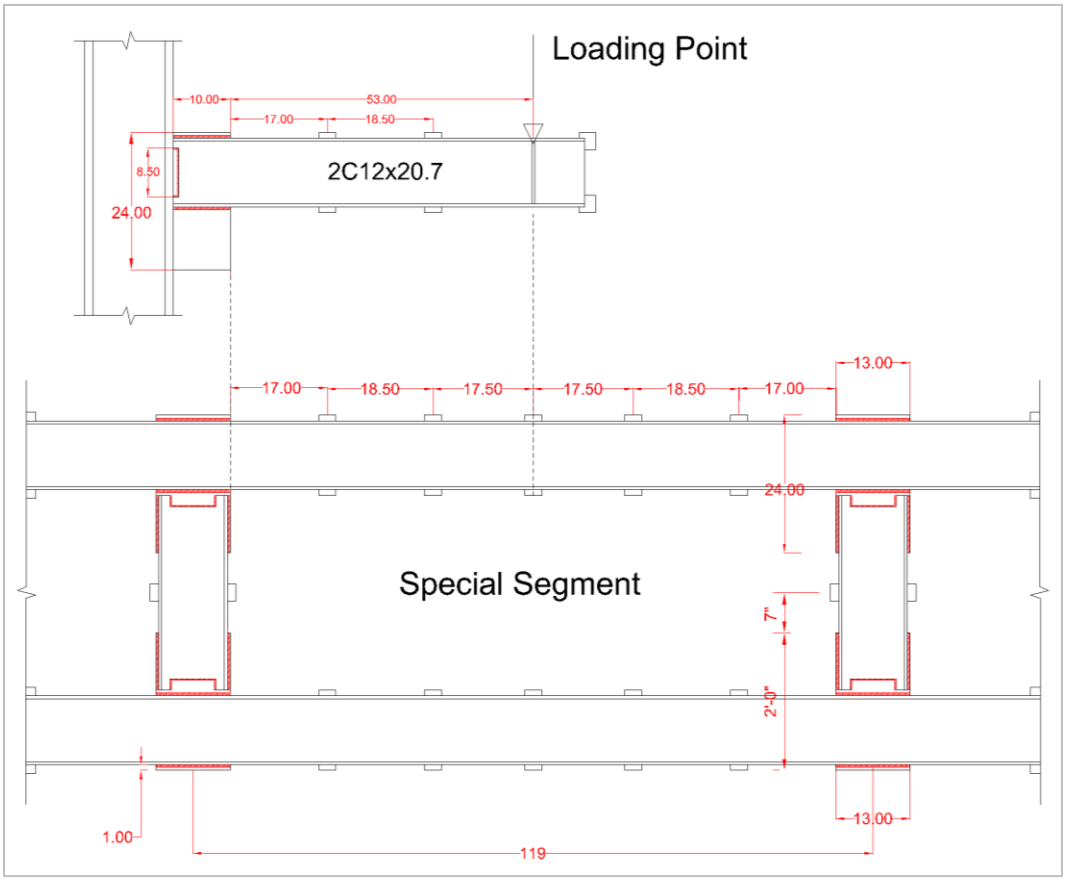

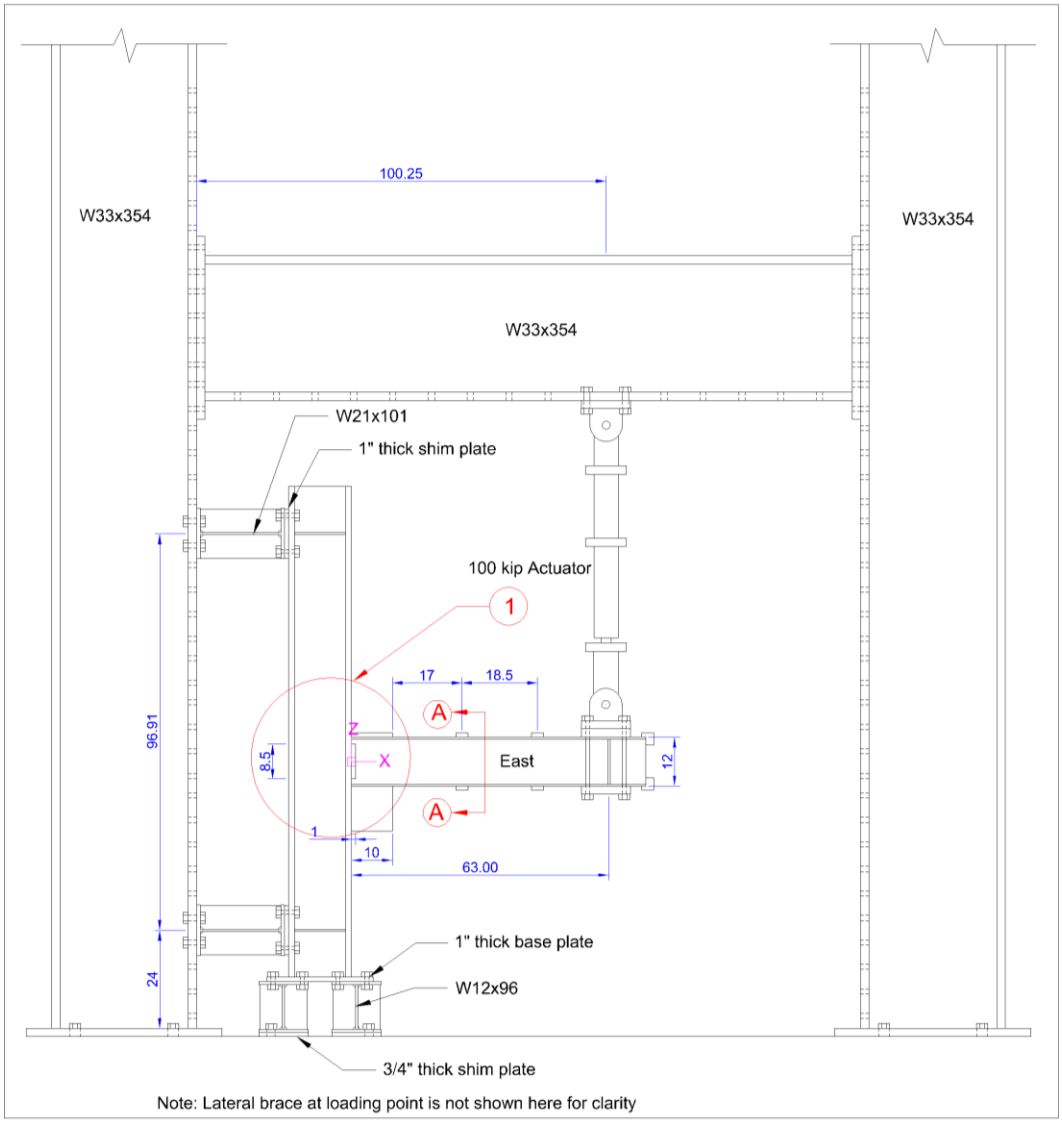
W33x354
100.25
W33x354
W33x354
W21x101
1" thick shim plate
100 kip Actuator
1
17
18.5
A
Z
X
East
12
8.5
A
96.91
1
10
63.00
1" thick base plate
W12x96
24
3/4" thick shim plate
Note: Lateral brace at loading point is not shown here for clarity

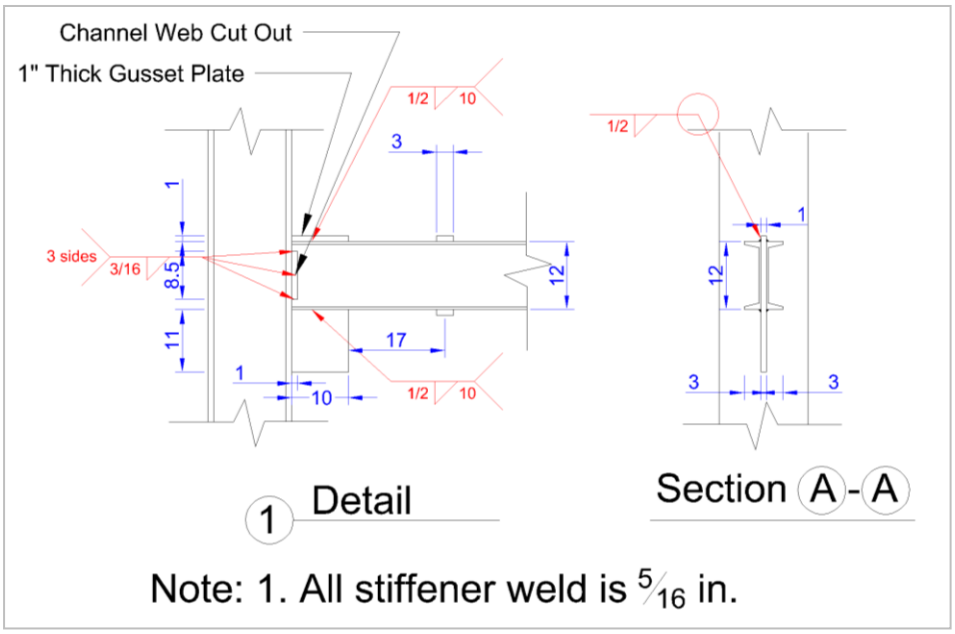
Channel Web Cut Out
1" Thick Gusset Plate
1/2
10
3
1
3 sides
3/16
8.5
11
12
17
1
10
1/2
10
1/2
1
12
3
3
1 Detail
Section A-A
Note: 1. All stiffener weld is 5/16 in.

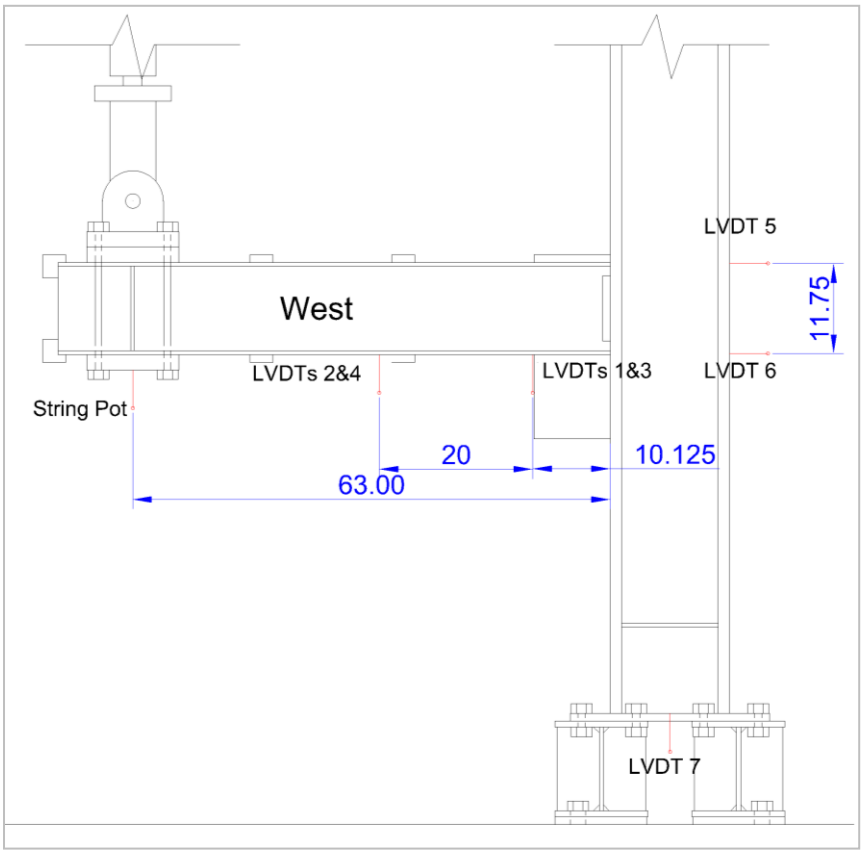
LVDT 5
11.75
West
LVDTs 2&4
LVDTs 1&3
LVDT 6
String Pot
20
10.125
63.00
LVDT 7

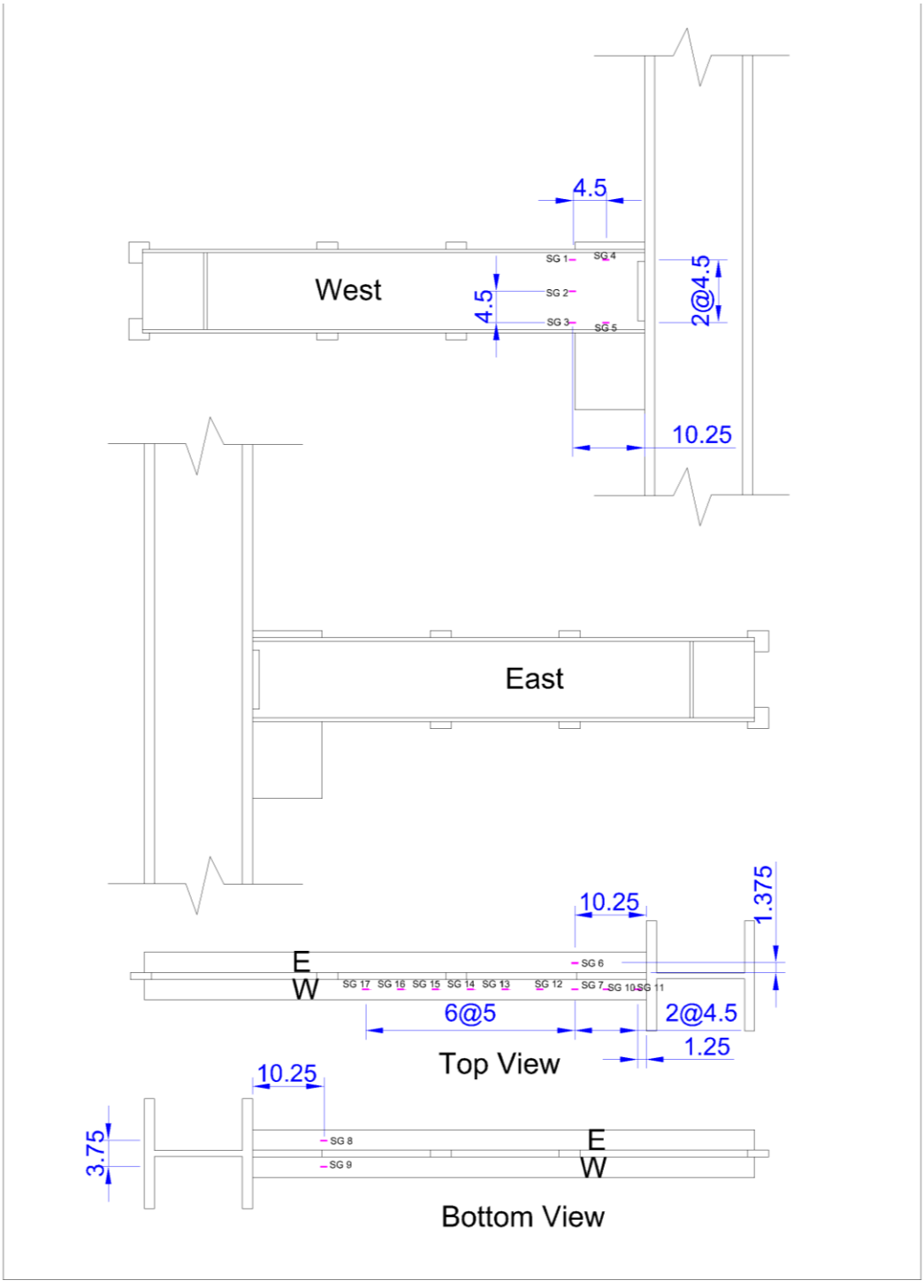
4.5
West
SG 1
SG 4
SG 2
SG 3
SG 5
4.5
2@4.5
10.25
East
10.25
1.375
E
W
SG 6
SG 17 SG 16 SG 15 SG 14 SG 13 SG 12 SG 7 SG 10 SG 11
6@5
2@4.5
1.25
Top View
10.25
3.75
SG 8
SG 9
E
W
Bottom View

Specimen 2C12-10-RBS

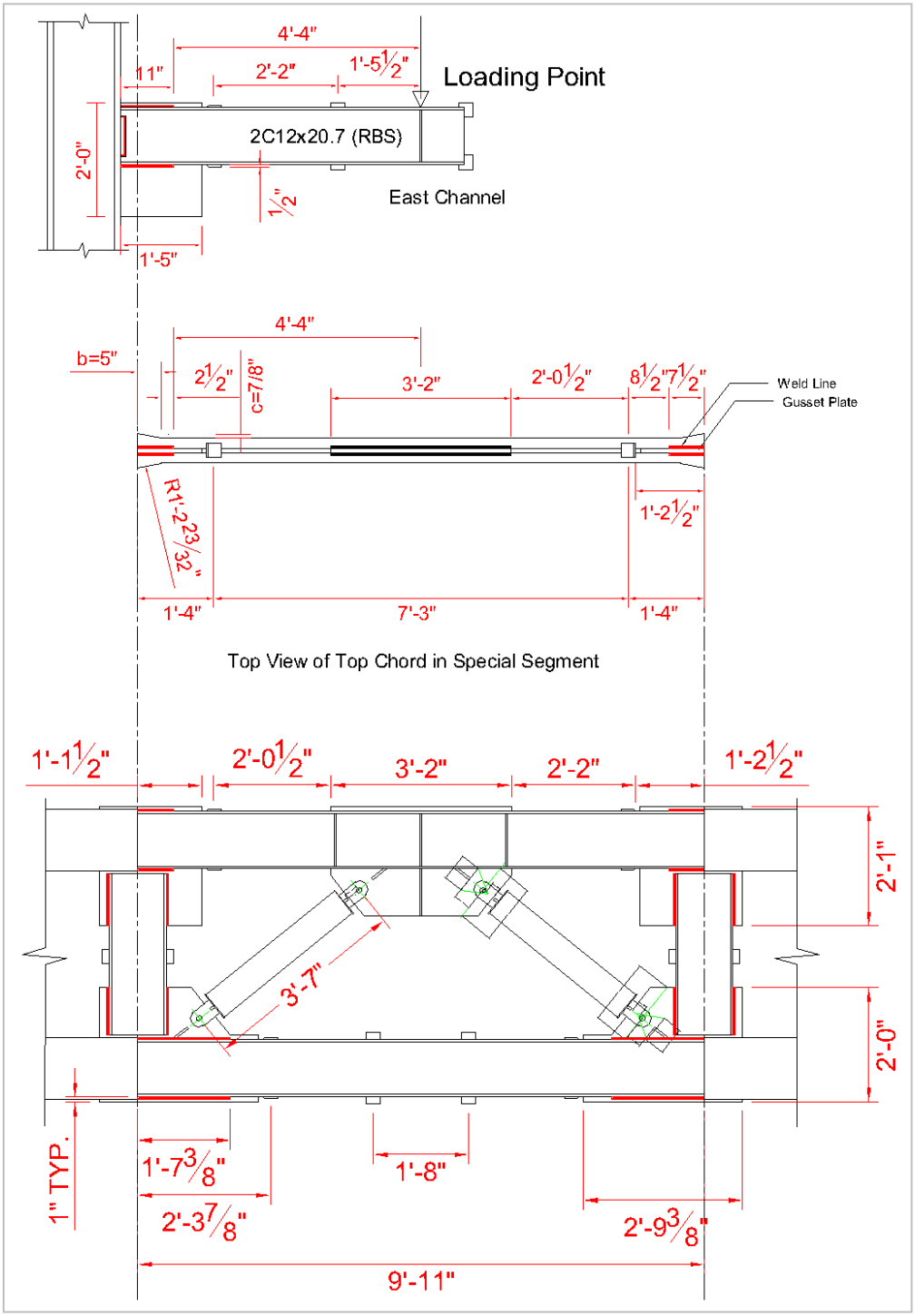

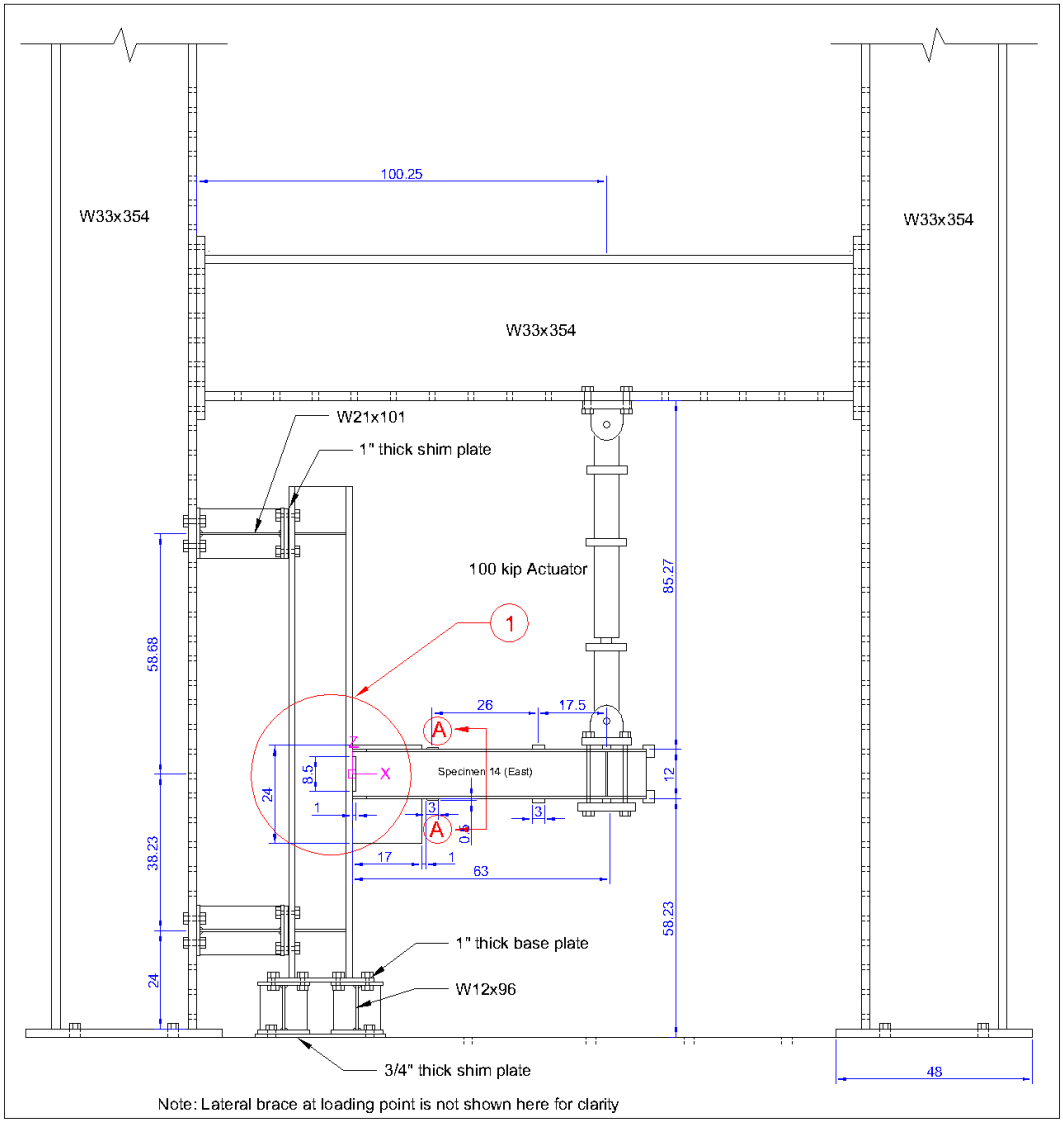
100.25
W33x354
W33x354
W33x354
W21x101
1" thick shim plate
100 kip Actuator
85.27
58.68
38.23
24
1
26
17.5
A
A
X
Specimen 14 (East)
8.5
24
12
1
3
3
0.5
17
1
63
58.23
1" thick base plate
W12x96
3/4" thick shim plate
48
Note: Lateral brace at loading point is not shown here for clarity

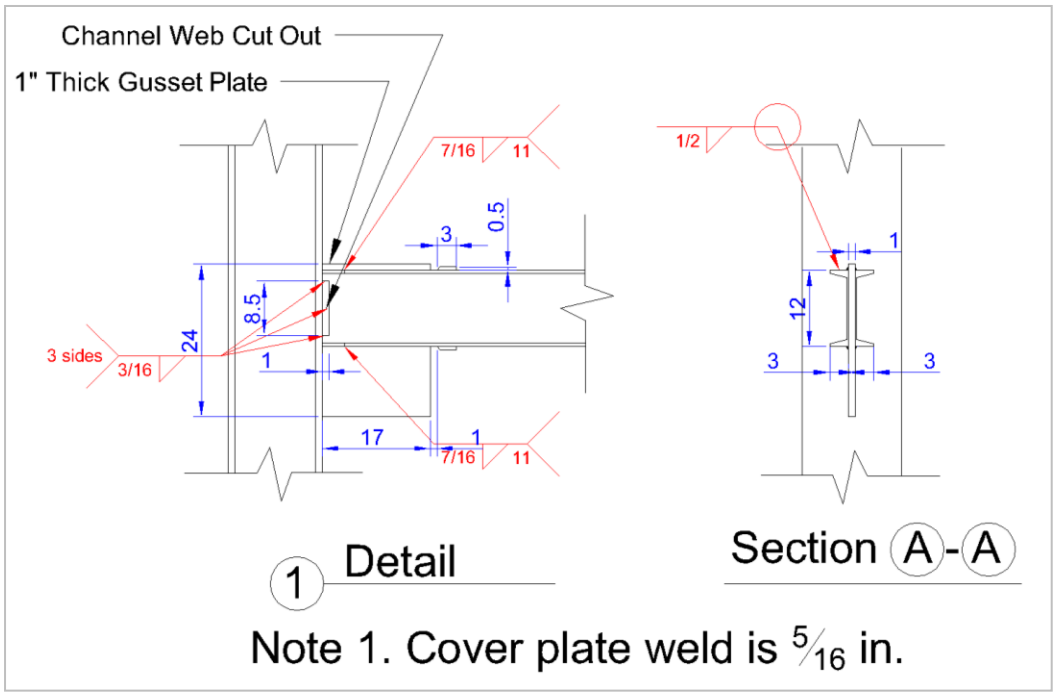
Channel Web Cut Out
1" Thick Gusset Plate
7/16
11
3
0.5
8.5
24
3 sides
3/16
1
17
1
7/16
11
1/2
1
12
3
3
1 Detail
Section A-A
Note 1. Cover plate weld is 5/16 in.

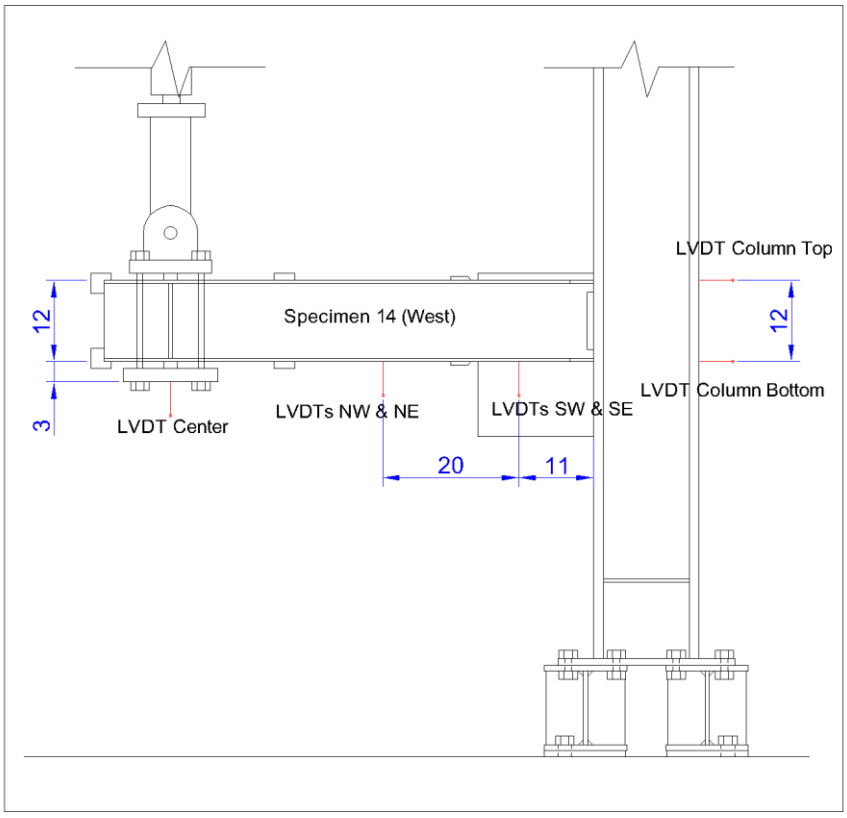
LVDT Column Top
12
Specimen 14 (West)
12
3
LVDT Center
LVDTs NW & NE
LVDTs SW & SE
LVDT Column Bottom
20
11

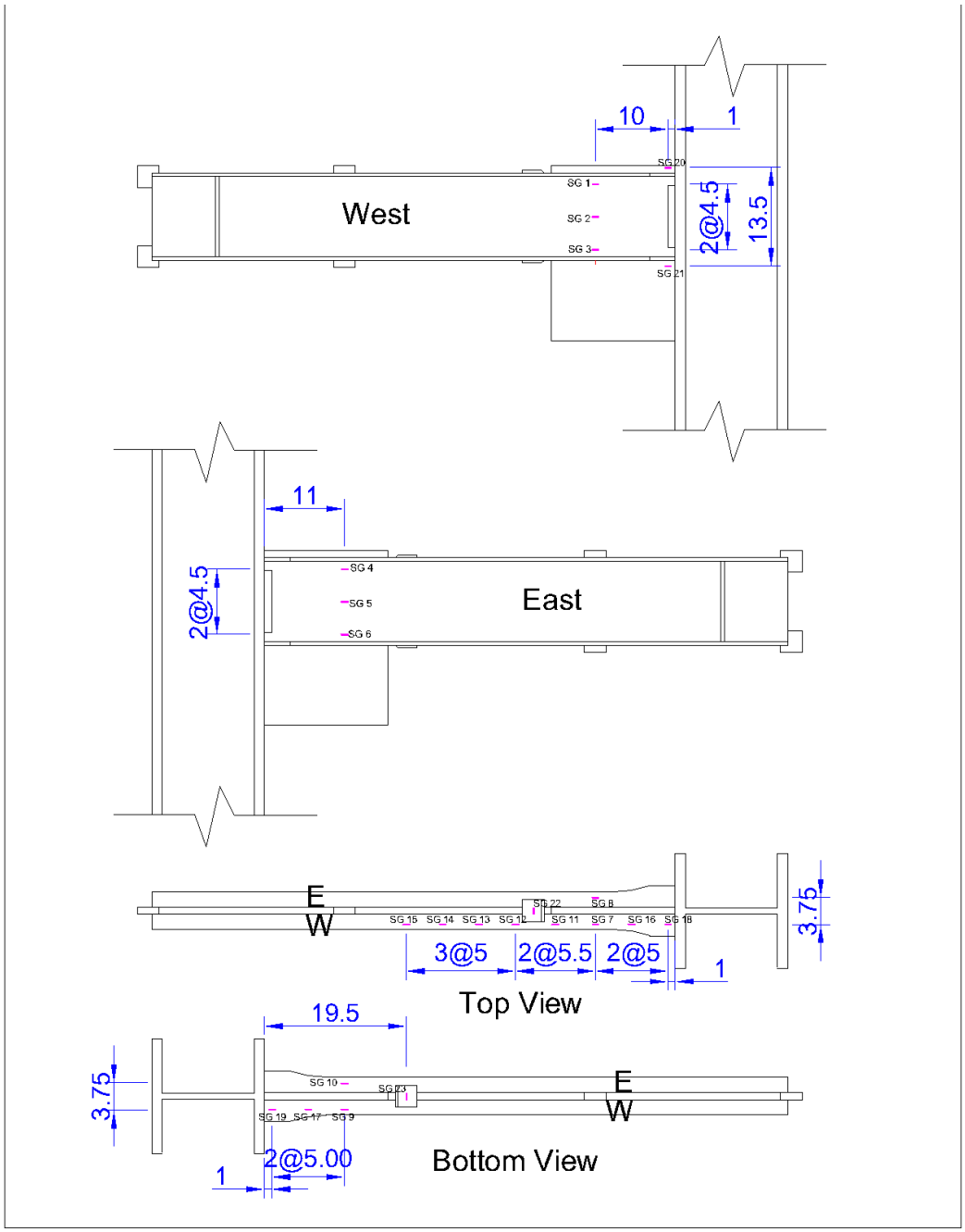
10
1
SG 20
SG 1
West
SG 2
SG 3
SG 21
2@4.5
13.5
11
2@4.5
SG 4
SG 5
East
SG 6
E
W
SG 22
SG 8
SG 15
SG 14
SG 13
SG 12
SG 11
SG 7
SG 16
SG 18
3@5
2@5.5
2@5
1
3.75
Top View
19.5
3.75
SG 10
SG 23
E
W
SG 19
SG 17
SG 9
2@5.00
1
Bottom View

Specimen 2C12-11-RBS

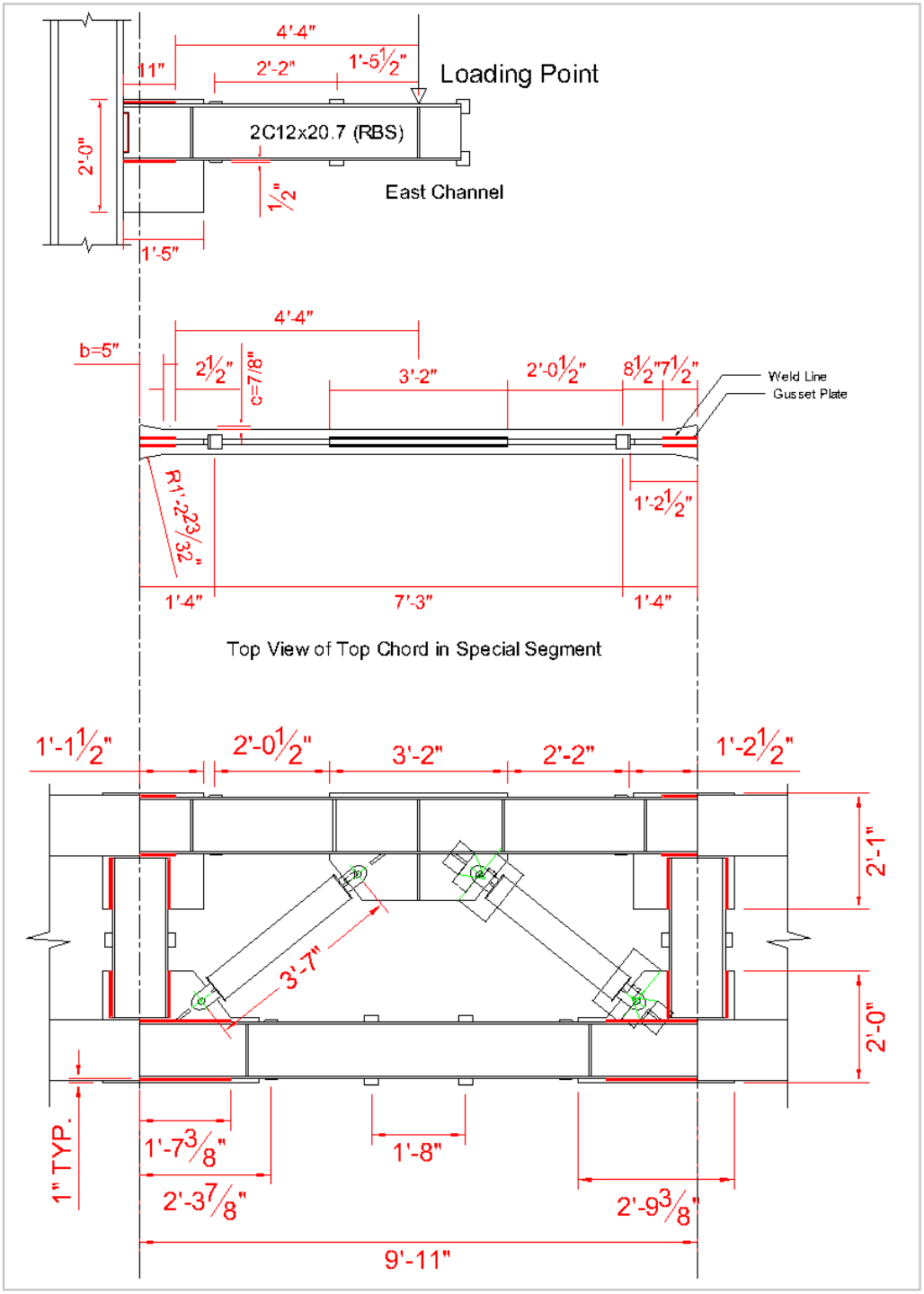

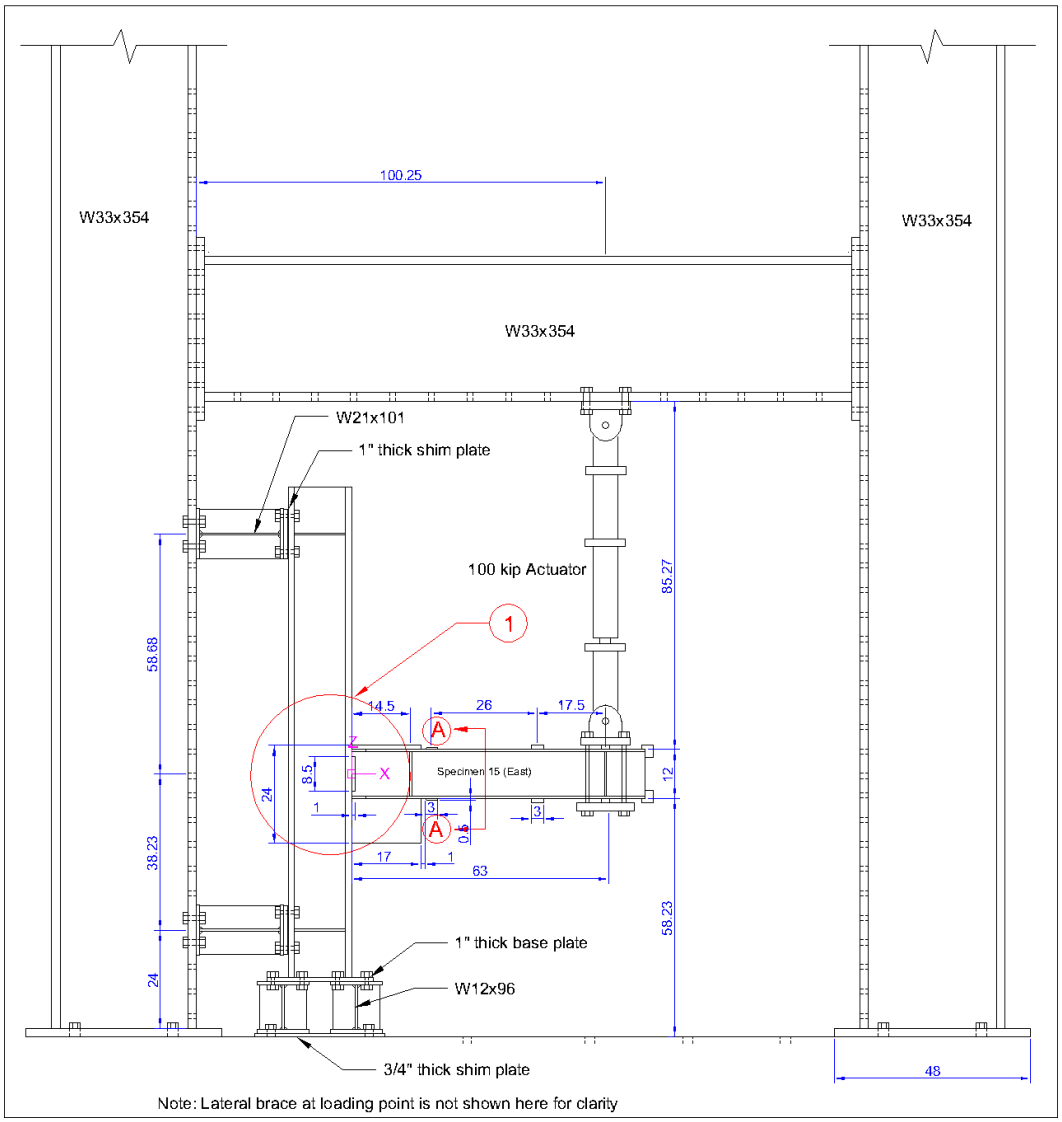
W33x354
100.25
W33x354
W33x354
W21x101
1" thick shim plate
100 kip Actuator
85.27
58.68
38.23
24
1
14.5
26
17.5
A
Z
X
8.5
24
Specimen 15 (East)
12
1
3
3
A
0.5
17
1
63
58.23
1" thick base plate
W12x96
3/4" thick shim plate
48
Note: Lateral brace at loading point is not shown here for clarity

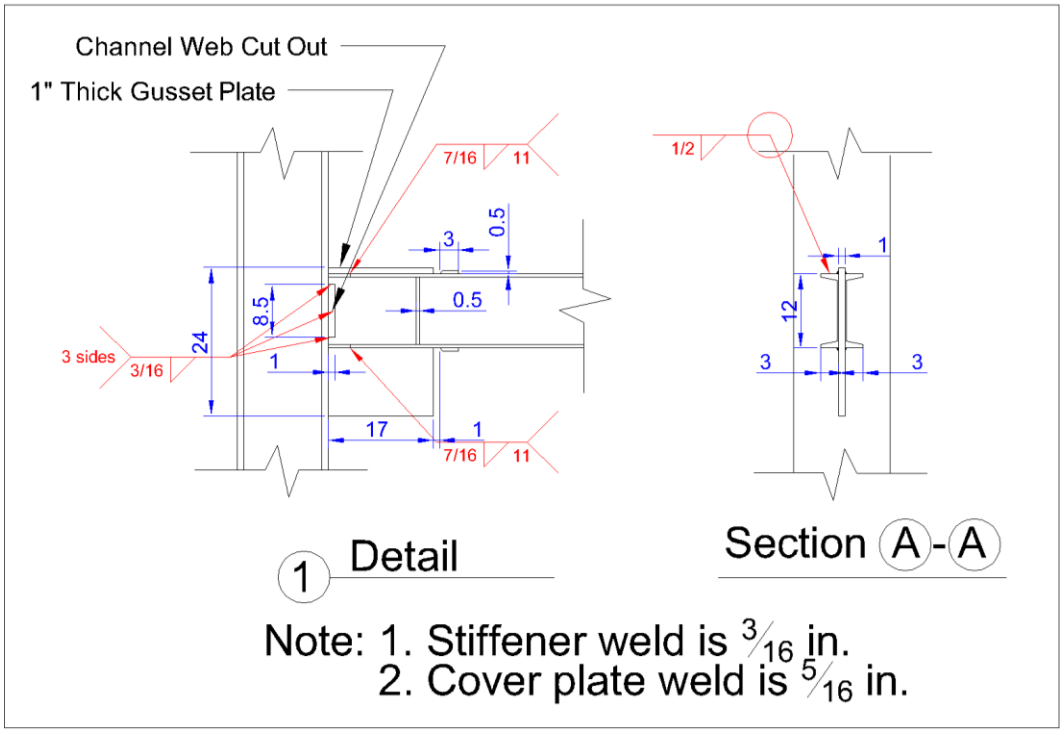
Channel Web Cut Out
1" Thick Gusset Plate
7/16
11
3
0.5
0.5
8.5
24
3 sides
3/16
1
17
1
7/16
11
1/2
1
12
3
3
1 Detail
Section A-A
Note: 1. Stiffener weld is 3/16 in.
2. Cover plate weld is 5/16 in.

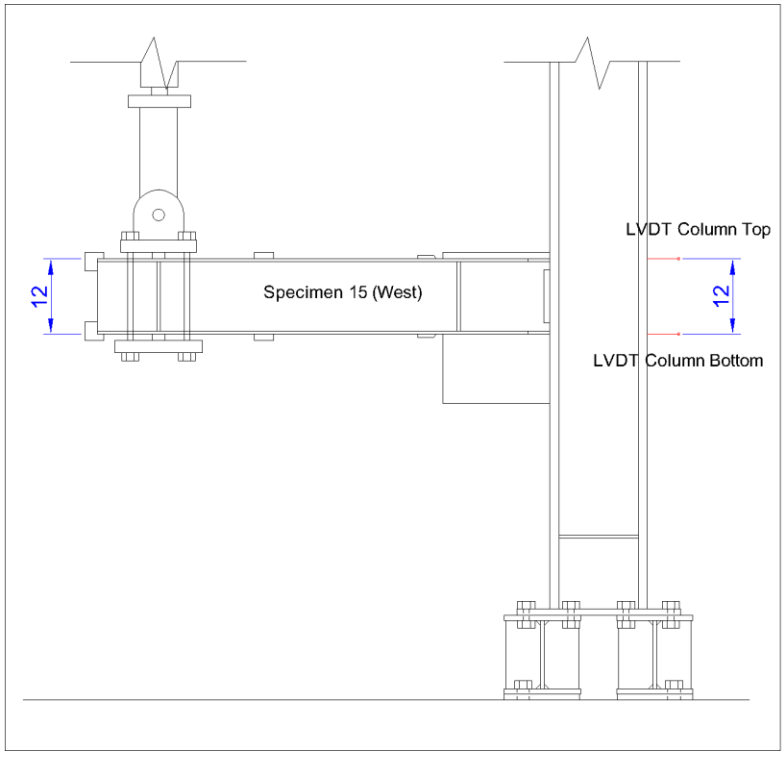
LVDT Column Top
12
Specimen 15 (West)
12
LVDT Column Bottom

Specimen 2C12-12

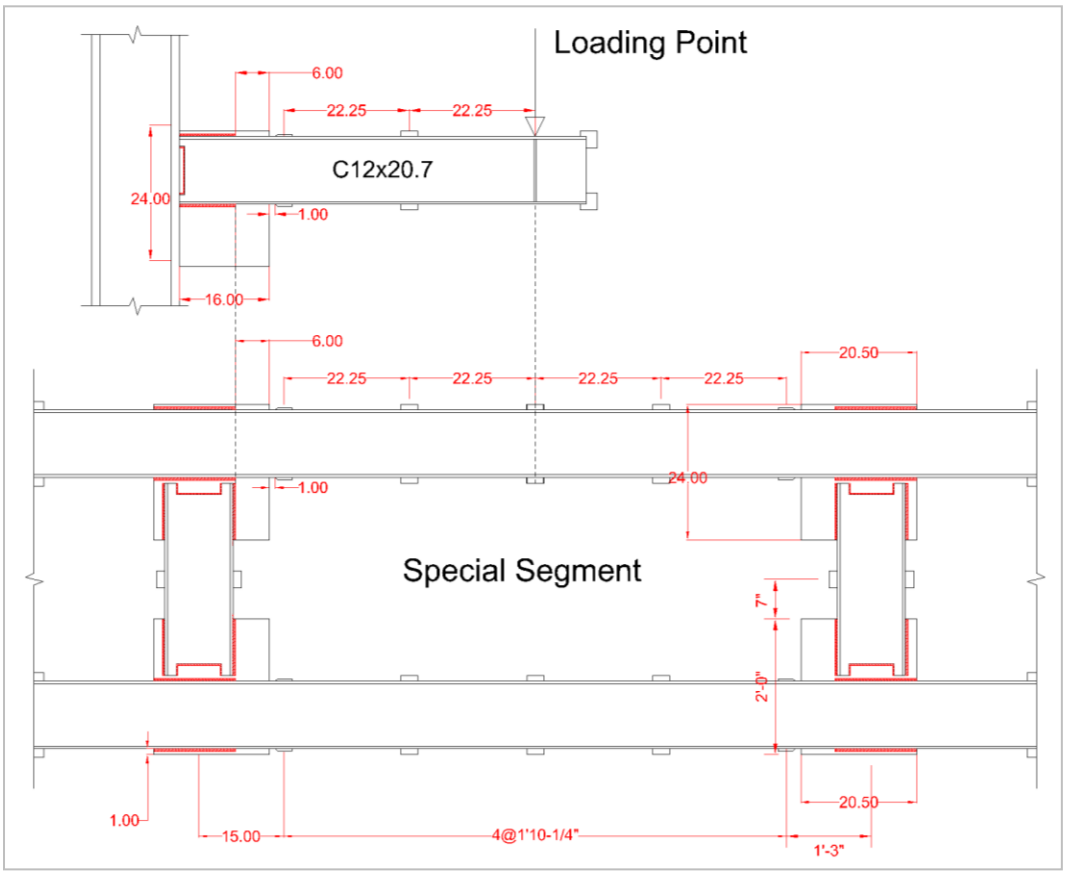

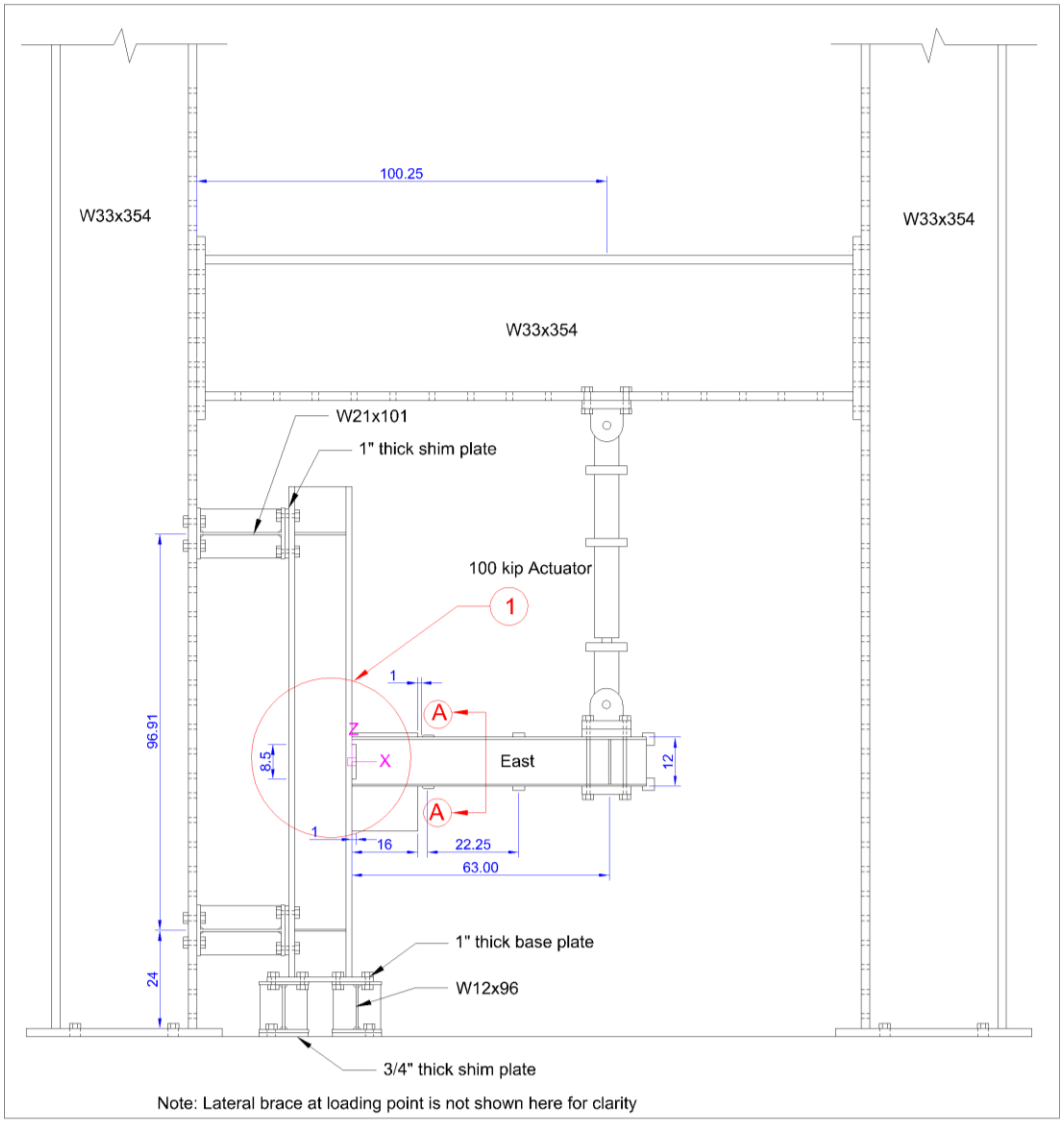
100.25
W33x354
W33x354
W33x354
W21x101
1" thick shim plate
100 kip Actuator
1
1
A
Z
X
East
12
8.5
A
1
16
22.25
63.00
96.91
24
1" thick base plate
W12x96
3/4" thick shim plate
Note: Lateral brace at loading point is not shown here for clarity

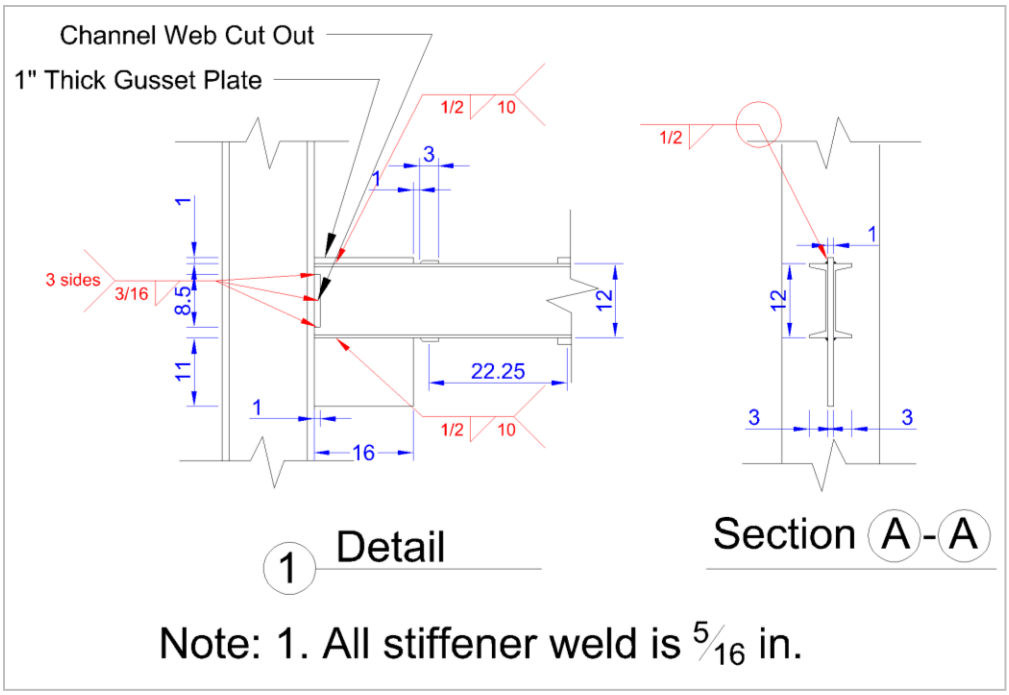
Channel Web Cut Out
1" Thick Gusset Plate
1/2
10
3
1
1
3 sides
3/16
8.5
11
12
22.25
1
16
1/2
10
1/2
1
12
3
3
1 Detail
Section A-A
Note: 1. All stiffener weld is 5/16 in.

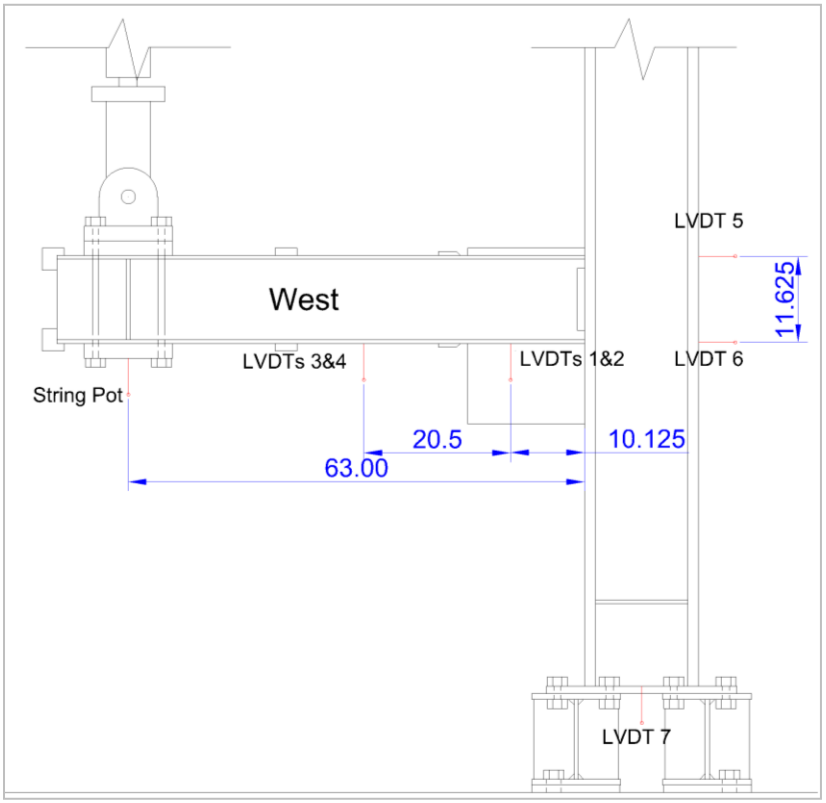
LVDT 5
11.625
West
LVDTs 3&4
LVDTs 1&2
LVDT 6
String Pot
20.5
10.125
63.00
LVDT 7

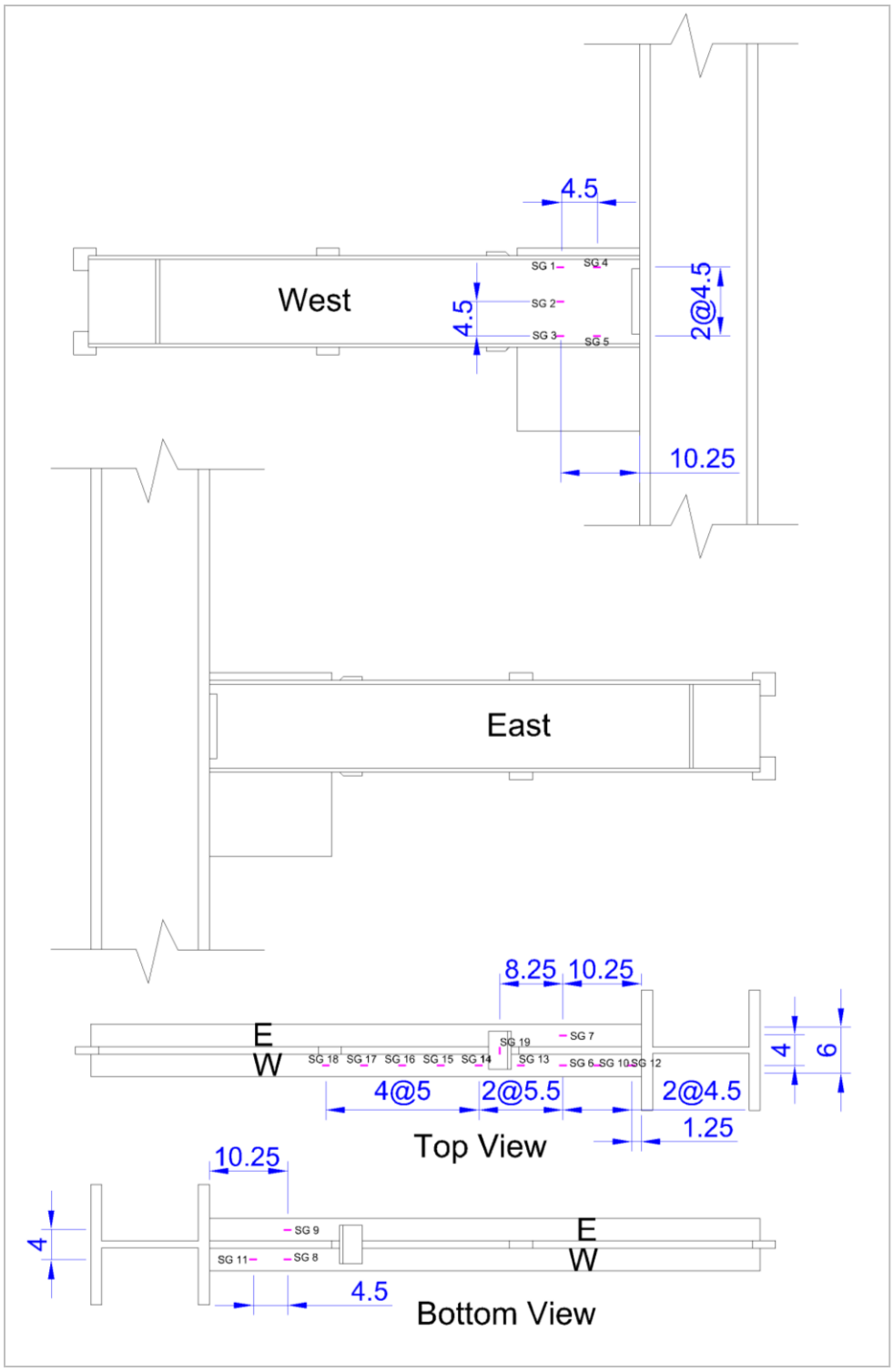
4.5
West
SG 1
SG 4
SG 2
SG 3
SG 5
4.5
2@4.5
10.25
East
8.25
10.25
E
W
SG 19
SG 7
SG 18
SG 17
SG 16
SG 15
SG 14
SG 13
SG 6
SG 10
SG 12
4
6
4@5
2@5.5
2@4.5
1.25
Top View
10.25
4
SG 9
SG 11
SG 8
E
W
4.5
Bottom View

Specimen 2C8-1

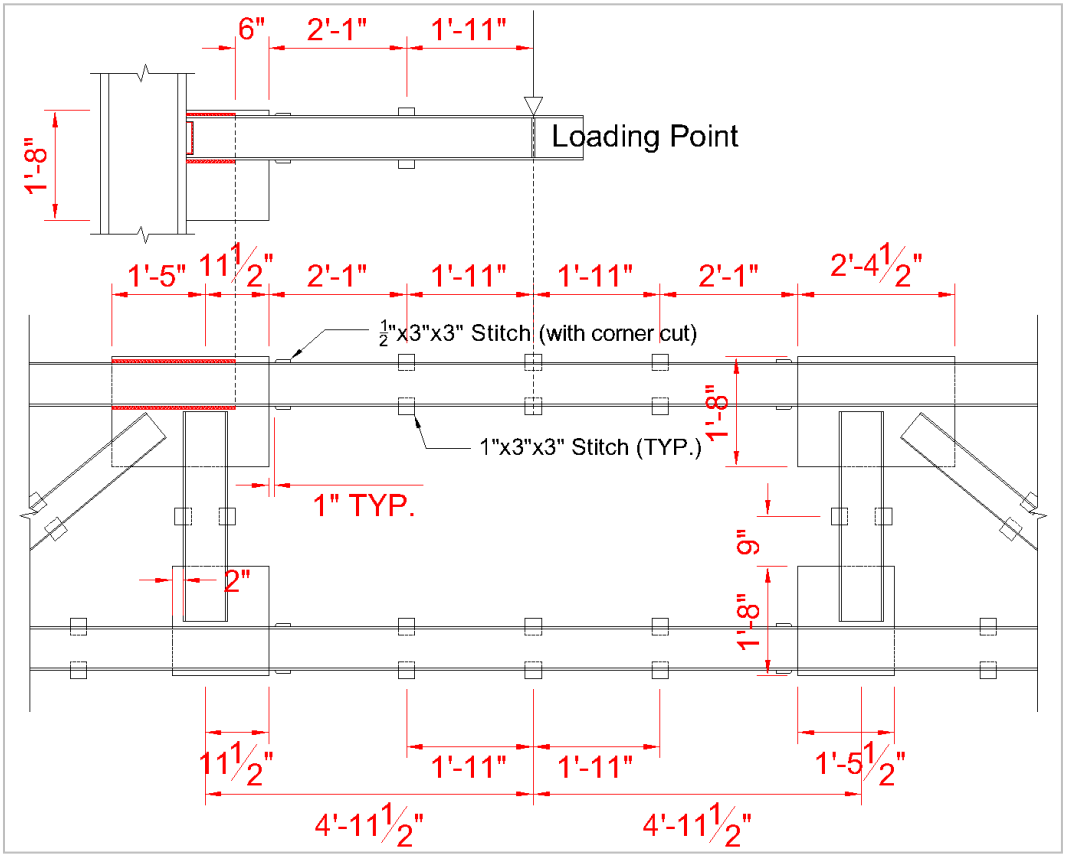

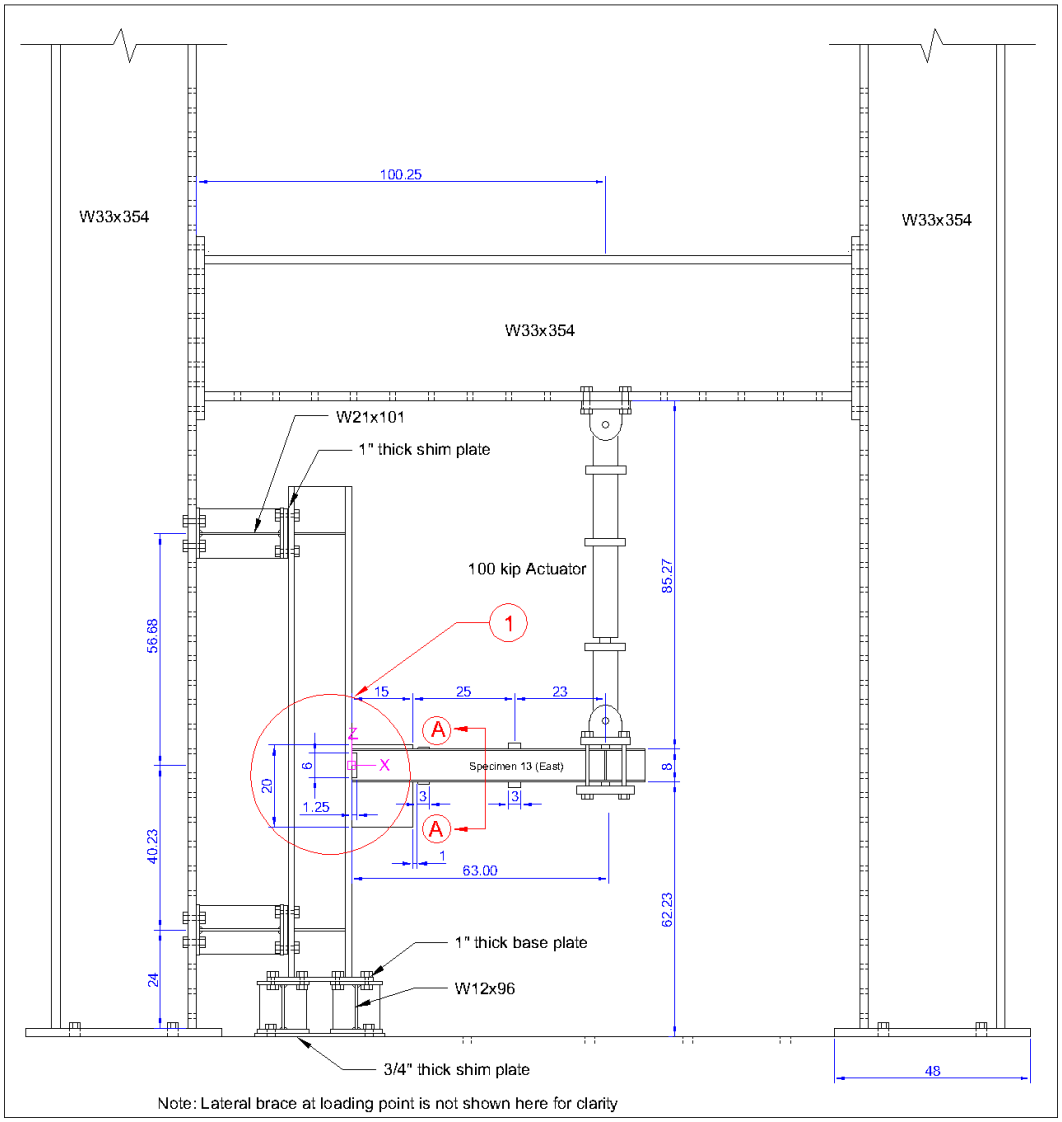
W33x354
100.25
W33x354
W33x354
W21x101
1" thick shim plate
100 kip Actuator
85.27
56.68
1
15
25
23
A
Z
X
6
20
Specimen 13 (East)
8
3
3
1.25
A
1
63.00
40.23
62.23
1" thick base plate
24
W12x96
3/4" thick shim plate
48
Note: Lateral brace at loading point is not shown here for clarity

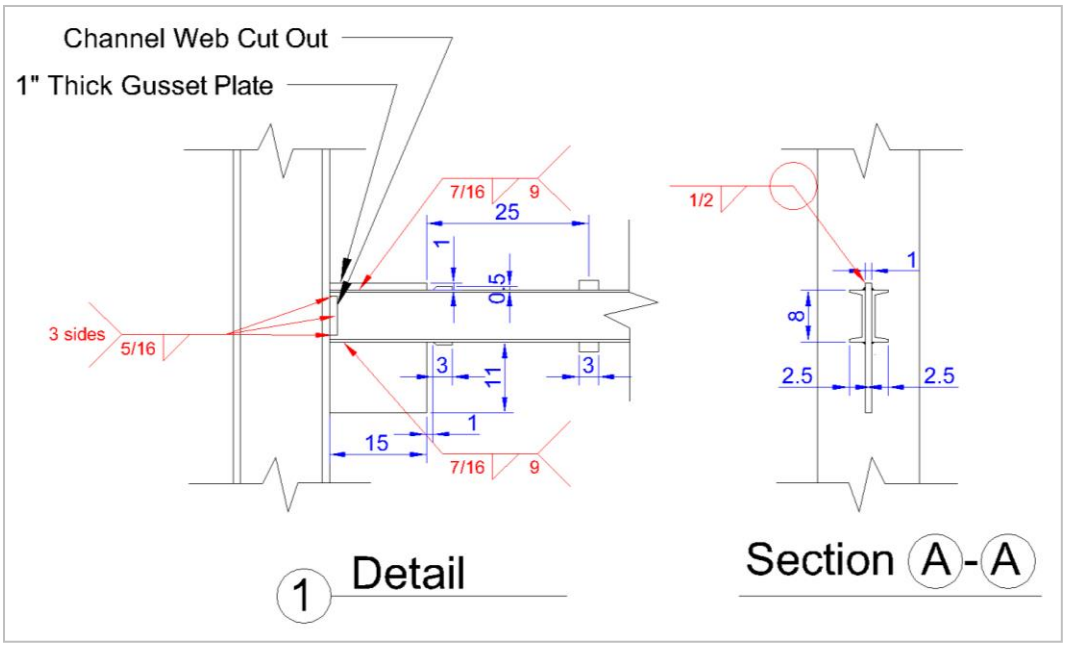
Channel Web Cut Out
1" Thick Gusset Plate
7/16
9
25
1
0.5
3 sides
5/16
3
11
3
1
15
7/16
9
1/2
1
8
2.5
2.5
1 Detail
Section A-A

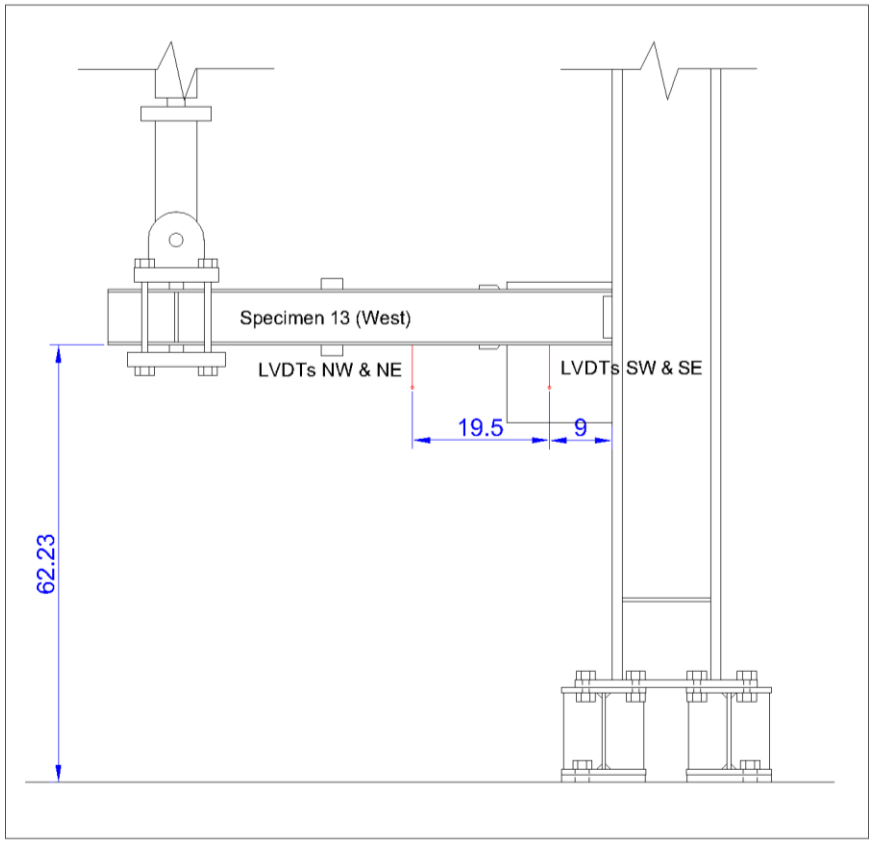
Specimen 13 (West)
LVDTs NW & NE
LVDTs SW & SE
19.5
9
62.23

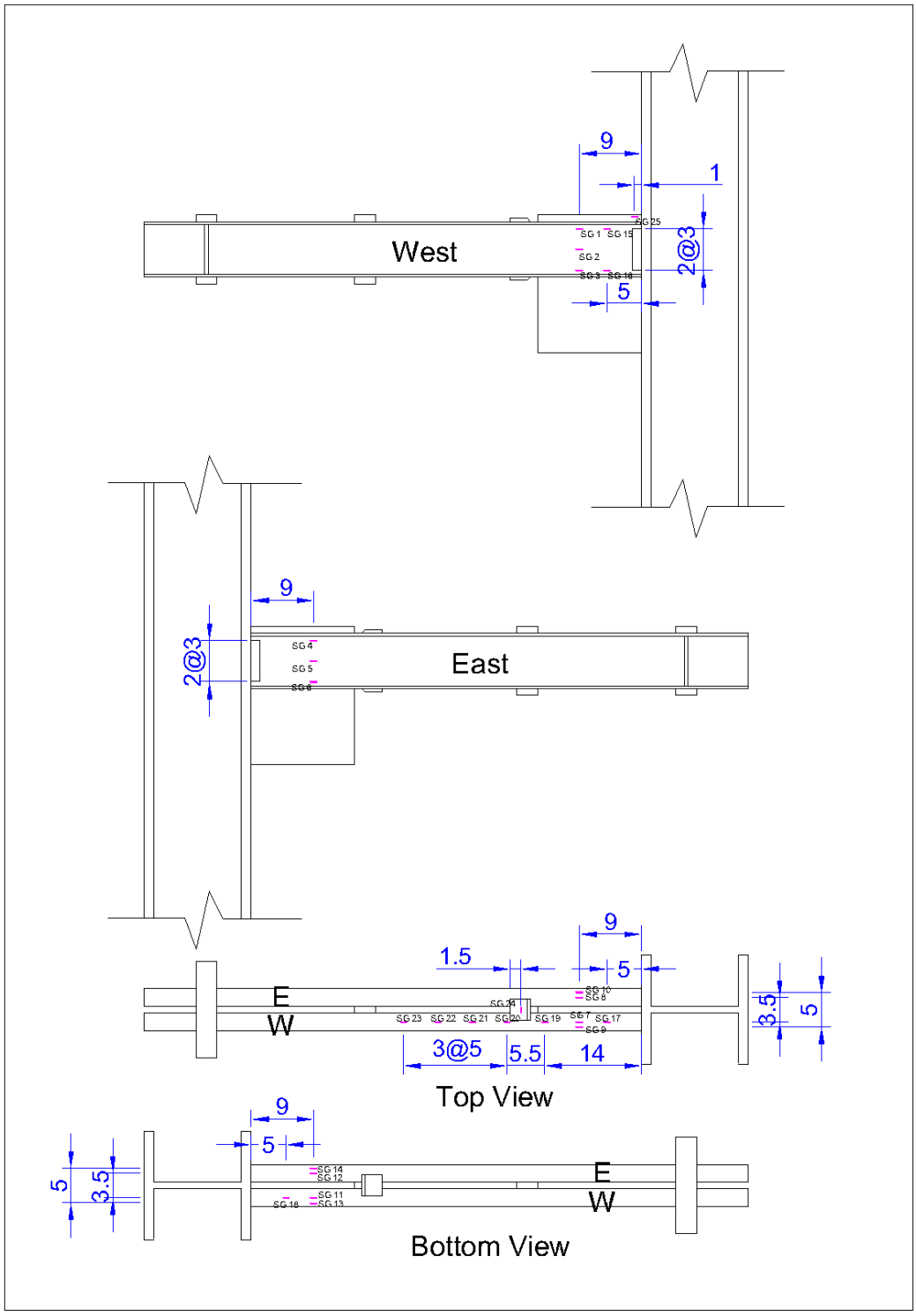
9
1
West
2@3
5
9
2@3
East
9
1.5
5
E
W
3@5
5.5
14
3.5
5
Top View
9
5
5
3.5
E
W
Bottom View

Specimen 2C6-1

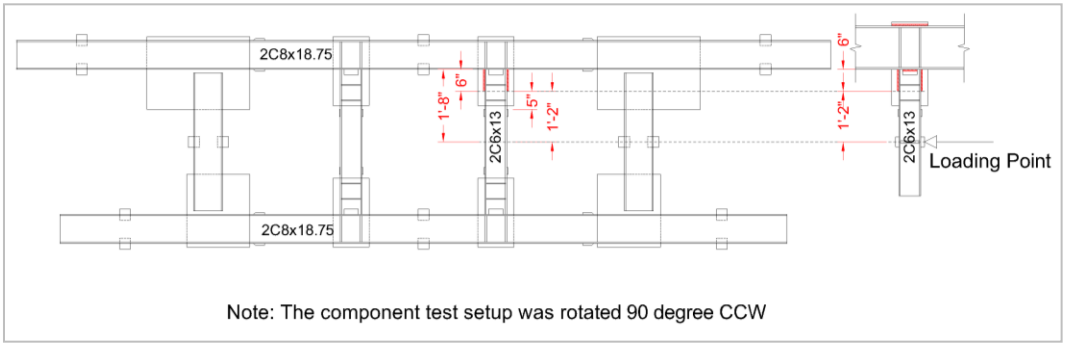

Note: The component test setup was rotated 90 degree CCW

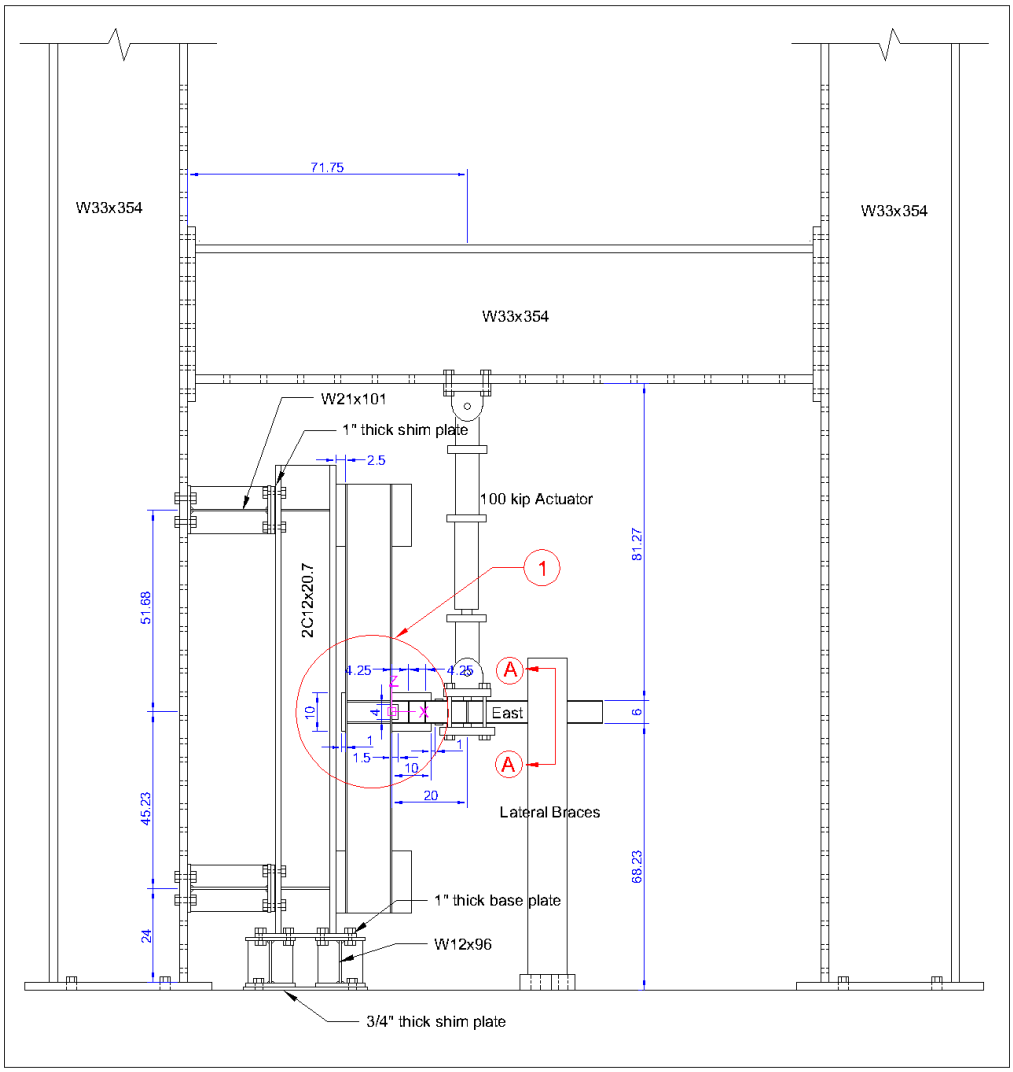

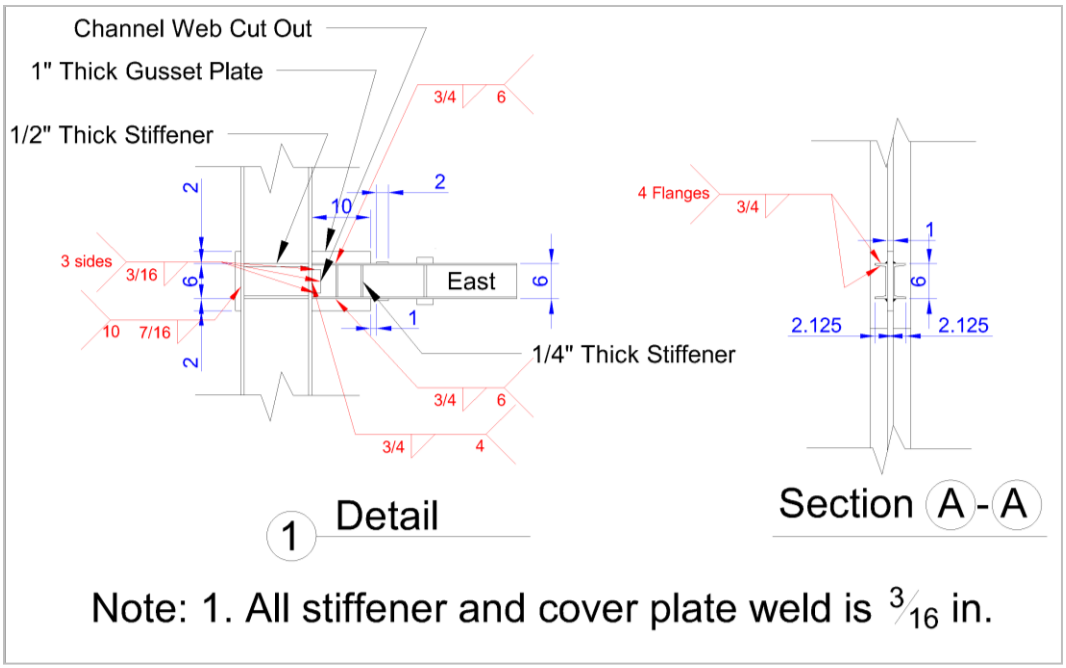
Channel Web Cut Out
1" Thick Gusset Plate
1/2" Thick Stiffener
3/4
6
2
10
2
3 sides
3/16
6
East
6
10
7/16
1
2
1/4" Thick Stiffener
3/4
6
3/4
4
1 Detail
4 Flanges
3/4
1
6
2.125
2.125
Section A-A
Note: 1. All stiffener and cover plate weld is 3/16 in.

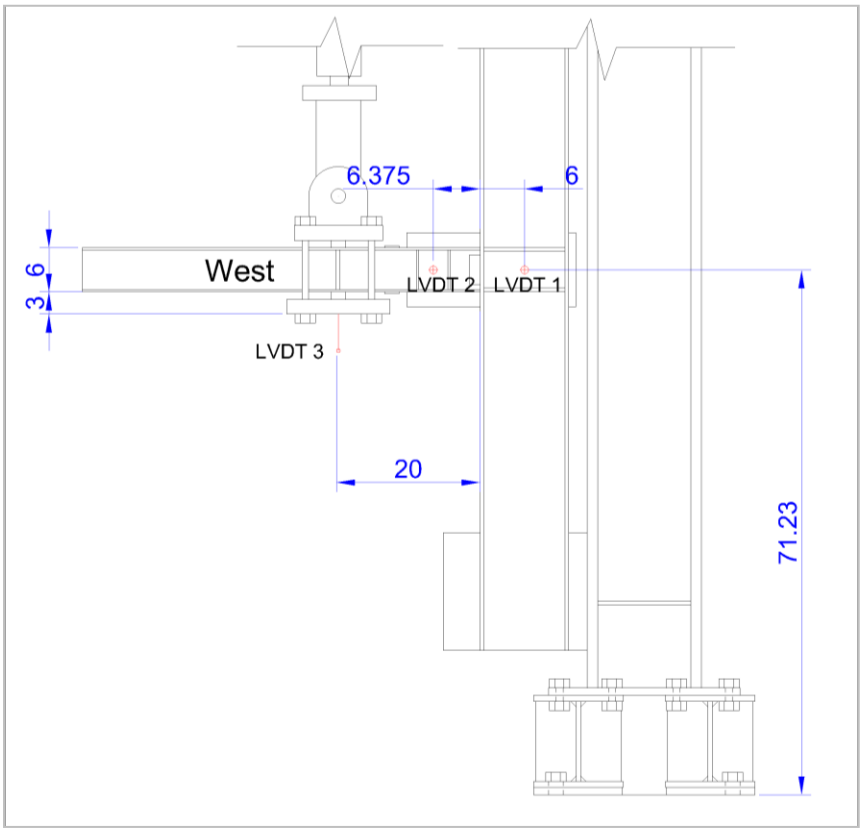
6.375
6
West
LVDT 2
LVDT 1
3
6
LVDT 3
20
71.23

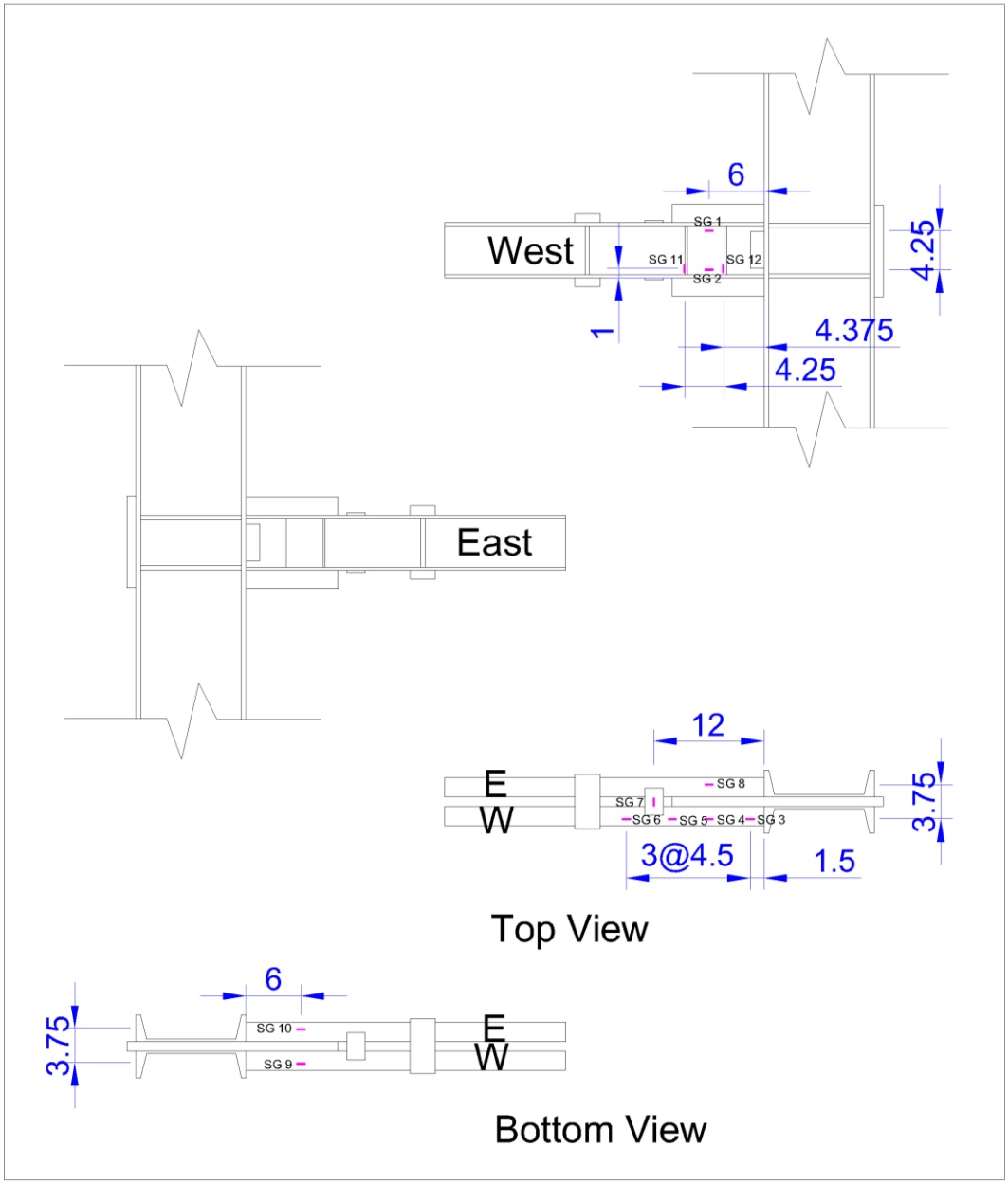
West
East
6
SG 1
SG 11
SG 12
SG 2
4.25
1
4.375
4.25
12
E
W
SG 8
SG 7
SG 6
SG 5
SG 4
SG 3
3.75
3@4.5
1.5
Top View
6
3.75
SG 10
SG 9
E
W
Bottom View

Specimen 2C6-2

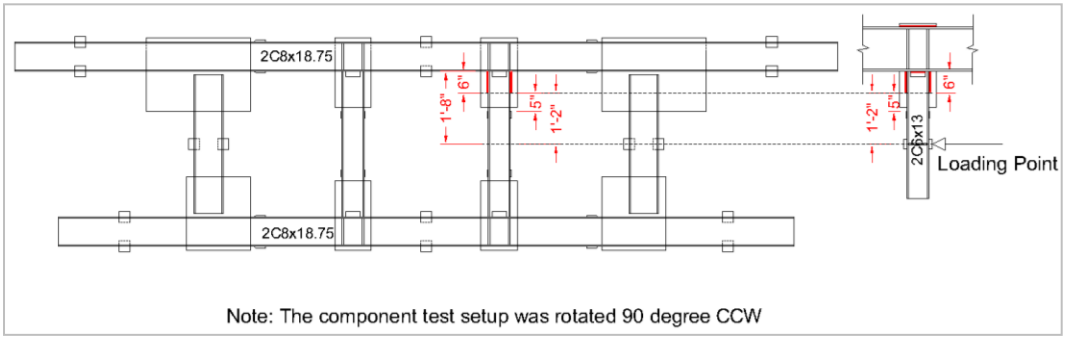

Note: The component test setup was rotated 90 degree CCW

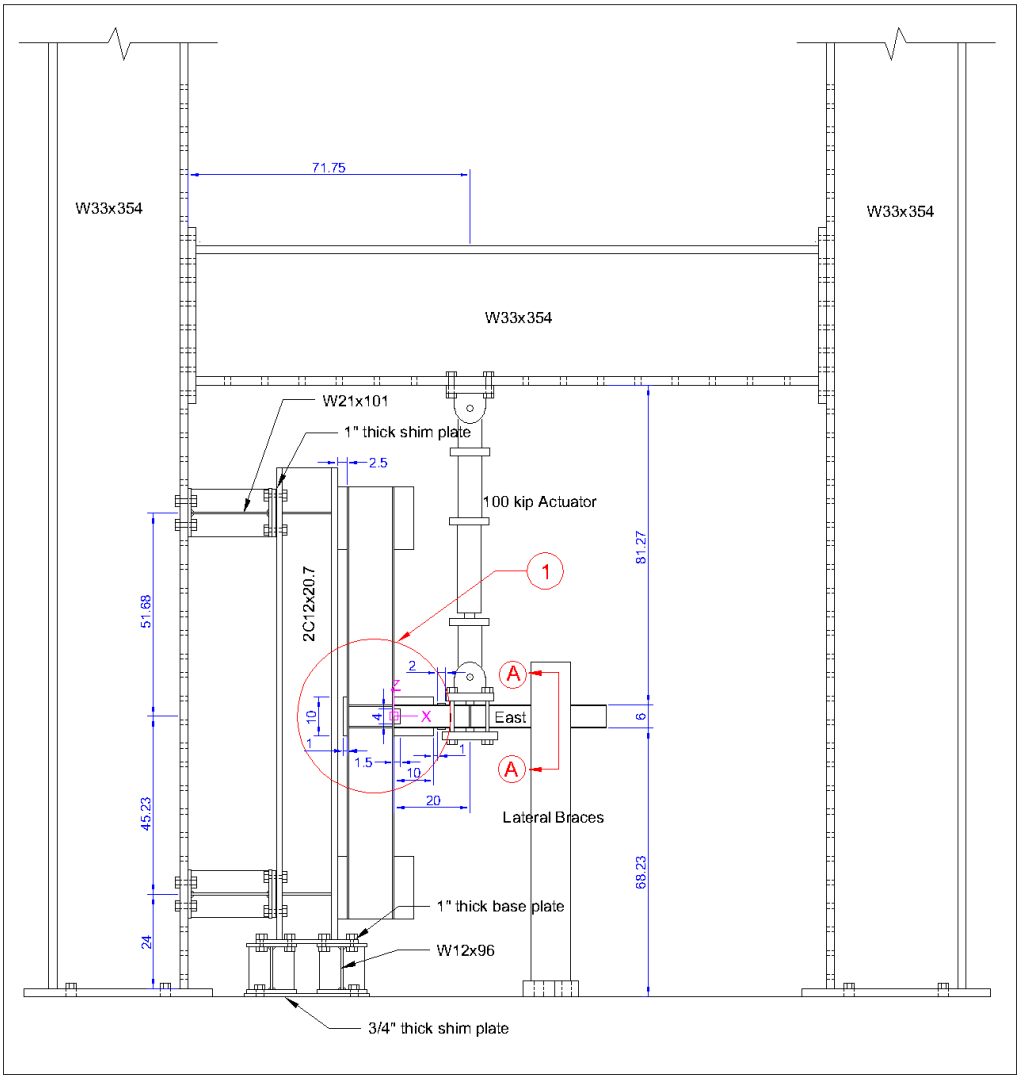

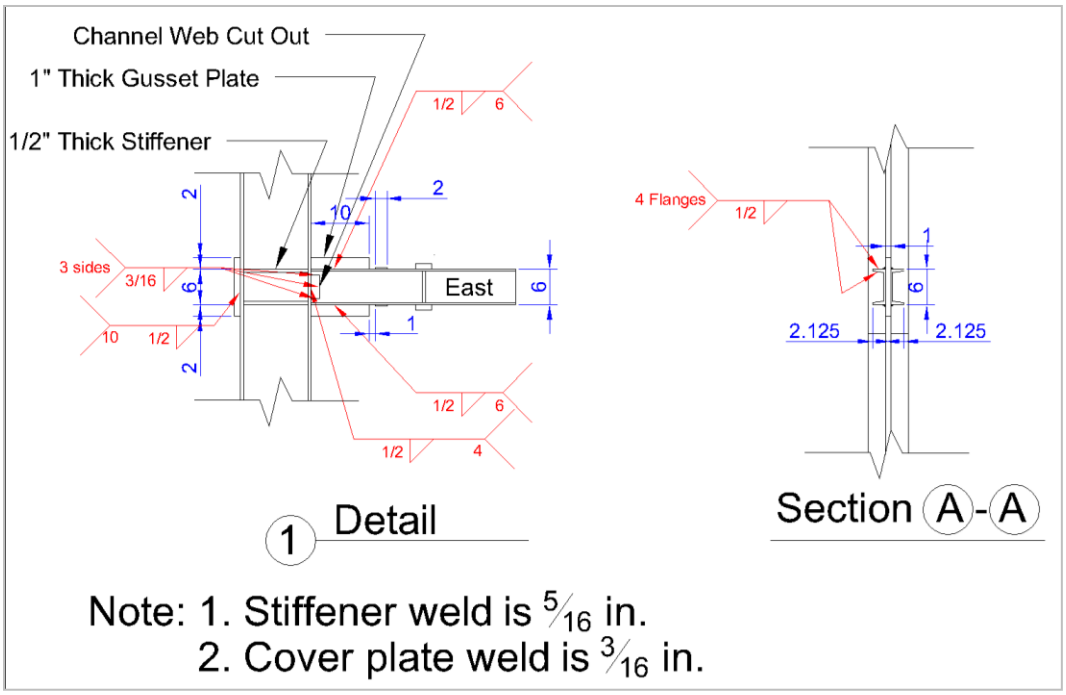
Channel Web Cut Out
1" Thick Gusset Plate
1/2" Thick Stiffener
East
3 sides
3/16
1/2
4 Flanges
2.125
2.125
1 Detail
Section A-A
Note: 1. Stiffener weld is 5/16 in.
2. Cover plate weld is 3/16 in.

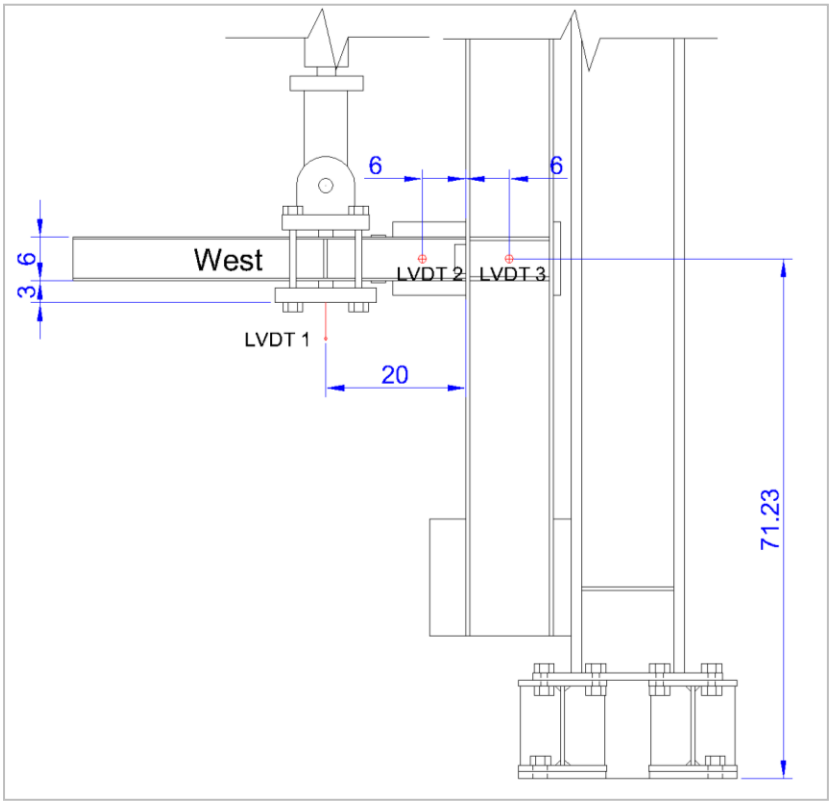
West
LVDT 1
LVDT 2
LVDT 3
20
71.23

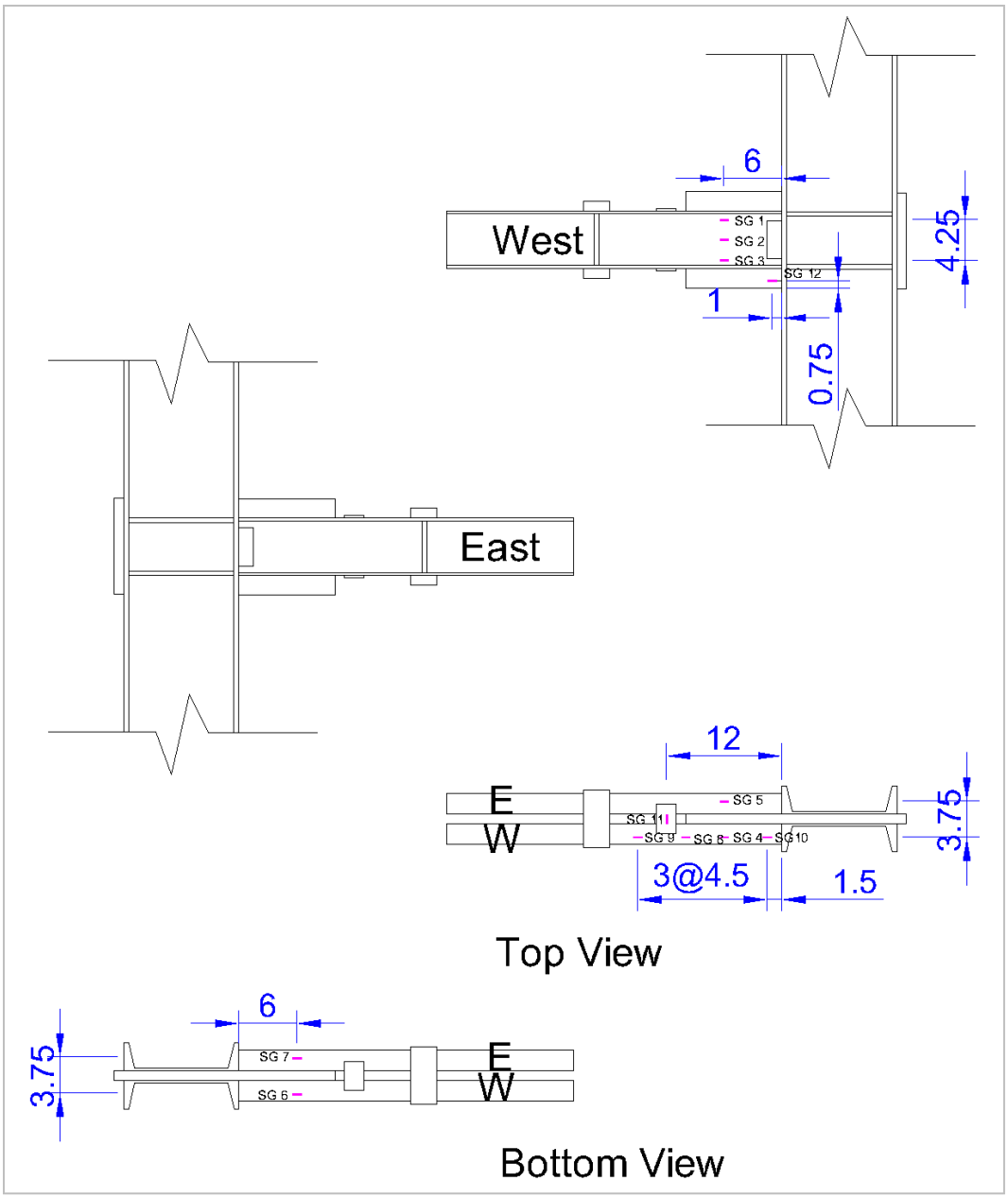
West
East
6
4.25
SG 1
SG 2
SG 3
SG 12
1
0.75
12
E
W
SG 5
SG 11
SG 9
SG 8
SG 4
SG 10
3.75
3@4.5
1.5
Top View
6
3.75
SG 7
SG 6
E
W
Bottom View

Specimen 2HSS8-1

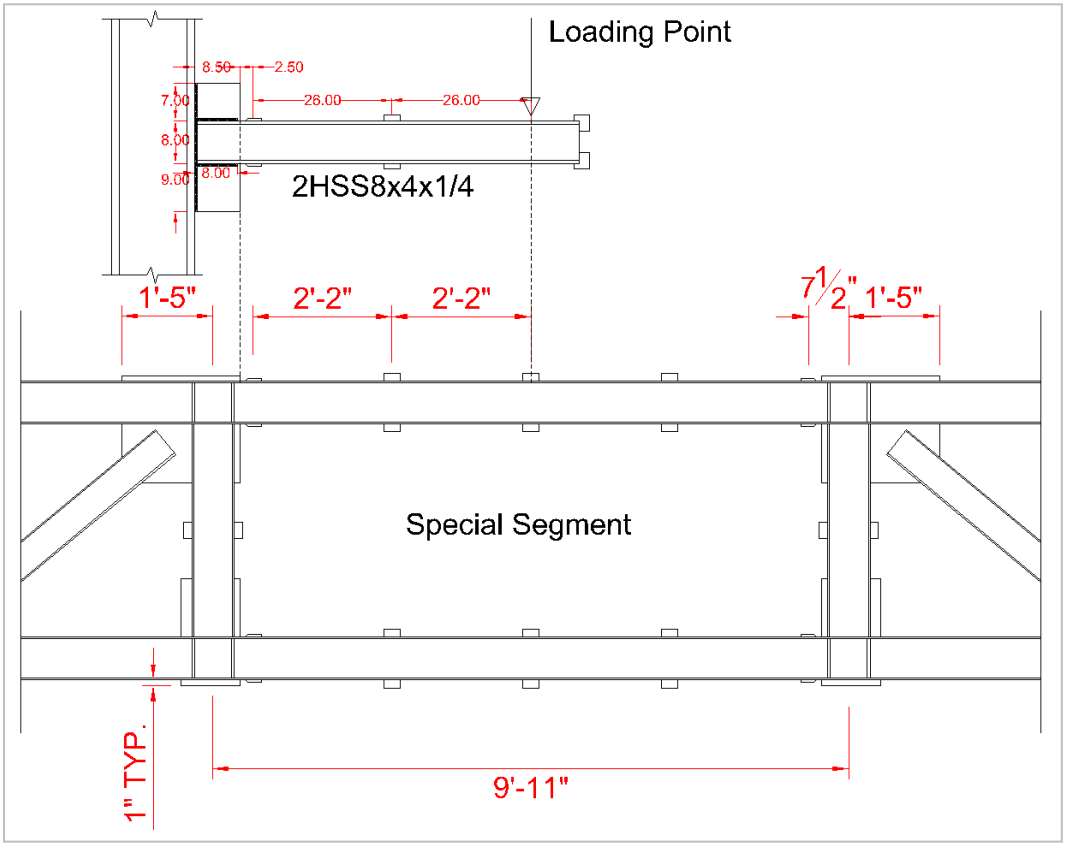

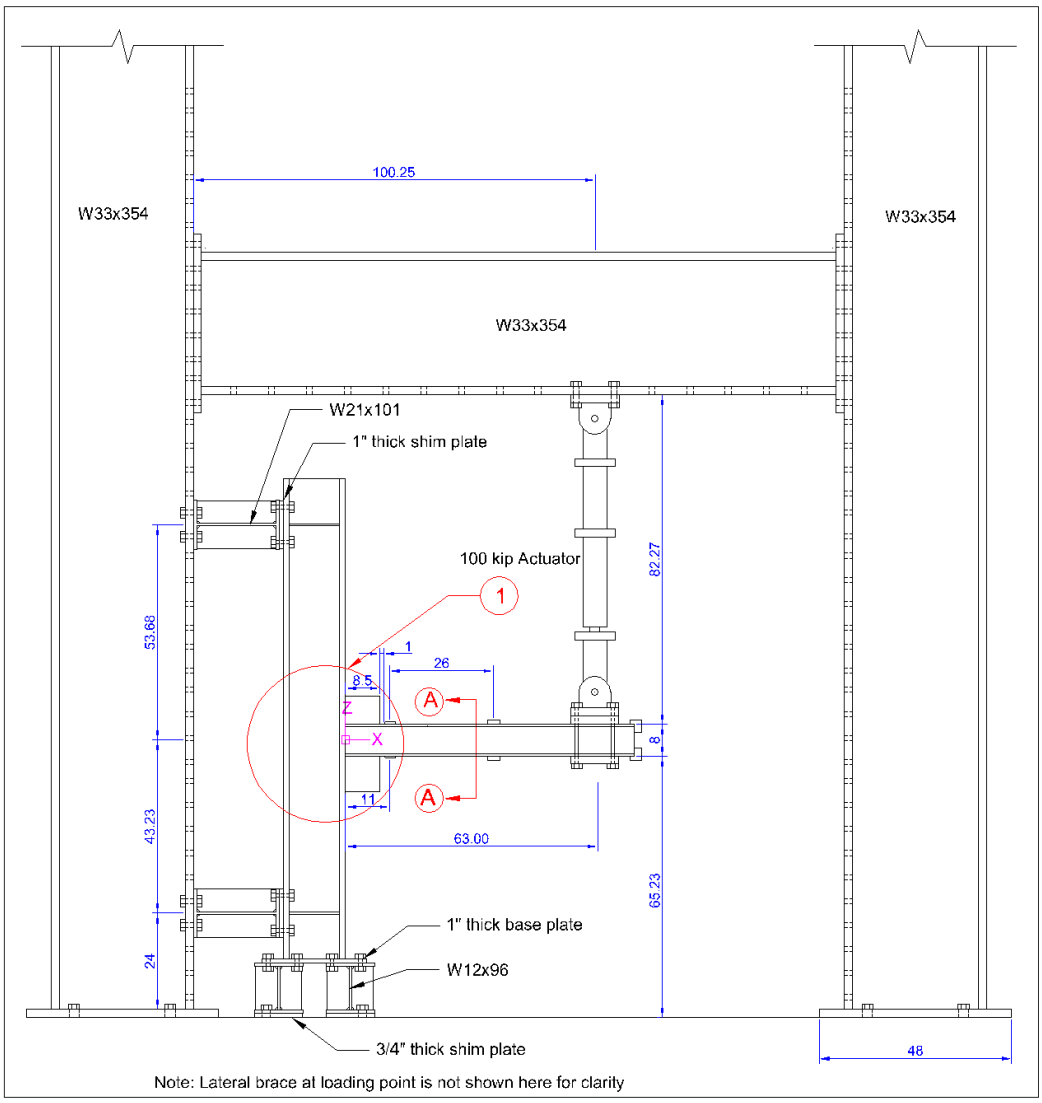
W33x354
100.25
W33x354
W33x354
W21x101
1" thick shim plate
100 kip Actuator
1
82.27
53.68
1
26
8.5
Z
X
A
A
8
11
43.23
63.00
65.23
1" thick base plate
W12x96
24
3/4" thick shim plate
48
Note: Lateral brace at loading point is not shown here for clarity

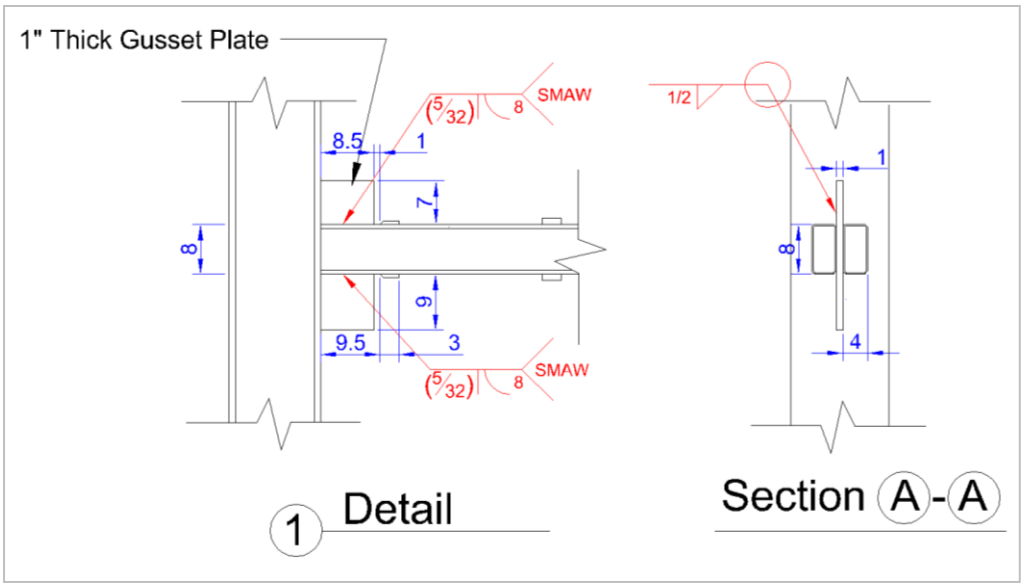
1" Thick Gusset Plate
(5/32)
8
SMAW
8.5
1
7
8
9
9.5
3
(5/32)
8
SMAW
1/2
1
8
4
1 Detail
Section A-A

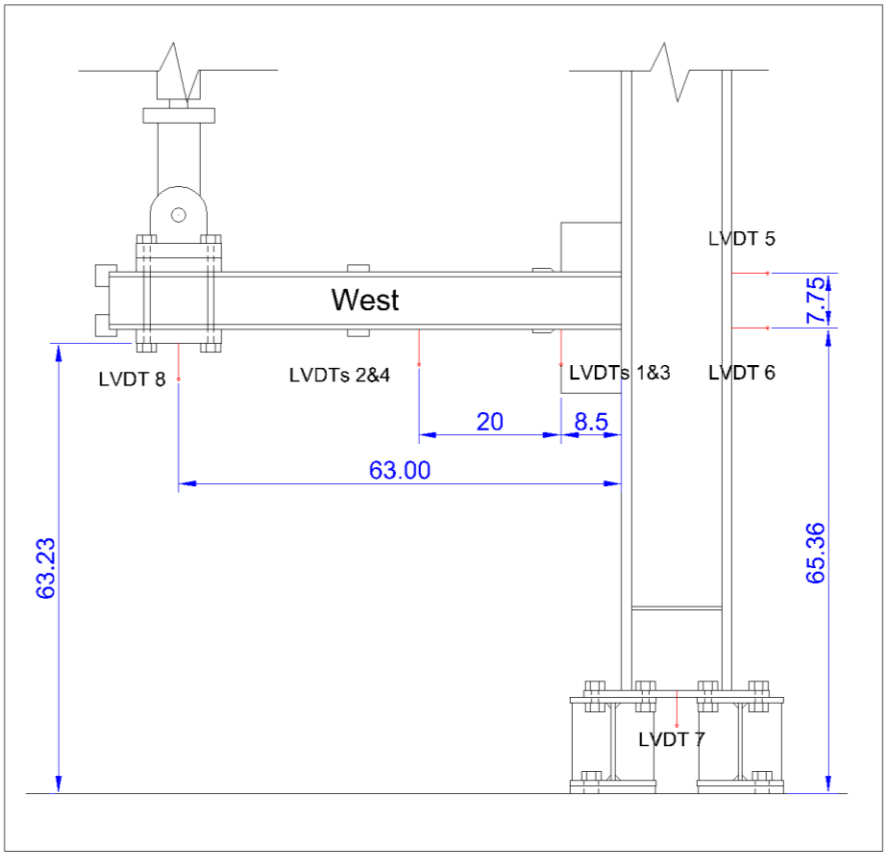
West
LVDT 5
7.75
LVDT 8
LVDTs 2&4
LVDTs 1&3
LVDT 6
20
8.5
63.00
63.23
65.36
LVDT 7

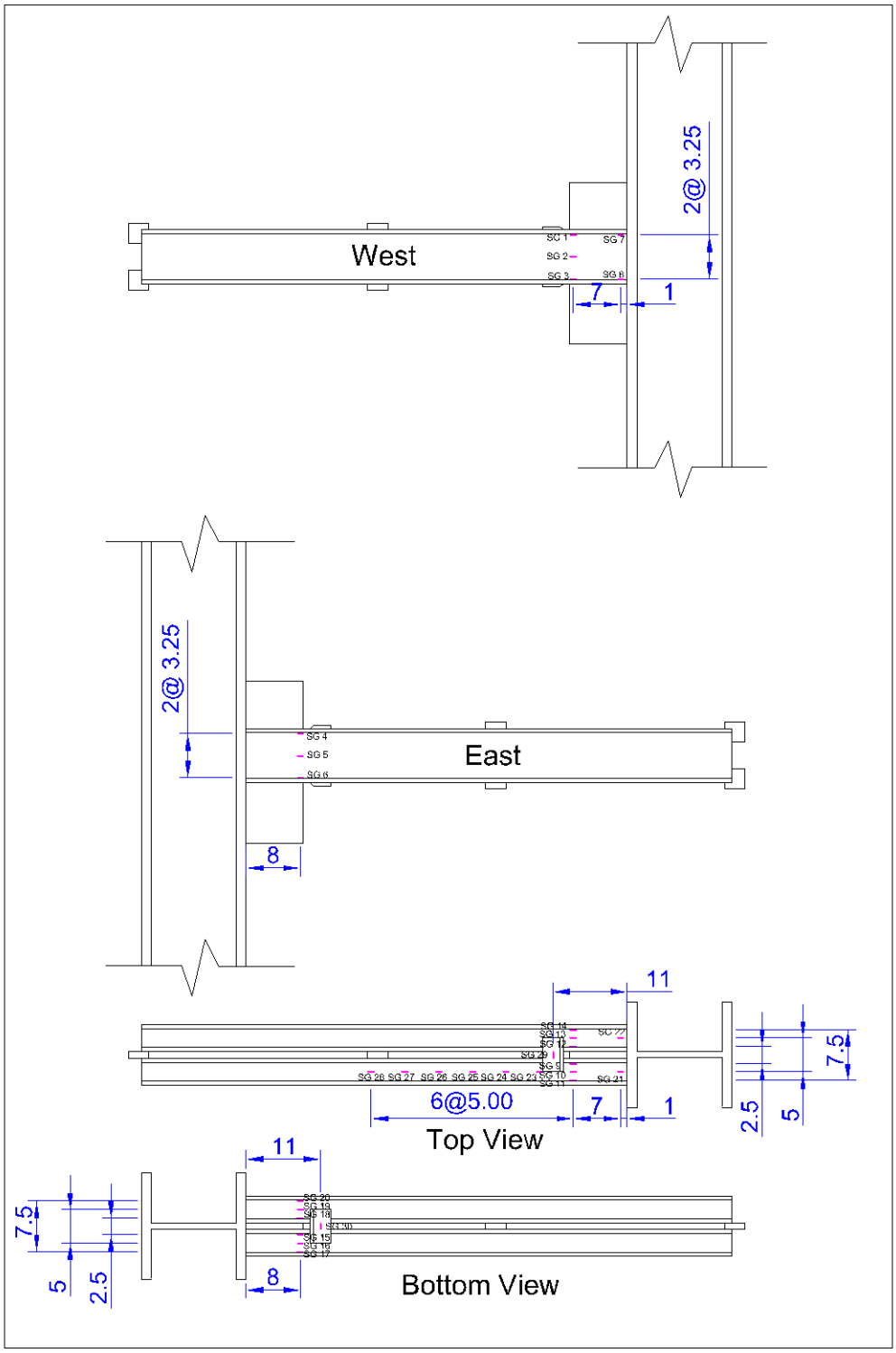
West
2@ 3.25
7
1
East
2@ 3.25
8
11
6@5.00
7
1
7.5
2.5
5
Top View
11
7.5
5
2.5
8
Bottom View

Specimen 2HSS8-2

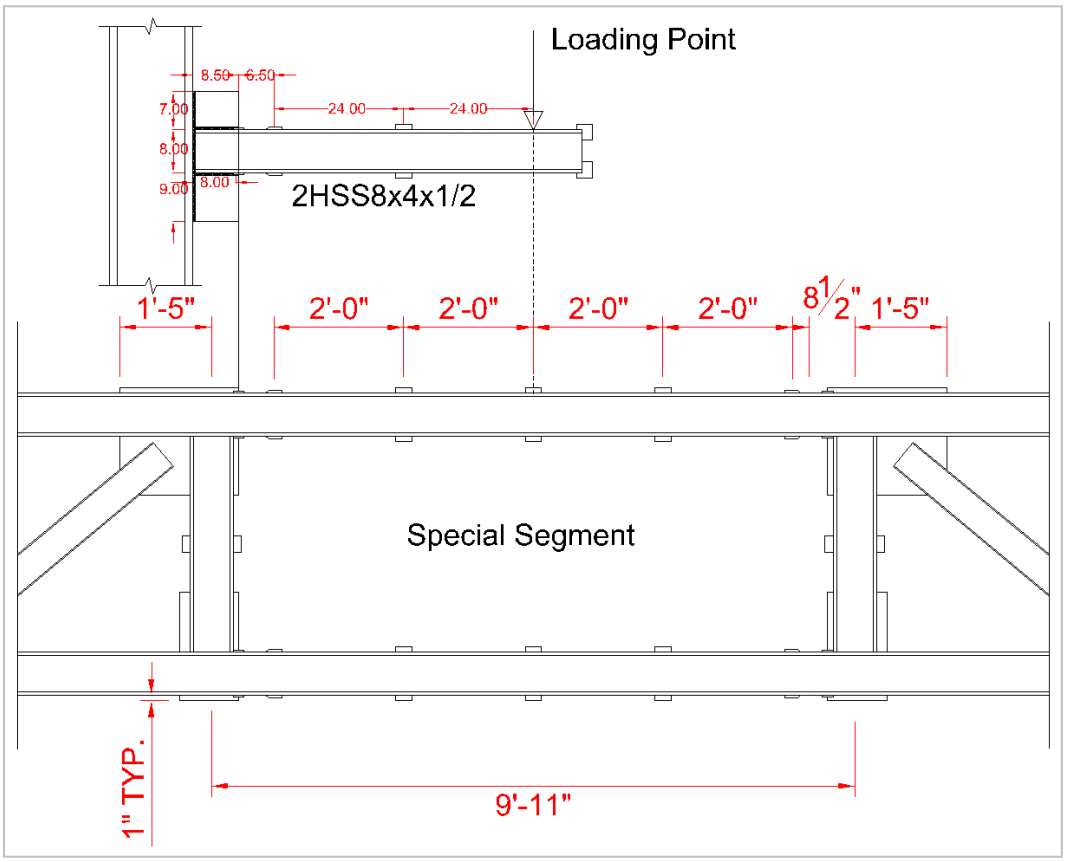

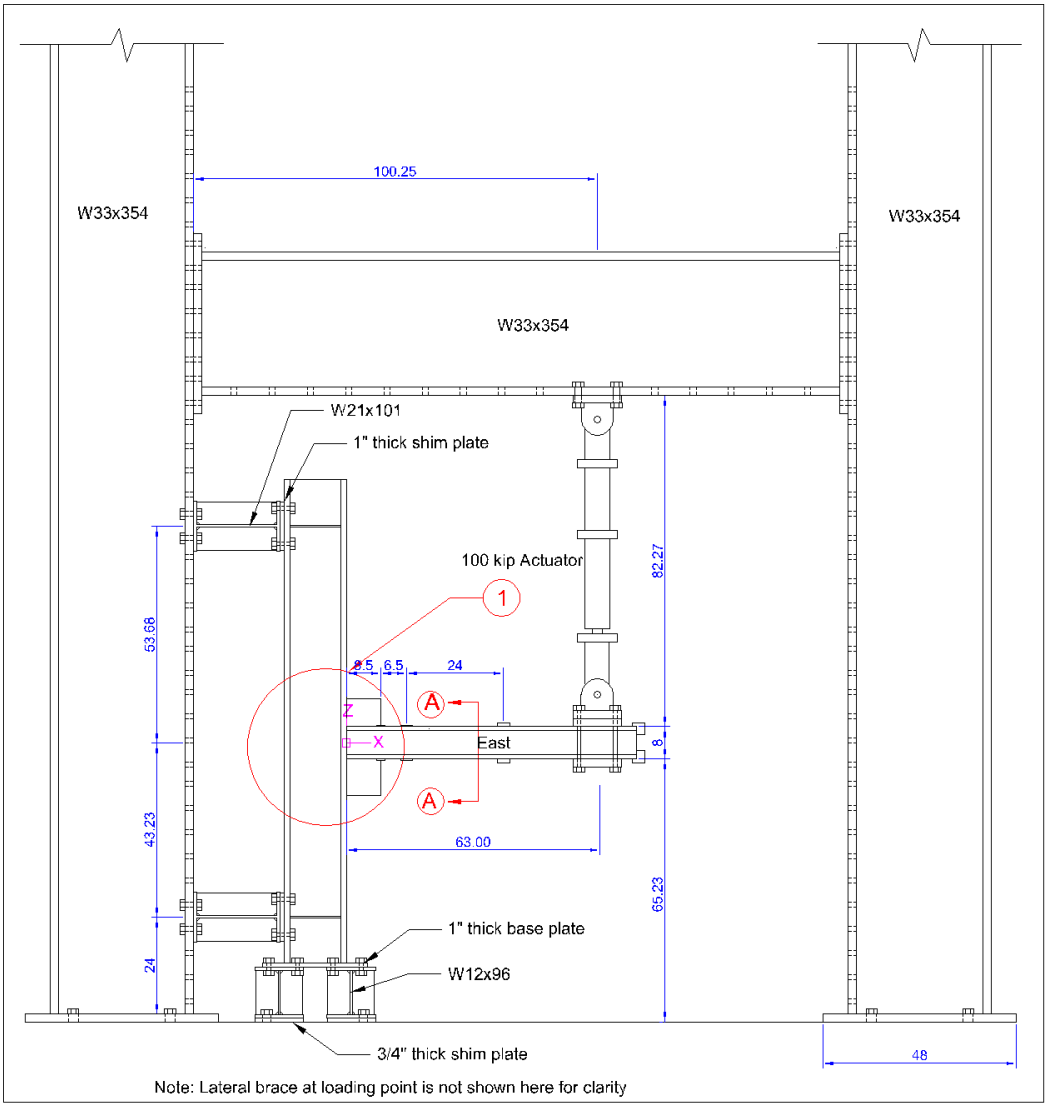
W33x354
100.25
W33x354
W33x354
W21x101
1" thick shim plate
100 kip Actuator
1
63.66
43.23
24
82.27
8
65.23
8.5
6.5
24
Z
X
East
A
A
63.00
1" thick base plate
W12x96
3/4" thick shim plate
48
Note: Lateral brace at loading point is not shown here for clarity

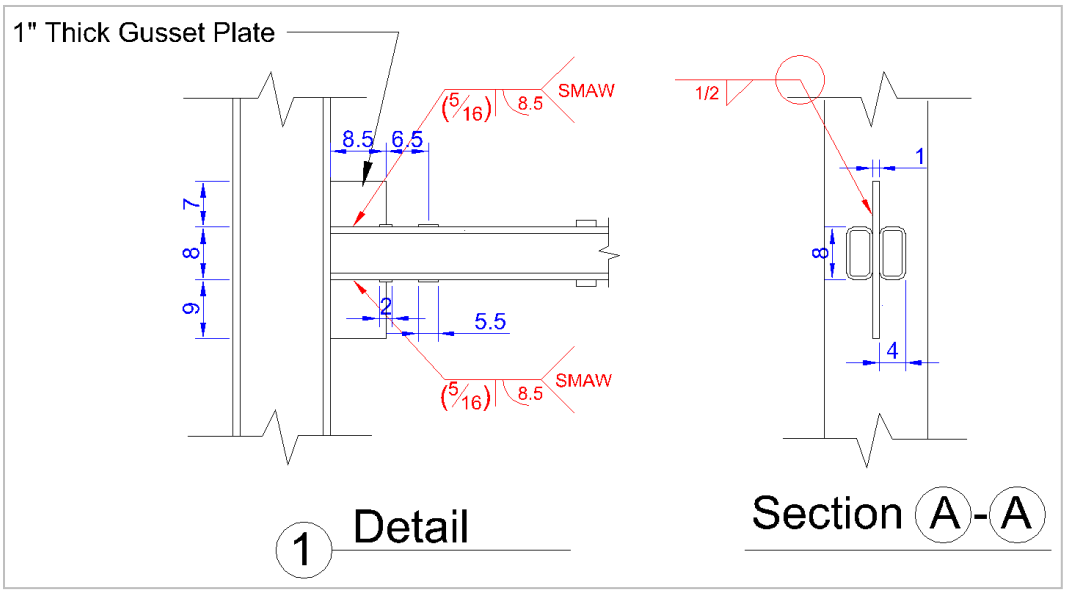
1" Thick Gusset Plate
(5/16)
8.5
SMAW
8.5
6.5
7
8
9
2
5.5
(5/16)
8.5
SMAW
1/2
1
8
4
1
Detail
Section A-A

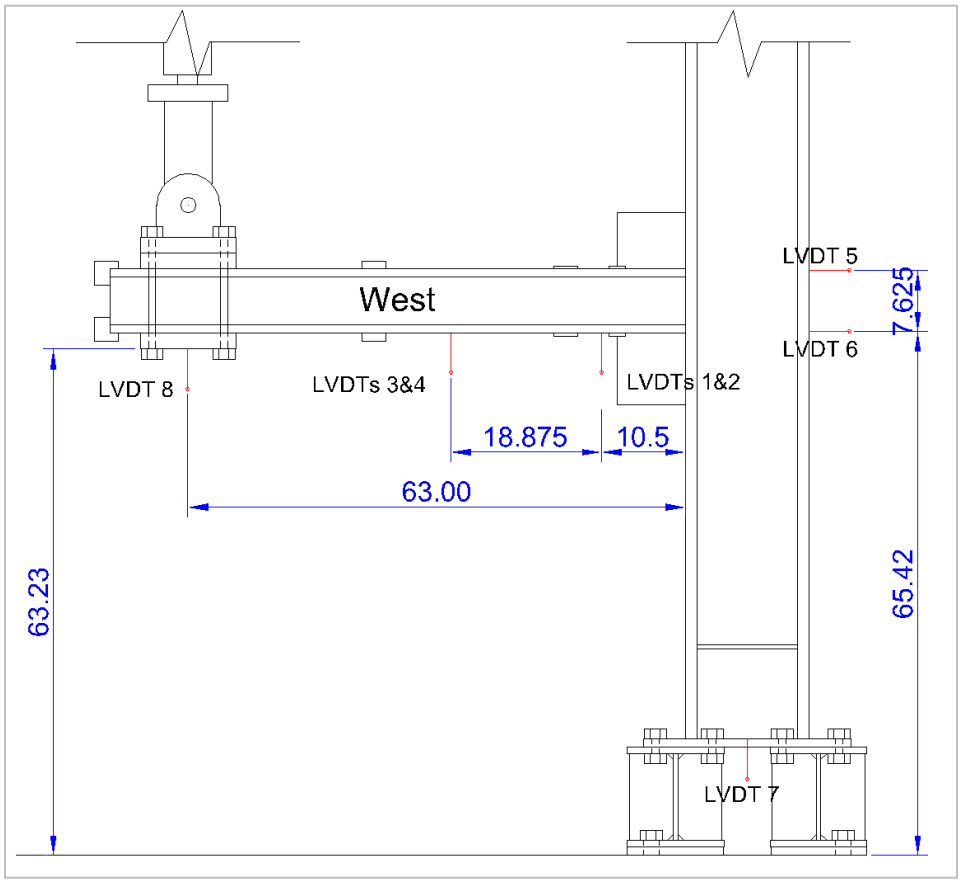
West
LVDT 5
LVDT 6
7.625
LVDT 8
LVDTs 3&4
LVDTs 1&2
18.875
10.5
63.00
63.23
65.42
LVDT 7

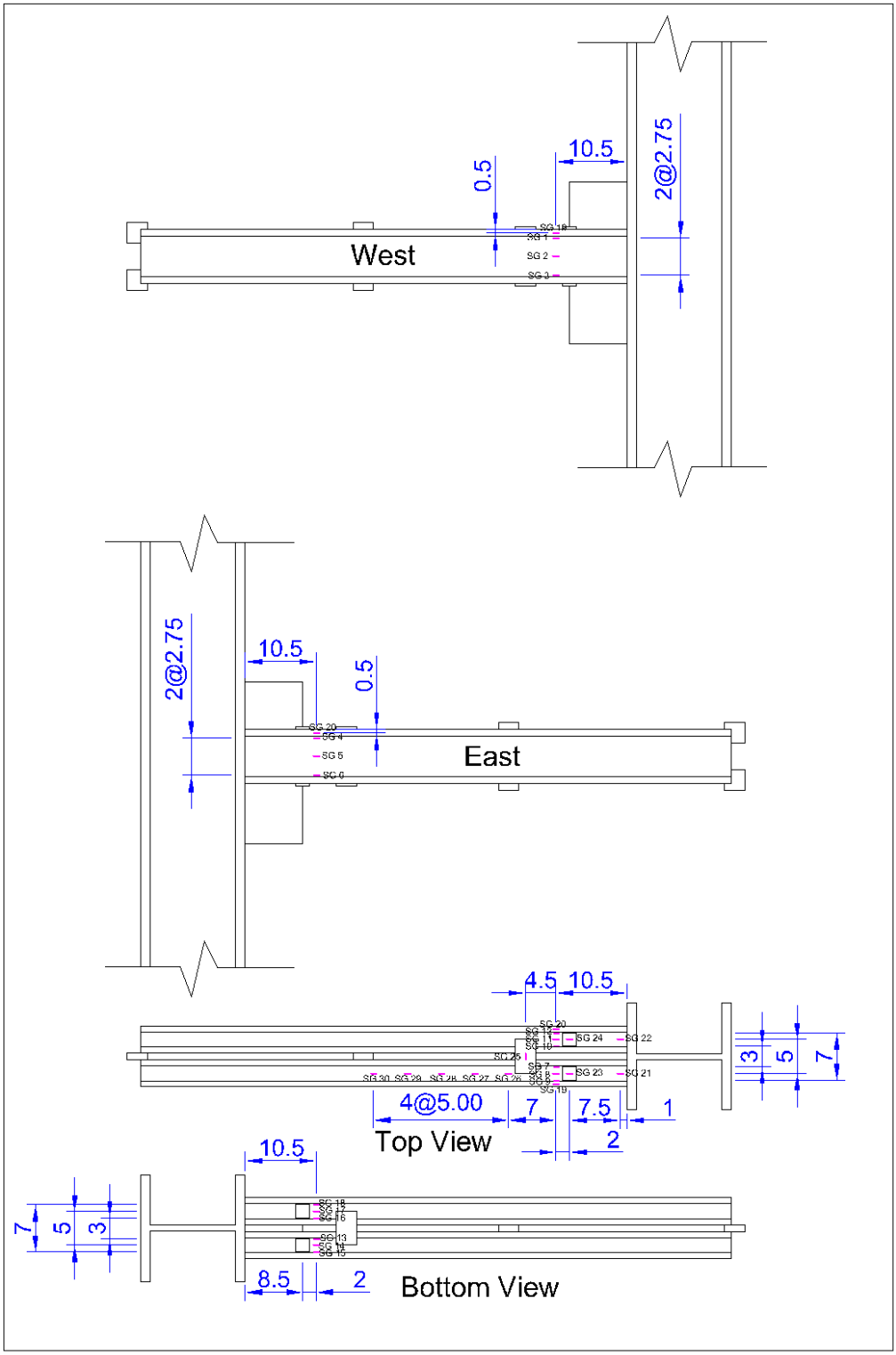
West
0.5
10.5
2@2.75
East
2@2.75
10.5
0.5
4.5
10.5
4@5.00
7
7.5
1
2
Top View
3
5
7
10.5
7
5
3
8.5
2
Bottom View

Specimen 2HSS8-3

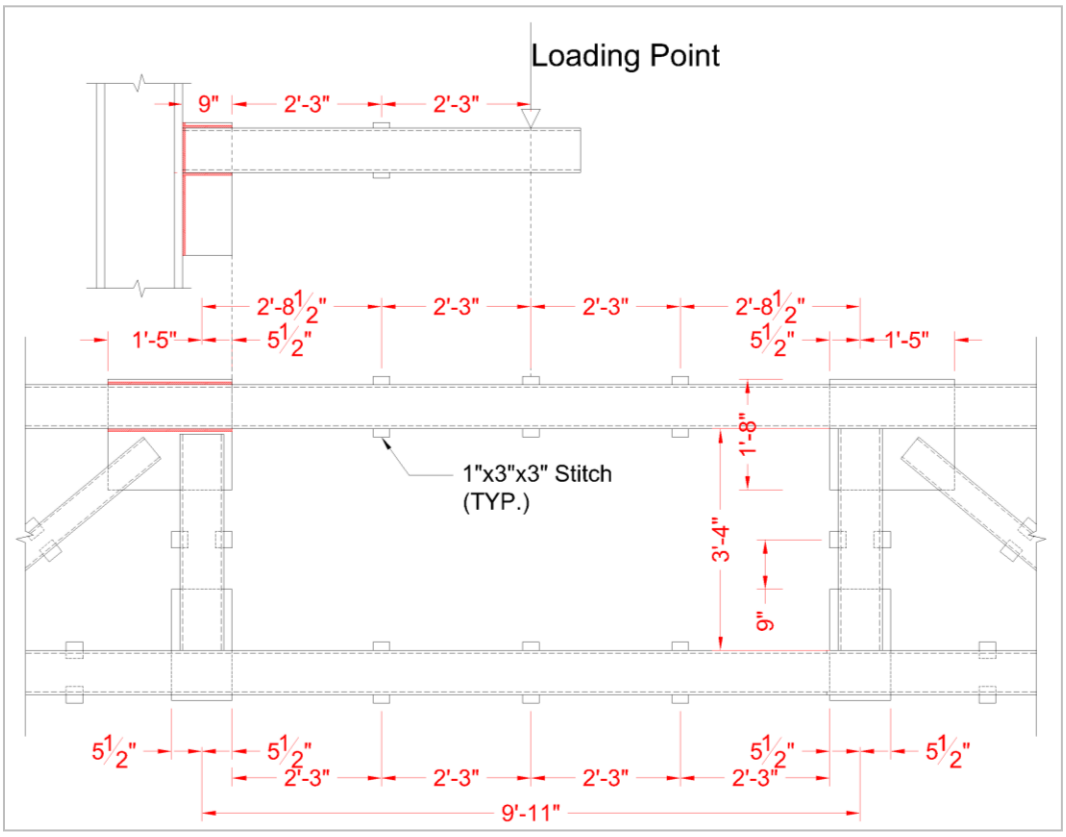

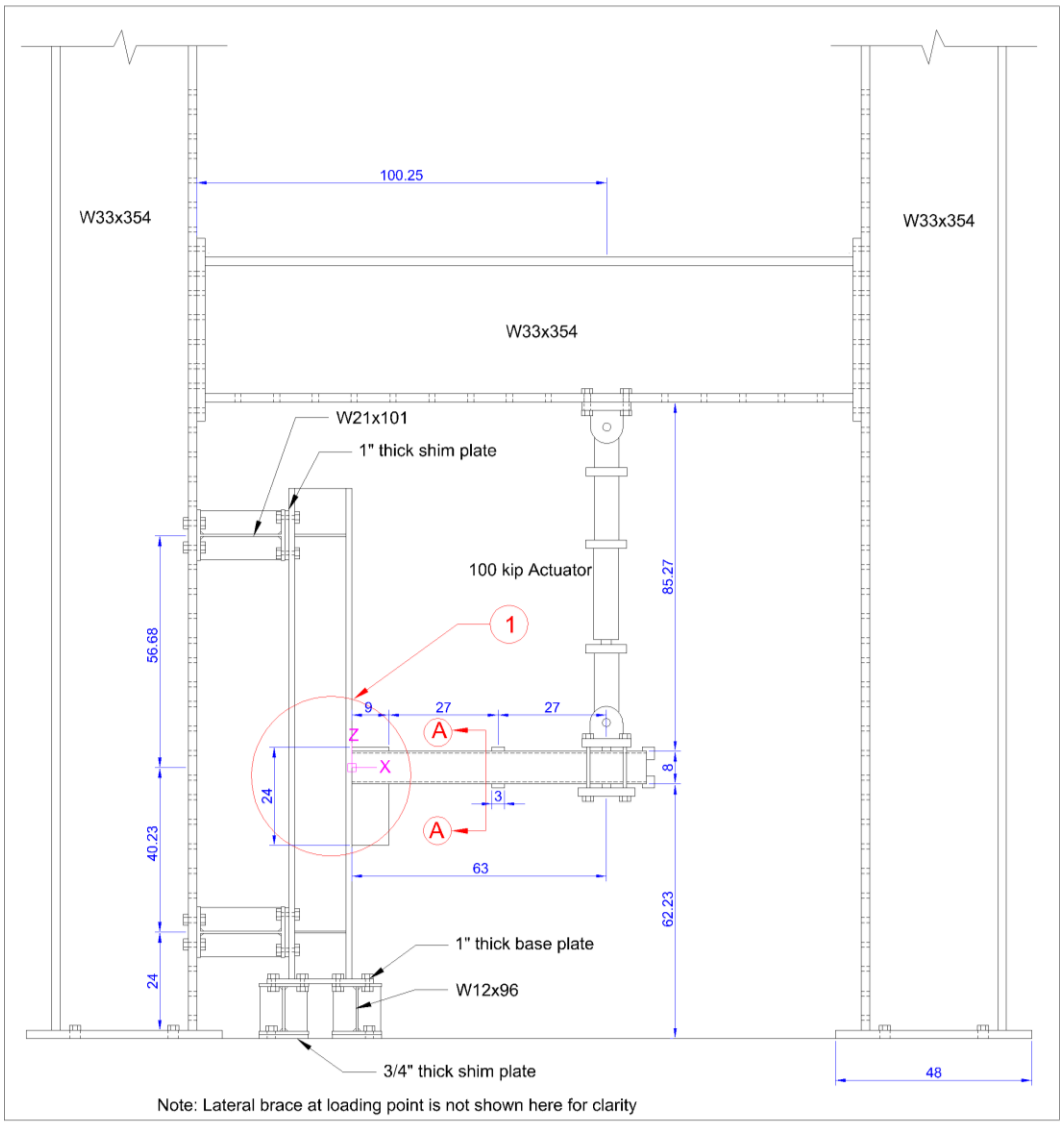
100.25
W33x354
W33x354
W33x354
W21x101
1" thick shim plate
100 kip Actuator
85.27
56.68
40.23
24
24
1
9
27
27
Z
X
A
A
24
8
3
63
62.23
1" thick base plate
W12x96
3/4" thick shim plate
48
Note: Lateral brace at loading point is not shown here for clarity

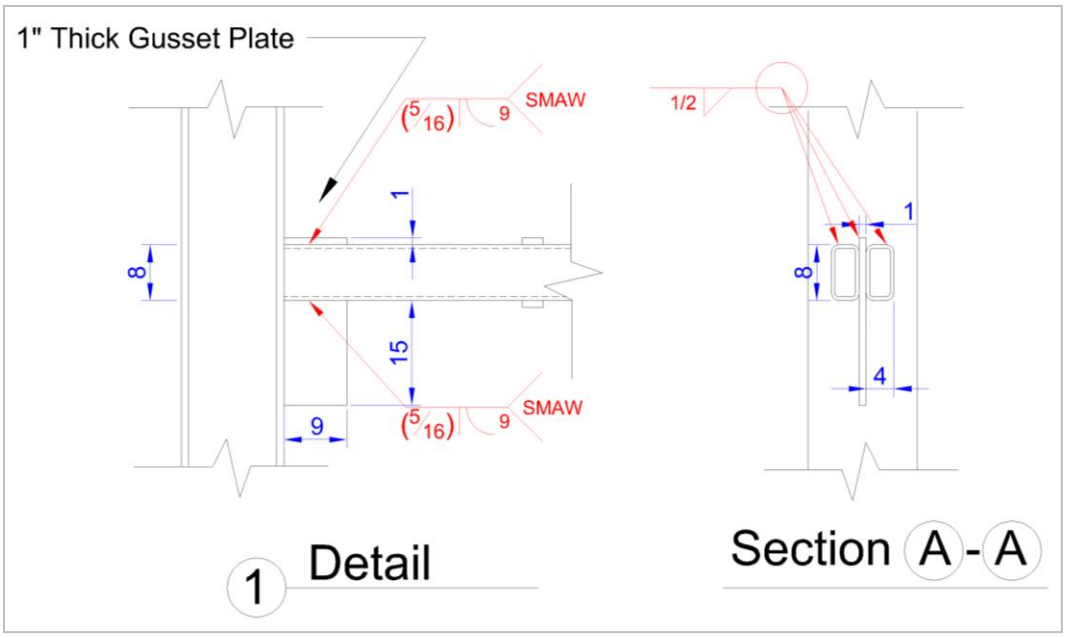
1" Thick Gusset Plate
(5/16)
9
SMAW
1
8
15
9
(5/16)
9
SMAW
1/2
1
8
4
1
Detail
Section A - A

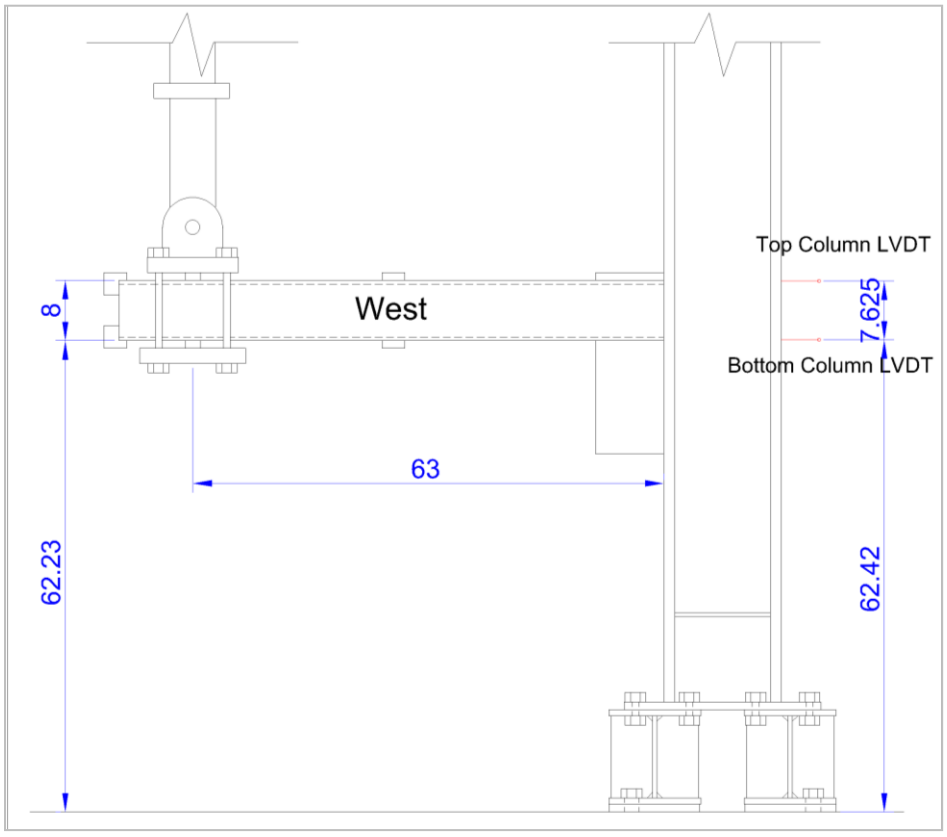
West
8
63
62.23
Top Column LVDT
7.625
Bottom Column LVDT
62.42

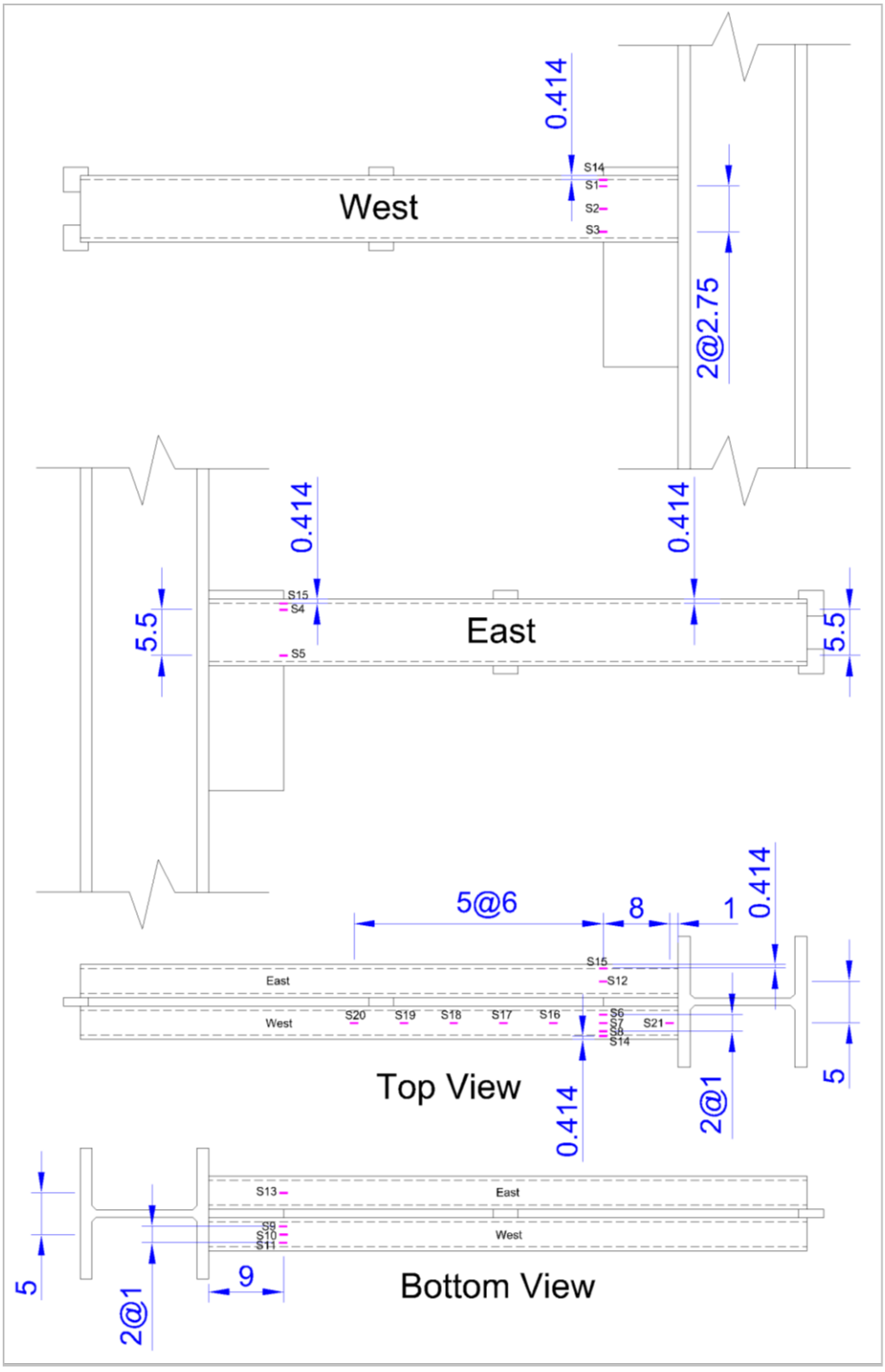
0.414
S14
S1
S2
S3
West
2@2.75
0.414
0.414
S15
S4
S5
East
5.5
5.5
5@6
8
1
0.414
S15
S12
East
West
S20
S19
S18
S17
S16
S6
S7
S8
S14
S21
Top View
0.414
2@1
5
S13
East
S9
S10
S11
West
5
2@1
9
Bottom View

Appendix E

Strain Gauge Data for Component Tests

Specimen 2C12-1

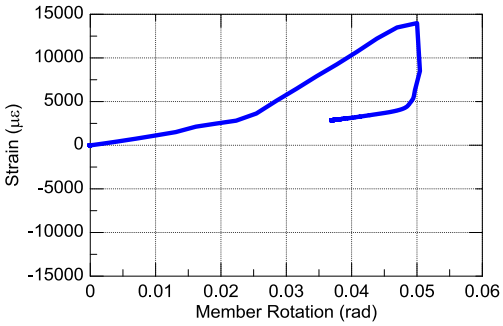

SG 1

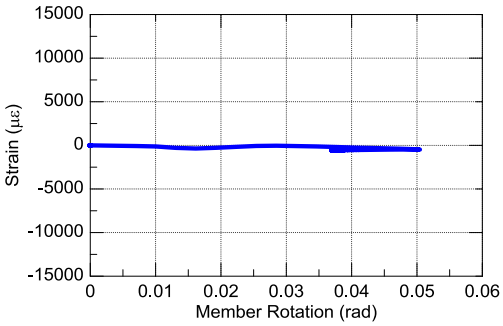

SG 2

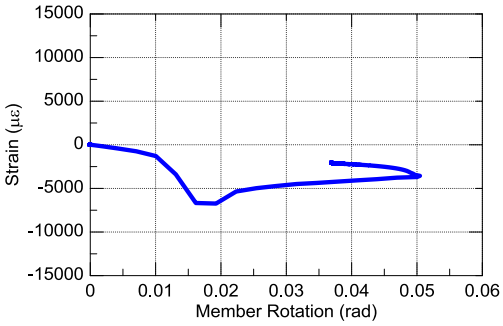

SG 3

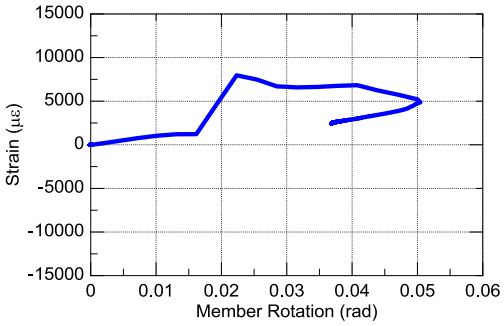

SG 4

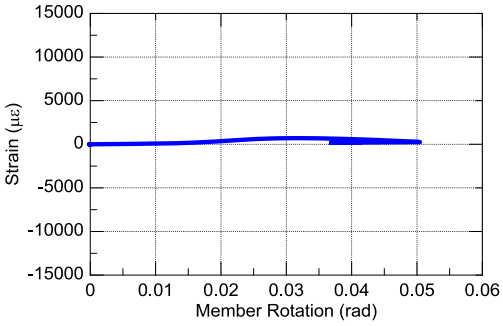

SG 5

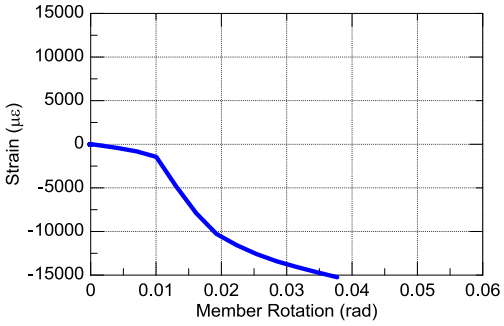

SG 6

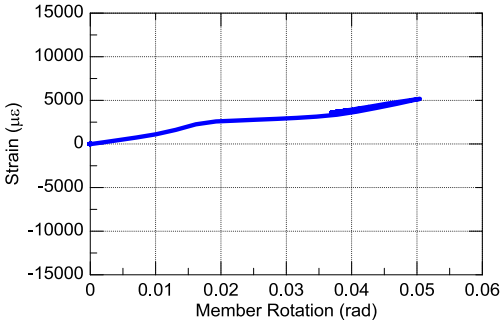

SG 7

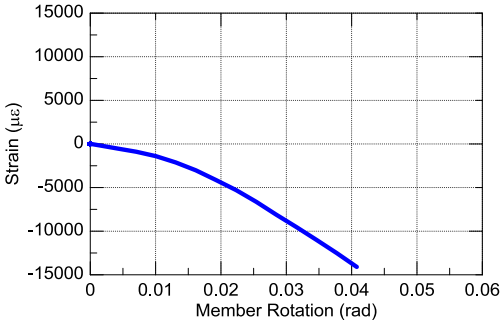

SG 8

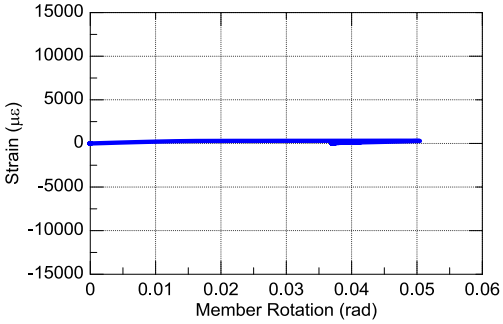

SG 9

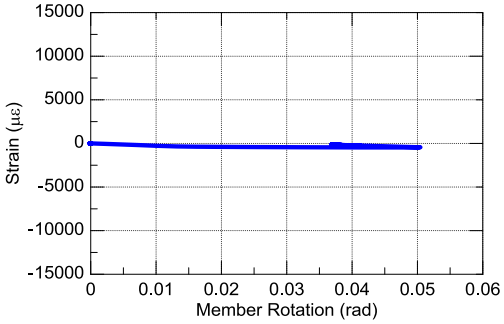

SG 10

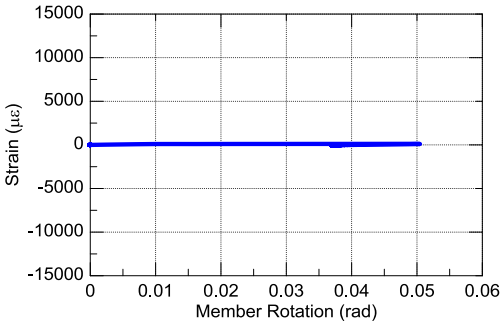

SG 11

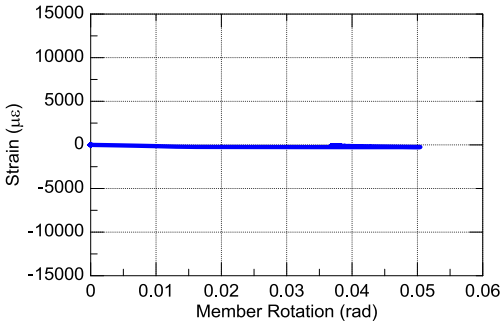

SG 12

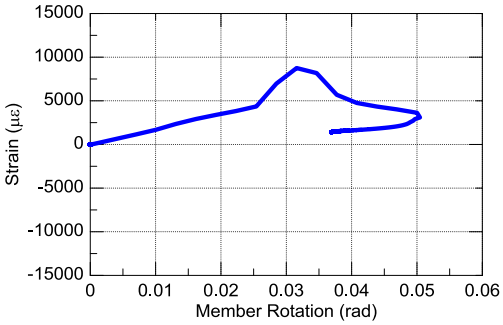

SG 13

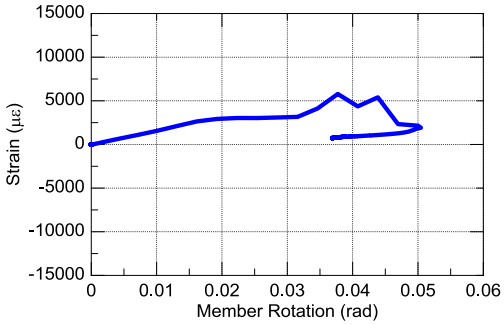

SG 14

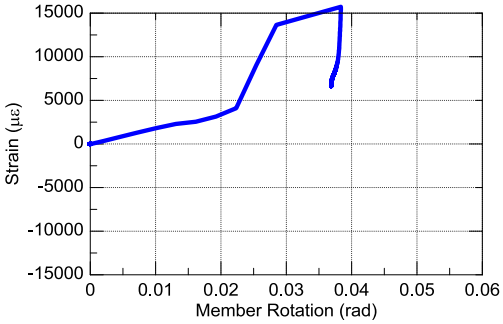

SG 15

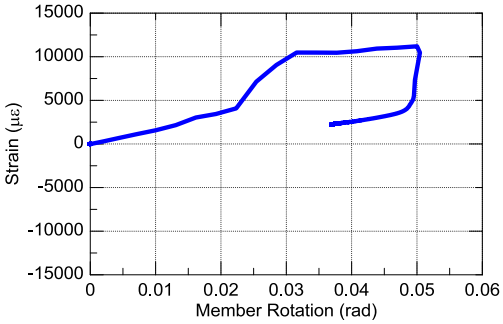

SG 16

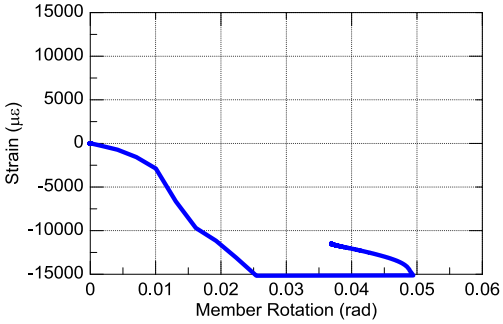

SG 17

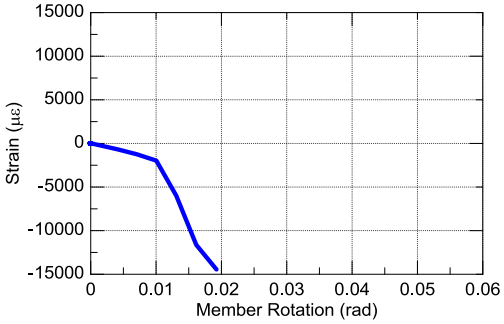

SG 18

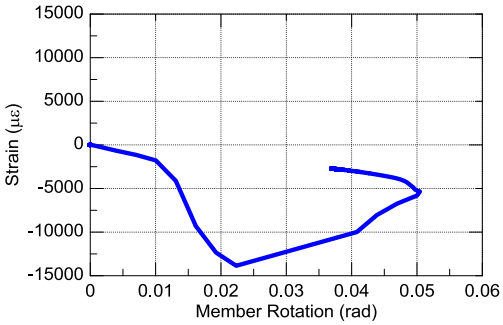

SG 19

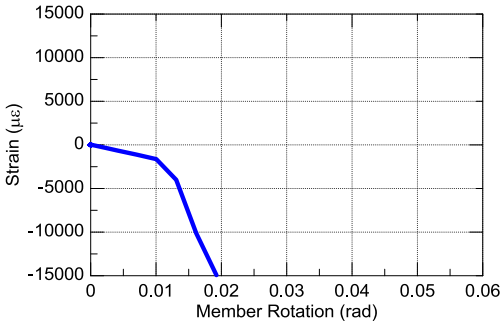

SG 20

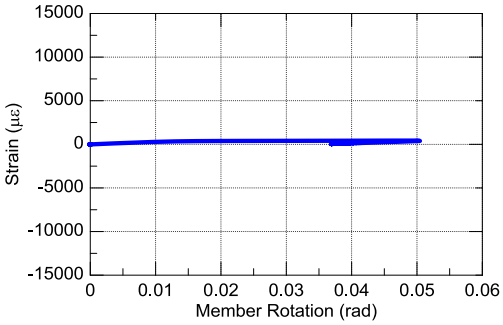

SG 21

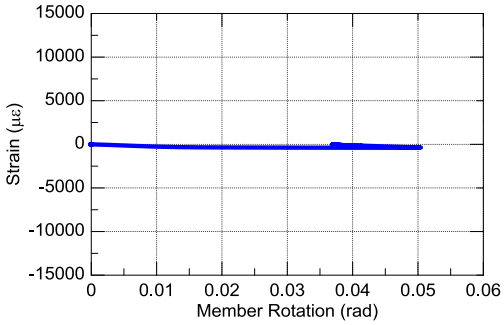

SG 22

Specimen 2C12-2

In this specimen, the displacement recorded in the data acquisition system was incorrect. As a result, the plots were made between load versus strain instead.

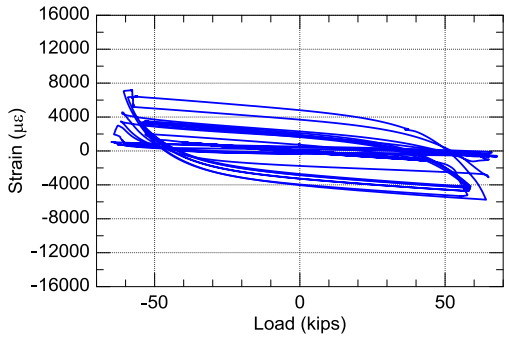

SG 1

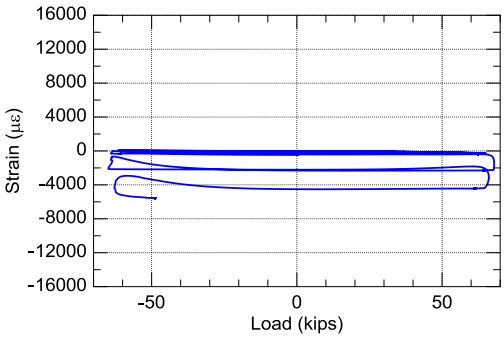

SG 2

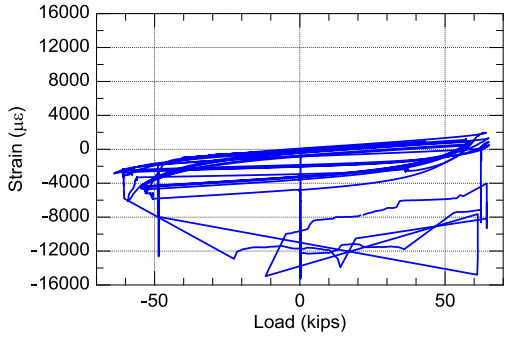

SG 3

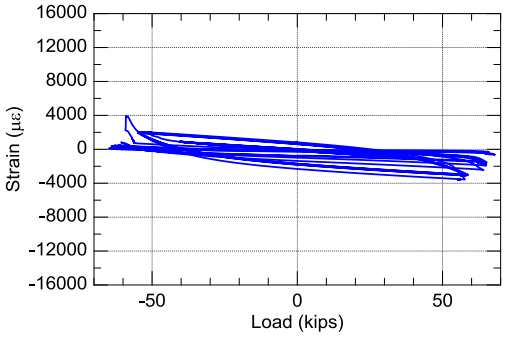

SG 4

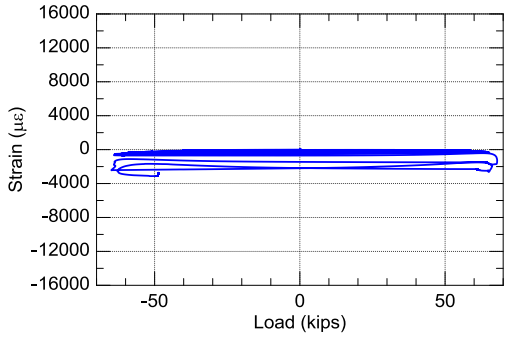

SG 5

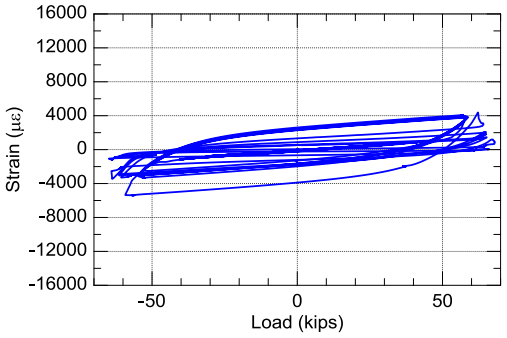

SG 6

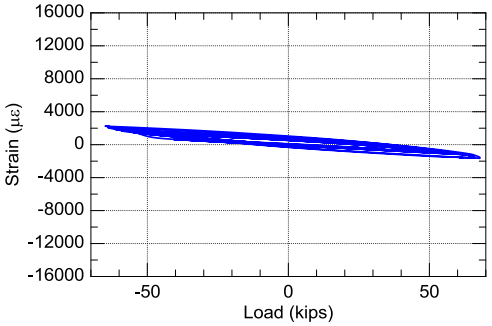

SG 7

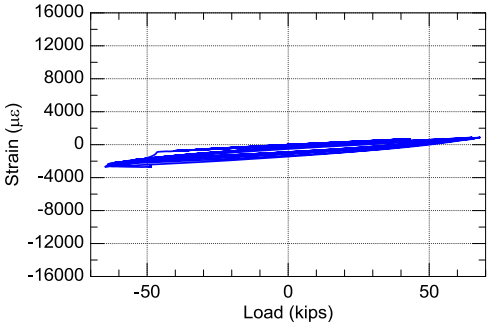

SG 8

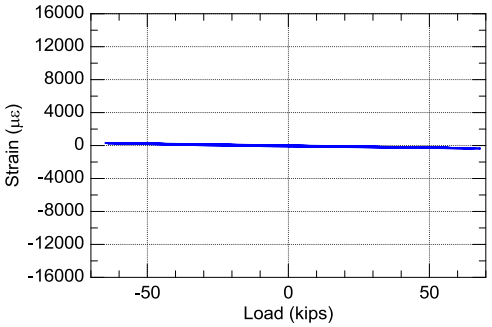

SG 9

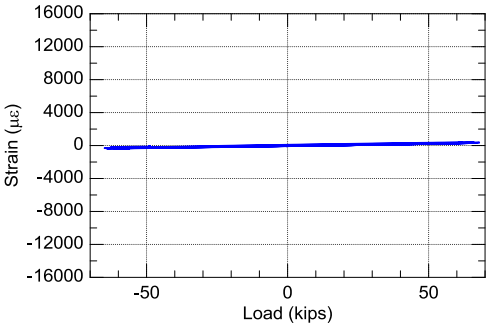

SG 10

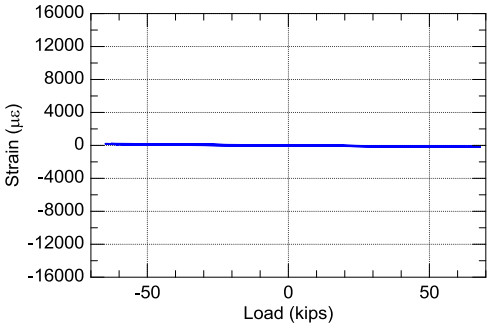

SG 11

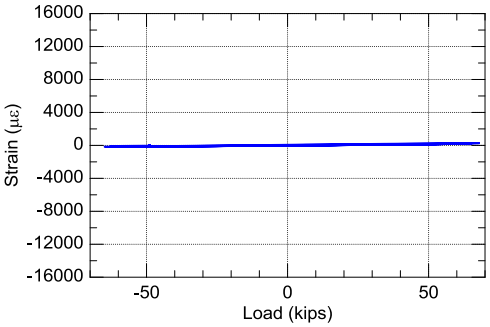

SG 12

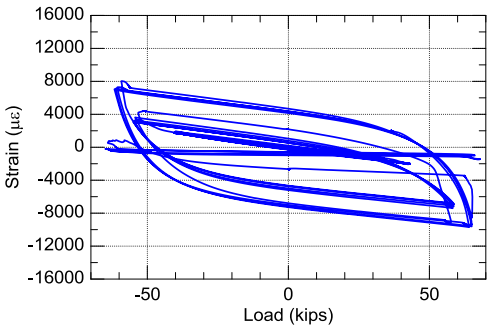

SG 13

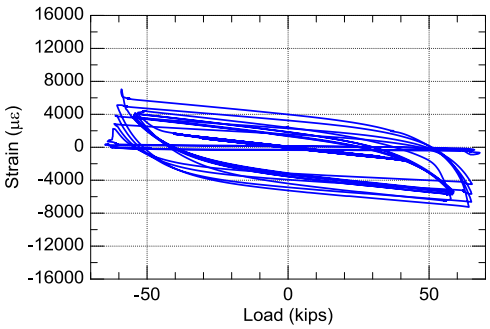

SG 14

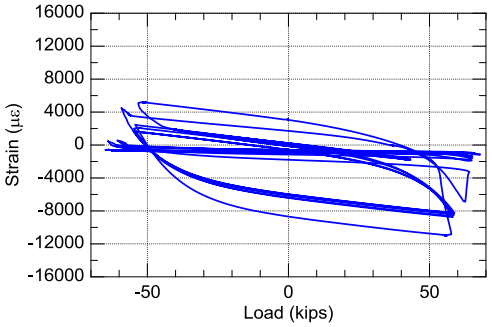

SG 15

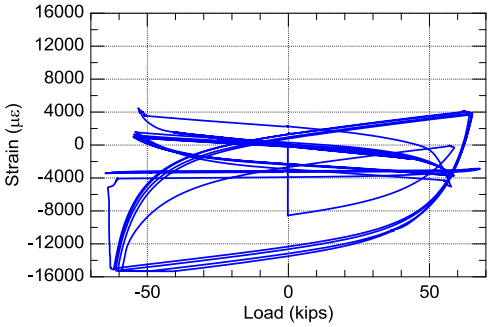

SG 16

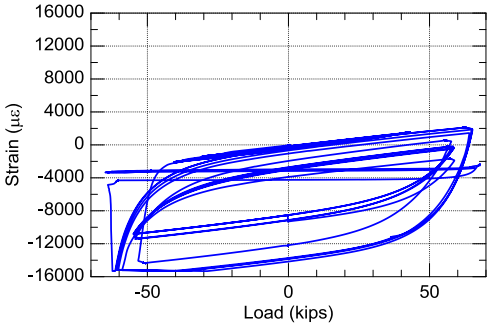

SG 17

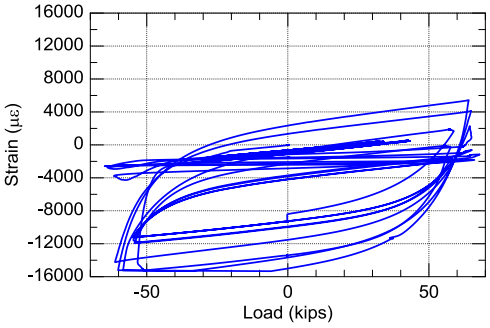

SG 18

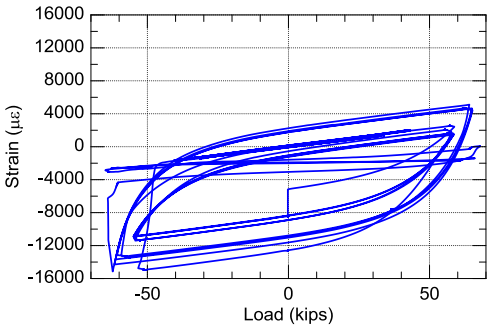

SG 19

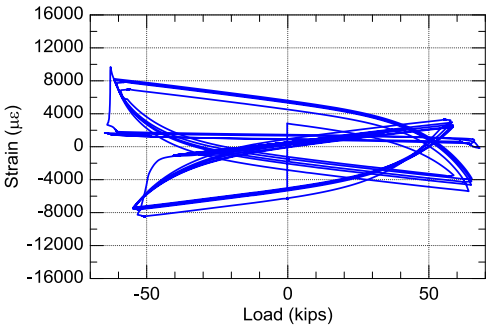

SG 20

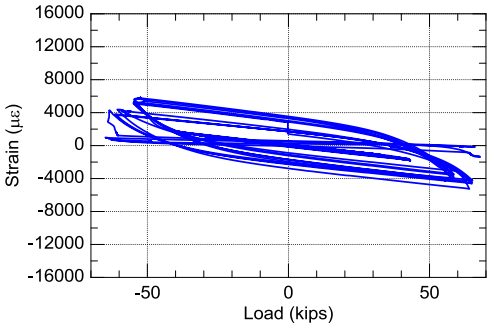

SG 21

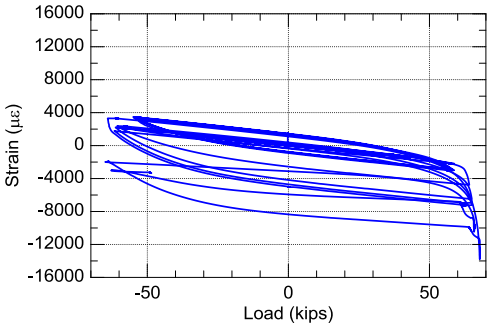

SG 22

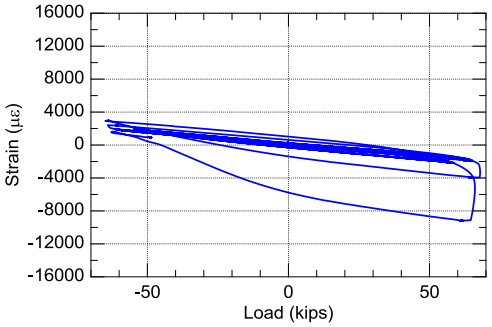

SG 23

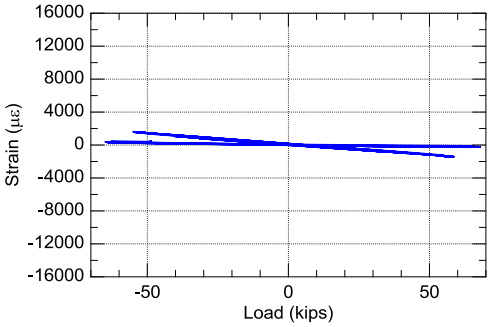

SG 24

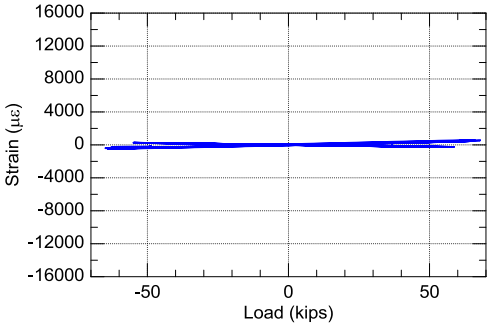

SG 25

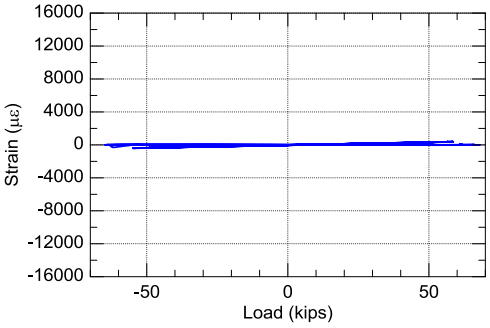

SG 26

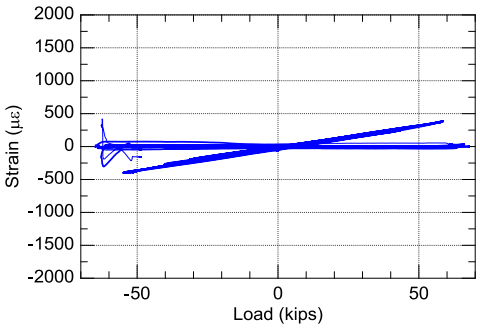

SG 1-1

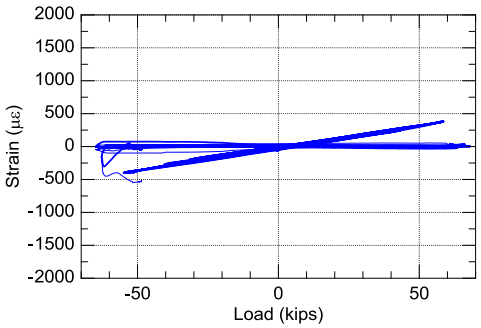

SG 1-2

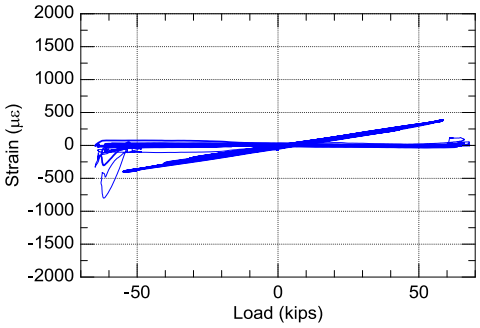

SG 1-3

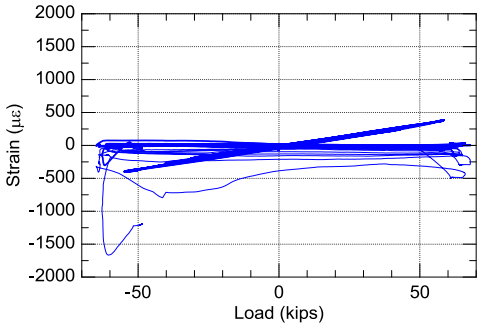

SG 1-4

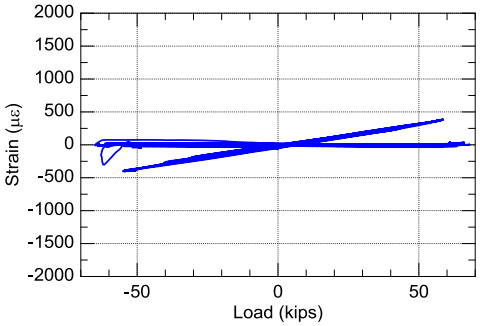

SG 2-1

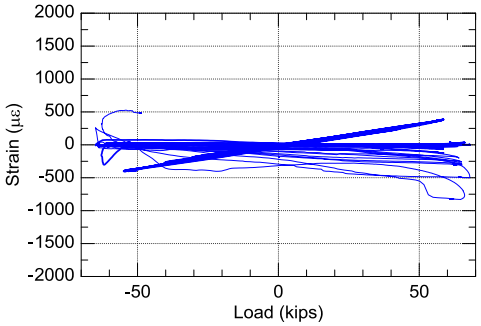

SG 2-2

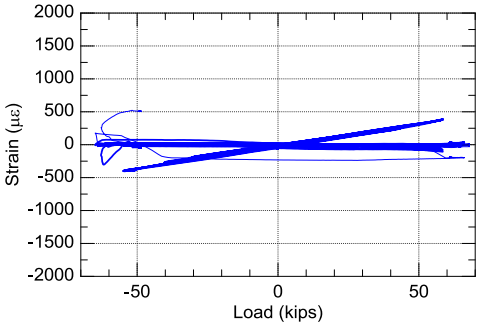

SG 2-3

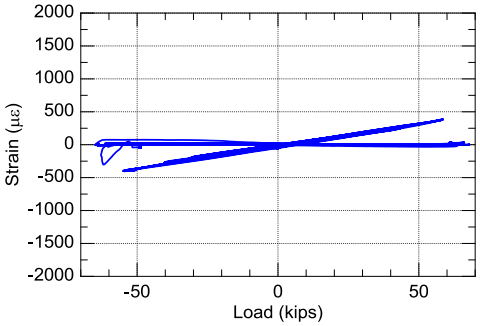

SG 2-4

Specimen 2C12-3

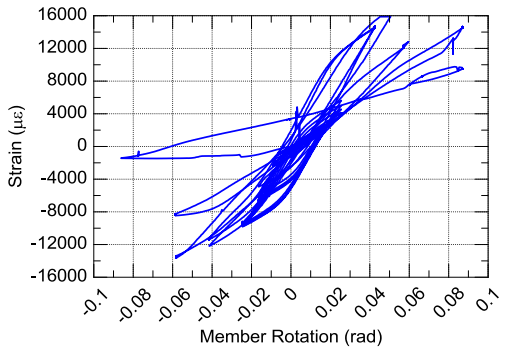

SG 1

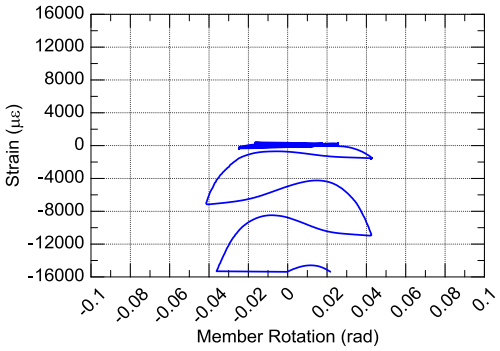

SG 2

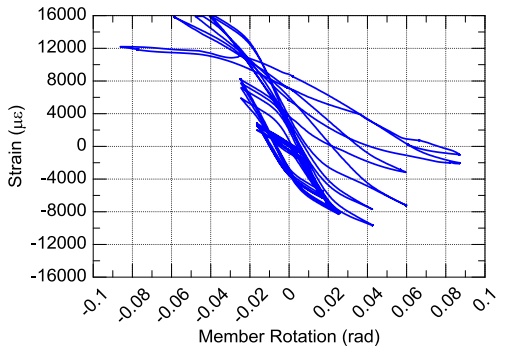

SG 3

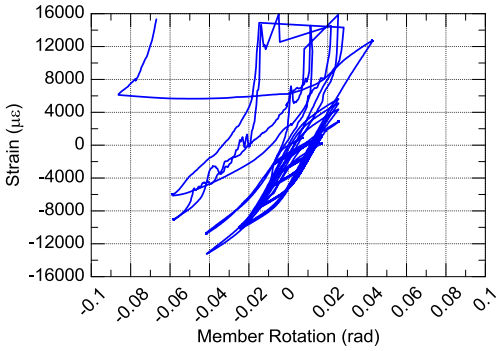

SG 4

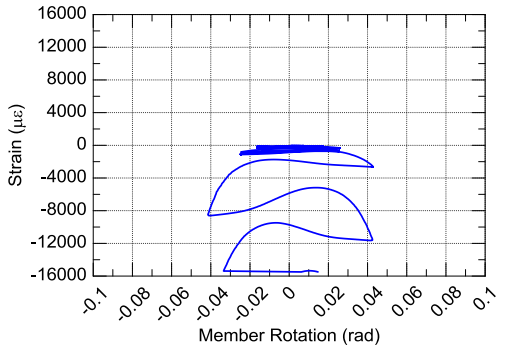

SG 5

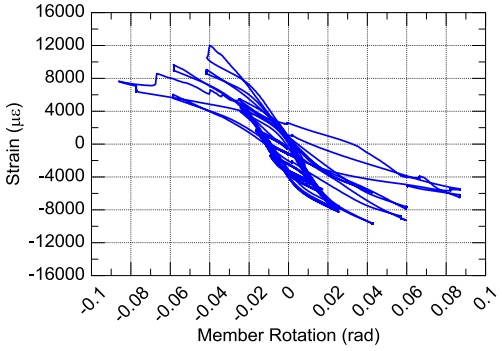

SG 6

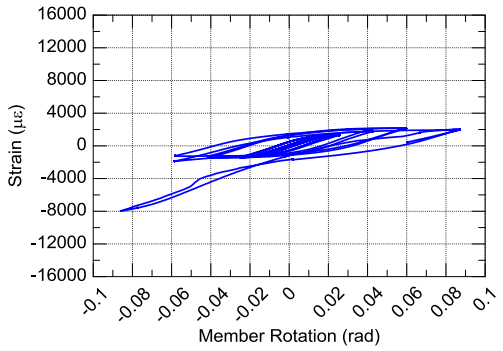

SG 7

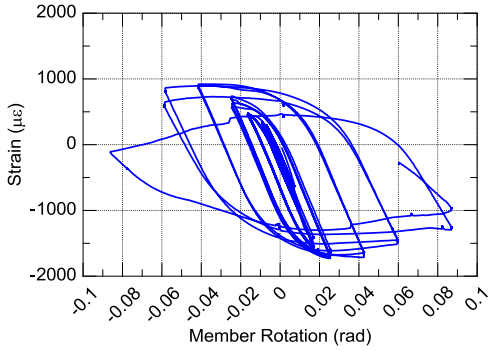

SG 8

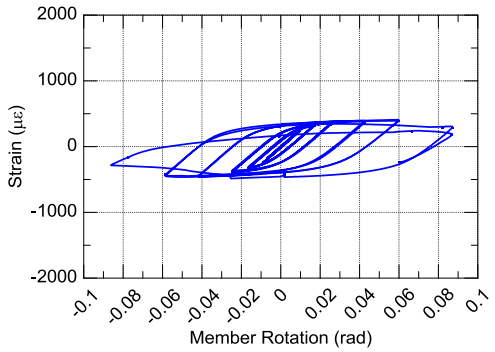

SG 9

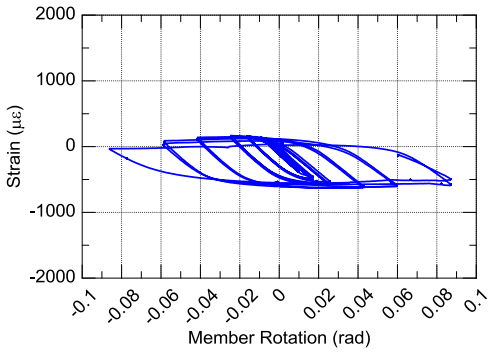

SG 10

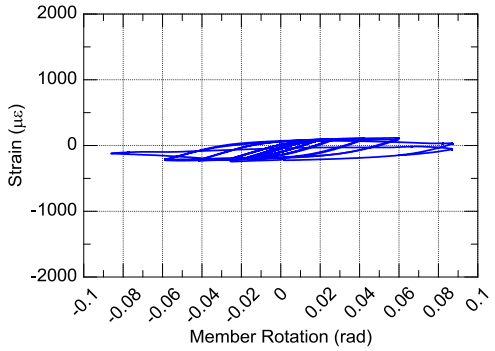

SG 11

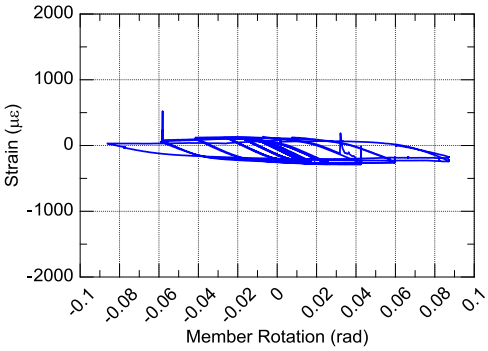

SG 12

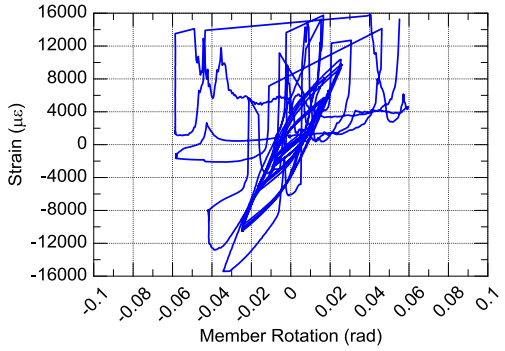

SG 13

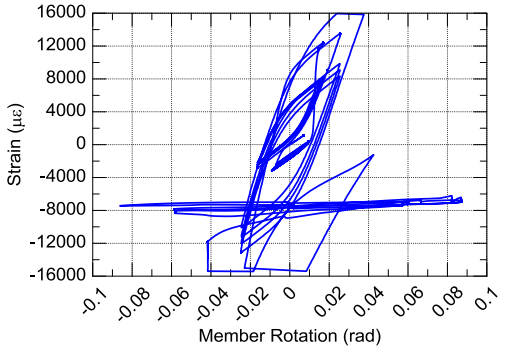

SG 14

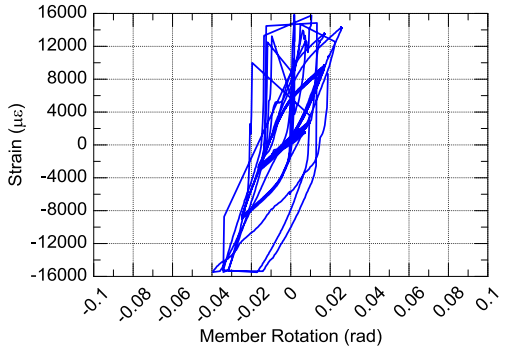

SG 15

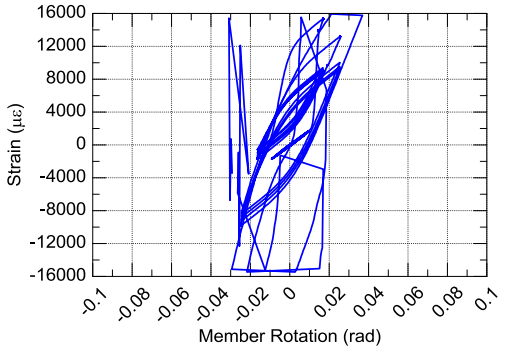

SG 16

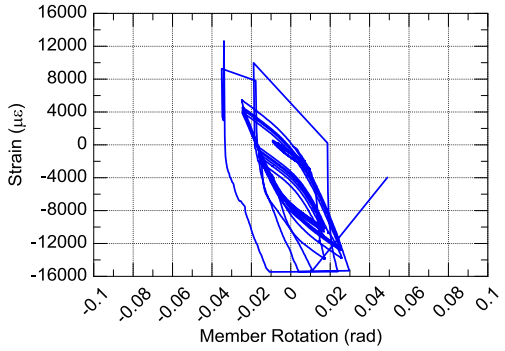

SG 17

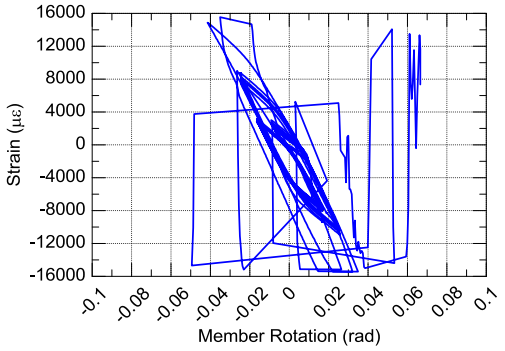

SG 18

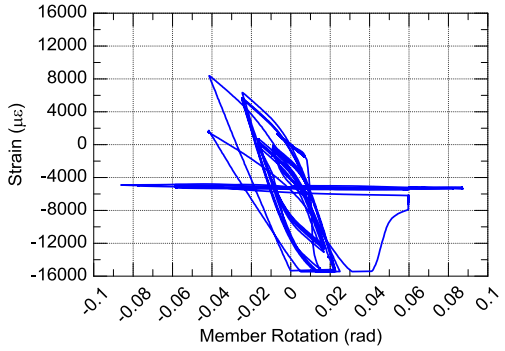

SG 19

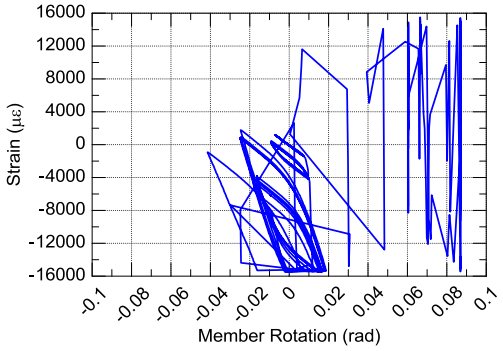

SG 20

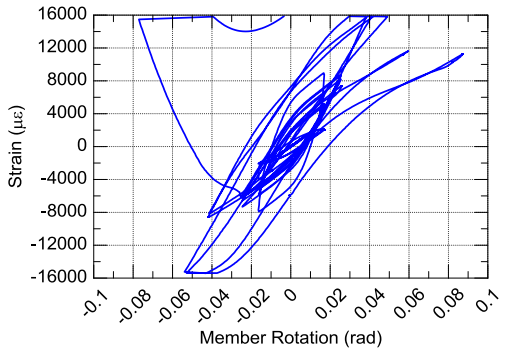

SG 21

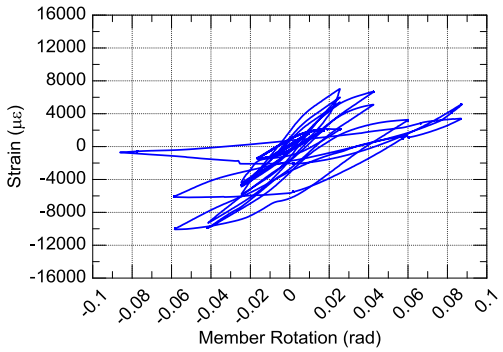

SG 22

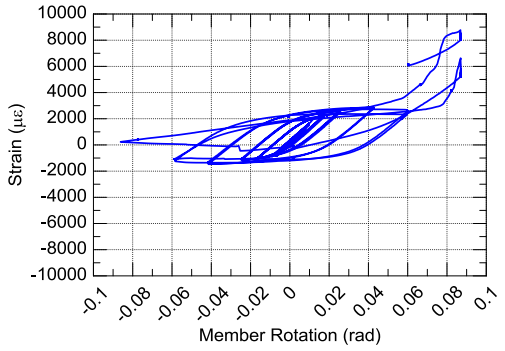

SG 23

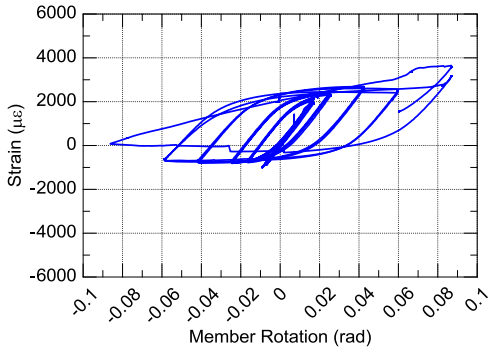

SG 24

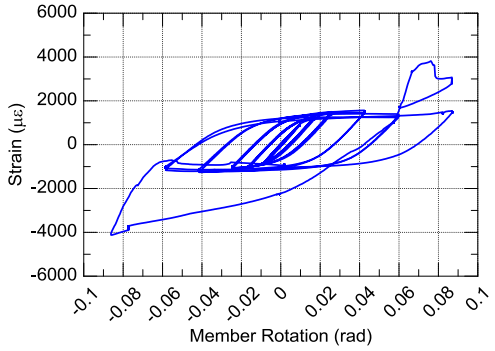

SG 25

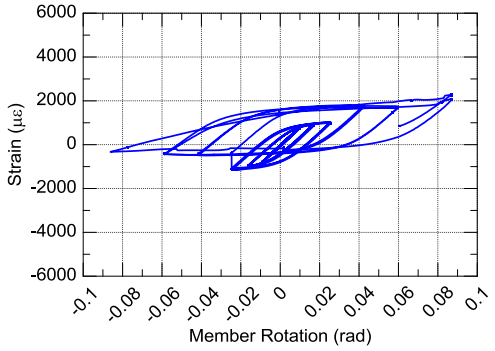

SG 26

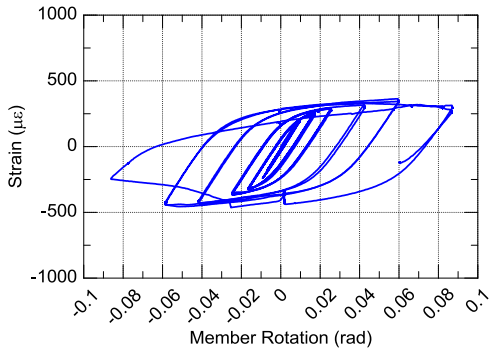

SG 27

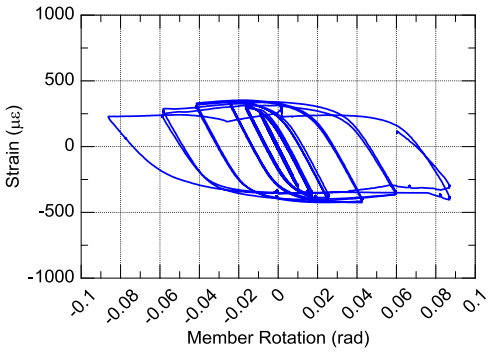

SG 28

Specimen 2C12-4

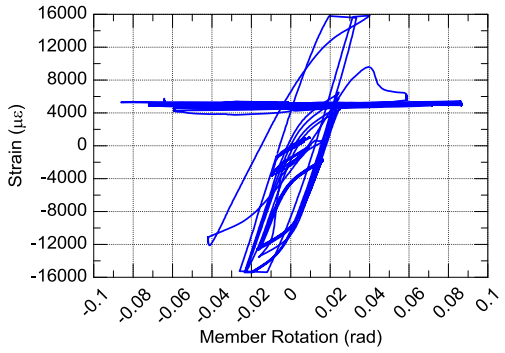

SG 1

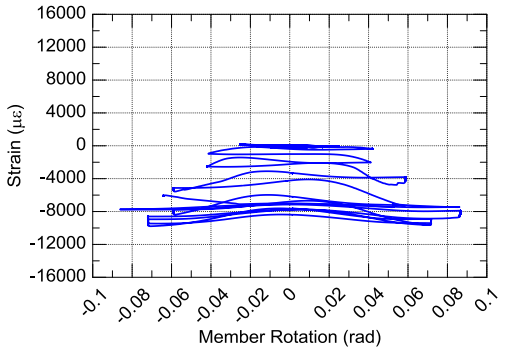

SG 2

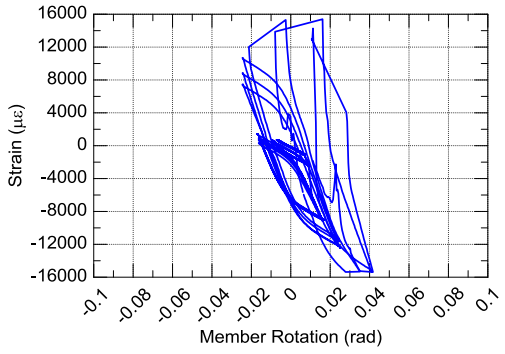

SG 3

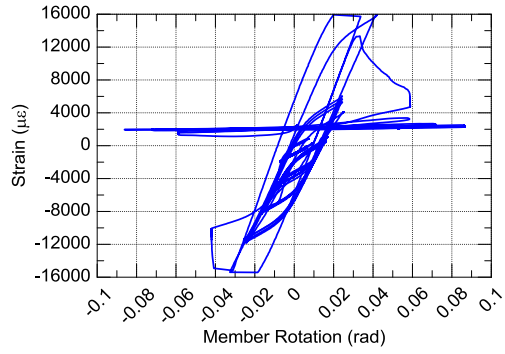

SG 4

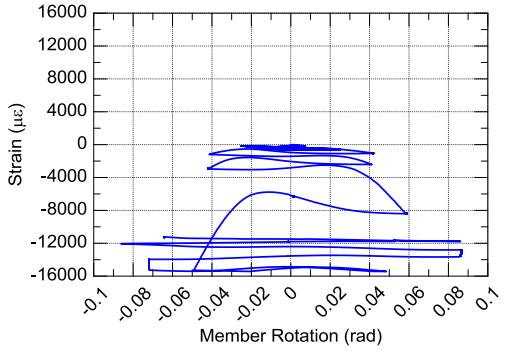

SG 5

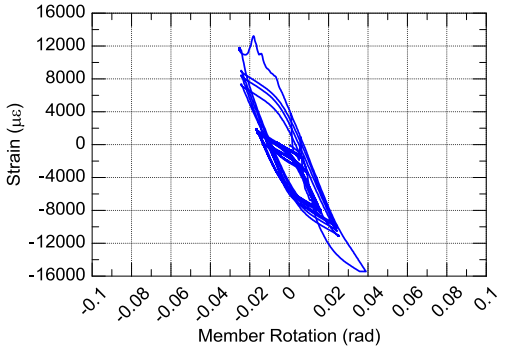

SG 6

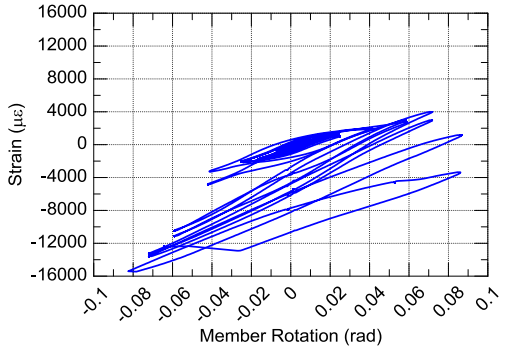

SG 7

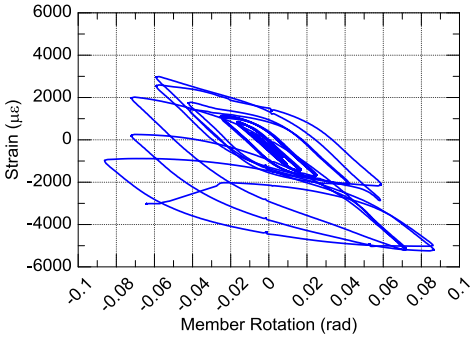

SG 8

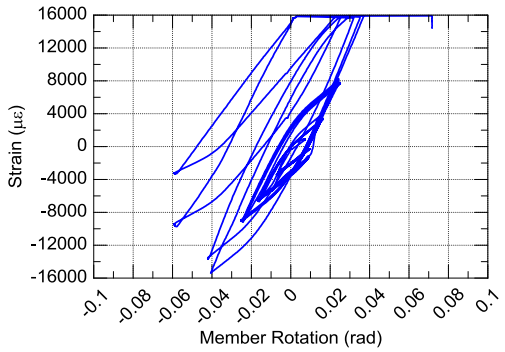

SG 9

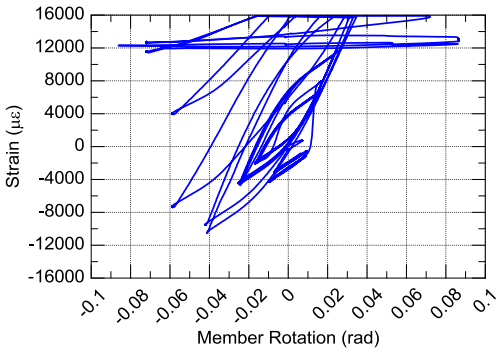

SG 10

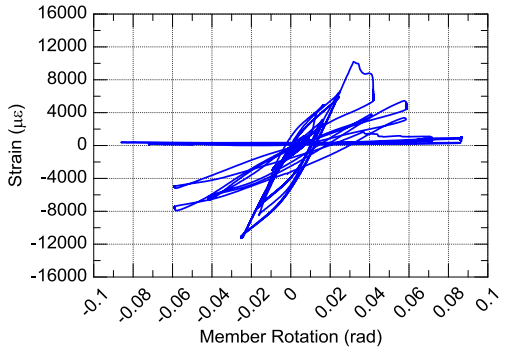

SG 11

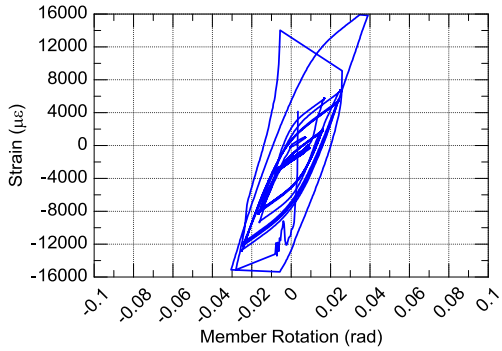

SG 12

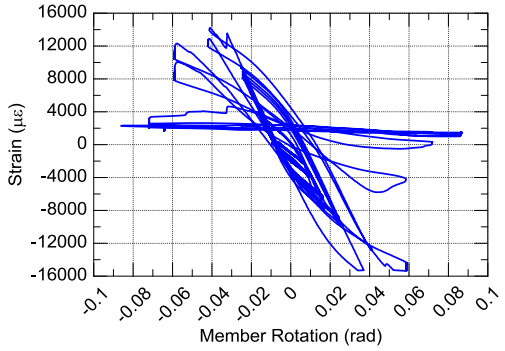

SG 13

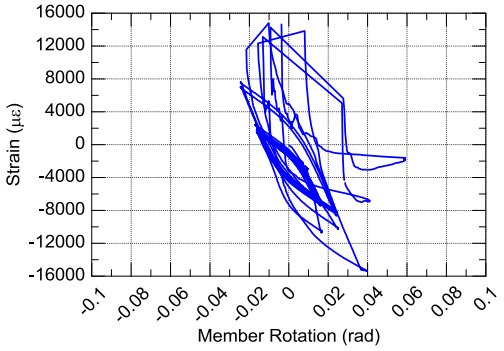

SG 14

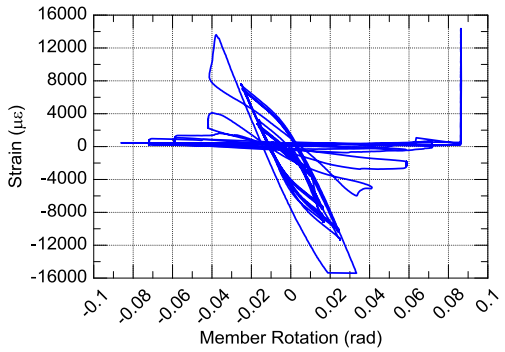

SG 15

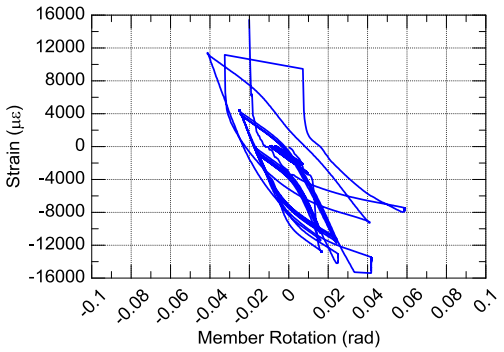

SG 16

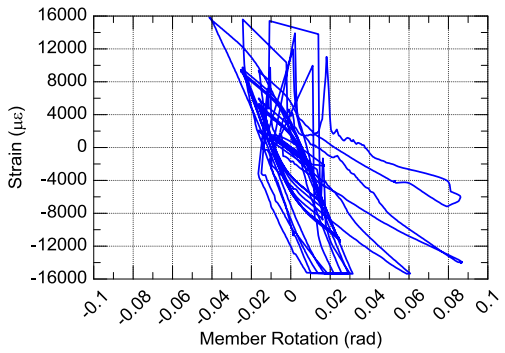

SG 17

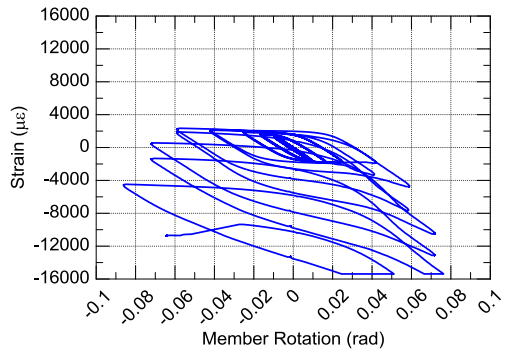

SG 18

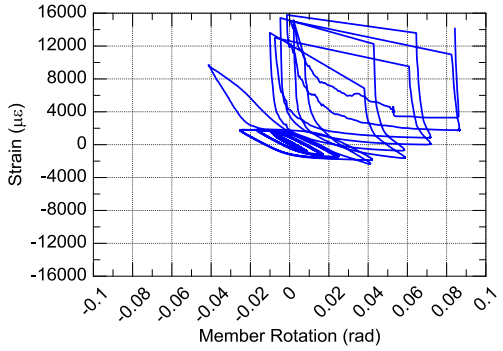

SG 19

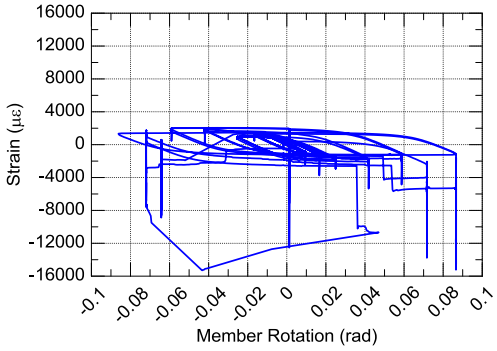

SG 20

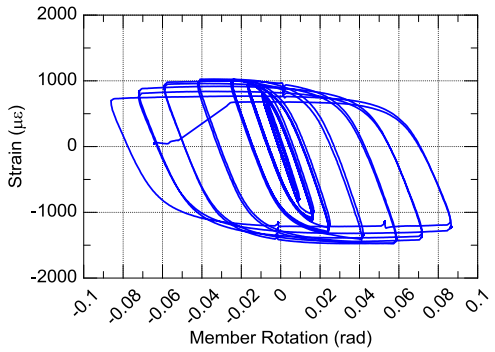

SG 21

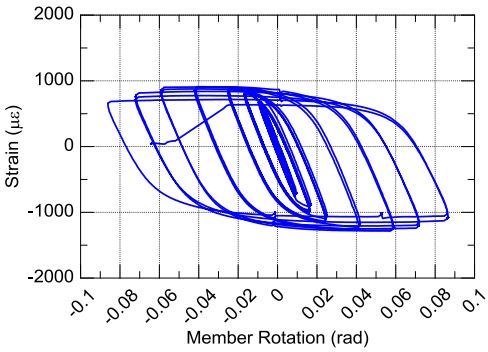

SG 22

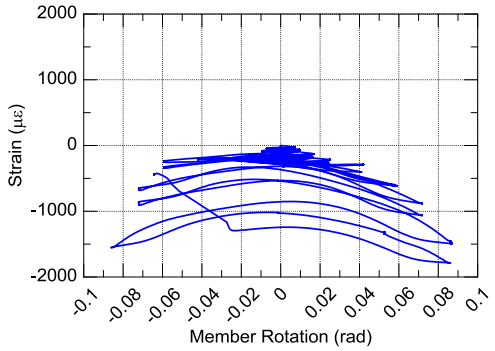

SG 23

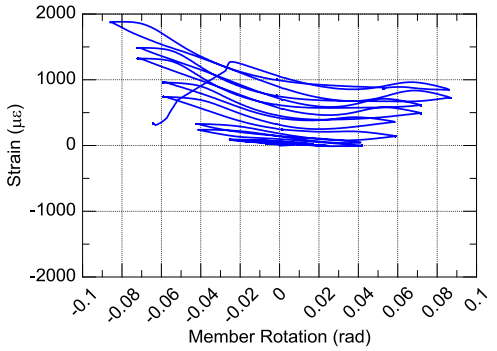

SG 24

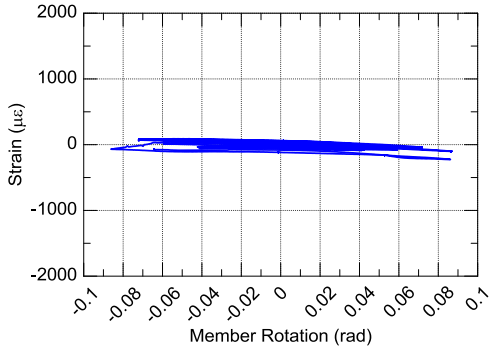

SG 25

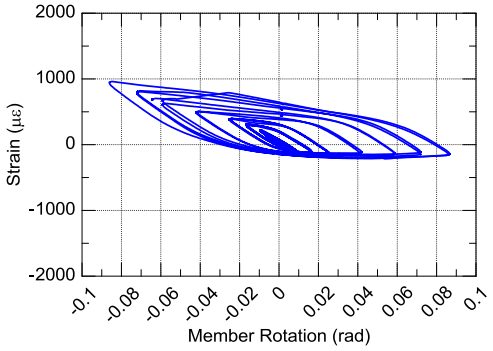

SG 26

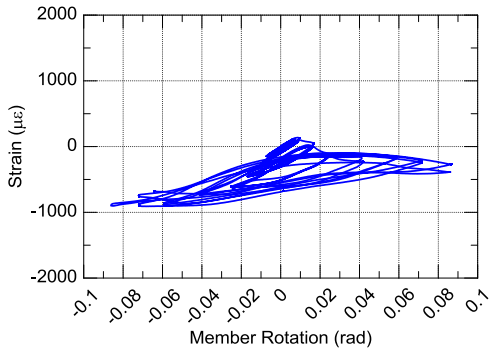

SG 27

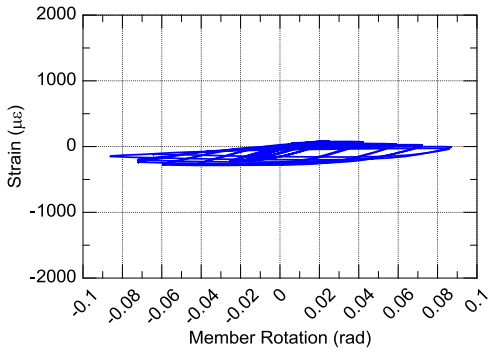

SG 28

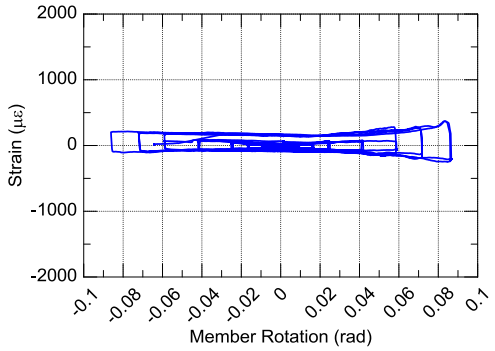

SG 29

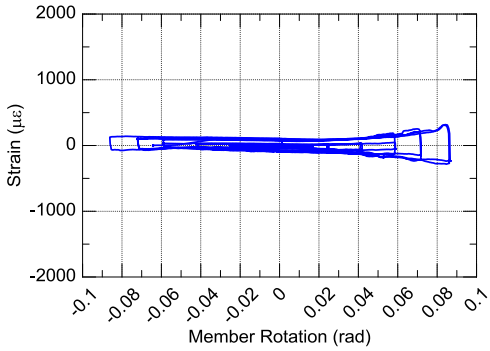

SG 30

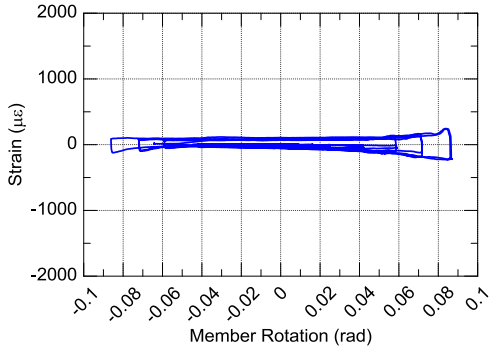

SG 31

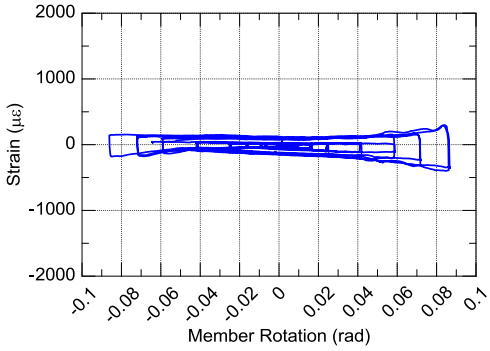

SG 32

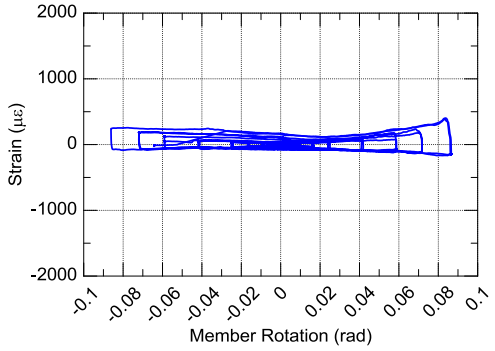

SG 33

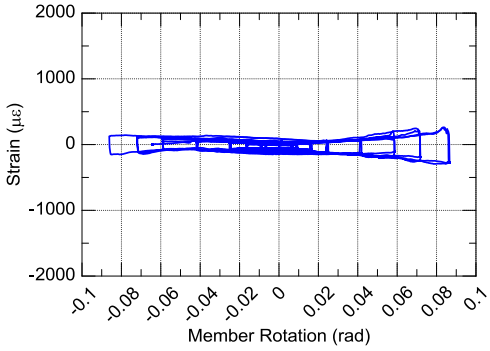

SG 34

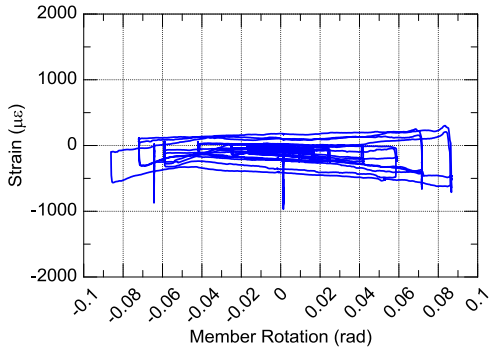

SG 35

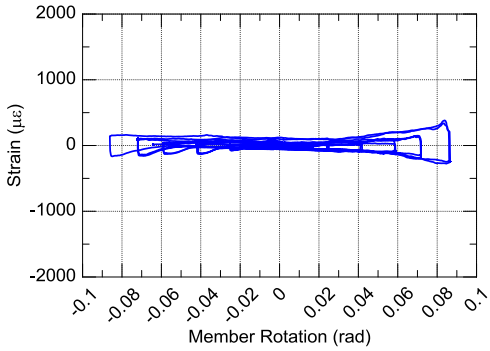

SG 36

Specimen 2C12-5

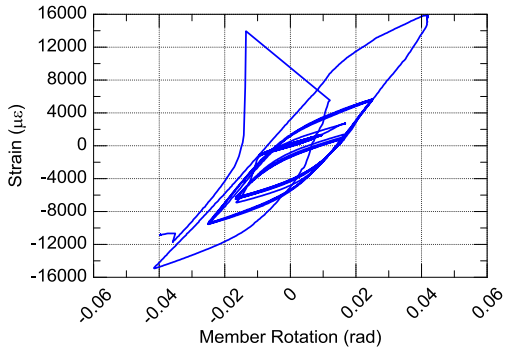

SG 1

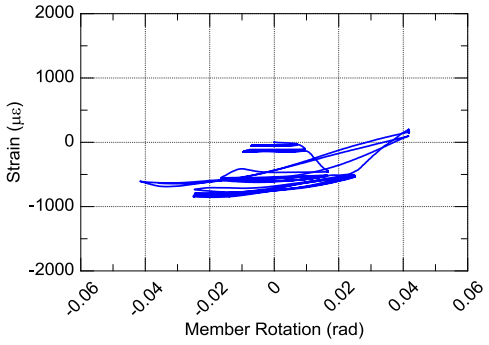

SG 2

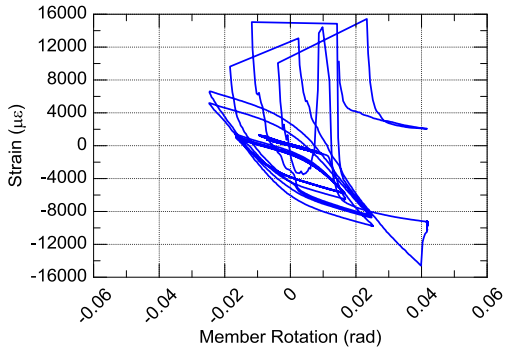

SG 3

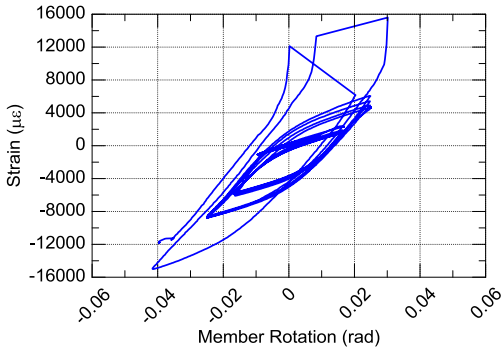

SG 4

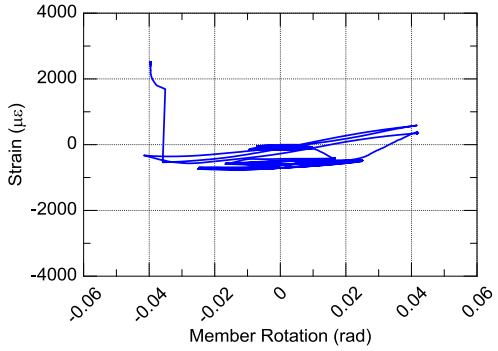

SG 5

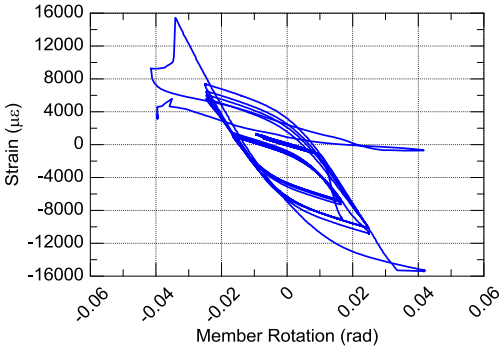

SG 6

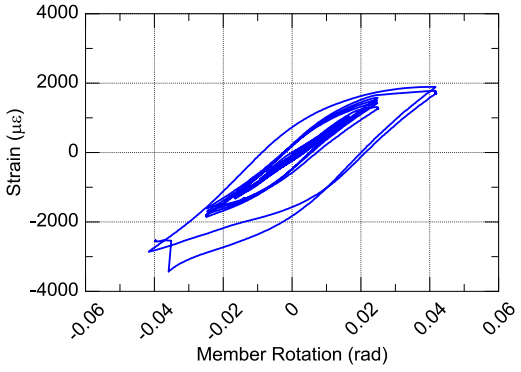

SG 7

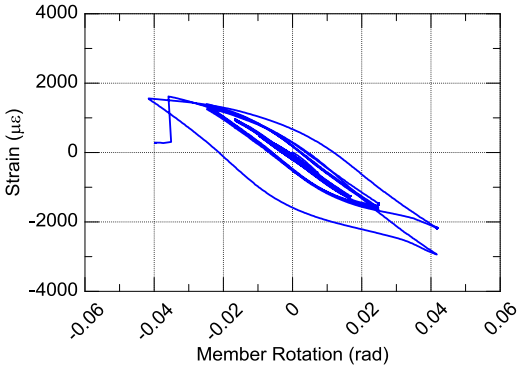

SG 8

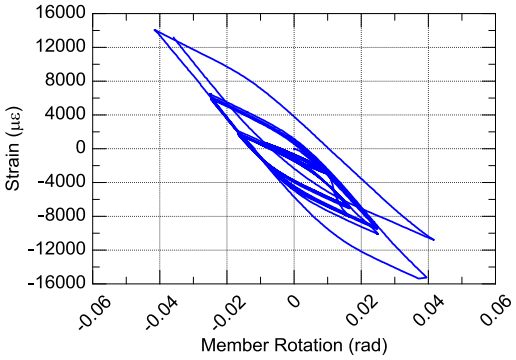

SG 9

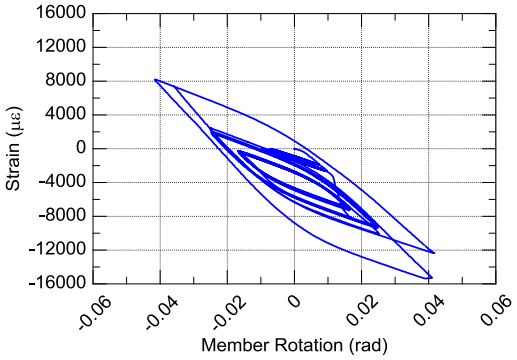

SG 10

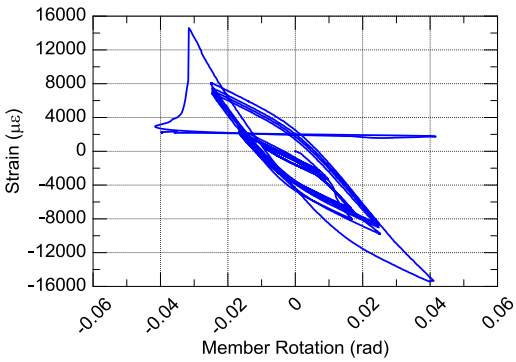

SG 11

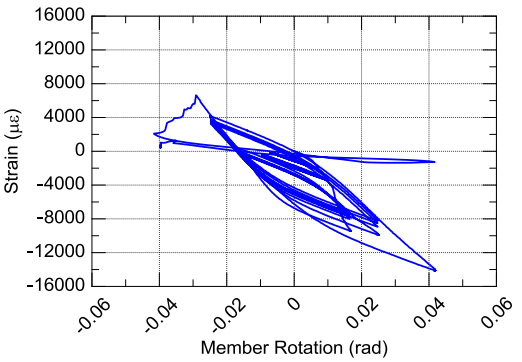

SG 12

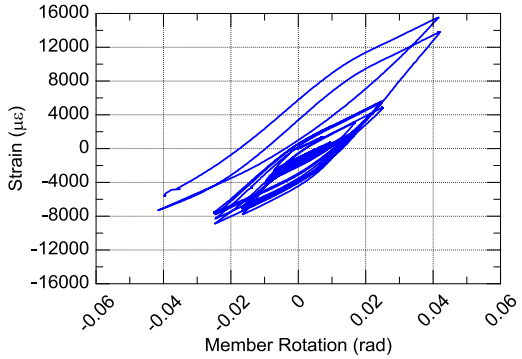

SG 13

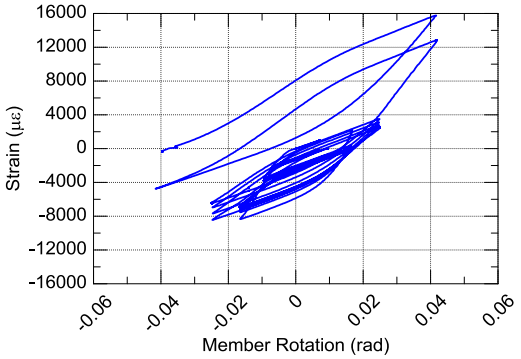

SG 14

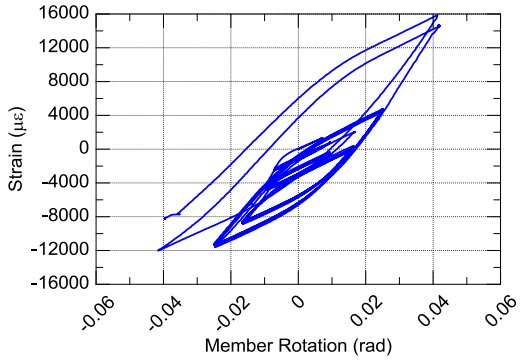

SG 15

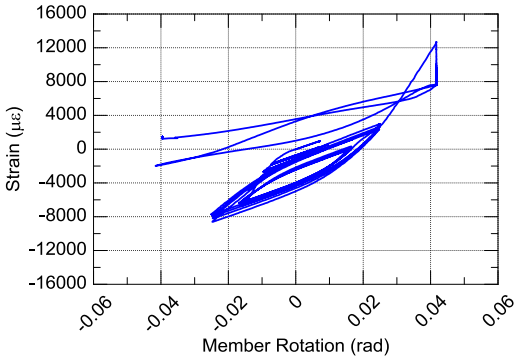

SG 16

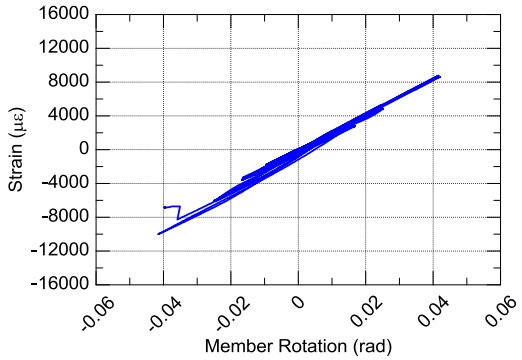

SG 17

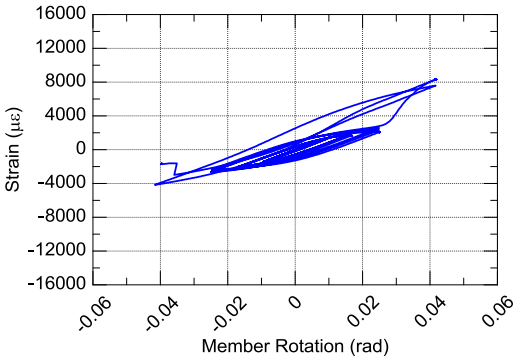

SG 18

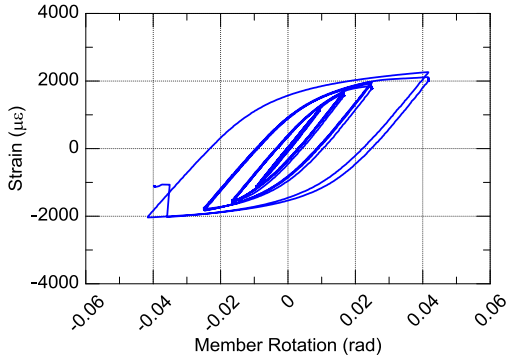

SG 19

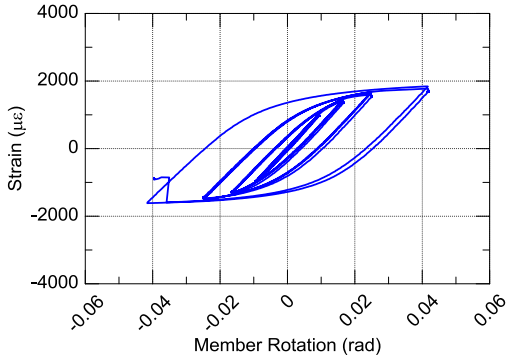

SG 20

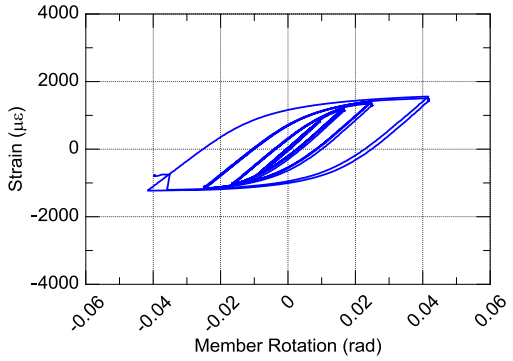

SG 21

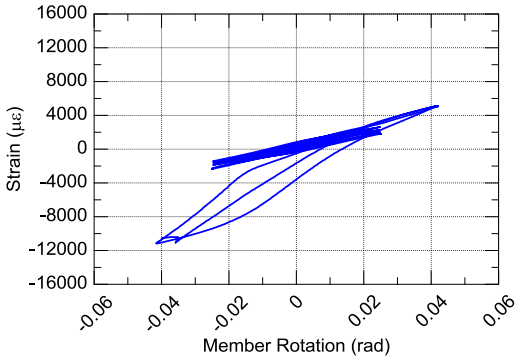

SG 23

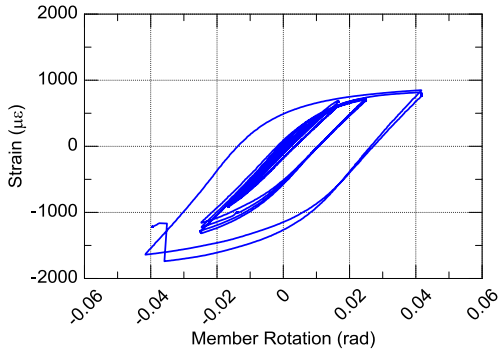

SG 24

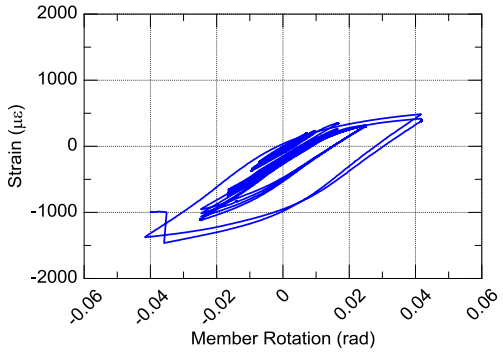

SG 25

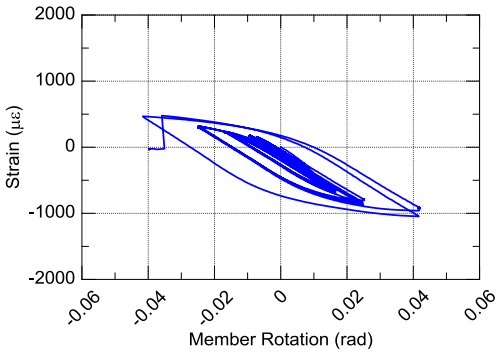

SG 26

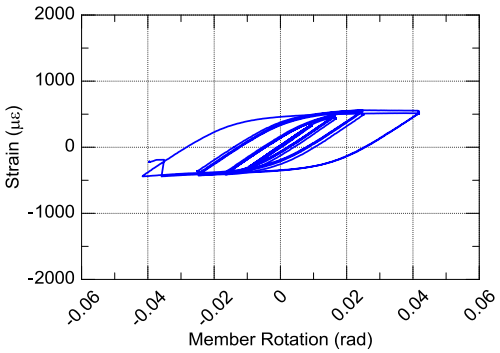

SG 27

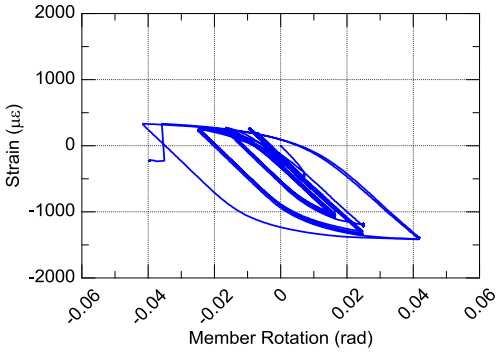

SG 28

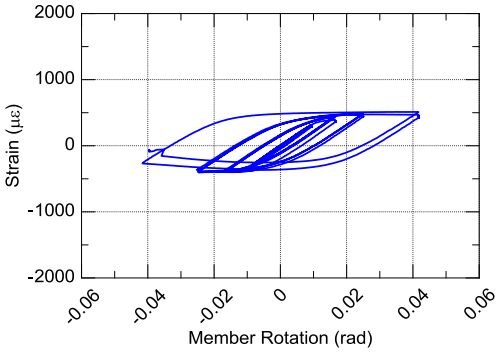

SG 29

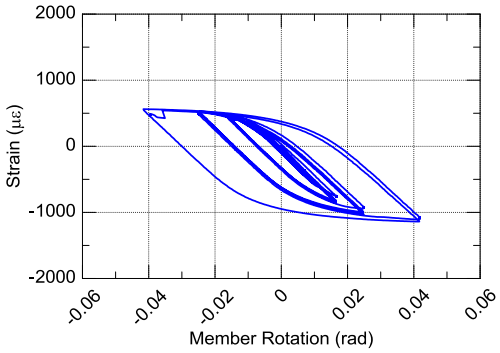

SG 30

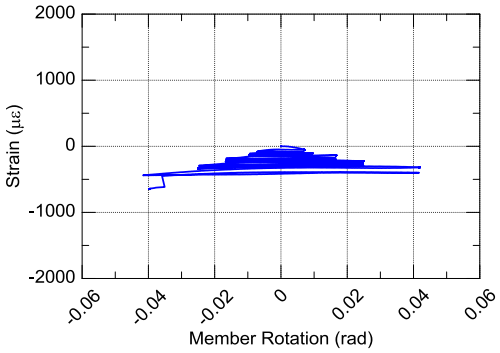

SG 31

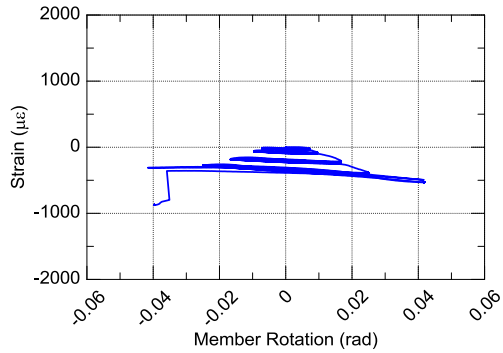

SG 32

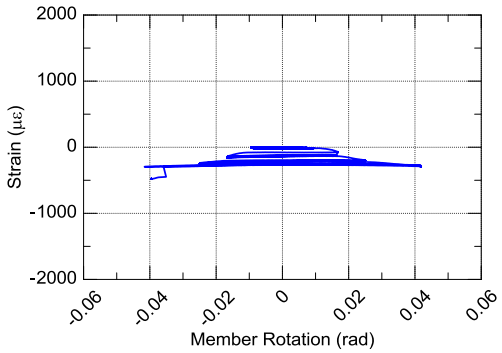

SG 33

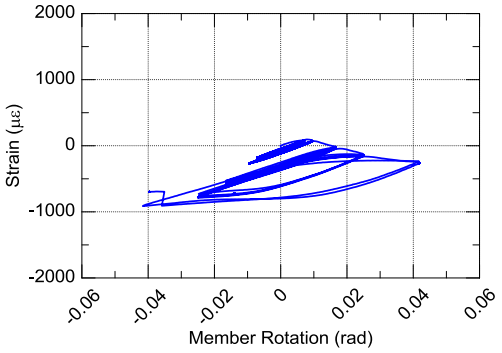

SG 34

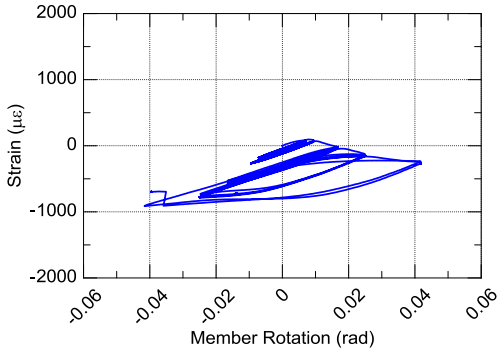

SG 35

Specimen 2C12-6

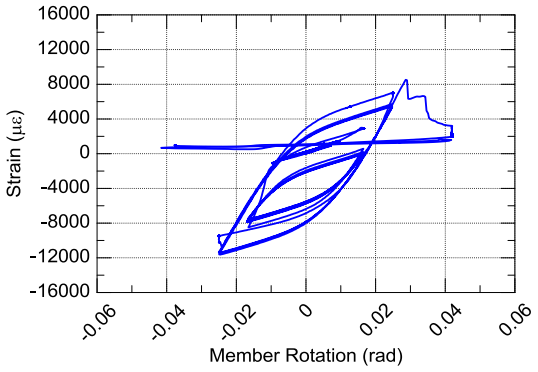

SG 1

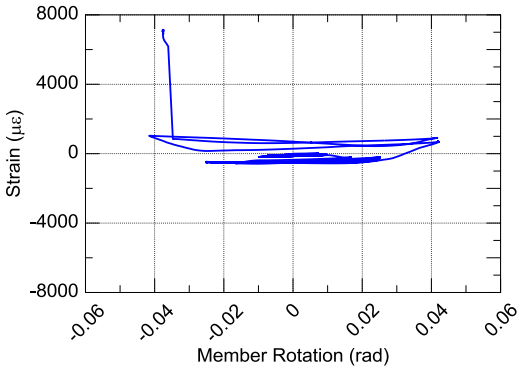

SG 2

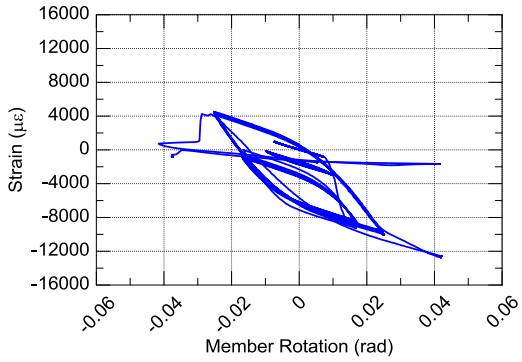

SG 3

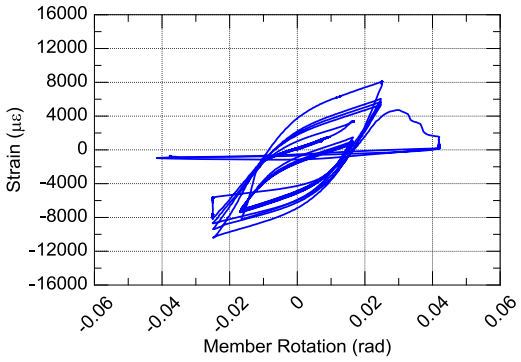

SG 4

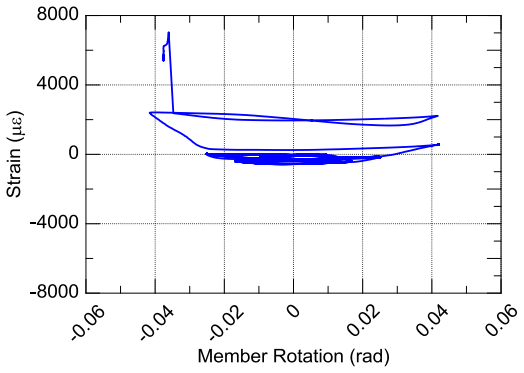

SG 5

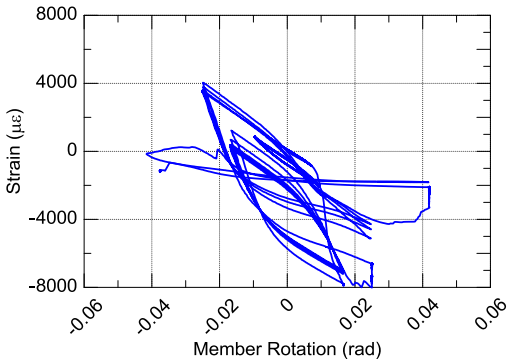

SG 6

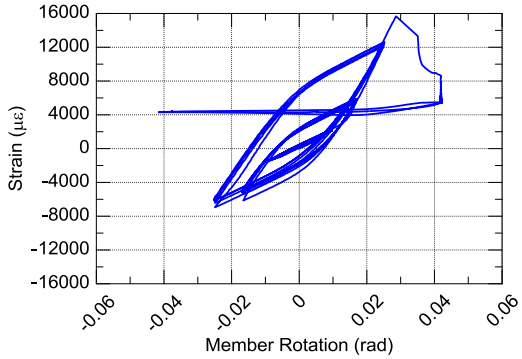

SG 7

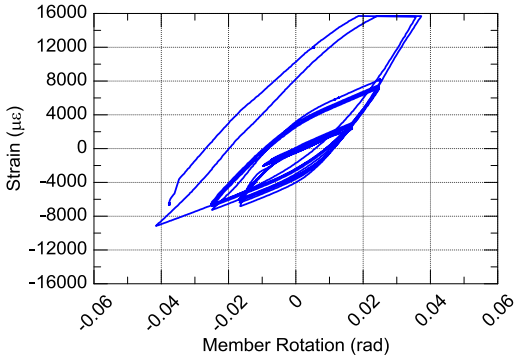

SG 8

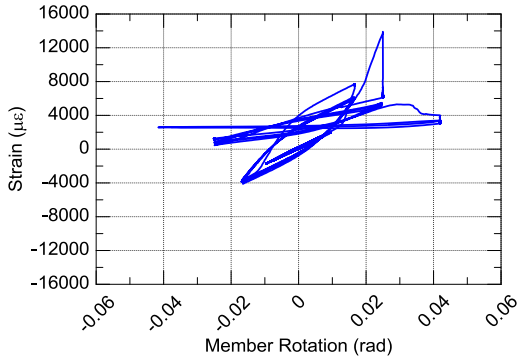

SG 9

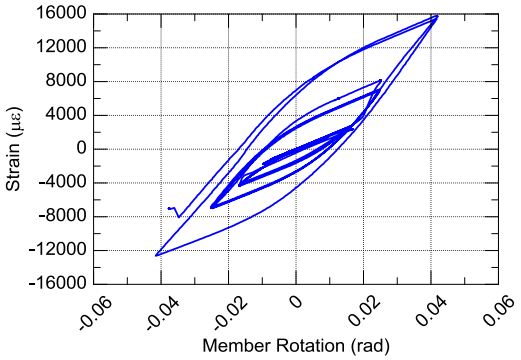

SG 10

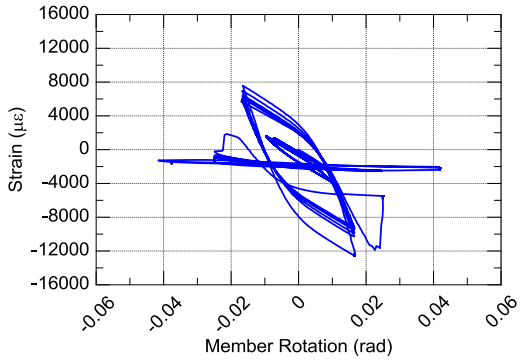

SG 11

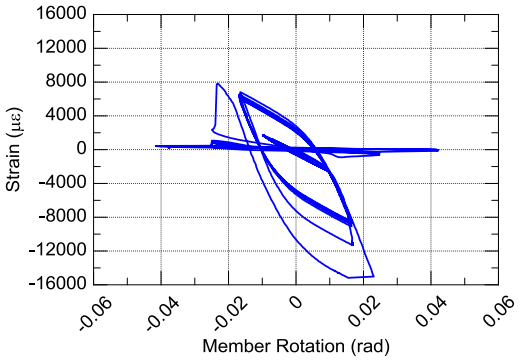

SG 12

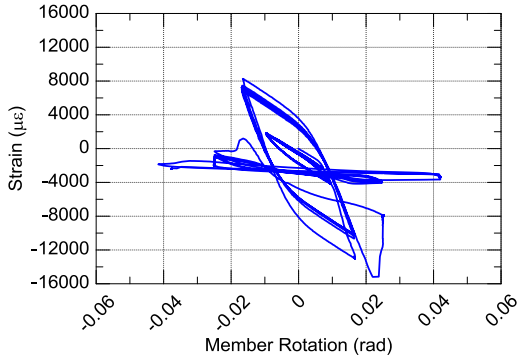

SG 13

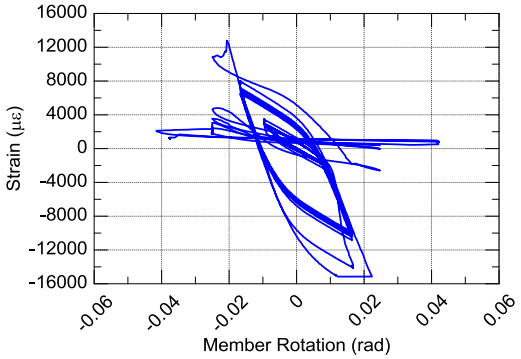

SG 14

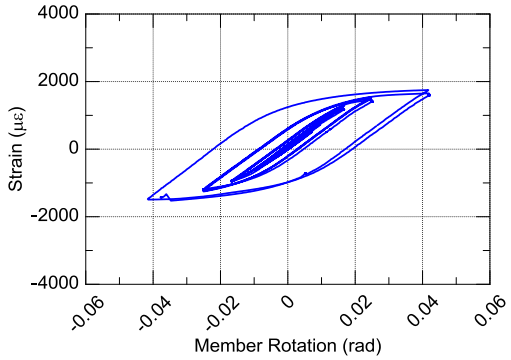

SG 15

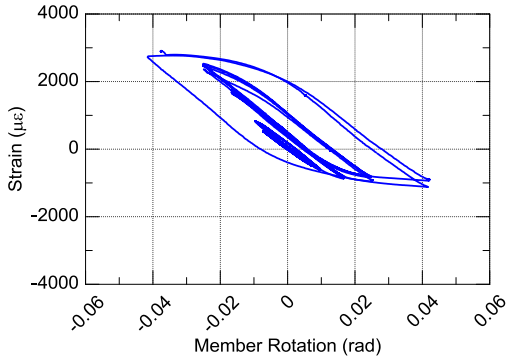

SG 16

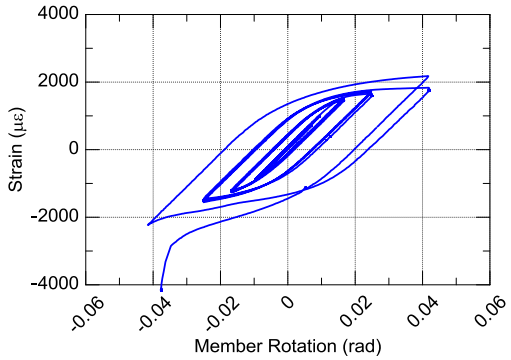

SG 17

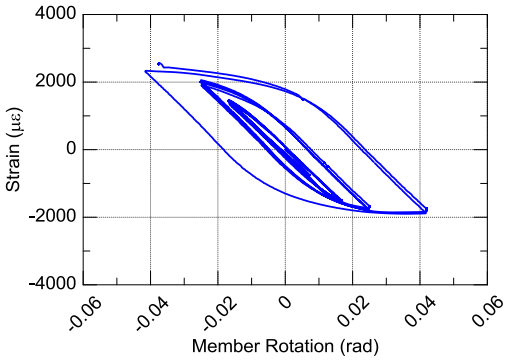

SG 18

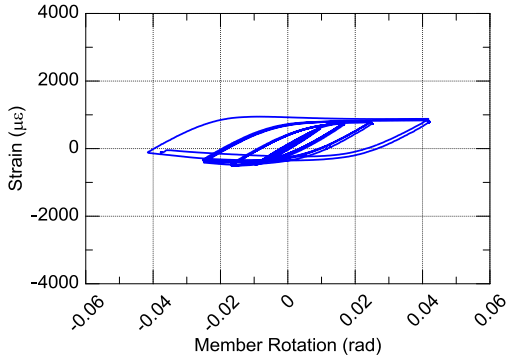

SG 19

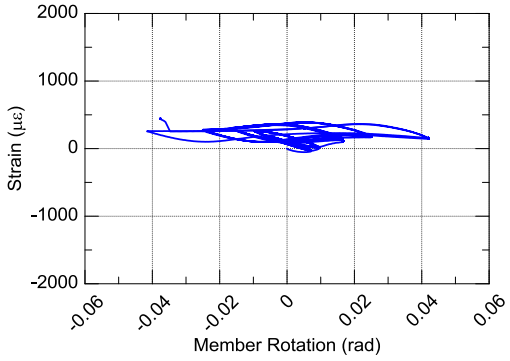

SG 20

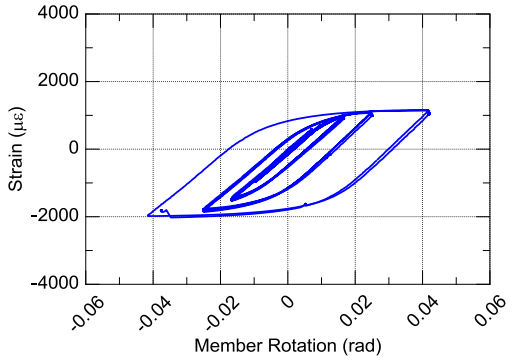

G 21

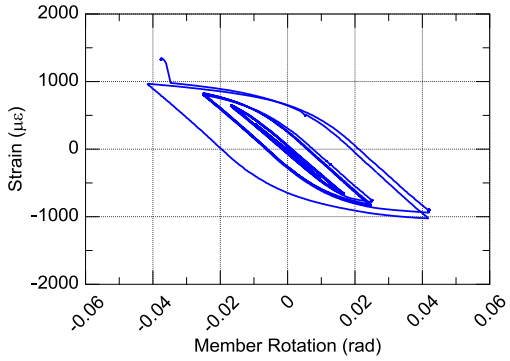

SG 22

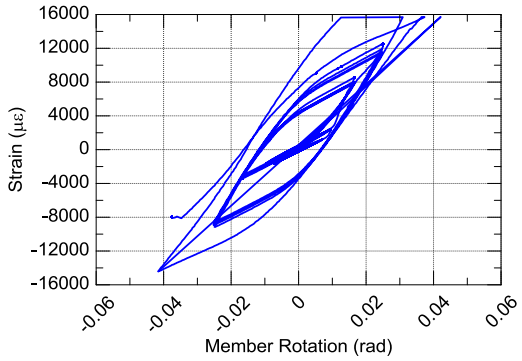

SG 23

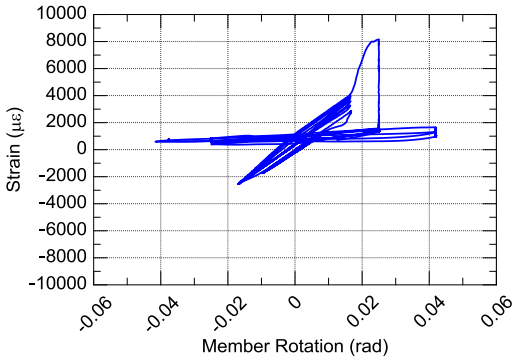

SG 24

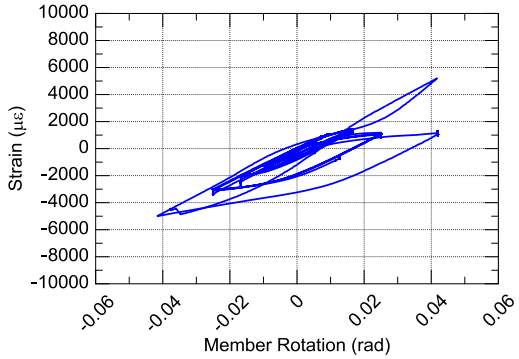

SG 25

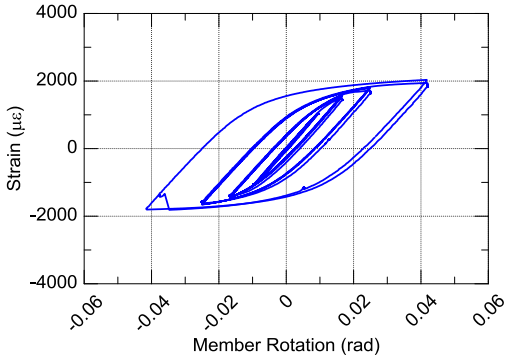

SG 26

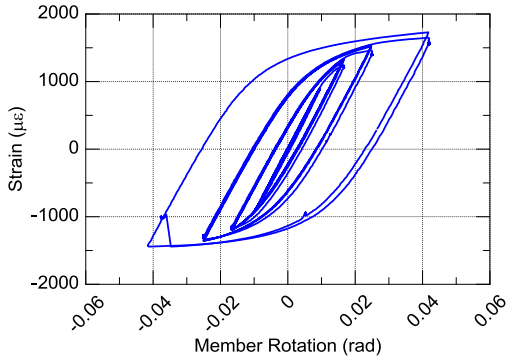

SG 27

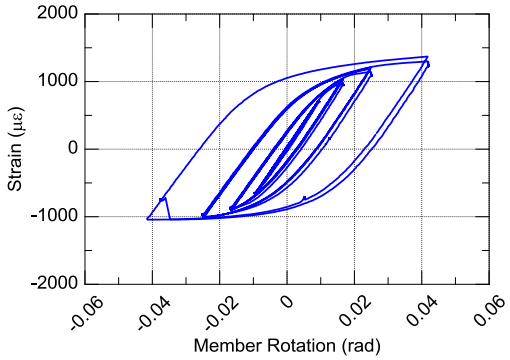

SG 28

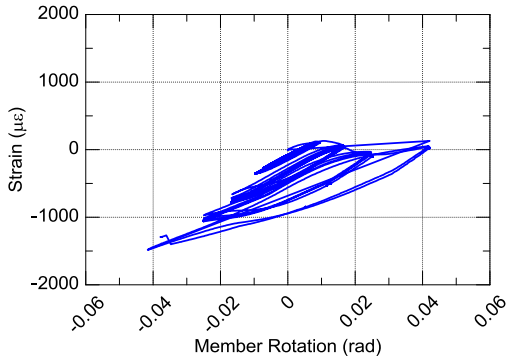

SG 29

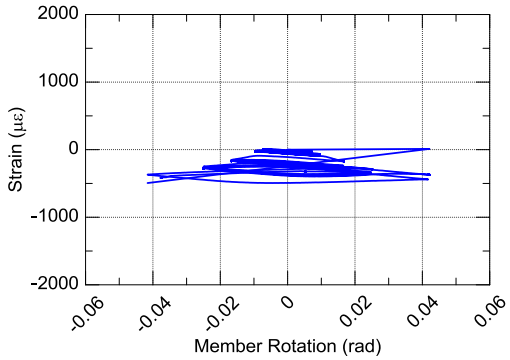

SG 30

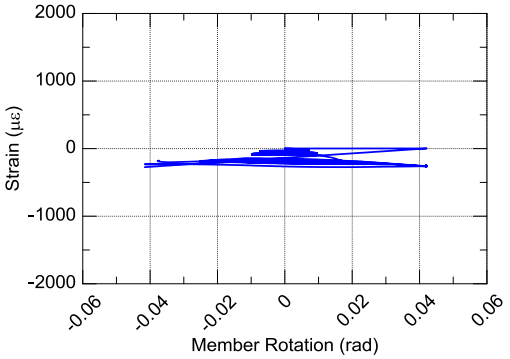
2000
1000
0
-1000
-2000
Strain (με)
-0.06
-0.04
-0.02
0
0.02
0.04
0.06
Member Rotation (rad)
SG 31

Specimen 2C12-7

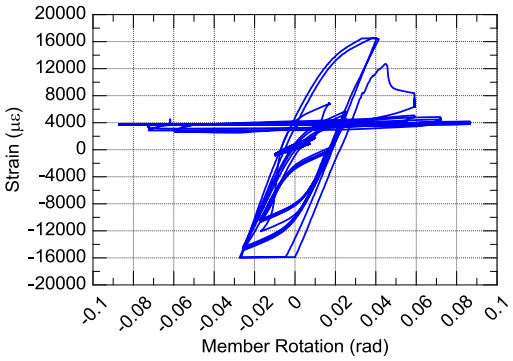

SG 1

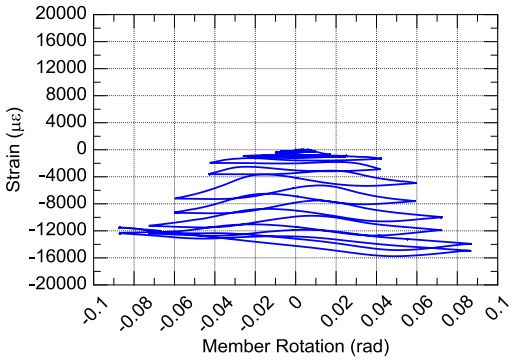

SG 2

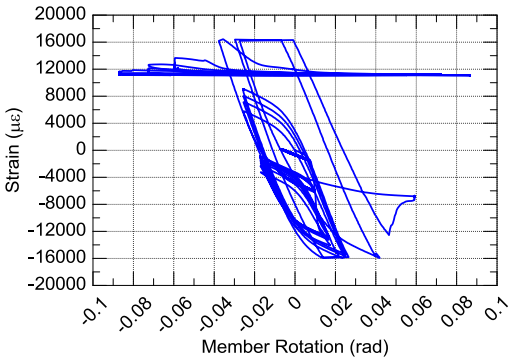

SG 3

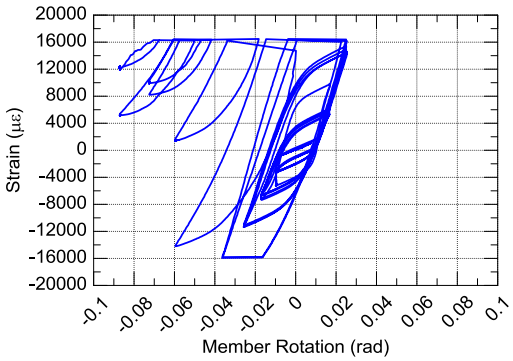

SG 4

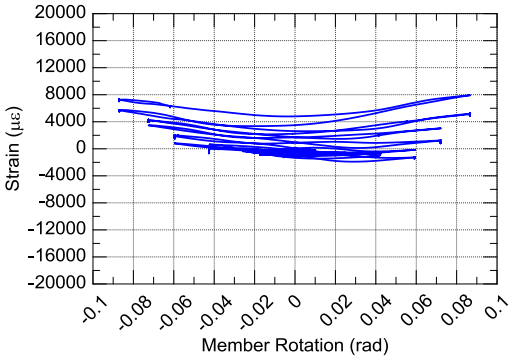

SG 5

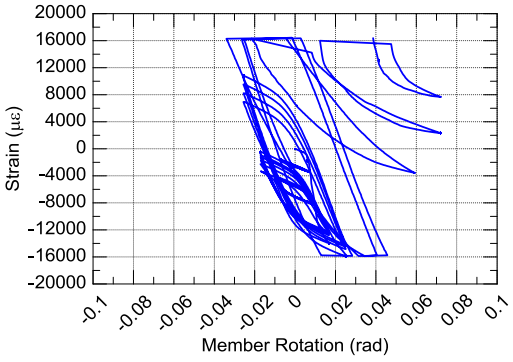

SG 6

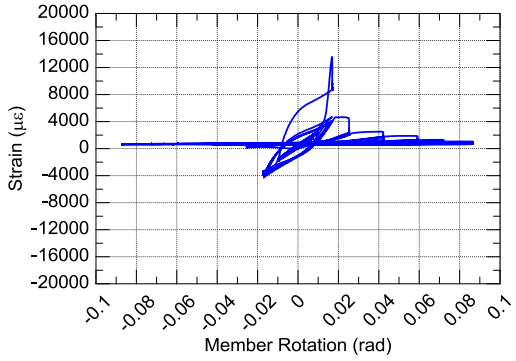

SG 7

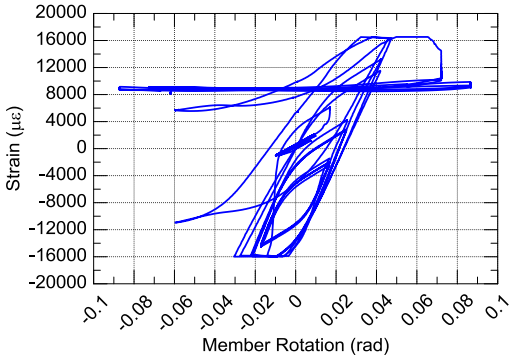

SG 8

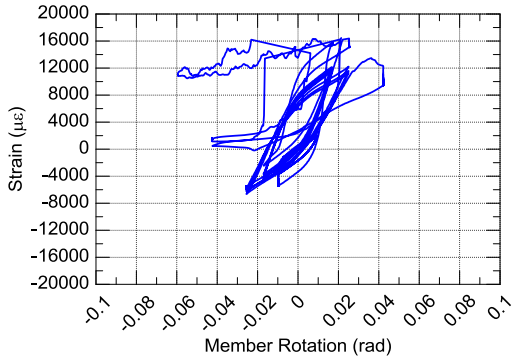

SG 9

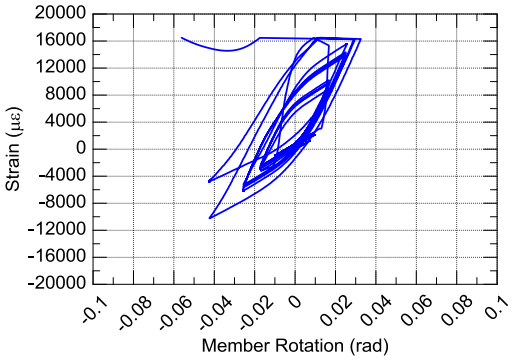

SG 10

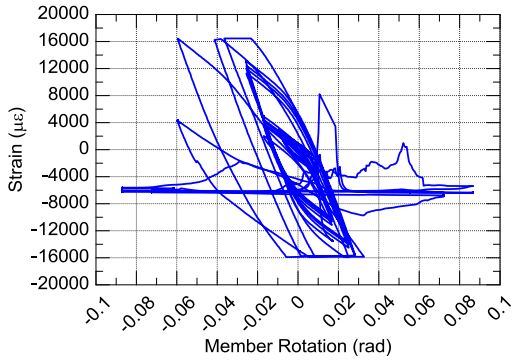

SG 11

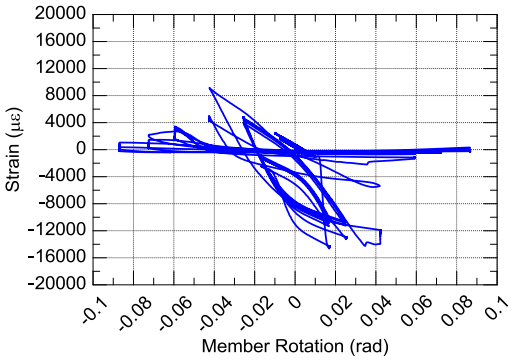

SG 12

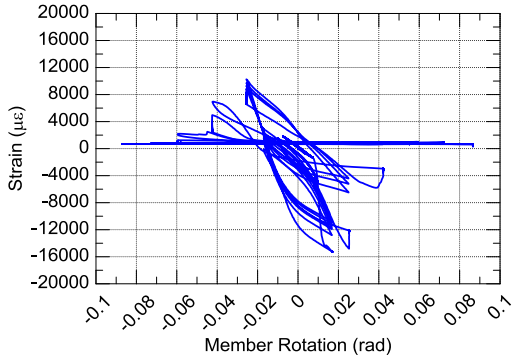

SG 13

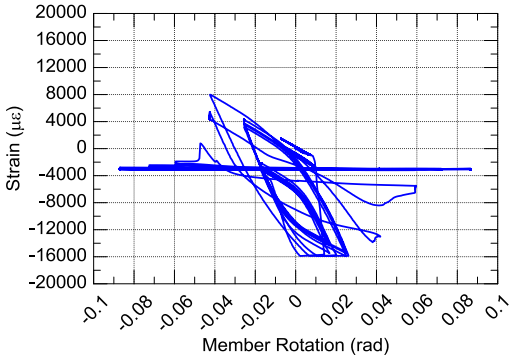

SG 14

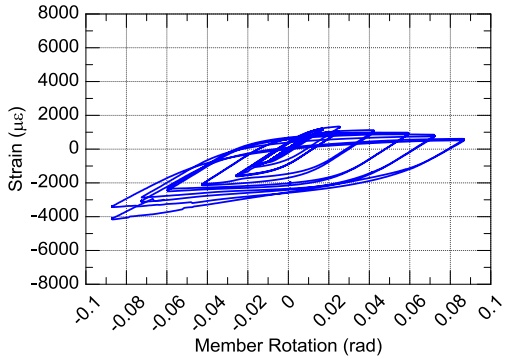

SG 15

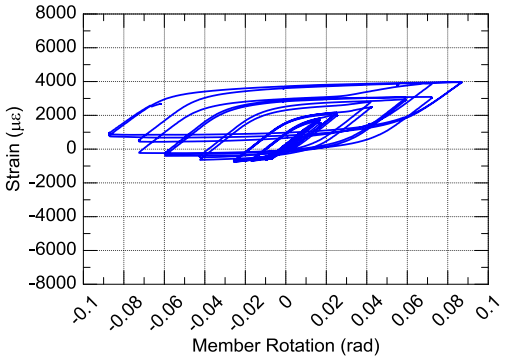

SG 16

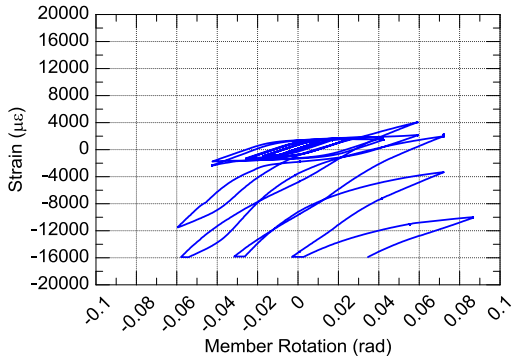

SG 17

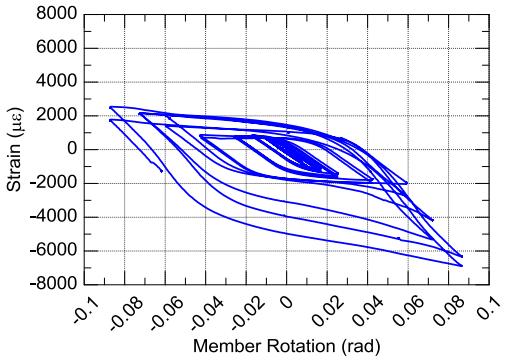

SG 18

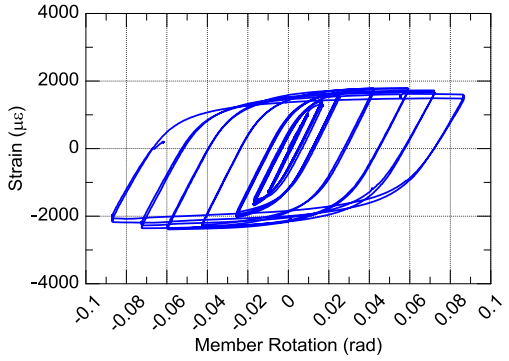

SG 19

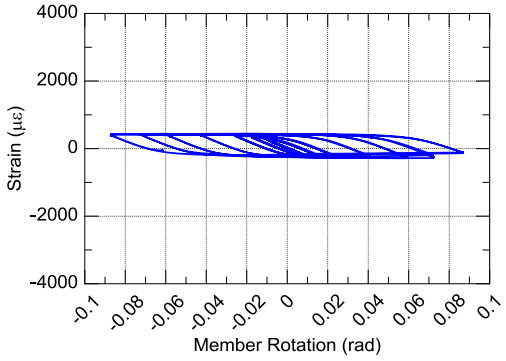

SG 20

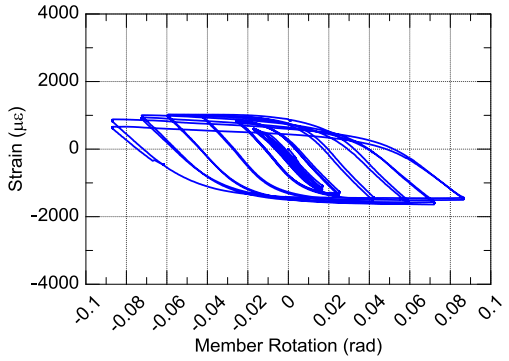

G 21

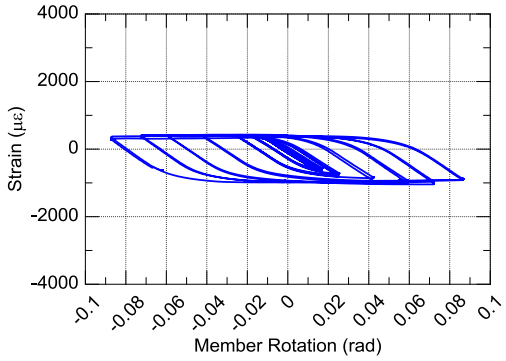

SG 22

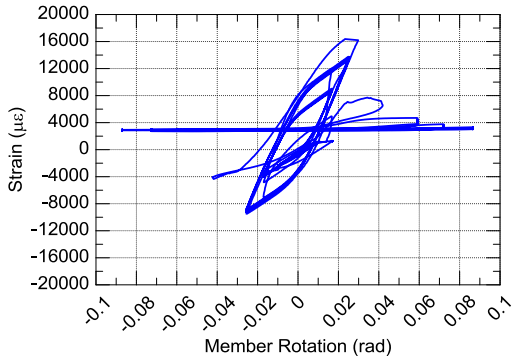

SG 23

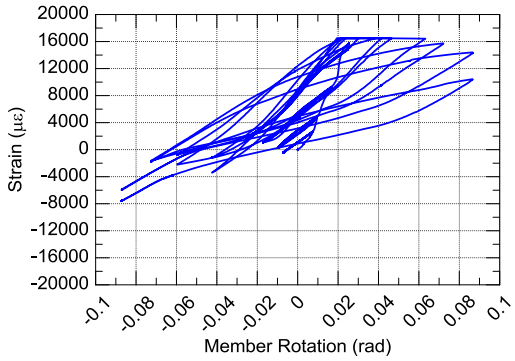

SG 24

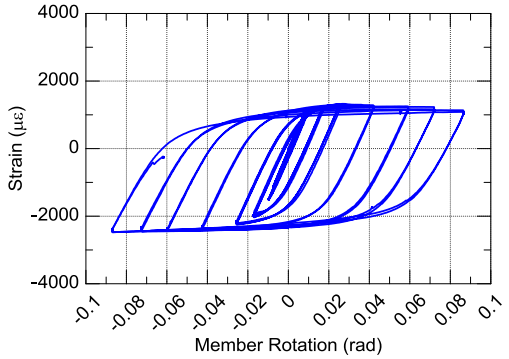

SG 25

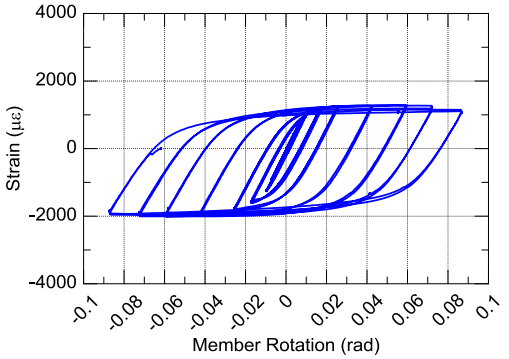

SG 26

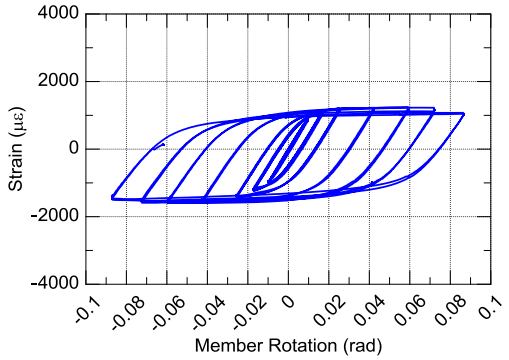

SG 27

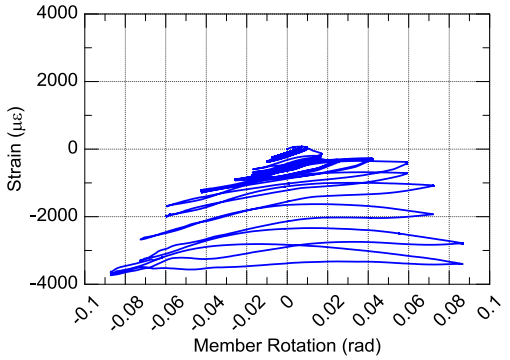

SG 28

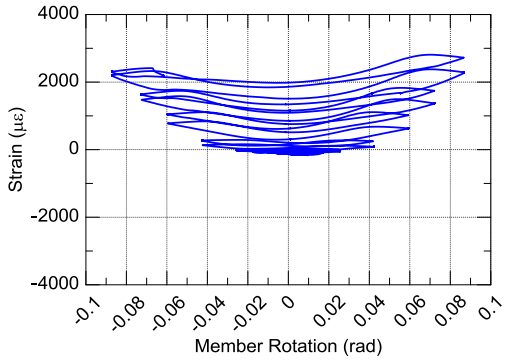

SG 29

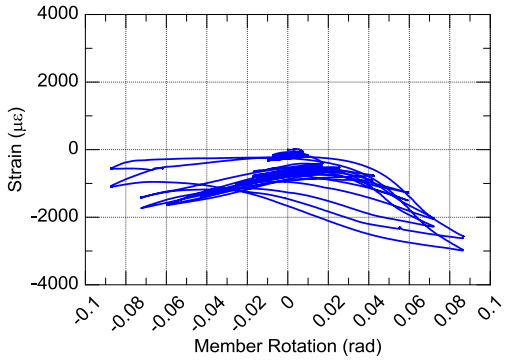

SG 30

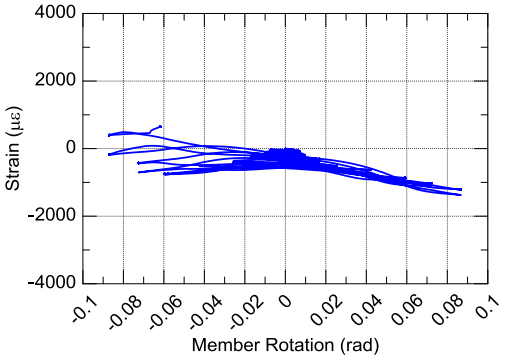
4000
2000
0
-2000
-4000
Strain (με)
-0.1
-0.08
-0.06
-0.04
-0.02
0
0.02
0.04
0.06
0.08
0.1
Member Rotation (rad)

SG 31

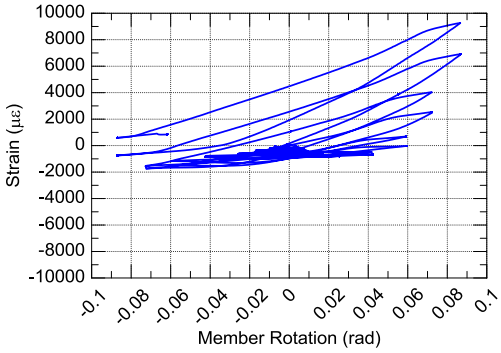
10000
8000
6000
4000
2000
0
-2000
-4000
-6000
-8000
-10000
Strain (με)
-0.1
-0.08
-0.06
-0.04
-0.02
0
0.02
0.04
0.06
0.08
0.1
Member Rotation (rad)

SG 32

Specimen 2C12-8

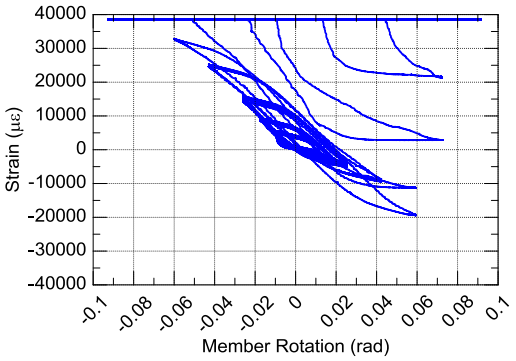

SG 1

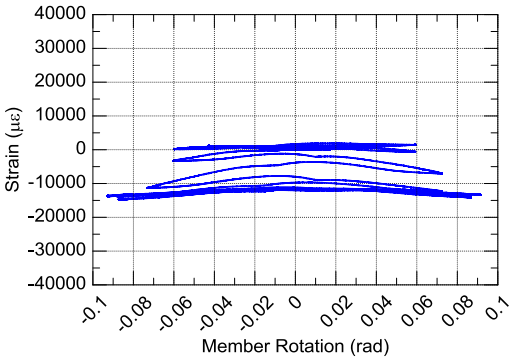

SG 2

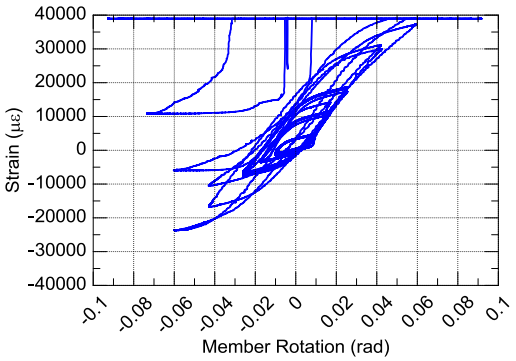

SG 3

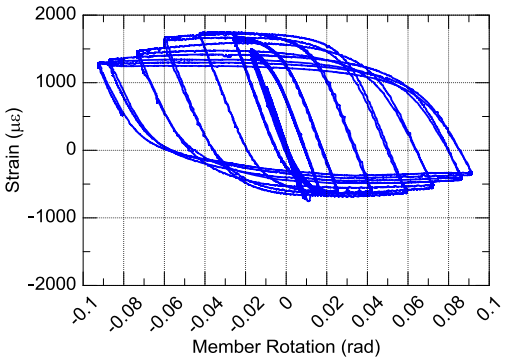

SG 4

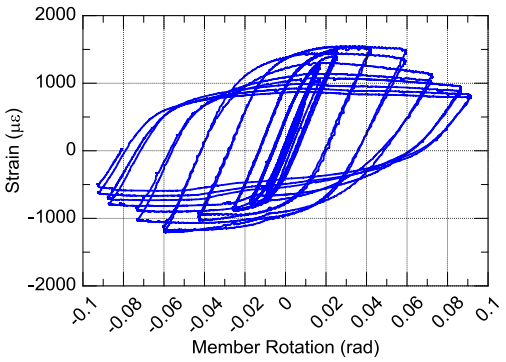

SG 5

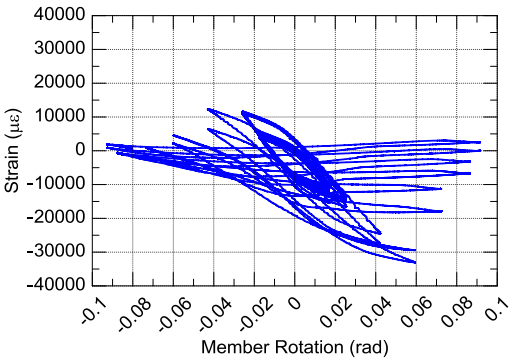

SG 6

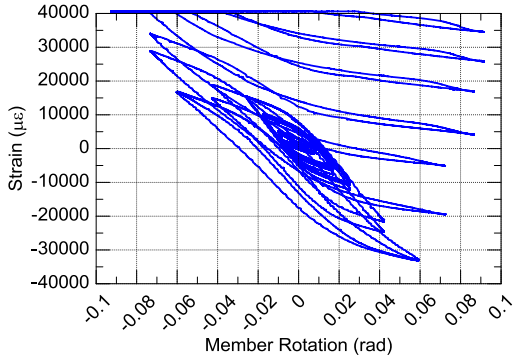

SG 7

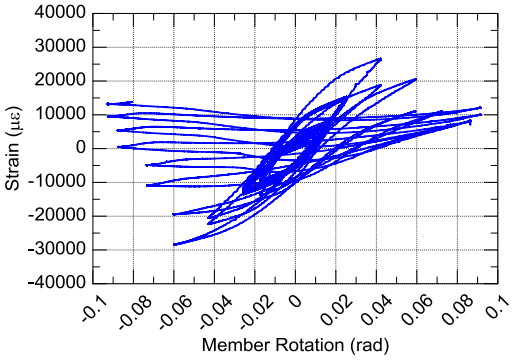

SG 8

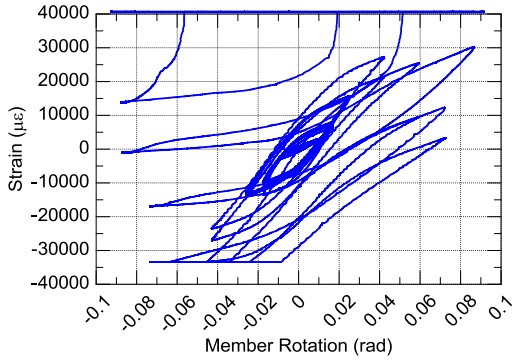

SG 9

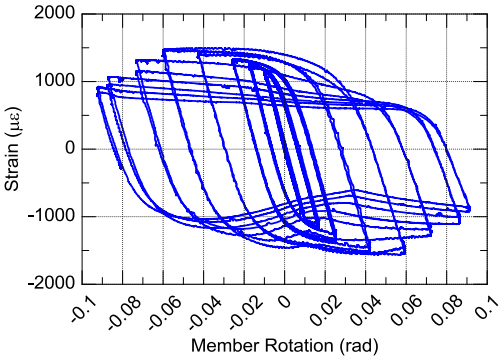

SG 10

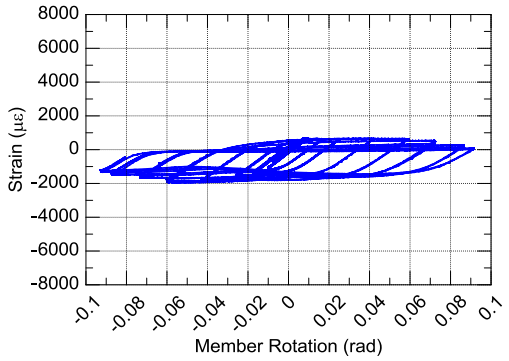

SG 11

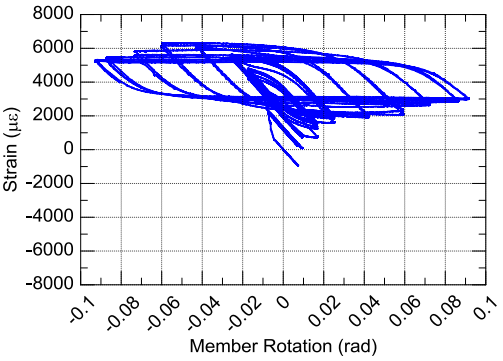

SG 12

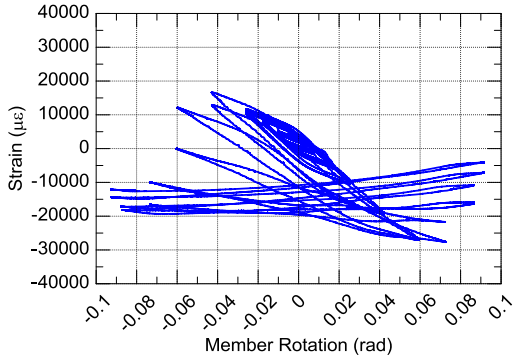

SG 13

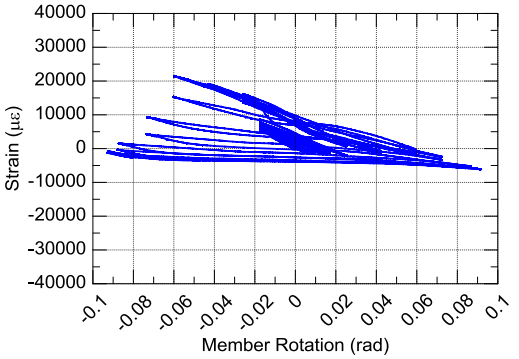

SG 14

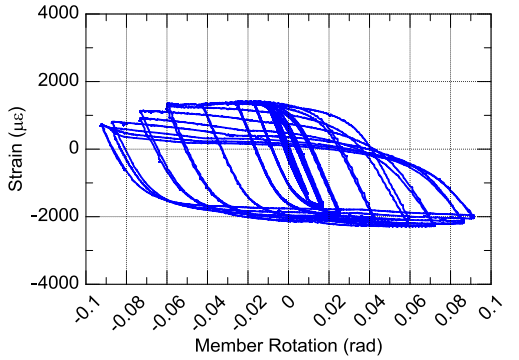

SG 15

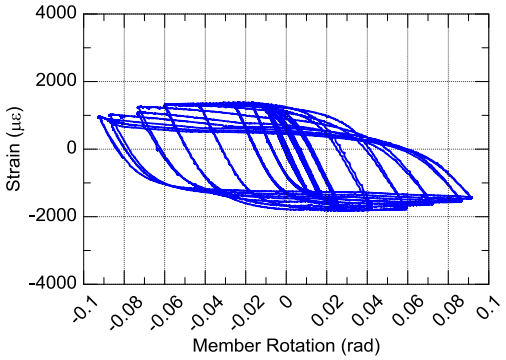

SG 16

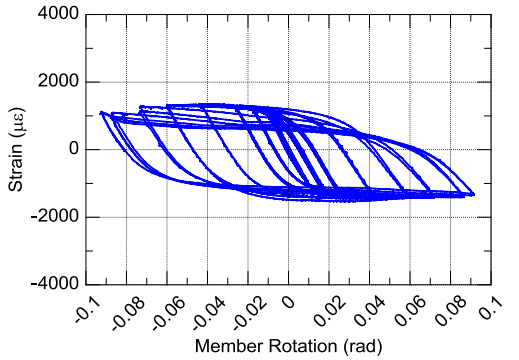

SG 17

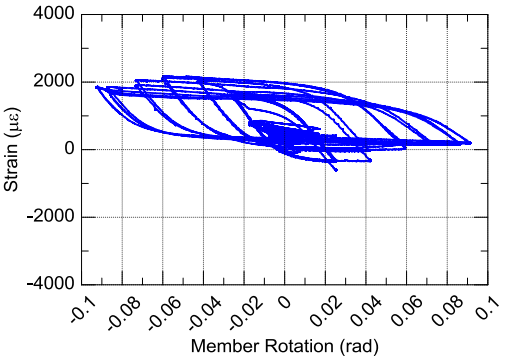

SG 18

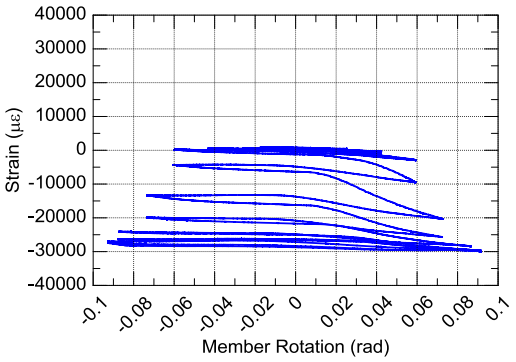
40000
30000
20000
10000
0
-10000
-20000
-30000
-40000
Strain (με)
-0.1
-0.08
-0.06
-0.04
-0.02
0
0.02
0.04
0.06
0.08
0.1
Member Rotation (rad)
SG 19

Specimen 2C12-9

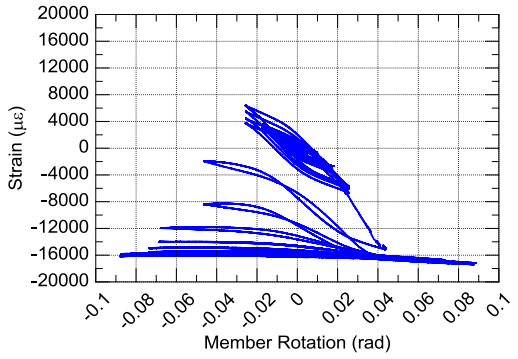

SG 1

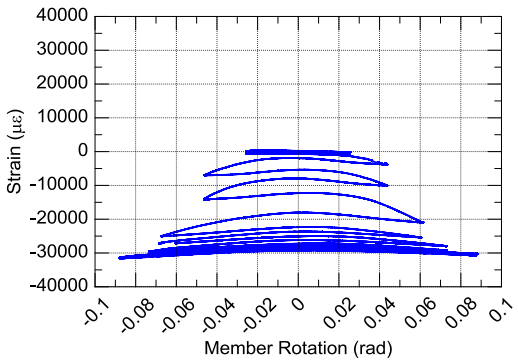

SG 2

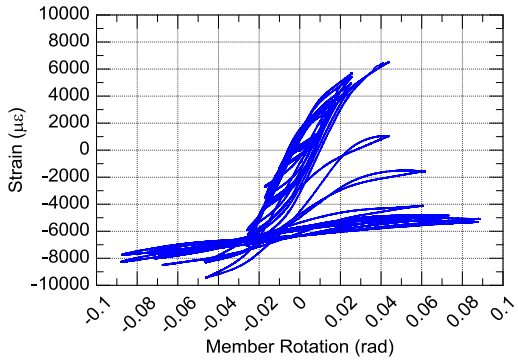

SG 3

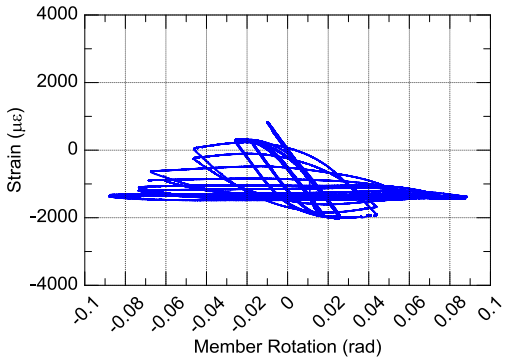

SG 4

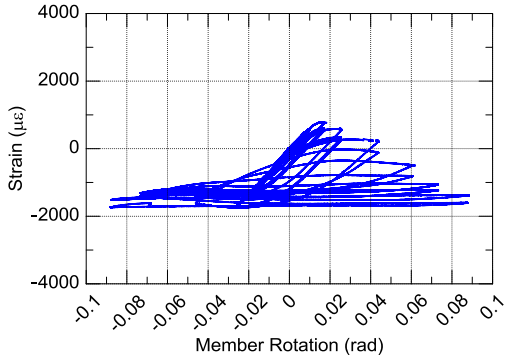

SG 5

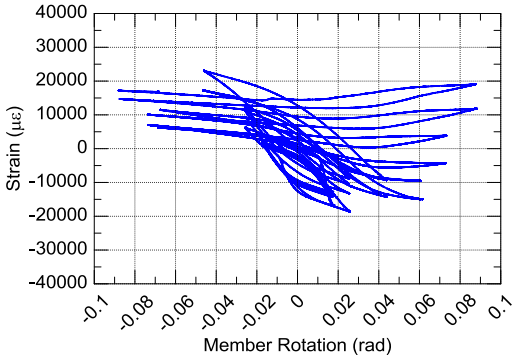

SG 6

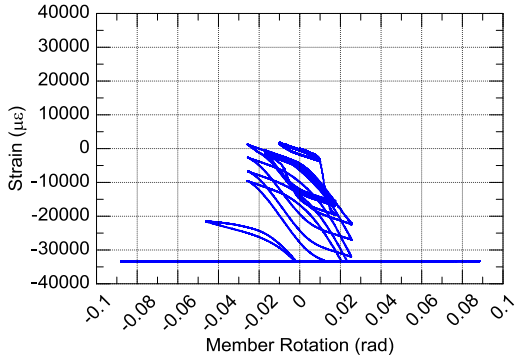

SG 7

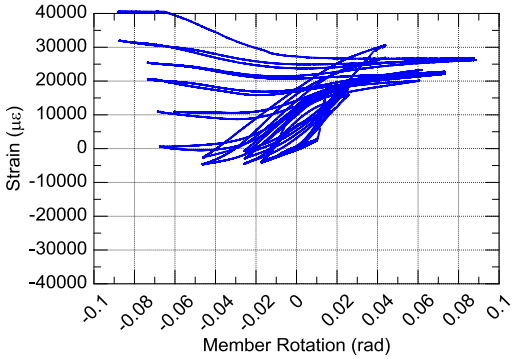

SG 8

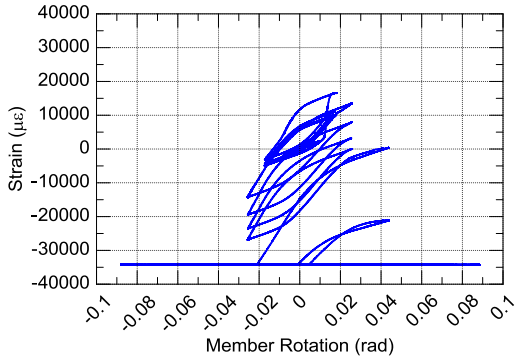

SG 9

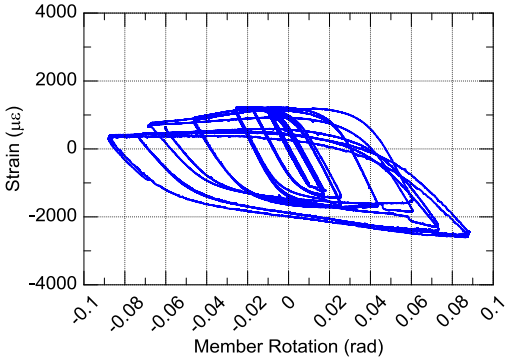

SG 10

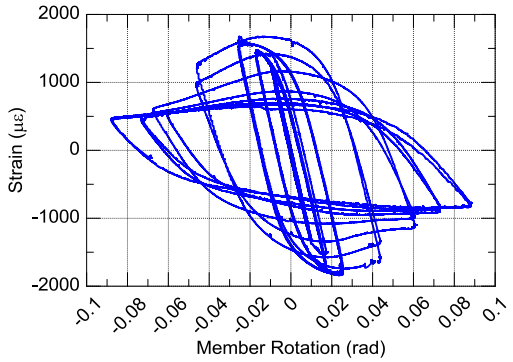

SG 11

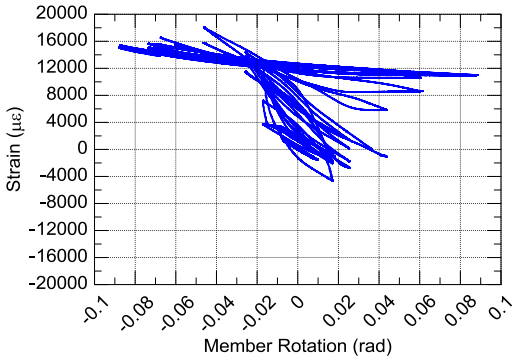

SG 12

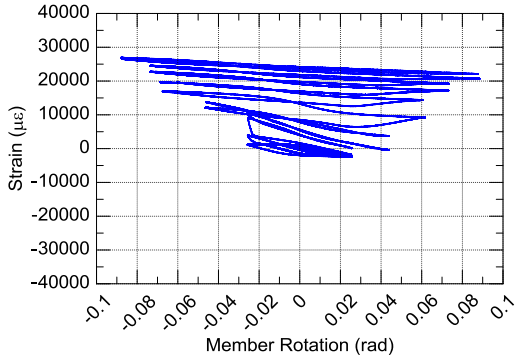

SG 13

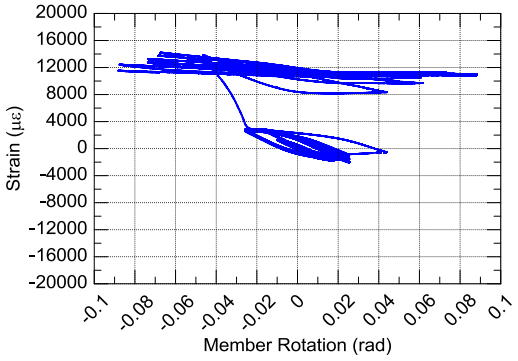

SG 14

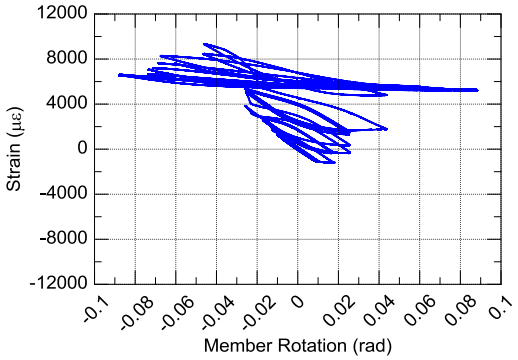

SG 15

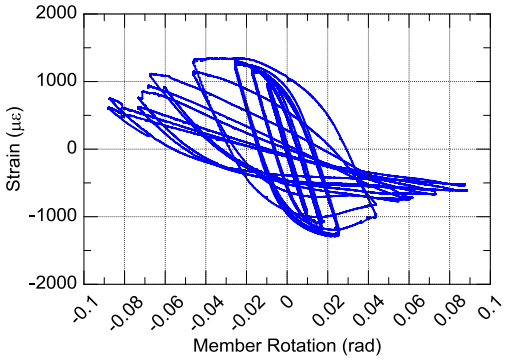

SG 16

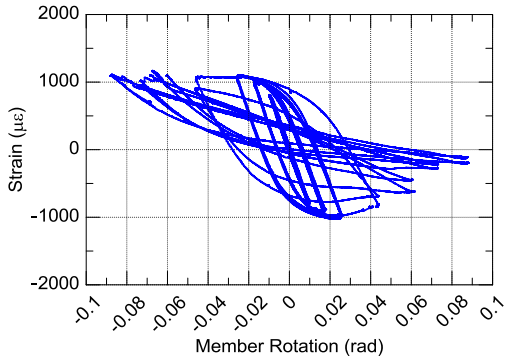

SG 17

Specimen 2C12-10-RBS

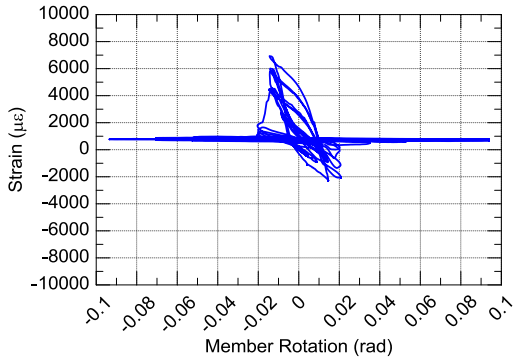

SG 1

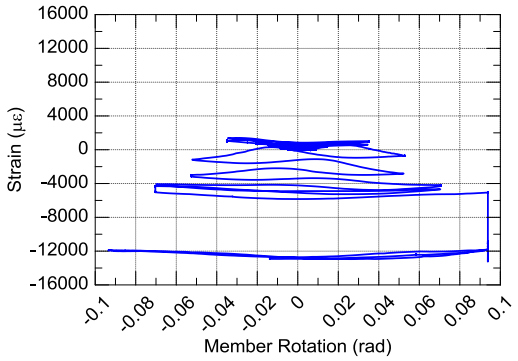

SG 2

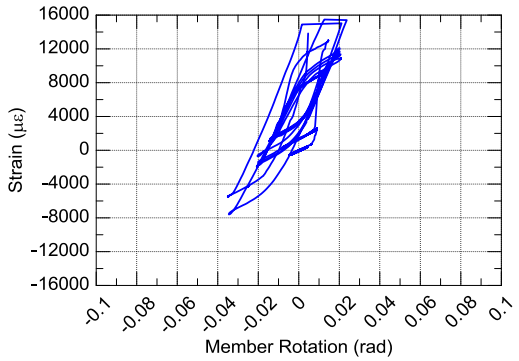

SG 3

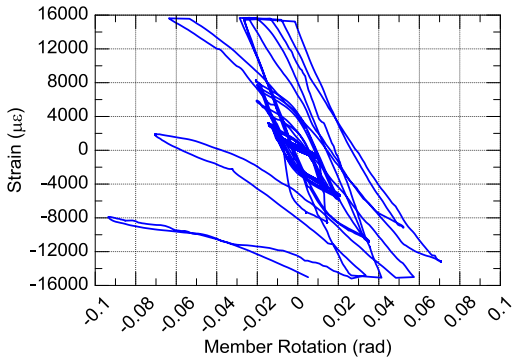

SG 4

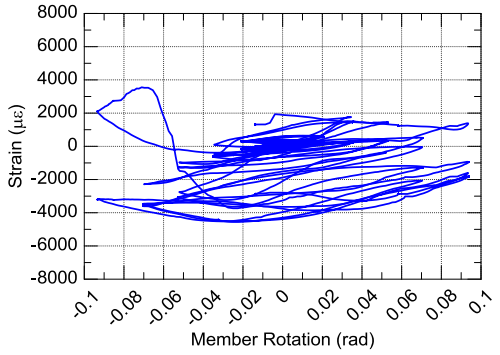

SG 5

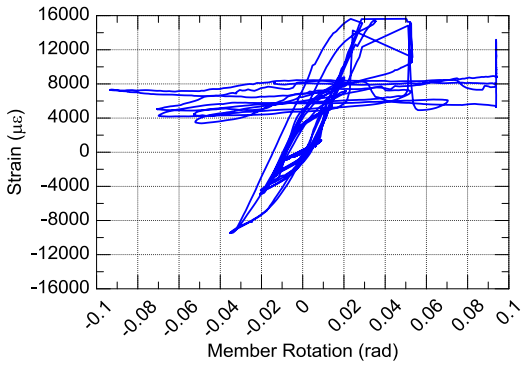

SG 6

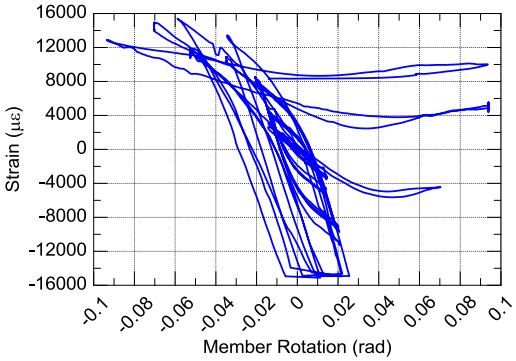

SG 7

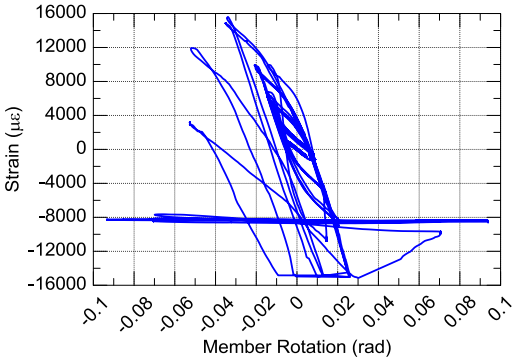

SG 8

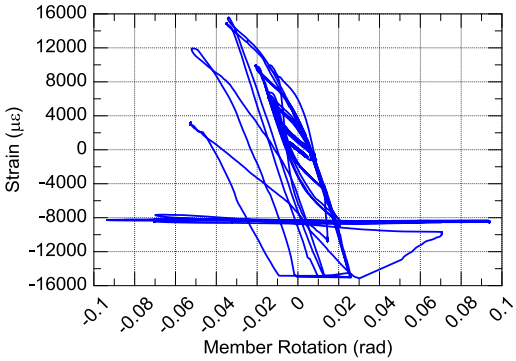

SG 9

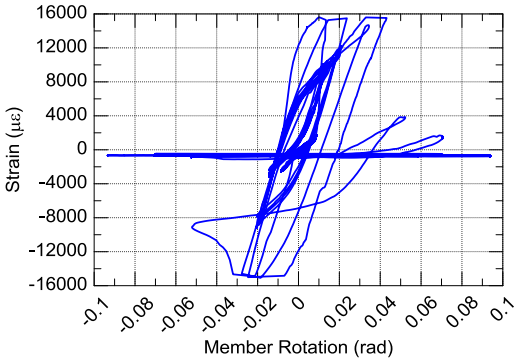

SG 10

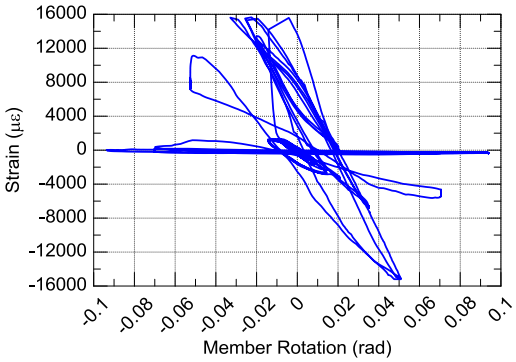

SG 11

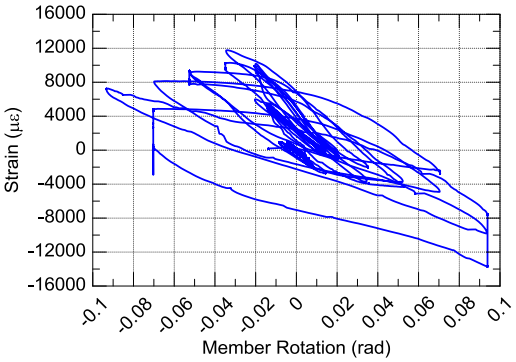

SG 12

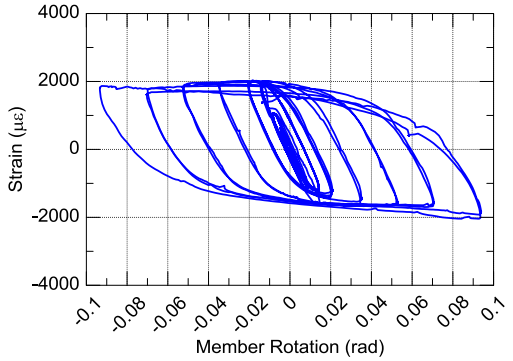

SG 13

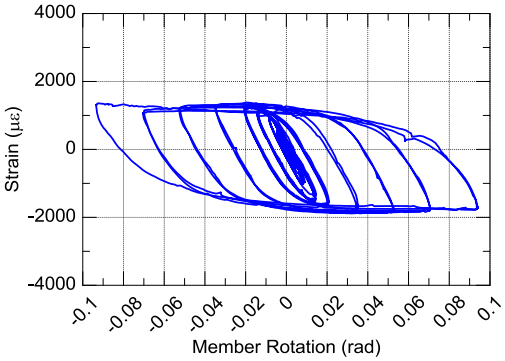

SG 14

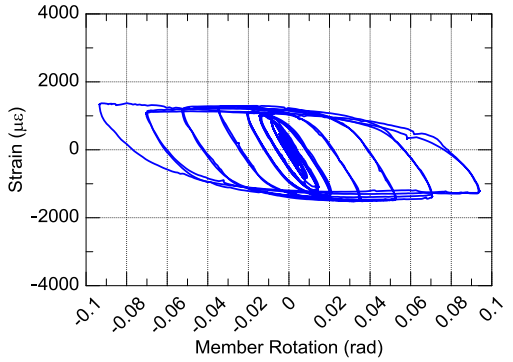

SG 15

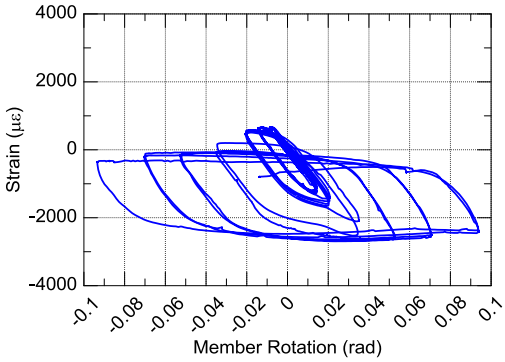

SG 16

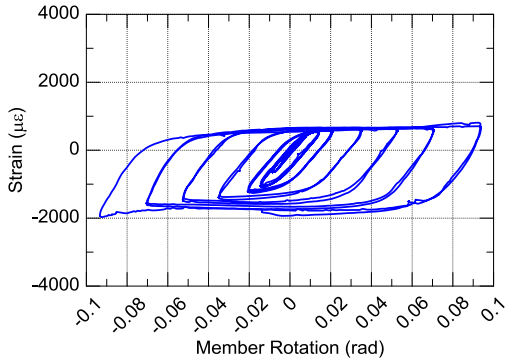

SG 17

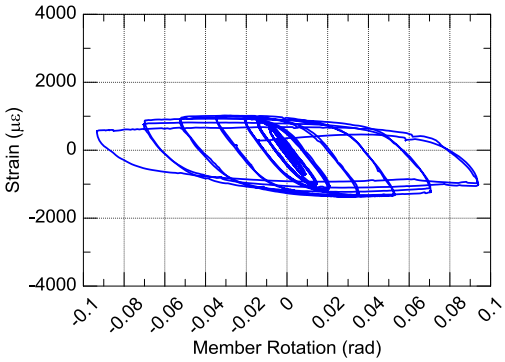

SG 18

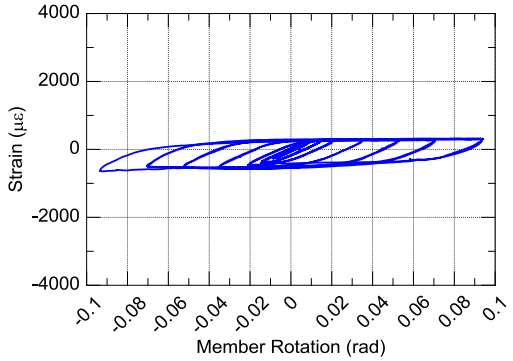

SG 19

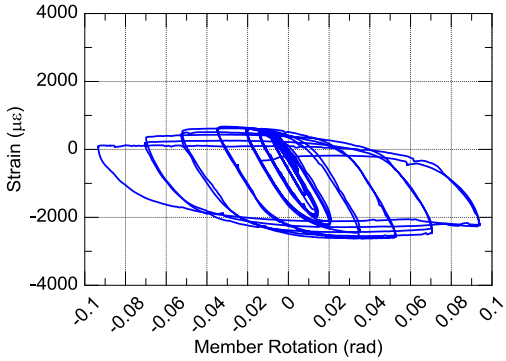

SG 20

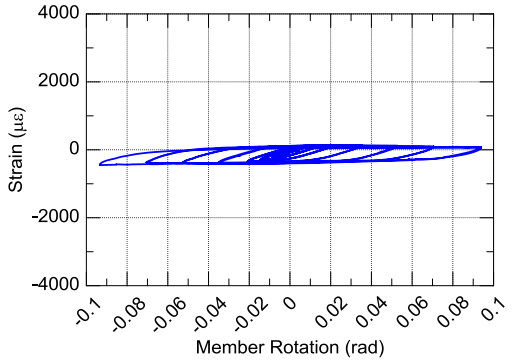

G 21

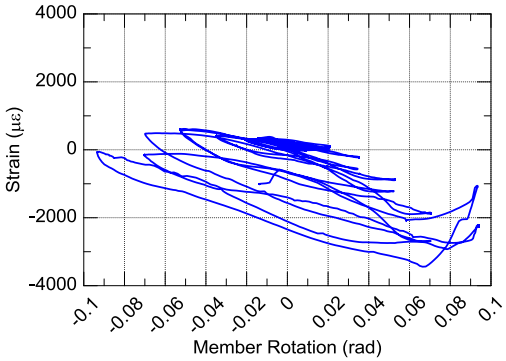

SG 22

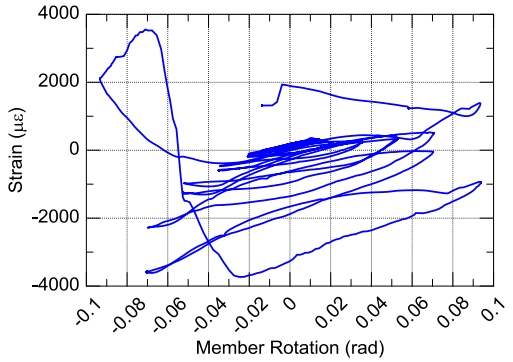

SG 23

Specimen 2C12-11-RBS

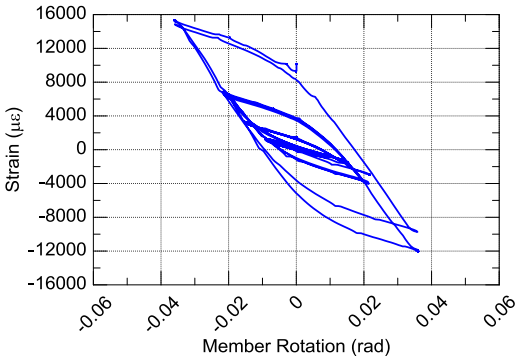

SG 1

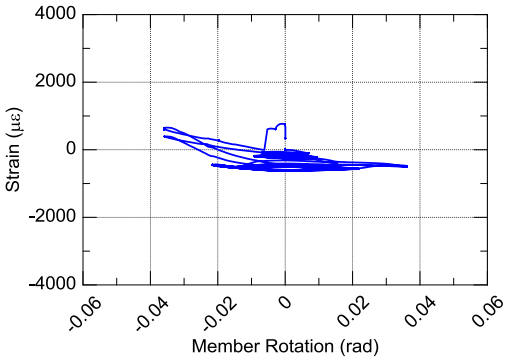

SG 2

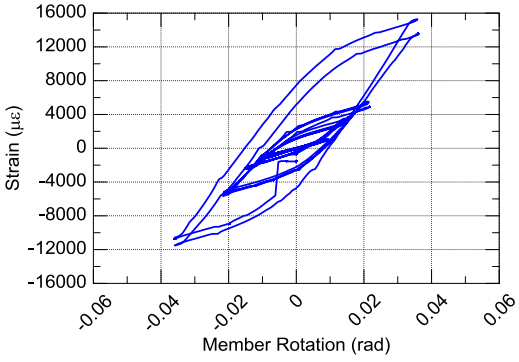

SG 3

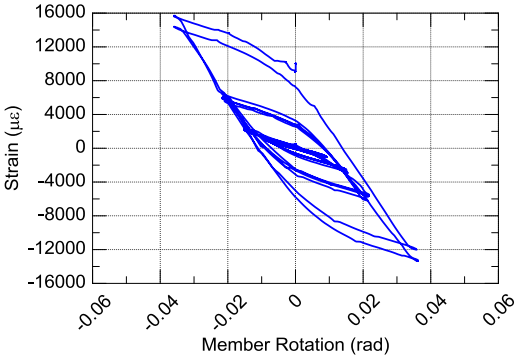

SG 4

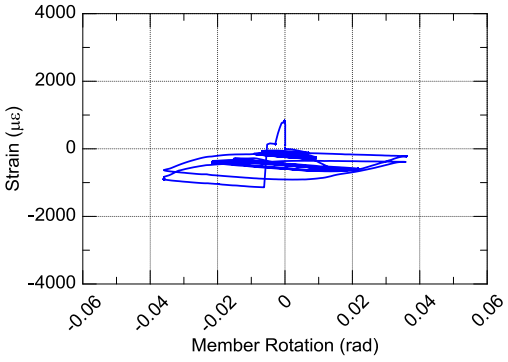

SG 5

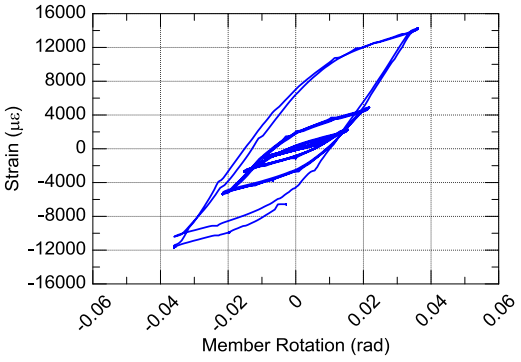

SG 6

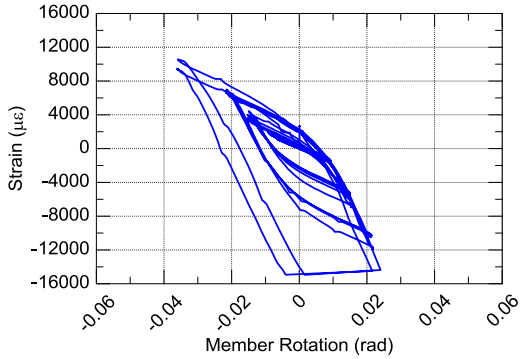

SG 7

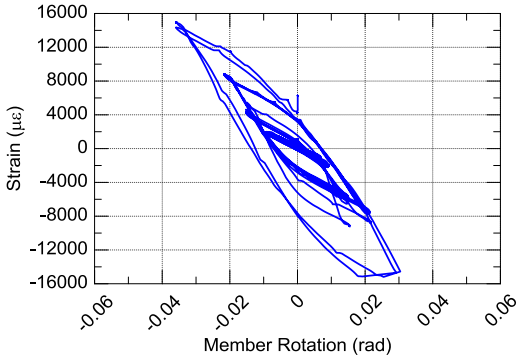

SG 8

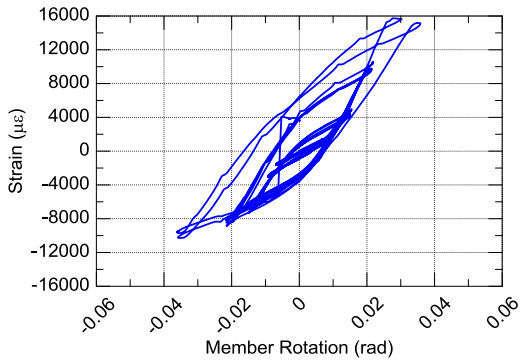

SG 9

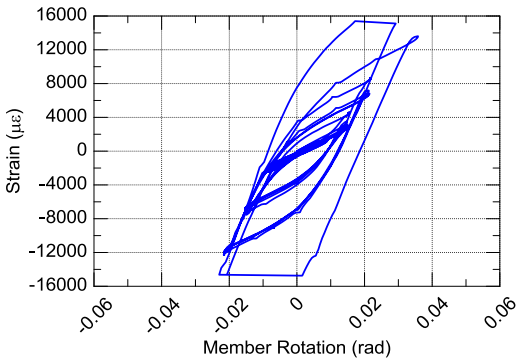

SG 10

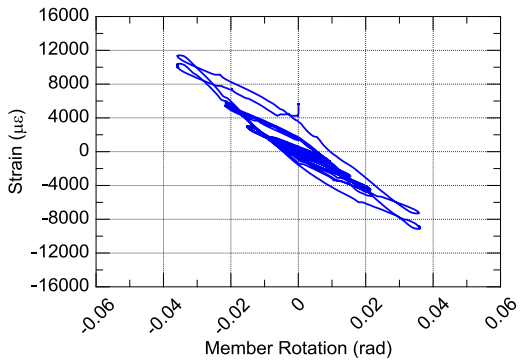

SG 11

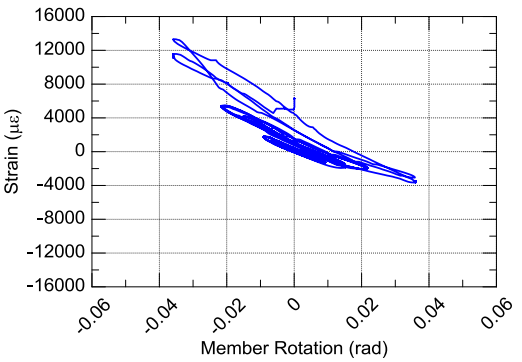

SG 12

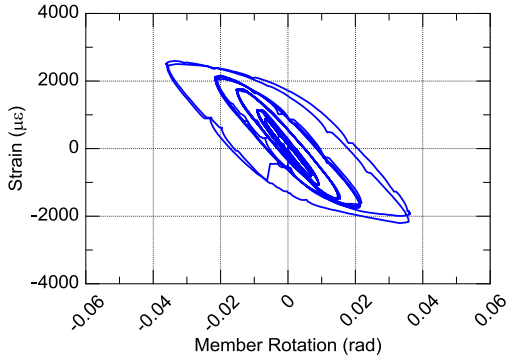

SG 13

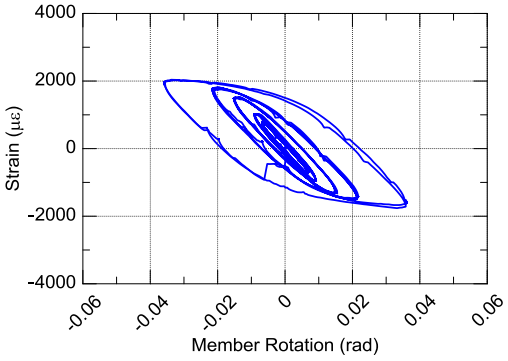

SG 14

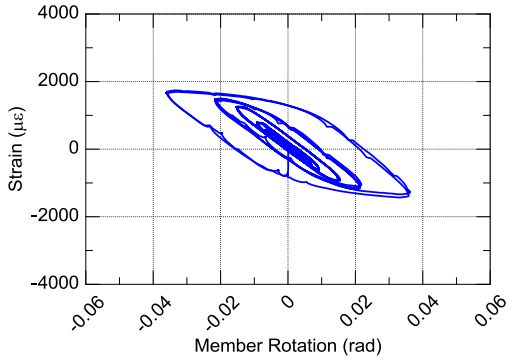

SG 15

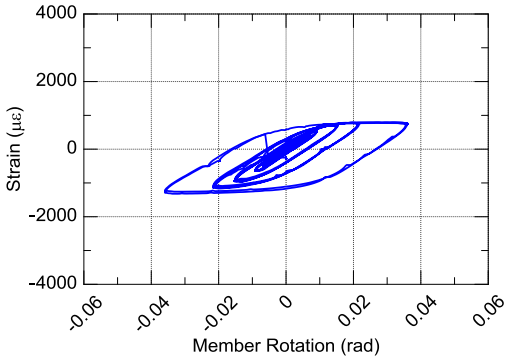

SG 16

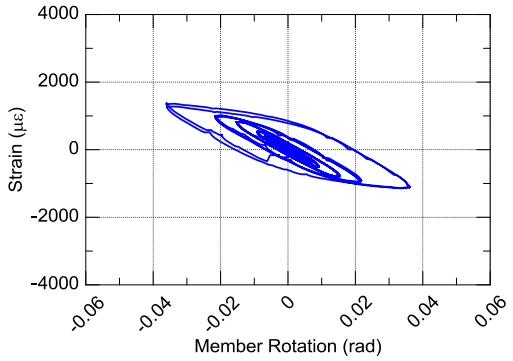

SG 17

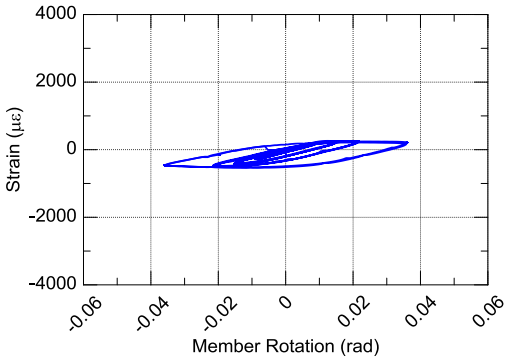

SG 18

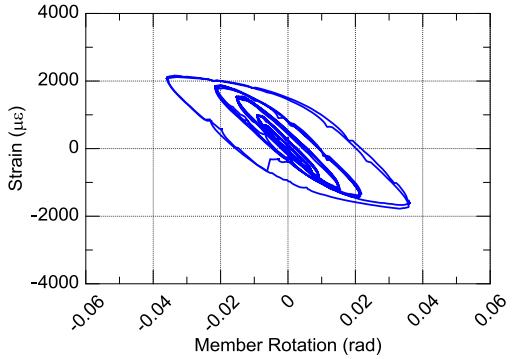

SG 19

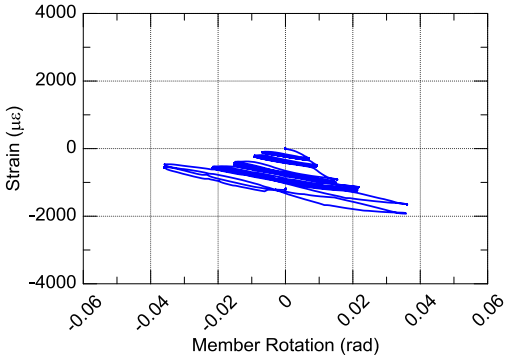

SG 20

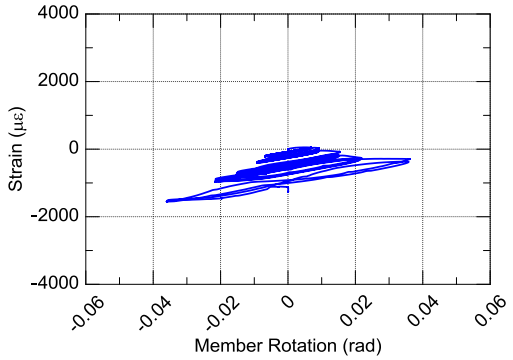

G 21

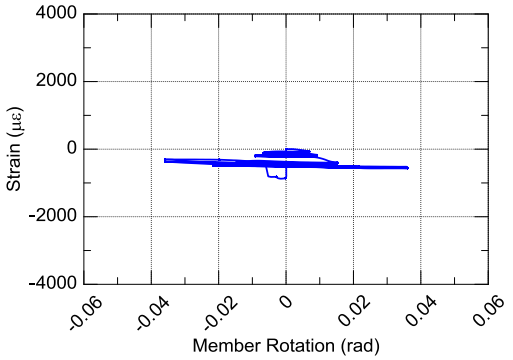

SG 22

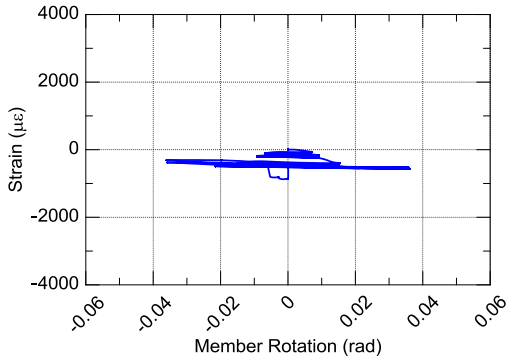

SG 23

Specimen 2C12-12

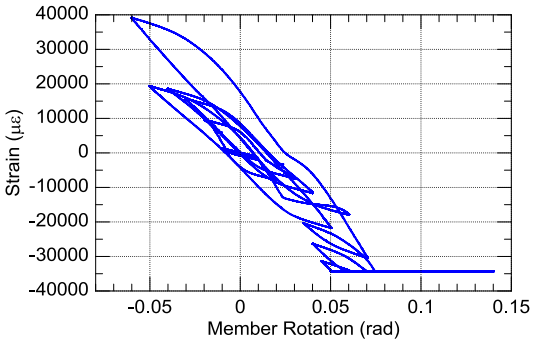

SG 1

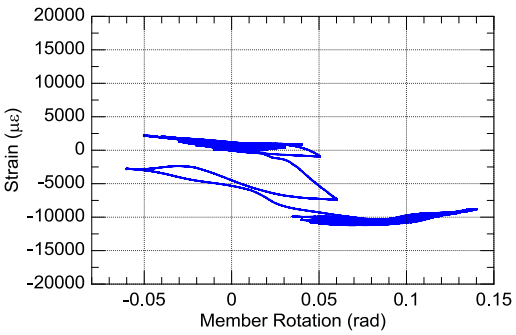

SG 2

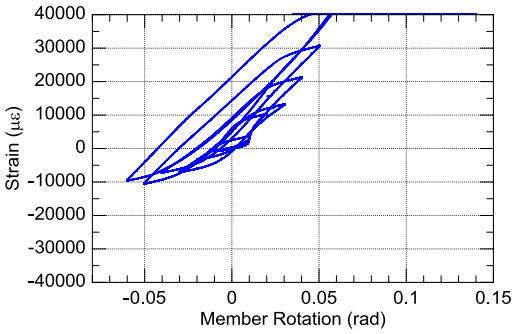

SG 3

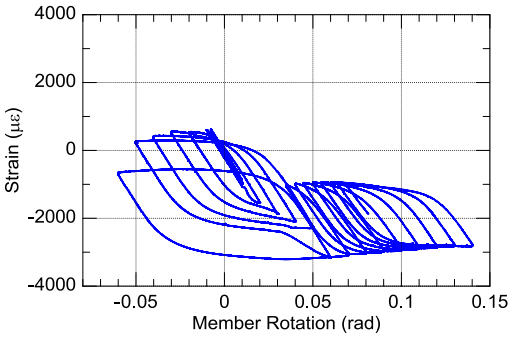

SG 4

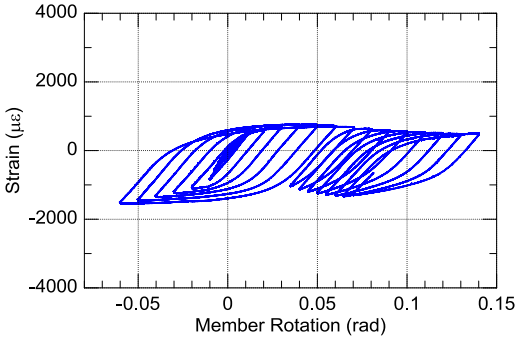

SG 5

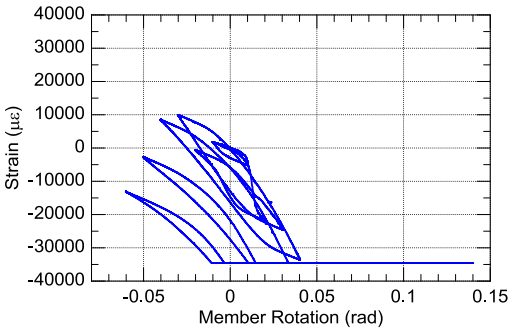

SG 6

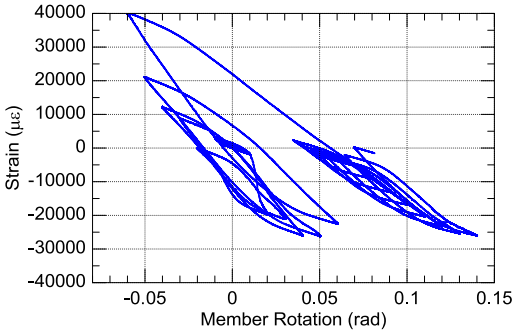

SG 7

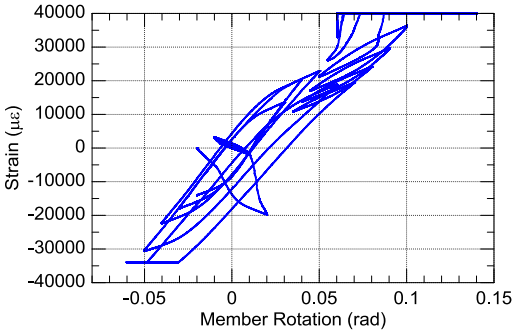

SG 8

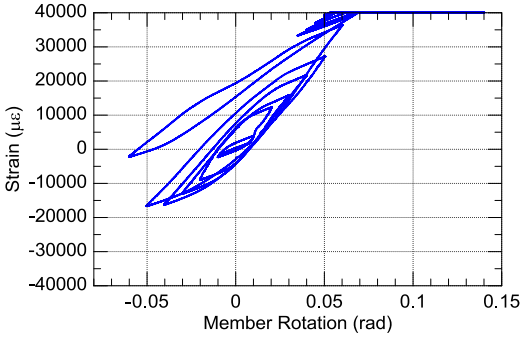

SG 9

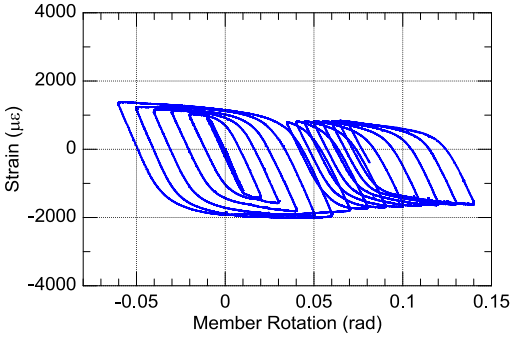

SG 10

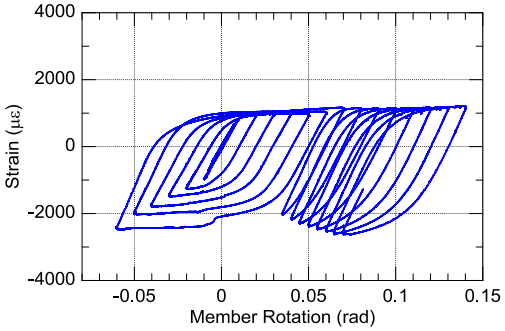

SG 11

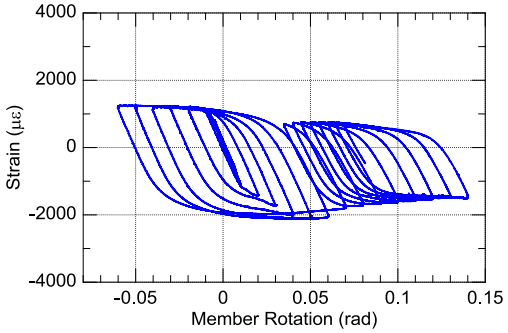

SG 12

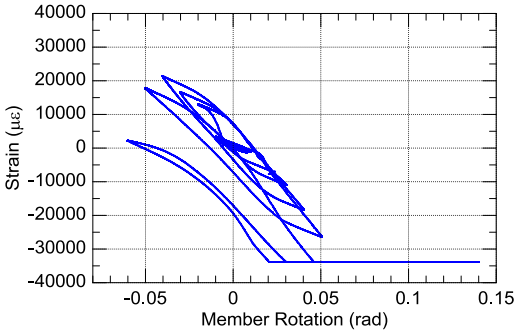

SG 13

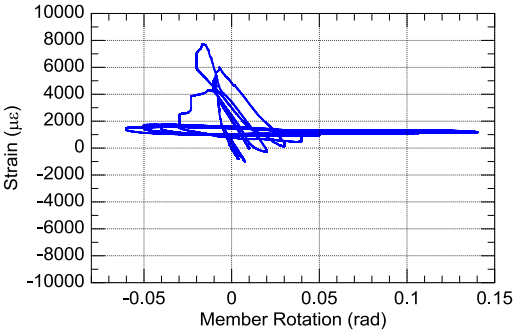

SG 14

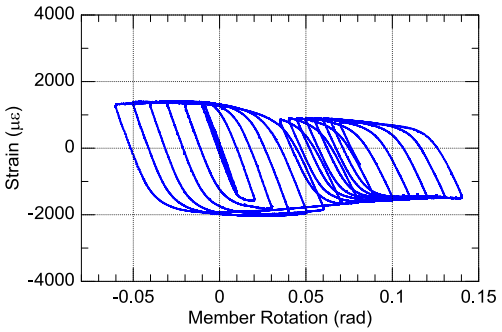

SG 15

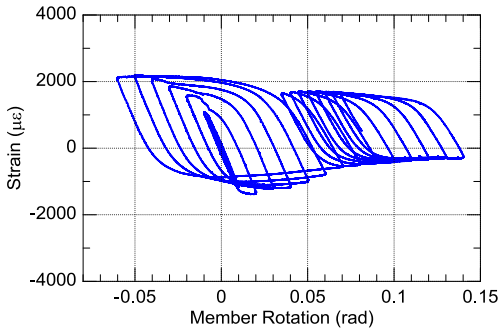

SG 16

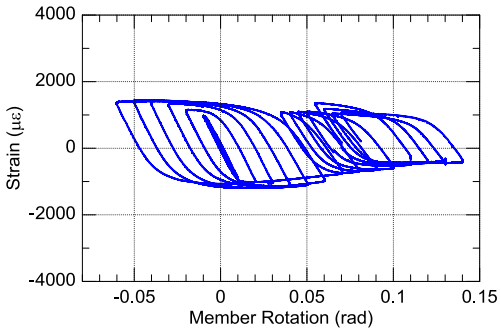

SG 17

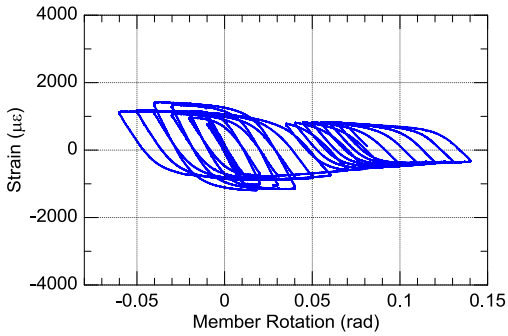

SG 18

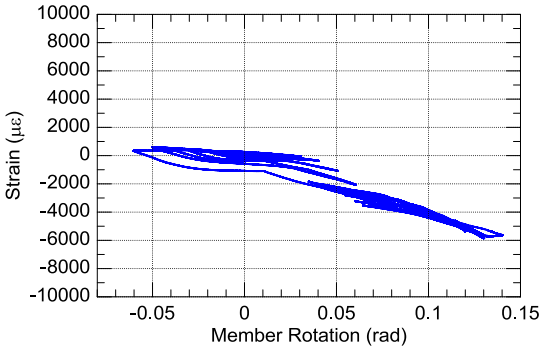

SG 19

Specimen 2C8-1

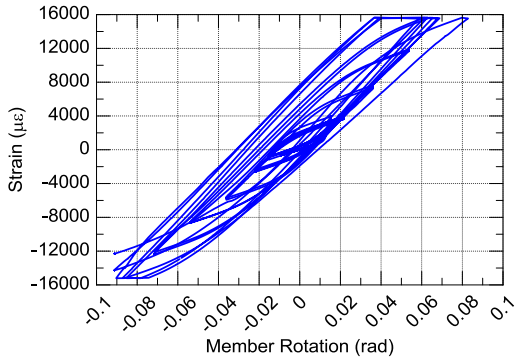

SG 1

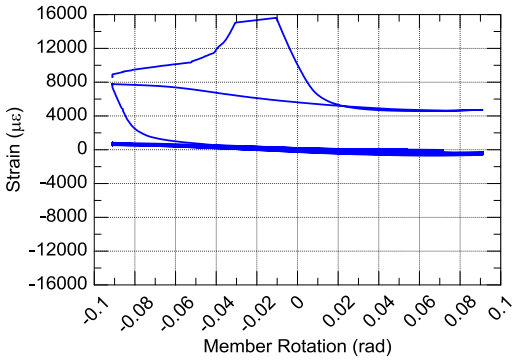

SG 2

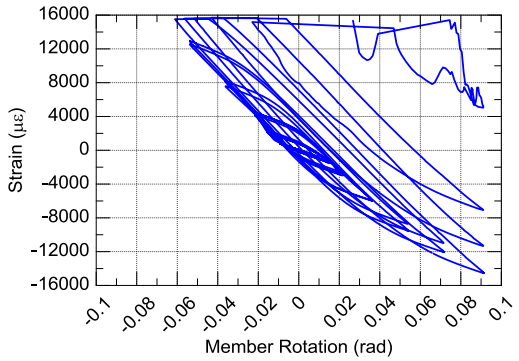

SG 3

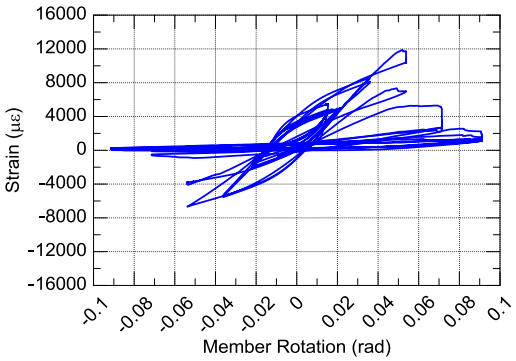

SG 4

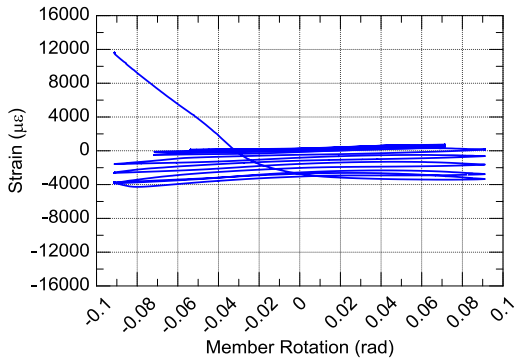

SG 5

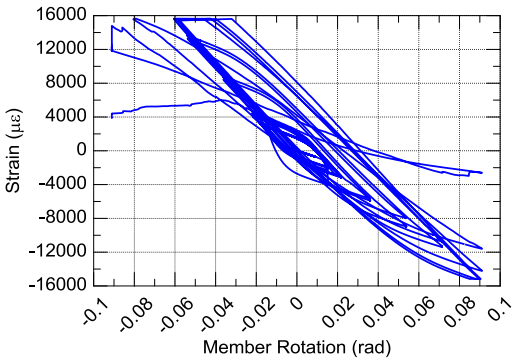

SG 6

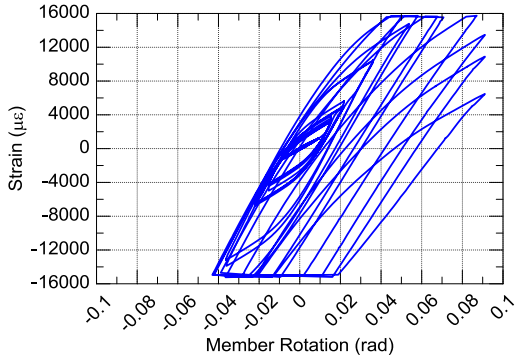

SG 7

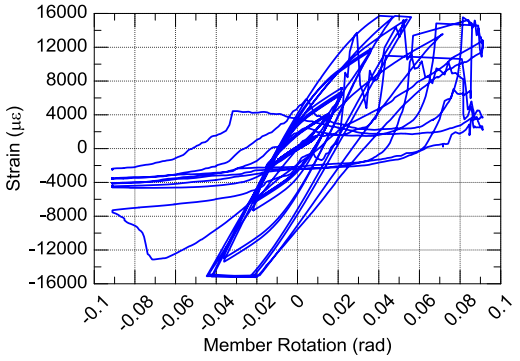

SG 8

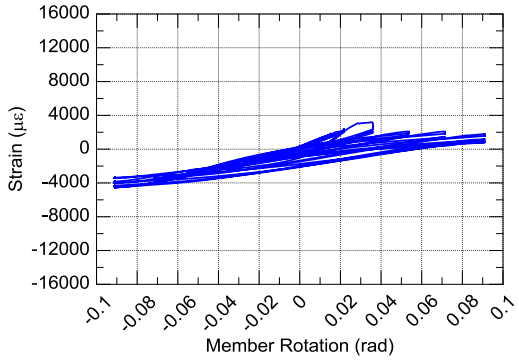

SG 9

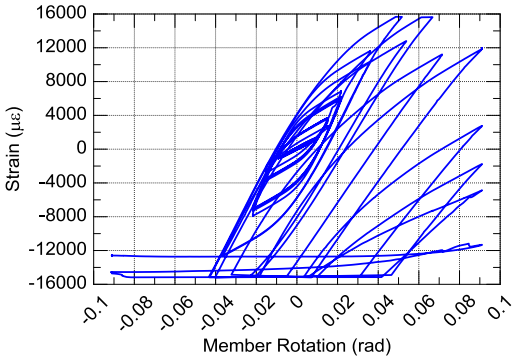

SG 10

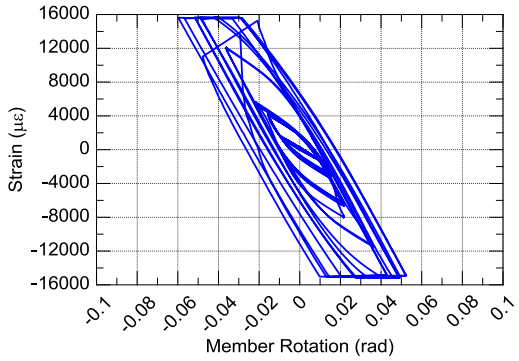

SG 11

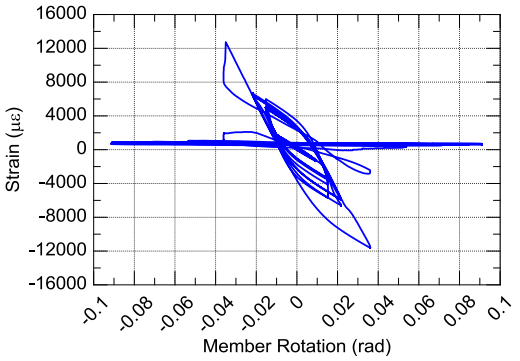

SG 12

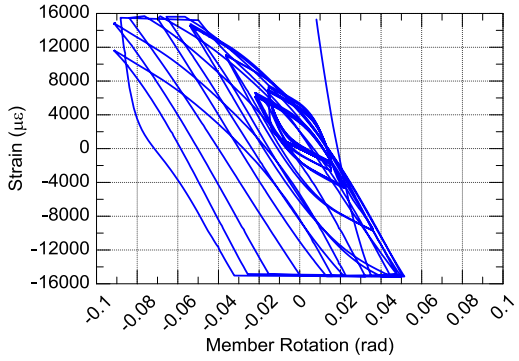

SG 13

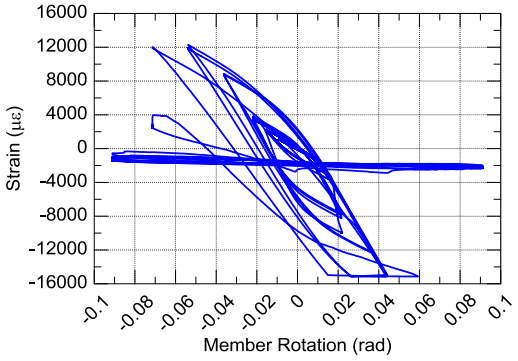

SG 14

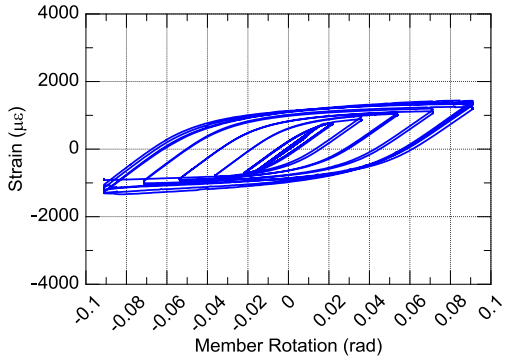

SG 15

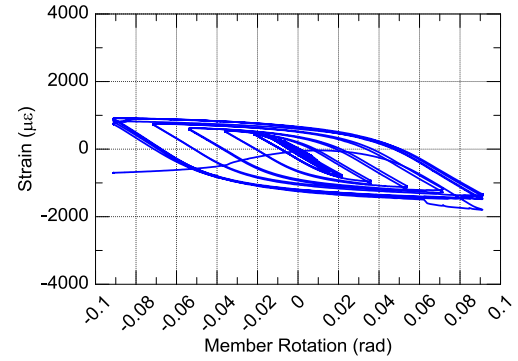

SG 16

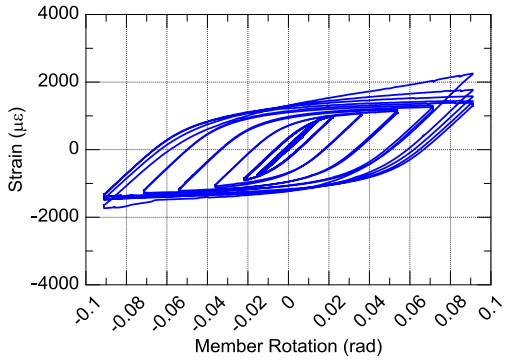

SG 17

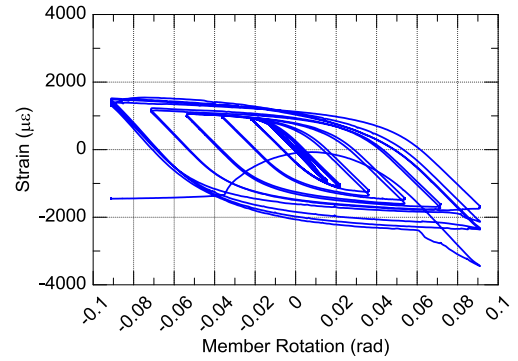

SG 18

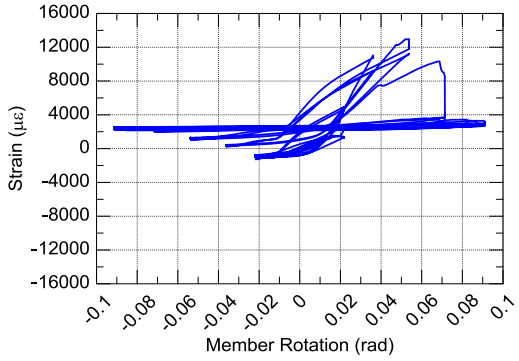

SG 19

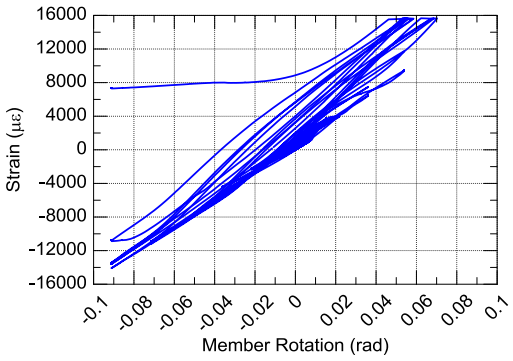

SG 20

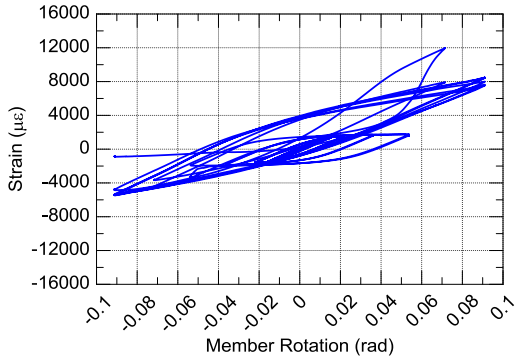

G 21

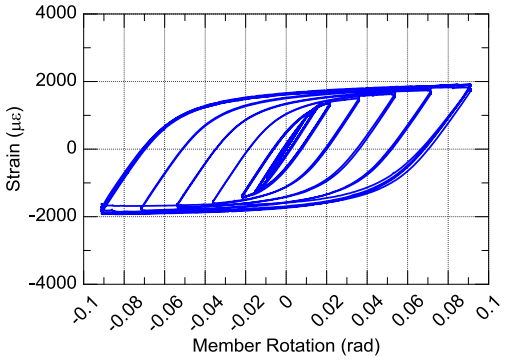

SG 22

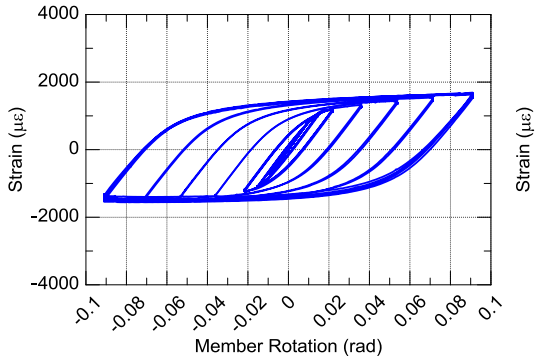

SG 23

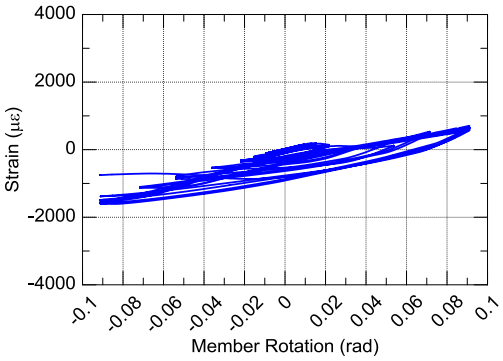

SG 24

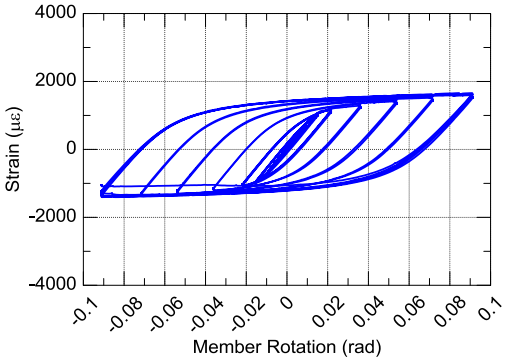
4000
2000
0
-2000
-4000
Strain (με)
-0.1
-0.08
-0.06
-0.04
-0.02
0
0.02
0.04
0.06
0.08
0.1
Member Rotation (rad)
SG 25

Specimen 2C6-1

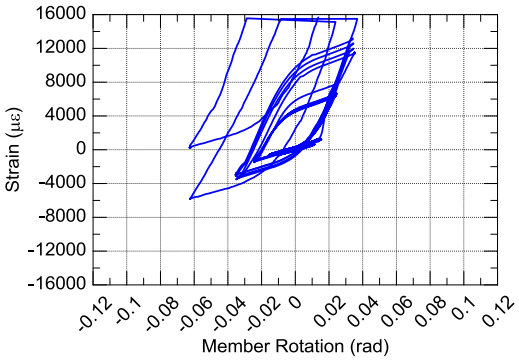

SG 1

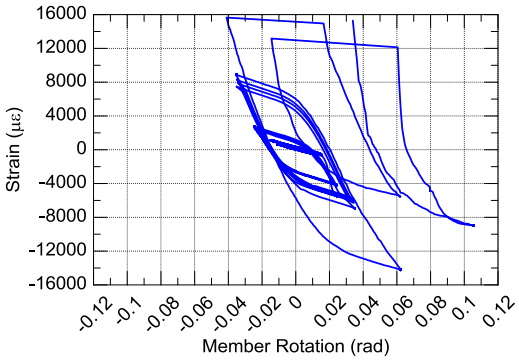

SG 2

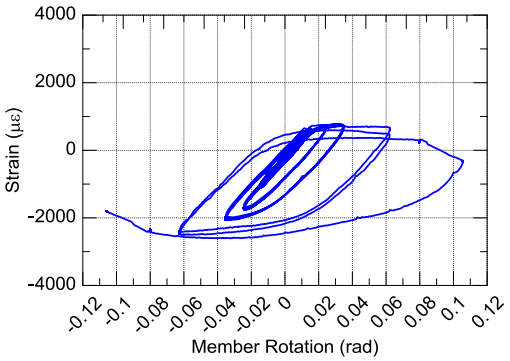

SG 3

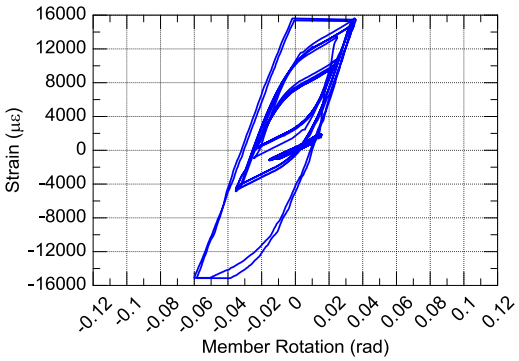

SG 4

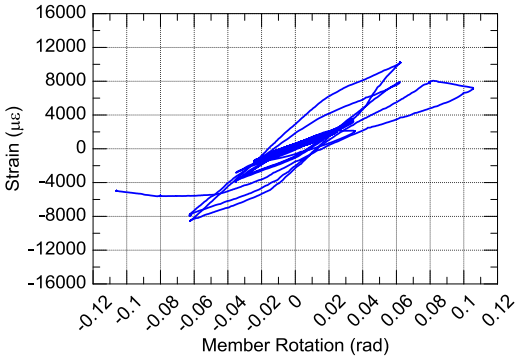

SG 5

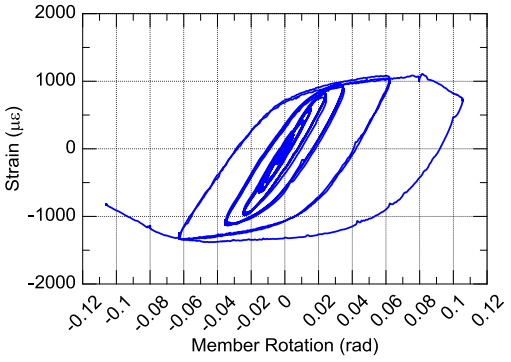

SG 6

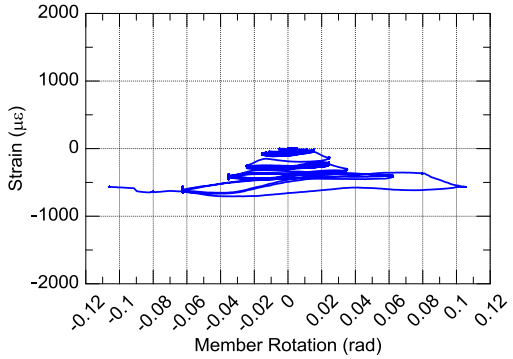

SG 7

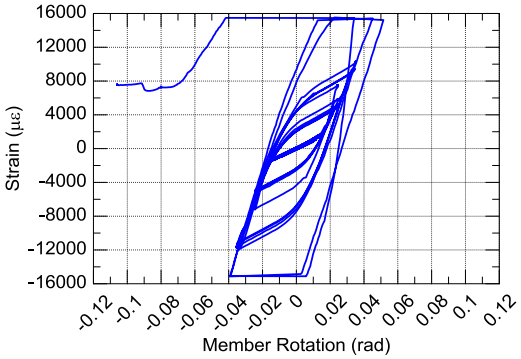

SG 8

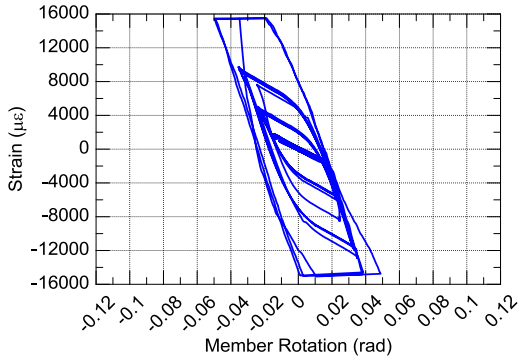

SG 9

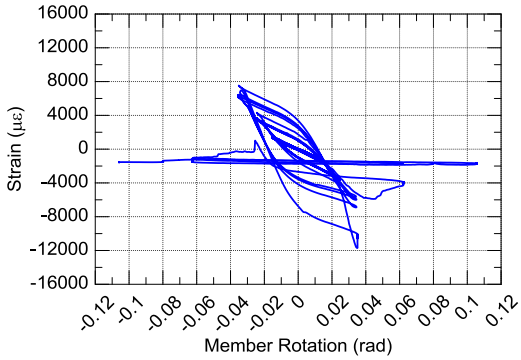

SG 10

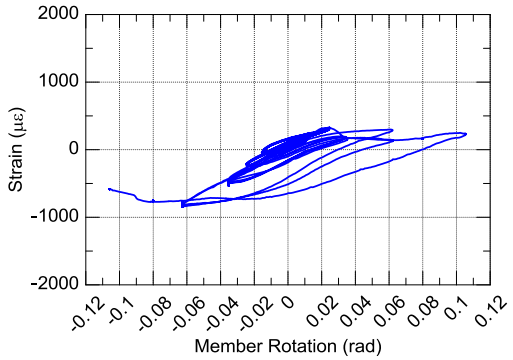

SG 11

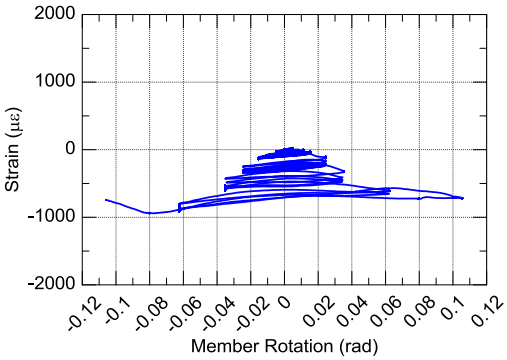

SG 12

Specimen 2C6-2

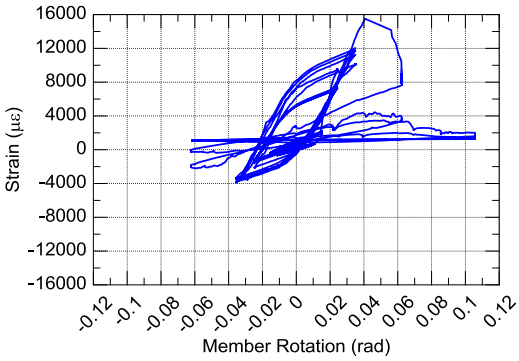

SG 1

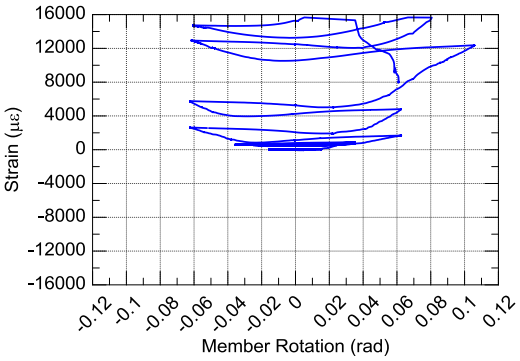

SG 2

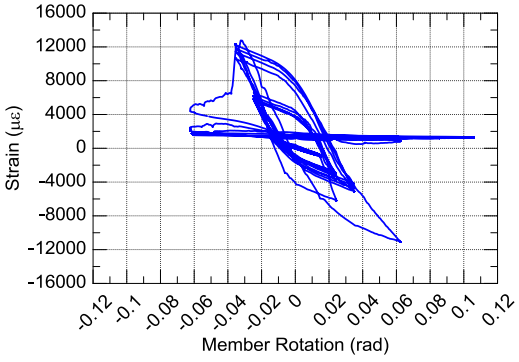

SG 3

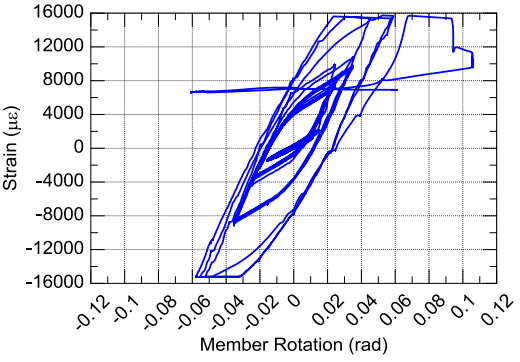

SG 4

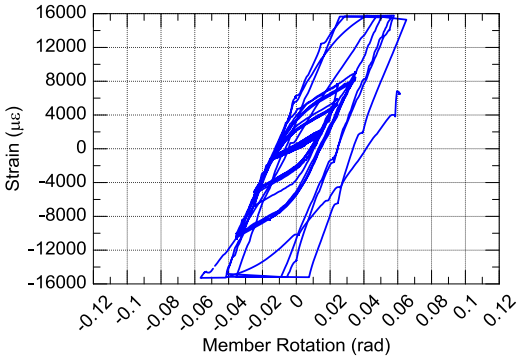

SG 5

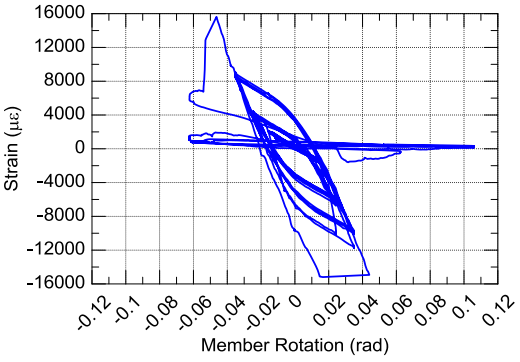

SG 6

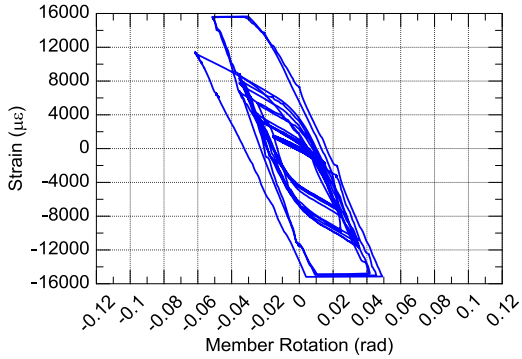

SG 7

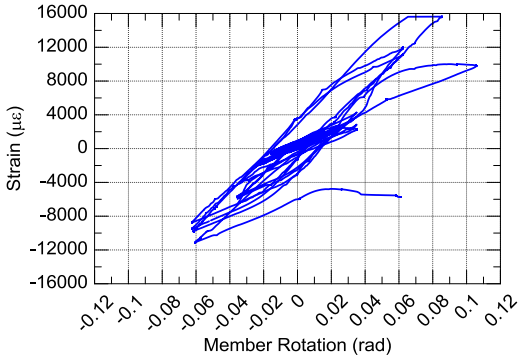

SG 8

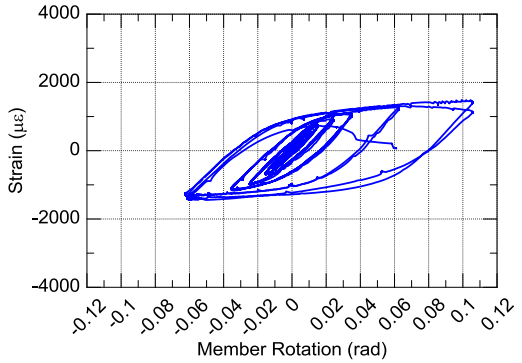

SG 9

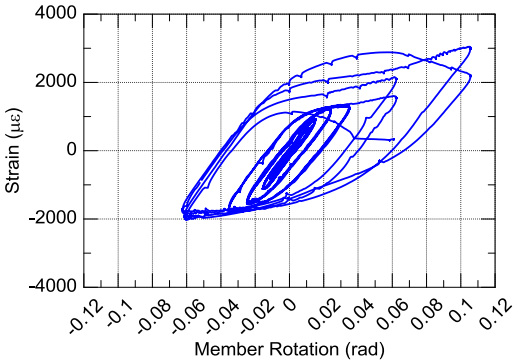

SG 10

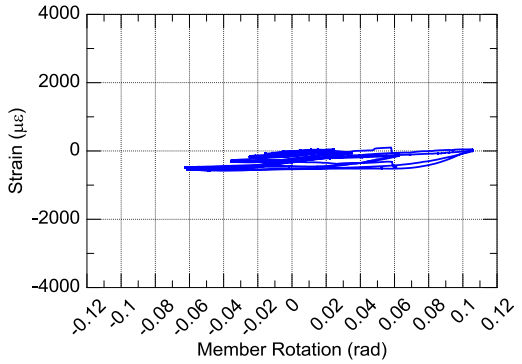

SG 11

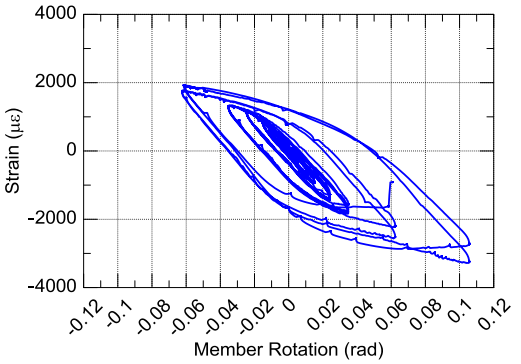

SG 12

Specimen 2HSS8-1

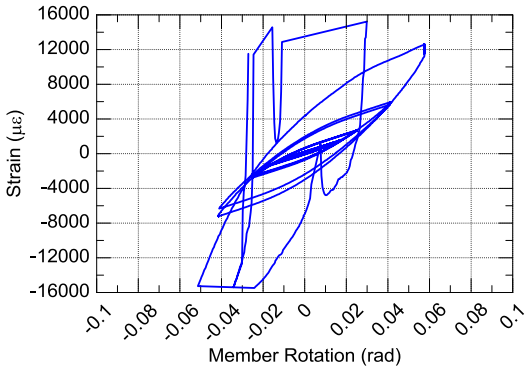

SG 1

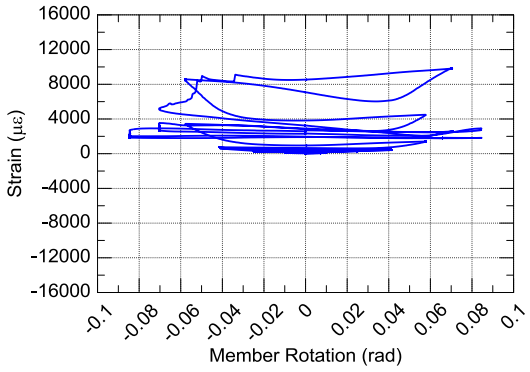

SG 2

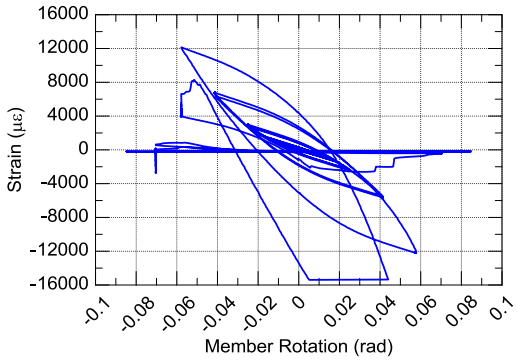

SG 3

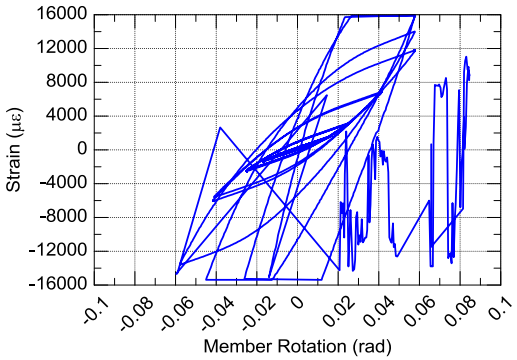

SG 4

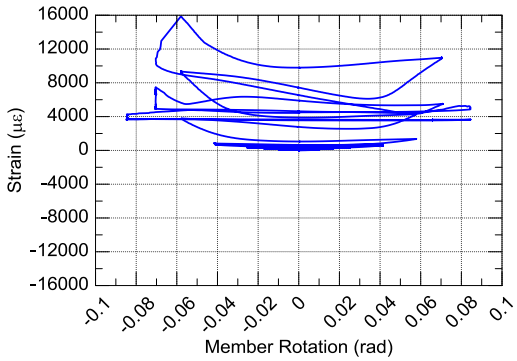

SG 5

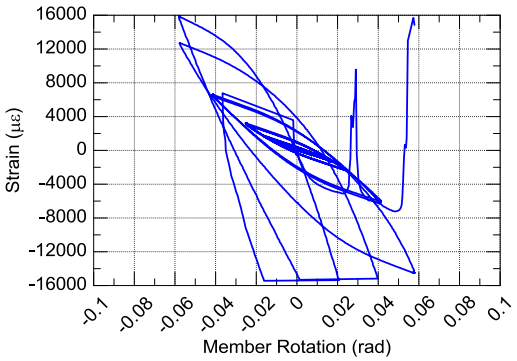

SG 6

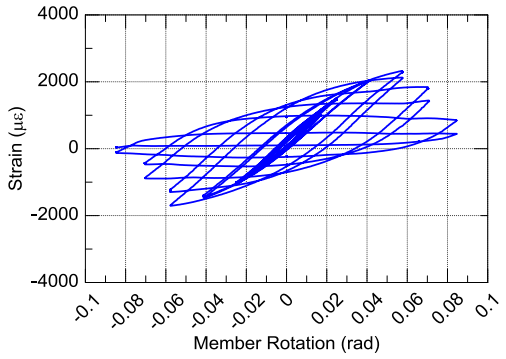

SG 7

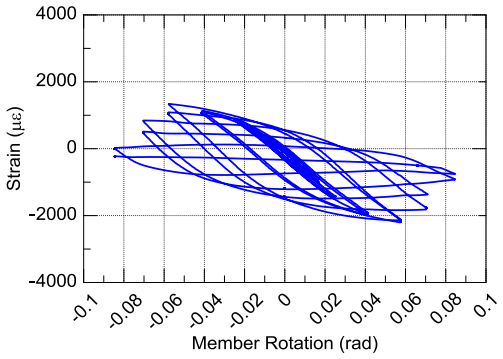

SG 8

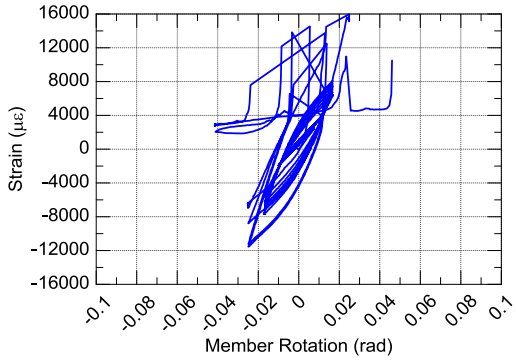

SG 9

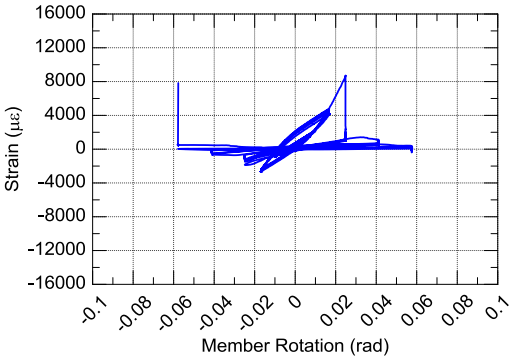

SG 10

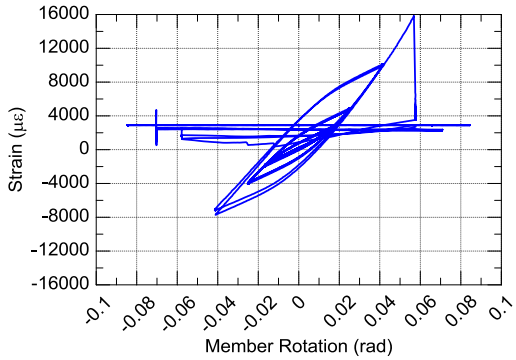

SG 11

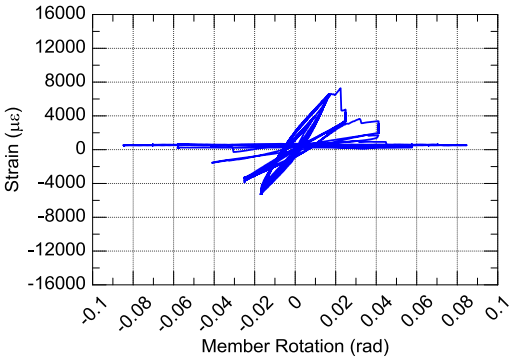

SG 12

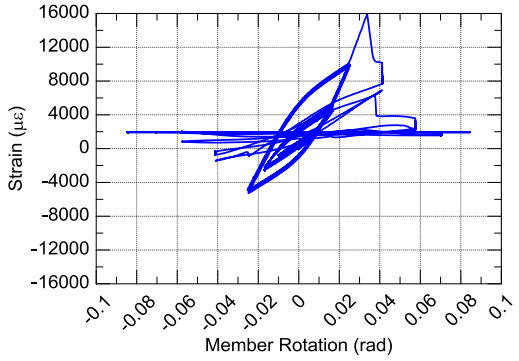

SG 13

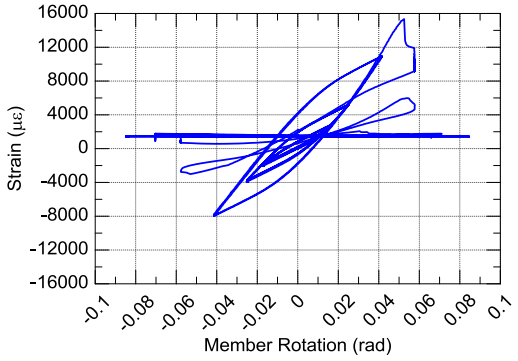

SG 14

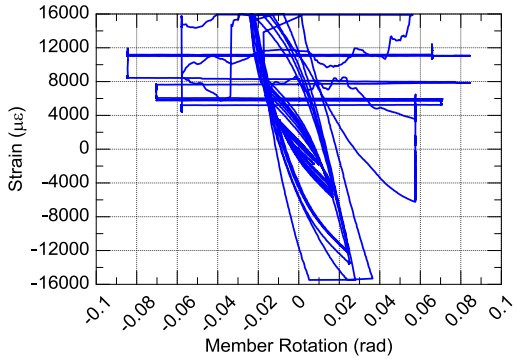

SG 15

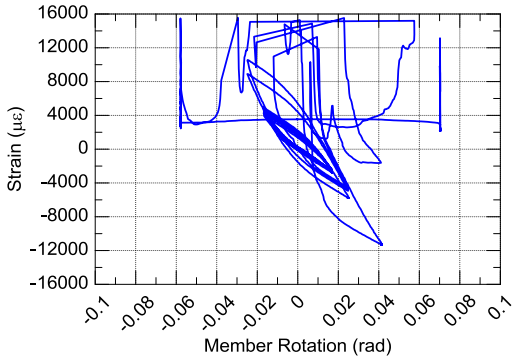

SG 16

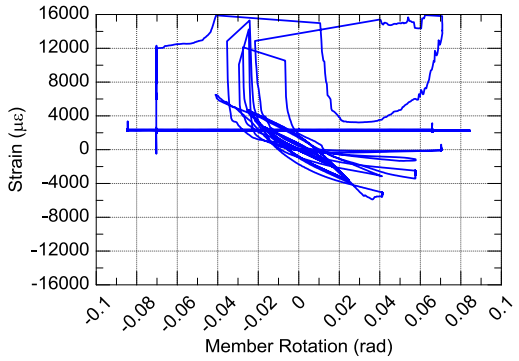

SG 17

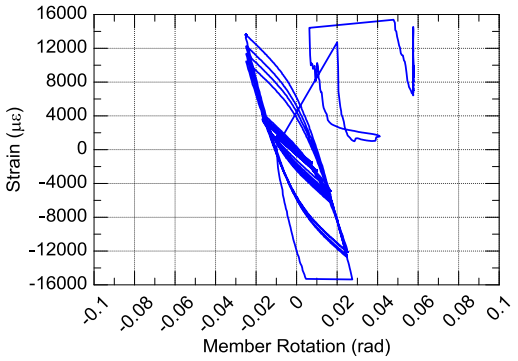

SG 18

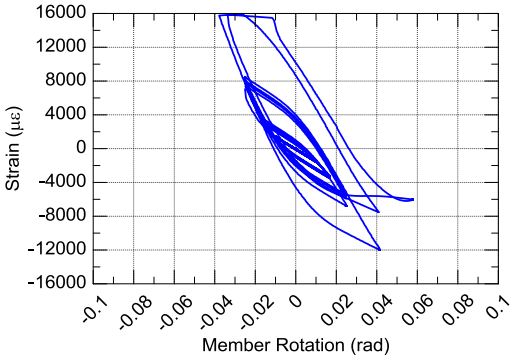

SG 19

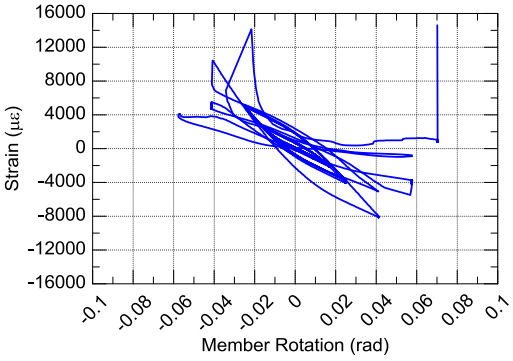

SG 20

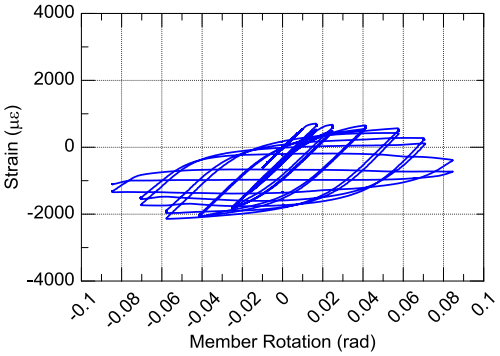

G 21

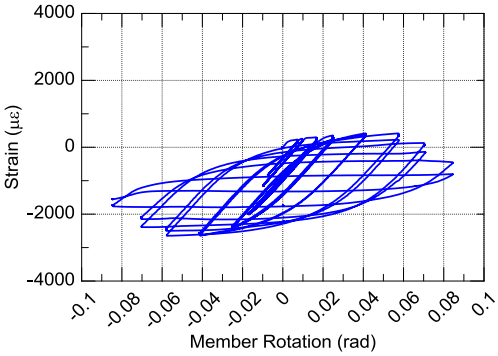

SG 22

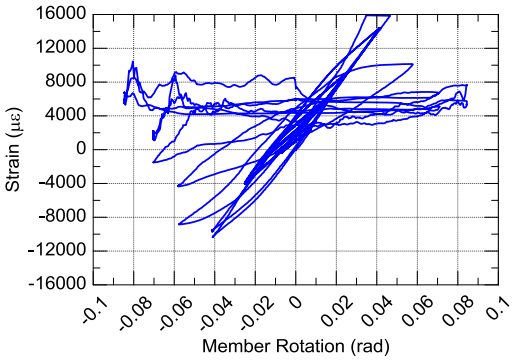

SG 23

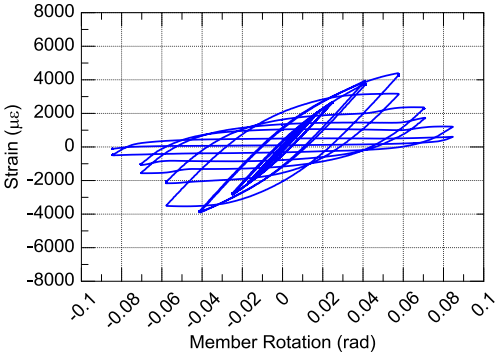

SG 24

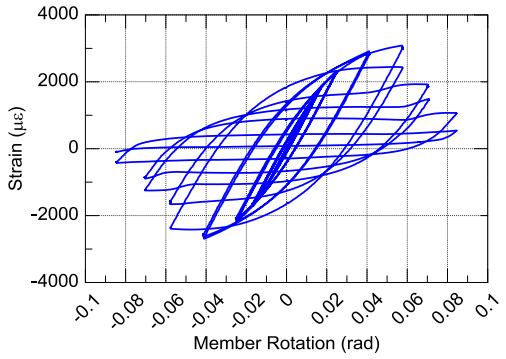

SG 25

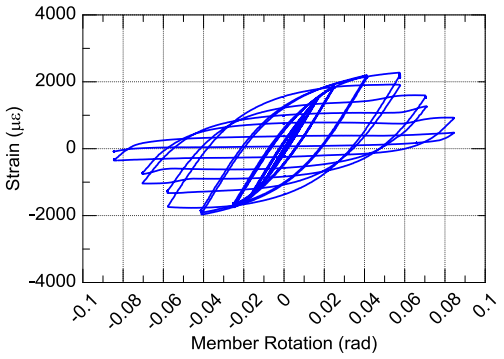

SG 26

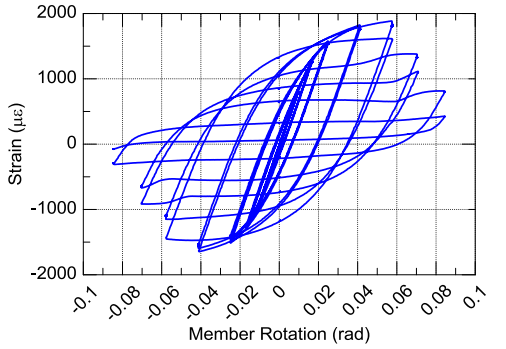

SG 27

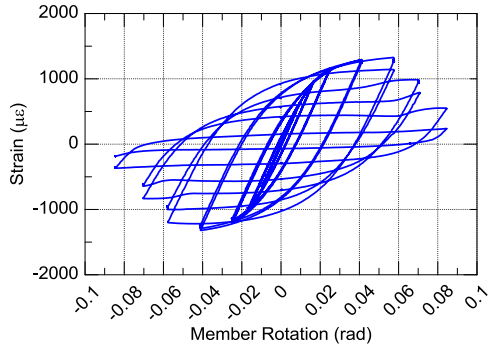

SG 28

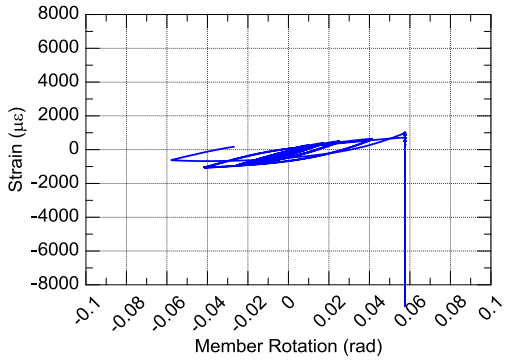

SG 29

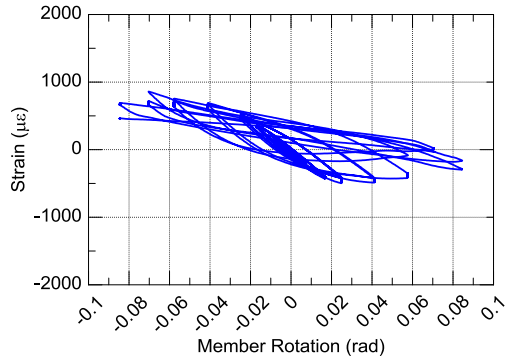

SG 30

Specimen 2HSS8-2

For this specimen, the data acquisition system recorded all strain gauge readings intermittently. This resulted in many straight line plots both vertically and horizontally. As a result, the plots are not shown here.

Specimen 2HSS8-3

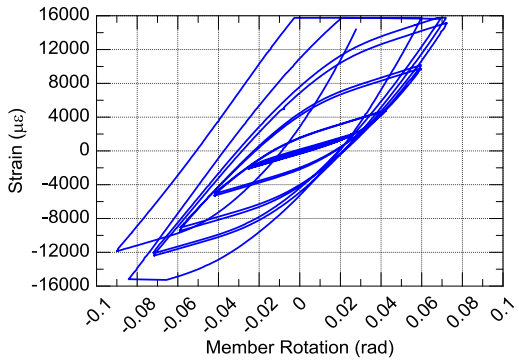

SG 1

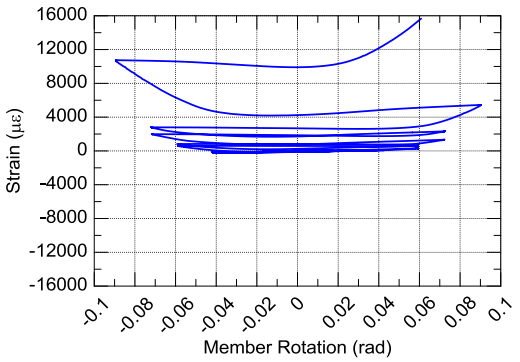

SG 2

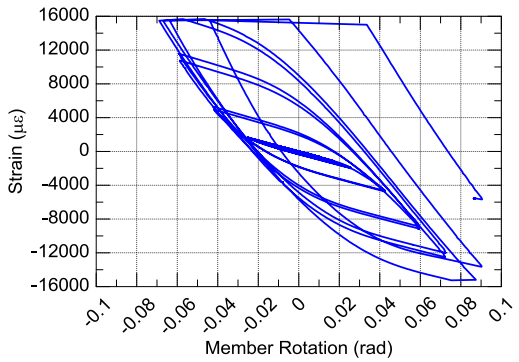

SG 3

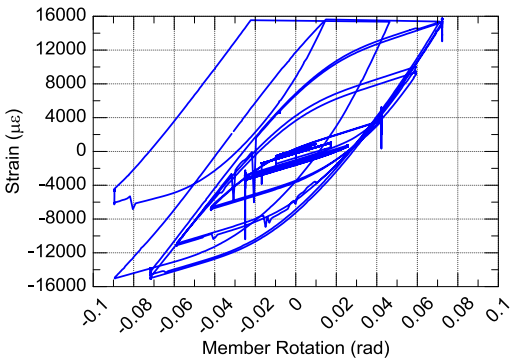

SG 4

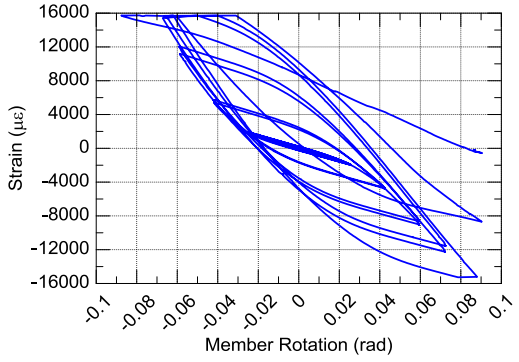

SG 5

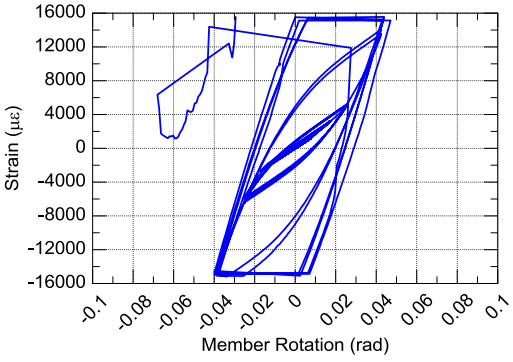

SG 6

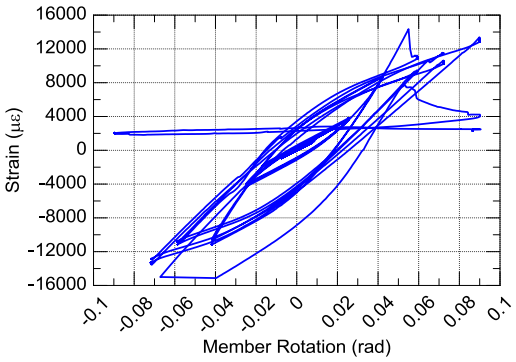

SG 7

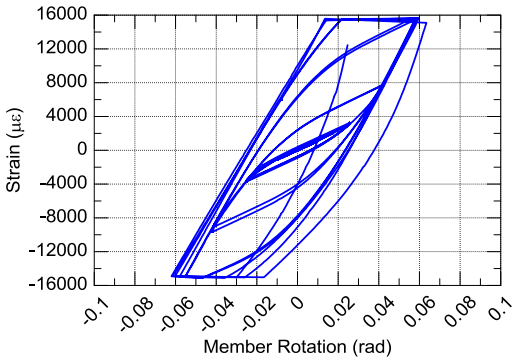

SG 8

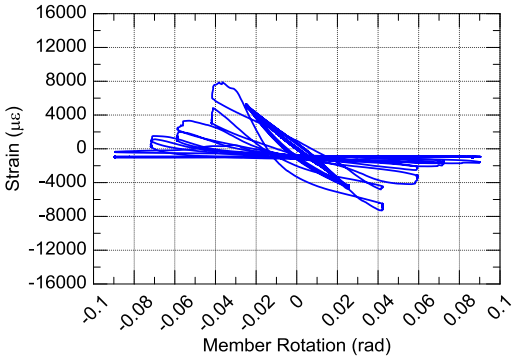

SG 9

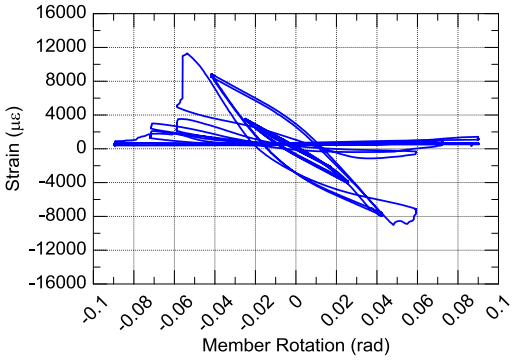

SG 10

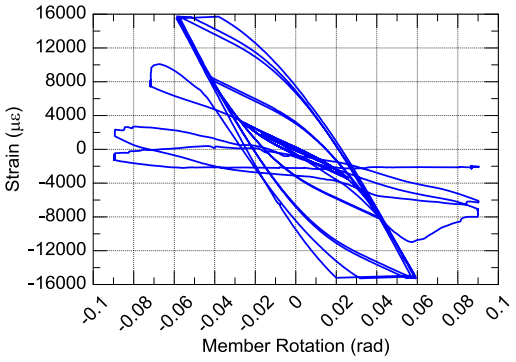

SG 11

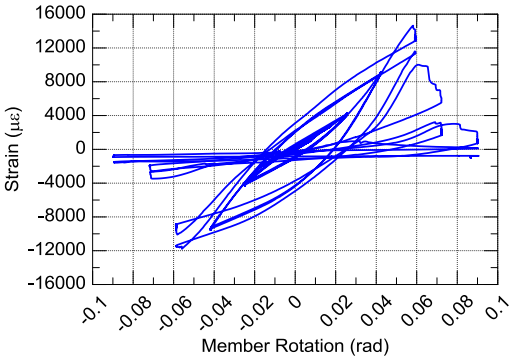

SG 12

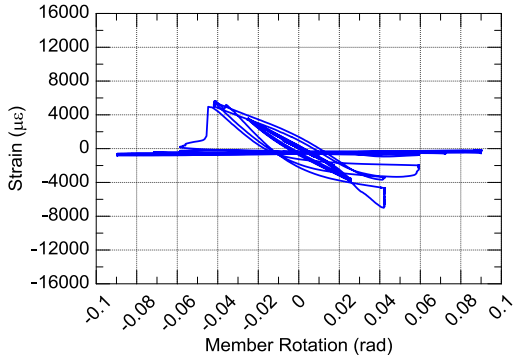

SG 13

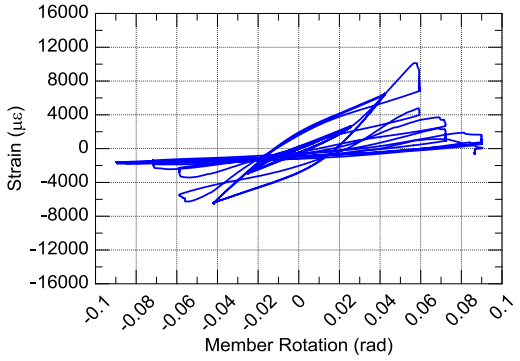

SG 14

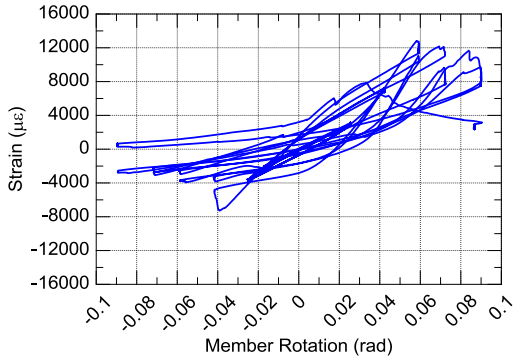

SG 15

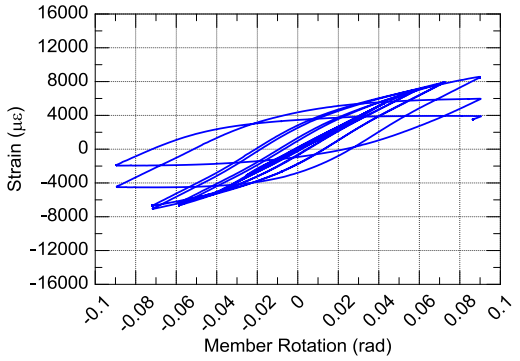

SG 16

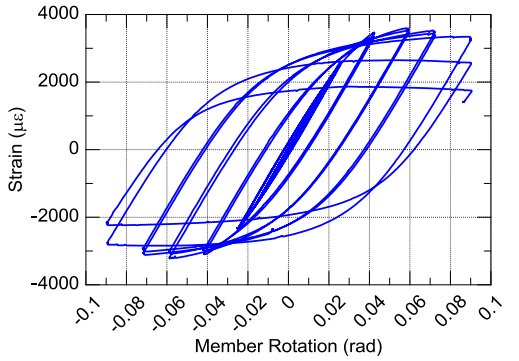

SG 17

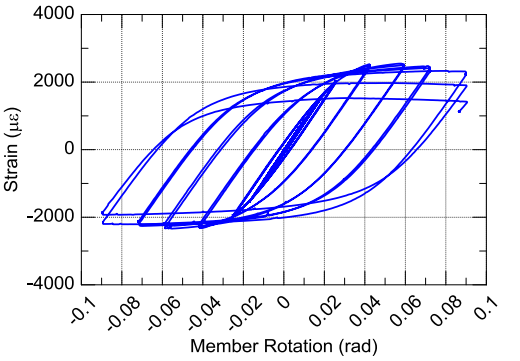

SG 18

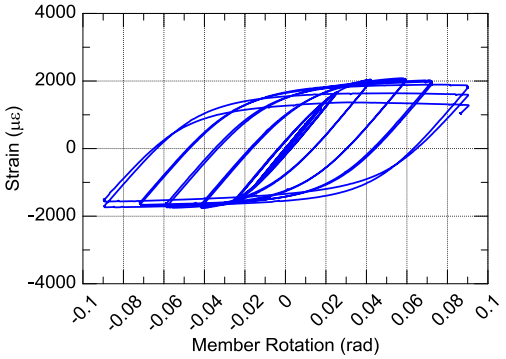

SG 19

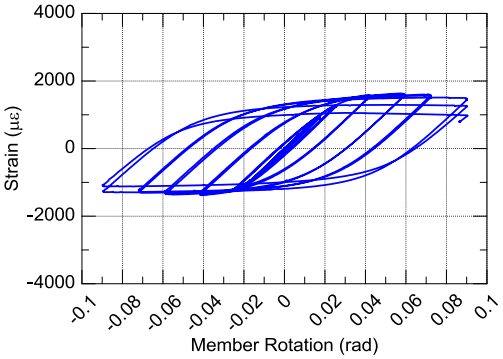

SG 20

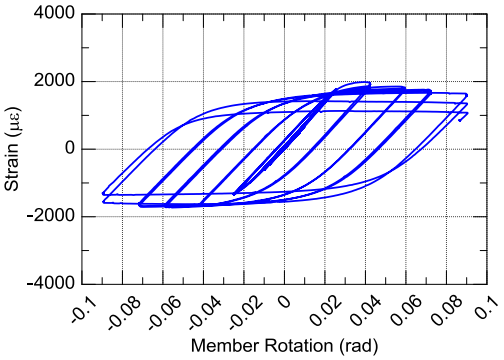

SG 21

Appendix F

Instrumentation and Strain Gauge Data for STMF Subassemblage Test

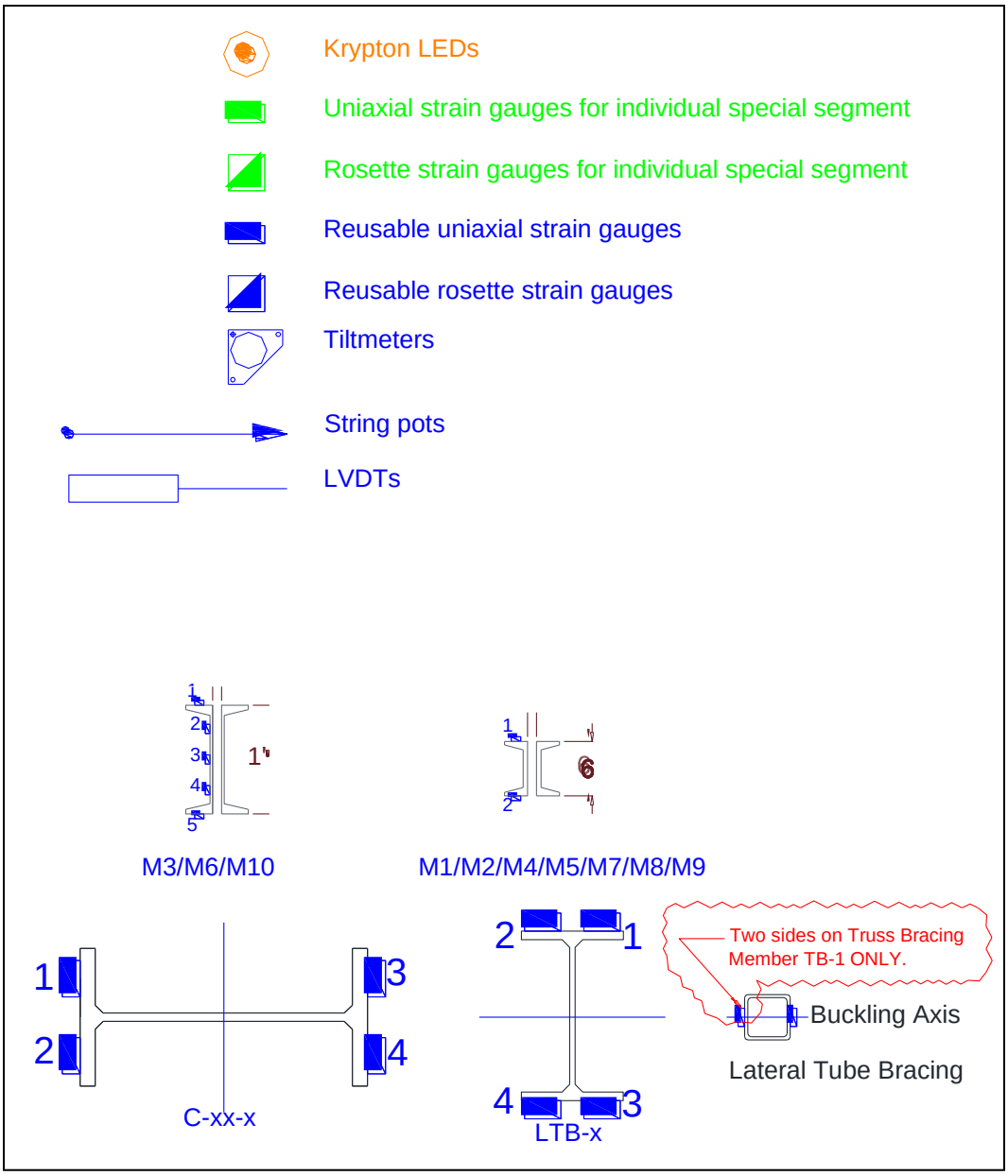

Instruments Legends

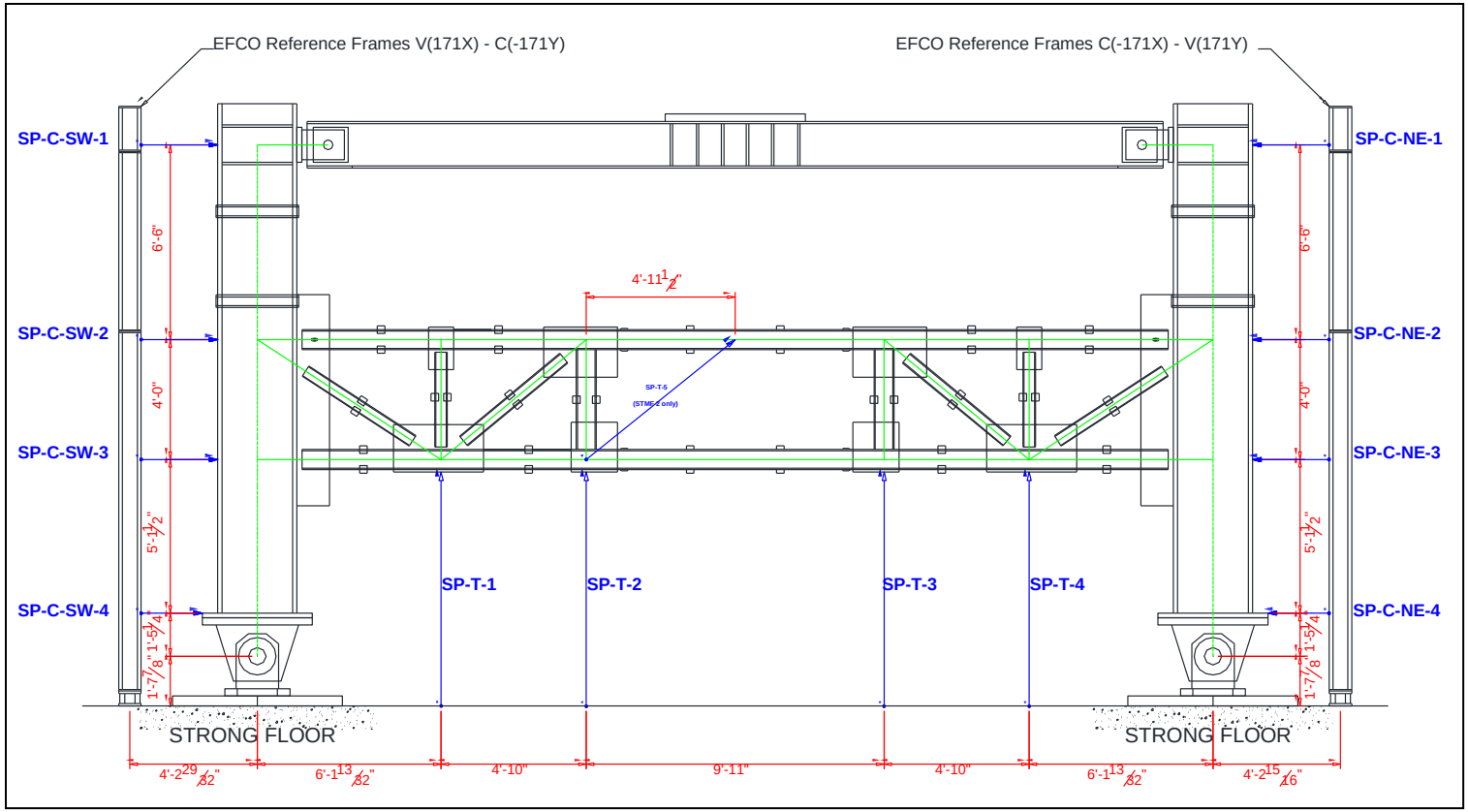

String Potentiometer Location

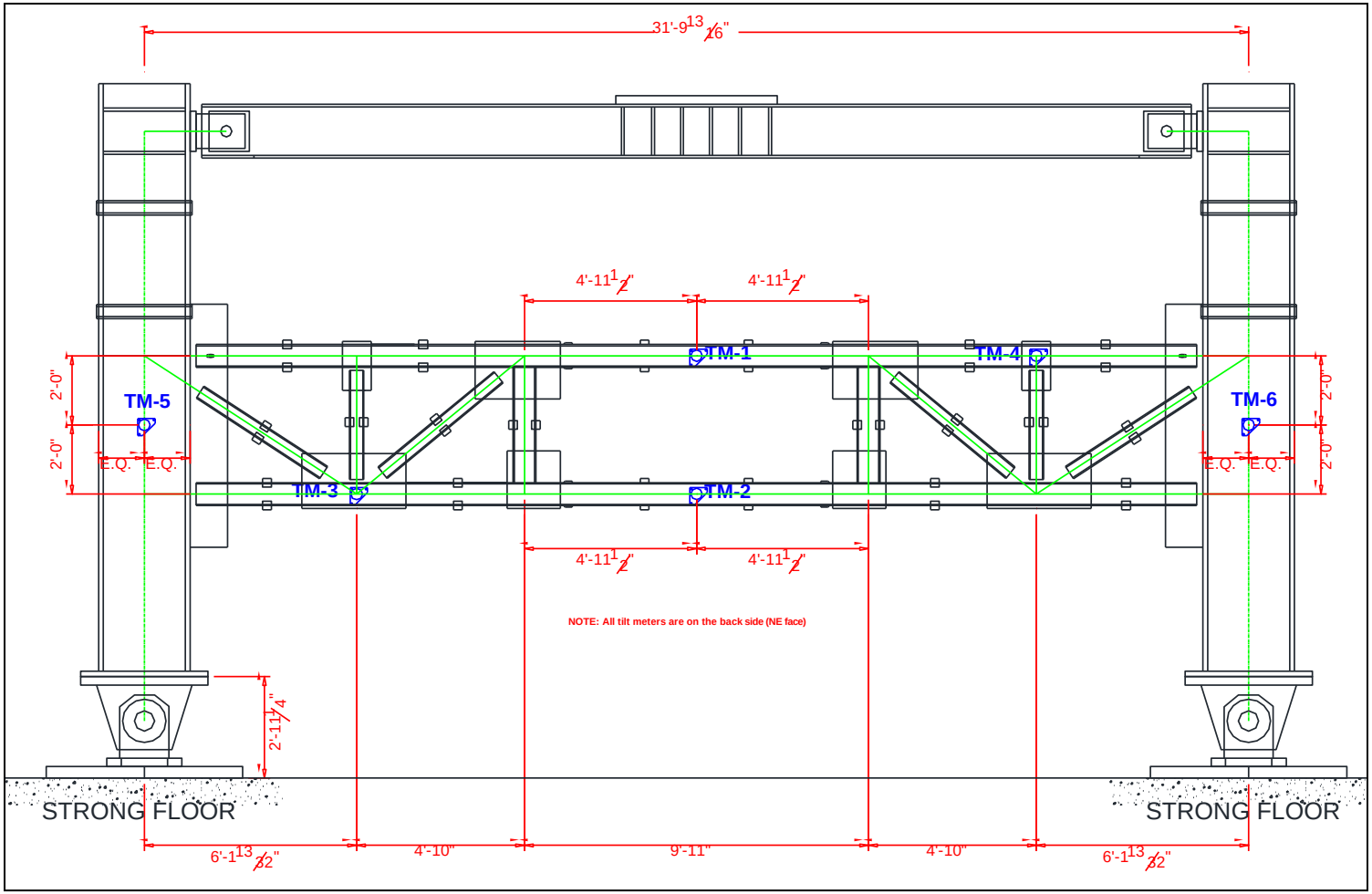

Tiltmeter Location

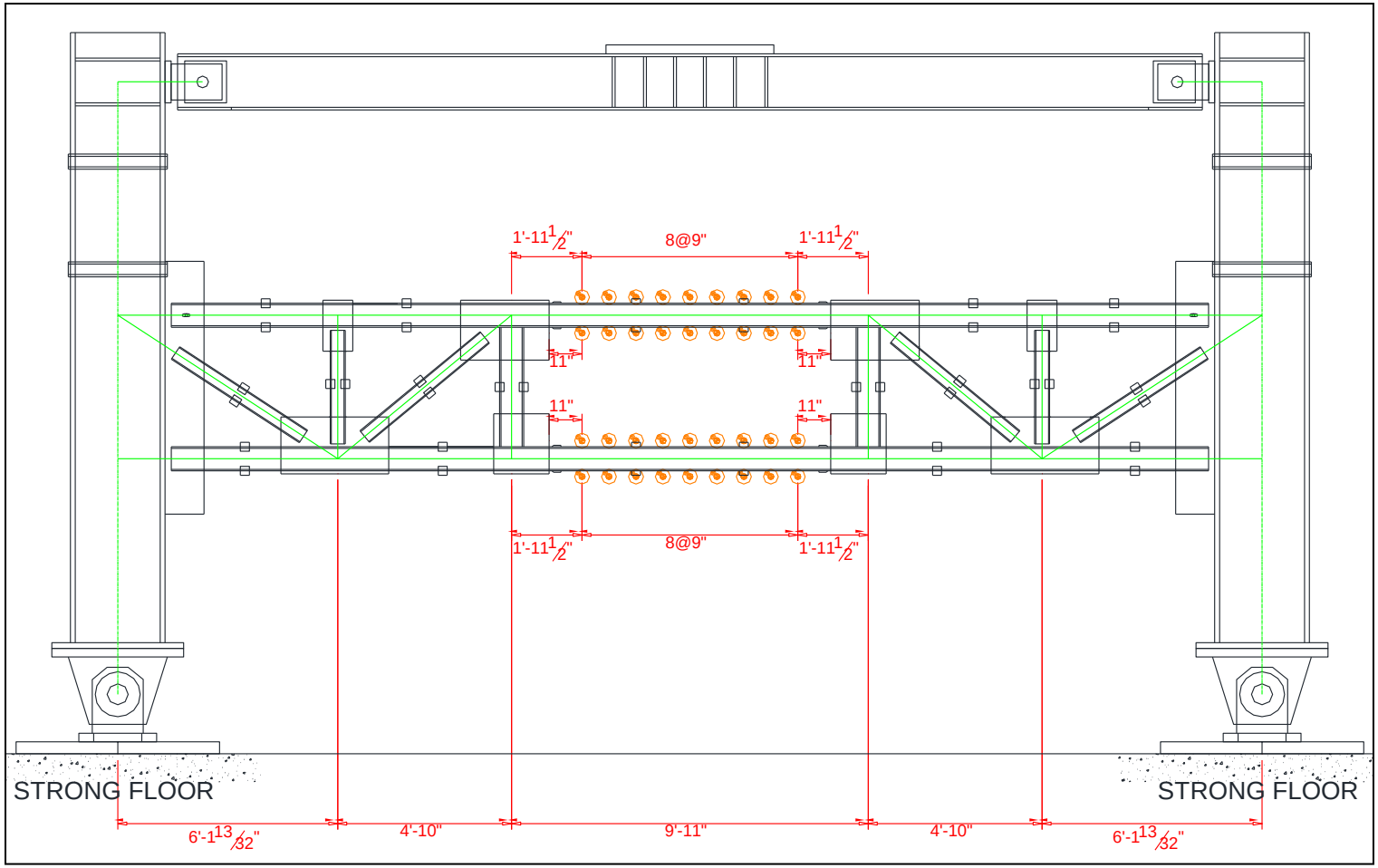

Krypton LED Sensor Location

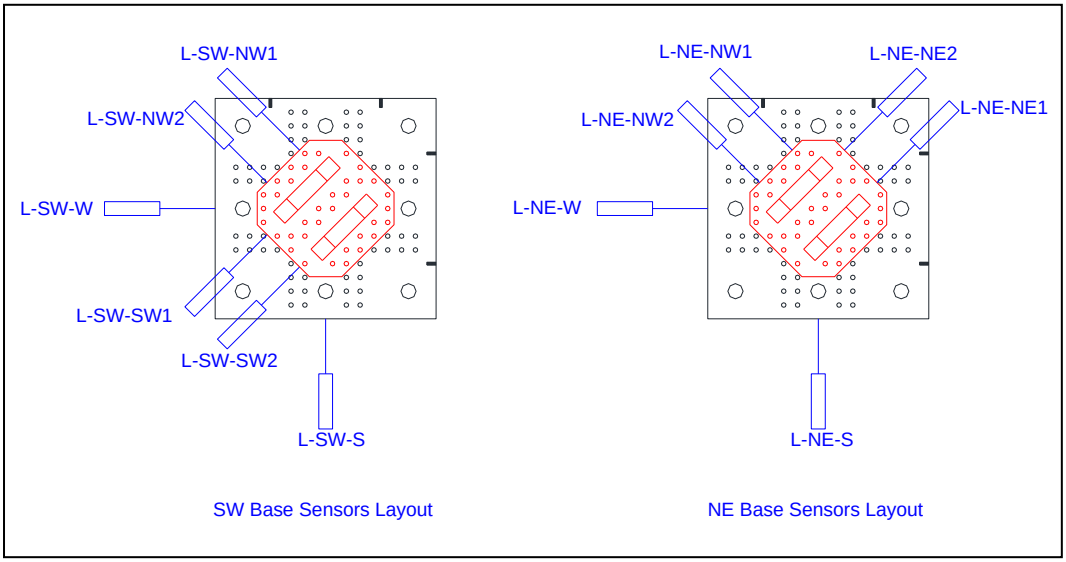

Displacement Sensors at Column Bases

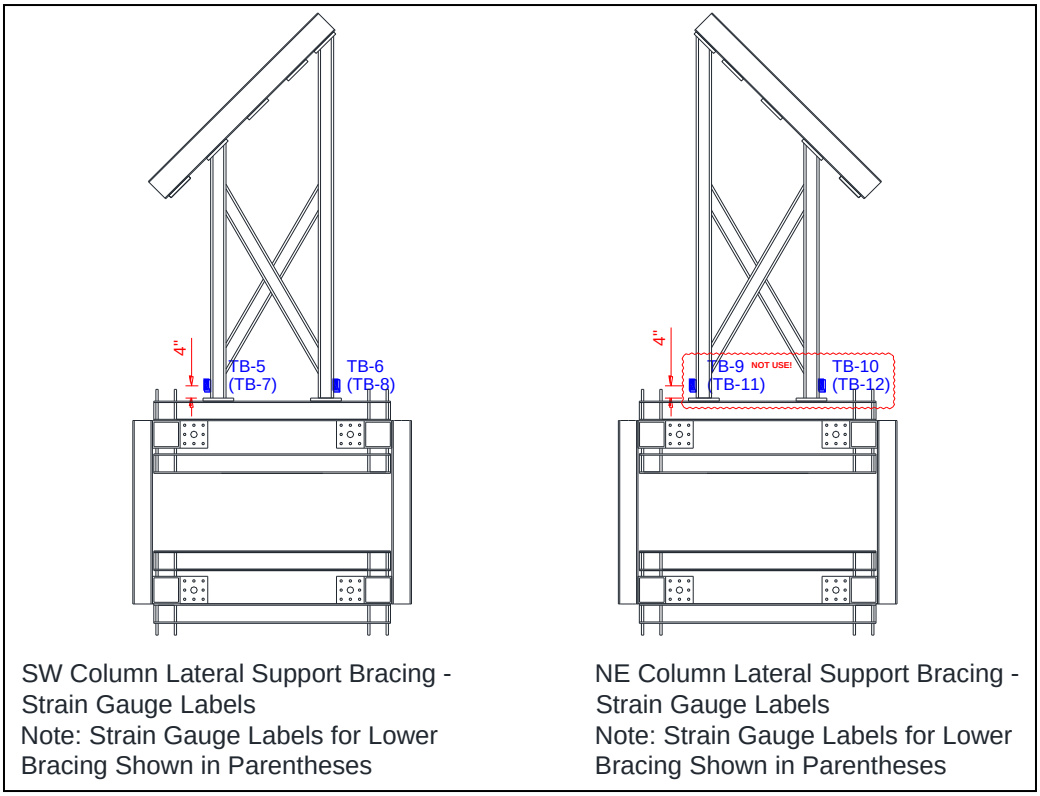

SW Column Lateral Support Bracing - Strain Gauge Labels
Note: Strain Gauge Labels for Lower Bracing Shown in Parentheses

NE Column Lateral Support Bracing - Strain Gauge Labels
Note: Strain Gauge Labels for Lower Bracing Shown in Parentheses

Column Braces

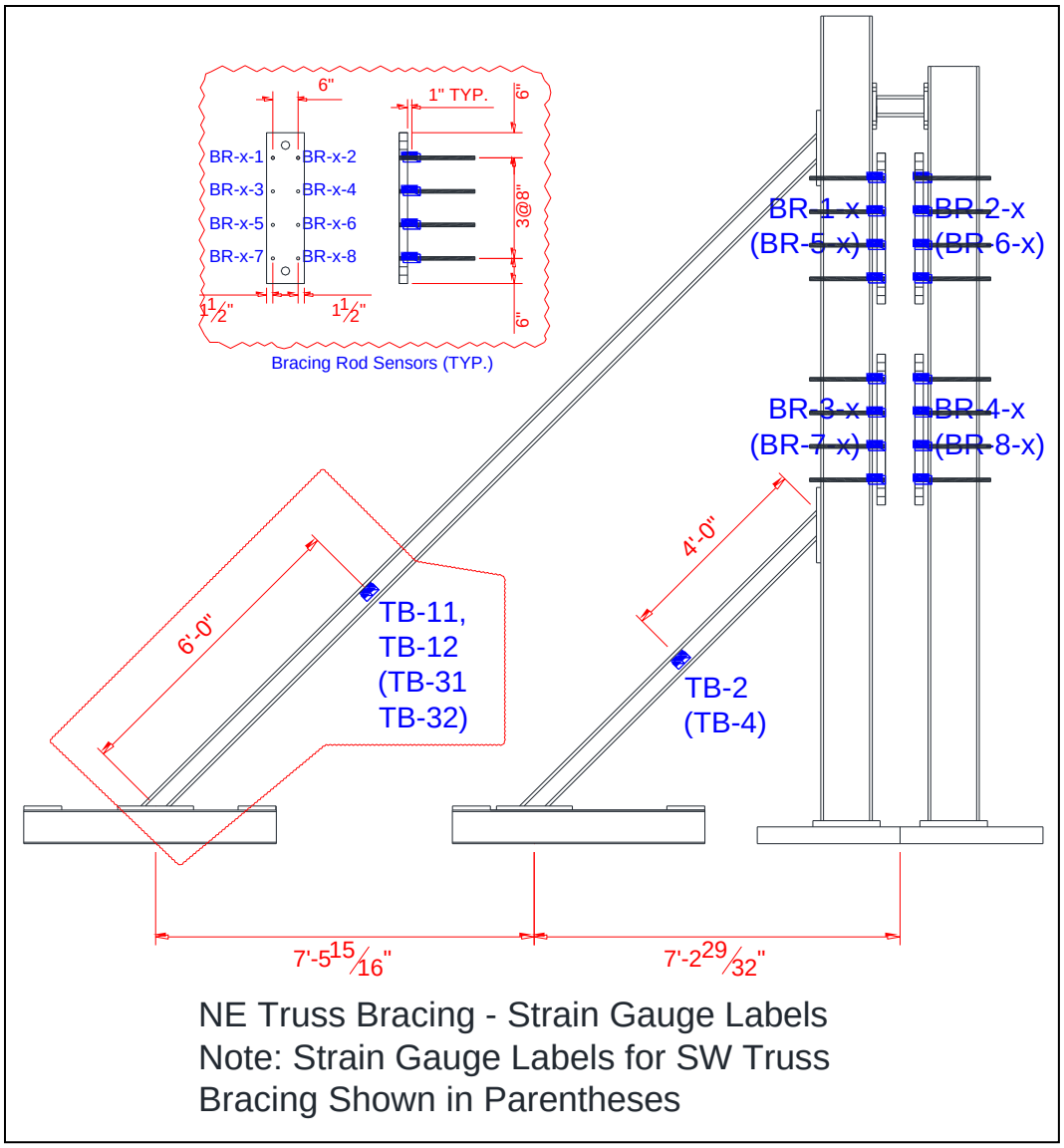

Truss Braces

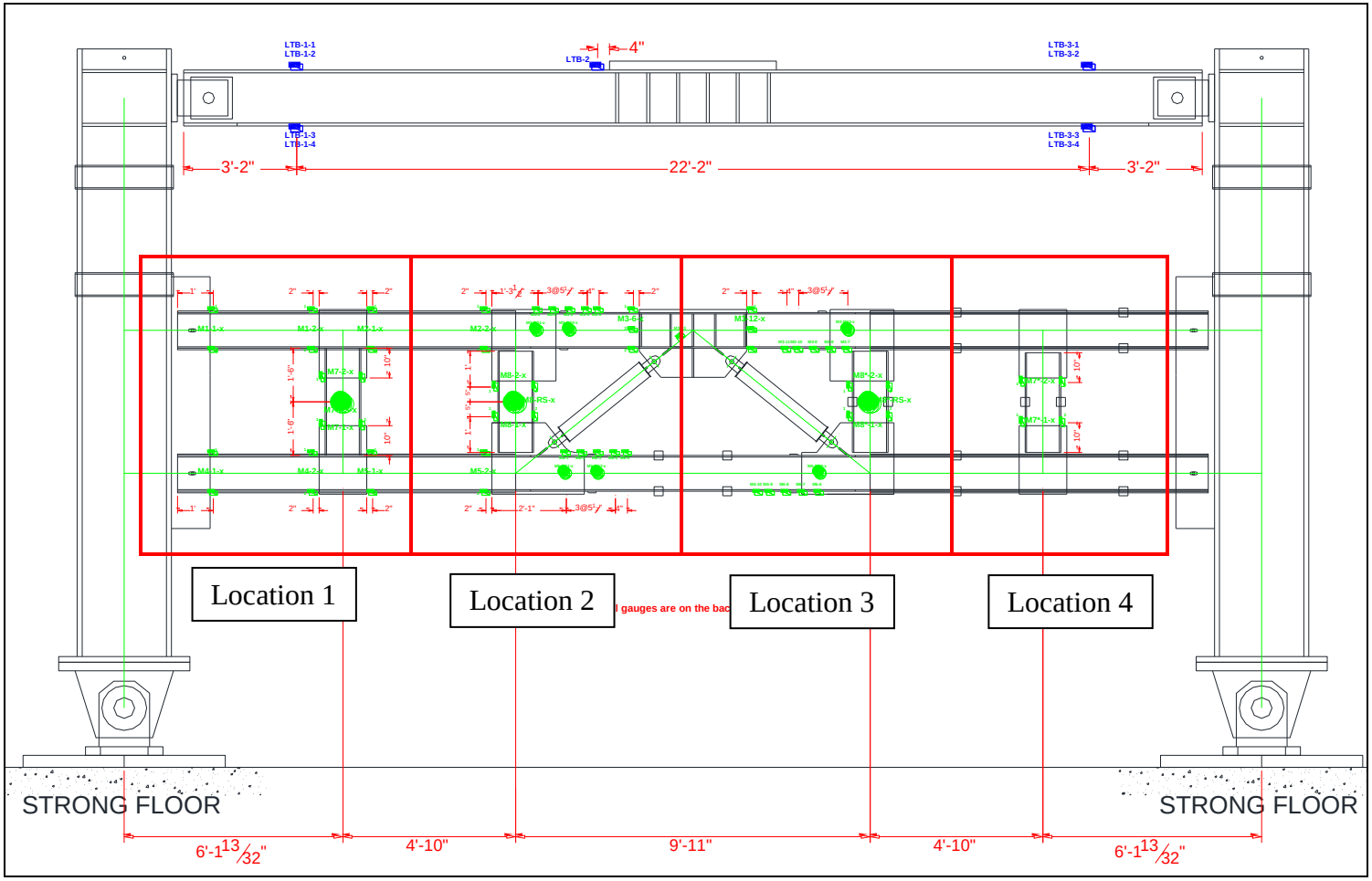

Strain Gauge Location

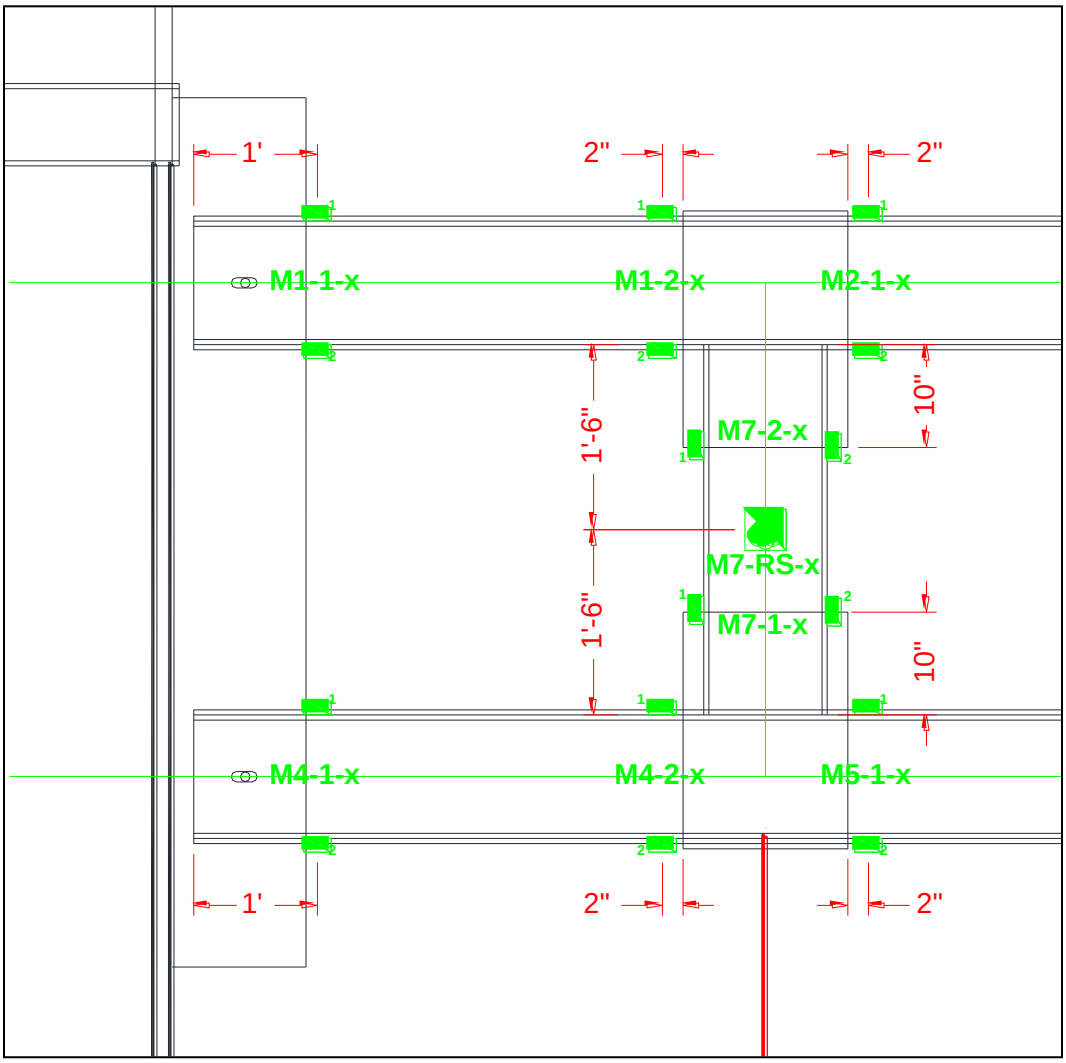
1'
2"
2"
M1-1-x
M1-2-x
M2-1-x
1'-6"
M7-2-x
10"
M7-RS-x
1'-6"
M7-1-x
10"
M4-1-x
M4-2-x
M5-1-x
1'
2"
2"

Location 1

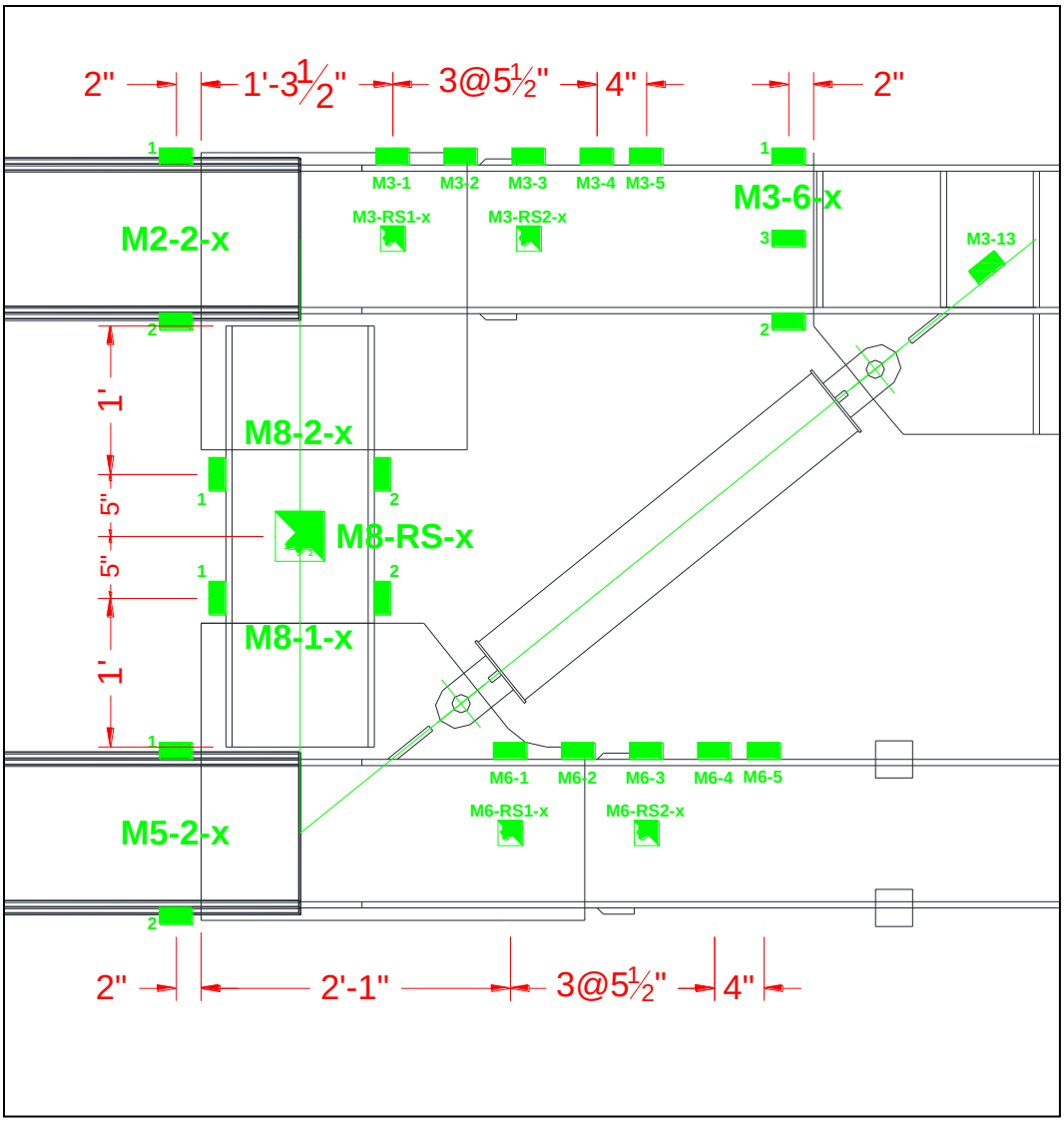
2"
1'-3½"
3@5½"
4"
2"
M3-1
M3-2
M3-3
M3-4
M3-5
M3-RS1-x
M3-RS2-x
M3-6-x
M3-13
M2-2-x
M8-2-x
M8-RS-x
M8-1-x
1'
5"
5"
1'
M6-1
M6-2
M6-3
M6-4
M6-5
M6-RS1-x
M6-RS2-x
M5-2-x
2"
2'-1"
3@5½"
4"

Location 2

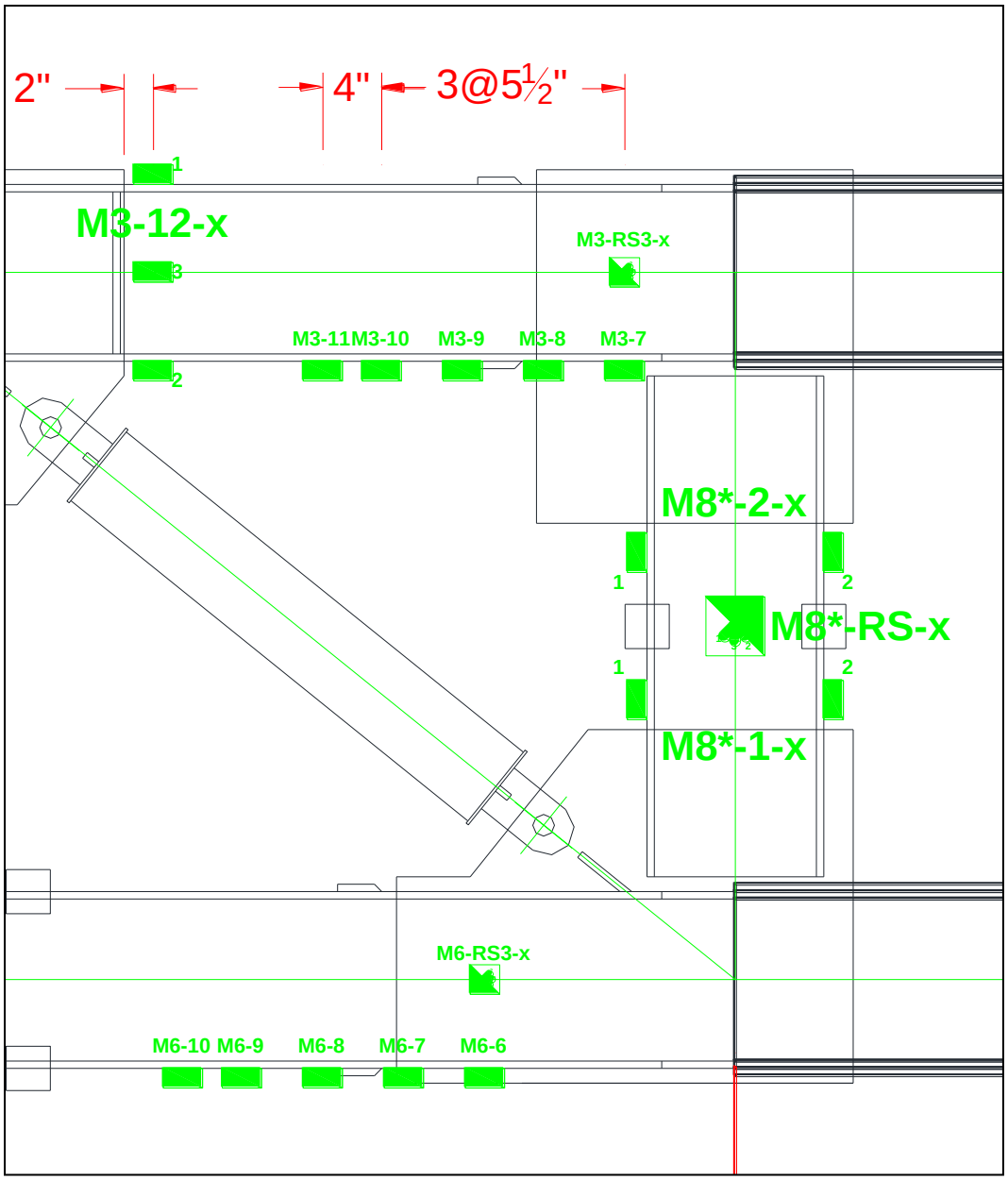
2"
4"
3@5½"
M3-12-x
M3-RS3-x
M3-11
M3-10
M3-9
M3-8
M3-7
M8*-2-x
M8*-RS-x
M8*-1-x
M6-RS3-x
M6-10
M6-9
M6-8
M6-7
M6-6

Location 3

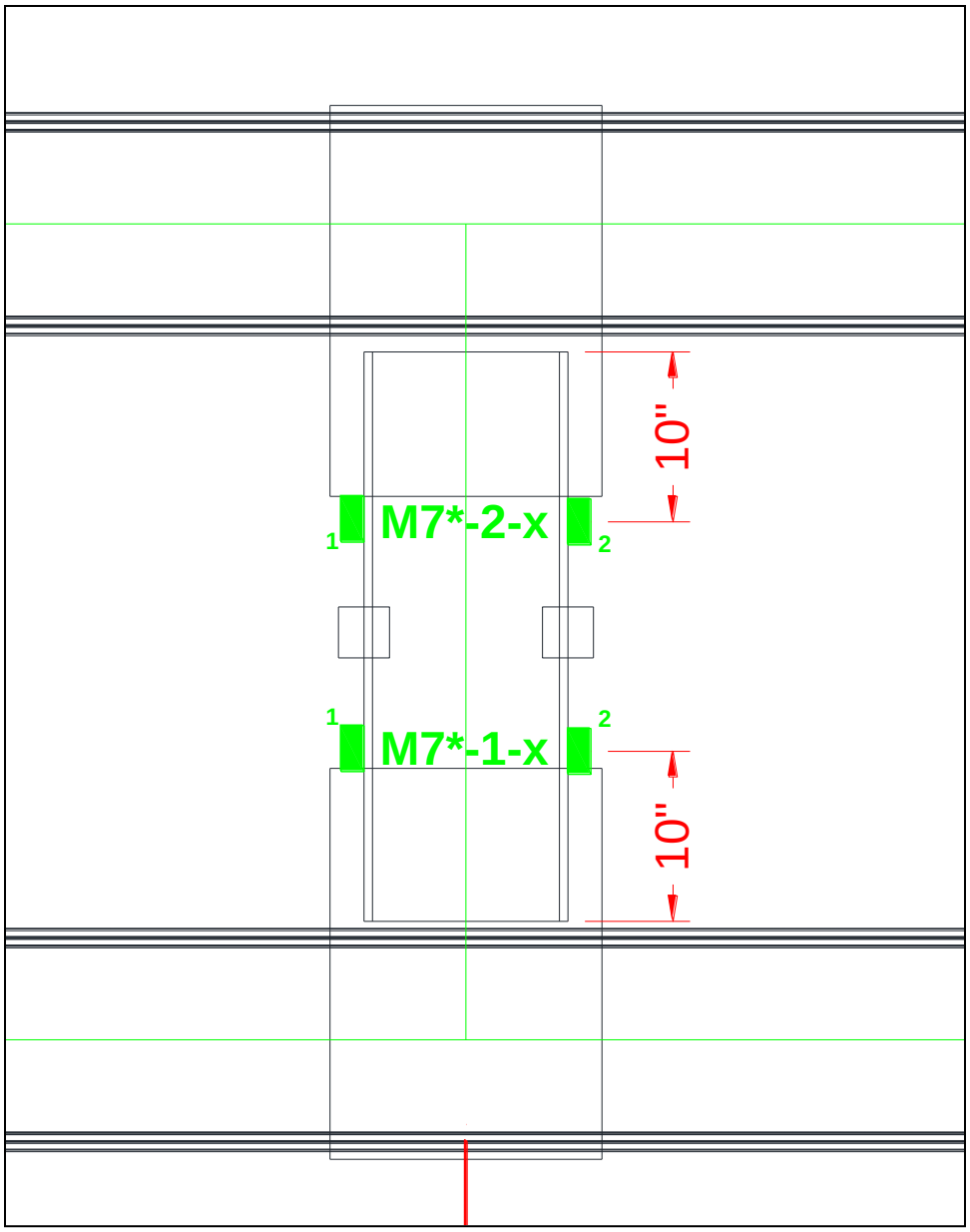

Location 4

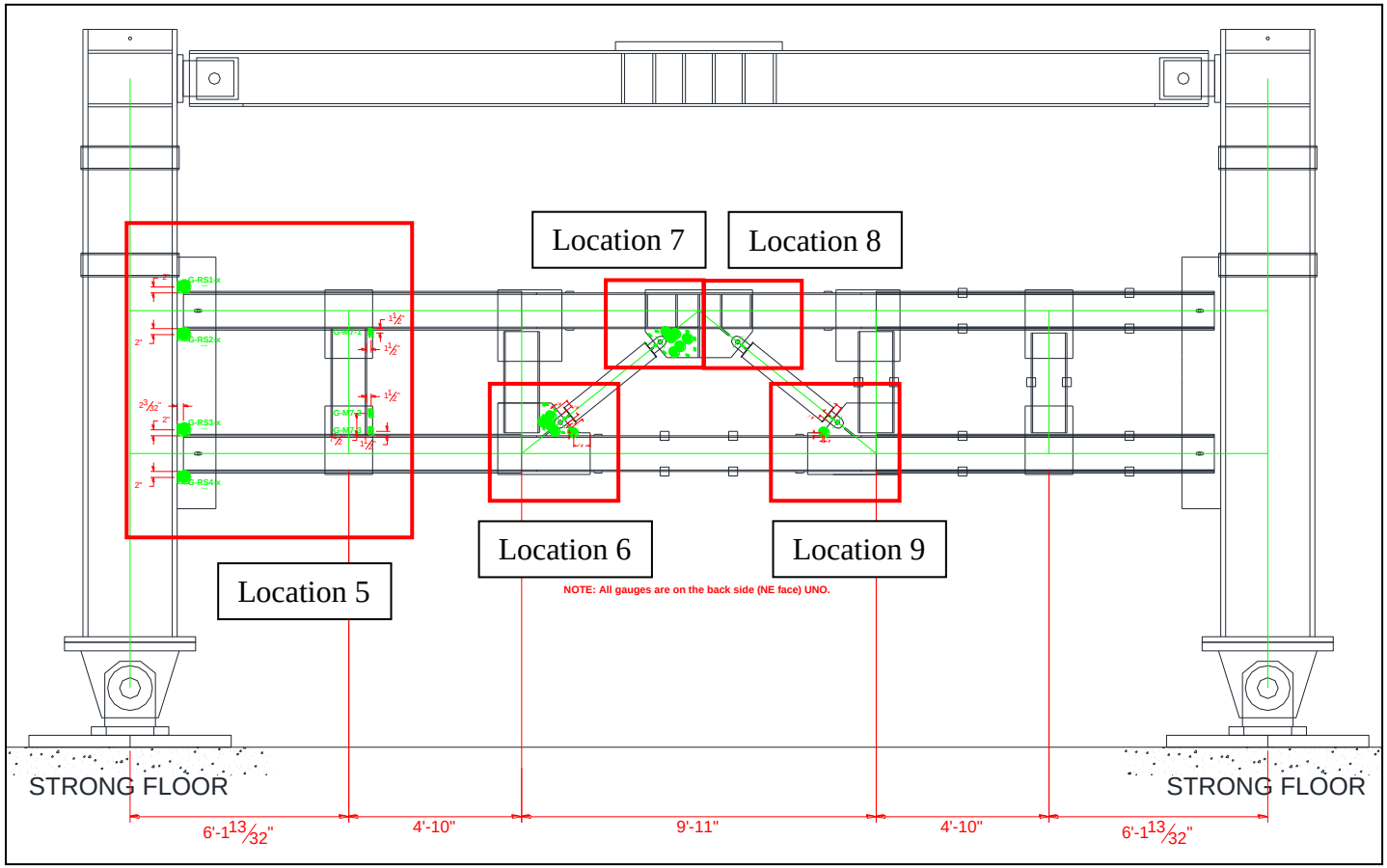

Gusset Plate and BRBs Strain Gauge Location

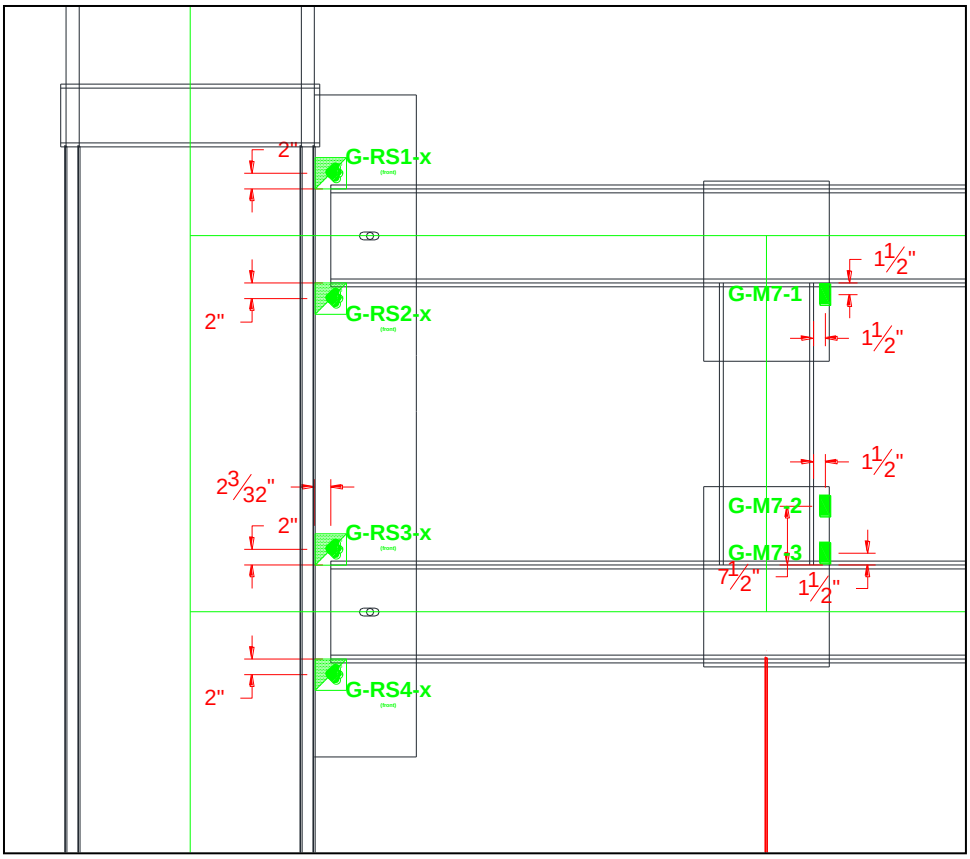
2"
G-RS1-x
(front)
2"
G-RS2-x
(front)
2 3/32"
2"
G-RS3-x
(front)
2"
G-RS4-x
(front)
1 1/2"
G-M7-1
1 1/2"
1 1/2"
G-M7-2
G-M7-3
7 1/2"
1 1/2"

Location 5

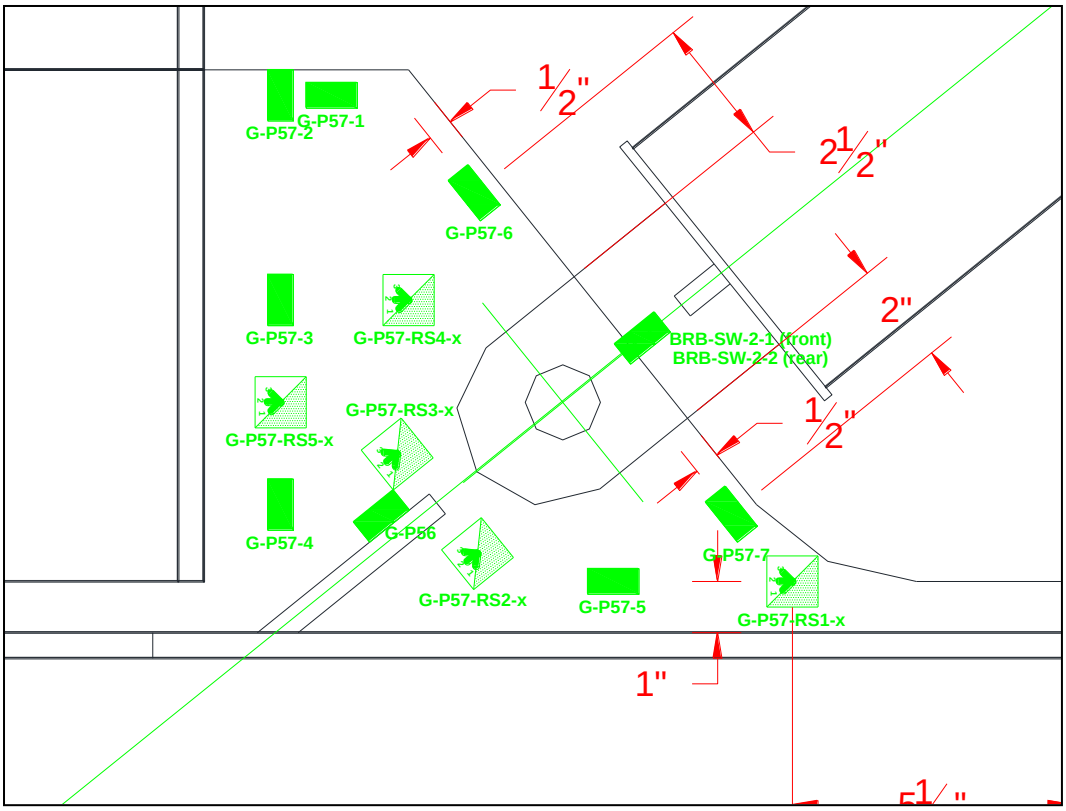

Location 6

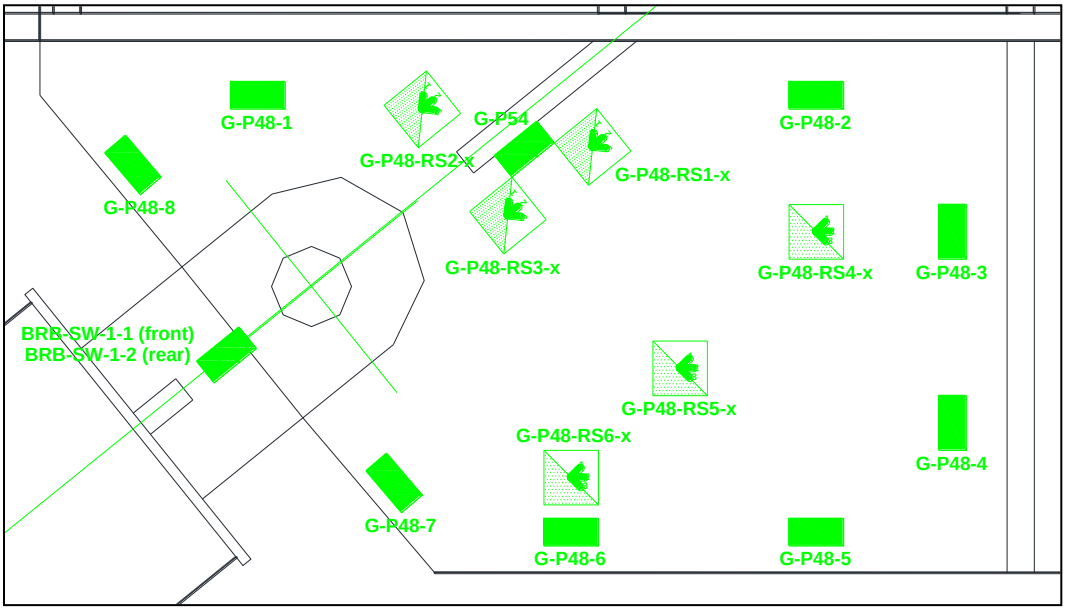

Location 7

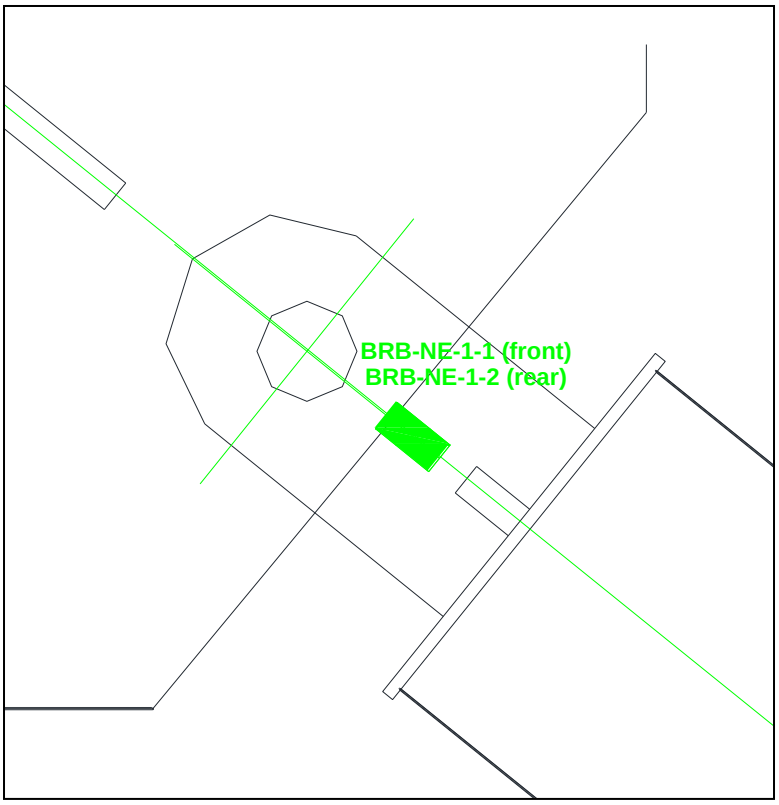

Location 8

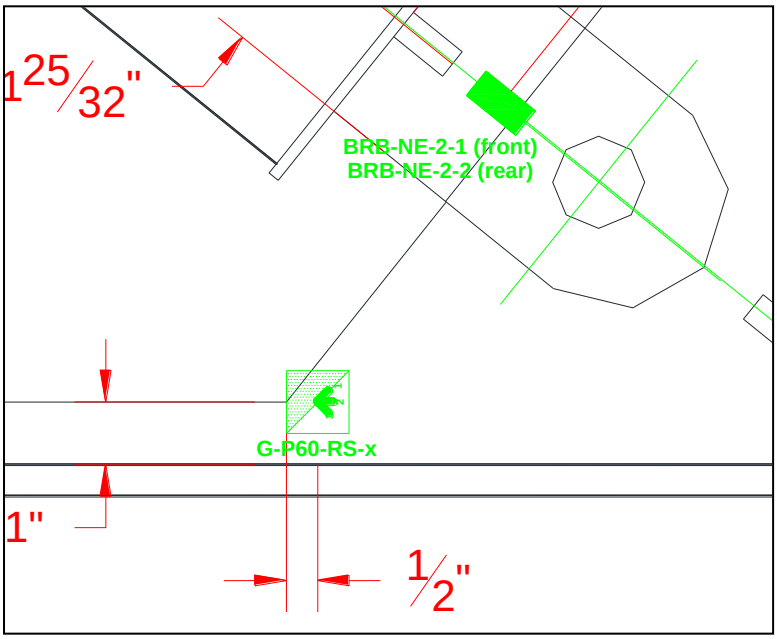

Location 9

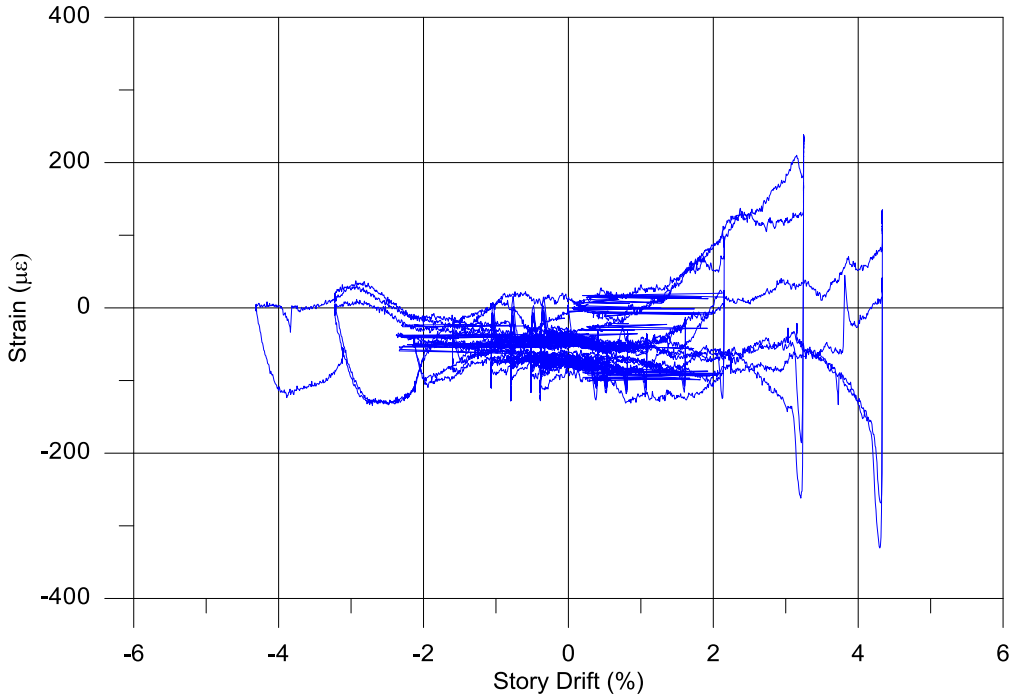
400
200
0
-200
-400
Strain (με)
-6
-4
-2
0
2
4
6
Story Drift (%)

BR-1-2

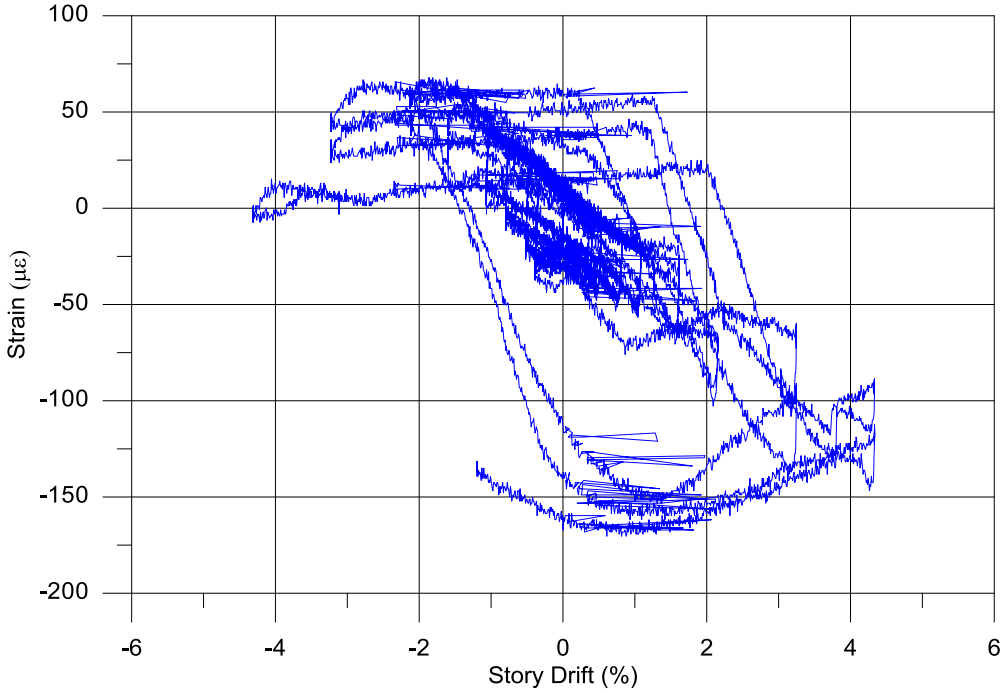
100
50
0
-50
-100
-150
-200
Strain (με)
-6
-4
-2
0
2
4
6
Story Drift (%)

BR-1-4

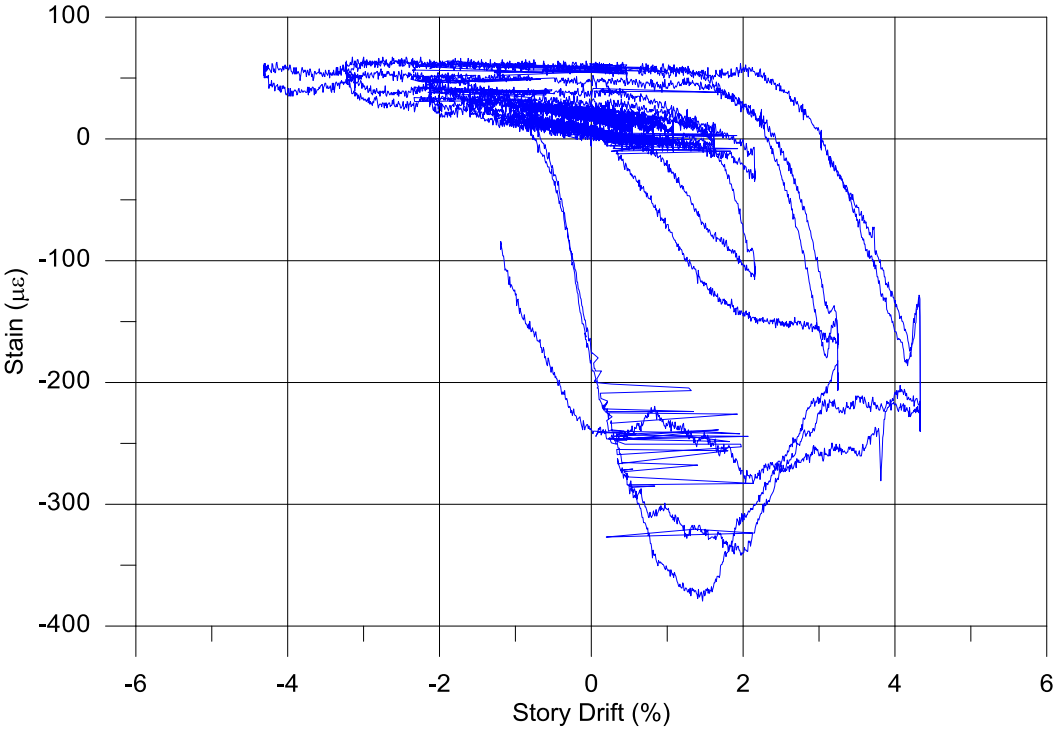
100
0
-100
-200
-300
-400
Stain (με)
-6
-4
-2
0
2
4
6
Story Drift (%)

BR-1-5

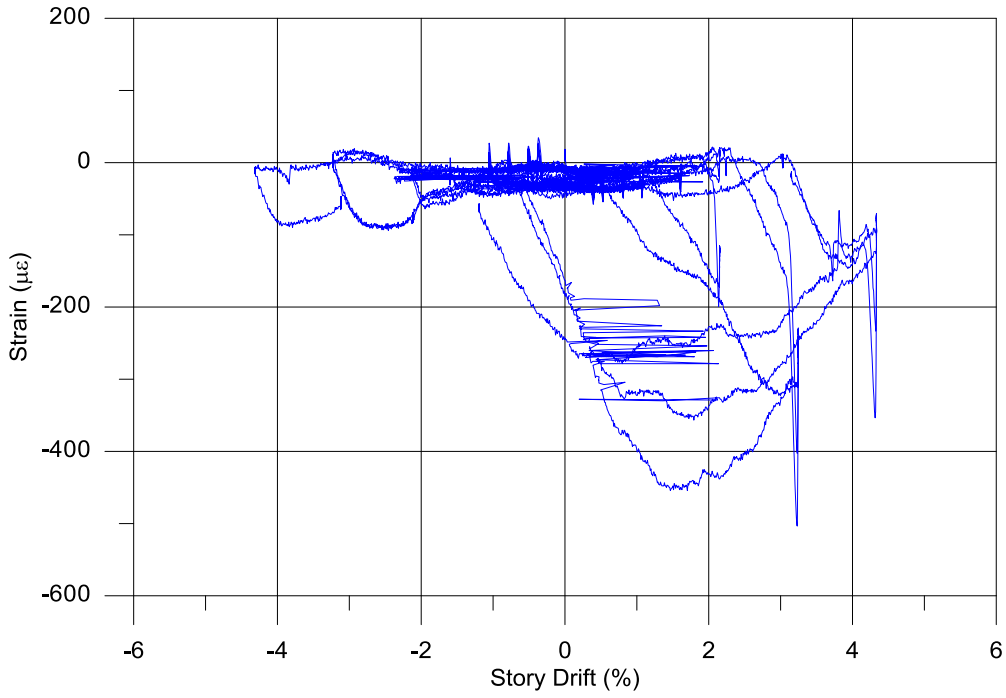
200
0
-200
-400
-600
Strain (με)
-6
-4
-2
0
2
4
6
Story Drift (%)

BR-1-6

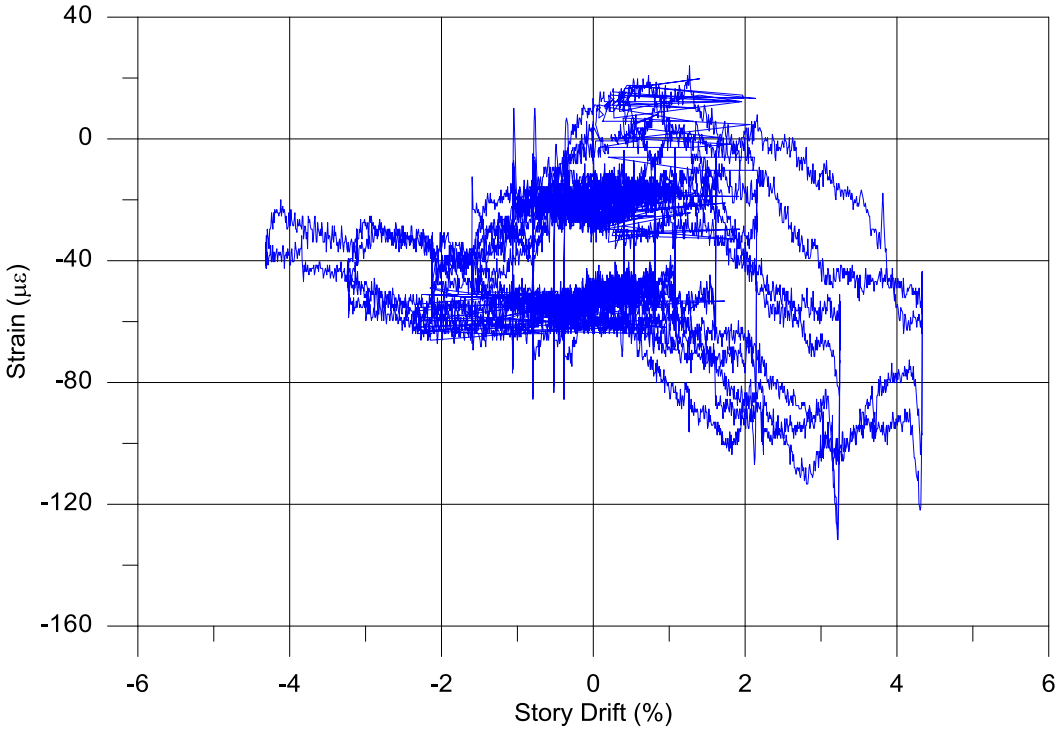
40
0
-40
-80
-120
-160
Strain (με)
-6
-4
-2
0
2
4
6
Story Drift (%)

BR-1-7

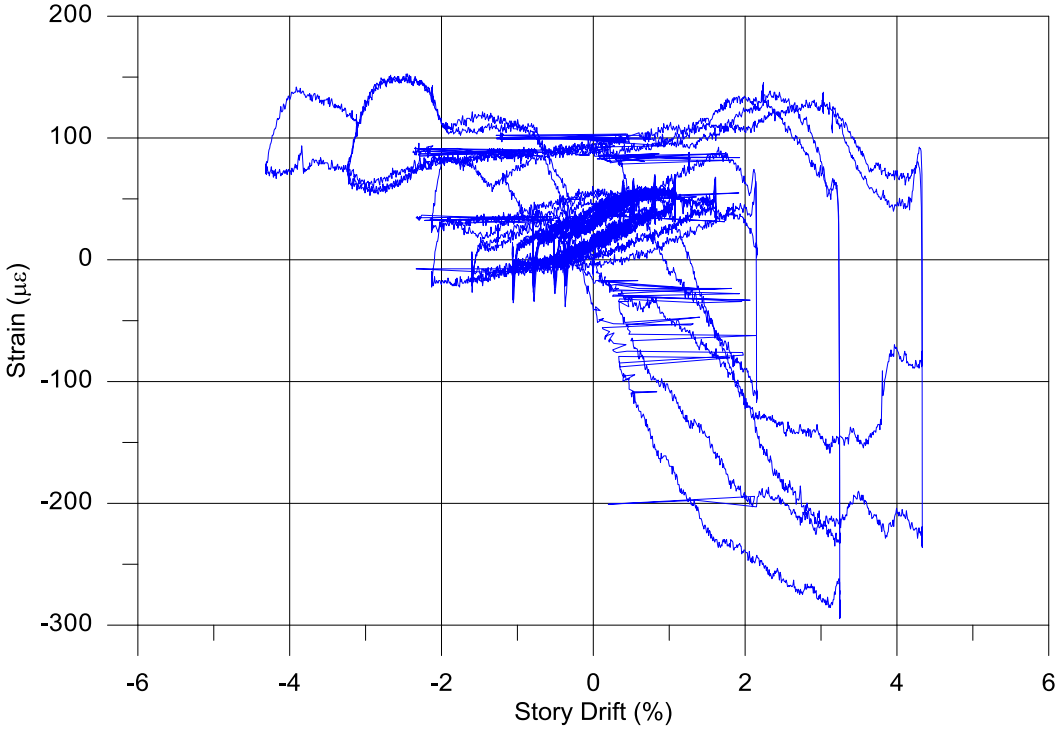
200
100
0
-100
-200
-300
Strain (με)
-6
-4
-2
0
2
4
6
Story Drift (%)

BR-1-8

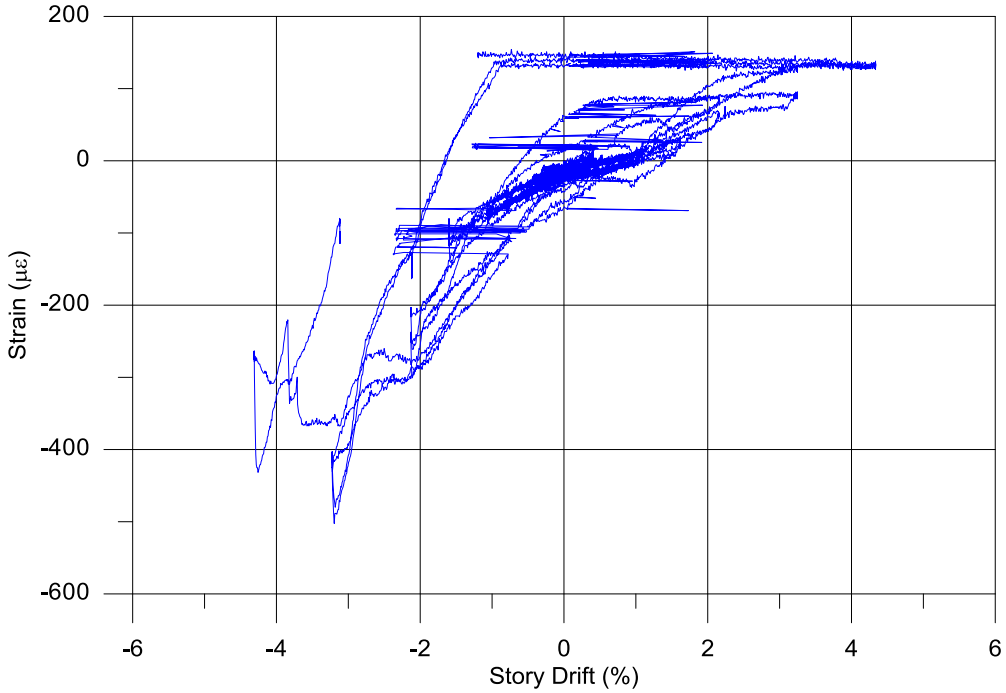
200
0
-200
-400
-600
Strain (με)
-6
-4
-2
0
2
4
6
Story Drift (%)

BR-2-1

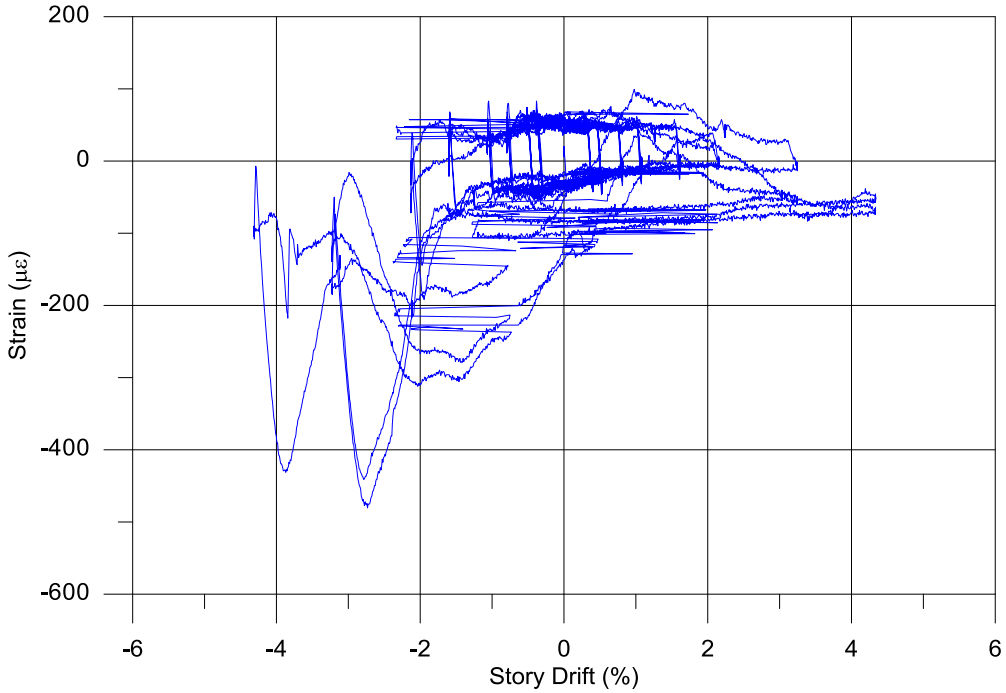
200
0
-200
-400
-600
Strain (με)
-6
-4
-2
0
2
4
6
Story Drift (%)

BR-2-2

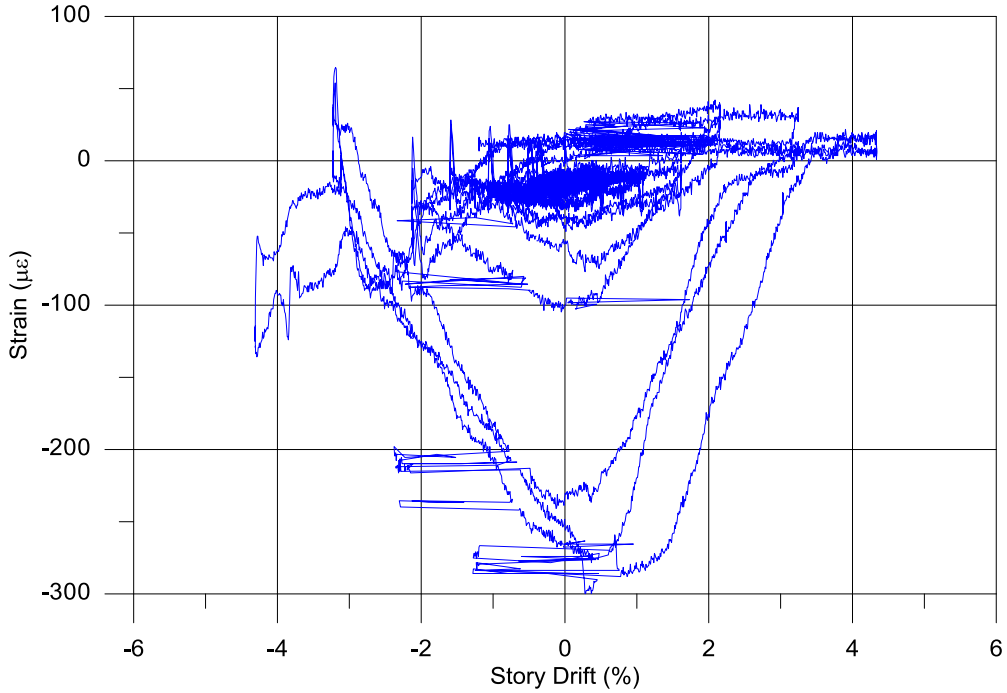
100
0
-100
-200
-300
Strain (με)
-6
-4
-2
0
2
4
6
Story Drift (%)

BR-2-3

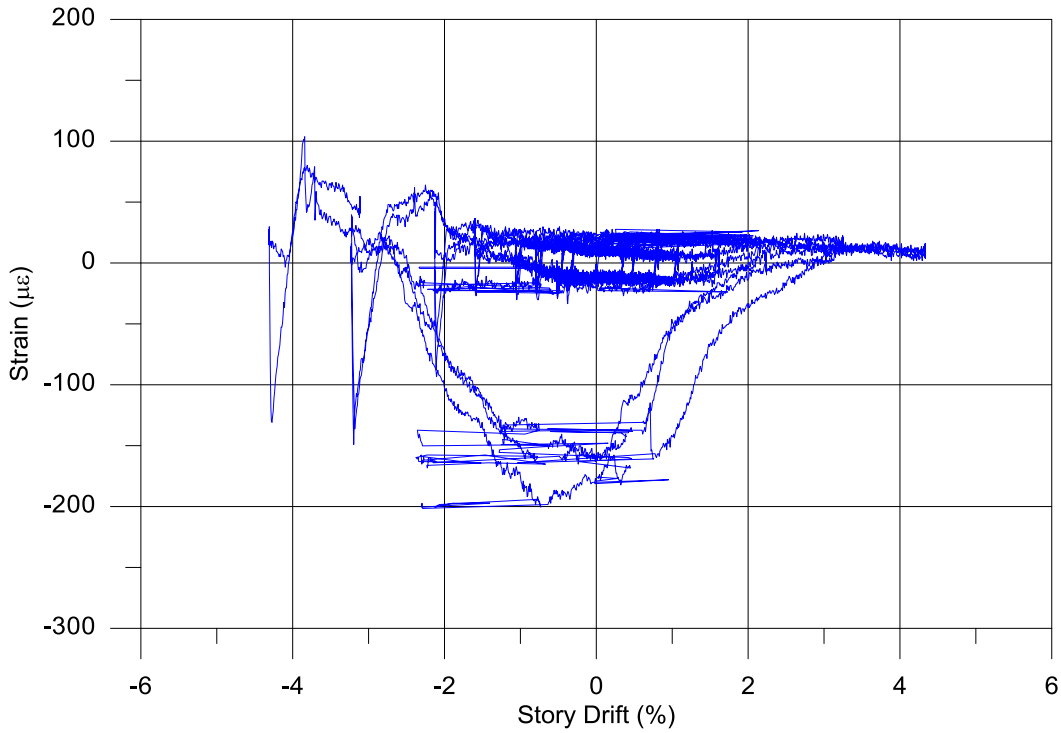
200
100
0
-100
-200
-300
Strain (με)
-6
-4
-2
0
2
4
6
Story Drift (%)

BR-2-4

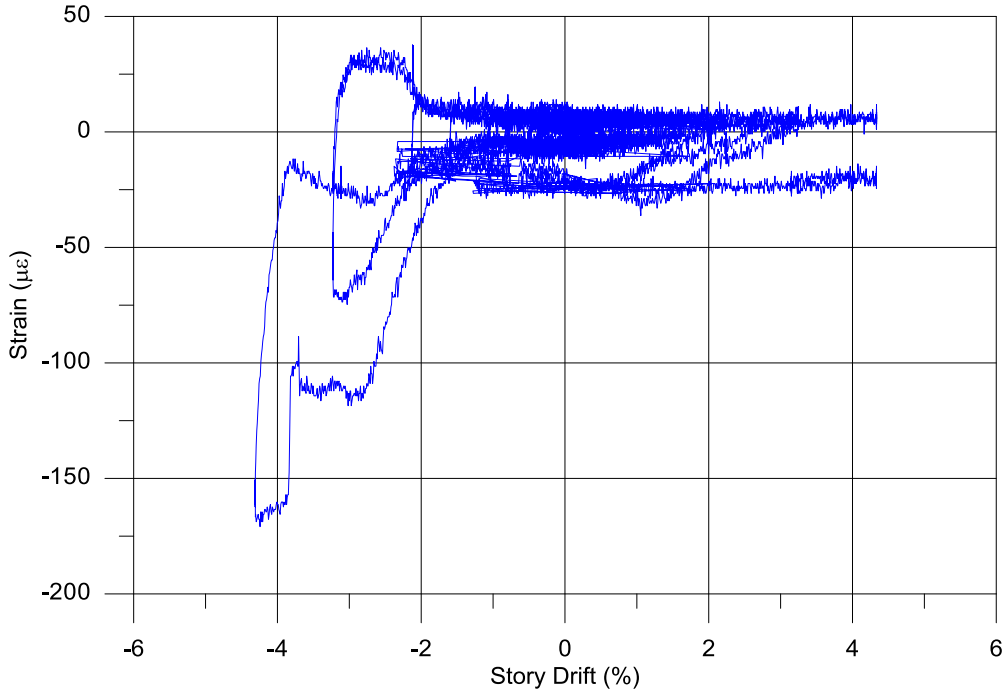
50
0
-50
-100
-150
-200
Strain (με)
-6
-4
-2
0
2
4
6
Story Drift (%)

BR-2-5

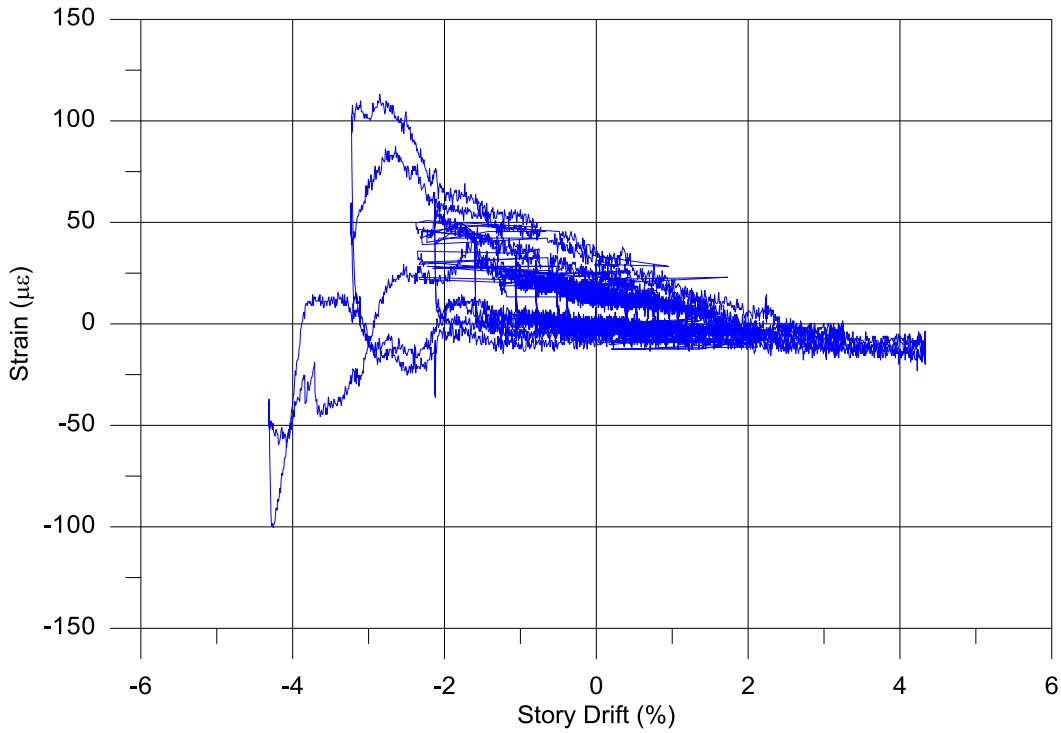
150
100
50
0
-50
-100
-150
Strain (με)
-6
-4
-2
0
2
4
6
Story Drift (%)

BR-2-6

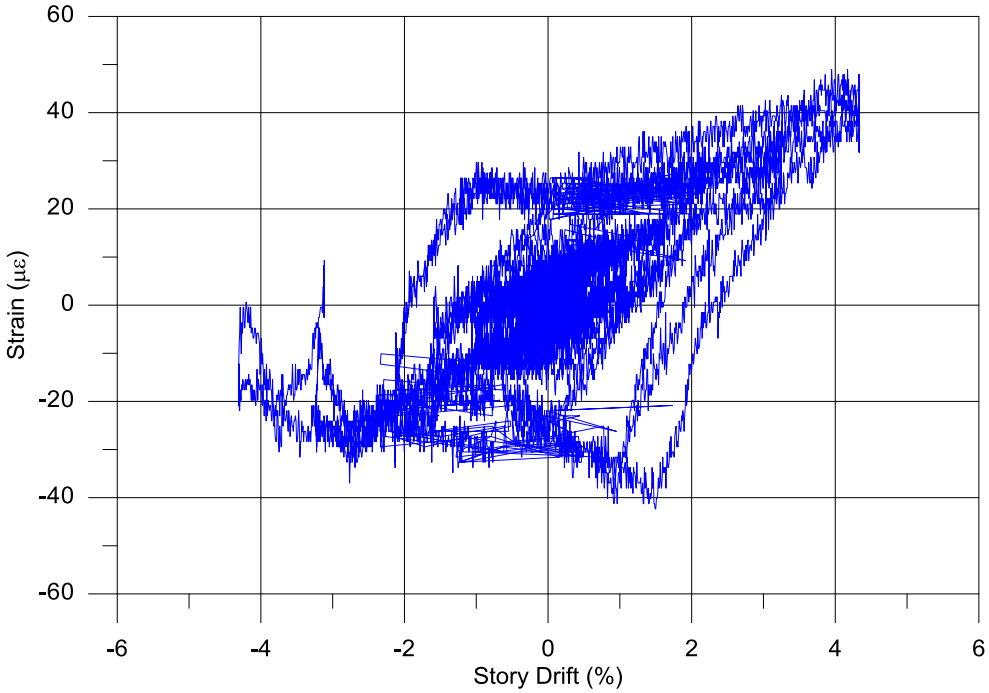
60
40
20
0
-20
-40
-60
Strain (με)
-6
-4
-2
0
2
4
6
Story Drift (%)

BR-2-7

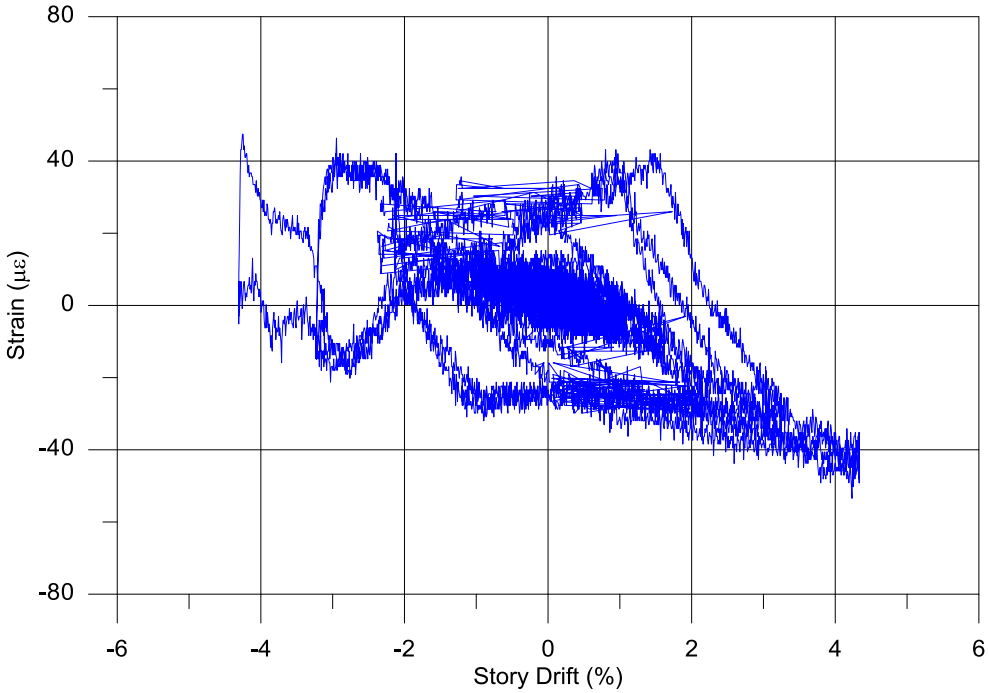
80
40
0
-40
-80
Strain (με)
-6
-4
-2
0
2
4
6
Story Drift (%)

BR-2-8

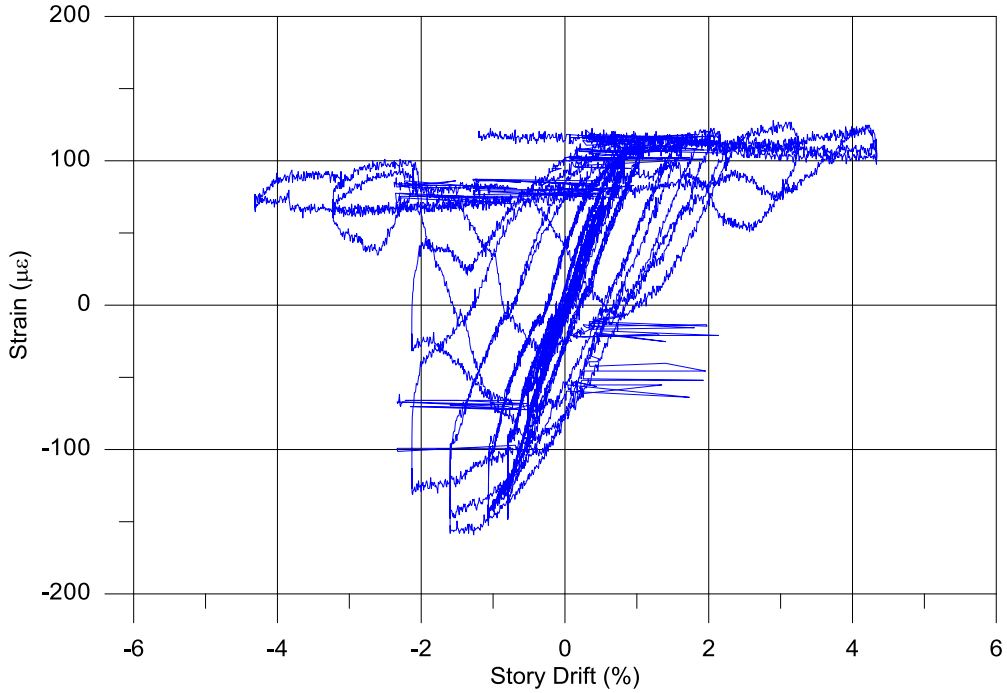
200
100
0
-100
-200
Strain (με)
-6
-4
-2
0
2
4
6
Story Drift (%)

BR-3-1

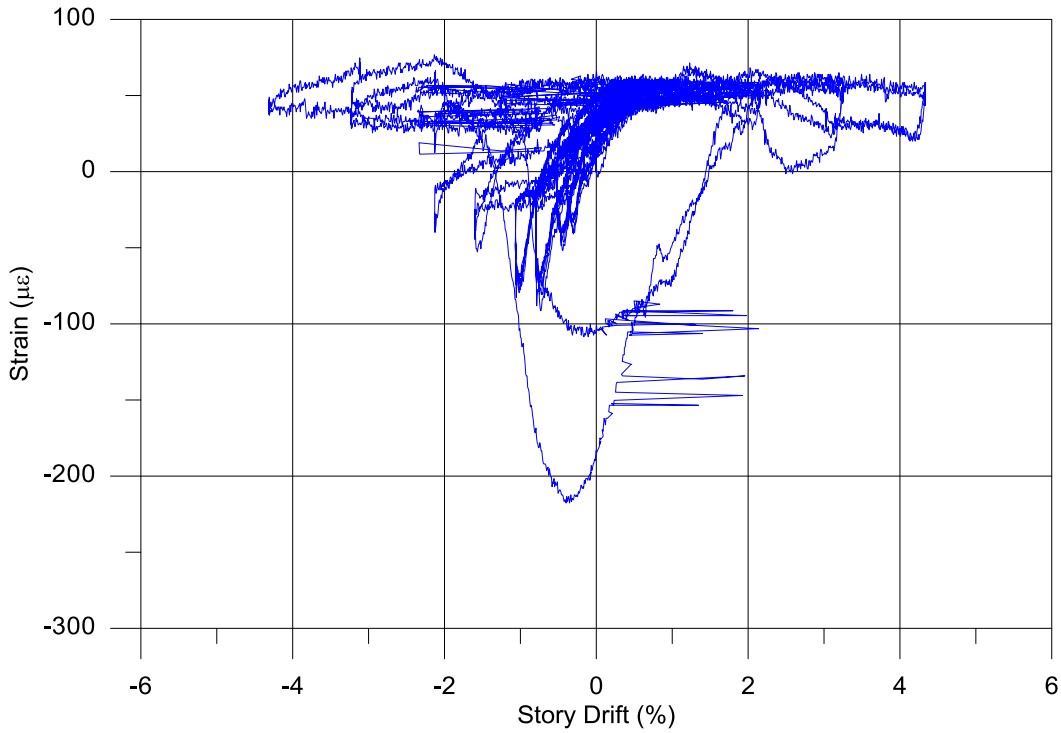
100
0
-100
-200
-300
Strain (με)
-6
-4
-2
0
2
4
6
Story Drift (%)

BR-3-2

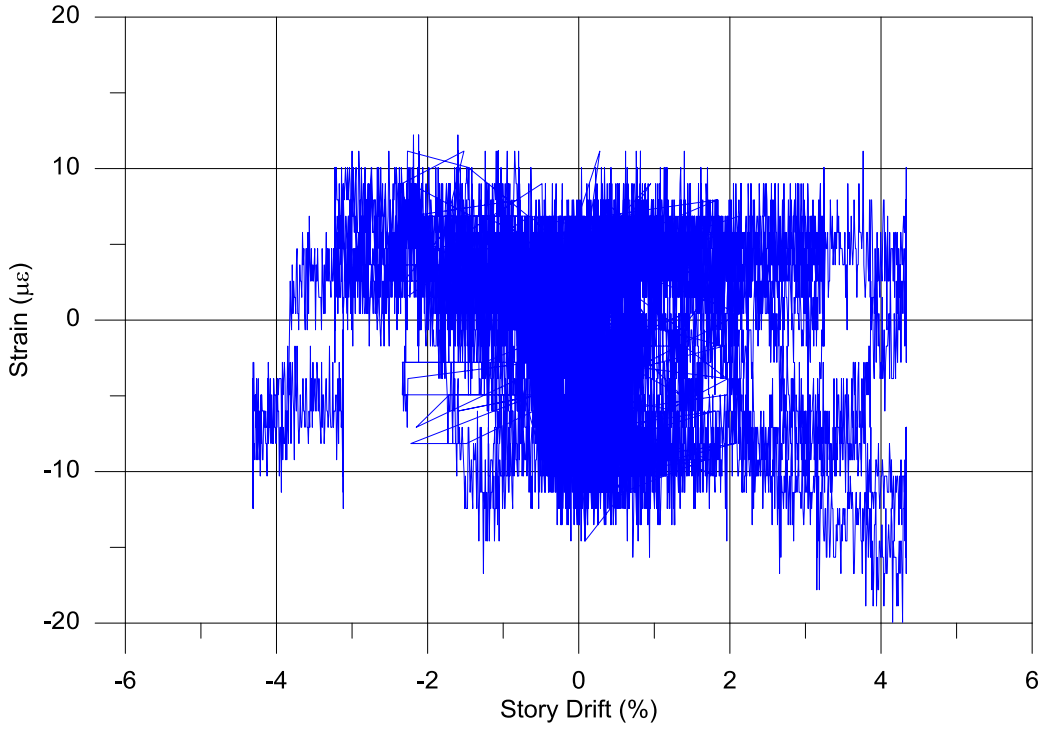
20
10
0
-10
-20
Strain (με)
-6
-4
-2
0
2
4
6
Story Drift (%)

BR-3-3

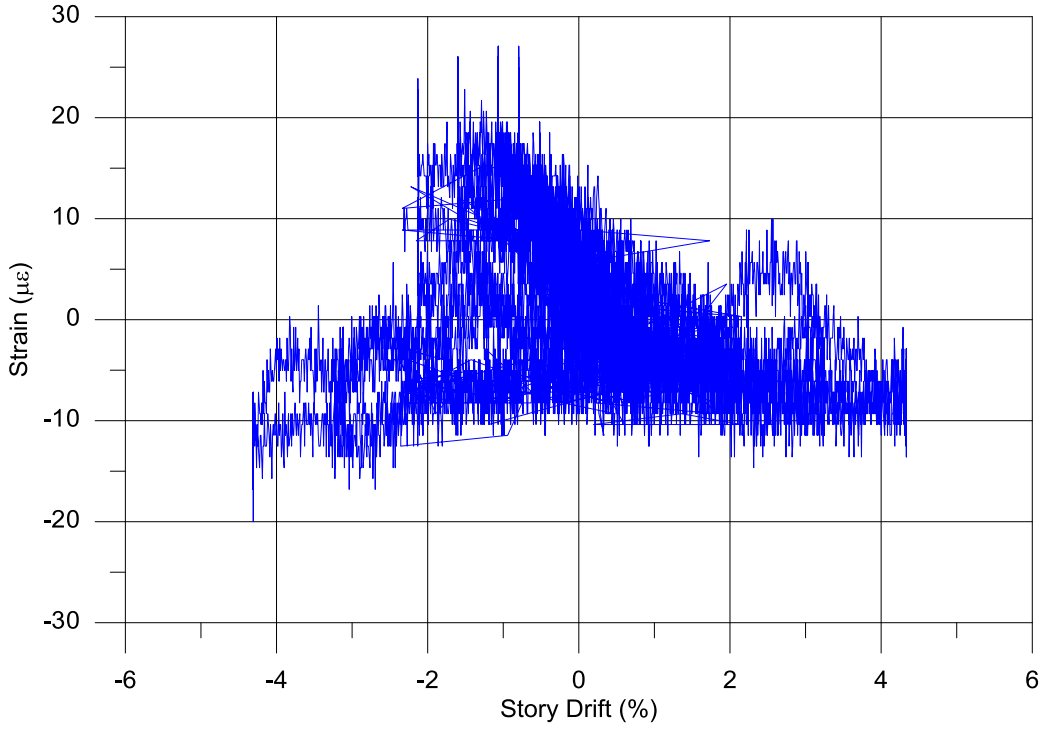
30
20
10
0
-10
-20
-30
Strain (με)
-6
-4
-2
0
2
4
6
Story Drift (%)

BR-3-4

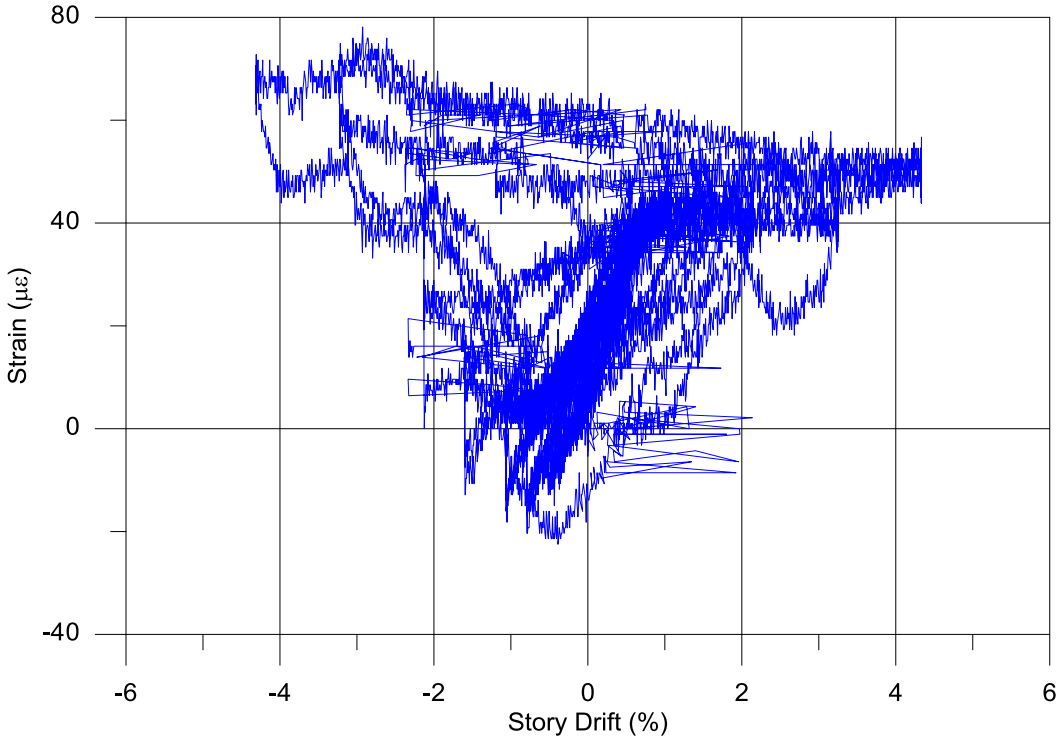
80
40
0
-40
Strain (με)
-6
-4
-2
0
2
4
6
Story Drift (%)

BR-3-5

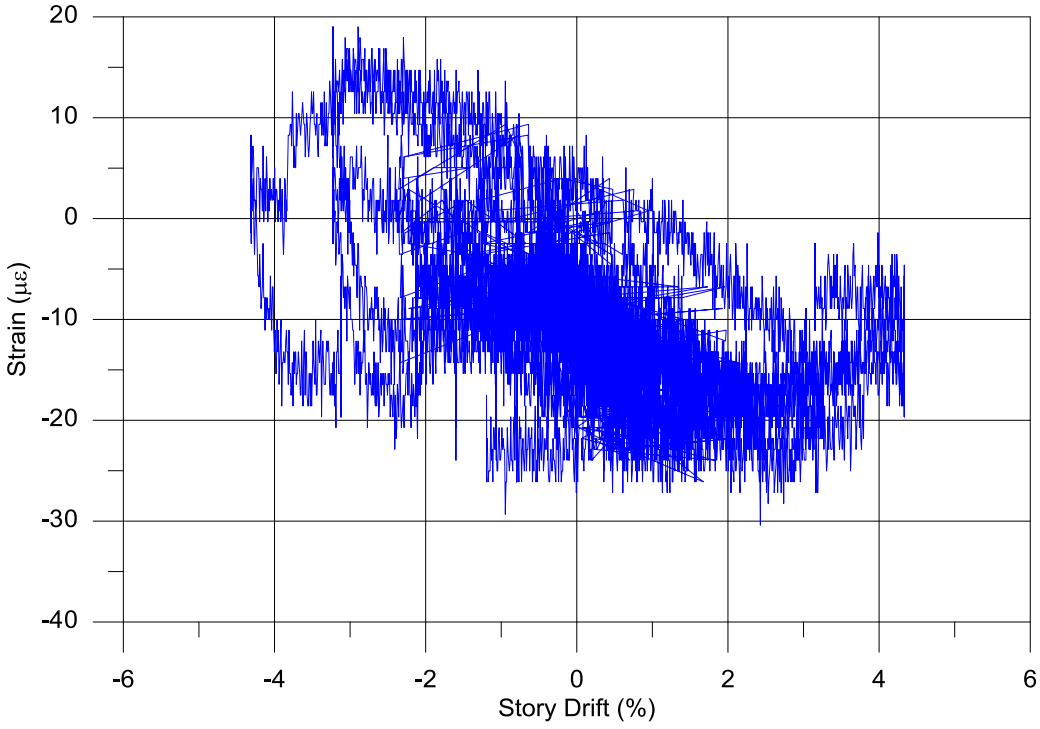
20
10
0
-10
-20
-30
-40
Strain (με)
-6
-4
-2
0
2
4
6
Story Drift (%)

BR-3-6

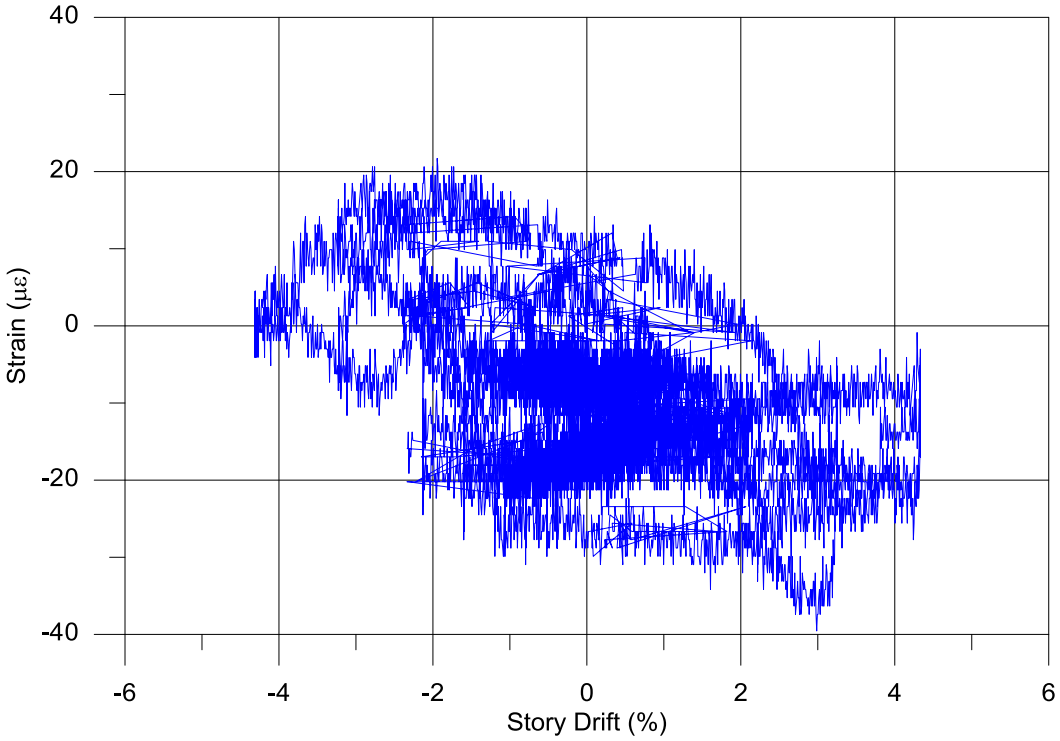
40
20
0
-20
-40
Strain (με)
-6
-4
-2
0
2
4
6
Story Drift (%)

BR-3-7

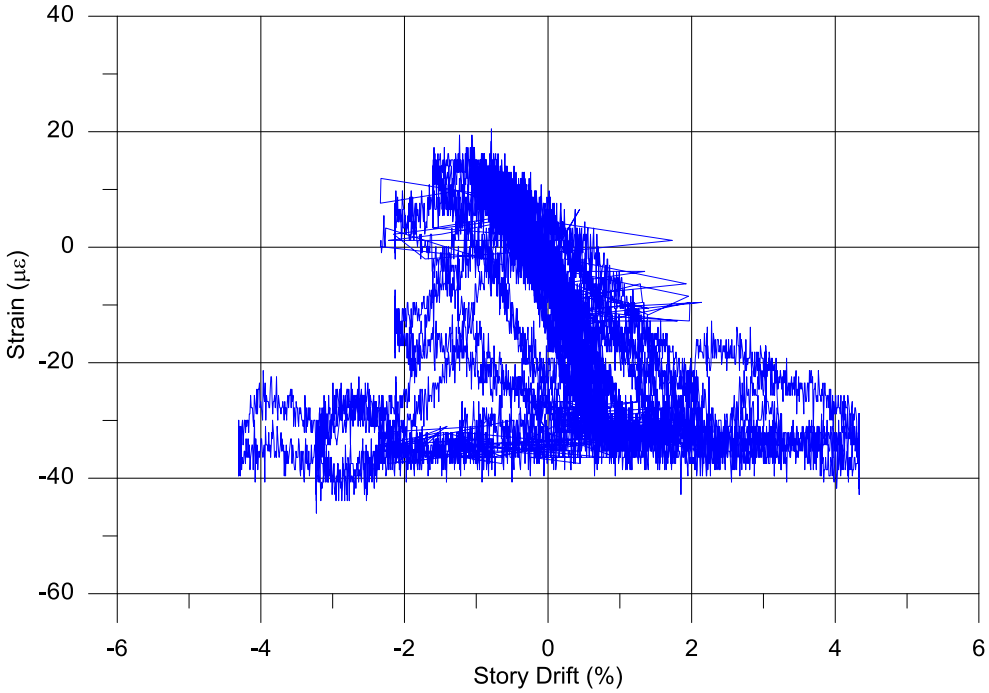
40
20
0
-20
-40
-60
Strain (με)
-6
-4
-2
0
2
4
6
Story Drift (%)

BR-3-8

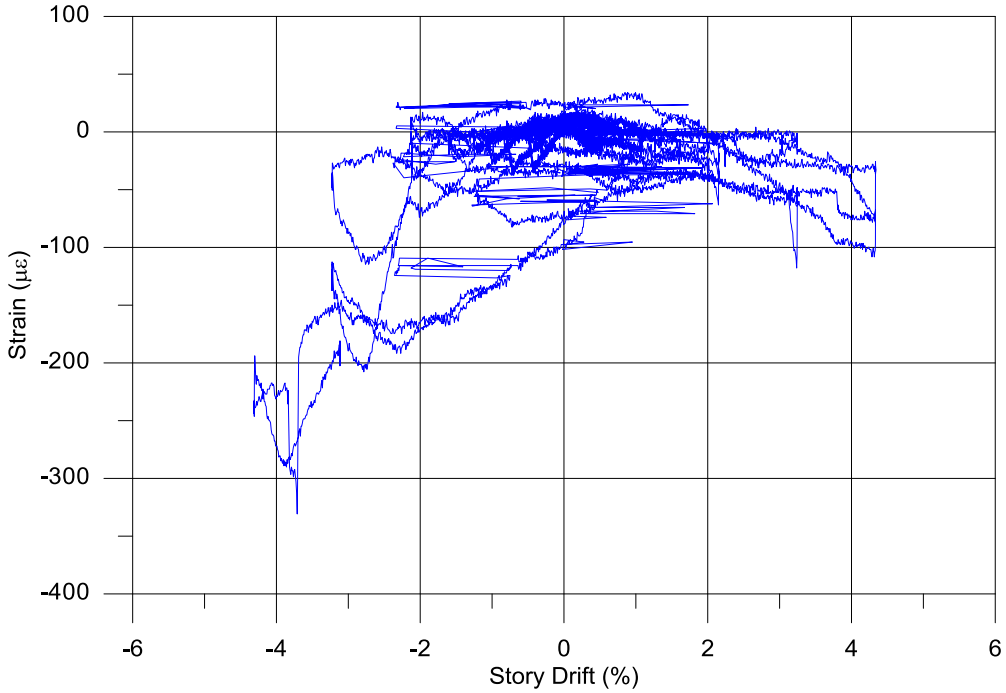
100
0
-100
-200
-300
-400
Strain (με)
-6
-4
-2
0
2
4
6
Story Drift (%)

BR-4-1

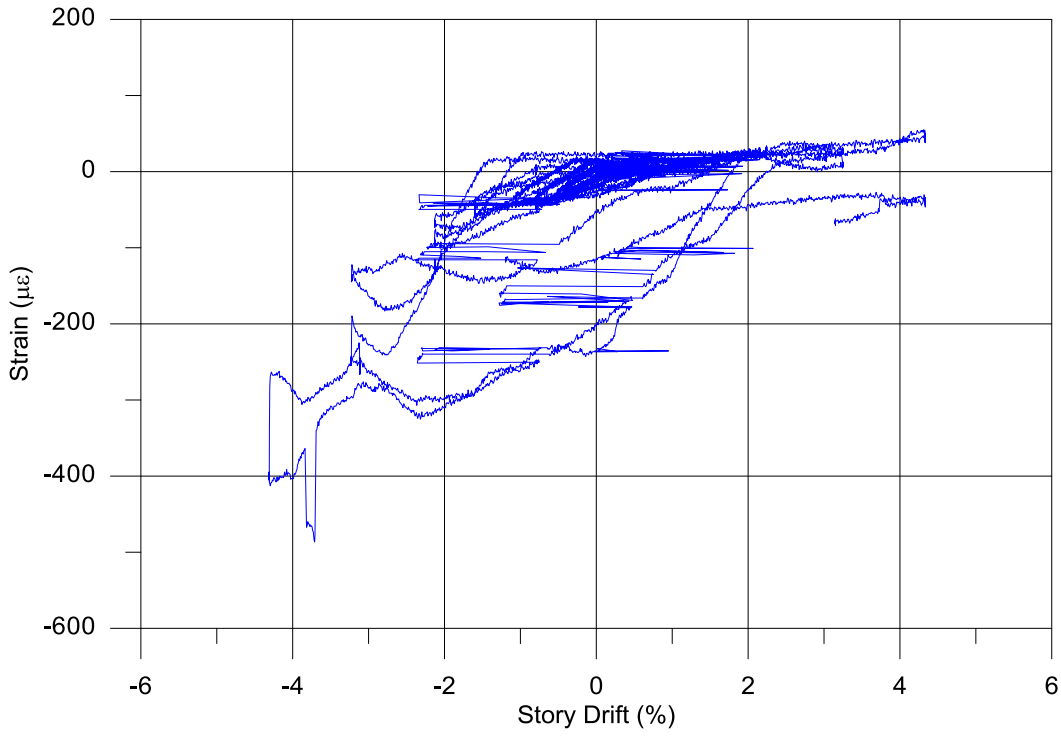
200
0
-200
-400
-600
Strain (με)
-6
-4
-2
0
2
4
6
Story Drift (%)

BR-4-2

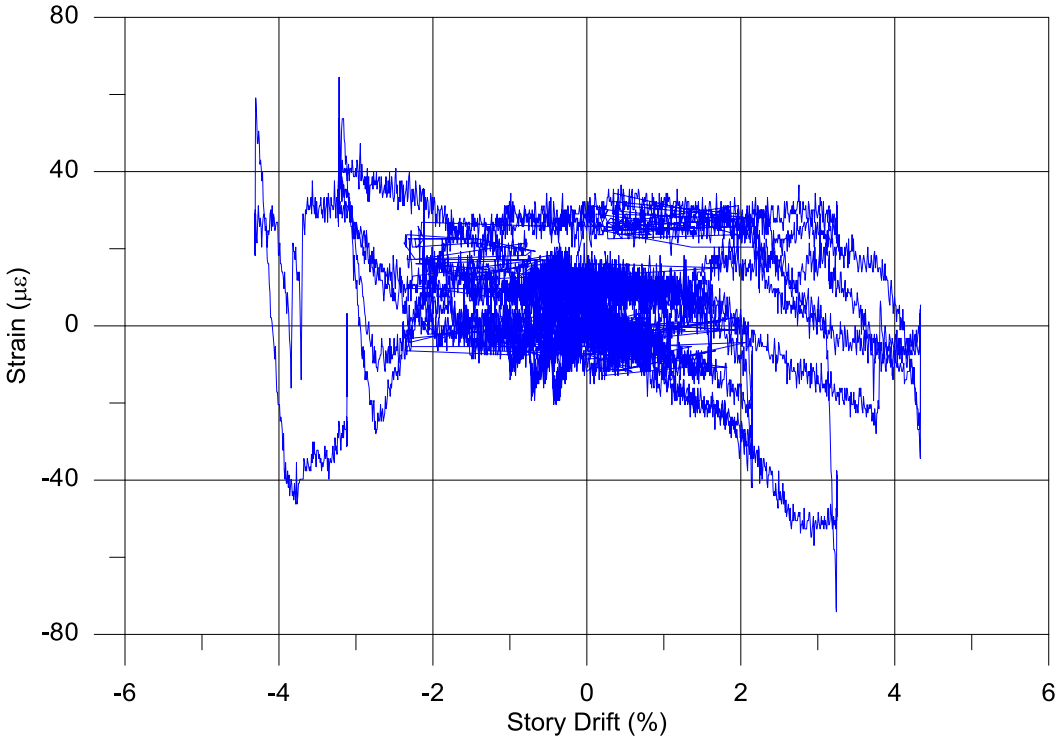
80
40
0
-40
-80
Strain (με)
-6
-4
-2
0
2
4
6
Story Drift (%)

BR-4-3

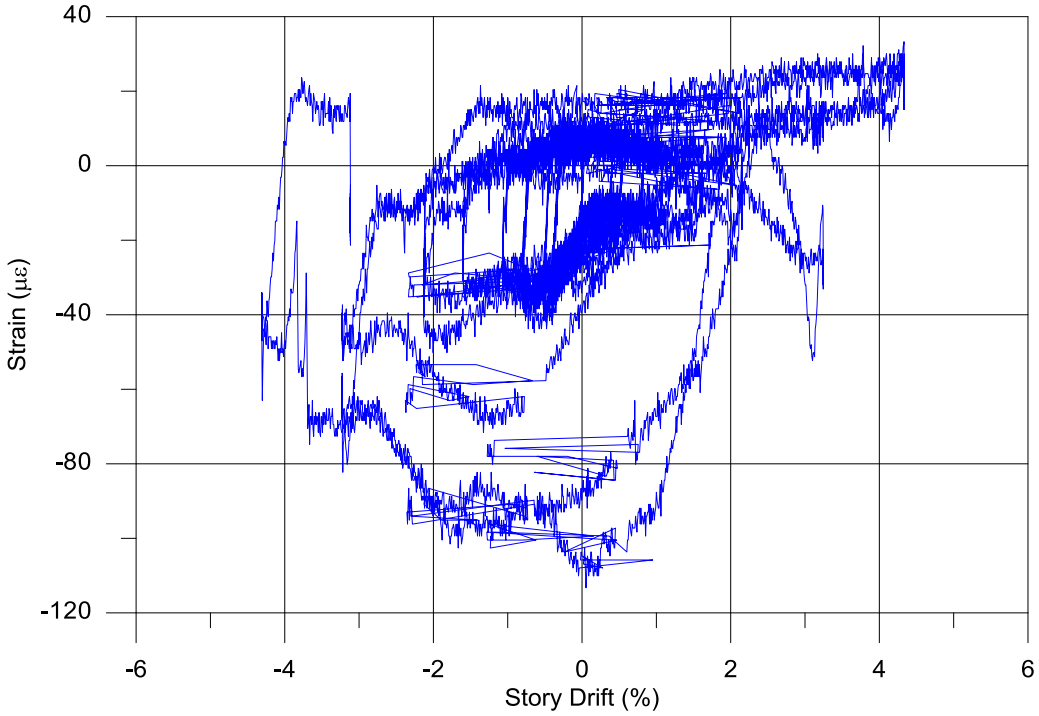
40
0
-40
-80
-120
Strain (με)
-6
-4
-2
0
2
4
6
Story Drift (%)

BR-4-4

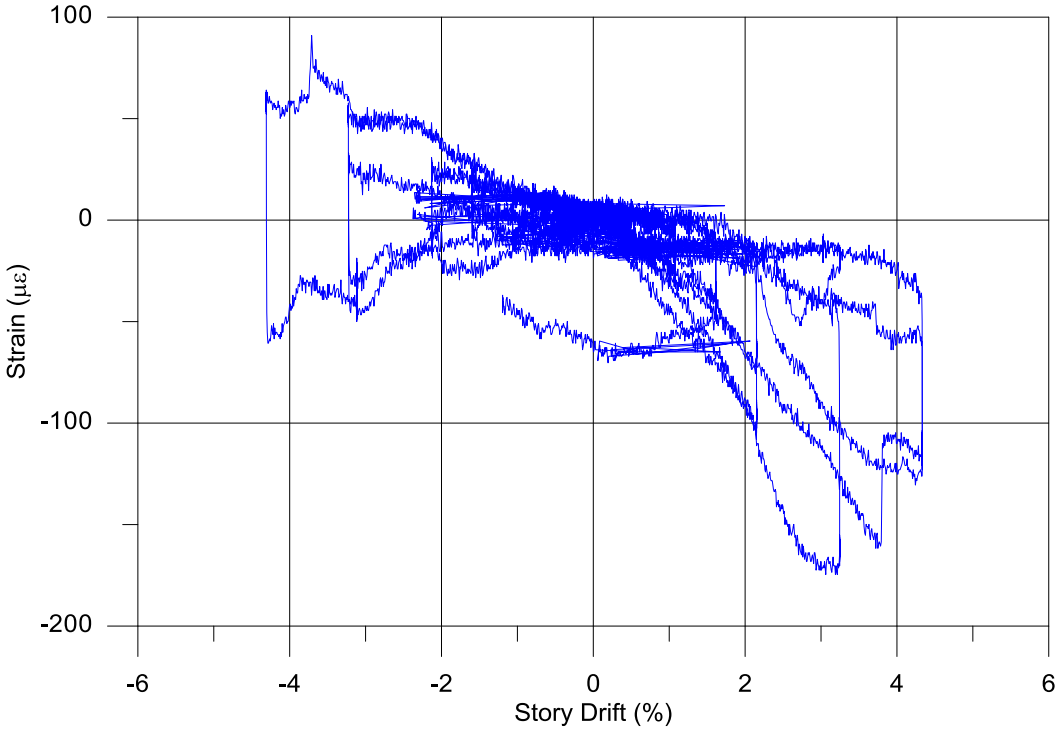
100
0
-100
-200
Strain (με)
-6
-4
-2
0
2
4
6
Story Drift (%)

BR-4-5

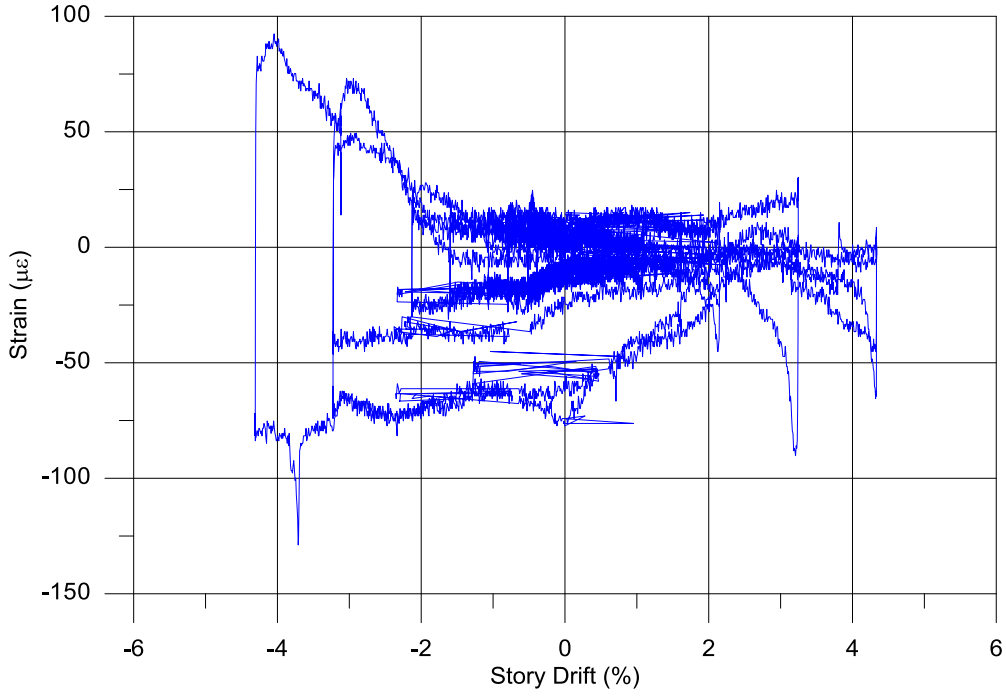
100
50
0
-50
-100
-150
Strain (με)
-6
-4
-2
0
2
4
6
Story Drift (%)

BR-4-6

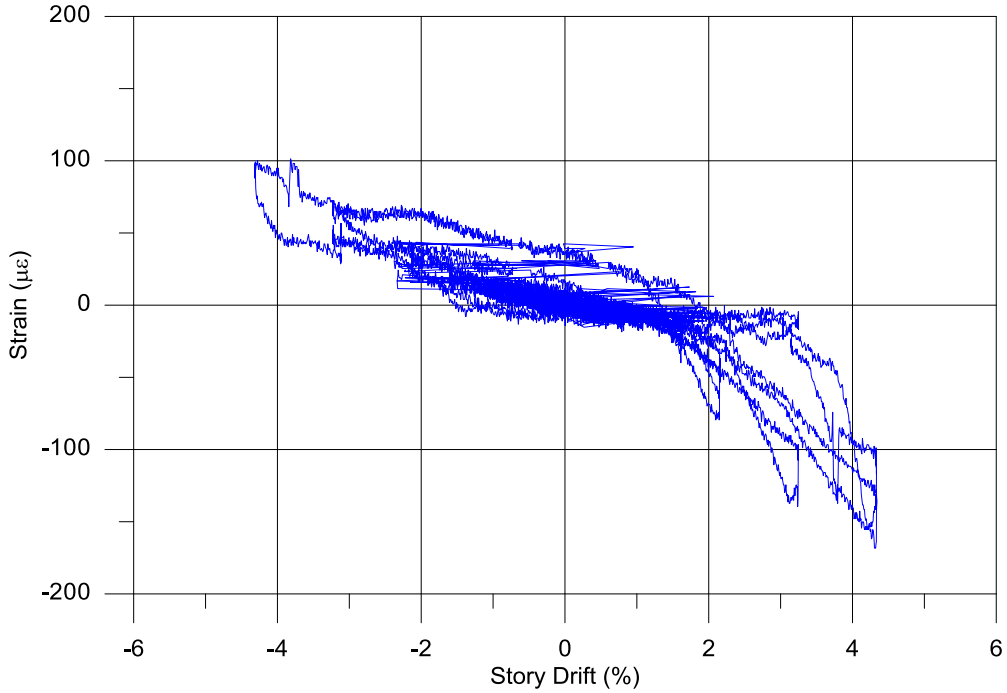
200
100
0
-100
-200
Strain (με)
-6
-4
-2
0
2
4
6
Story Drift (%)

BR-4-7

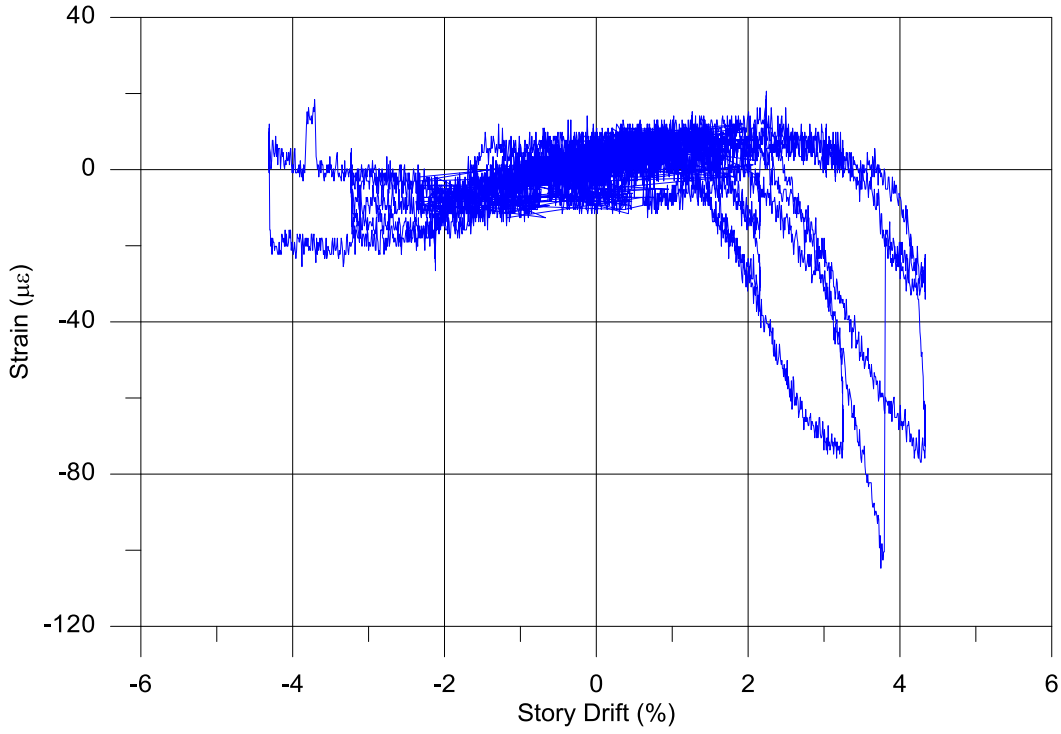
40
0
-40
-80
-120
Strain (με)
-6
-4
-2
0
2
4
6
Story Drift (%)

BR-4-8

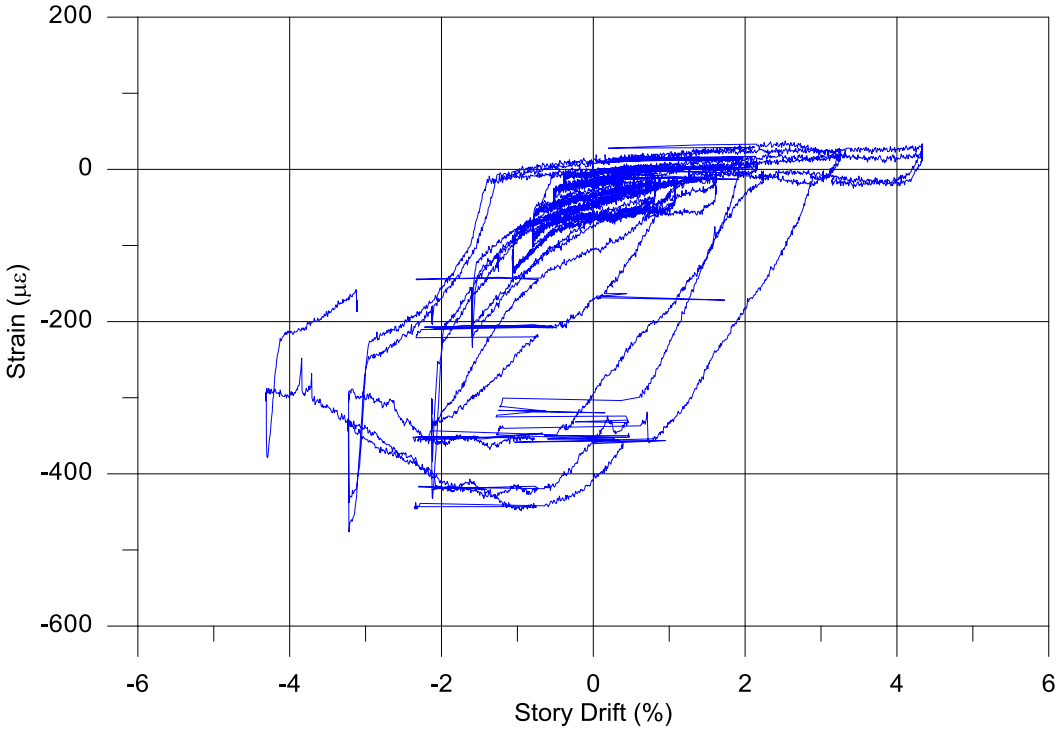
200
0
-200
-400
-600
Strain (με)
-6
-4
-2
0
2
4
6
Story Drift (%)

BR-5-1

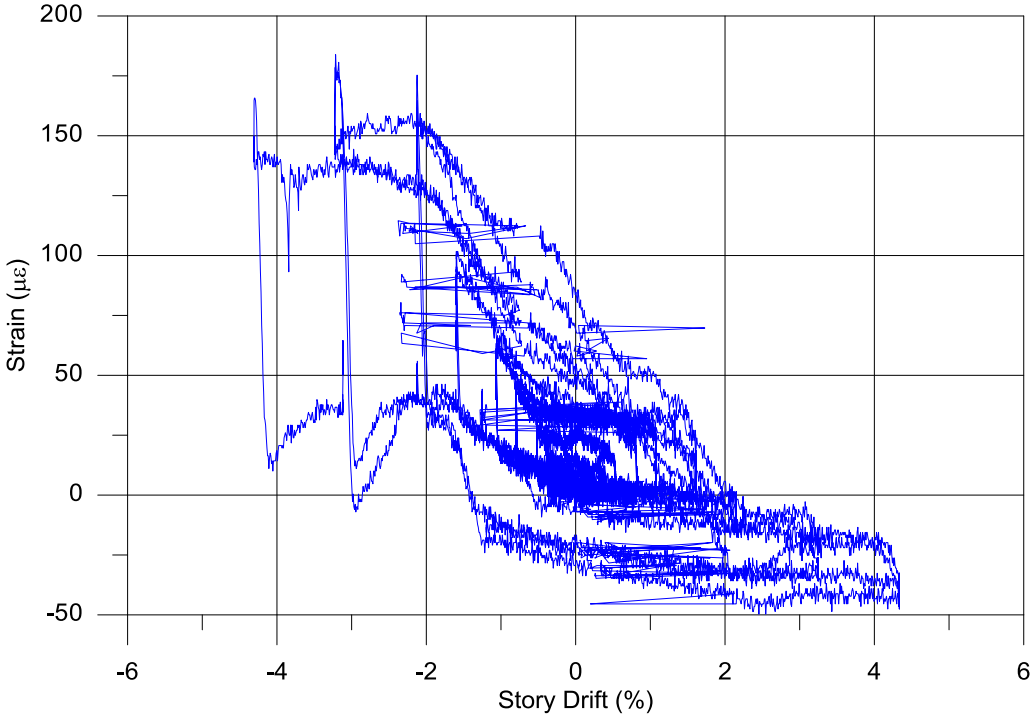
200
150
100
50
0
-50
Strain (με)
-6
-4
-2
0
2
4
6
Story Drift (%)

BR-5-2

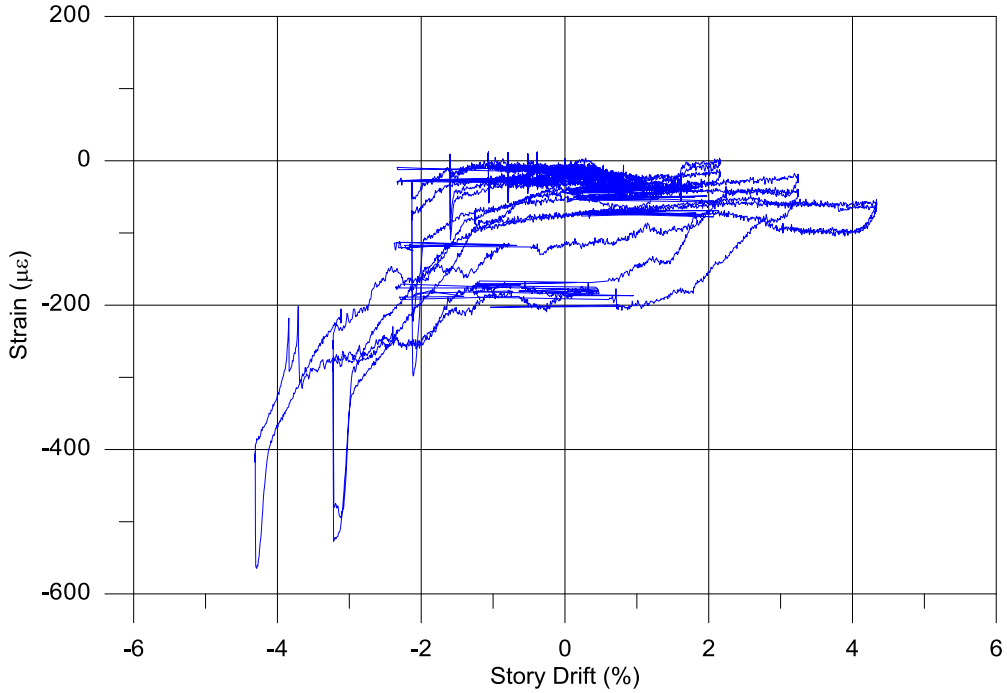
200
0
-200
-400
-600
Strain (με)
-6
-4
-2
0
2
4
6
Story Drift (%)

BR-5-3

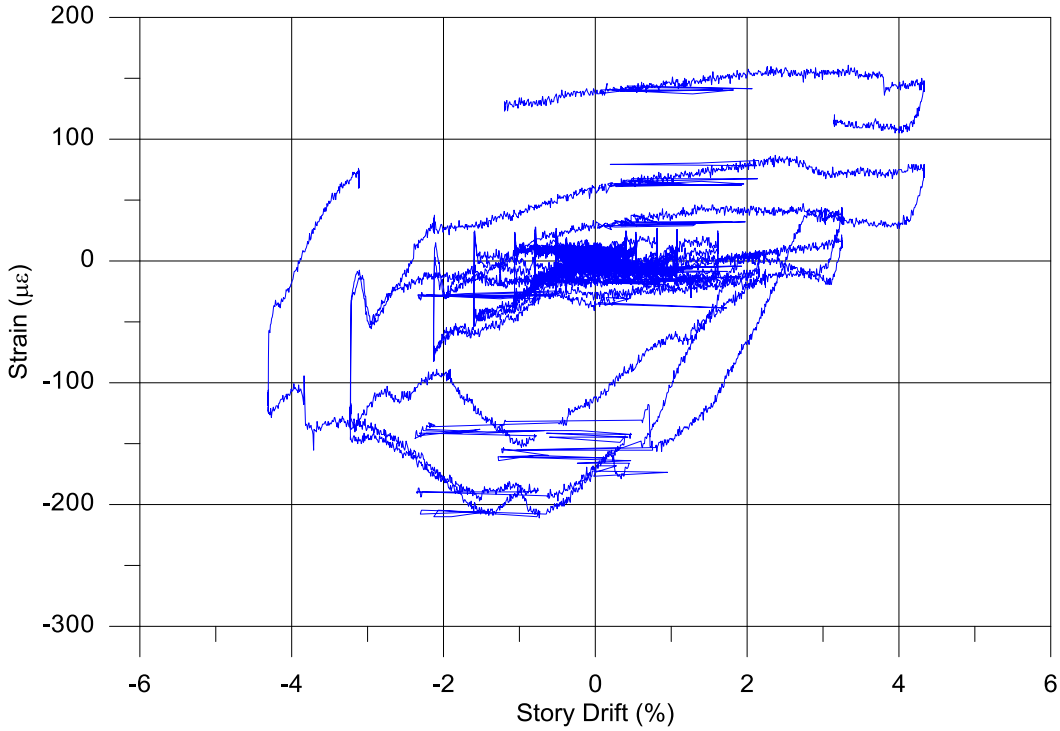
200
100
0
-100
-200
-300
Strain (με)
-6
-4
-2
0
2
4
6
Story Drift (%)

BR-5-4

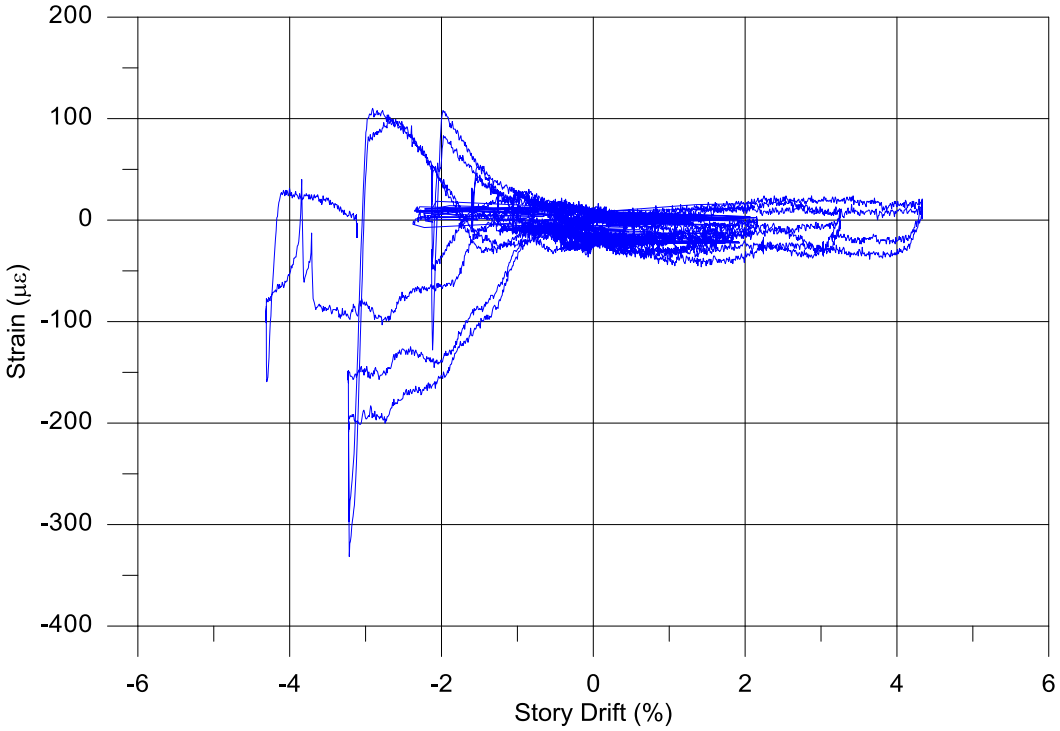
200
100
0
-100
-200
-300
-400
Strain (με)
-6
-4
-2
0
2
4
6
Story Drift (%)

BR-5-5

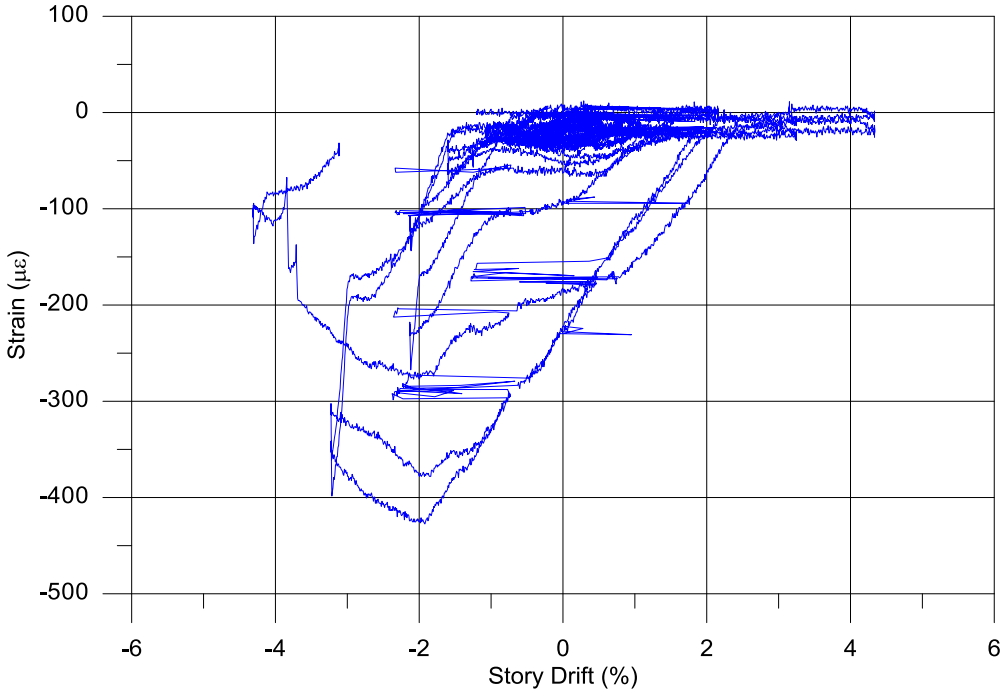
100
0
-100
-200
-300
-400
-500
Strain (με)
-6
-4
-2
0
2
4
6
Story Drift (%)

BR-5-6

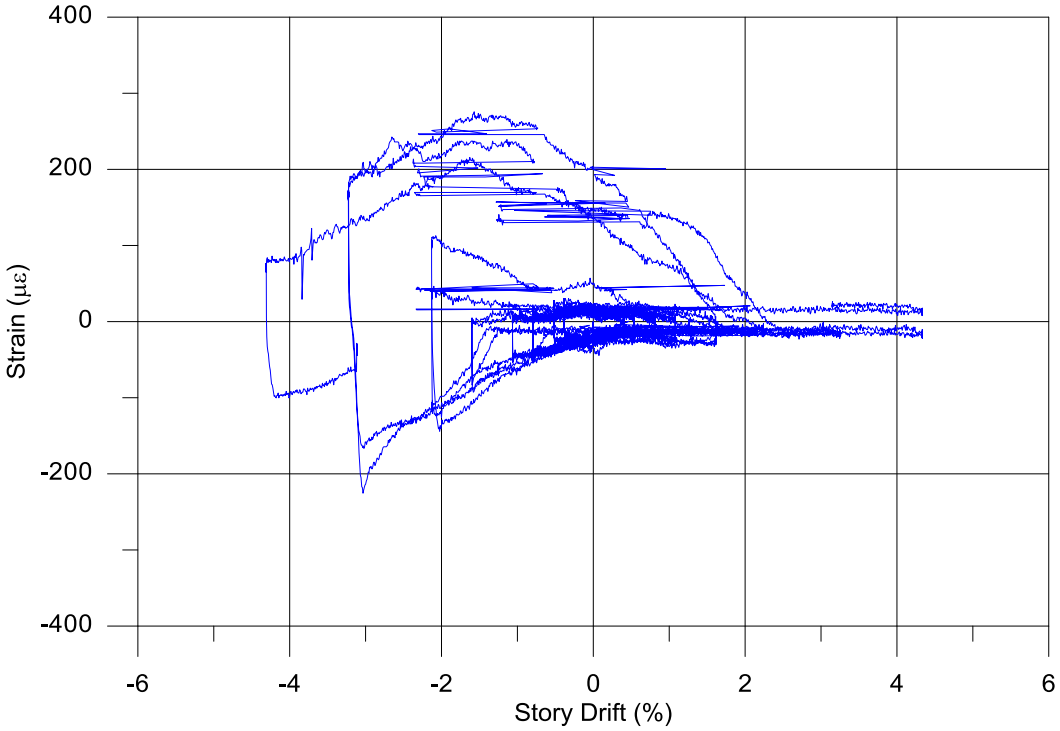
400
200
0
-200
-400
Strain (με)
-6
-4
-2
0
2
4
6
Story Drift (%)

BR-5-7

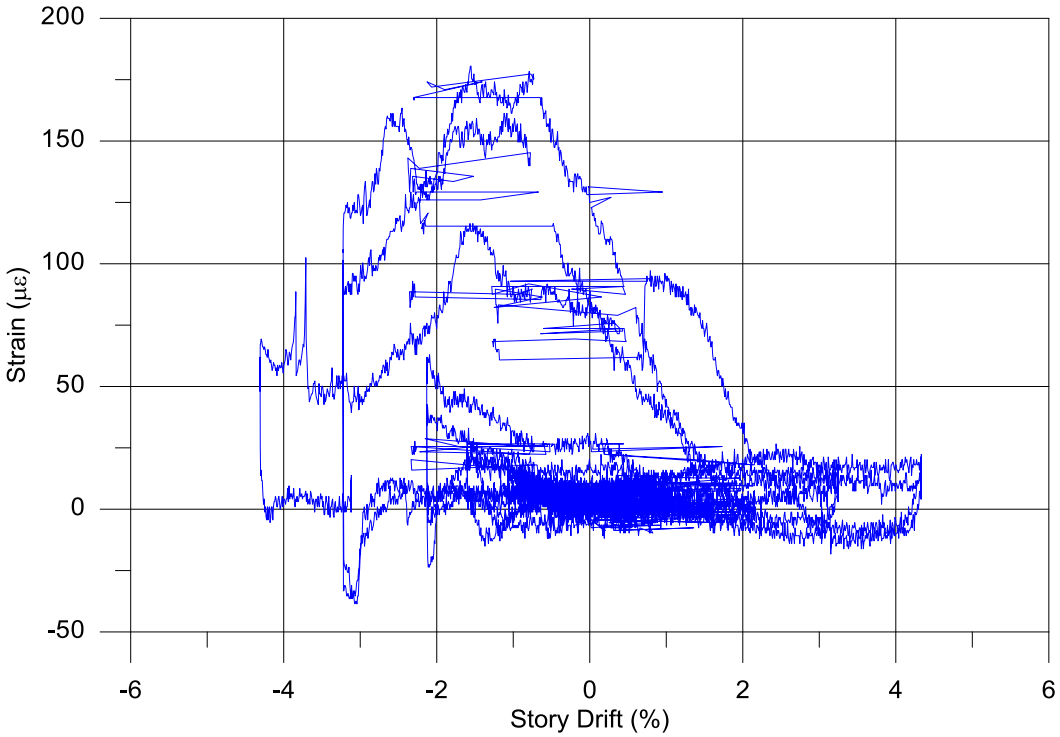
200
150
100
50
0
-50
Strain (με)
-6
-4
-2
0
2
4
6
Story Drift (%)

BR-5-8

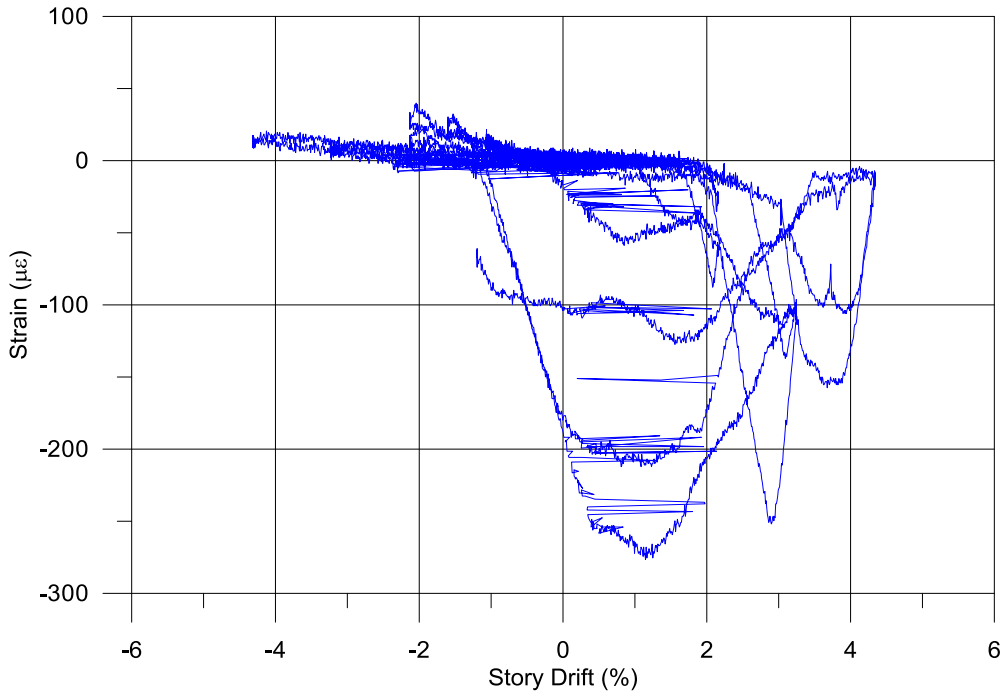
100
0
-100
-200
-300
Strain (με)
-6
-4
-2
0
2
4
6
Story Drift (%)

BR-6-1

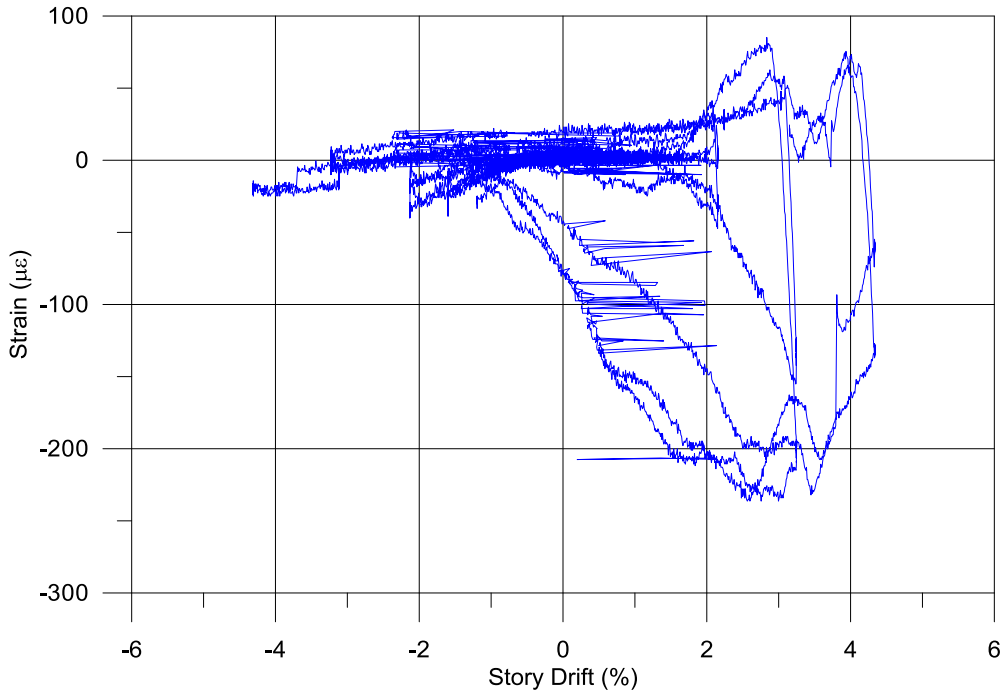
100
0
-100
-200
-300
Strain (με)
-6
-4
-2
0
2
4
6
Story Drift (%)

BR-6-2

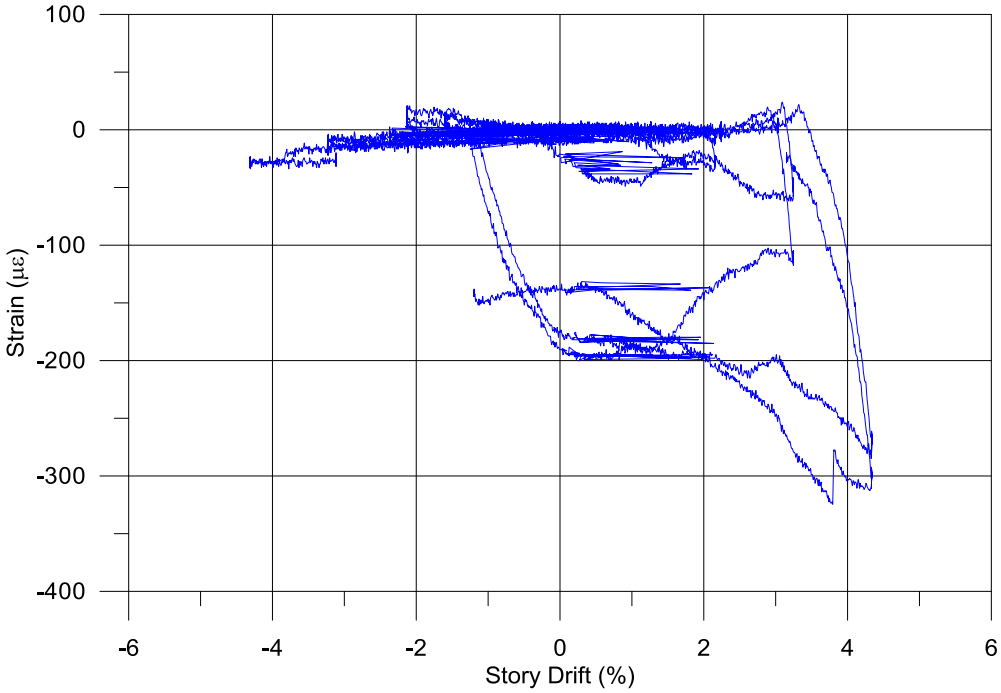
100
0
-100
-200
-300
-400
Strain (με)
-6
-4
-2
0
2
4
6
Story Drift (%)

BR-6-3

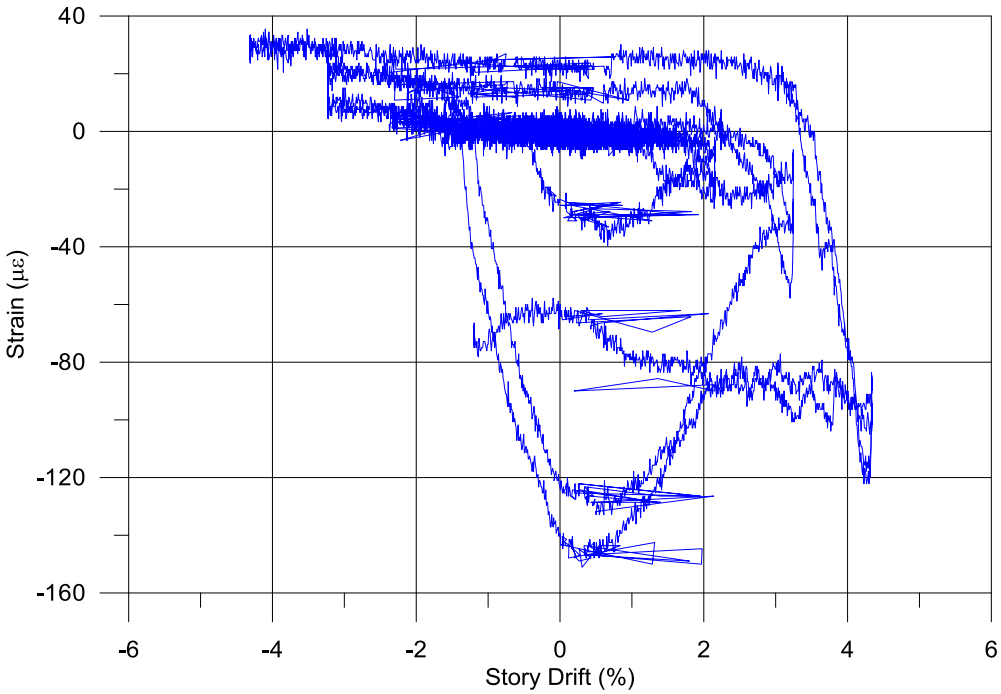
40
0
-40
-80
-120
-160
Strain (με)
-6
-4
-2
0
2
4
6
Story Drift (%)

BR-6-4

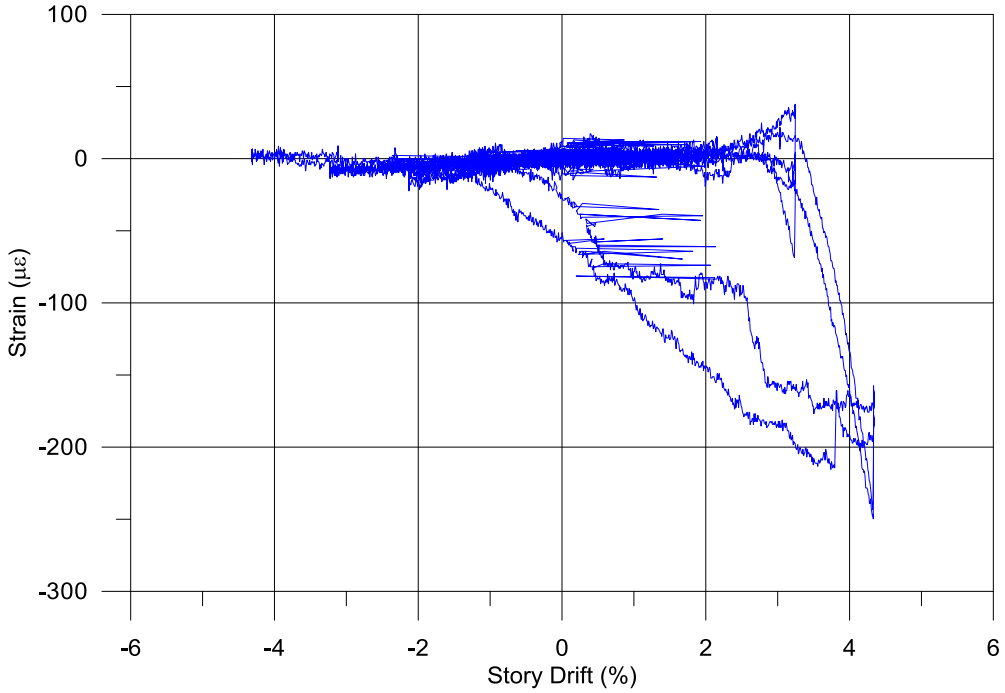
100
0
-100
-200
-300
Strain (με)
-6
-4
-2
0
2
4
6
Story Drift (%)

BR-6-5

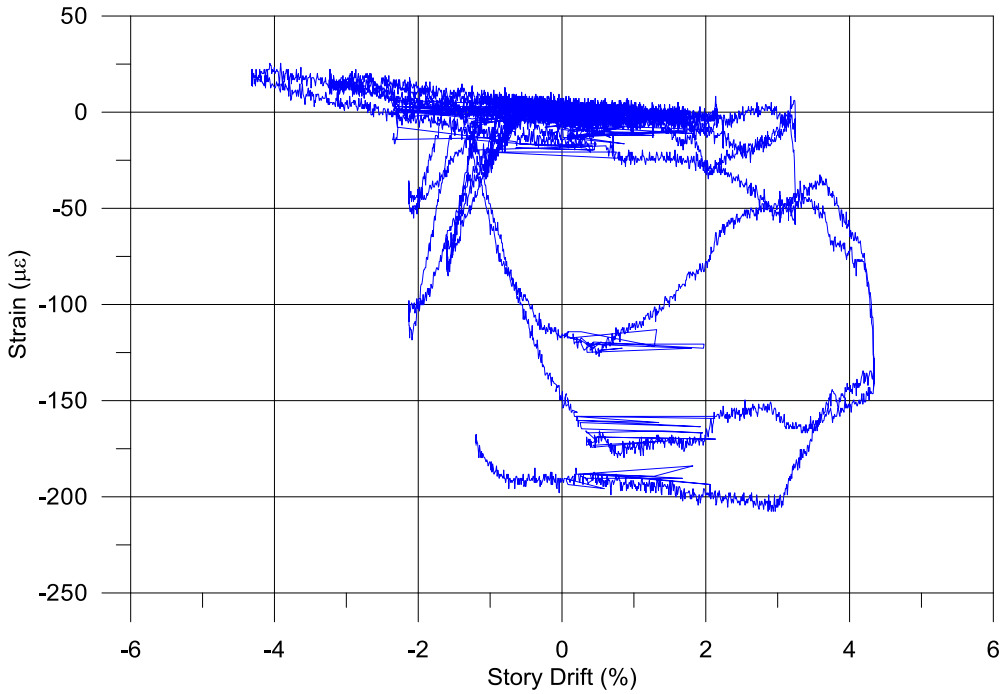
50
0
-50
-100
-150
-200
-250
Strain (με)
-6
-4
-2
0
2
4
6
Story Drift (%)

BR-6-6

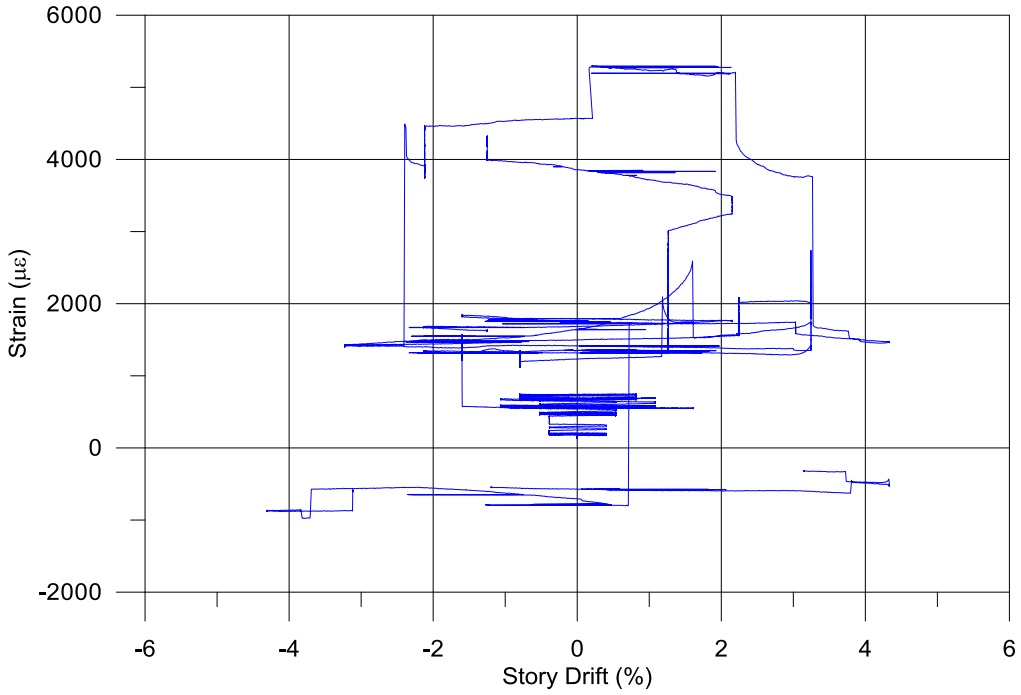
6000
4000
2000
0
-2000
Strain (με)
-6
-4
-2
0
2
4
6
Story Drift (%)

BR-6-7

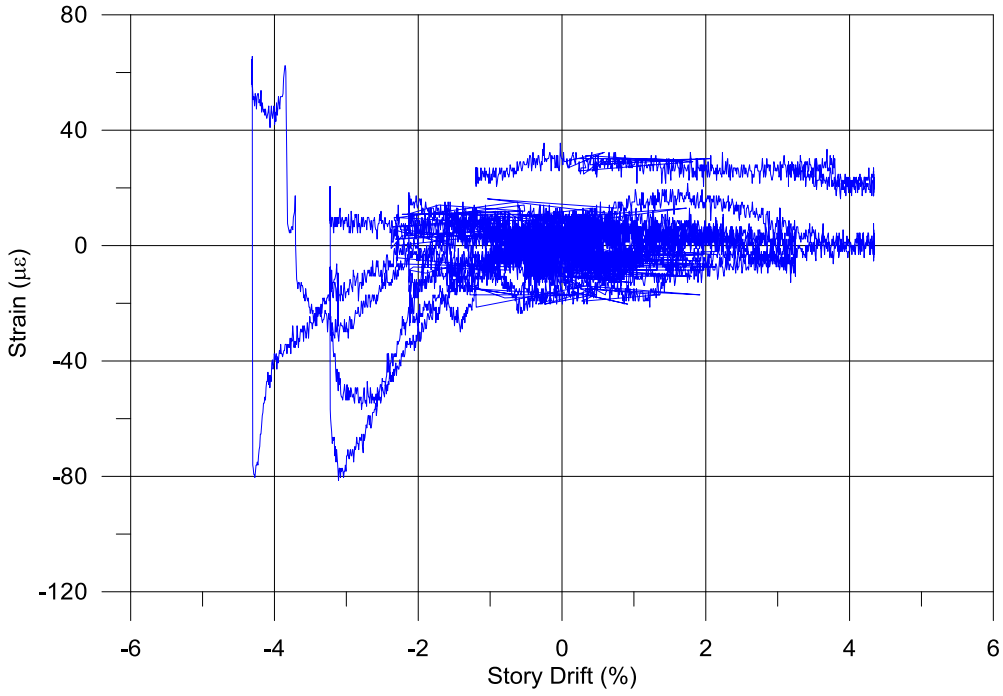
80
40
0
-40
-80
-120
Strain (με)
-6
-4
-2
0
2
4
6
Story Drift (%)

BR-7-1

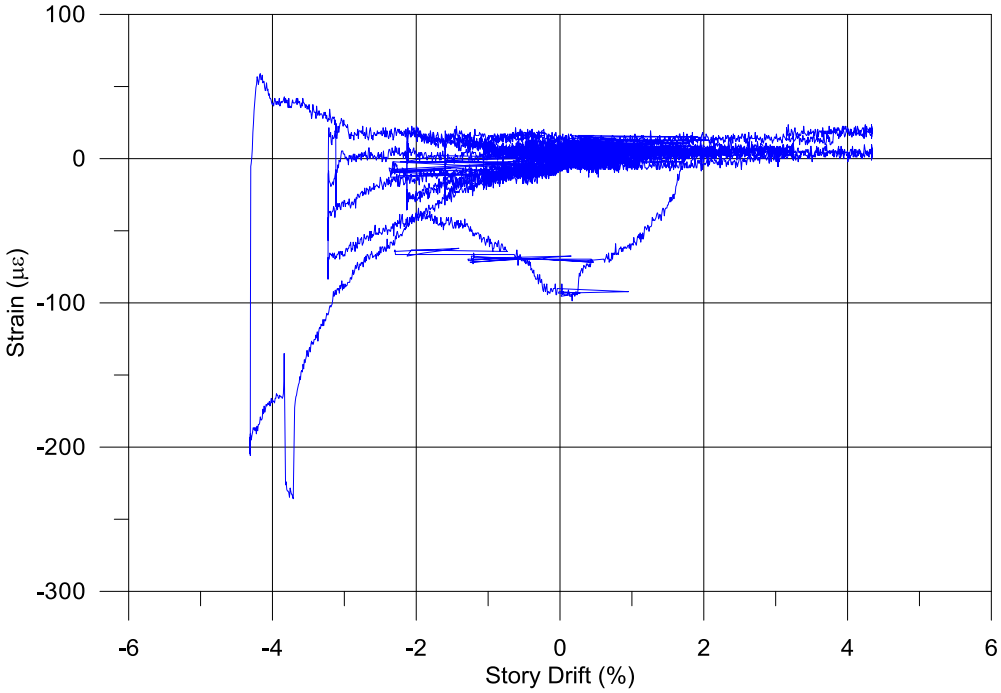
100
0
-100
-200
-300
Strain (με)
-6
-4
-2
0
2
4
6
Story Drift (%)

BR-7-3

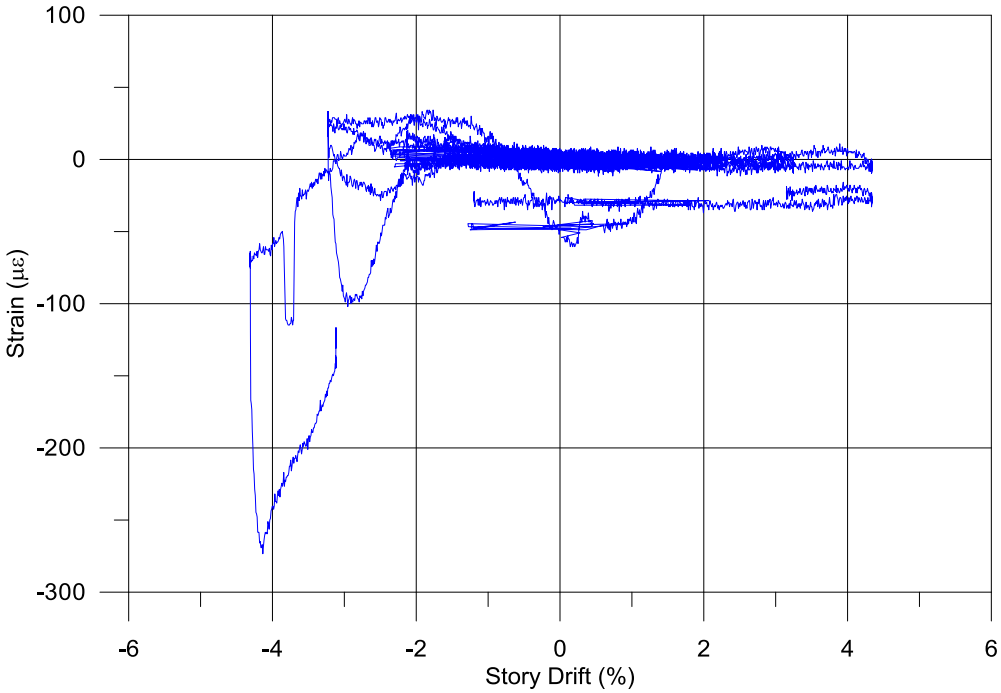
100
0
-100
-200
-300
Strain (με)
-6
-4
-2
0
2
4
6
Story Drift (%)

BR-7-4

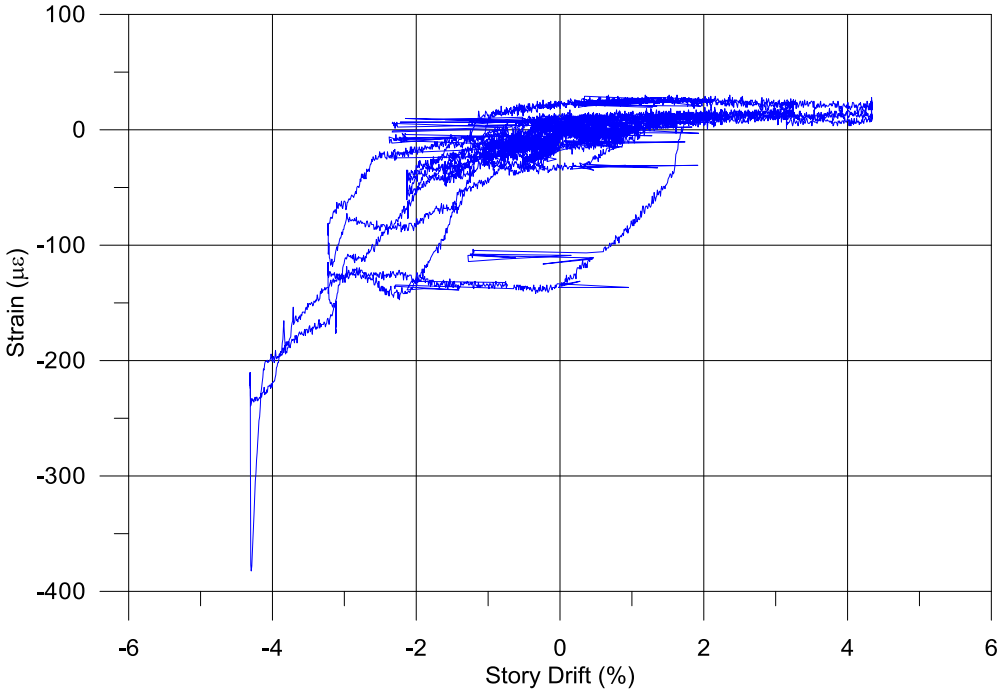
100
0
-100
-200
-300
-400
Strain (με)
-6
-4
-2
0
2
4
6
Story Drift (%)

BR-7-5

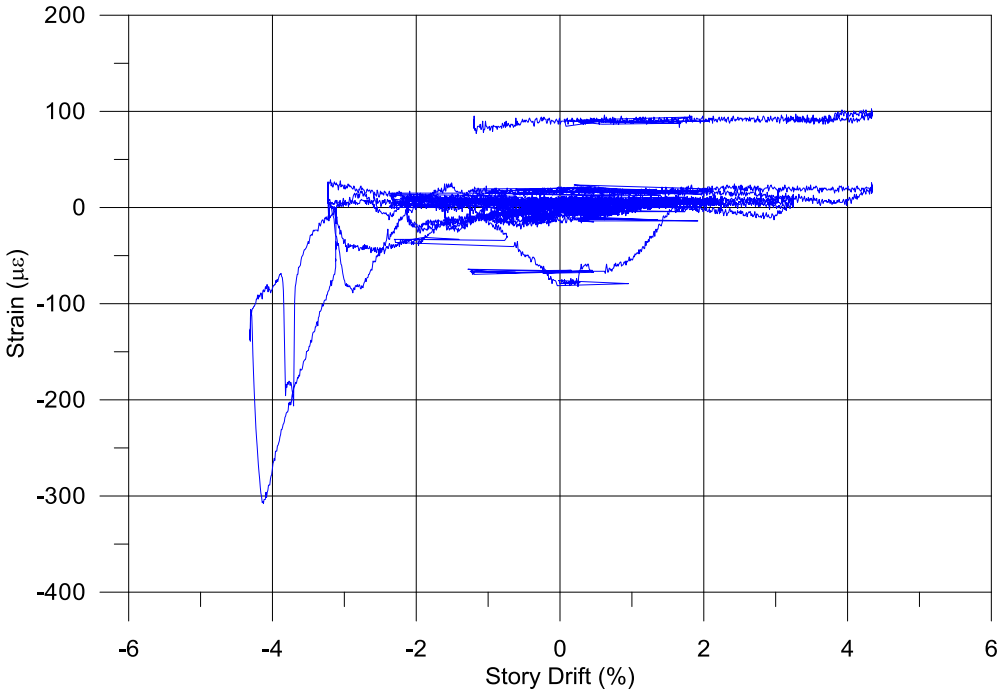
200
100
0
-100
-200
-300
-400
Strain (με)
-6
-4
-2
0
2
4
6
Story Drift (%)

BR-7-6

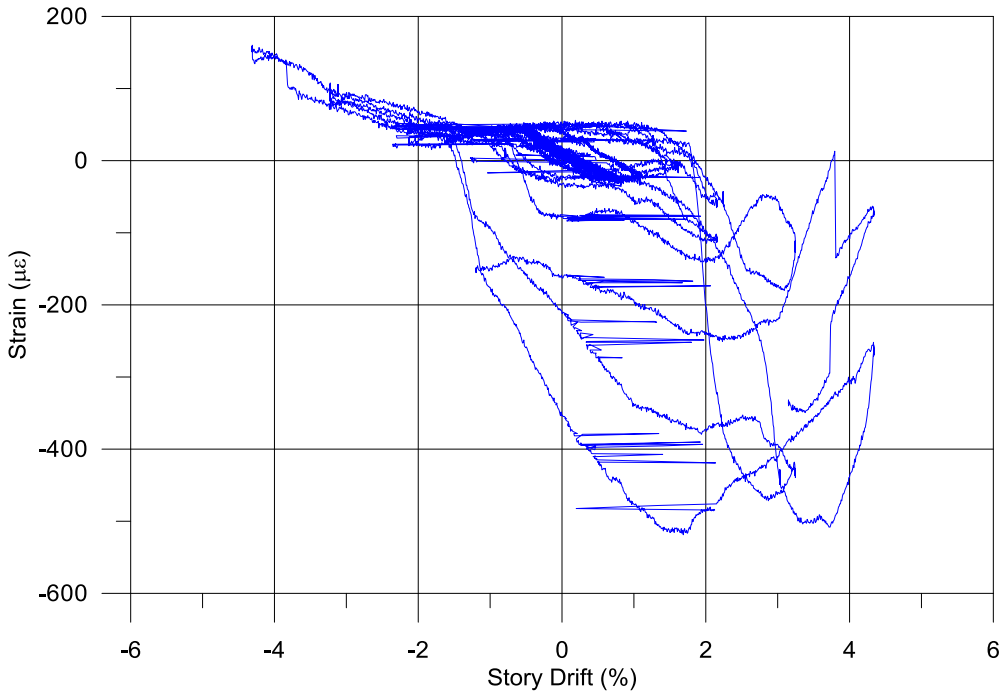
200
0
-200
-400
-600
Strain (με)
-6
-4
-2
0
2
4
6
Story Drift (%)

BR-8-1

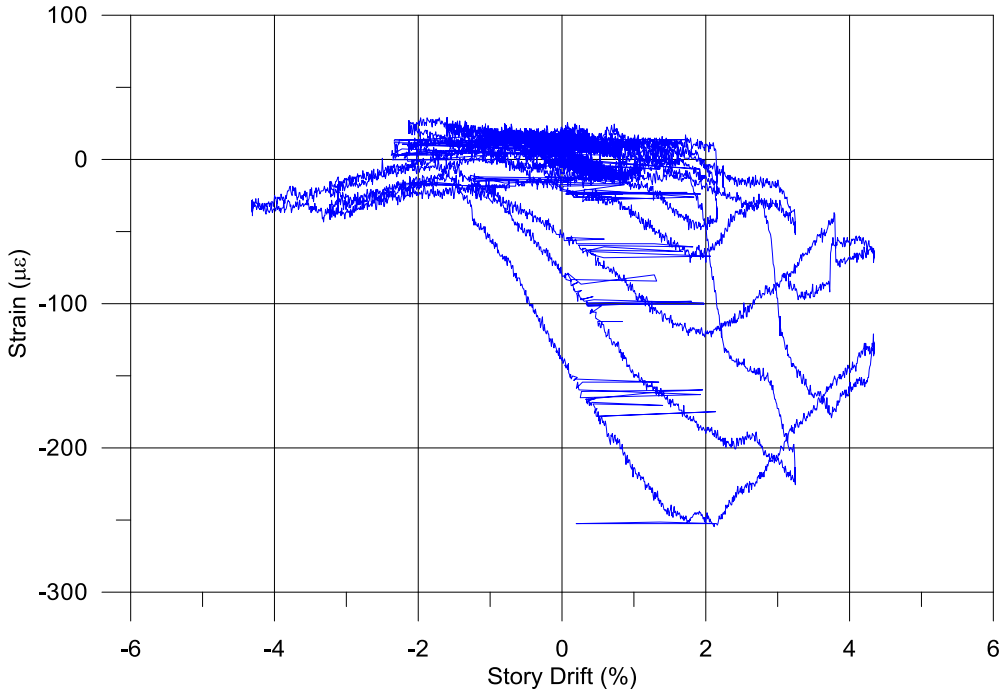
100
0
-100
-200
-300
Strain (με)
-6
-4
-2
0
2
4
6
Story Drift (%)

BR-8-2

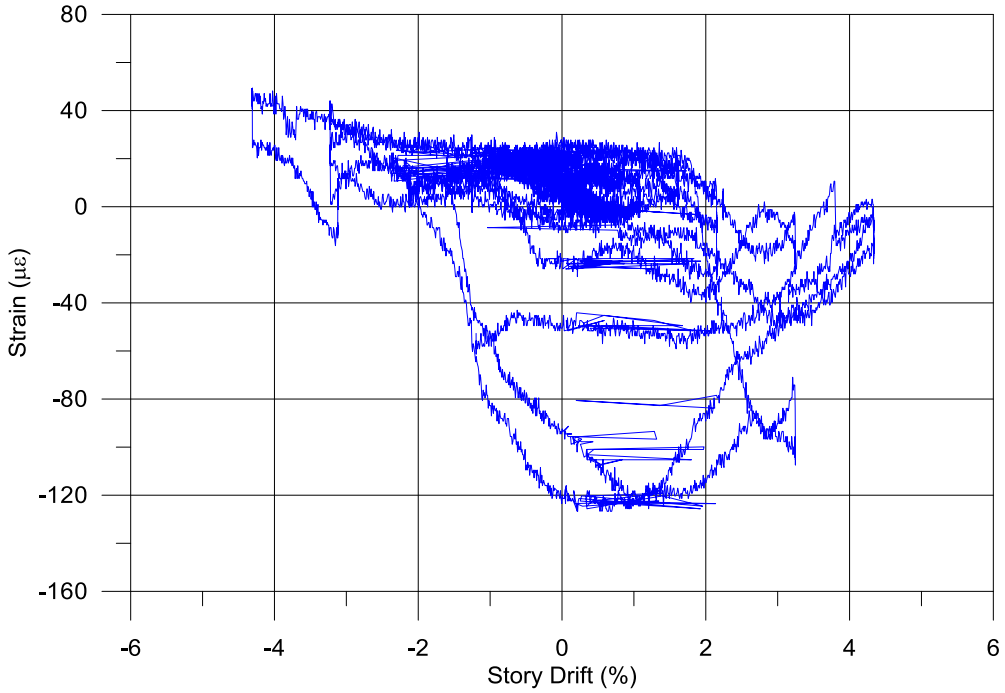
80
40
0
-40
-80
-120
-160
Strain (με)
-6
-4
-2
0
2
4
6
Story Drift (%)

BR-8-3

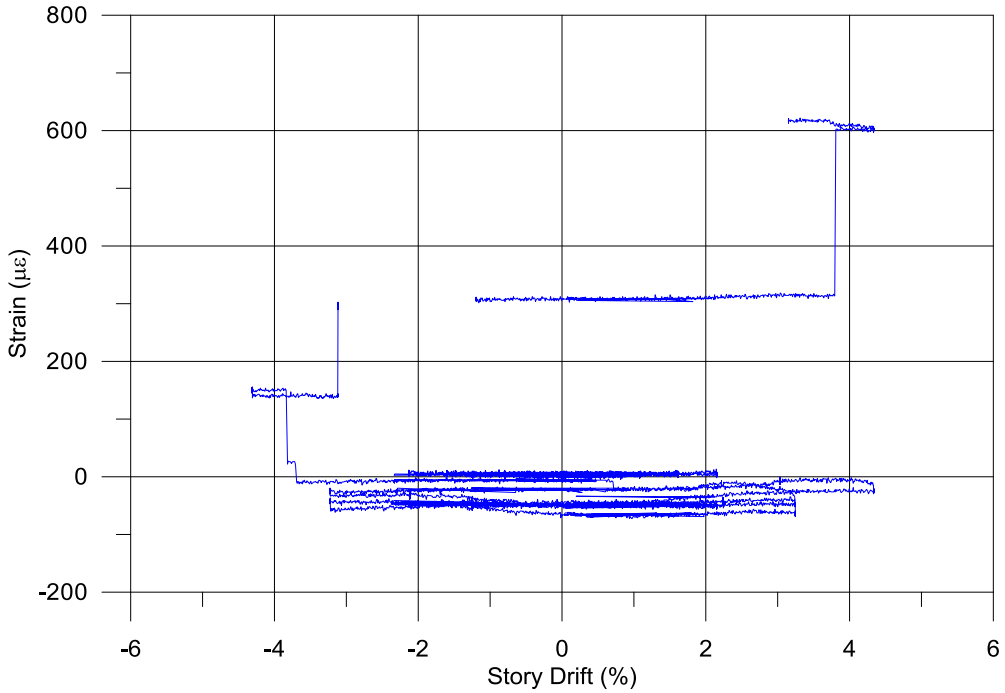
800
600
400
200
0
-200
Strain (με)
-6
-4
-2
0
2
4
6
Story Drift (%)

BR-8-4

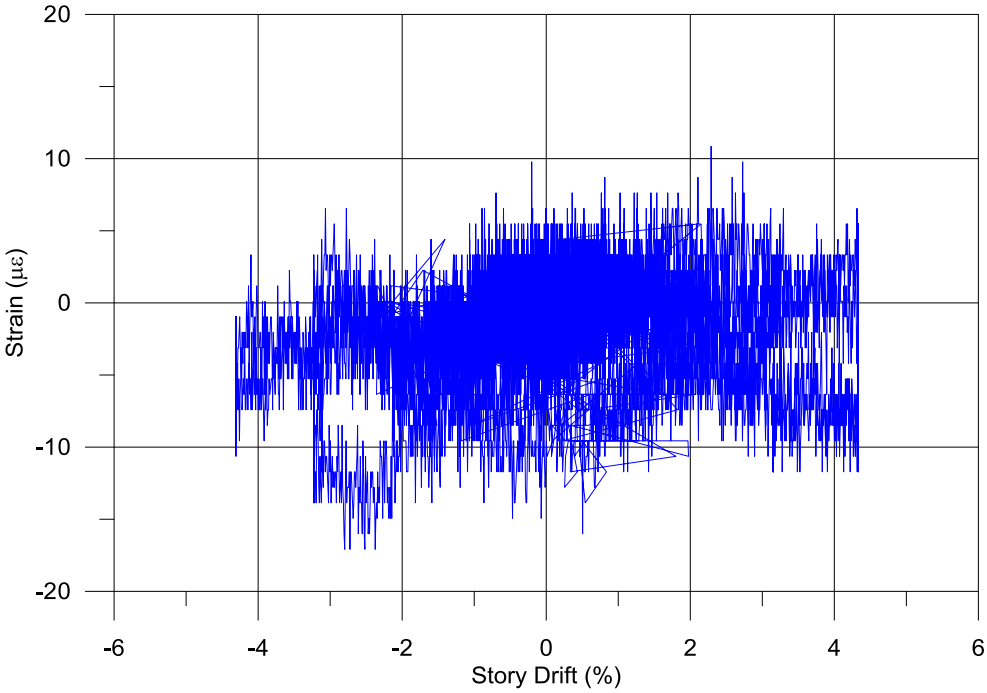
20
10
0
-10
-20
Strain (με)
-6
-4
-2
0
2
4
6
Story Drift (%)

BR-8-5

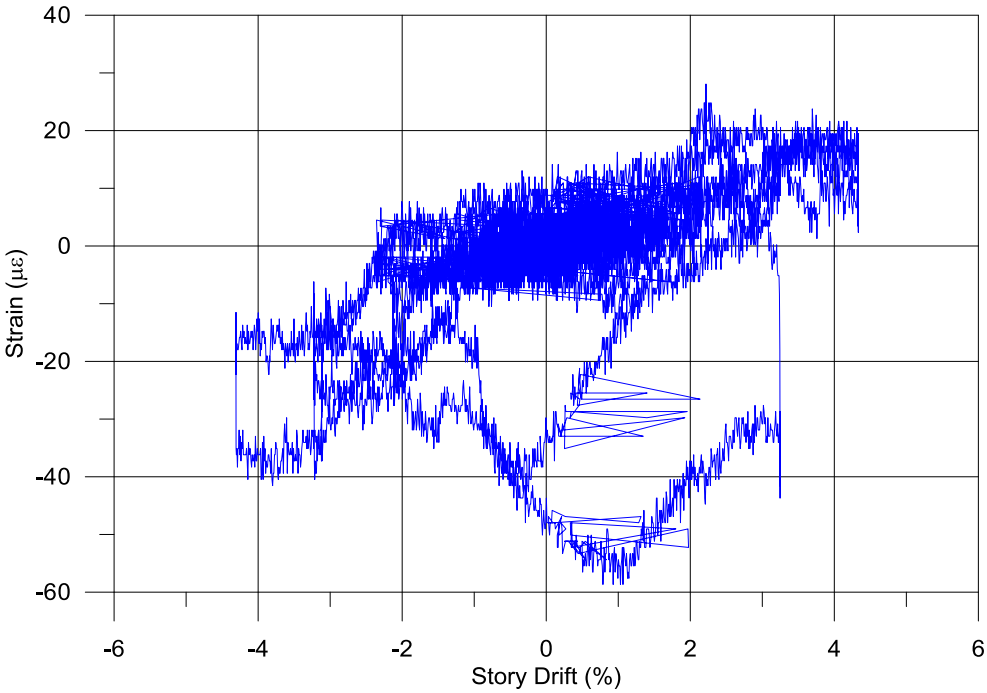
40
20
0
-20
-40
-60
Strain (με)
-6
-4
-2
0
2
4
6
Story Drift (%)

BR-8-6

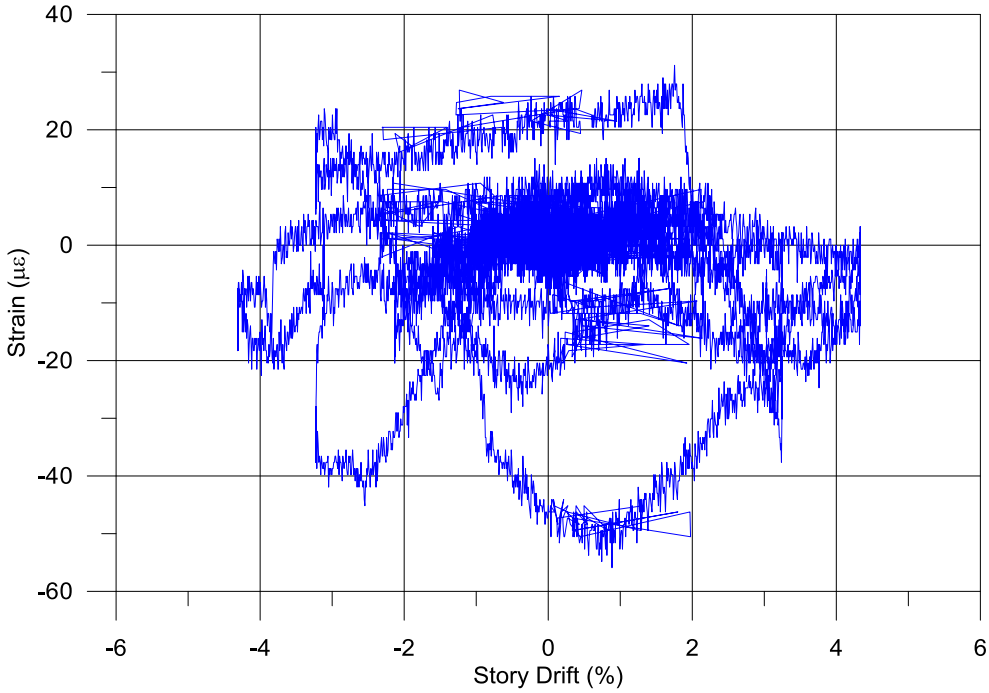
40
20
0
-20
-40
-60
Strain (με)
-6
-4
-2
0
2
4
6
Story Drift (%)

BR-8-7

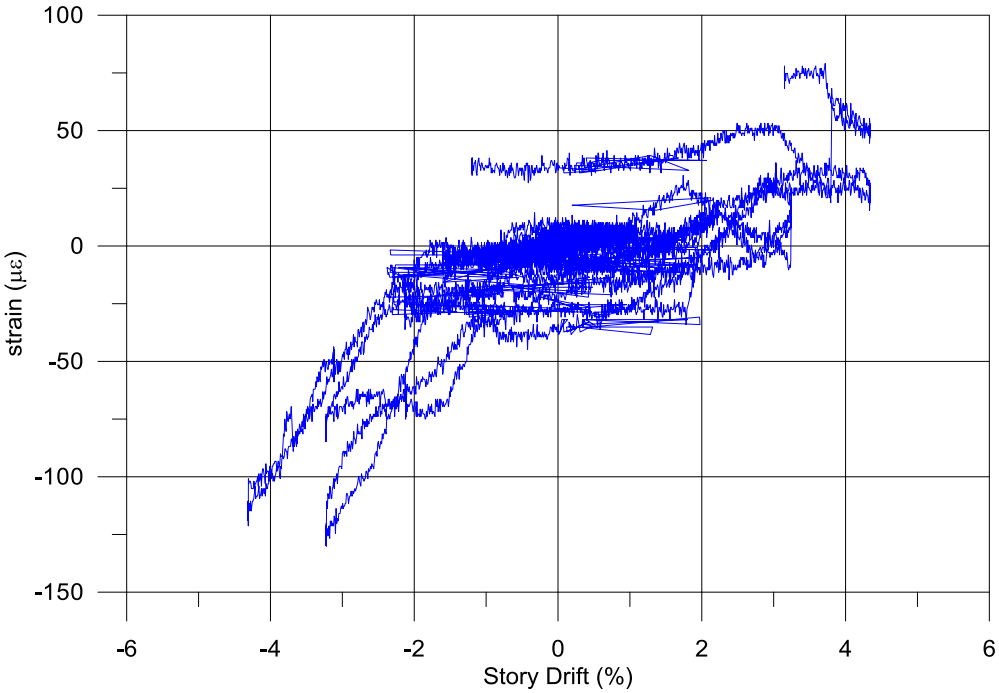
100
50
0
-50
-100
-150
strain (με)
-6
-4
-2
0
2
4
6
Story Drift (%)

BR-8-8

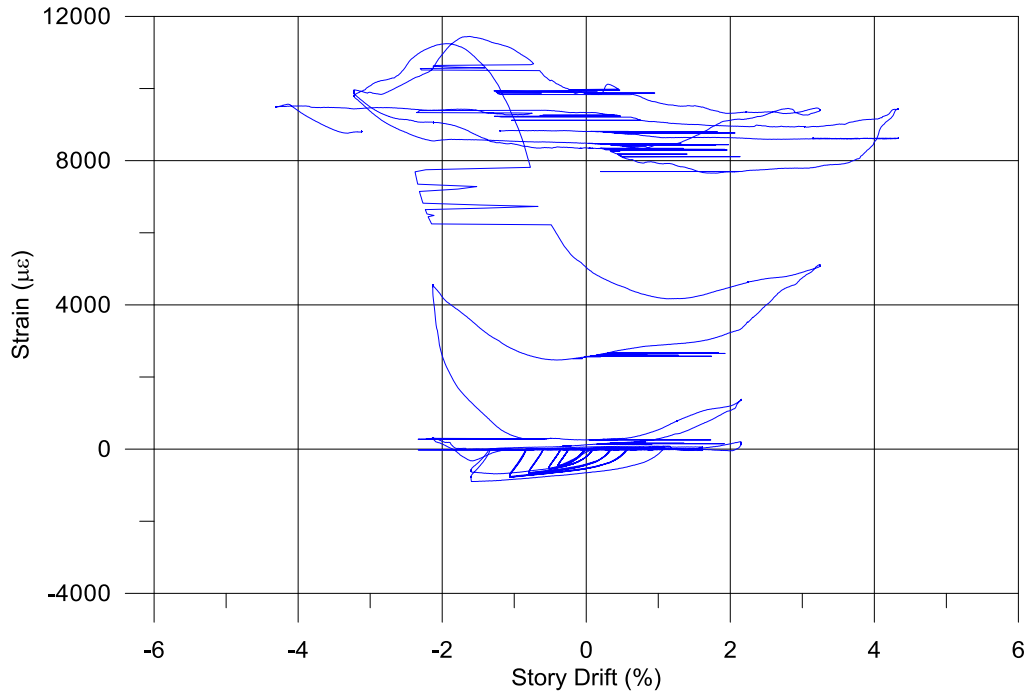

BRB-NE-1-1

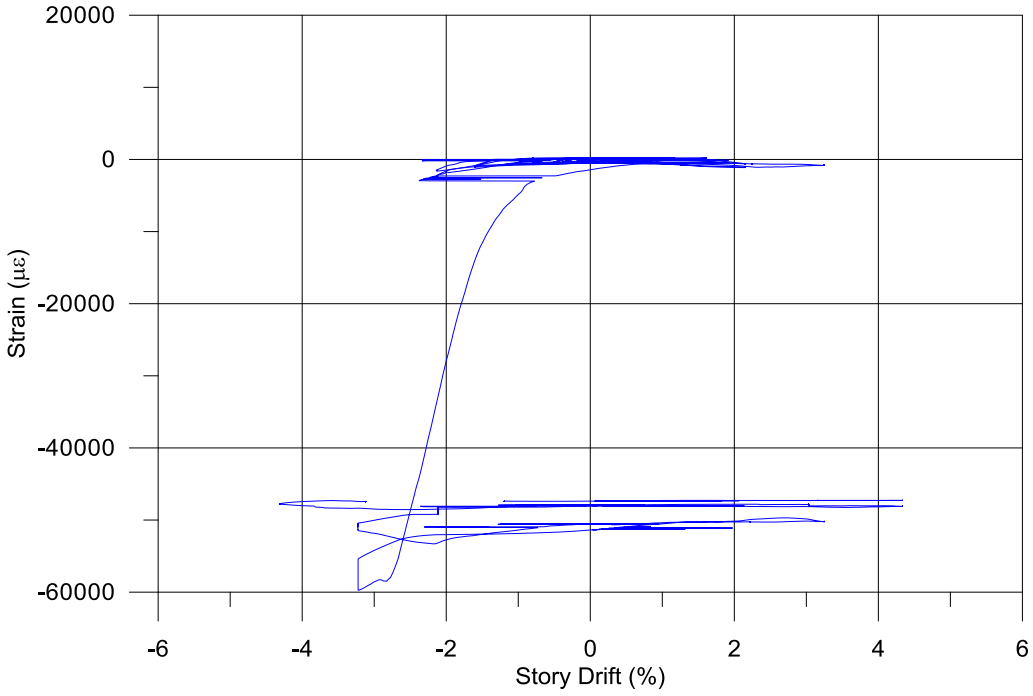

BRB-NE-1-2

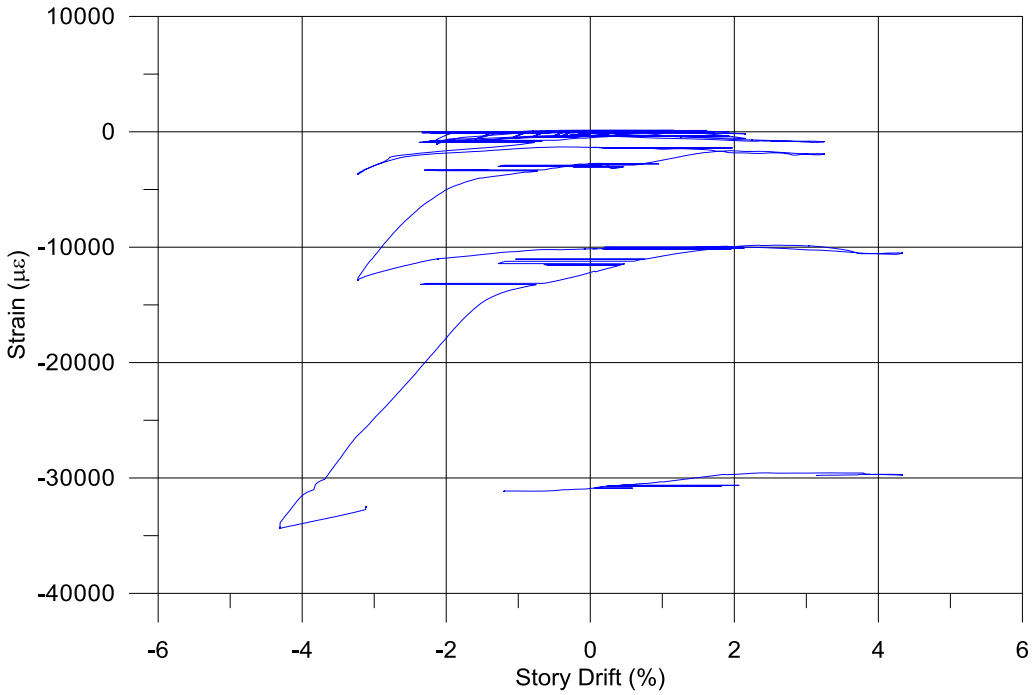

BRB-NE-2-1

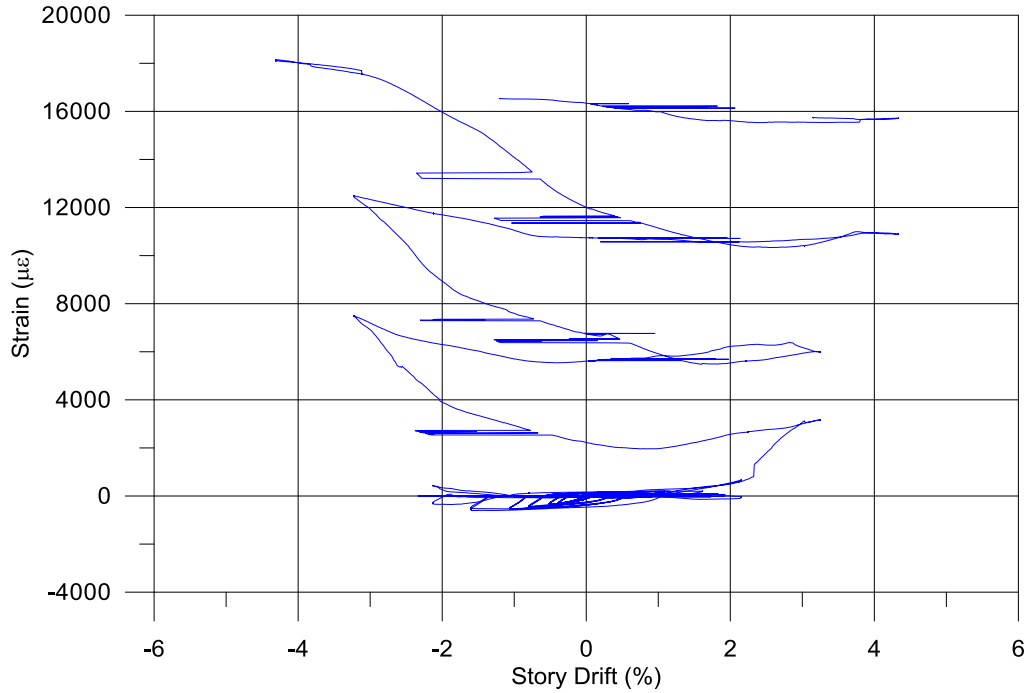

BRB-NE-2-2

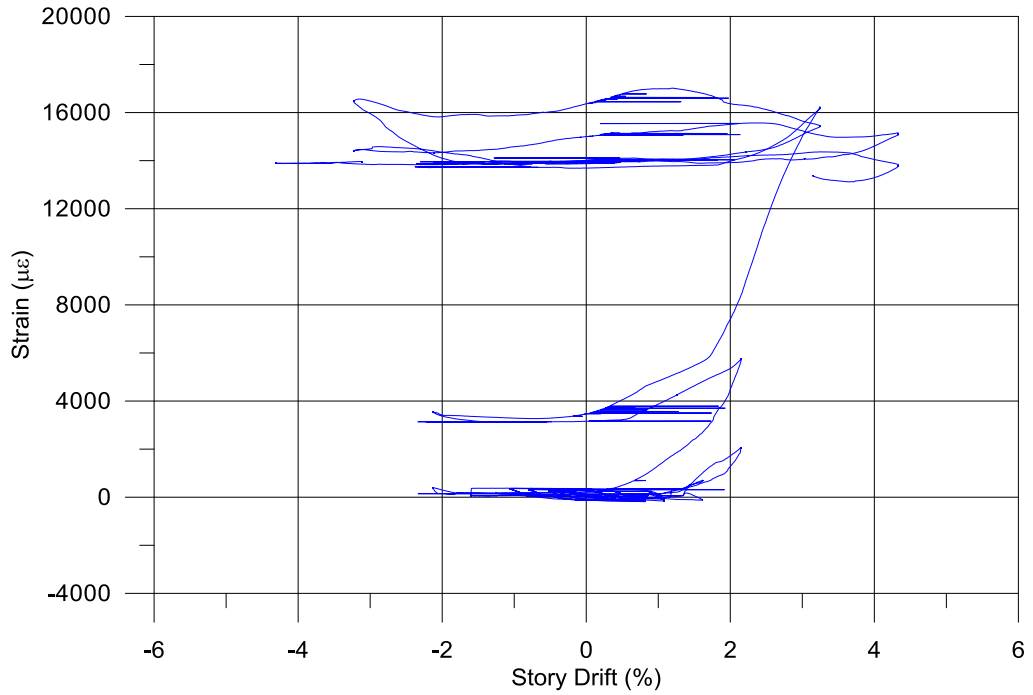

BRB-SW-1-1

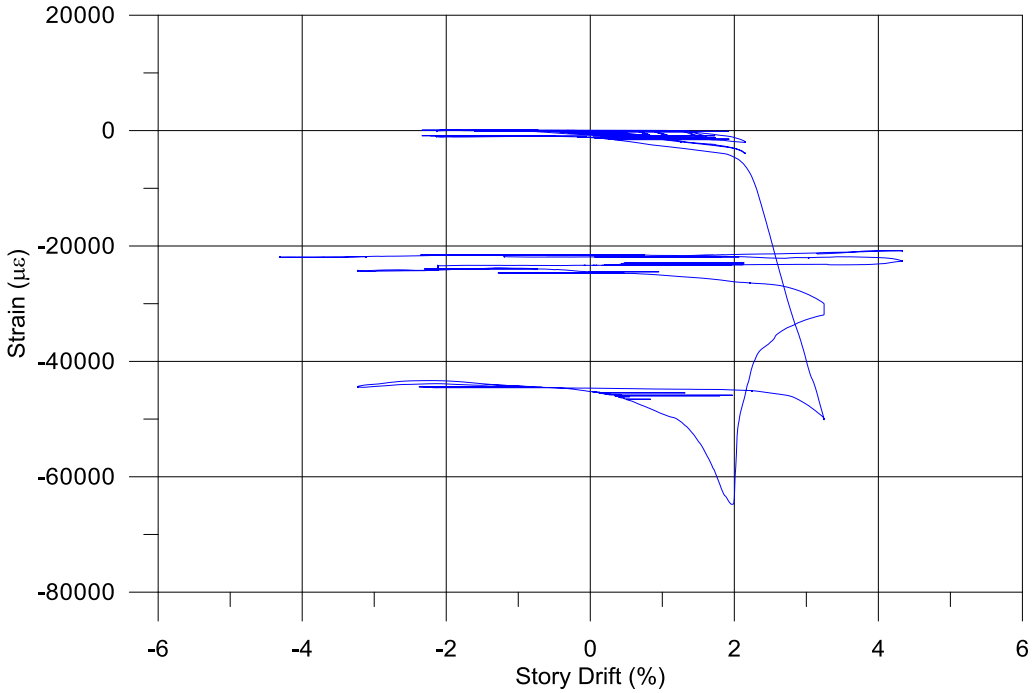

BRB-SW-1-2

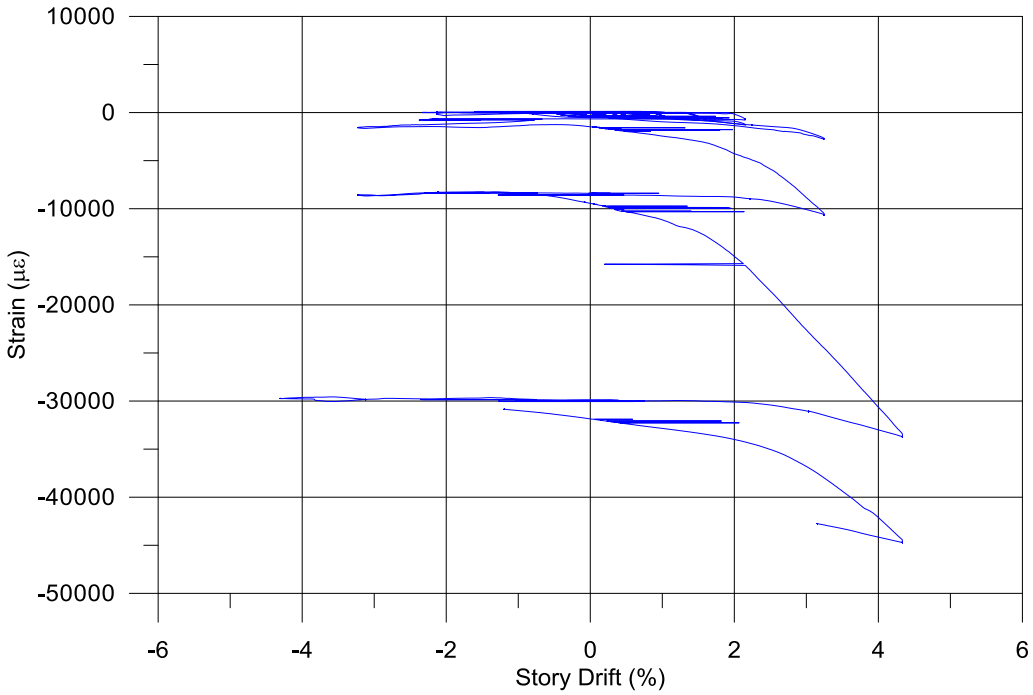

BRB-SW-2-1

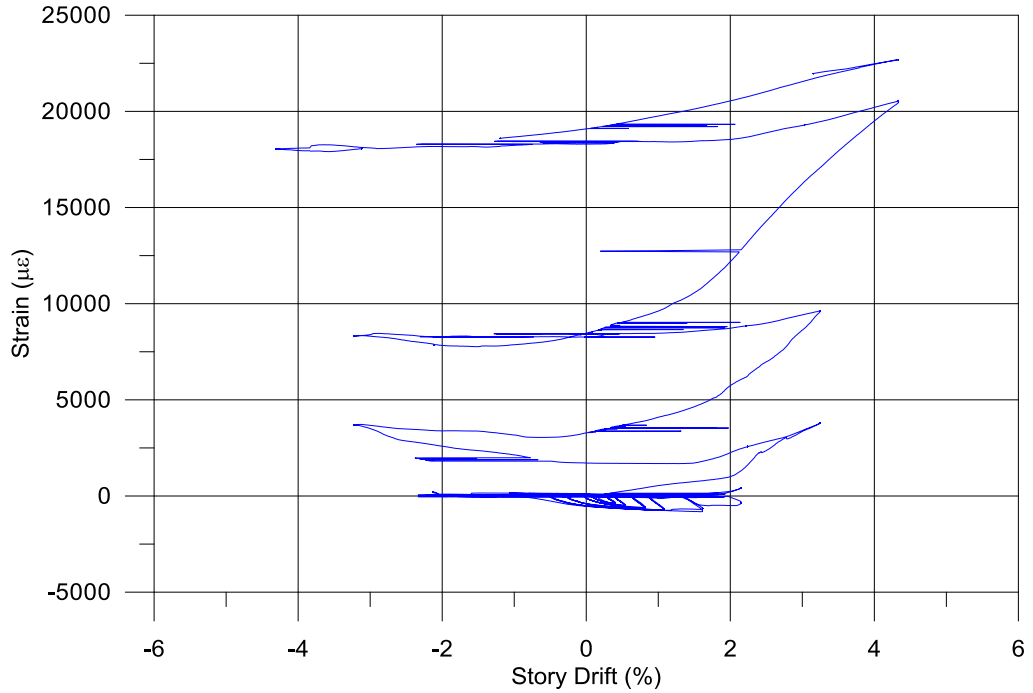

BRB-SW-2-2

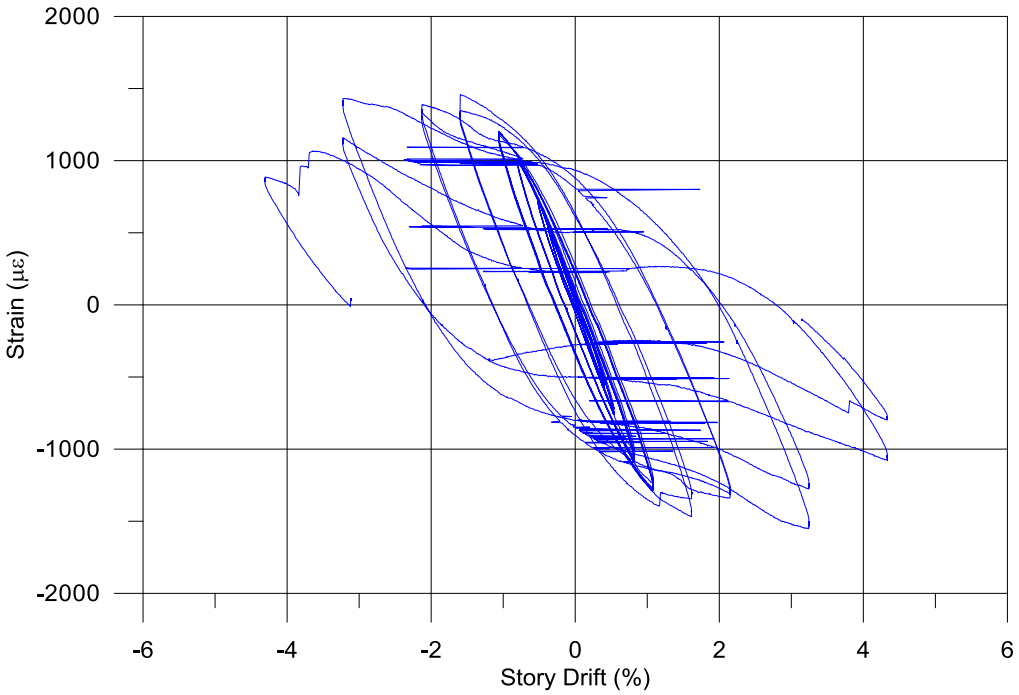
2000
1000
0
-1000
-2000
Strain (με)
-6
-4
-2
0
2
4
6
Story Drift (%)

G-M7-1

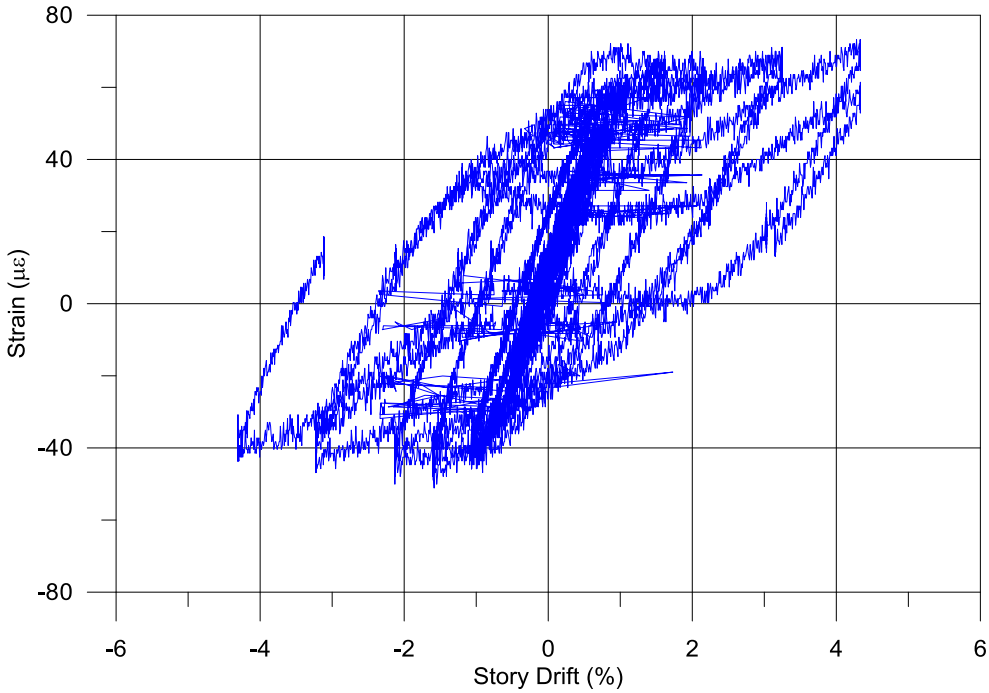
80
40
0
-40
-80
Strain (με)
-6
-4
-2
0
2
4
6
Story Drift (%)

G-M7-2

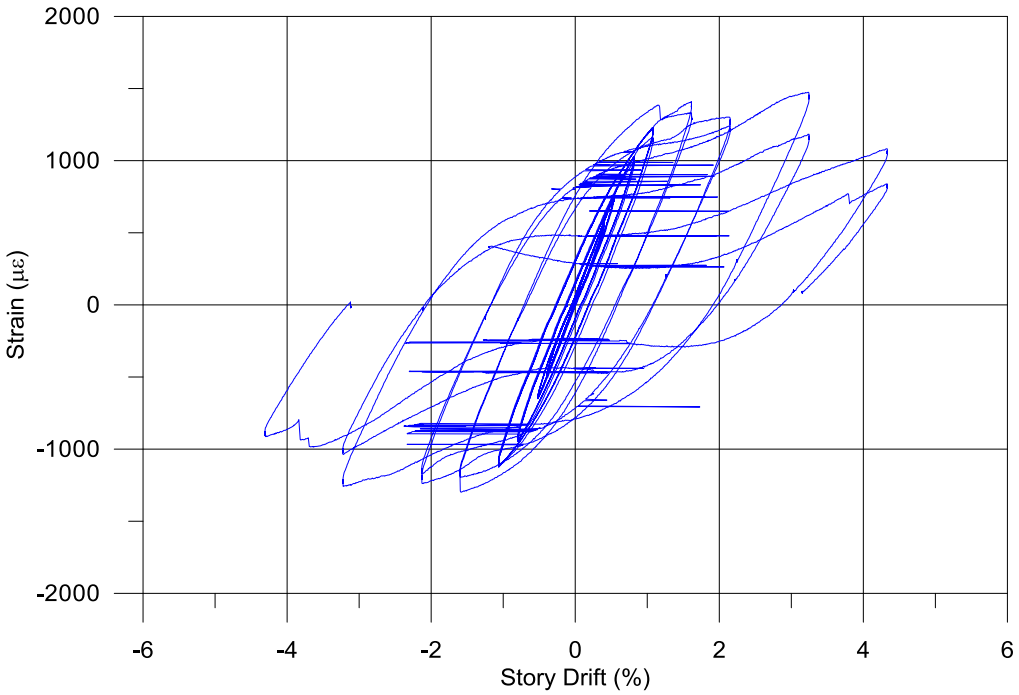
2000
1000
0
-1000
-2000
Strain (με)
-6
-4
-2
0
2
4
6
Story Drift (%)

G-M7-3

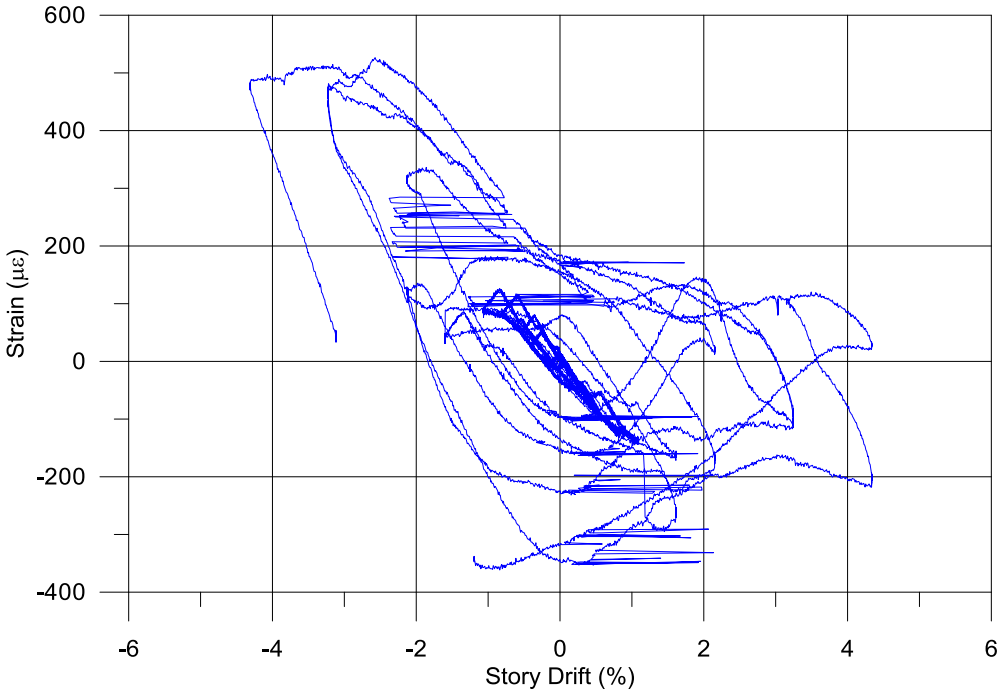
600
400
200
0
-200
-400
Strain (με)
-6
-4
-2
0
2
4
6
Story Drift (%)

G-P48-1

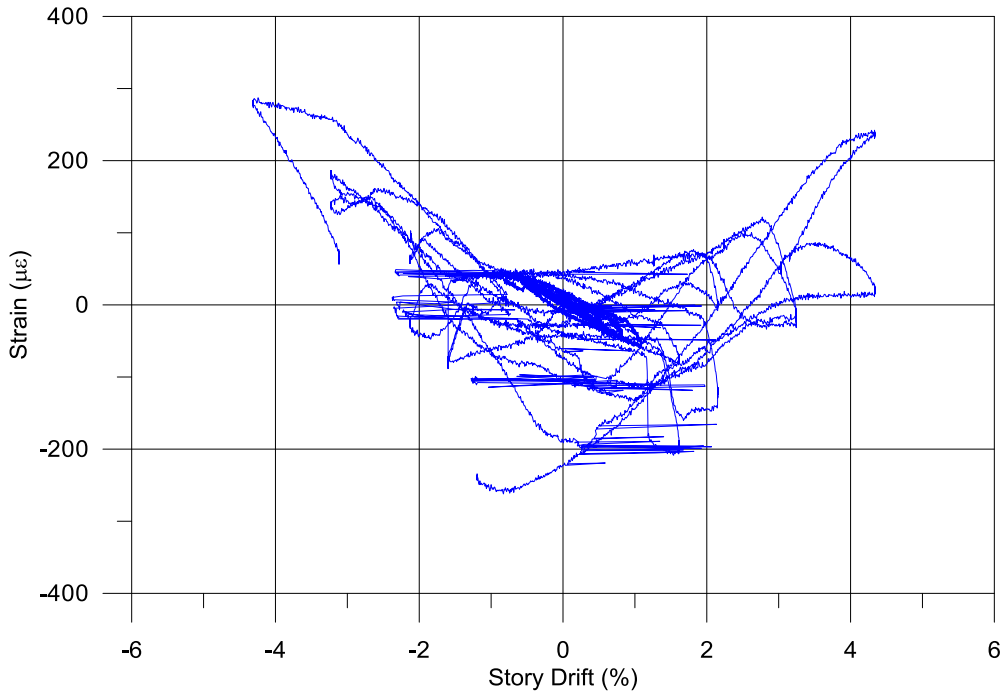
400
200
0
-200
-400
Strain (με)
-6
-4
-2
0
2
4
6
Story Drift (%)

G-P48-2

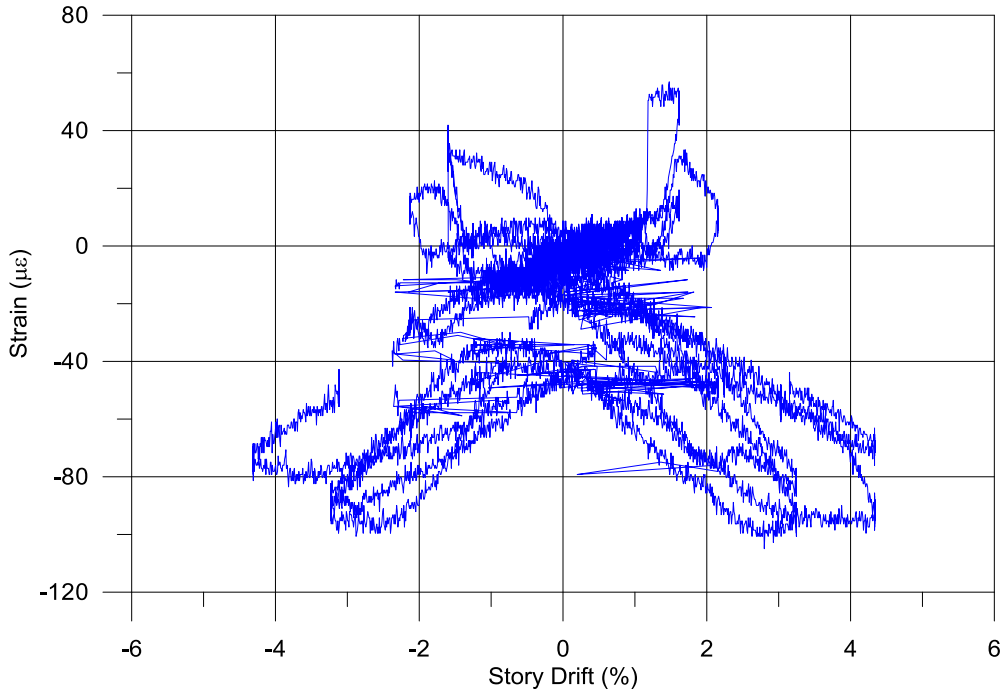
80
40
0
-40
-80
-120
Strain (με)
-6
-4
-2
0
2
4
6
Story Drift (%)

G-P48-3

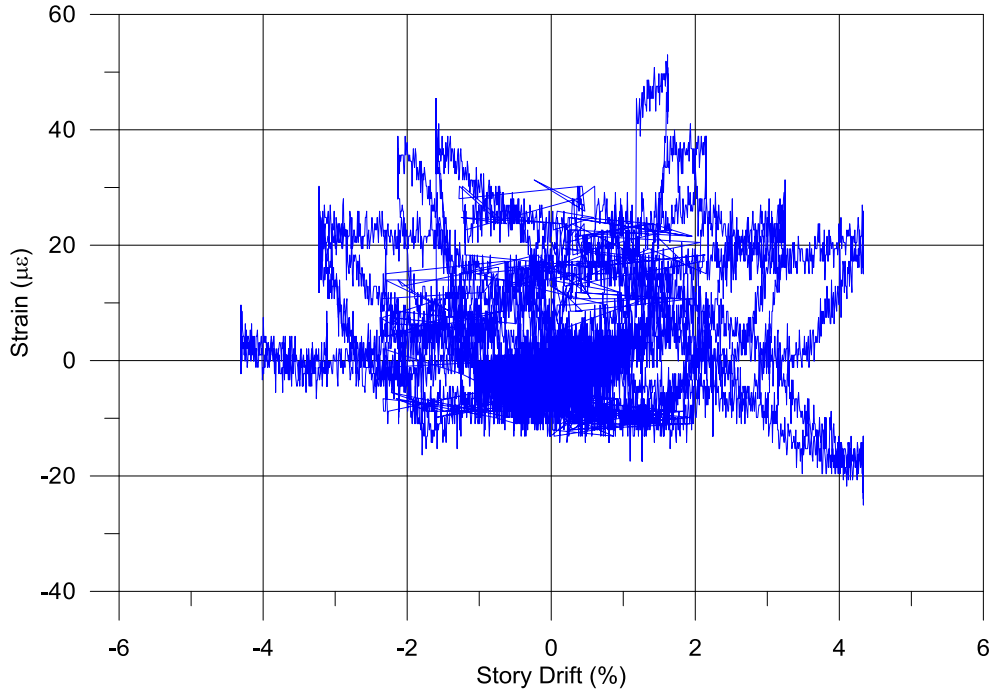
60
40
20
0
-20
-40
Strain (με)
-6
-4
-2
0
2
4
6
Story Drift (%)

G-P48-4

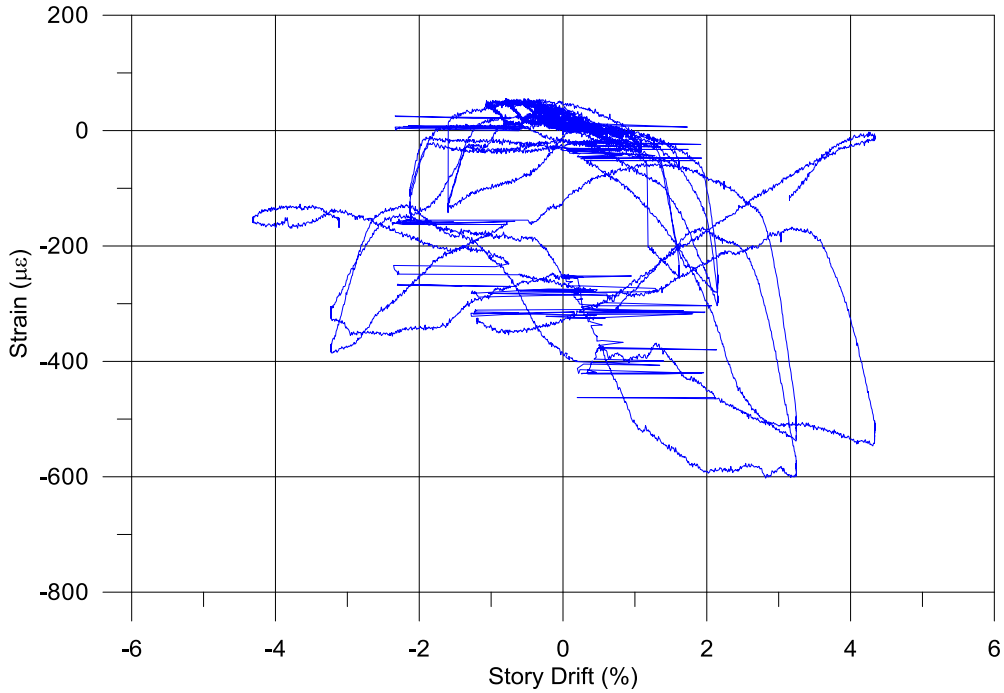
200
0
-200
-400
-600
-800
Strain (με)
-6
-4
-2
0
2
4
6
Story Drift (%)

G-P48-5

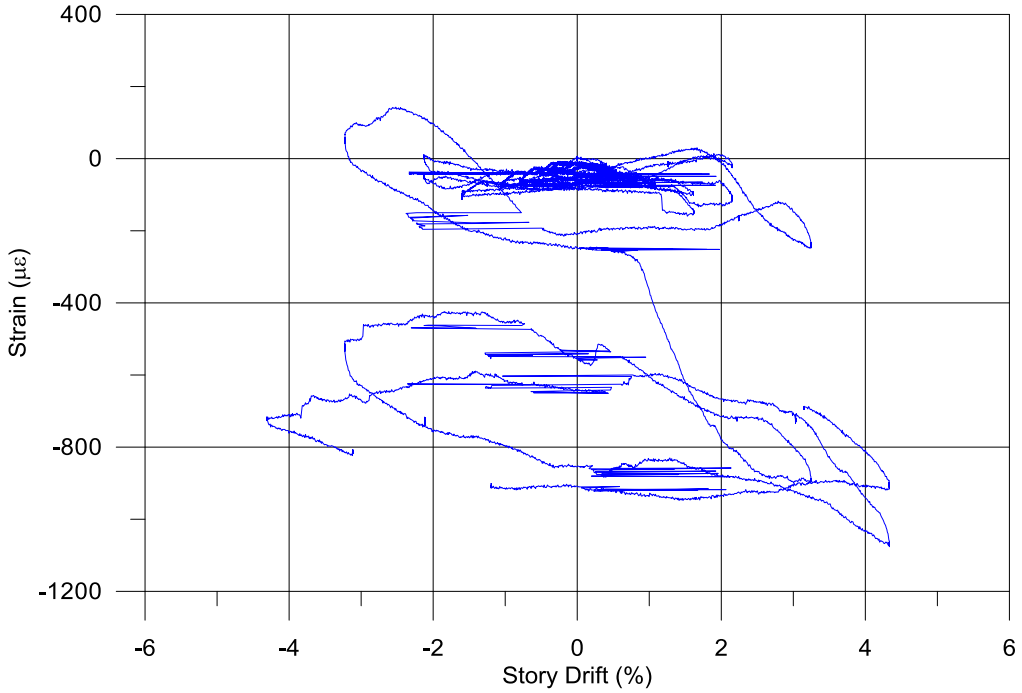
400
0
-400
-800
-1200
Strain (με)
-6
-4
-2
0
2
4
6
Story Drift (%)

G-P48-7

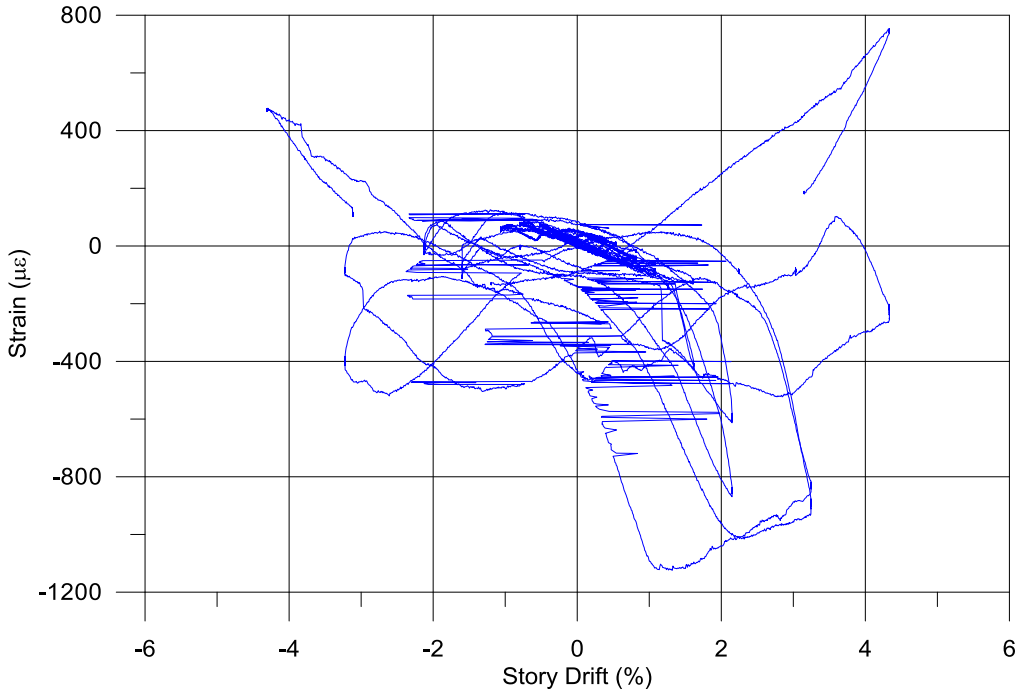
800
400
0
-400
-800
-1200
Strain (με)
-6
-4
-2
0
2
4
6
Story Drift (%)

G-P48-8

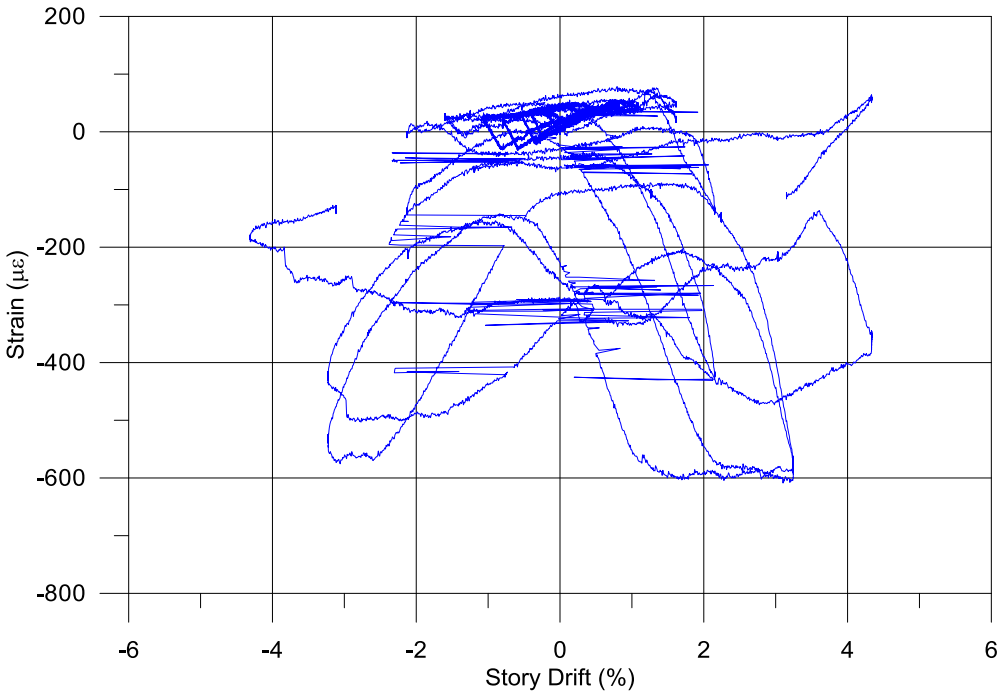

G-P48-RS1-1

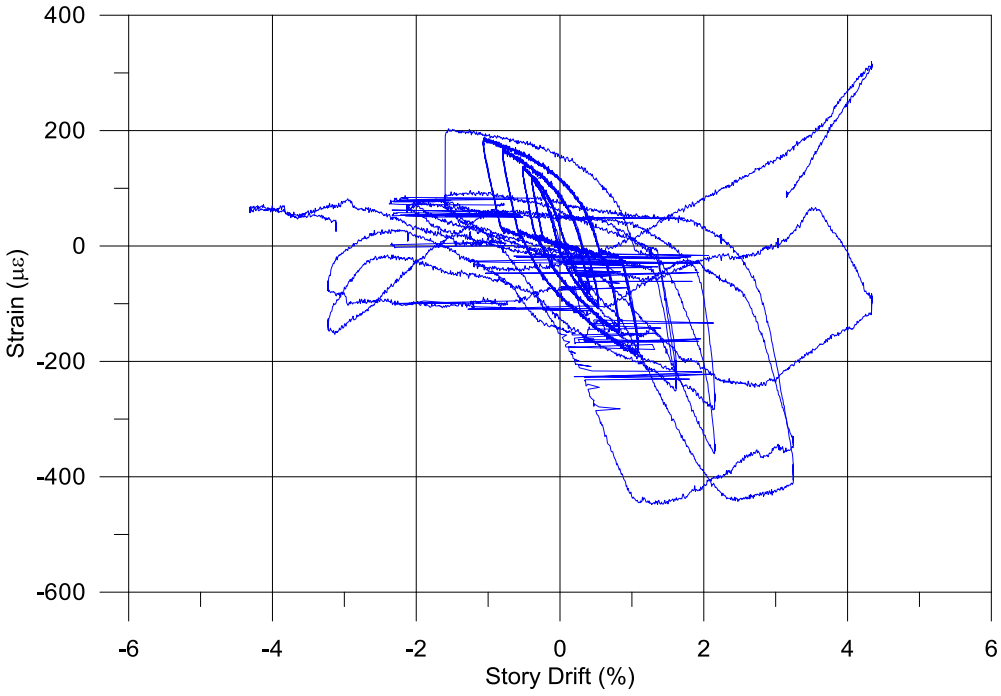

G-P48-RS1-2

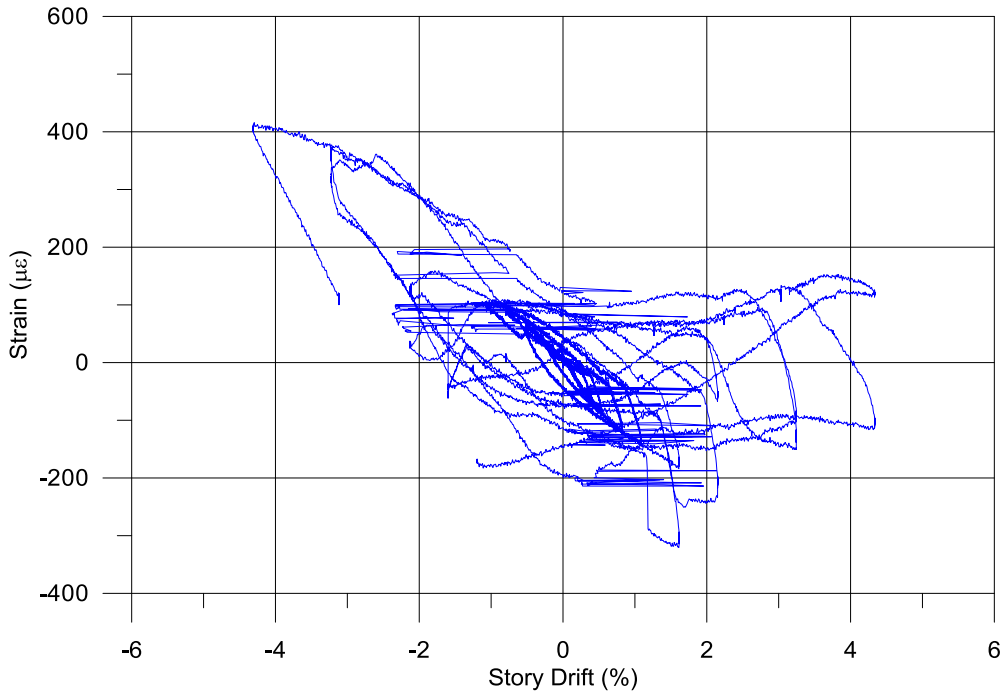

G-P48-RS1-3

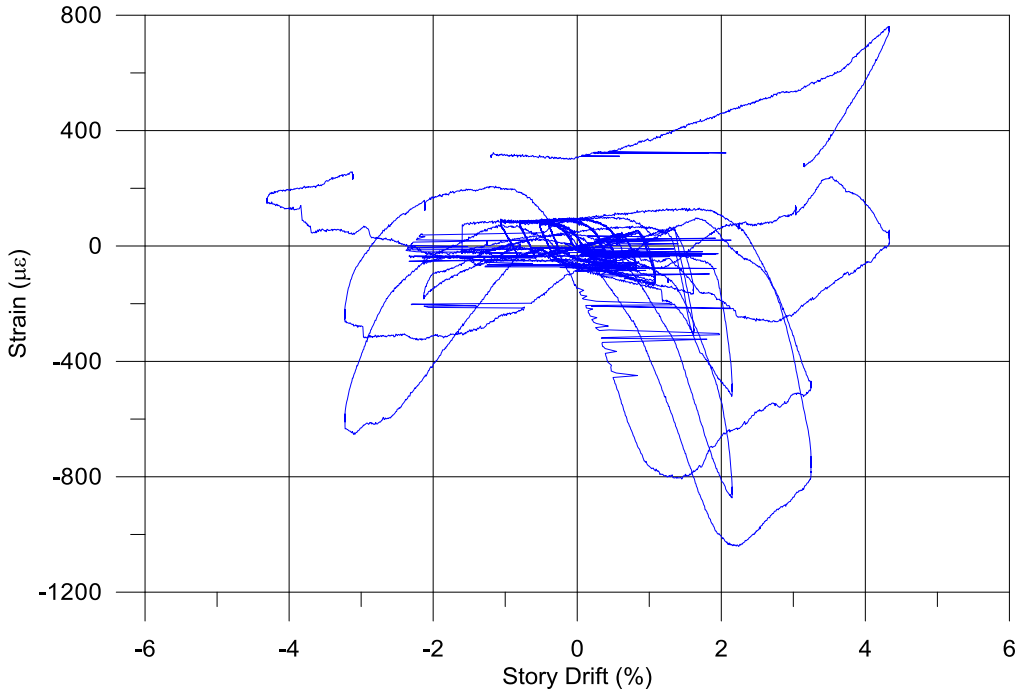

G-P48-RS2-1

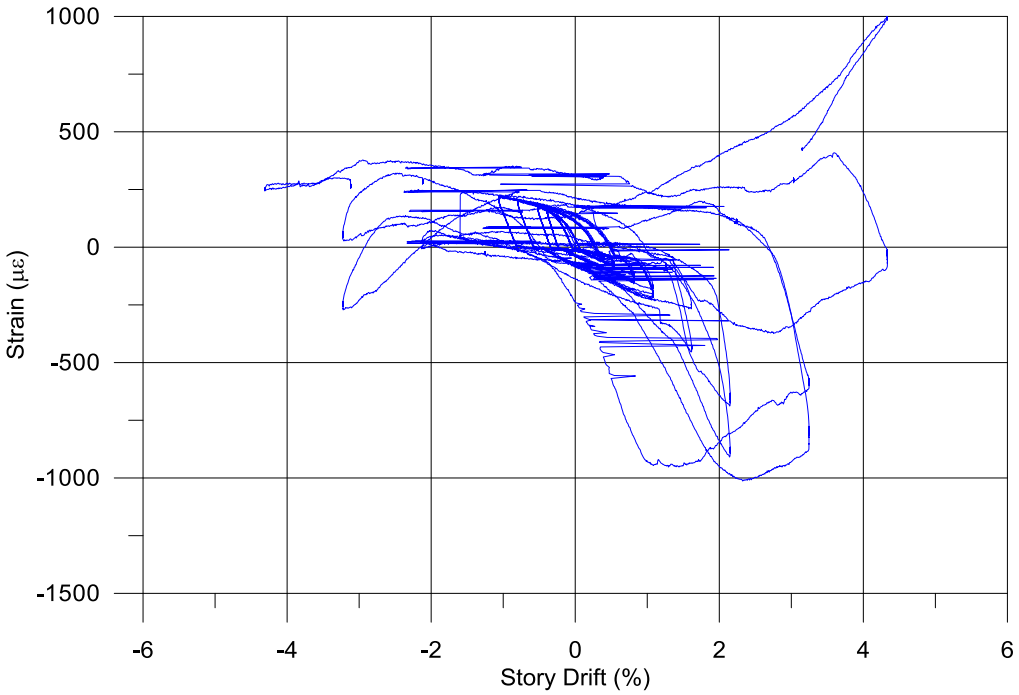

G-P48-RS2-2

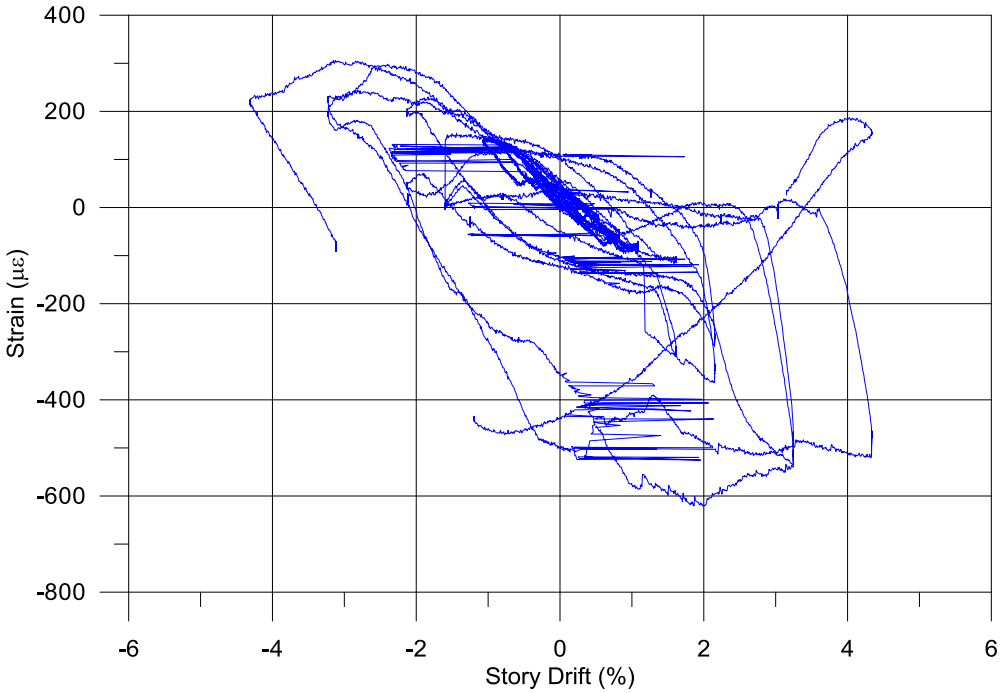

G-P48-RS2-3

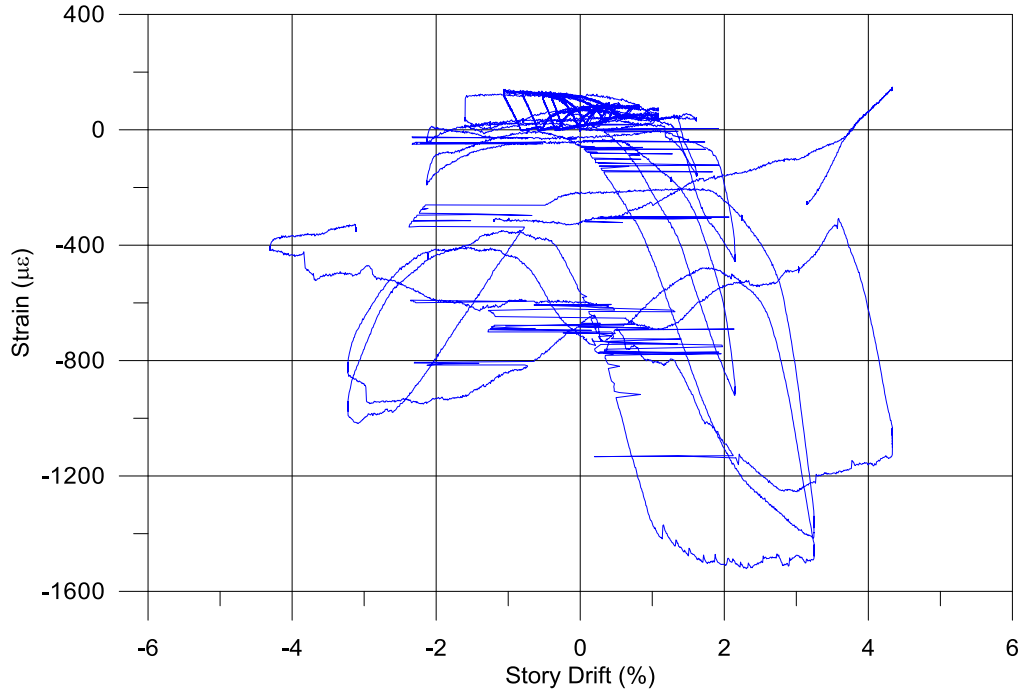

G-P48-RS3-1

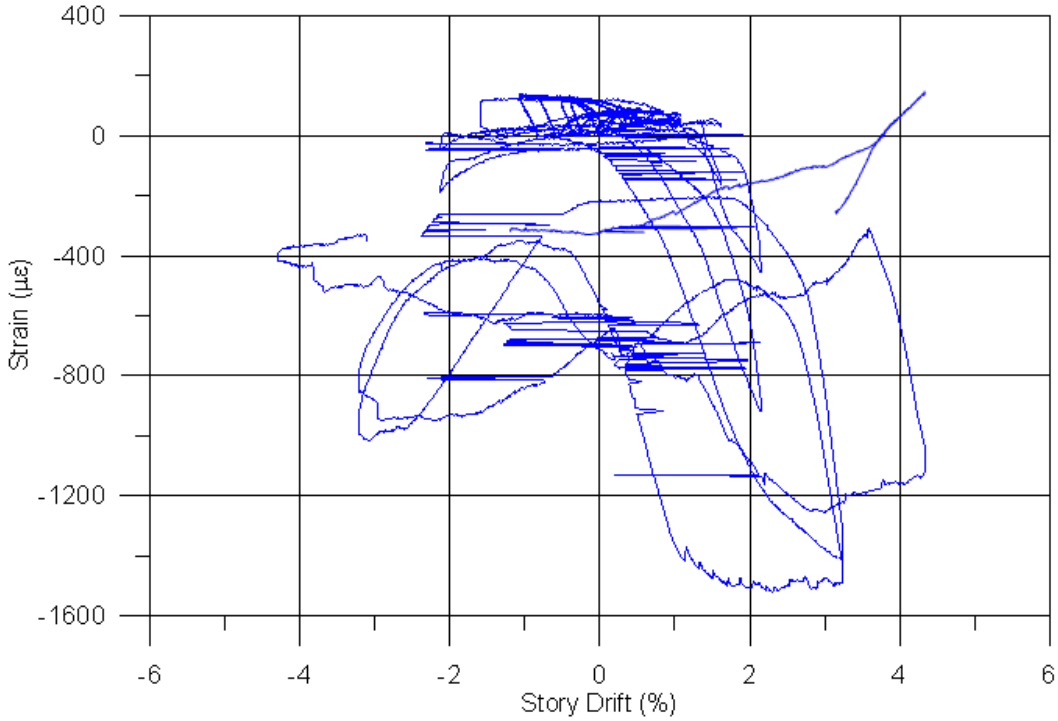

G-P48-RS3-2

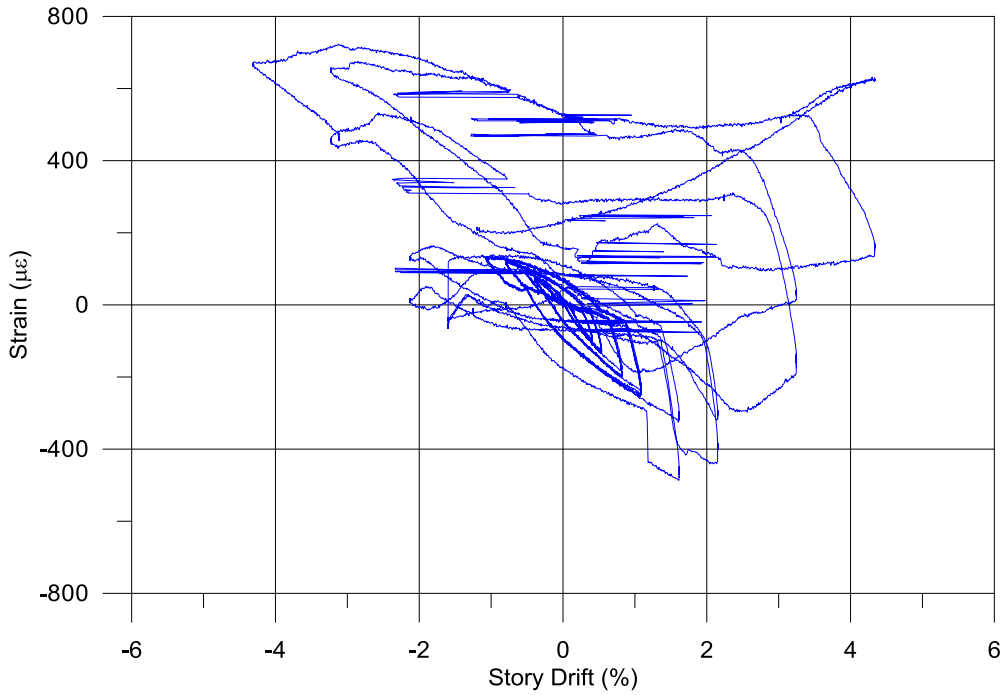

G-P48-RS3-3

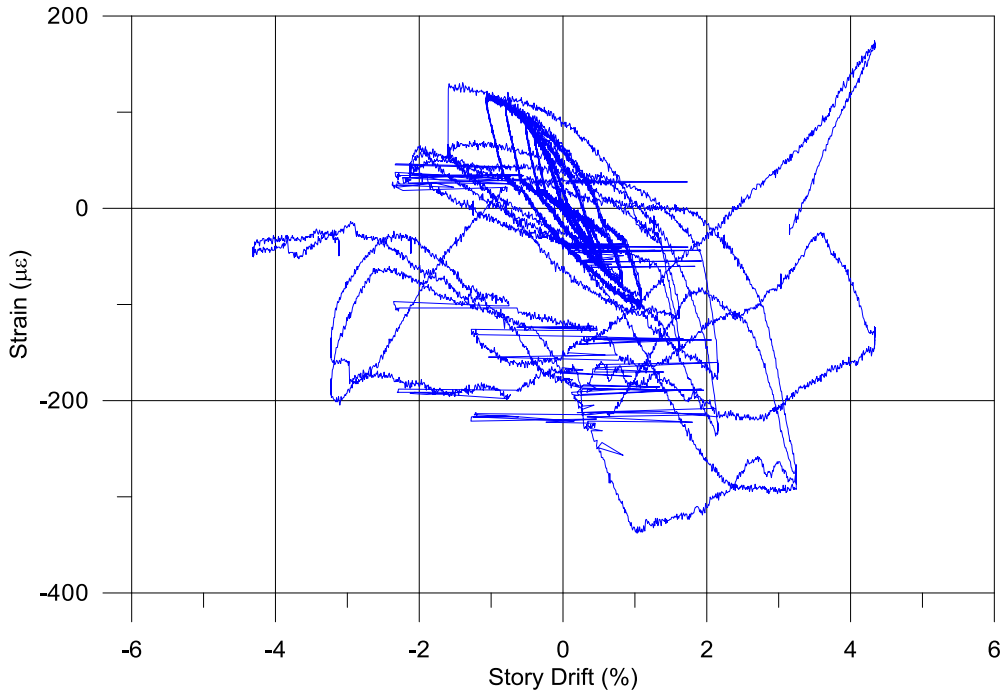

G-P48-RS4-1

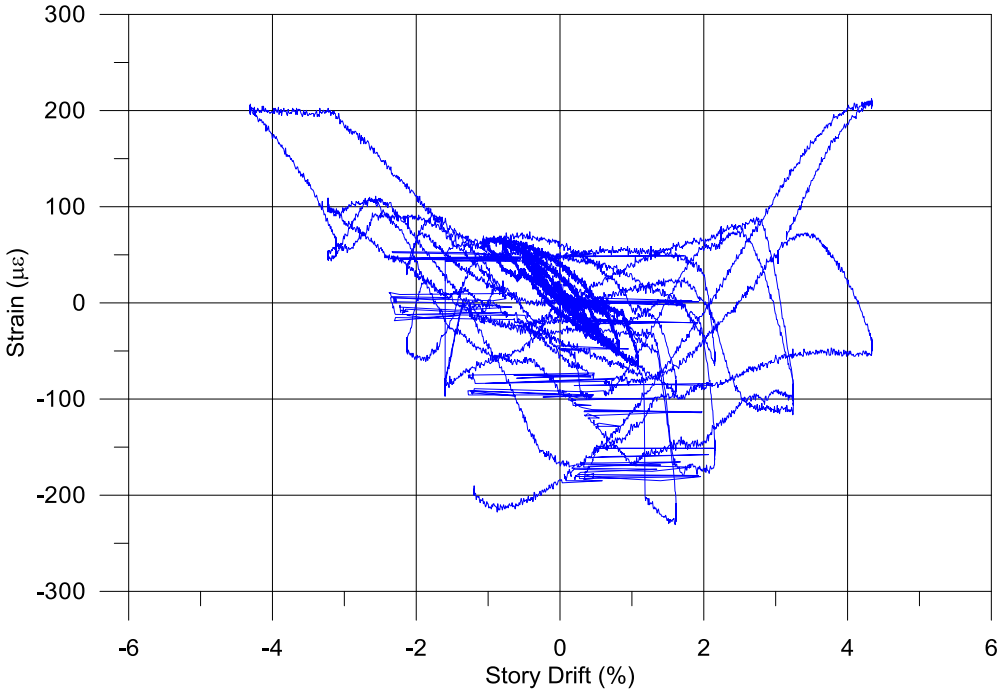

G-P48-RS4-2

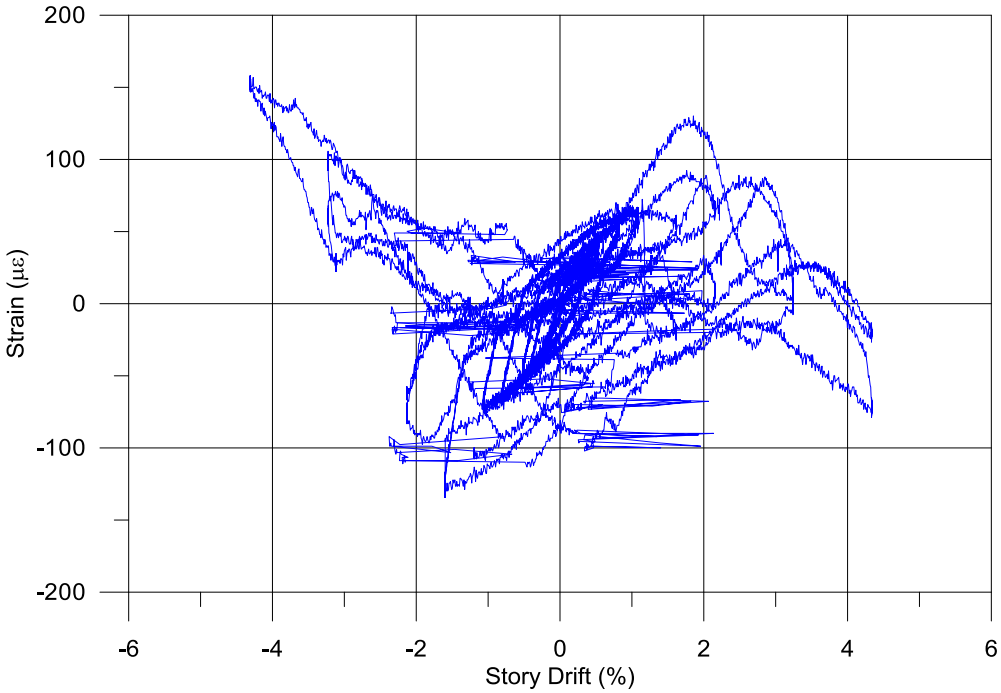

G-P48-RS4-3

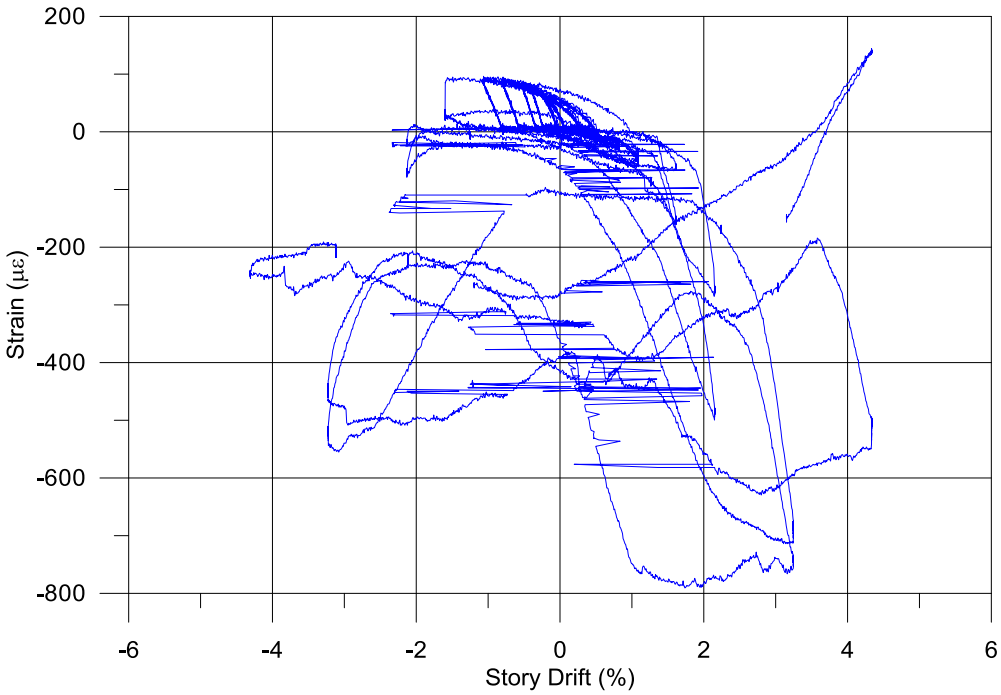

G-P48-RS5-1

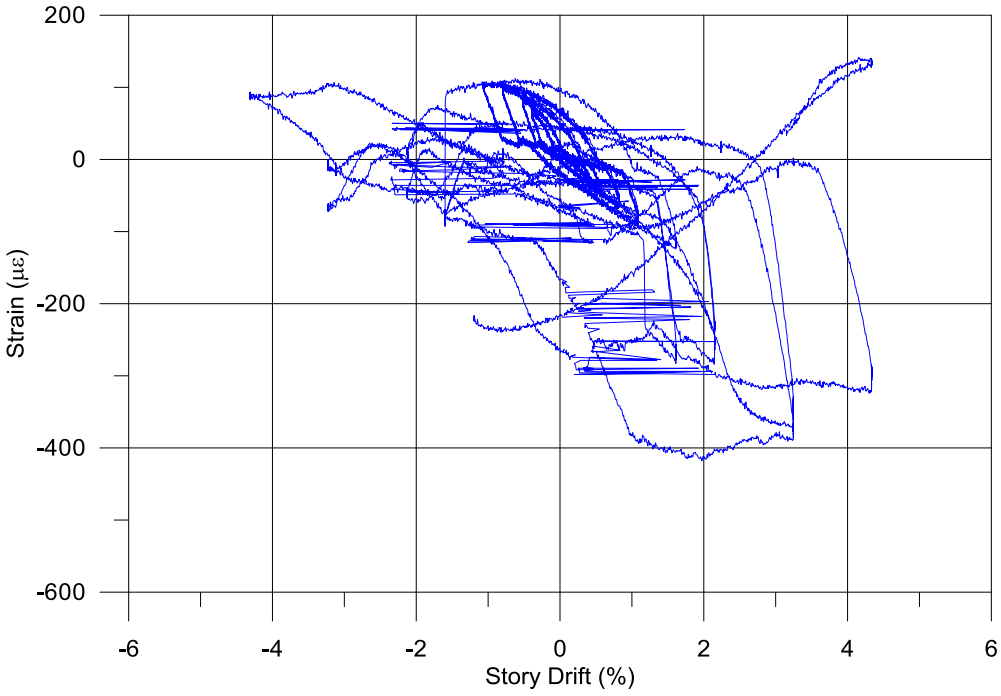

G-P48-RS5-2

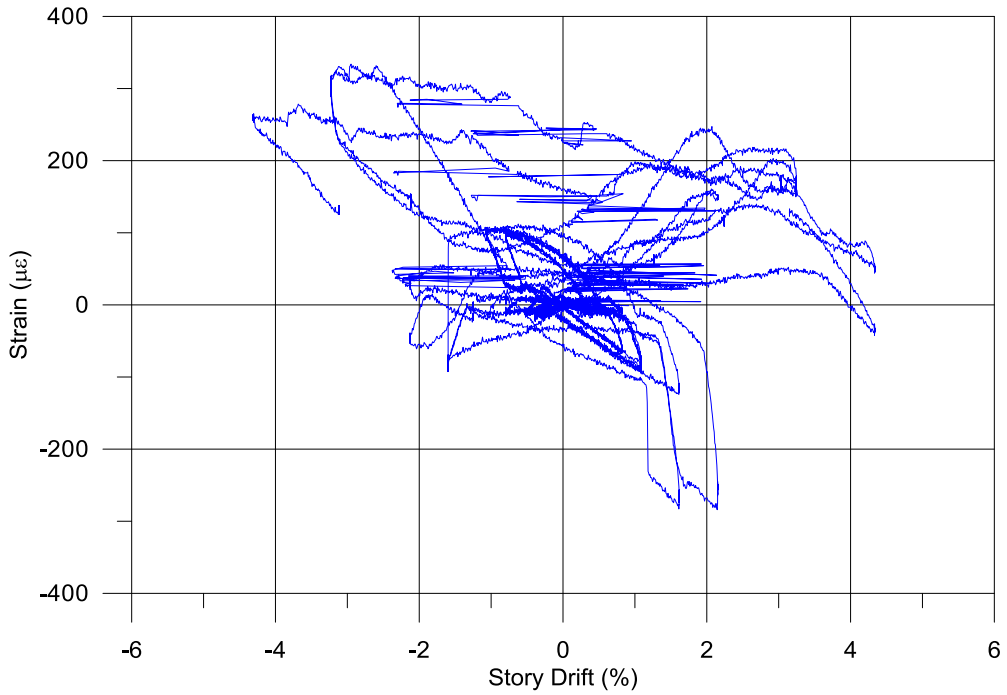

G-P48-RS5-3

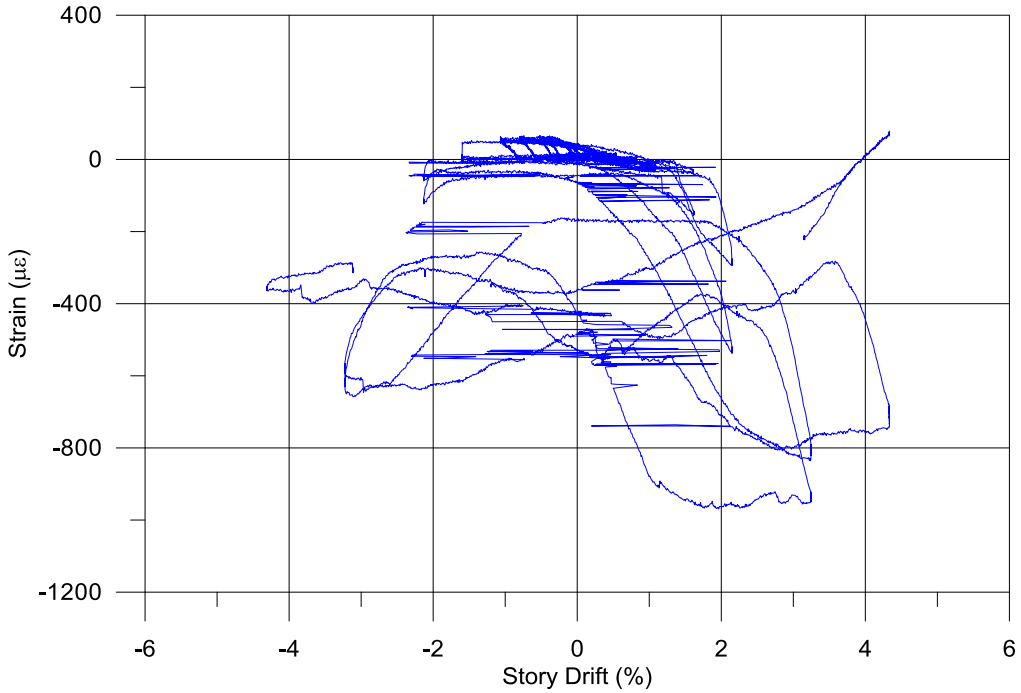

G-P48-RS6-1

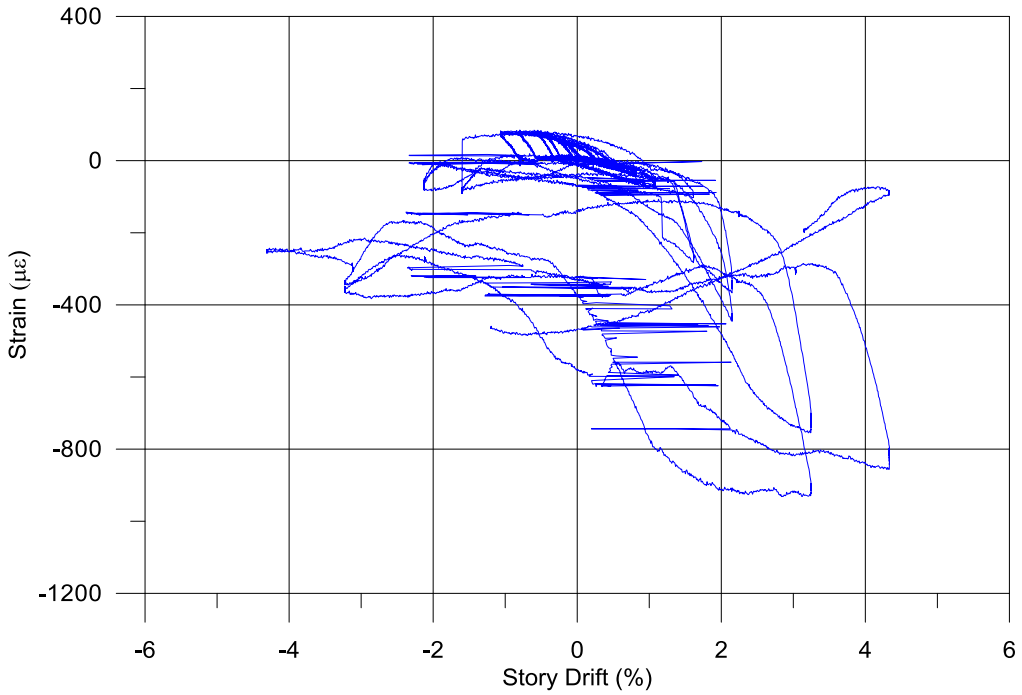

G-P48-RS6-2

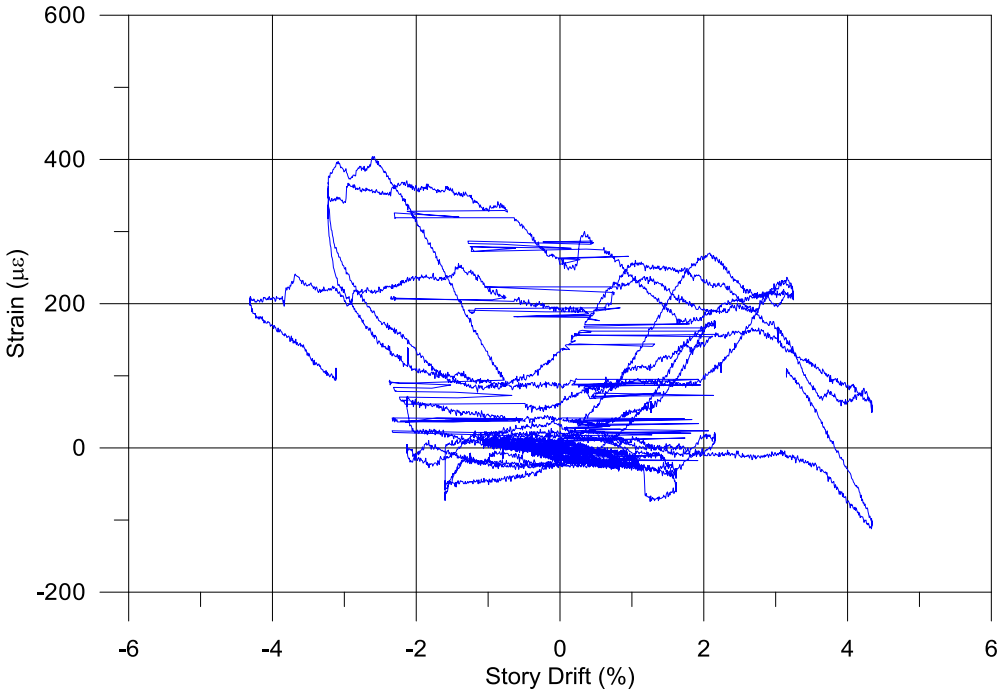

G-P48-RS6-3

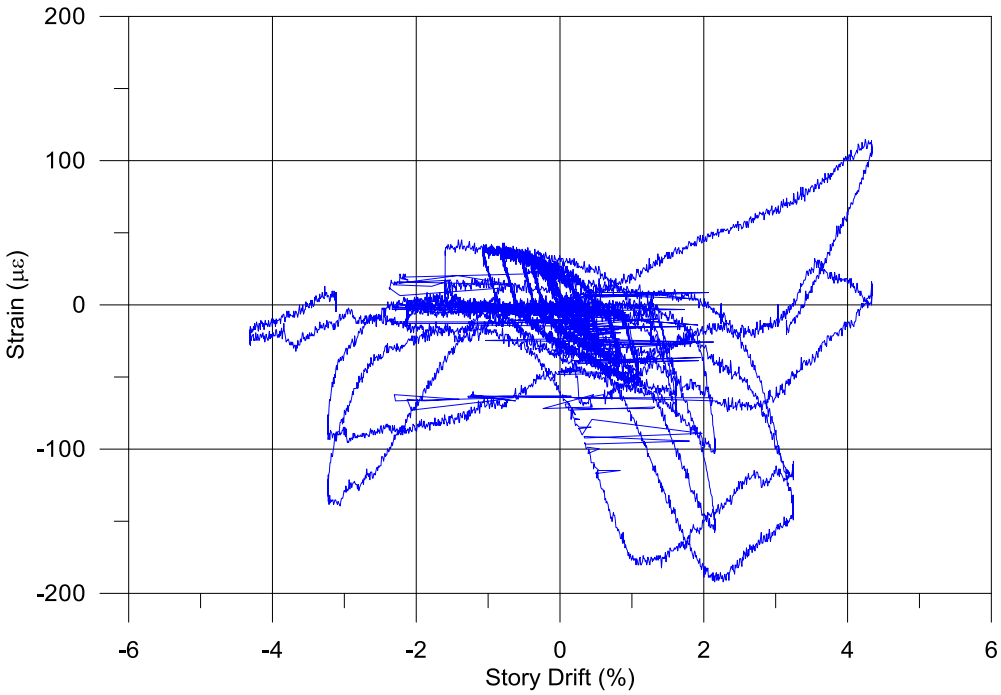
200
100
0
-100
-200
Strain (με)
-6
-4
-2
0
2
4
6
Story Drift (%)

G-P54

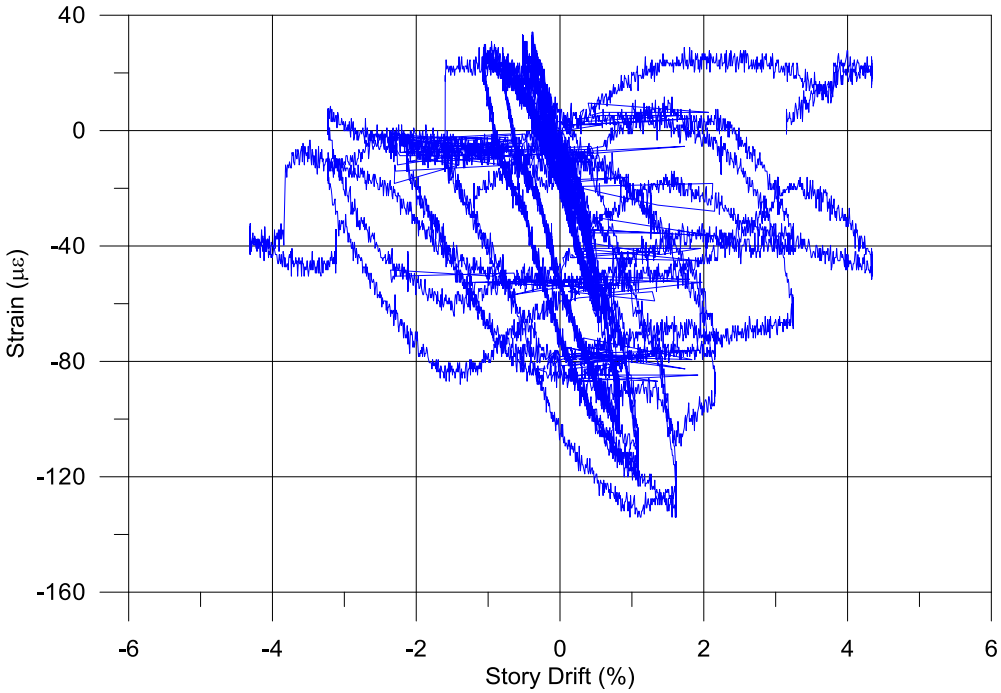
40
0
-40
-80
-120
-160
Strain (με)
-6
-4
-2
0
2
4
6
Story Drift (%)

G-P56

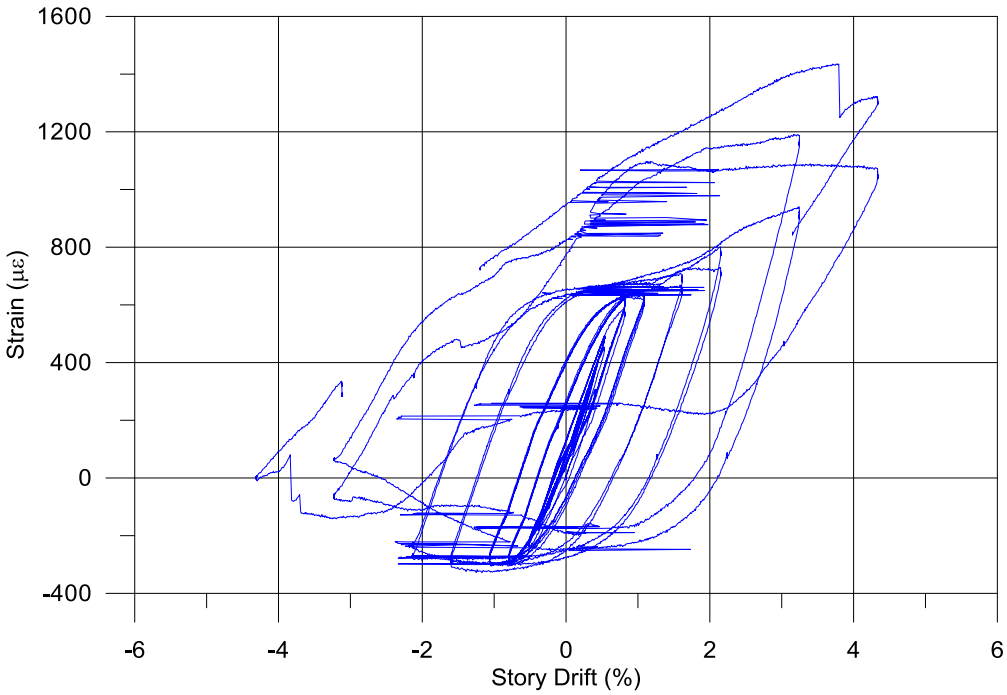
1600
1200
800
400
0
-400
Strain (με)
-6
-4
-2
0
2
4
6
Story Drift (%)

G-P57-1

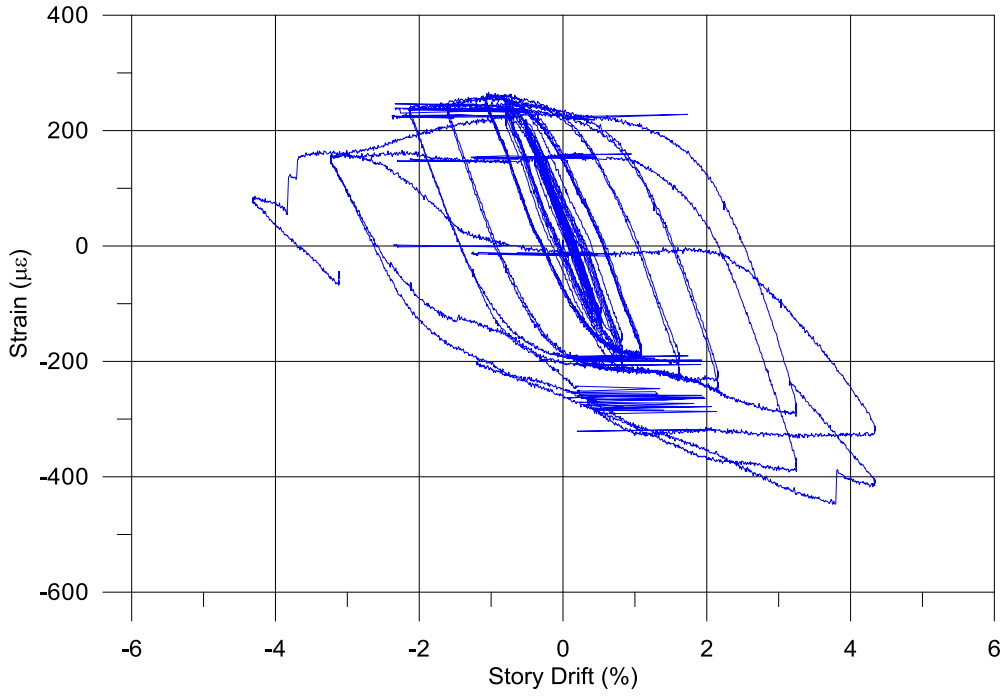
400
200
0
-200
-400
-600
Strain (με)
-6
-4
-2
0
2
4
6
Story Drift (%)

G-P57-2

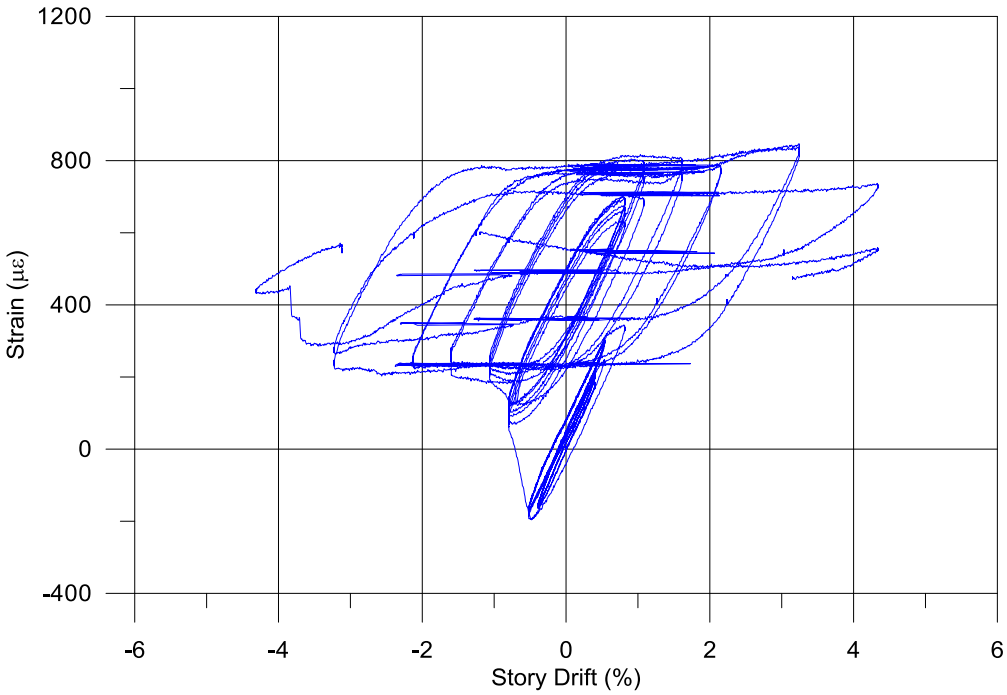
1200
800
400
0
-400
Strain (με)
-6
-4
-2
0
2
4
6
Story Drift (%)

G-P57-3

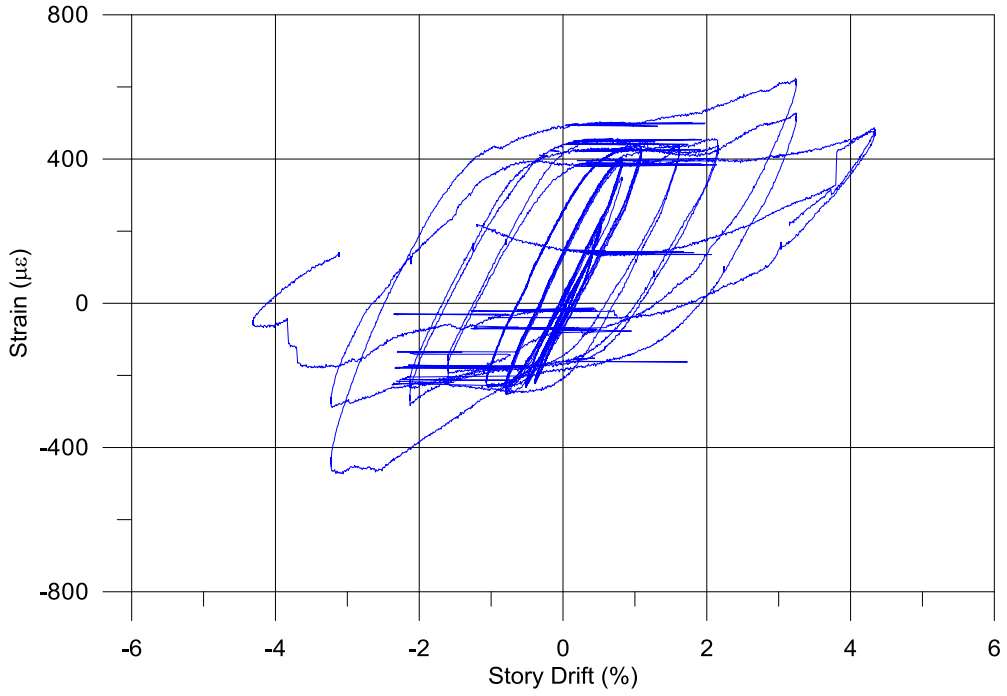
800
400
0
-400
-800
Strain (με)
-6
-4
-2
0
2
4
6
Story Drift (%)

G-P57-4

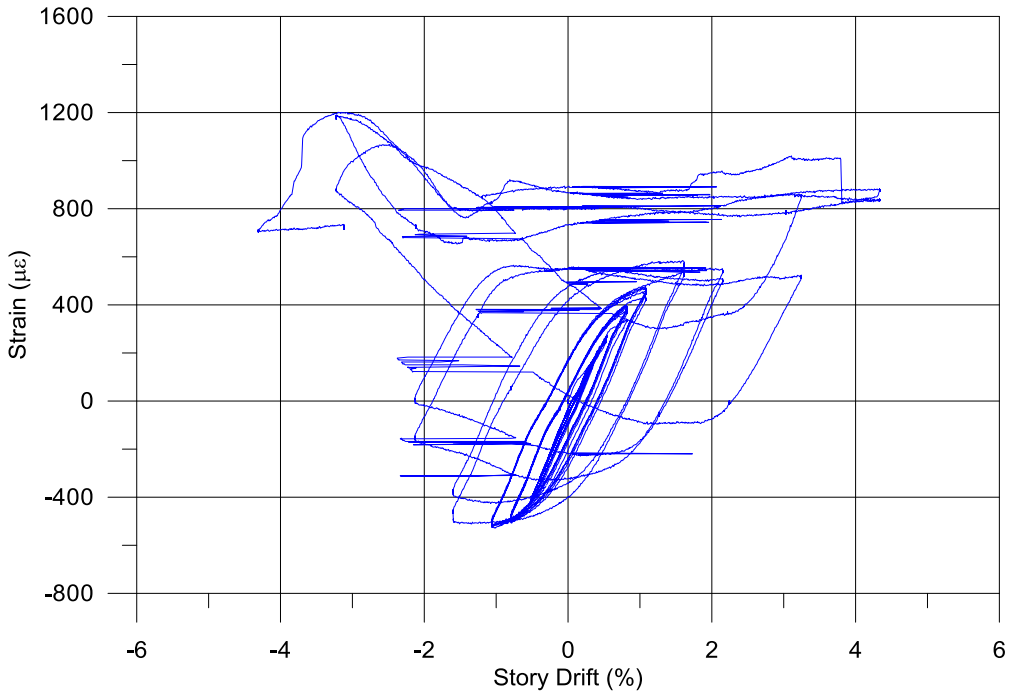
1600
1200
800
400
0
-400
-800
Strain (με)
-6
-4
-2
0
2
4
6
Story Drift (%)

G-P57-5

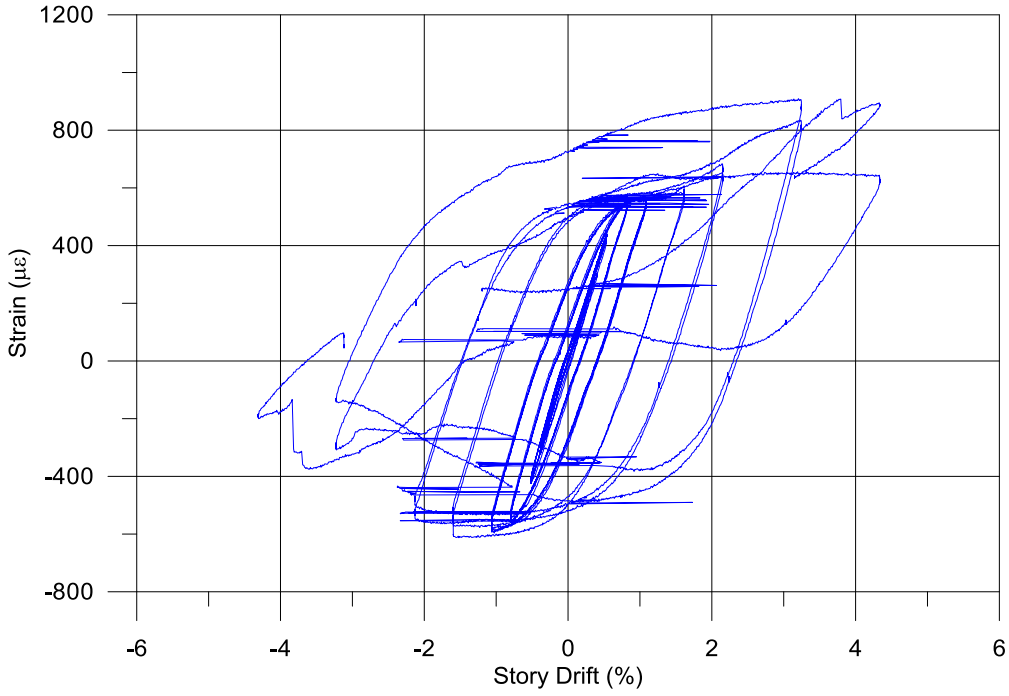
1200
800
400
0
-400
-800
Strain (με)
-6
-4
-2
0
2
4
6
Story Drift (%)

G-P57-6

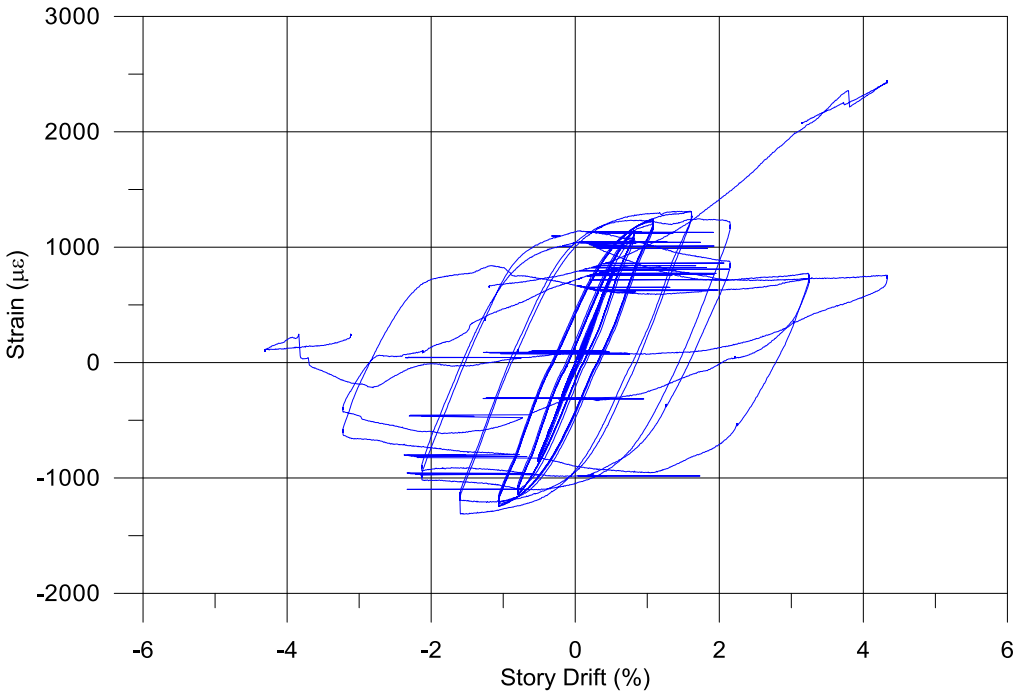

G-P57-7

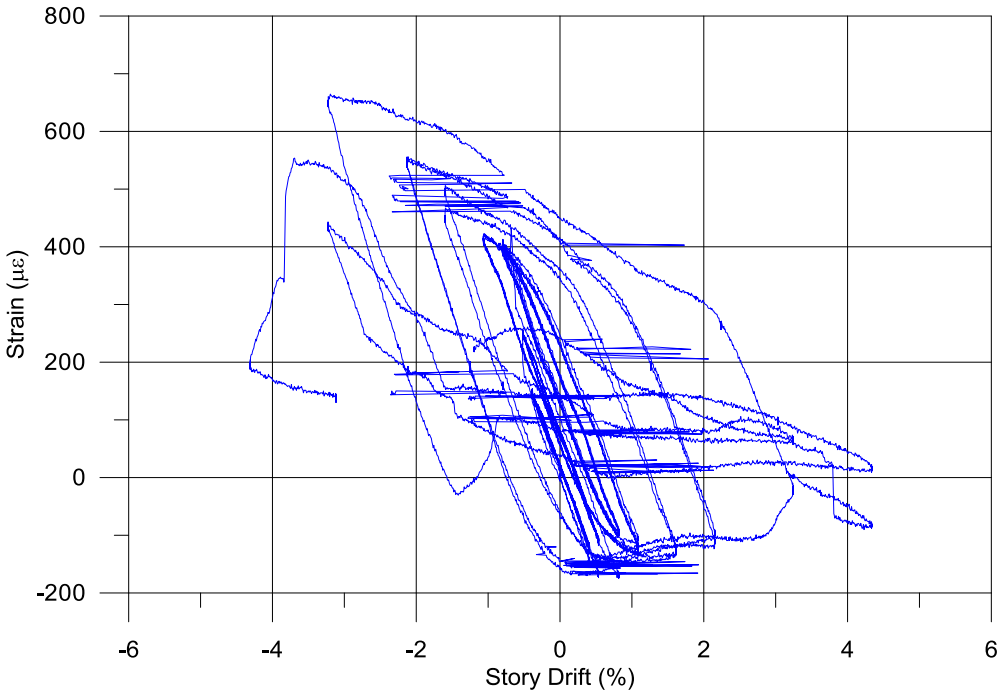

G-P57-RS1-1

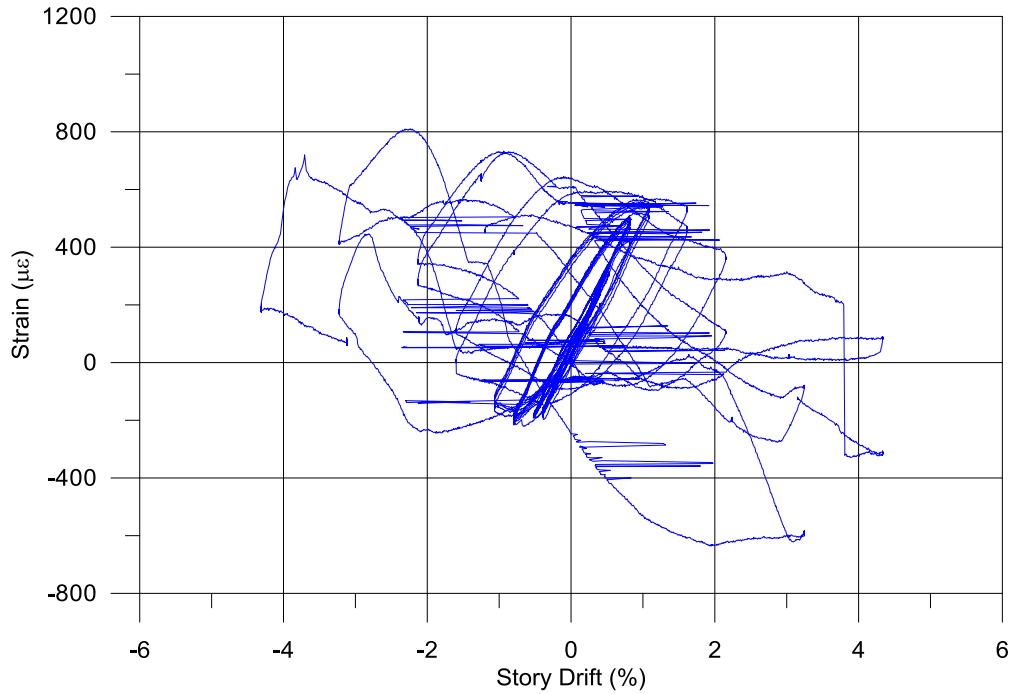

G-P57-RS1-2

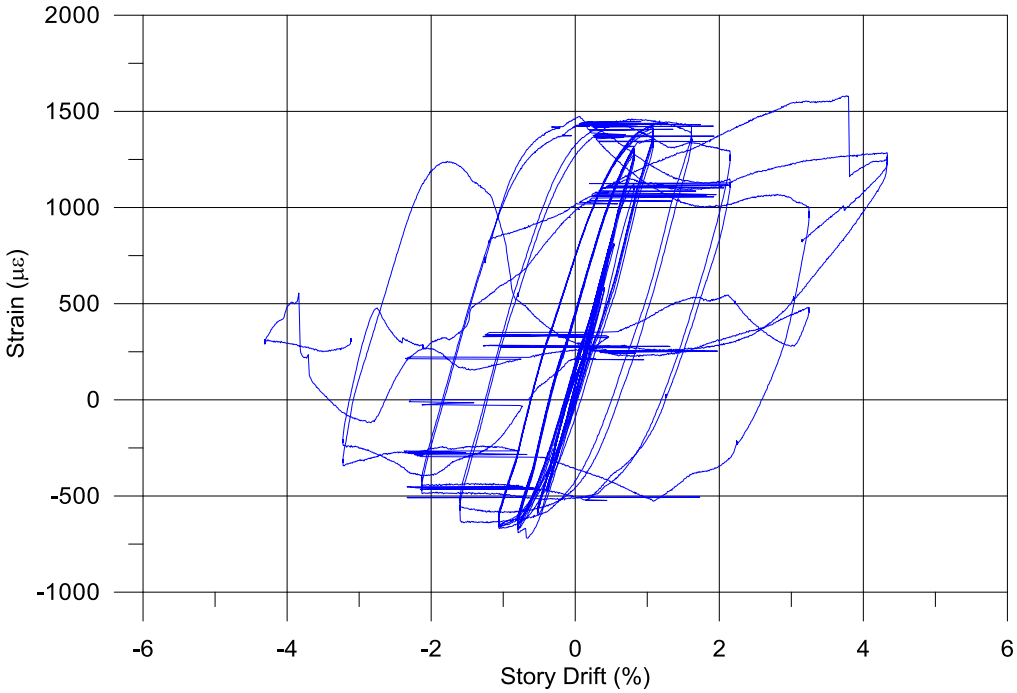

G-P57-RS1-3

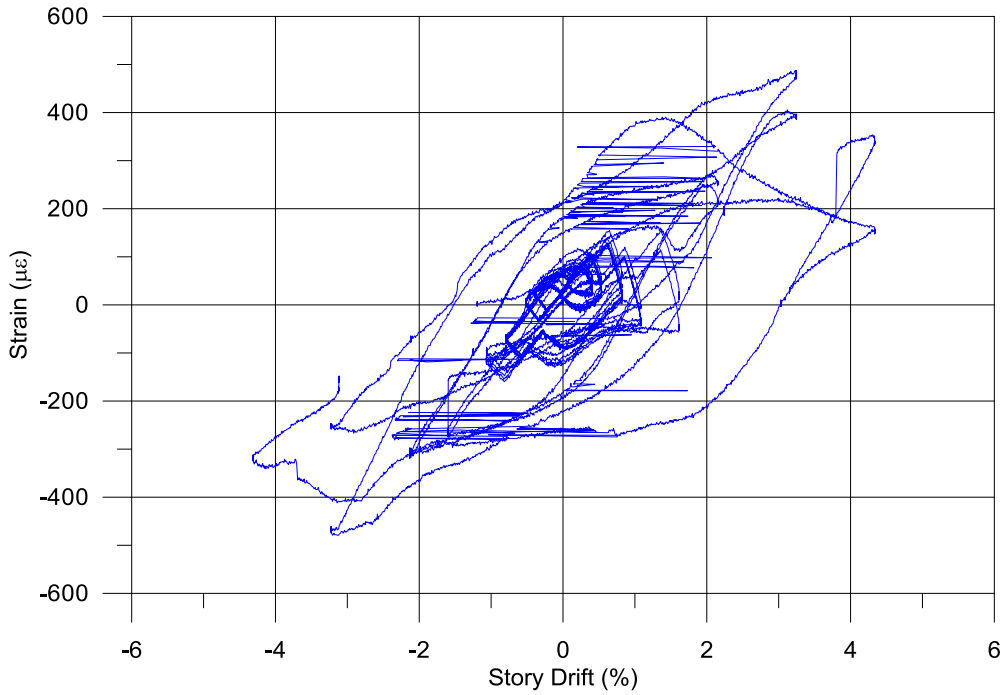

G-P57-RS2-1

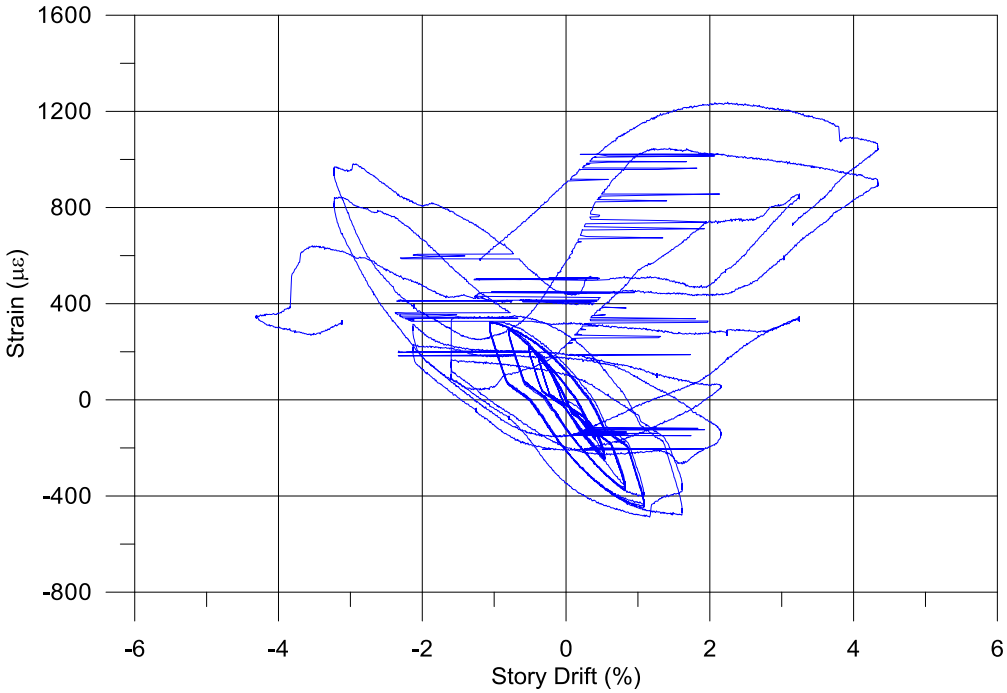

G-P57-RS2-2

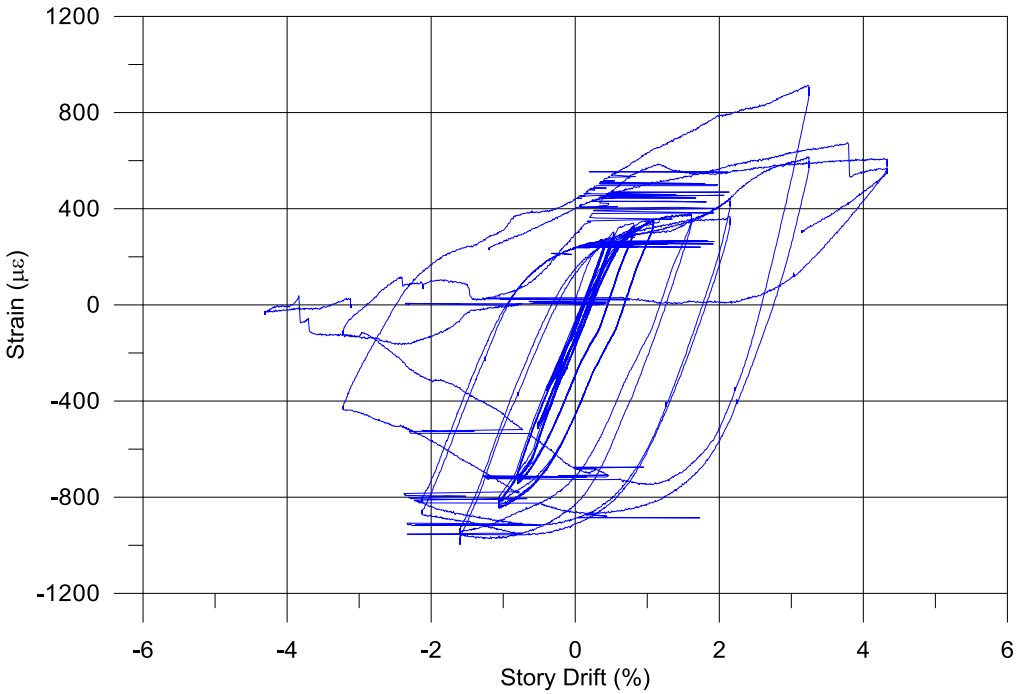

G-P57-RS2-3

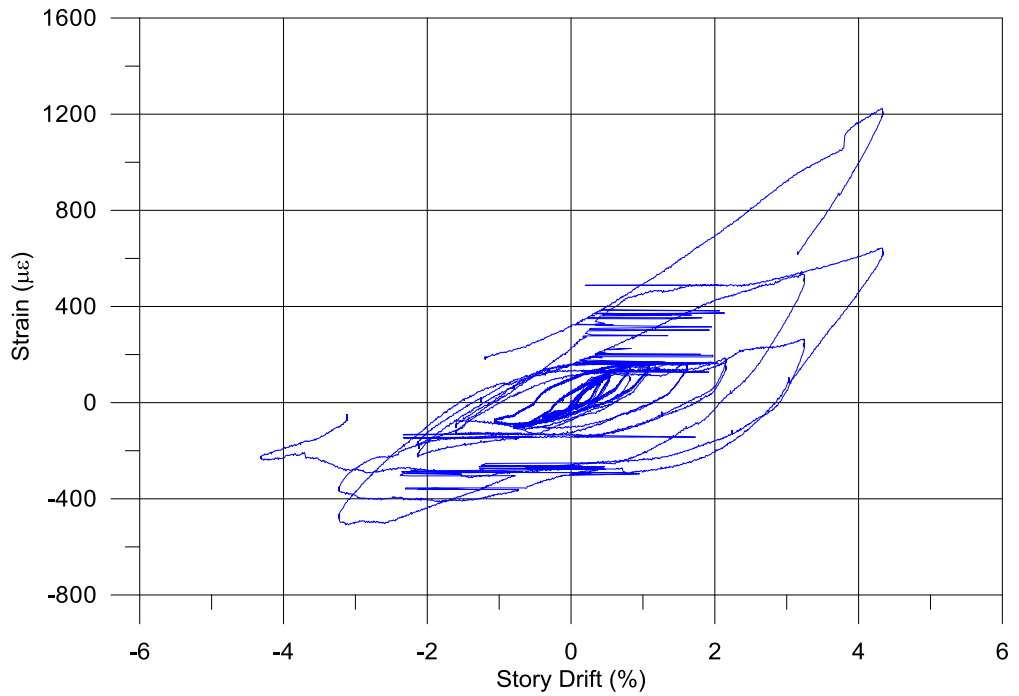

G-P57-RS3-1

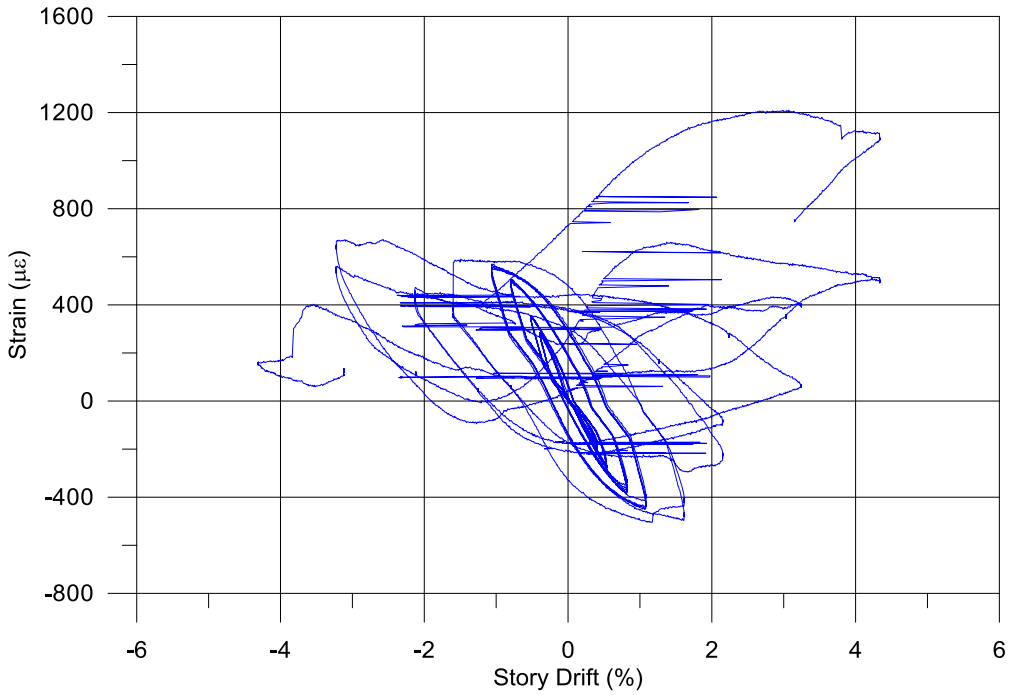

G-P57-RS3-2

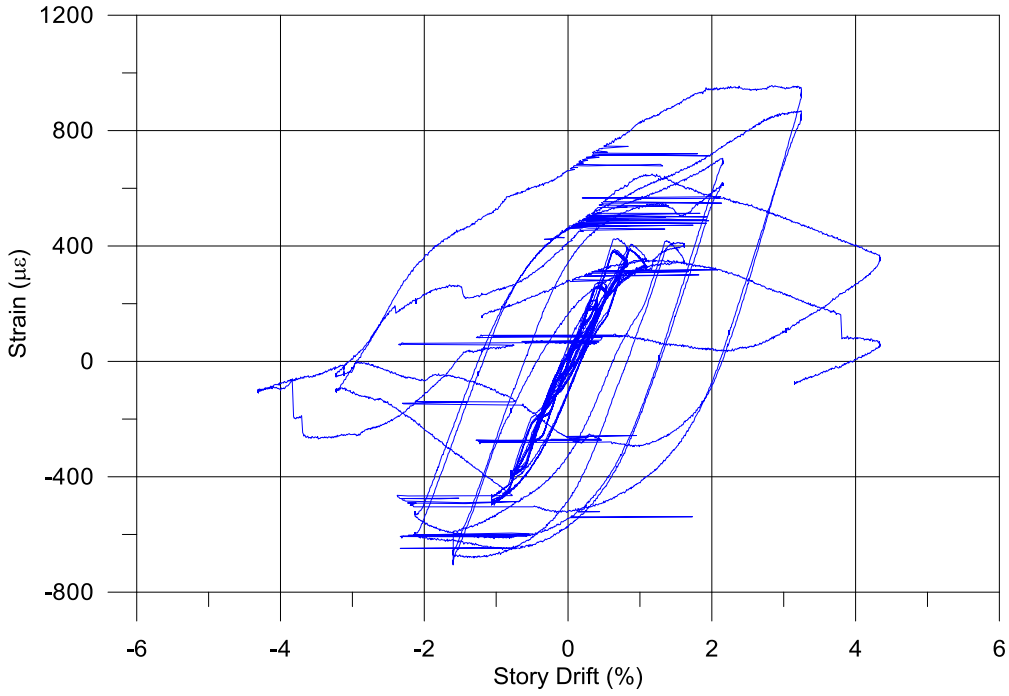

G-P57-RS3-3

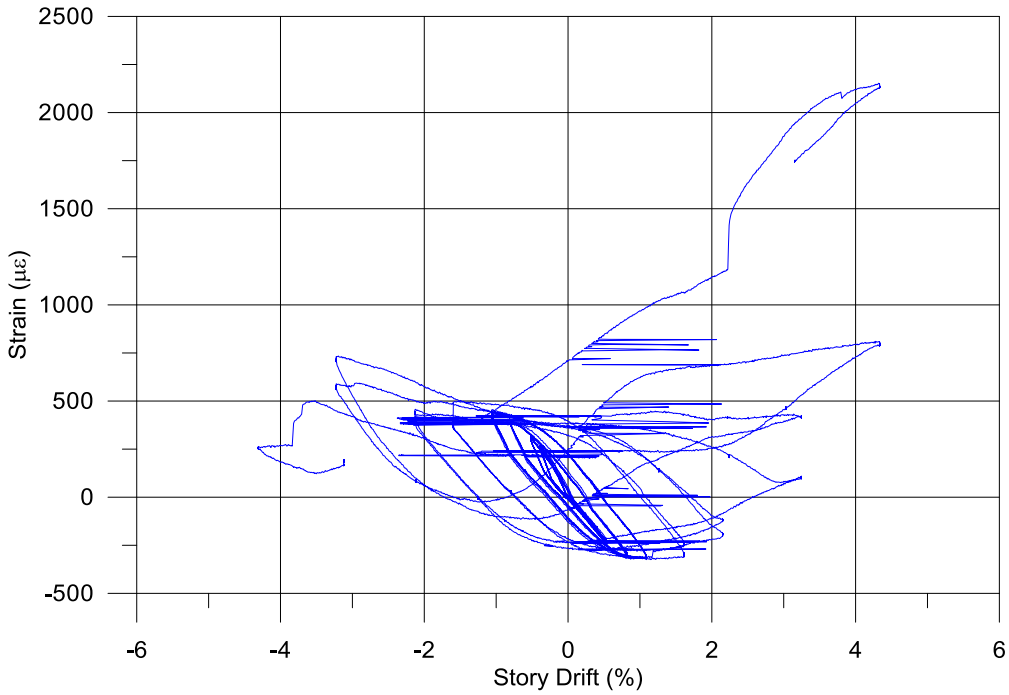

G-P57-RS4-1

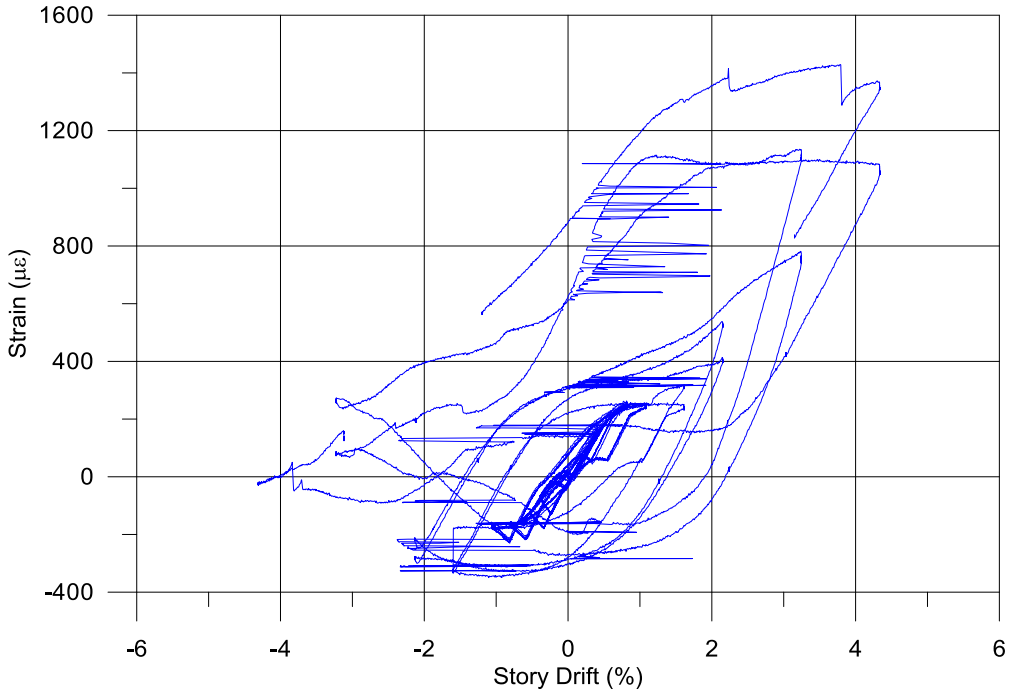

G-P57-RS4-2

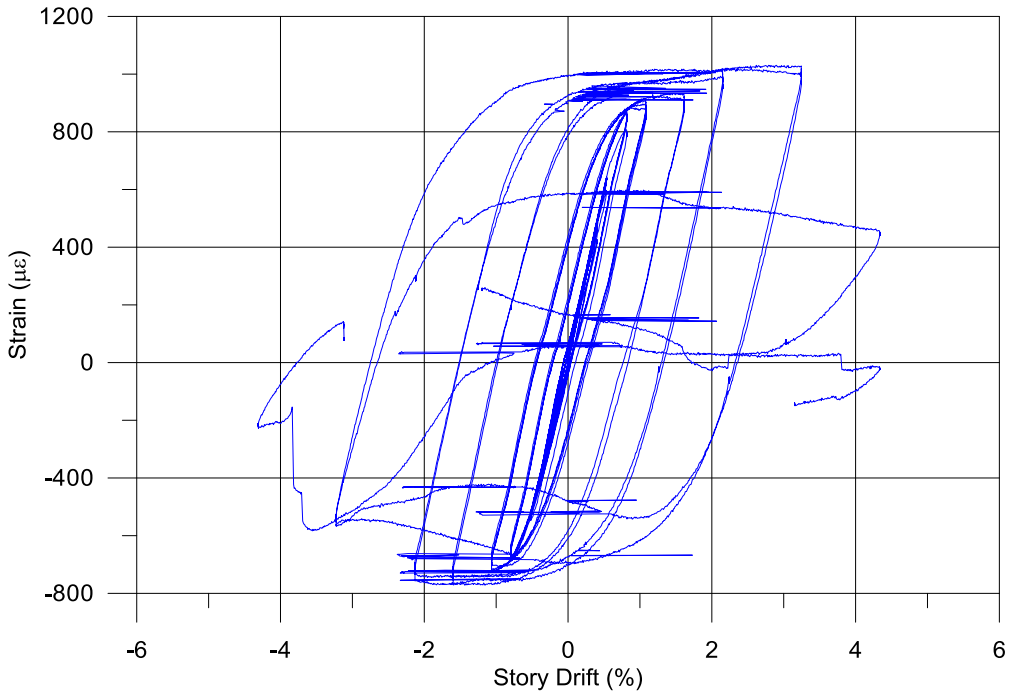

G-P57-RS4-3

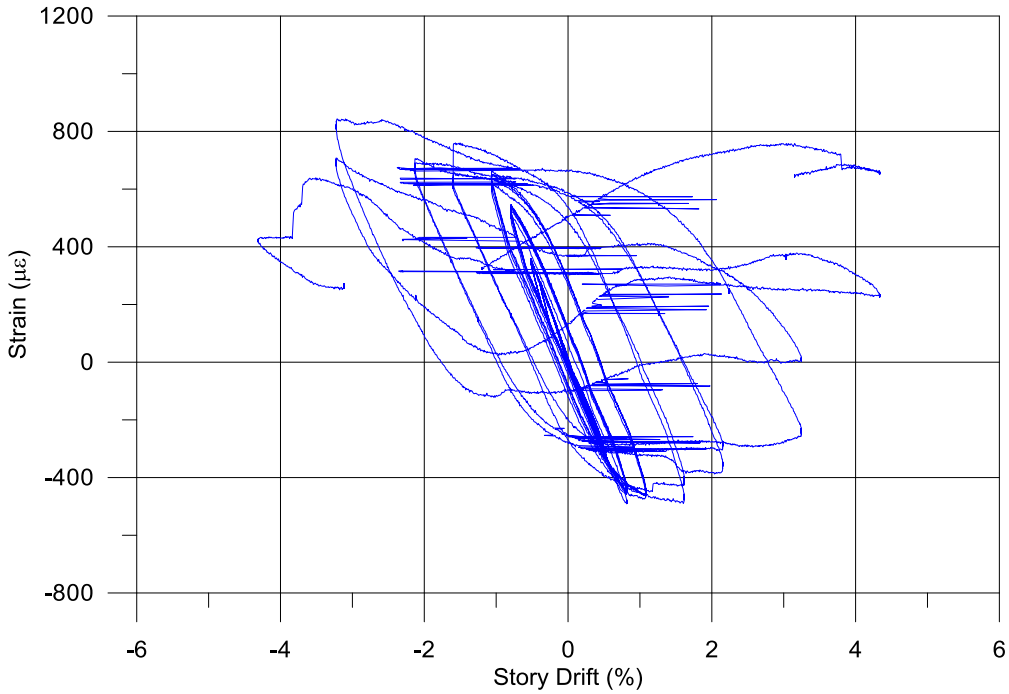

G-P57-RS5-1

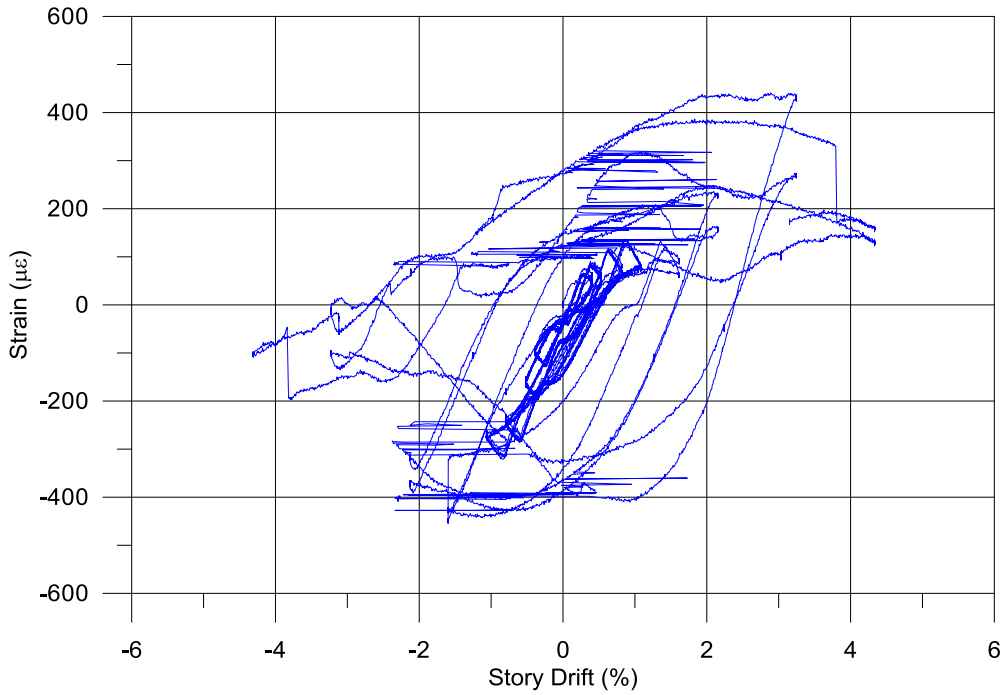

G-P57-RS5-2

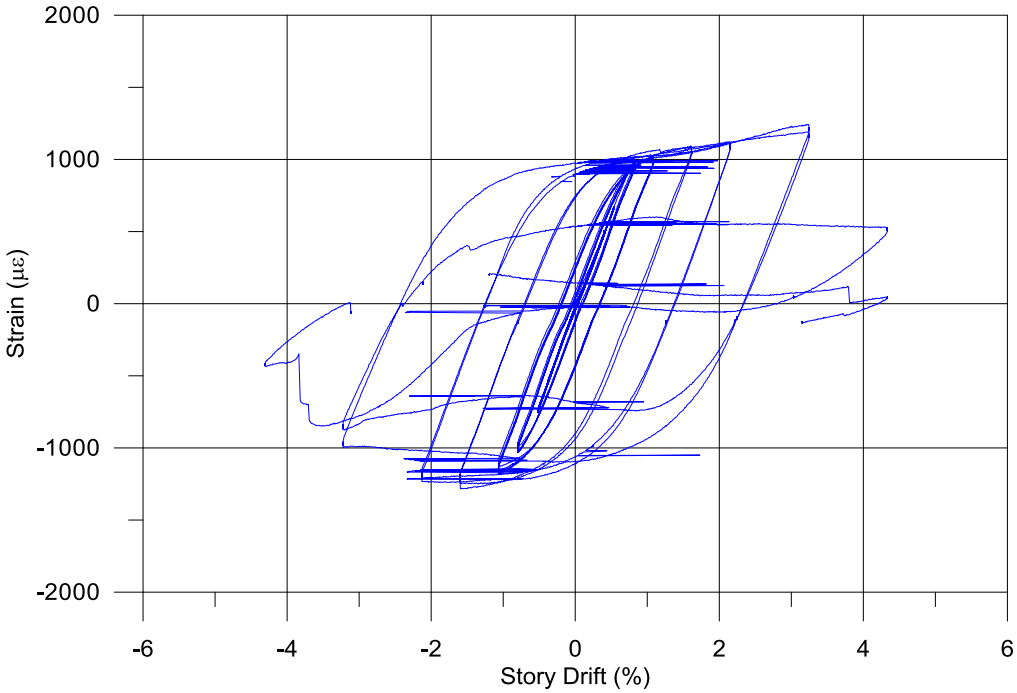

G-P57-RS5-3

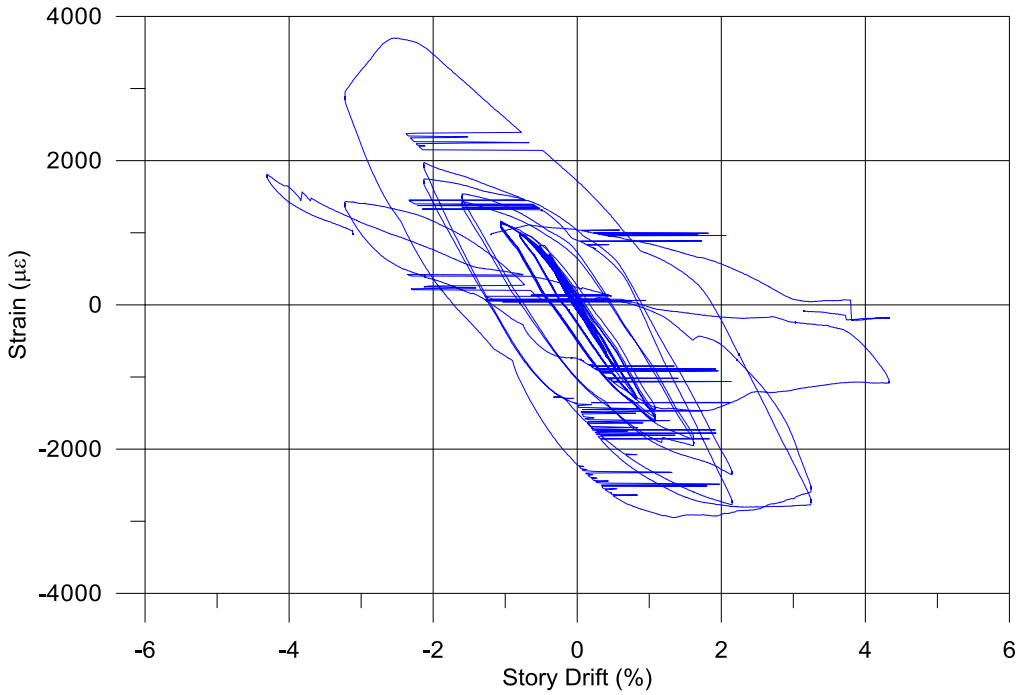

G-P60-RS1

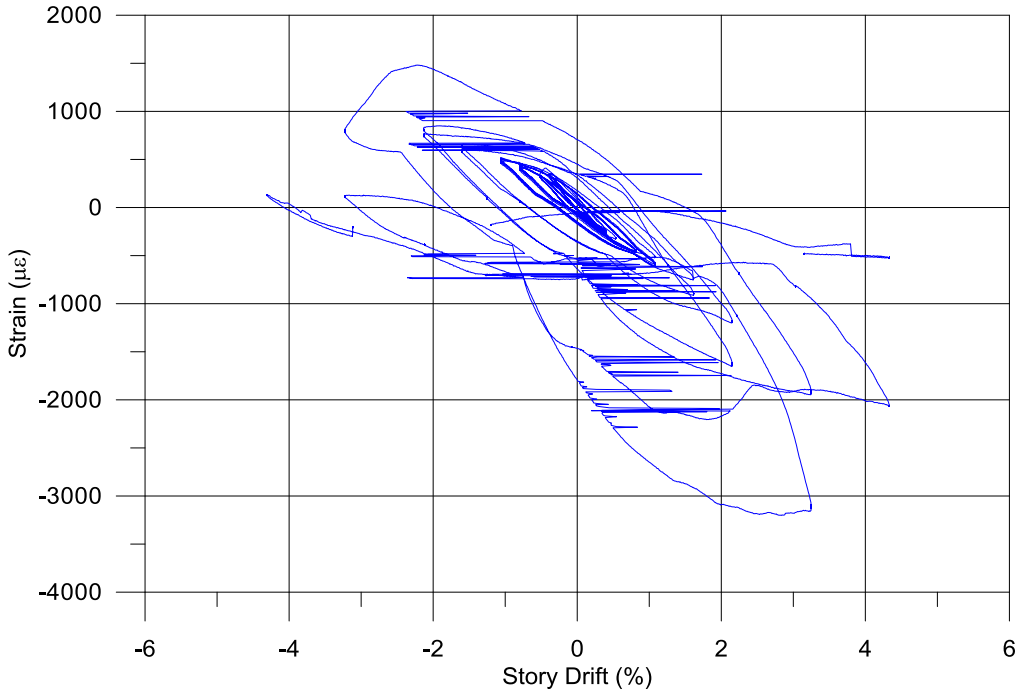

G-P60-RS2

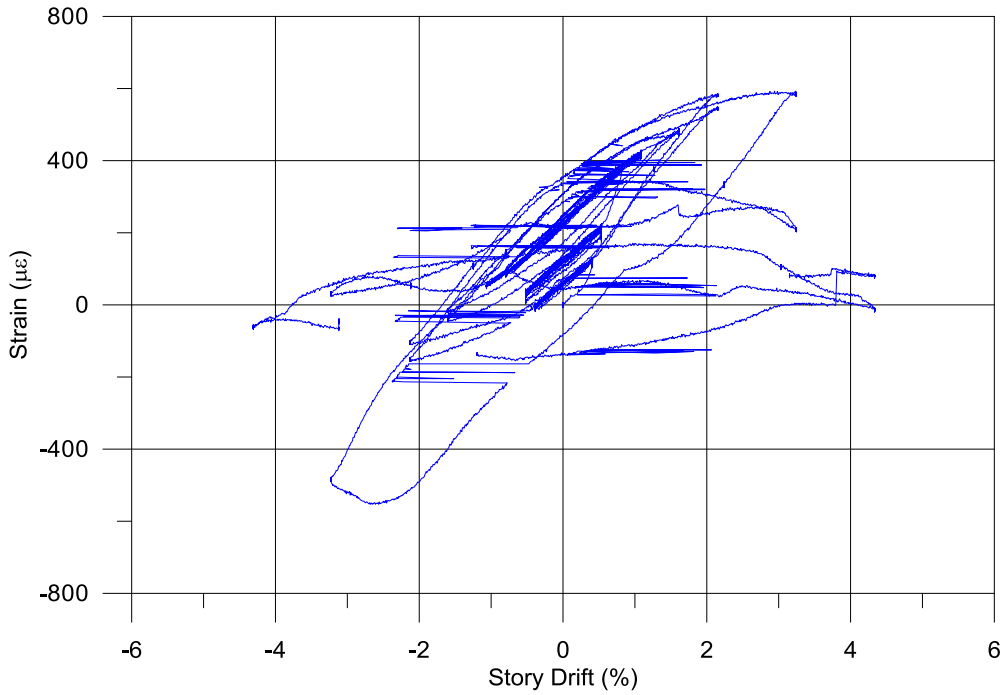

G-P60-RS3

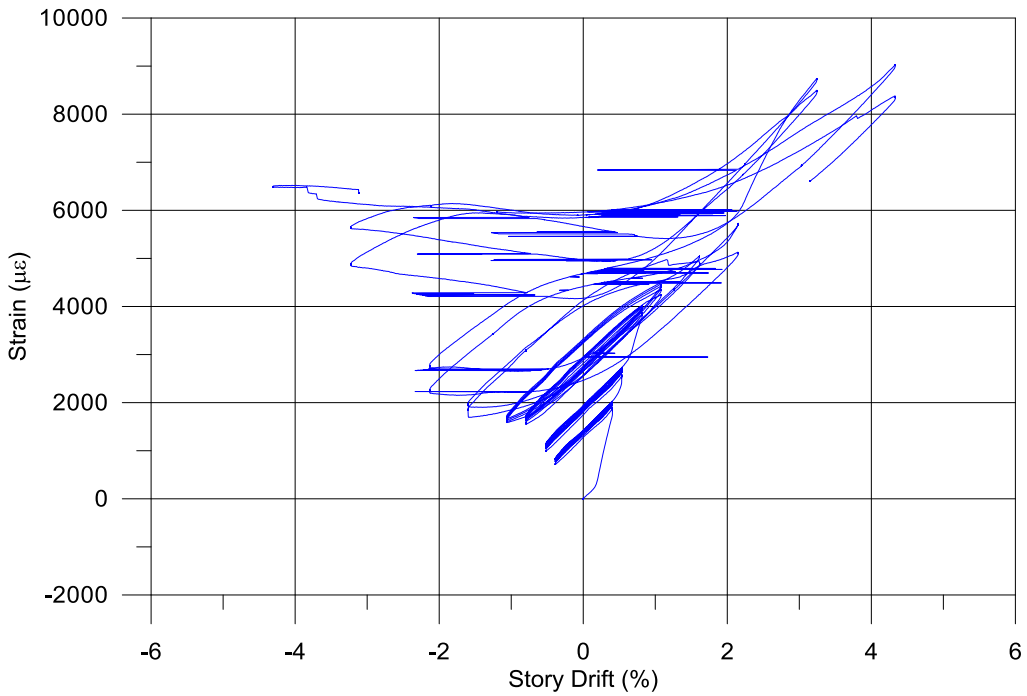

G-RS1-1

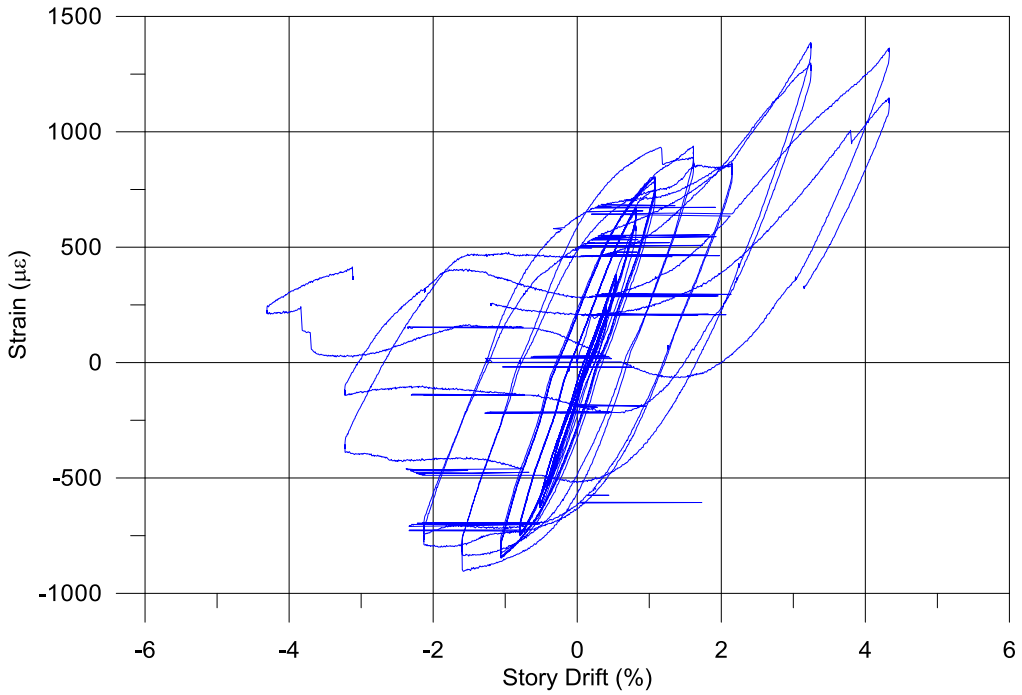
1500
1000
500
0
-500
-1000
Strain (με)
-6
-4
-2
0
2
4
6
Story Drift (%)

G-RS1-2

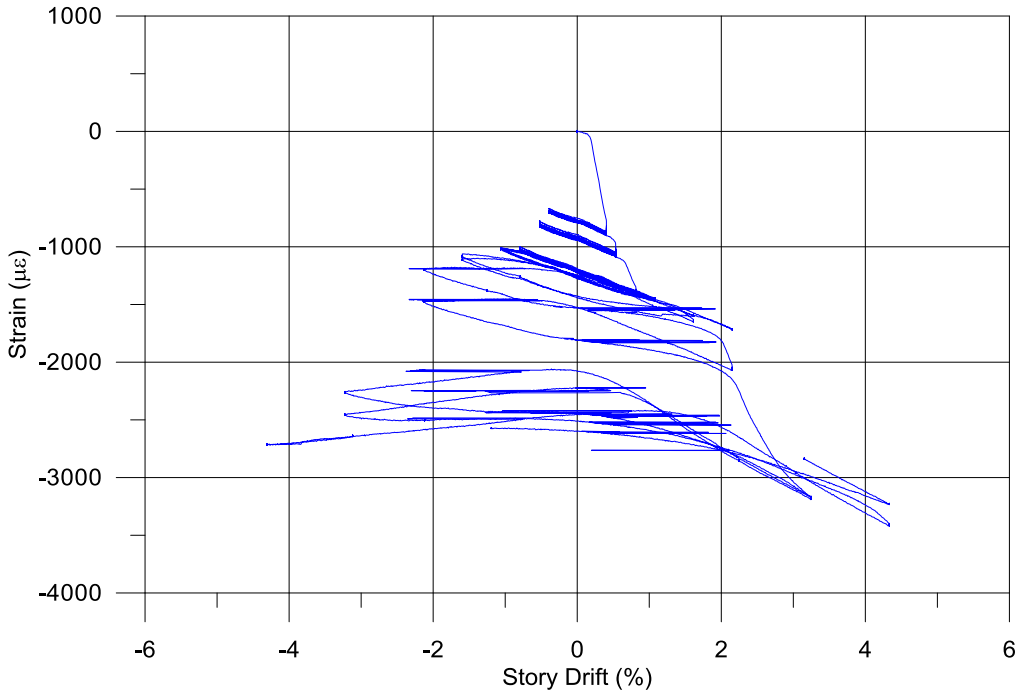
1000
0
-1000
-2000
-3000
-4000
Strain (με)
-6
-4
-2
0
2
4
6
Story Drift (%)

G-RS1-3

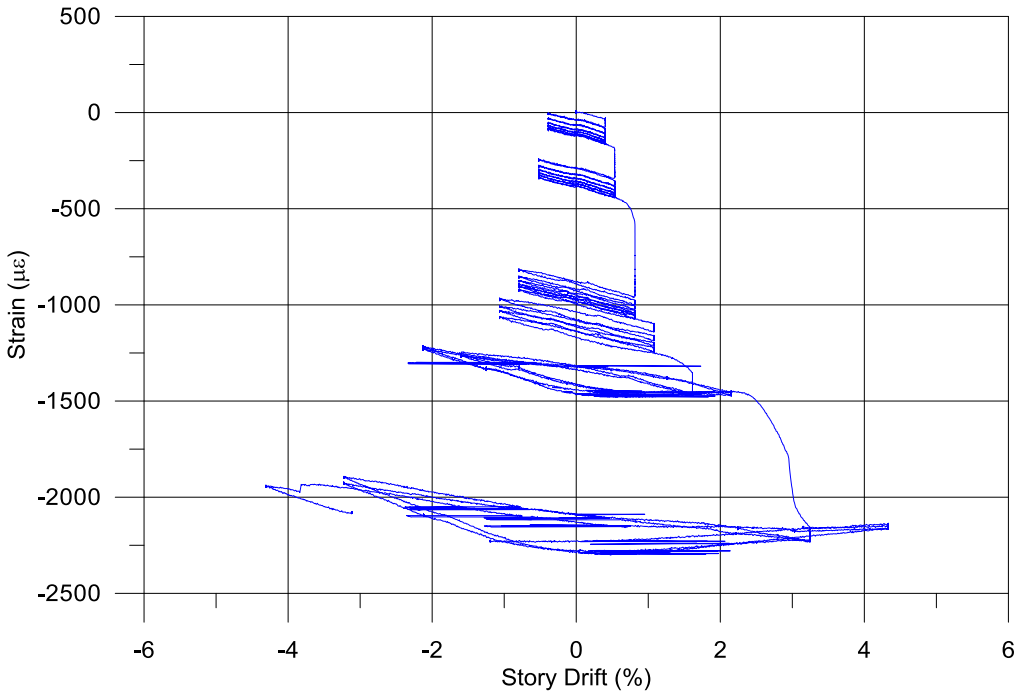
500
0
-500
-1000
-1500
-2000
-2500
Strain (με)
-6
-4
-2
0
2
4
6
Story Drift (%)

G-RS2-1

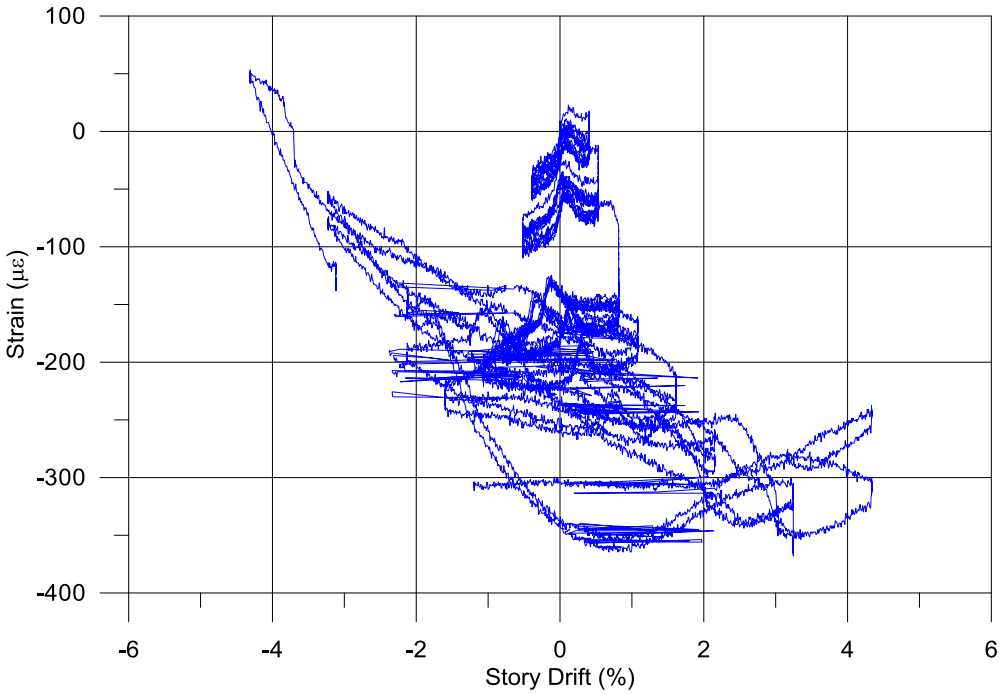
100
0
-100
-200
-300
-400
Strain (με)
-6
-4
-2
0
2
4
6
Story Drift (%)

G-RS2-2

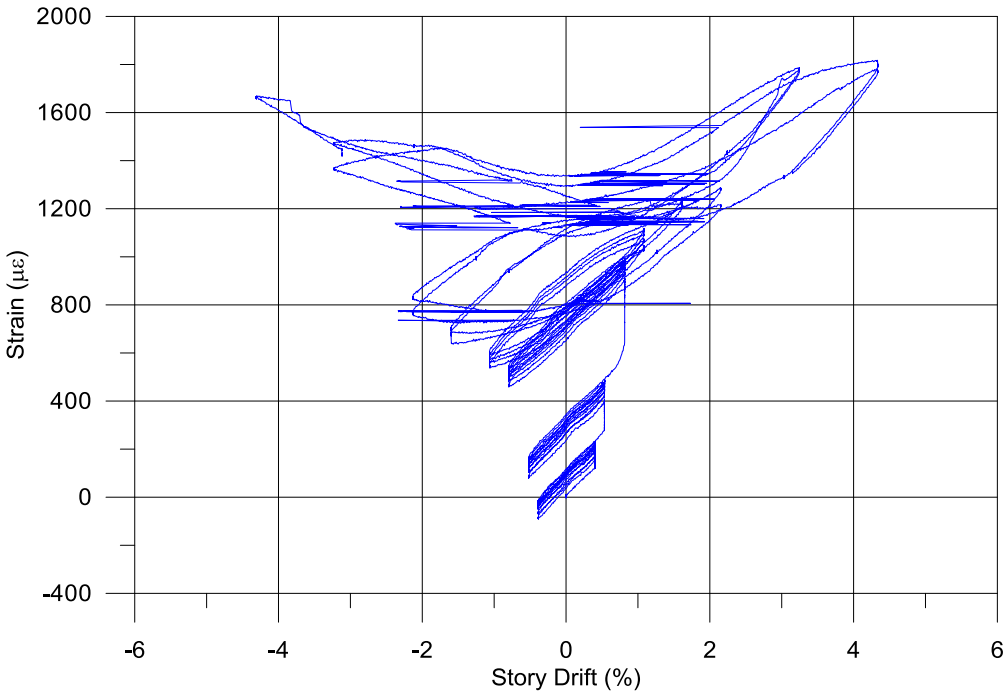
2000
1600
1200
800
400
0
-400
Strain (με)
-6
-4
-2
0
2
4
6
Story Drift (%)

G-RS2-3

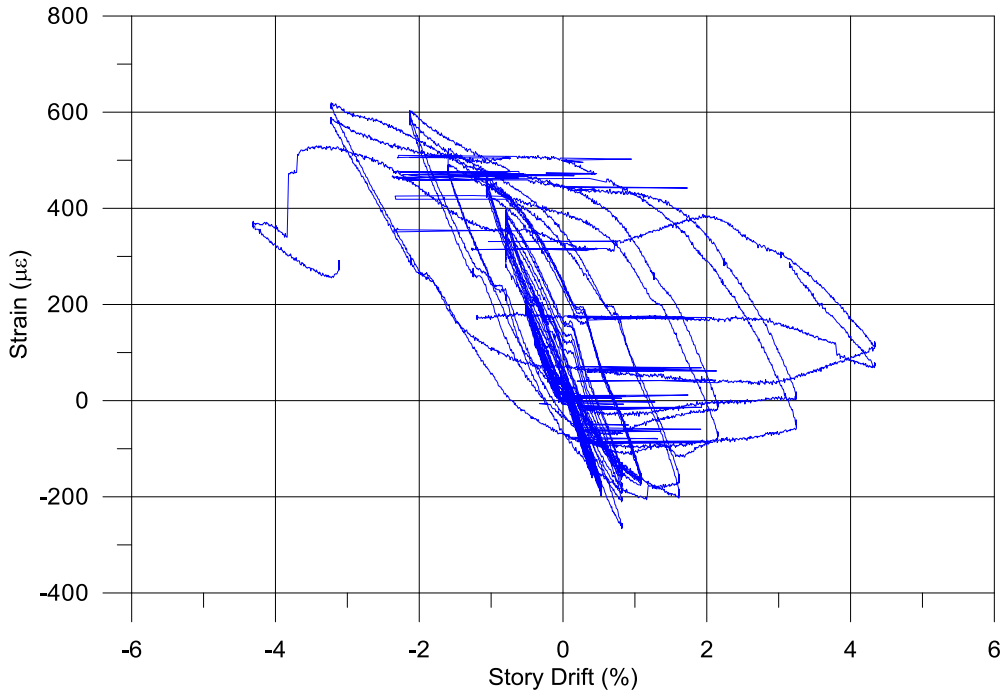
800
600
400
200
0
-200
-400
Strain (με)
-6
-4
-2
0
2
4
6
Story Drift (%)

G-RS3-1

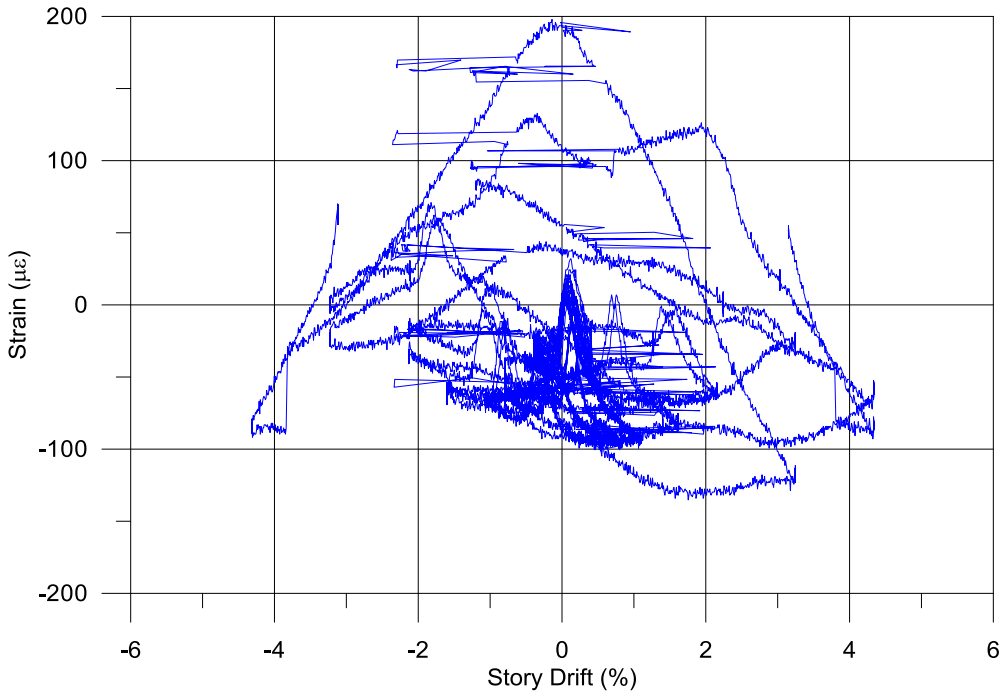
200
100
0
-100
-200
Strain (με)
-6
-4
-2
0
2
4
6
Story Drift (%)

G-RS3-2

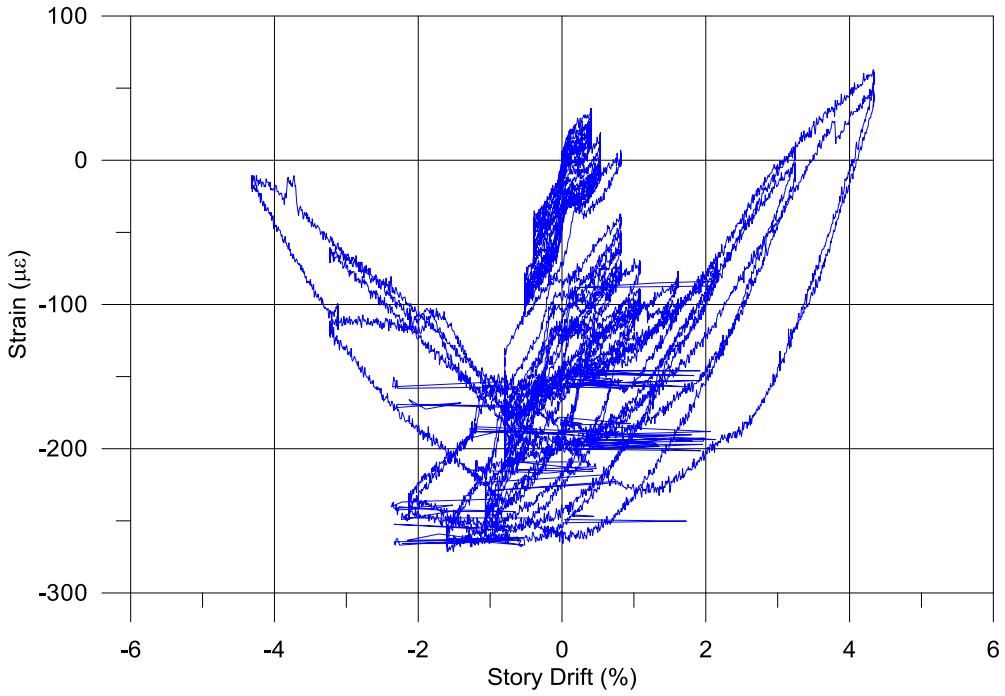
100
0
-100
-200
-300
Strain (με)
-6
-4
-2
0
2
4
6
Story Drift (%)

G-RS3-3

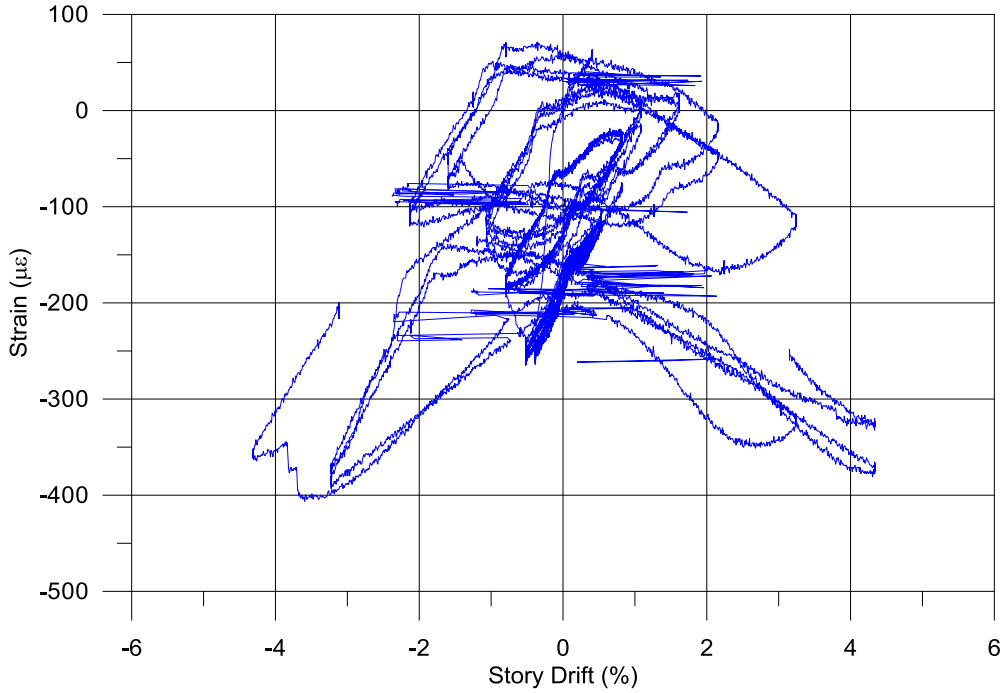
100
0
-100
-200
-300
-400
-500
Strain (με)
-6
-4
-2
0
2
4
6
Story Drift (%)

G-RS4-1

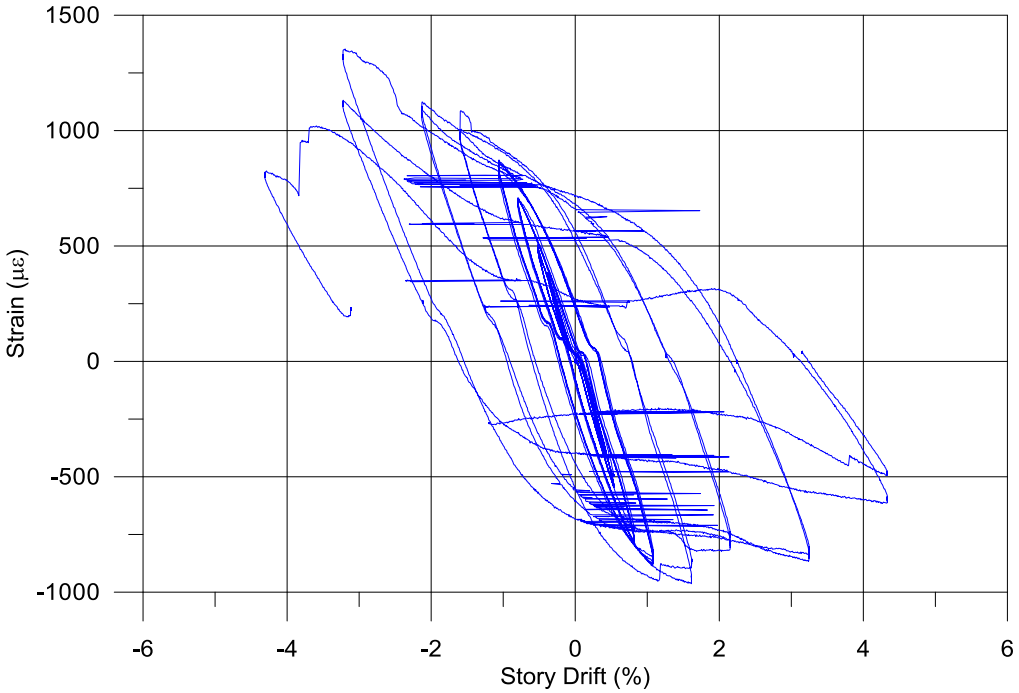
1500
1000
500
0
-500
-1000
Strain (με)
-6
-4
-2
0
2
4
6
Story Drift (%)

G-RS4-2

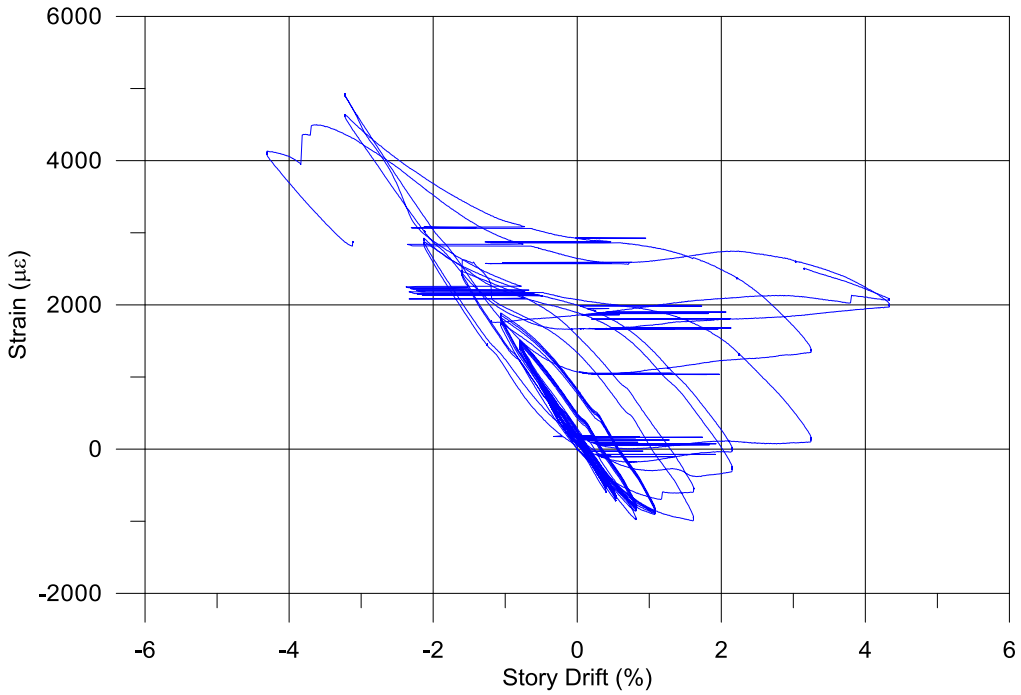
6000
4000
2000
0
-2000
Strain (με)
-6
-4
-2
0
2
4
6
Story Drift (%)

G-RS4-3

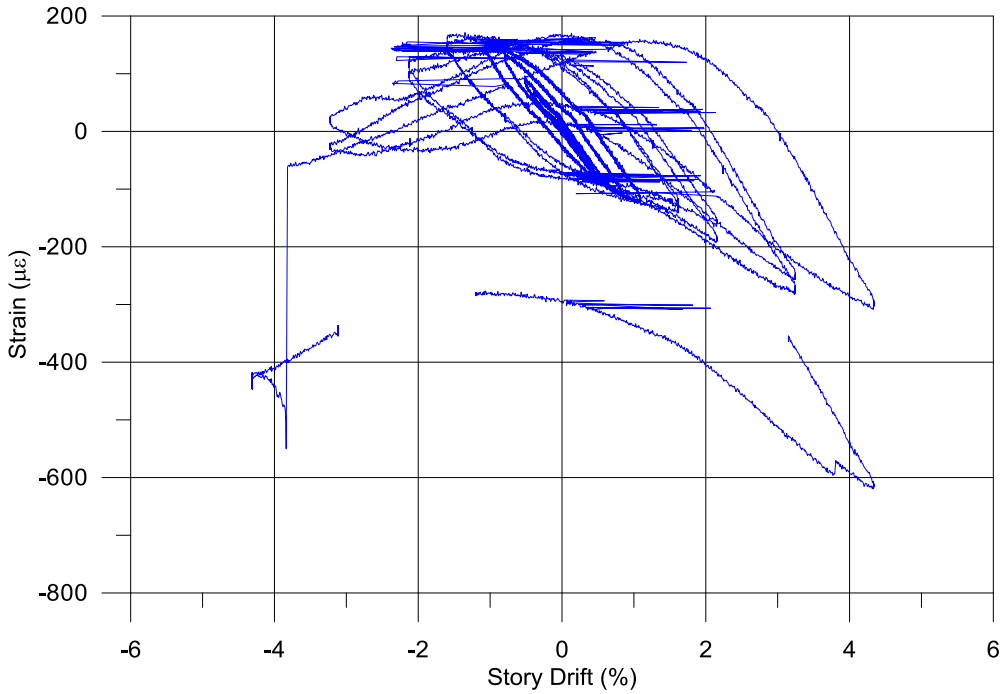
200
0
-200
-400
-600
-800
Strain (με)
-6
-4
-2
0
2
4
6
Story Drift (%)

LTB-1-1

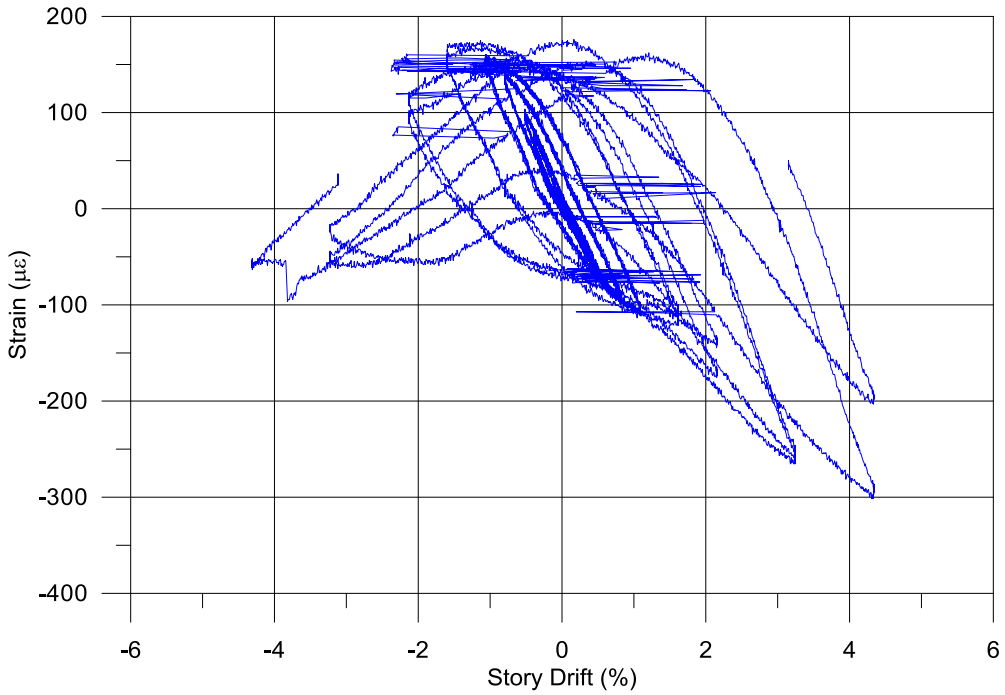
200
100
0
-100
-200
-300
-400
Strain (με)
-6
-4
-2
0
2
4
6
Story Drift (%)

LTB-1-2

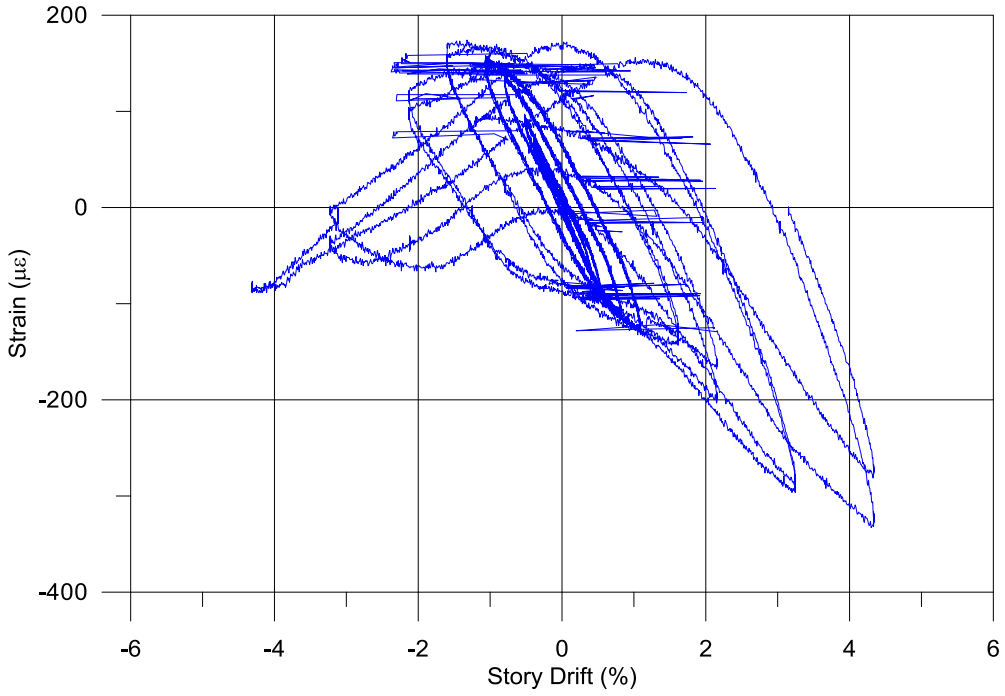
200
0
-200
-400
Strain (με)
-6
-4
-2
0
2
4
6
Story Drift (%)

LTB-1-3

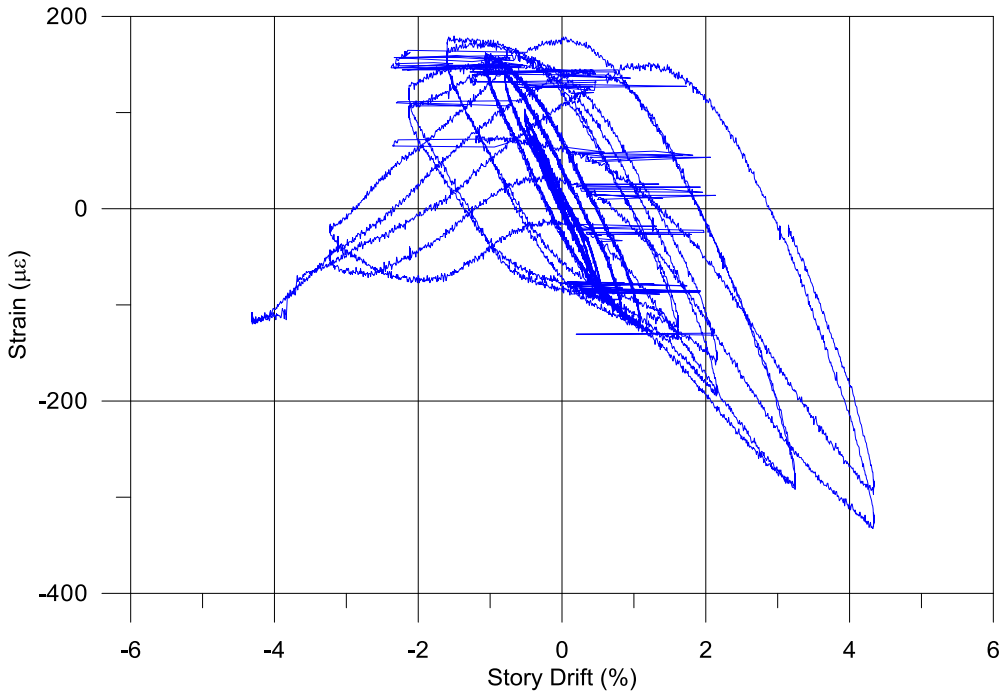
200
0
-200
-400
Strain (με)
-6
-4
-2
0
2
4
6
Story Drift (%)

LTB-1-4

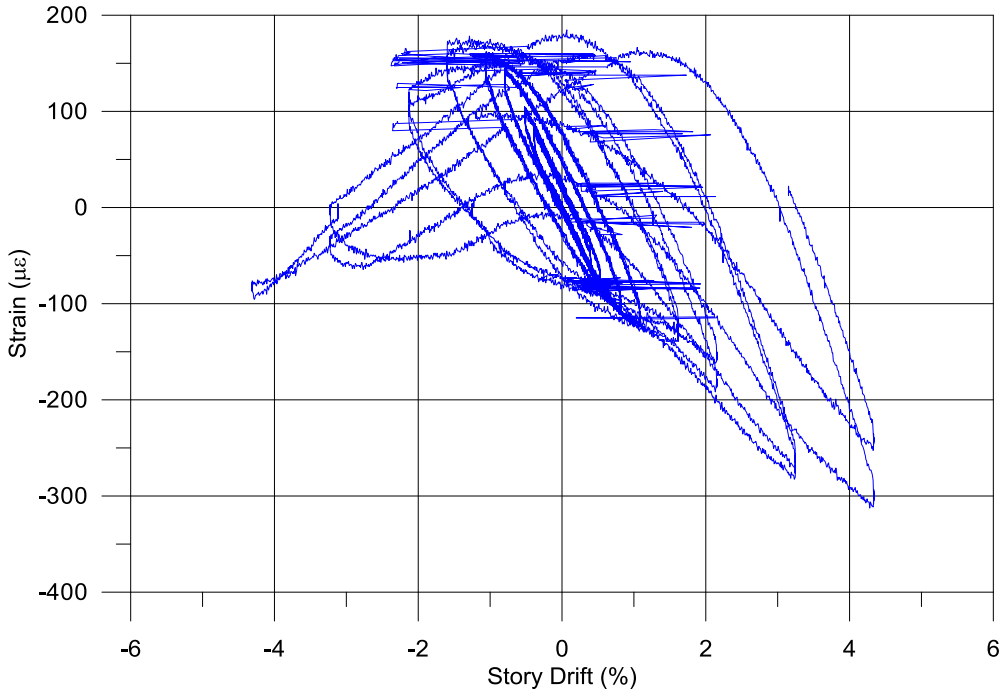
200
100
0
-100
-200
-300
-400
Strain (με)
-6
-4
-2
0
2
4
6
Story Drift (%)

LTB-2

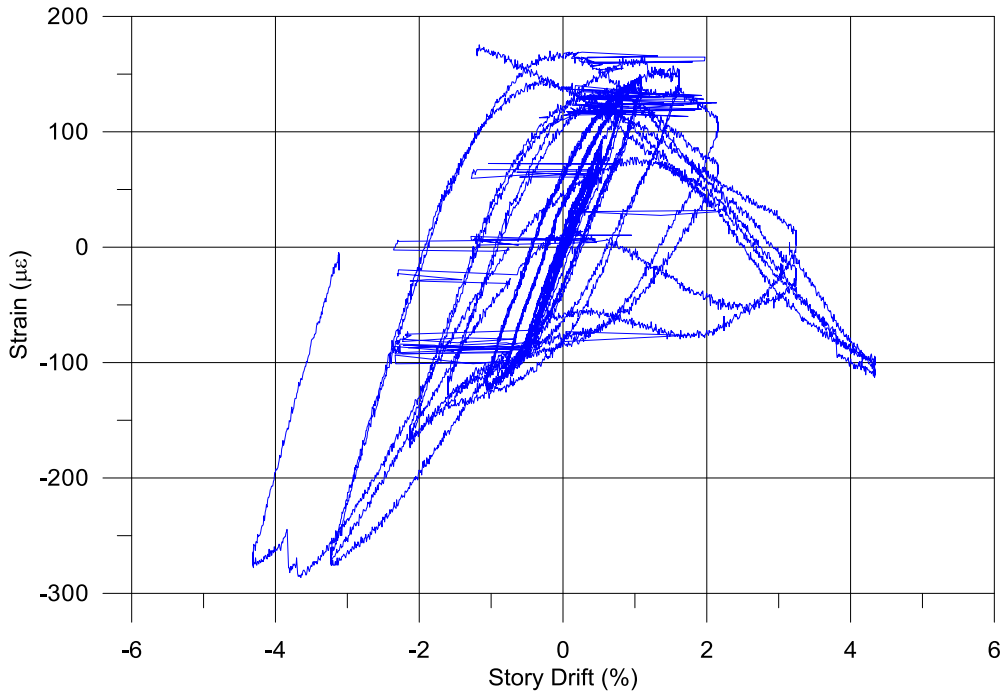
200
100
0
-100
-200
-300
Strain (με)
-6
-4
-2
0
2
4
6
Story Drift (%)

LTB-3-1

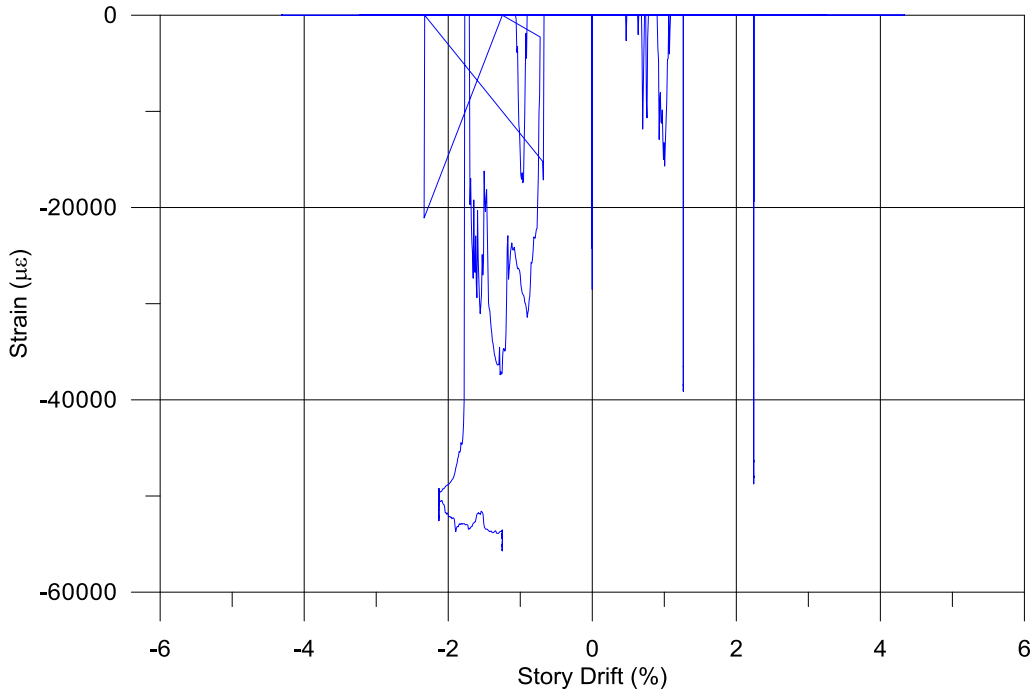
0
-20000
-40000
-60000
Strain (με)
-6
-4
-2
0
2
4
6
Story Drift (%)

LTB-3-2

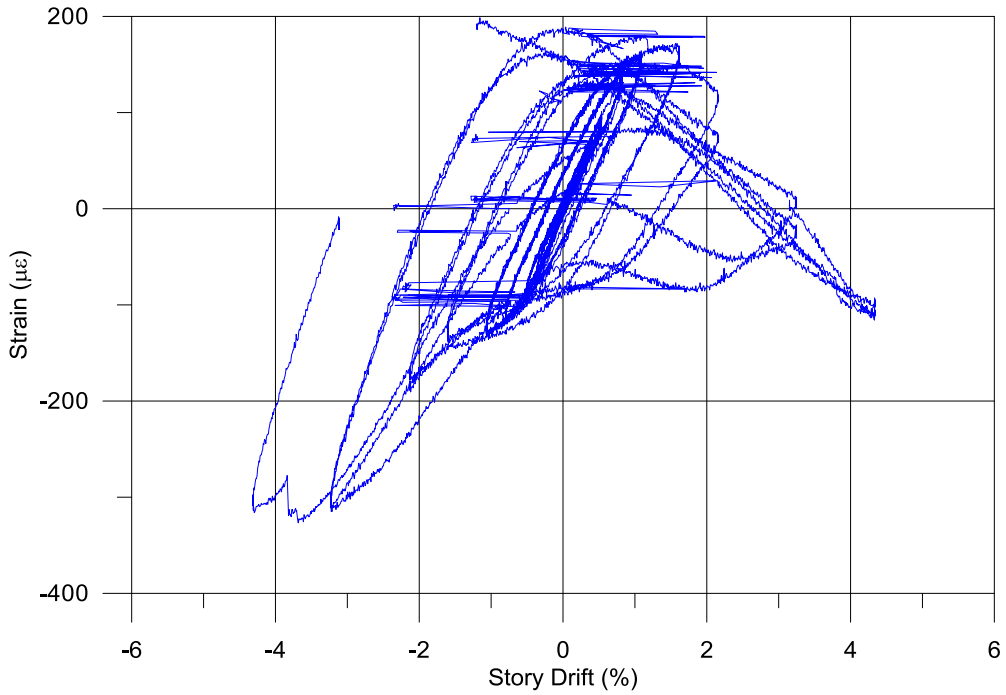
200
0
-200
-400
Strain (με)
-6
-4
-2
0
2
4
6
Story Drift (%)

LTB-3-3

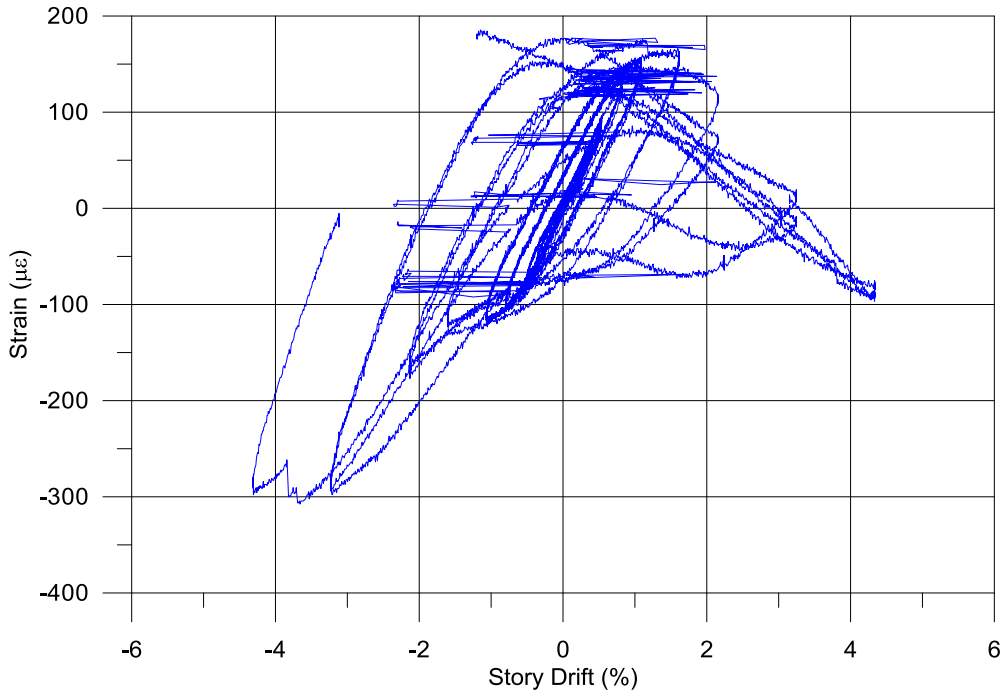
200
100
0
-100
-200
-300
-400
Strain (με)
-6
-4
-2
0
2
4
6
Story Drift (%)

LTB-3-4

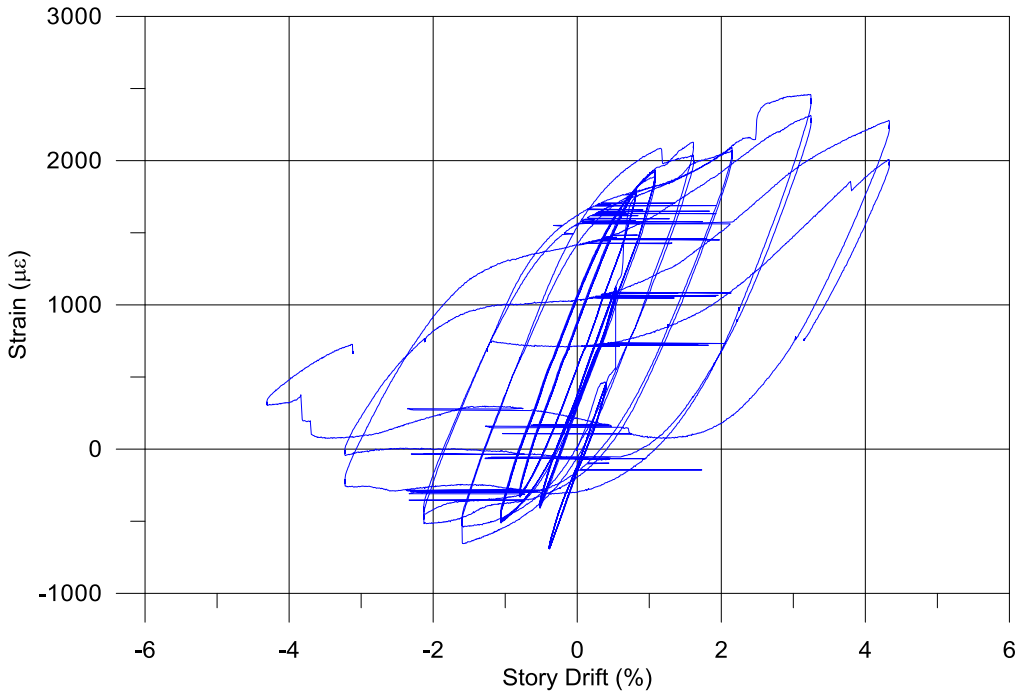
3000
2000
1000
0
-1000
Strain (με)
-6
-4
-2
0
2
4
6
Story Drift (%)

M1-1-1

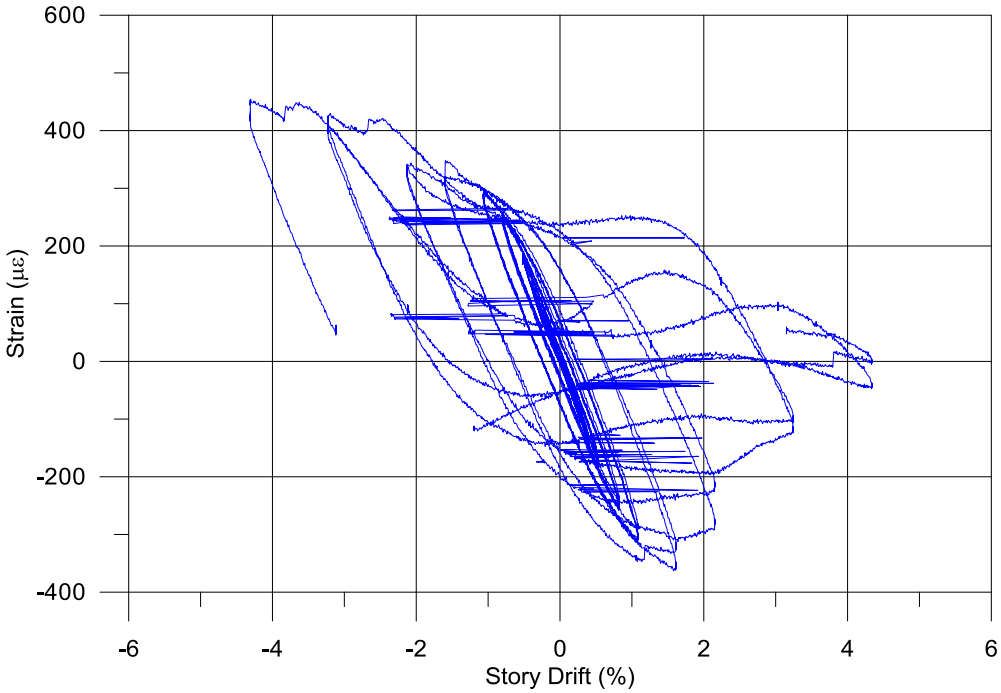
600
400
200
0
-200
-400
Strain (με)
-6
-4
-2
0
2
4
6
Story Drift (%)

M1-1-2

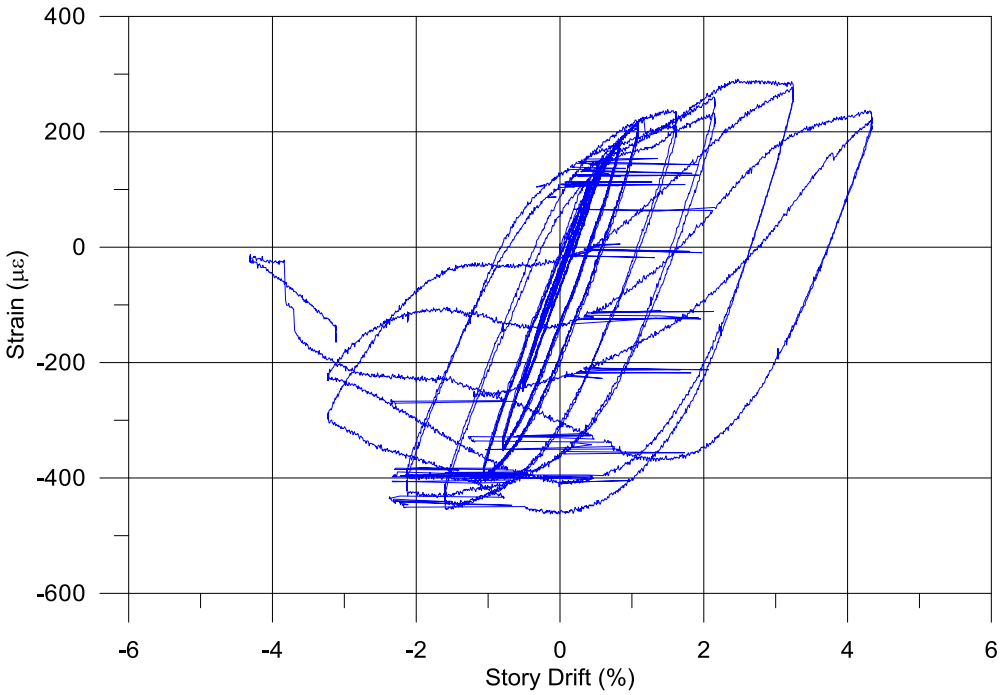
400
200
0
-200
-400
-600
Strain (με)
-6
-4
-2
0
2
4
6
Story Drift (%)

M1-2-1

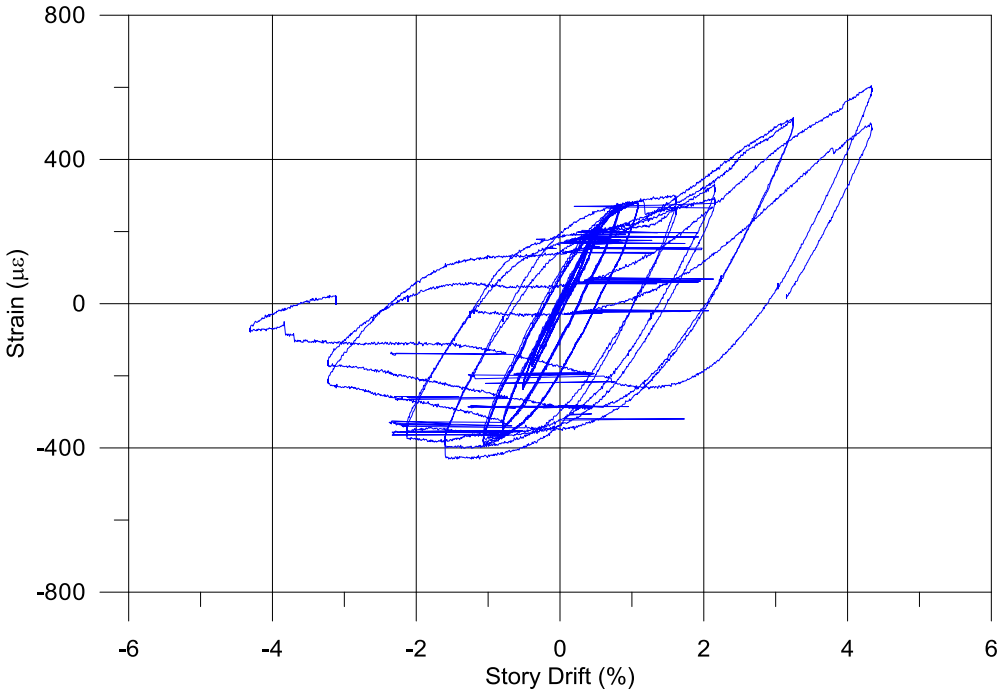
800
400
0
-400
-800
Strain (με)
-6
-4
-2
0
2
4
6
Story Drift (%)

M1-2-2

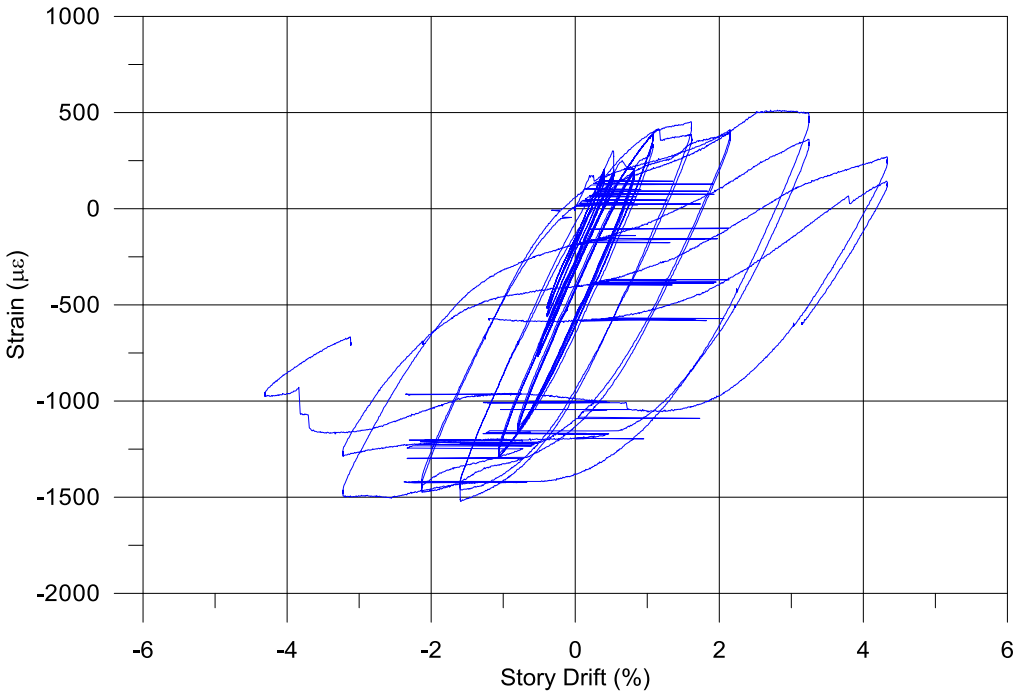
1000
500
0
-500
-1000
-1500
-2000
Strain (με)
-6
-4
-2
0
2
4
6
Story Drift (%)

M2-1-1

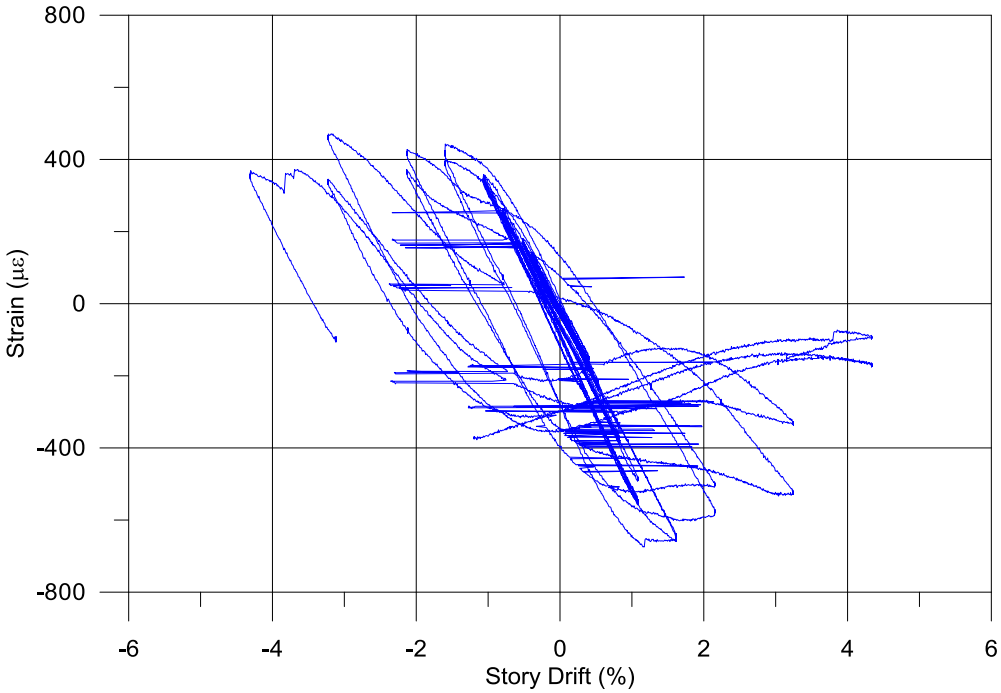
800
400
0
-400
-800
Strain (με)
-6
-4
-2
0
2
4
6
Story Drift (%)

M2-1-2

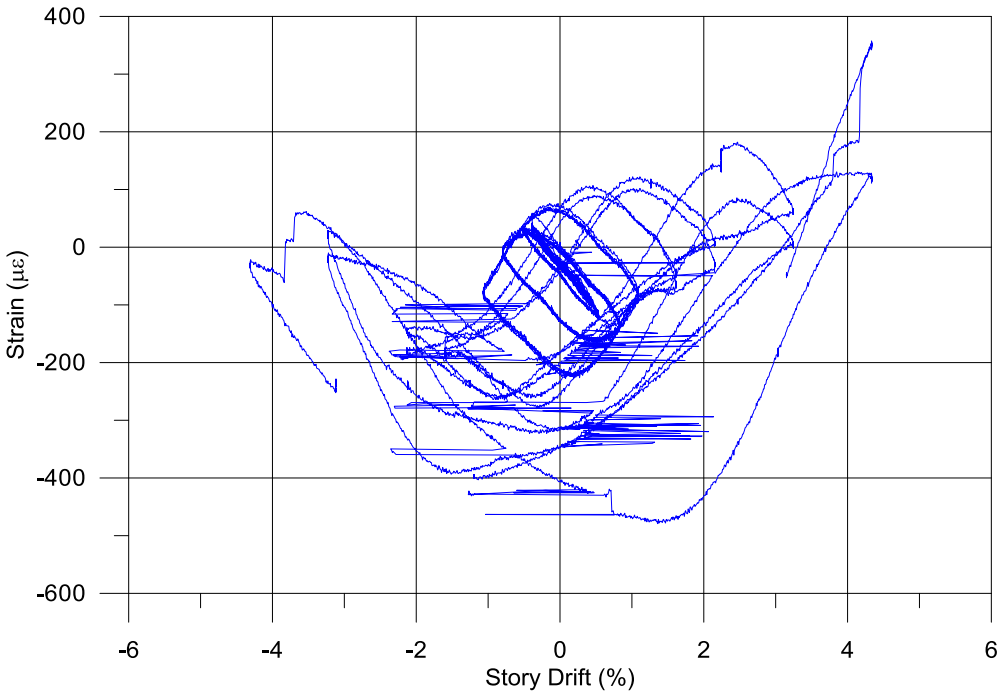
400
200
0
-200
-400
-600
Strain (με)
-6
-4
-2
0
2
4
6
Story Drift (%)

M2-2-1

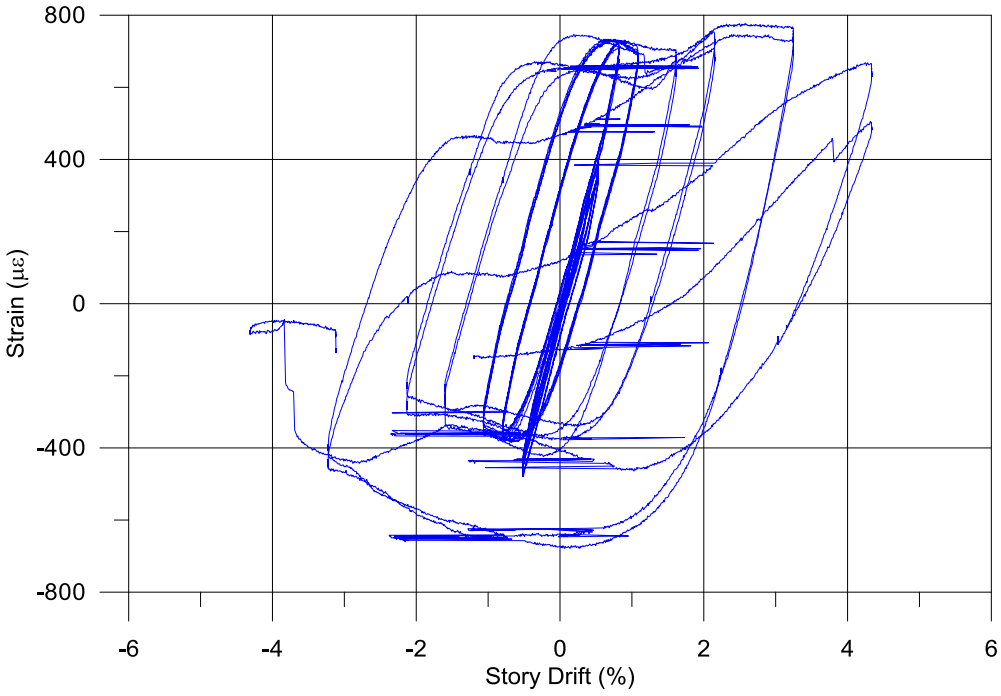
800
400
0
-400
-800
Strain (με)
-6
-4
-2
0
2
4
6
Story Drift (%)

M2-2-2

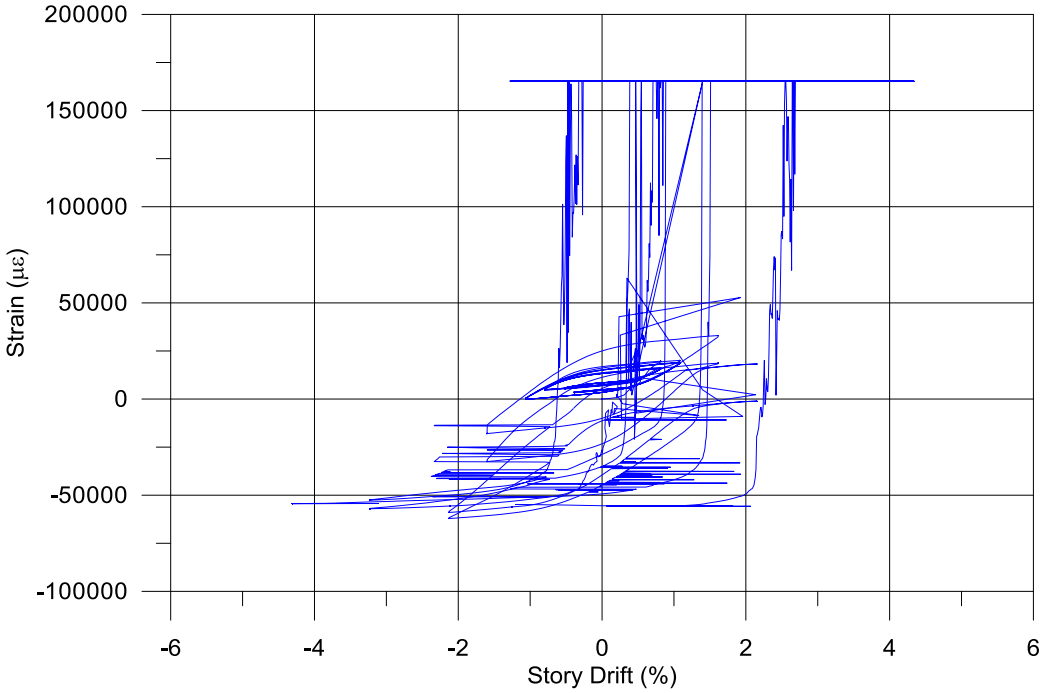
200000
150000
100000
50000
0
-50000
-100000
Strain (με)
-6
-4
-2
0
2
4
6
Story Drift (%)

M3-1

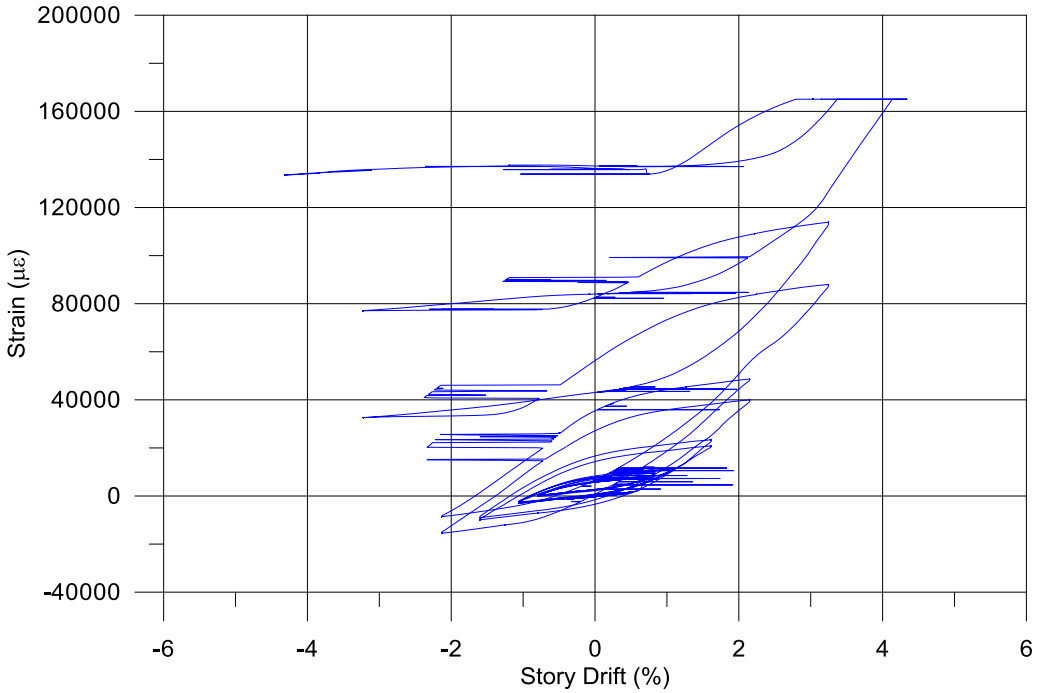
200000
160000
120000
80000
40000
0
-40000
Strain (με)
-6
-4
-2
0
2
4
6
Story Drift (%)

M3-2

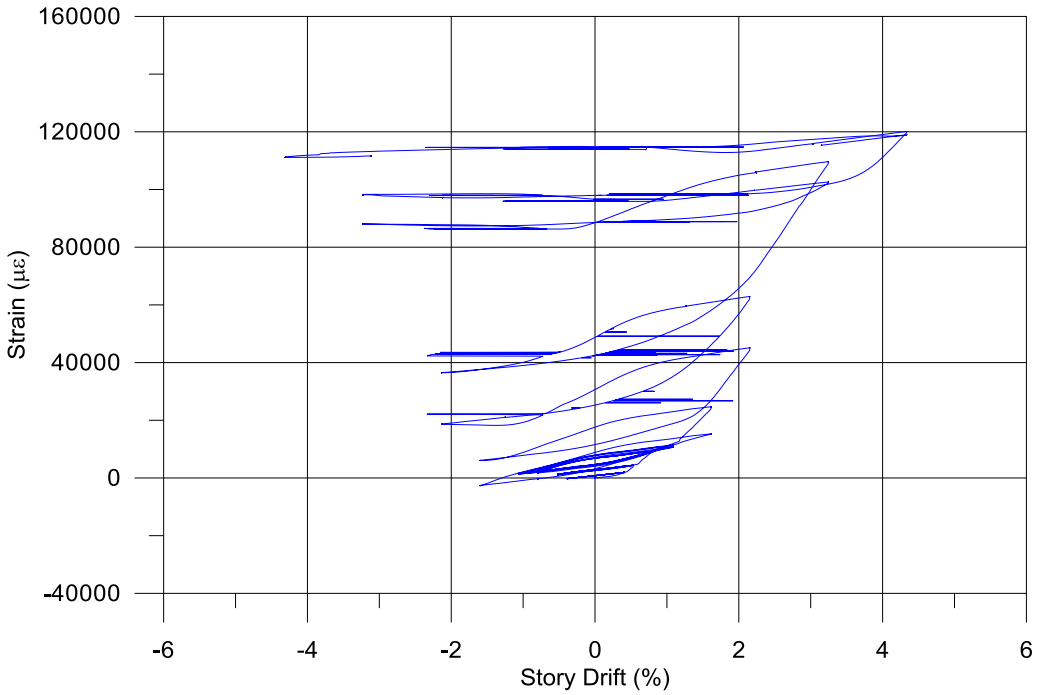
160000
120000
80000
40000
0
-40000
Strain (με)
-6
-4
-2
0
2
4
6
Story Drift (%)

M3-3

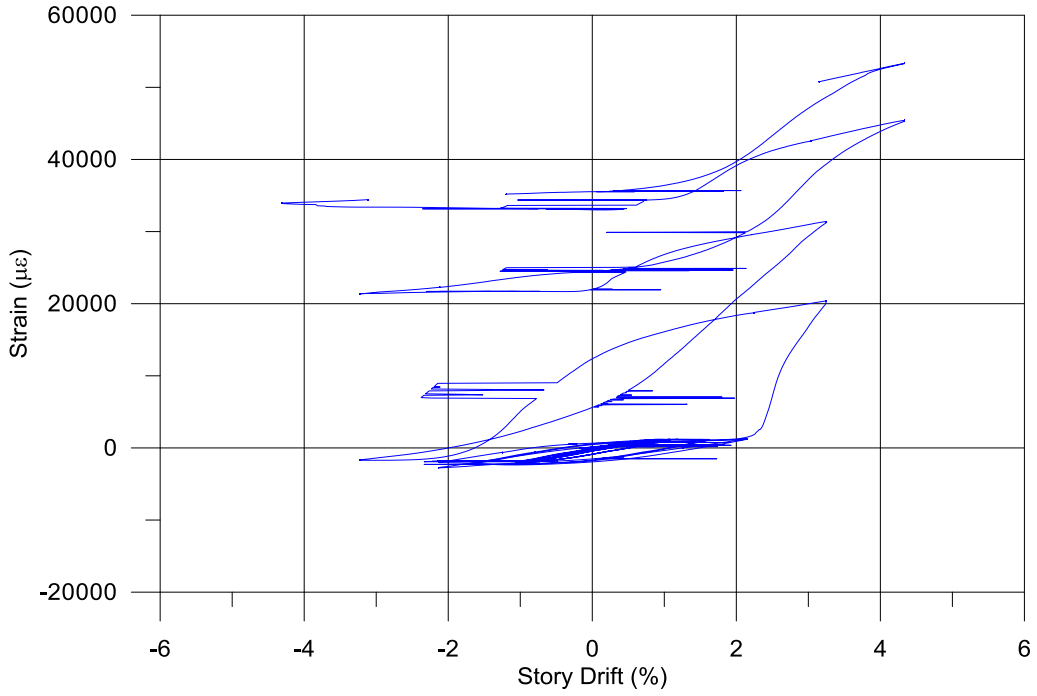
60000
40000
20000
0
-20000
Strain (με)
-6
-4
-2
0
2
4
6
Story Drift (%)

M3-4

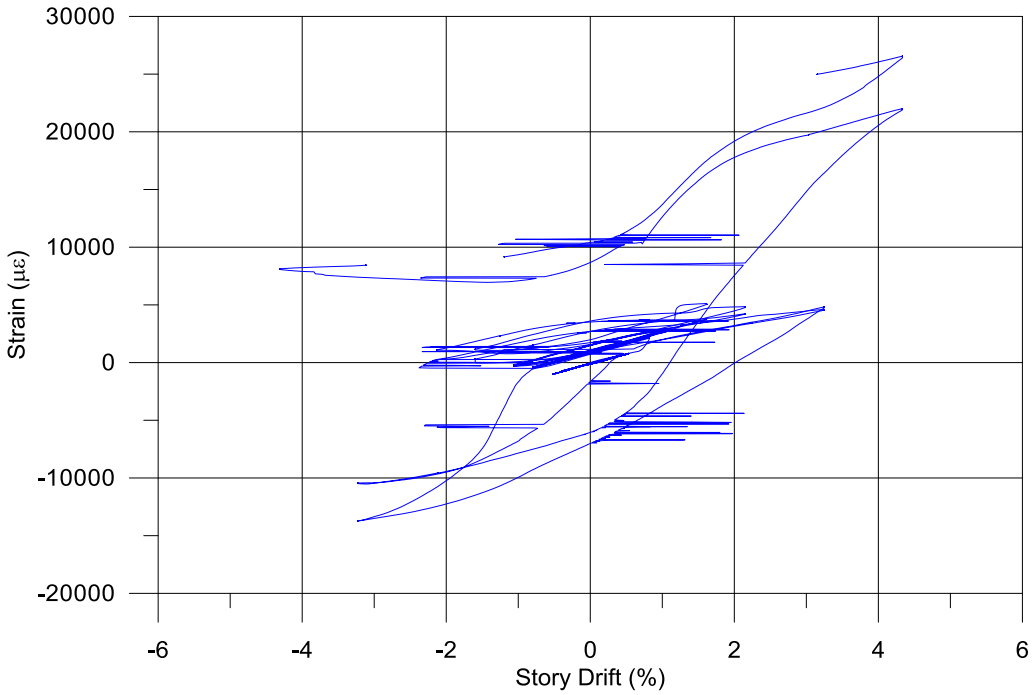
30000
20000
10000
0
-10000
-20000
Strain (με)
-6
-4
-2
0
2
4
6
Story Drift (%)

M3-5

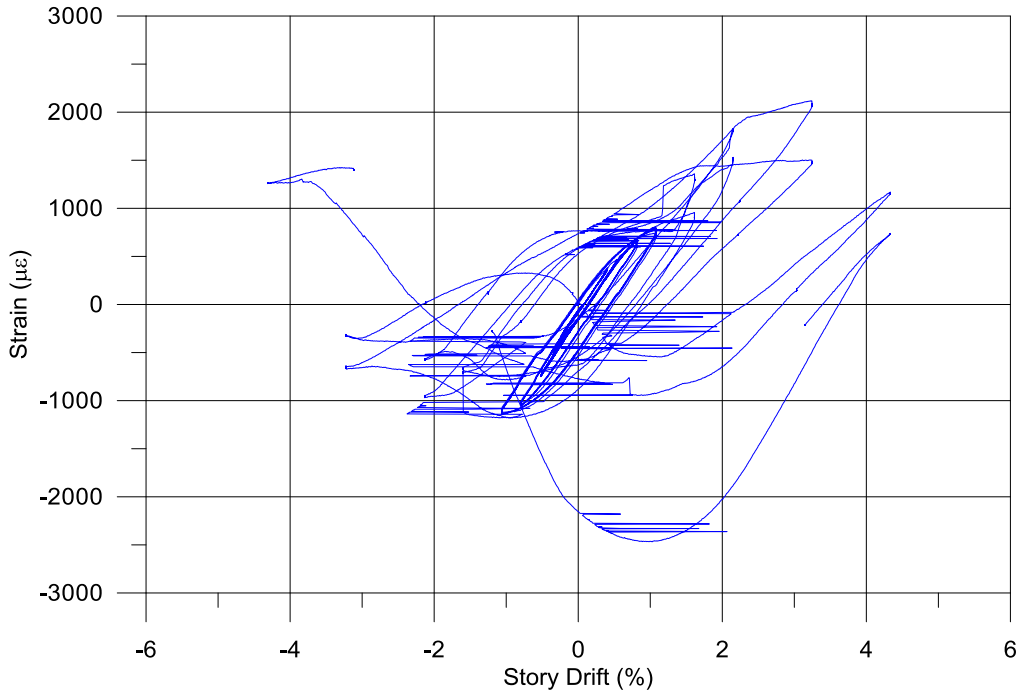
3000
2000
1000
0
-1000
-2000
-3000
Strain (με)
-6
-4
-2
0
2
4
6
Story Drift (%)

M3-6-1

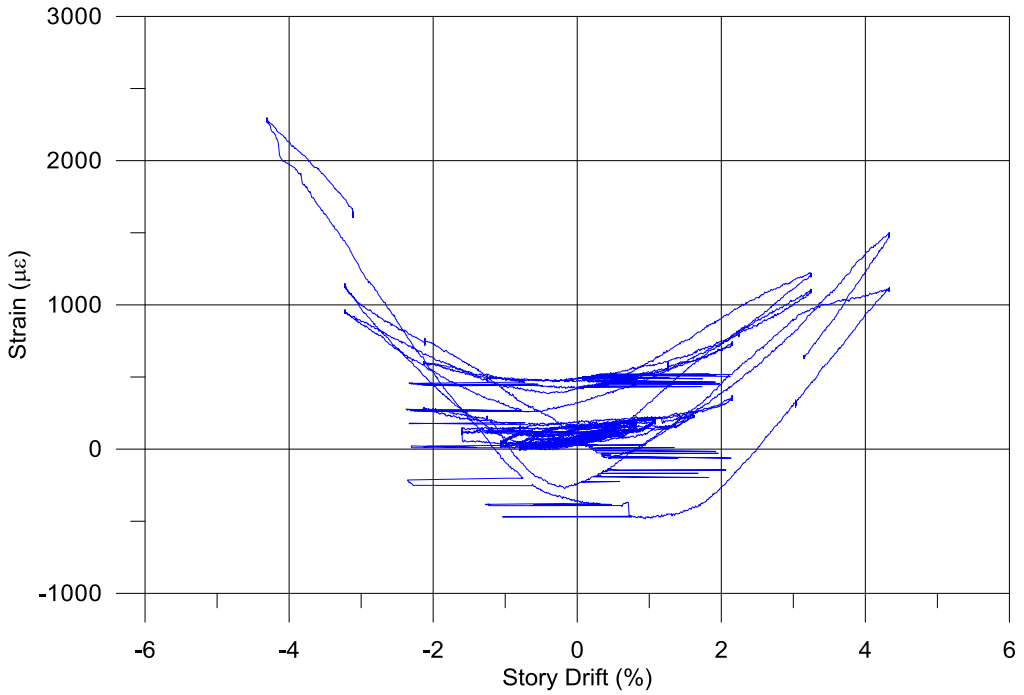
3000
2000
1000
0
-1000
Strain (με)
-6
-4
-2
0
2
4
6
Story Drift (%)

M3-6-2

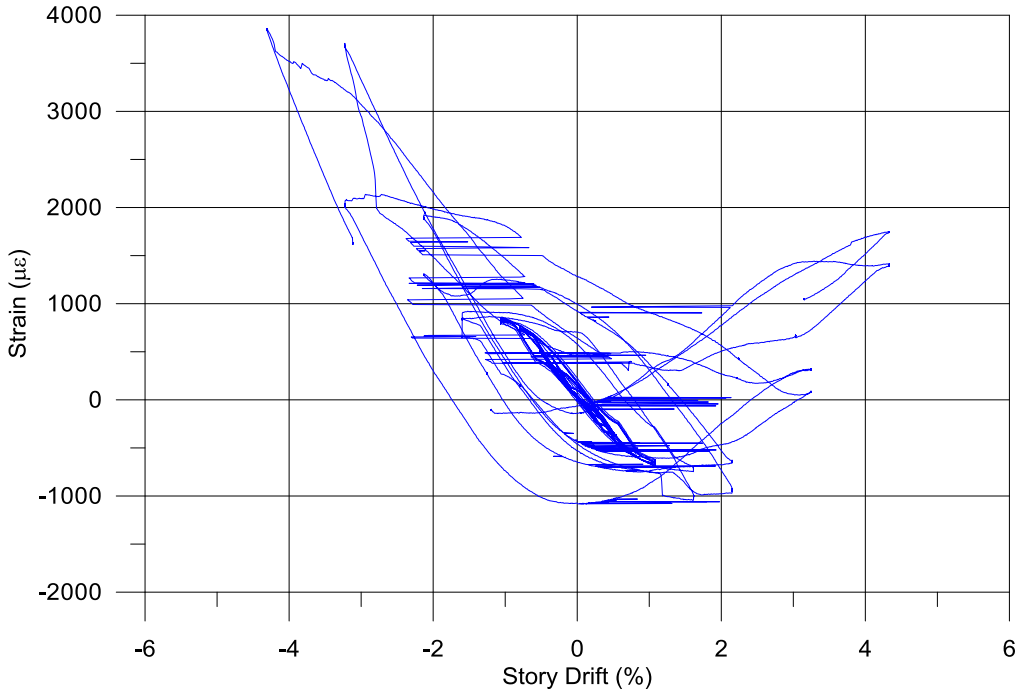
4000
3000
2000
1000
0
-1000
-2000
Strain (με)
-6
-4
-2
0
2
4
6
Story Drift (%)

M3-6-3

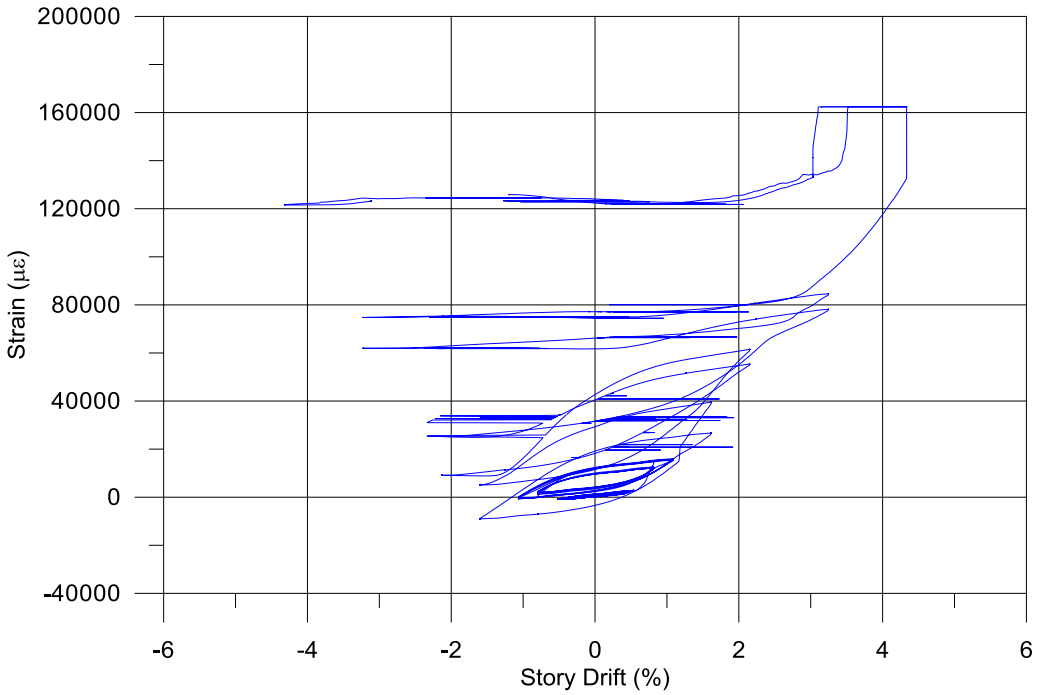
200000
160000
120000
80000
40000
0
-40000
Strain (με)
-6
-4
-2
0
2
4
6
Story Drift (%)

M3-7

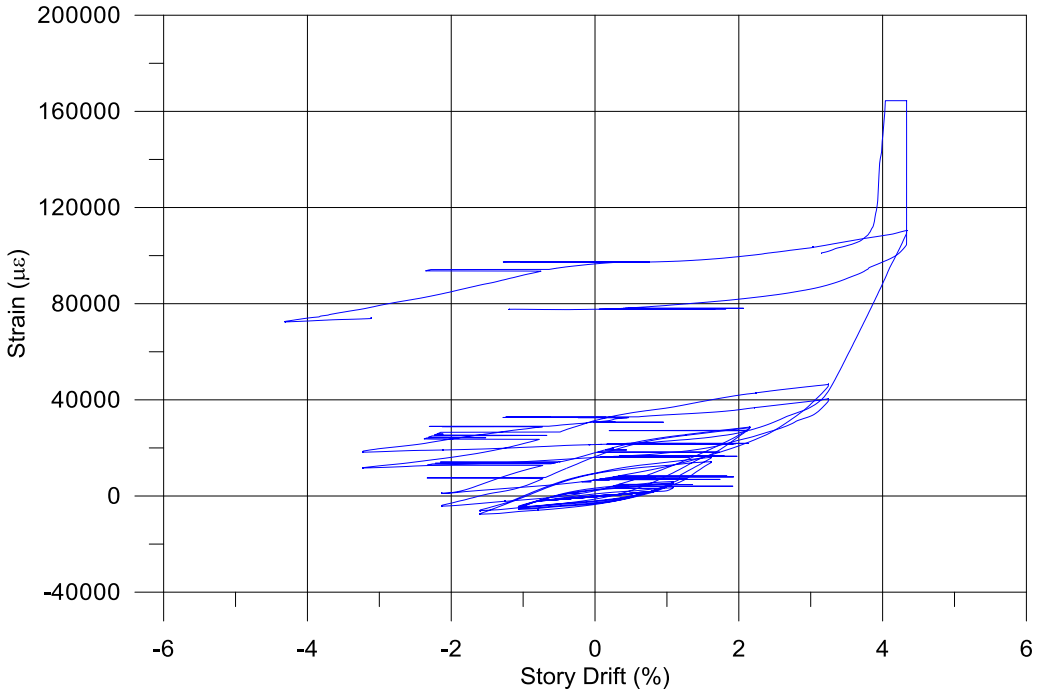
200000
160000
120000
80000
40000
0
-40000
Strain (με)
-6
-4
-2
0
2
4
6
Story Drift (%)

M3-8

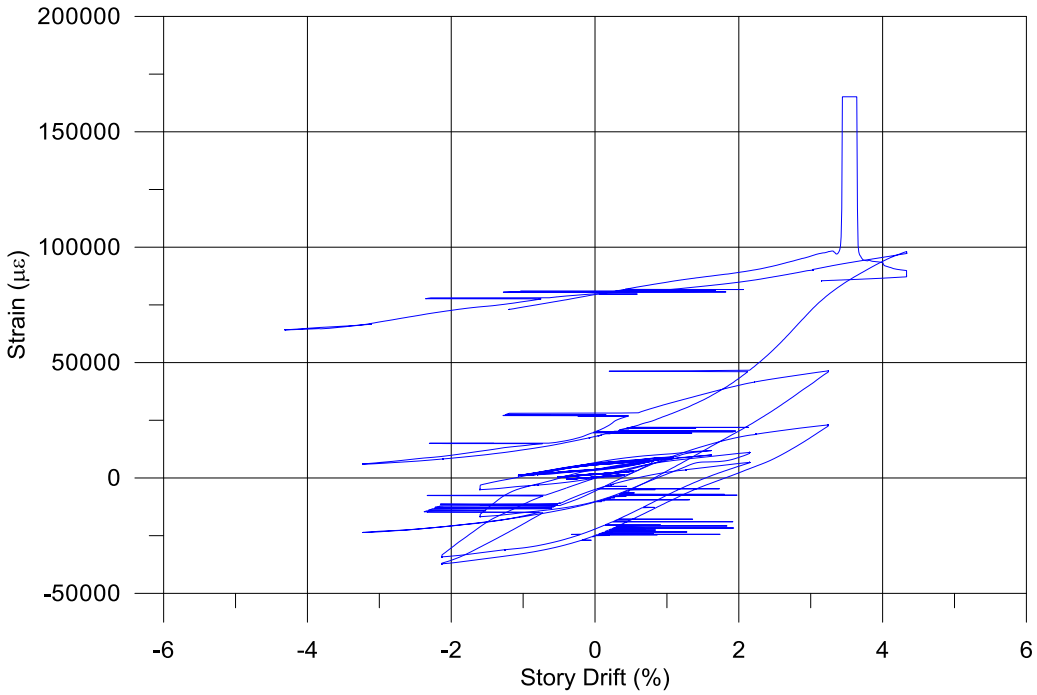
200000
150000
100000
50000
0
-50000
Strain (με)
-6
-4
-2
0
2
4
6
Story Drift (%)

M3-9

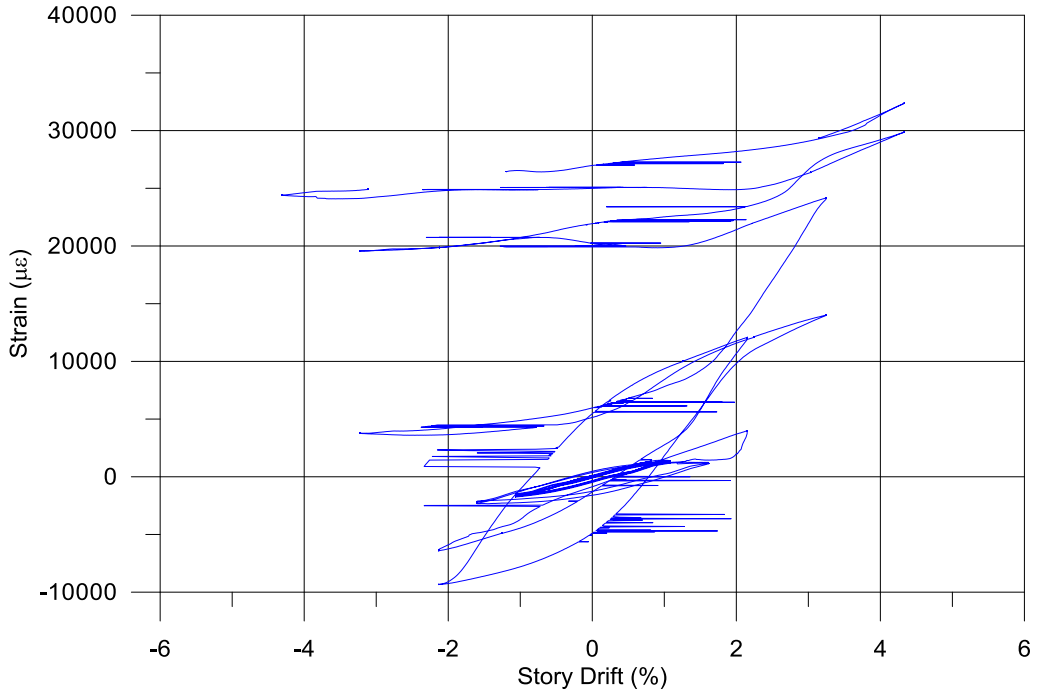
40000
30000
20000
10000
0
-10000
Strain (με)
-6
-4
-2
0
2
4
6
Story Drift (%)

M3-10

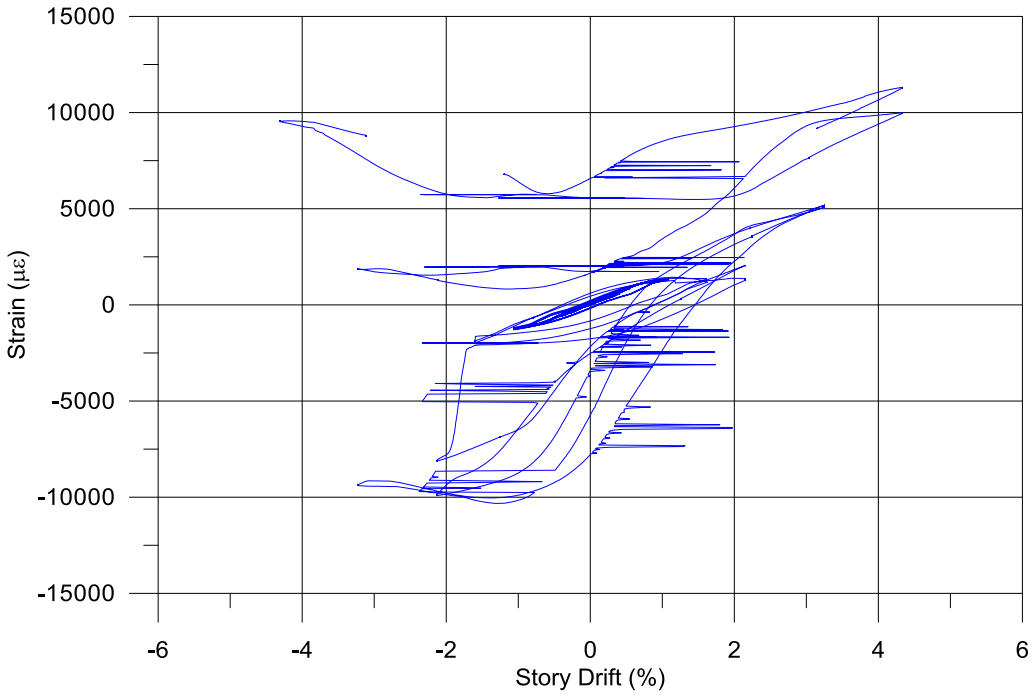
15000
10000
5000
0
-5000
-10000
-15000
Strain (με)
-6
-4
-2
0
2
4
6
Story Drift (%)

M3-11

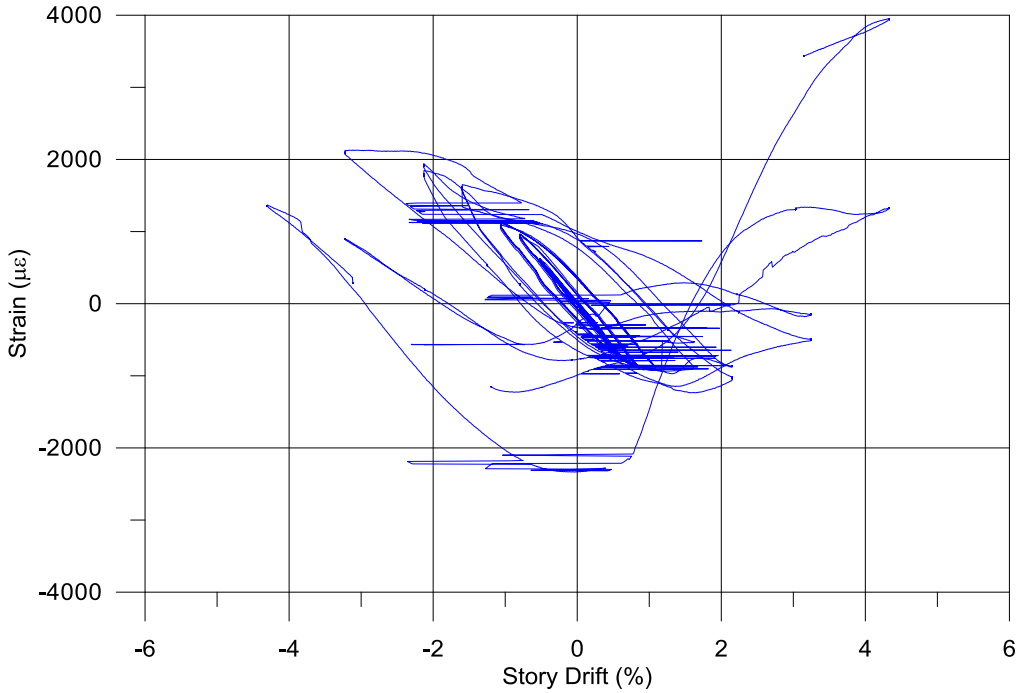
4000
2000
0
-2000
-4000
Strain (με)
-6
-4
-2
0
2
4
6
Story Drift (%)

M3-12-1

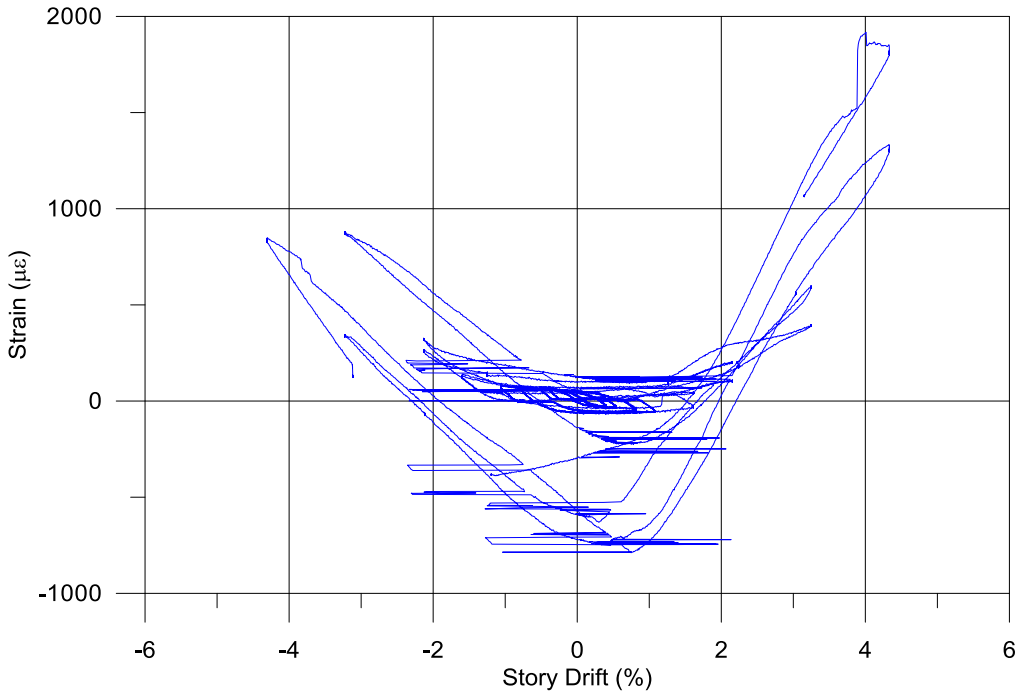
2000
1000
0
-1000
Strain (με)
-6
-4
-2
0
2
4
6
Story Drift (%)

M3-12-2

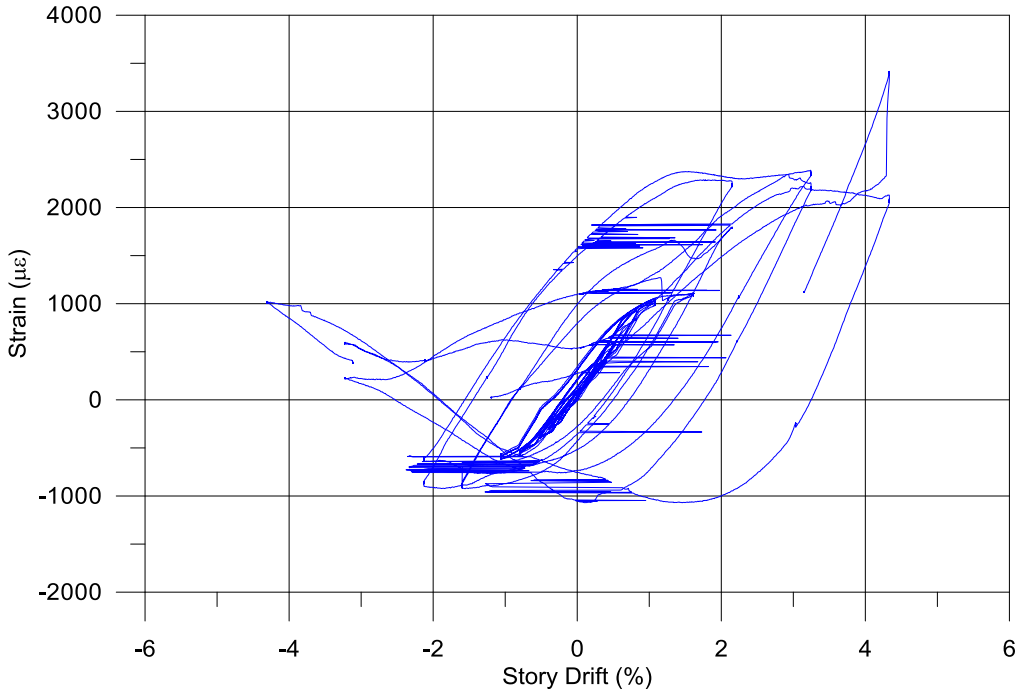
4000
3000
2000
1000
0
-1000
-2000
Strain (με)
-6
-4
-2
0
2
4
6
Story Drift (%)

M3-12-3

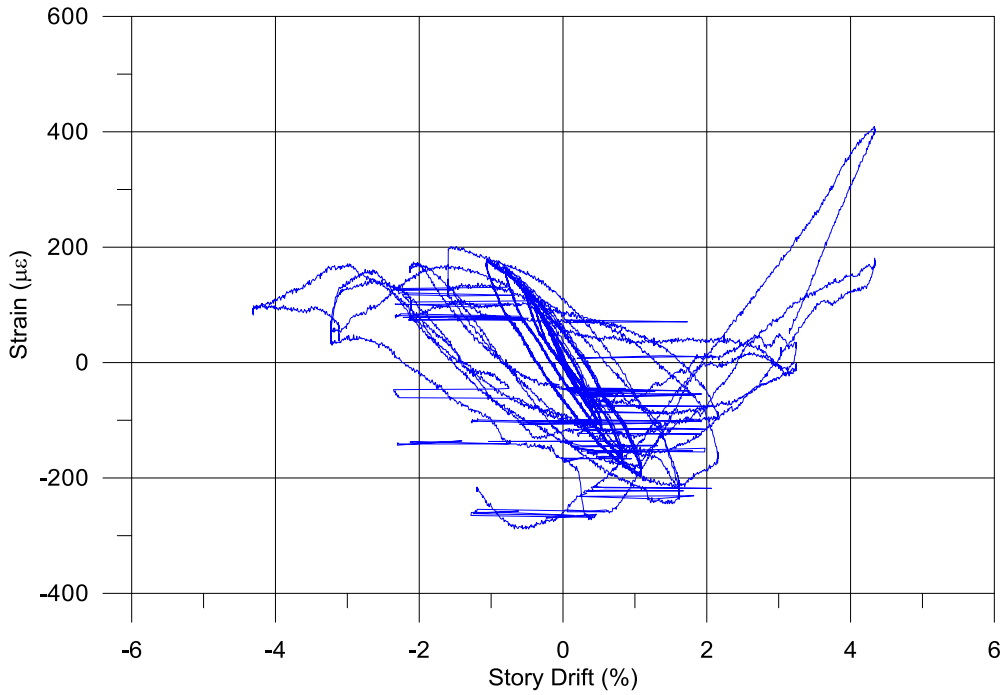
600
400
200
0
-200
-400
Strain (με)
-6
-4
-2
0
2
4
6
Story Drift (%)

M3-13

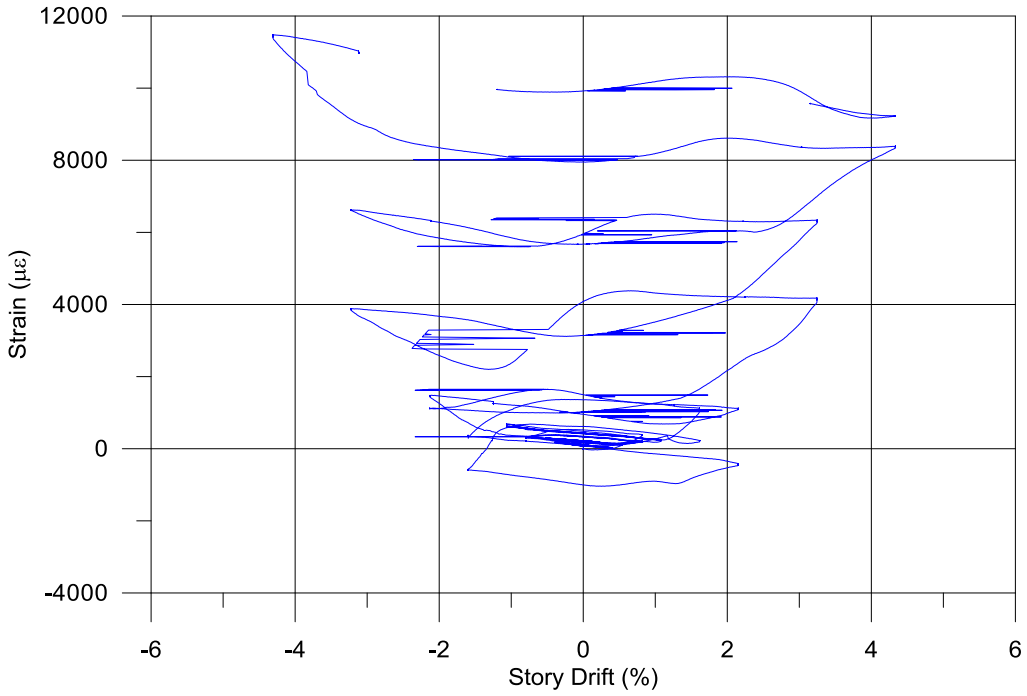
12000
8000
4000
0
-4000
Strain (με)
-6
-4
-2
0
2
4
6
Story Drift (%)

M3-RS1-1

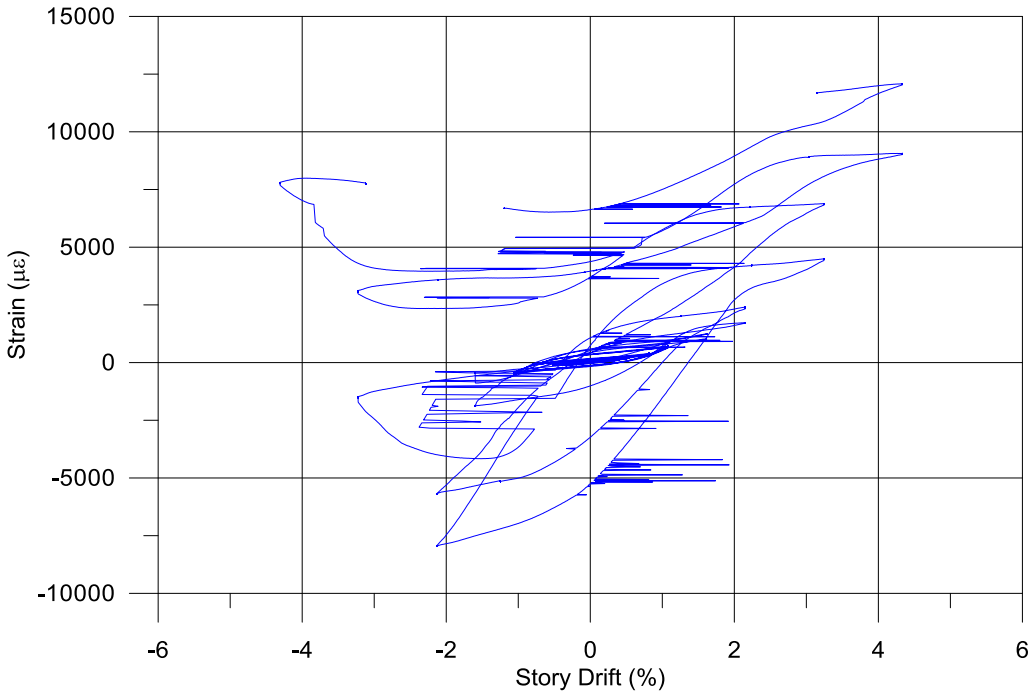

M3-RS1-2

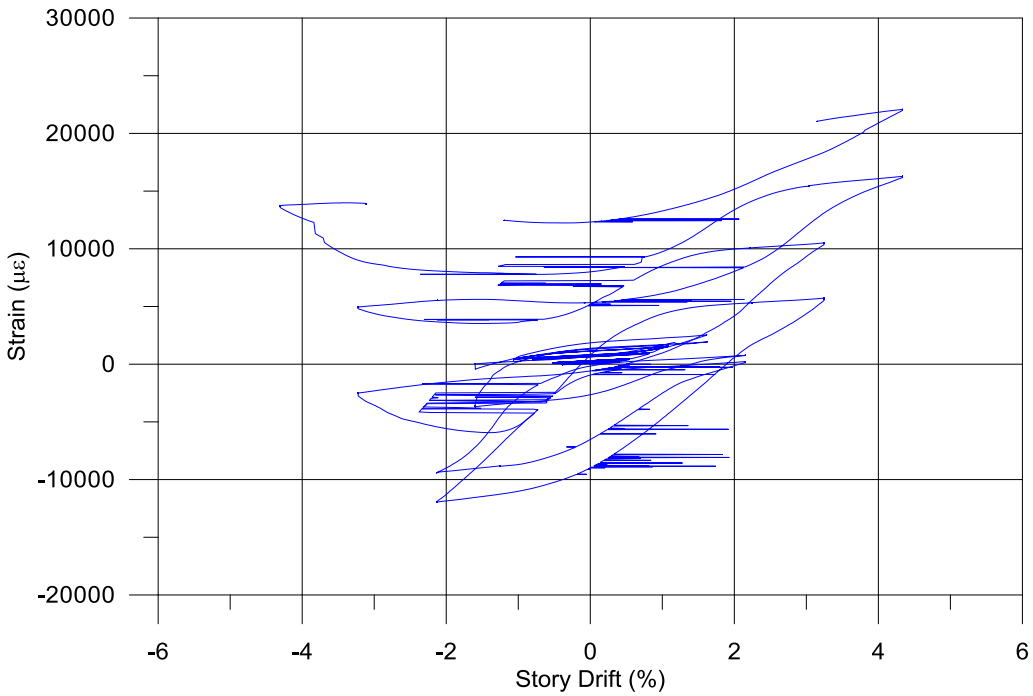

M3-RS1-3

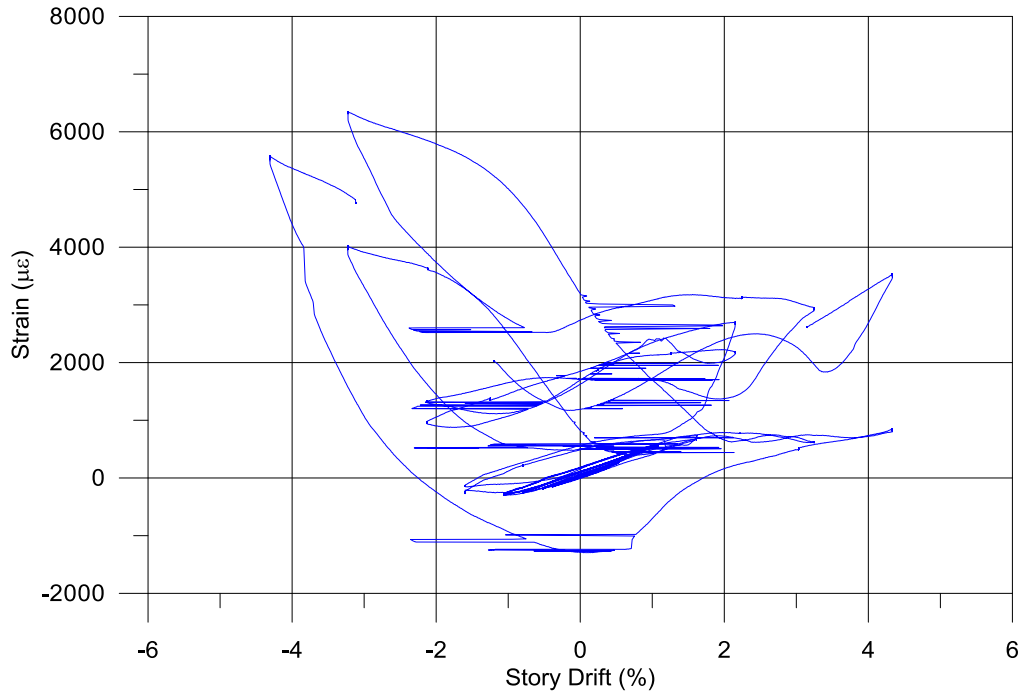

M3-RS2-1

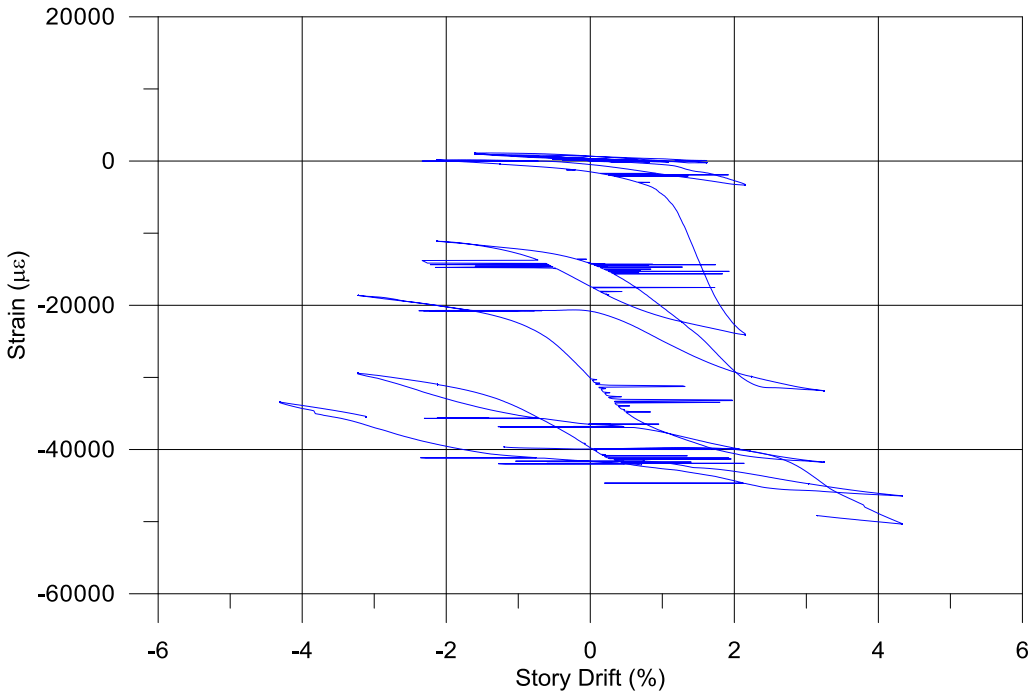

M3-RS2-2

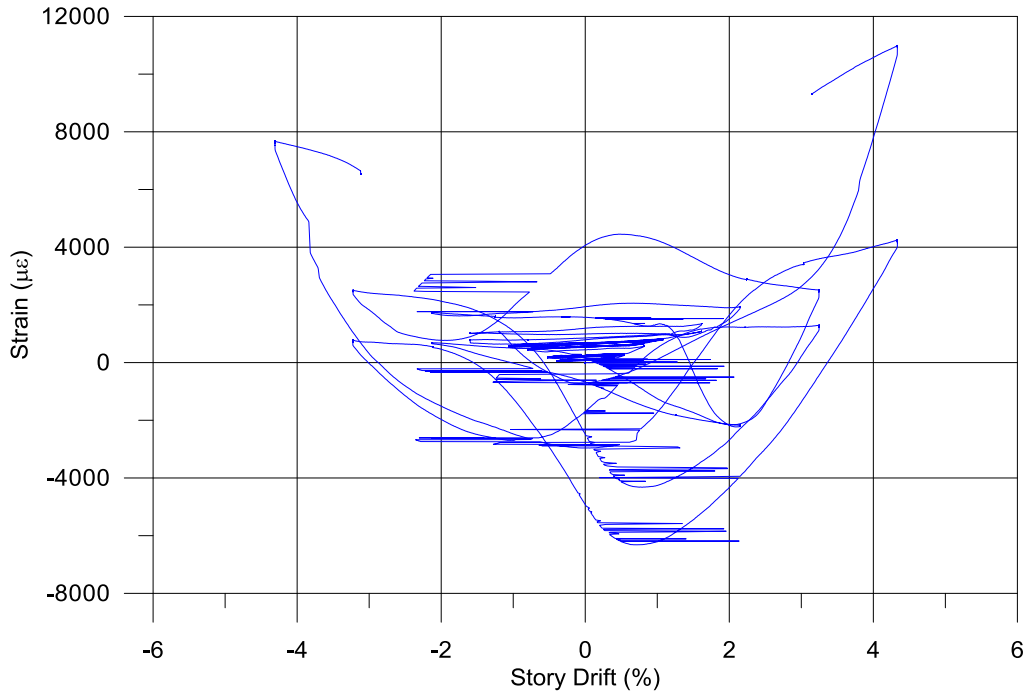

M3-RS2-3

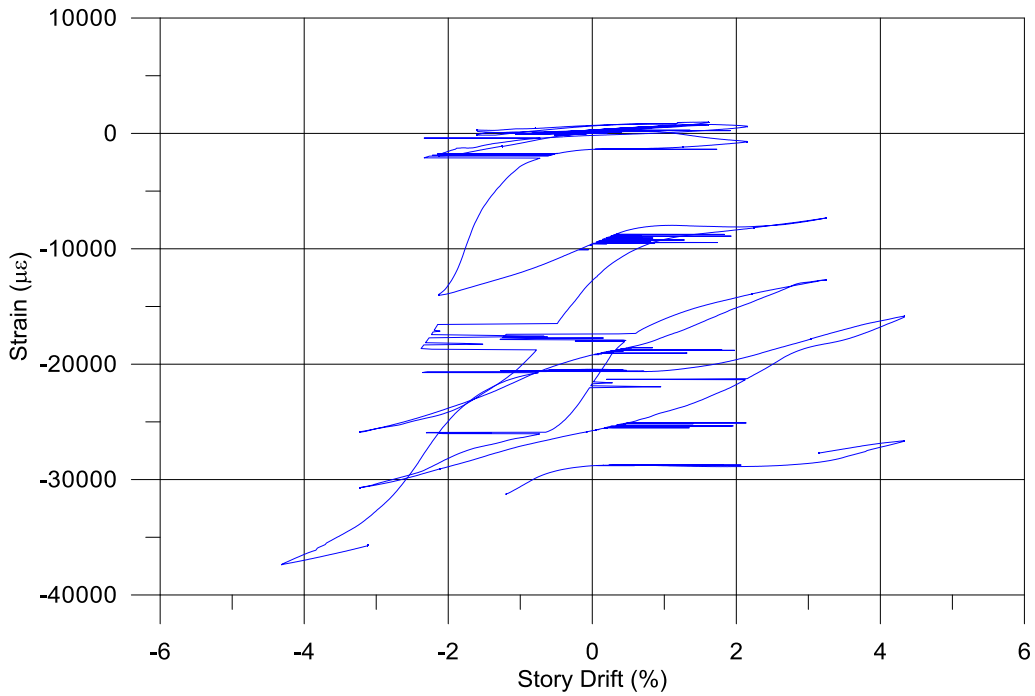

M3-RS3-1

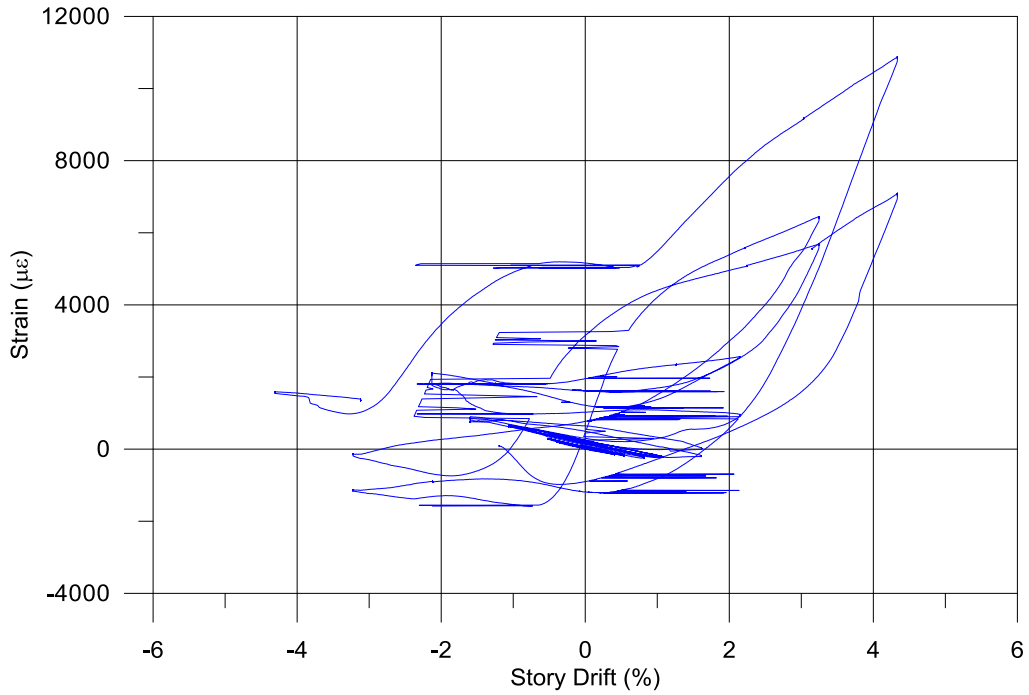

M3-RS3-2

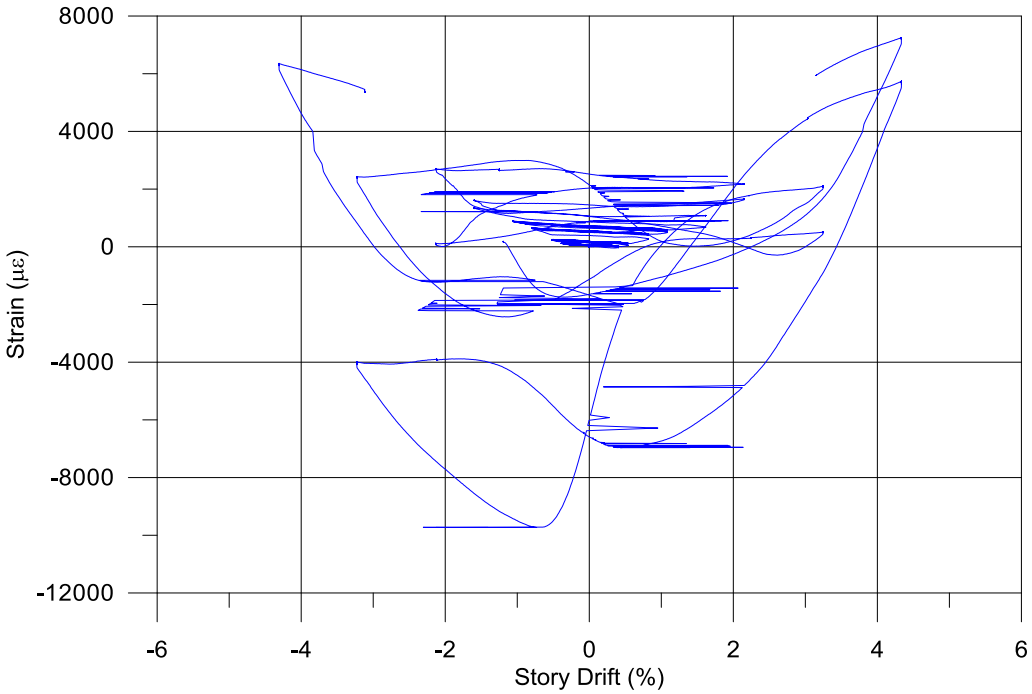

M3-RS3-3

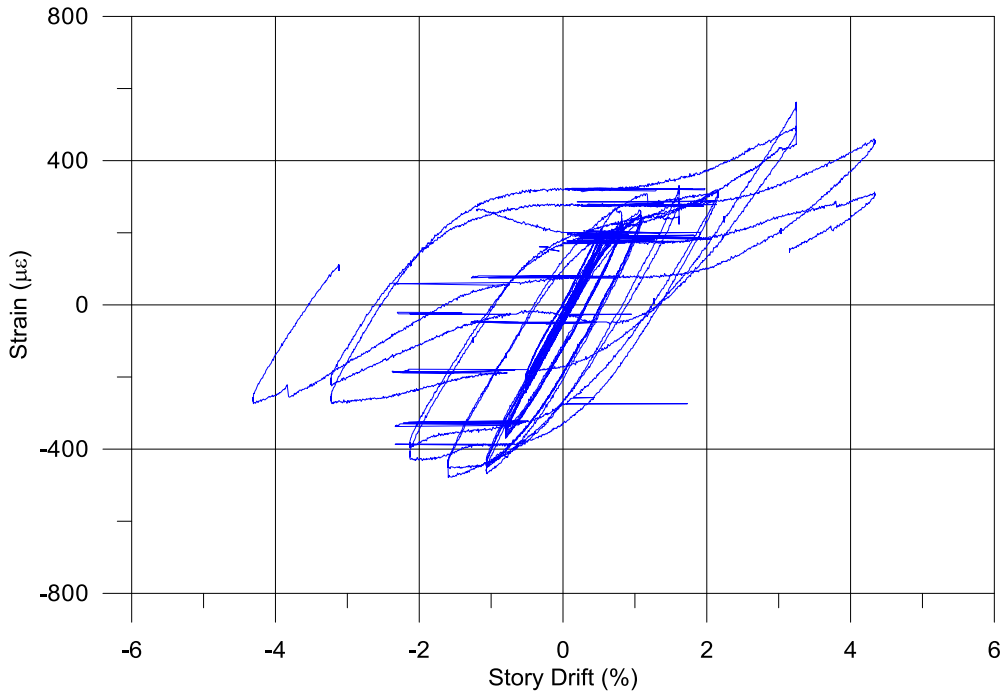
800
400
0
-400
-800
Strain (με)
-6
-4
-2
0
2
4
6
Story Drift (%)

M4-1-1

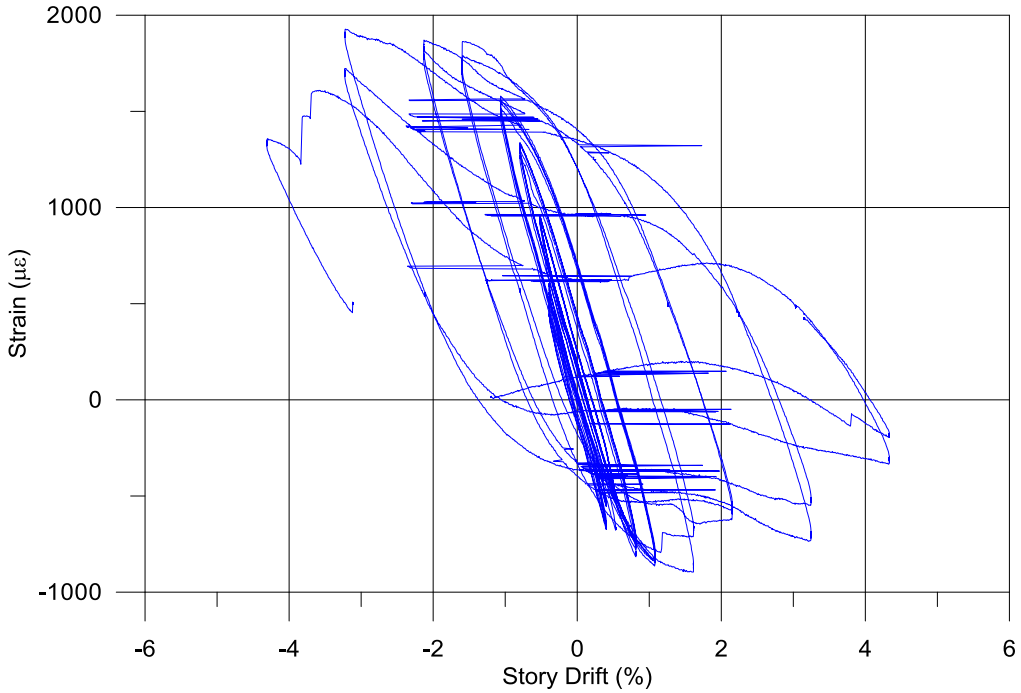
2000
1000
0
-1000
Strain (με)
-6
-4
-2
0
2
4
6
Story Drift (%)

M4-1-2

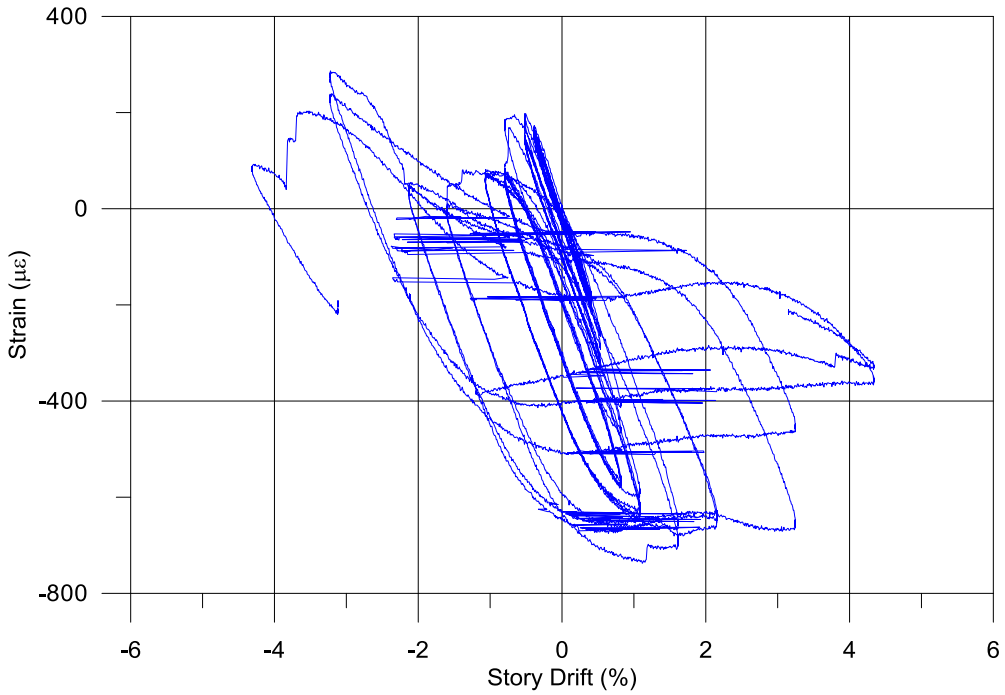
400
0
-400
-800
Strain (με)
-6
-4
-2
0
2
4
6
Story Drift (%)

M4-2-1

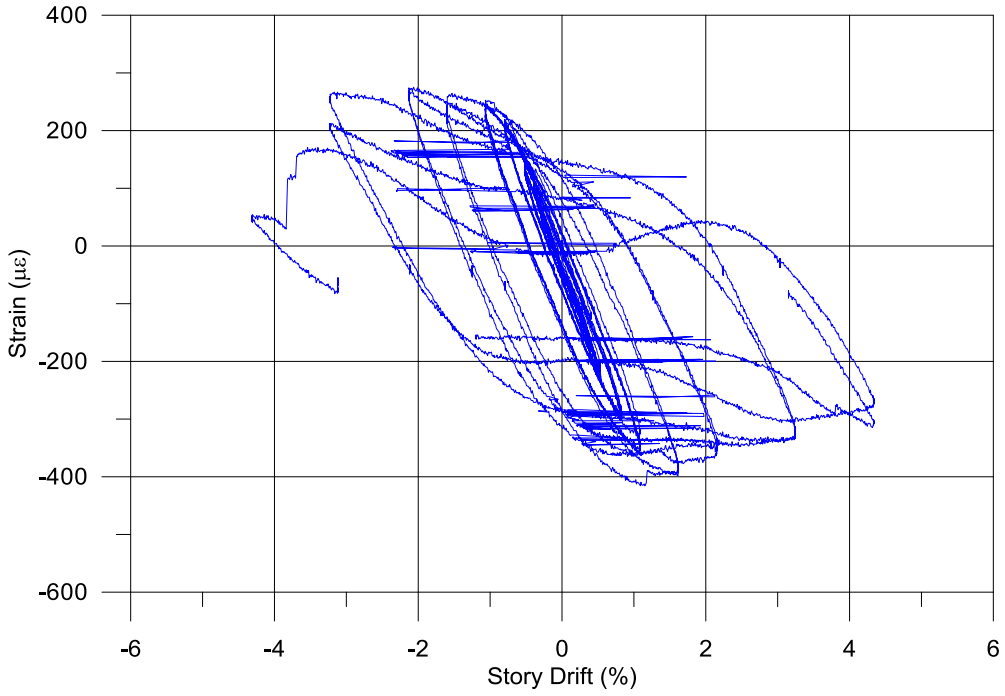
400
200
0
-200
-400
-600
Strain (με)
-6
-4
-2
0
2
4
6
Story Drift (%)

M4-2-2

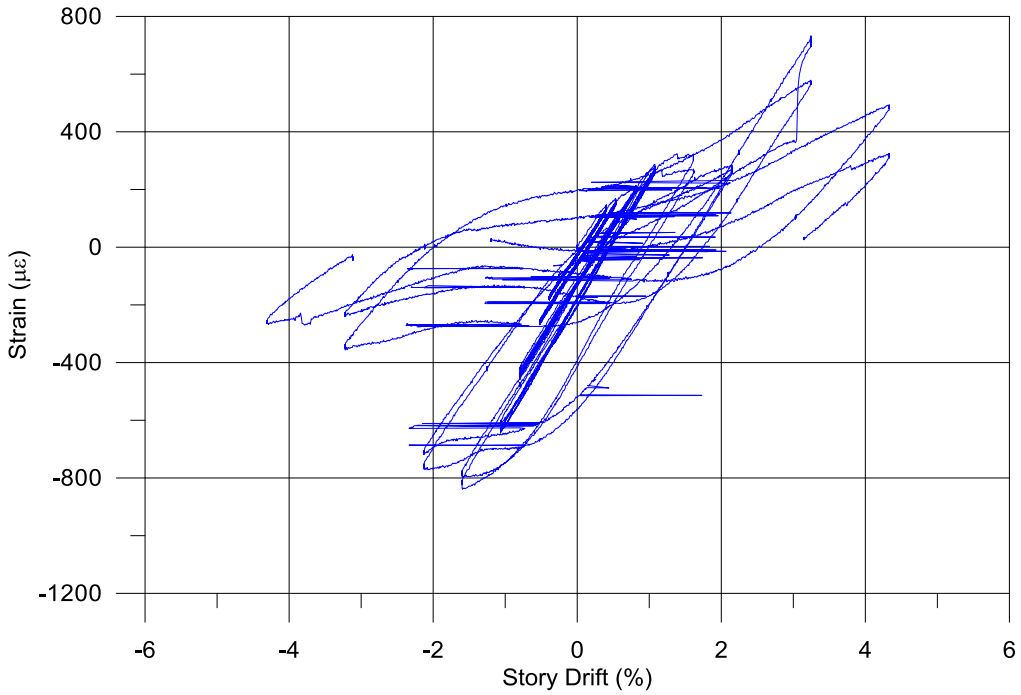
800
400
0
-400
-800
-1200
Strain (με)
-6
-4
-2
0
2
4
6
Story Drift (%)

M5-1-1

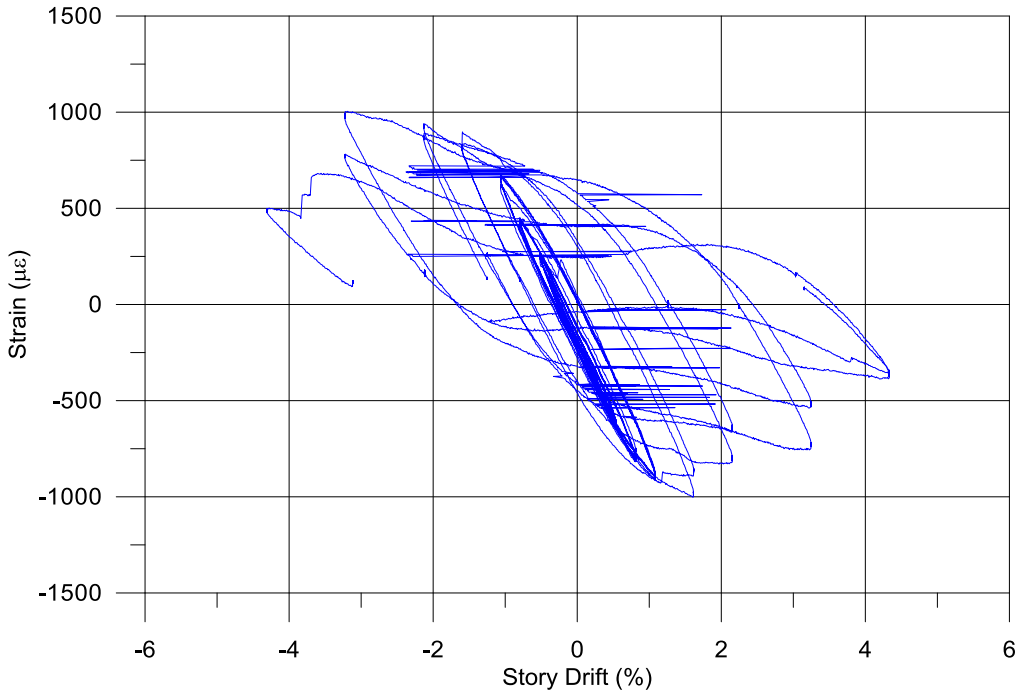
1500
1000
500
0
-500
-1000
-1500
Strain (με)
-6
-4
-2
0
2
4
6
Story Drift (%)

M5-1-2

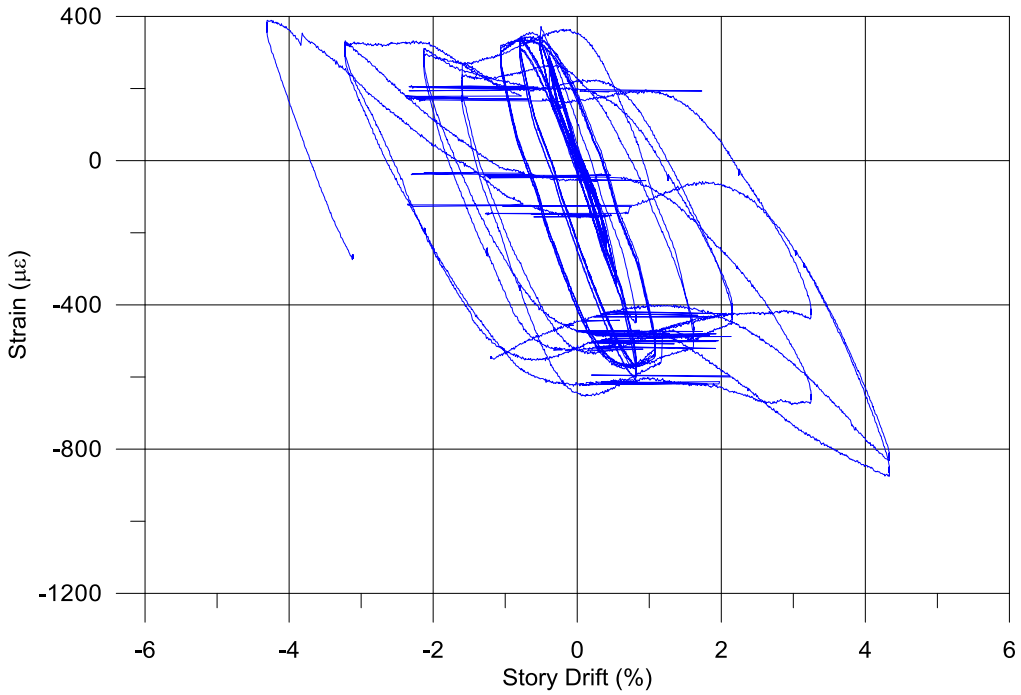
400
0
-400
-800
-1200
Strain (με)
-6
-4
-2
0
2
4
6
Story Drift (%)

M5-2-1

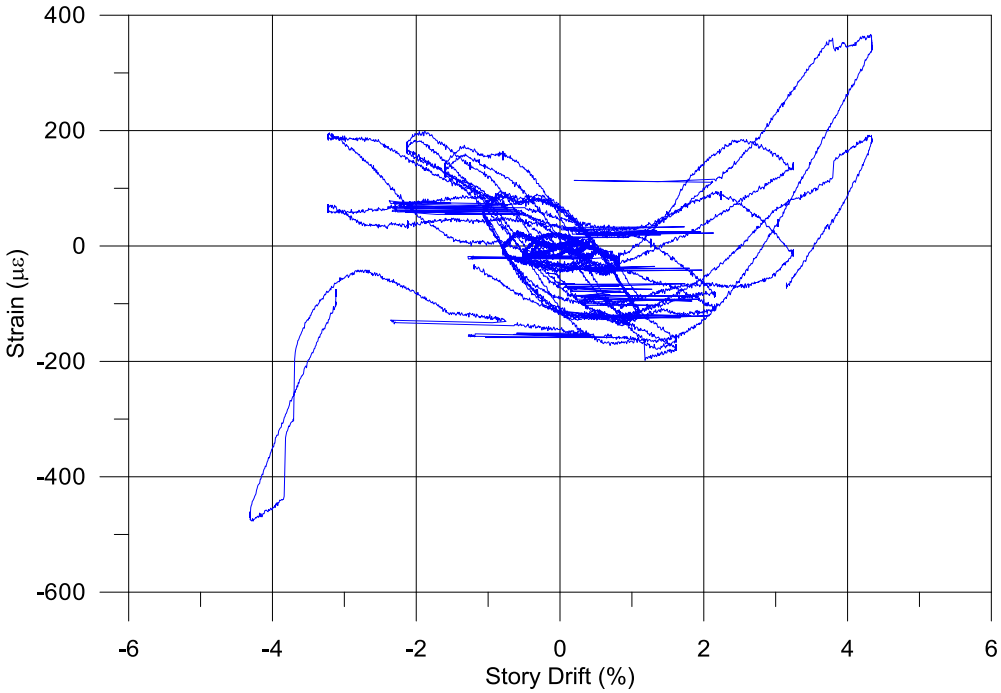
400
200
0
-200
-400
-600
Strain (με)
-6
-4
-2
0
2
4
6
Story Drift (%)

M5-2-2

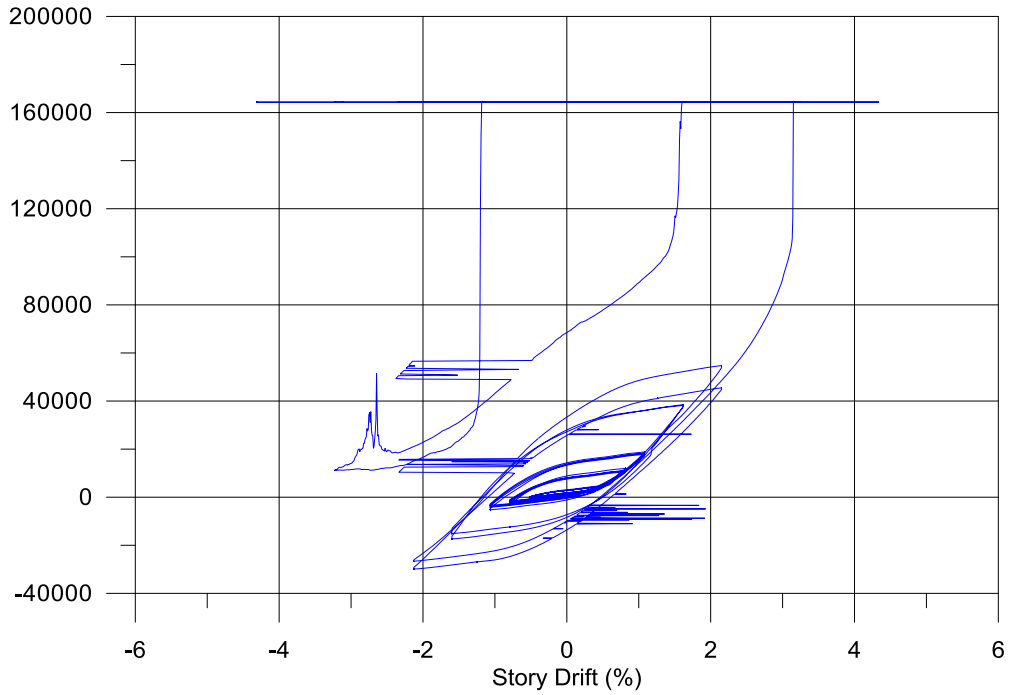
200000
160000
120000
80000
40000
0
-40000
-6
-4
-2
0
2
4
6
Story Drift (%)

M6-1

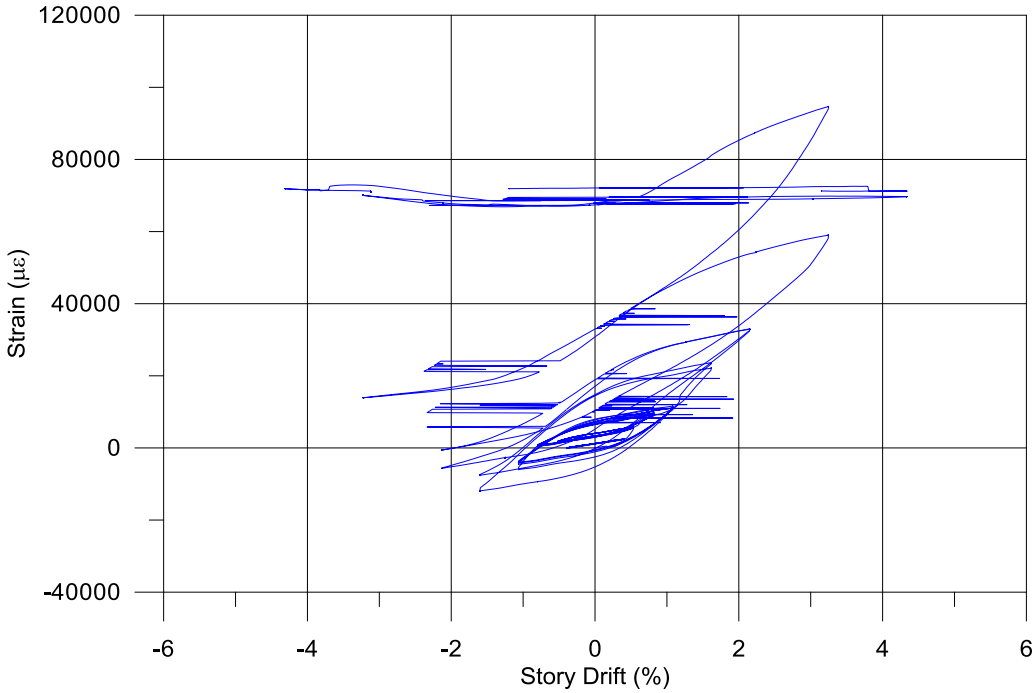
120000
80000
40000
0
-40000
Strain (με)
-6
-4
-2
0
2
4
6
Story Drift (%)

M6-2

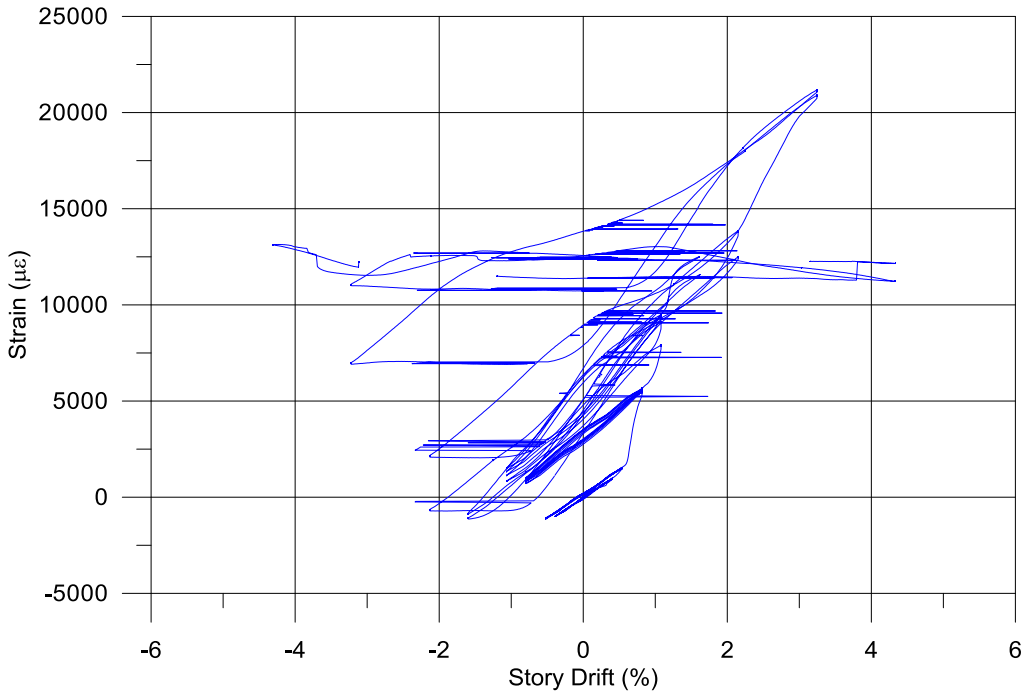
25000
20000
15000
10000
5000
0
-5000
Strain (με)
-6
-4
-2
0
2
4
6
Story Drift (%)

M6-3

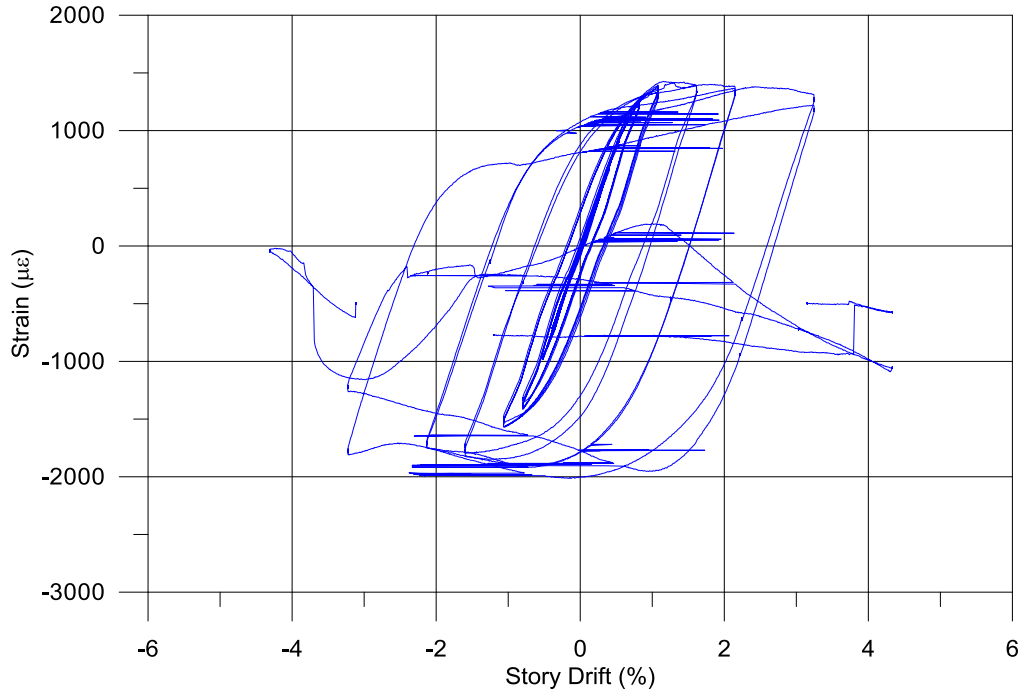
2000
1000
0
-1000
-2000
-3000
Strain (με)
-6
-4
-2
0
2
4
6
Story Drift (%)

M6-4

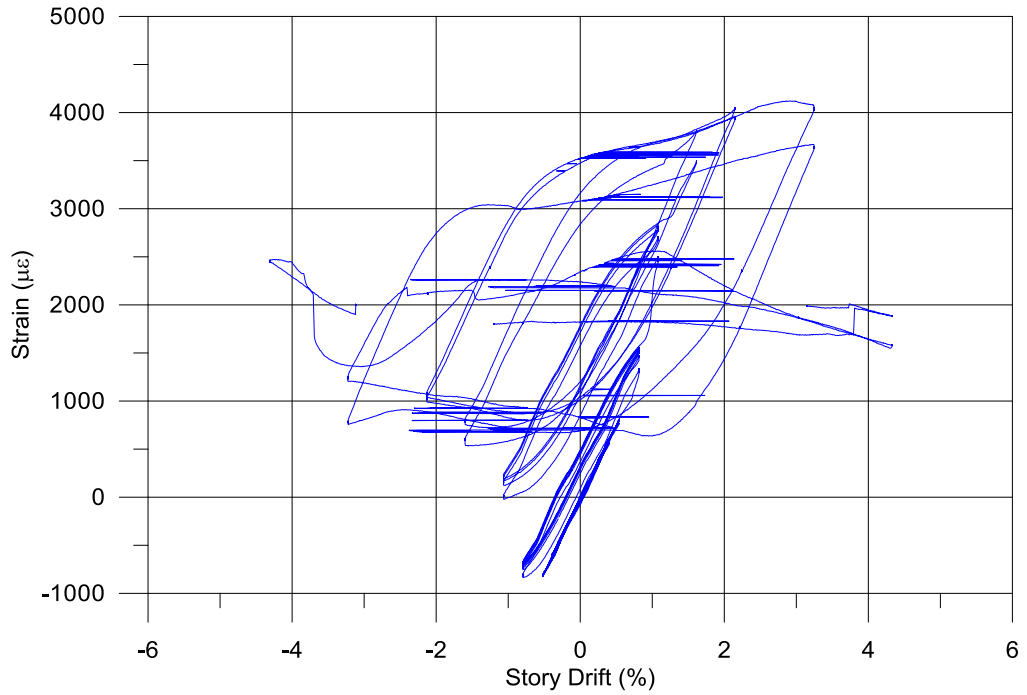
5000
4000
3000
2000
1000
0
-1000
Strain (με)
-6
-4
-2
0
2
4
6
Story Drift (%)

M6-5

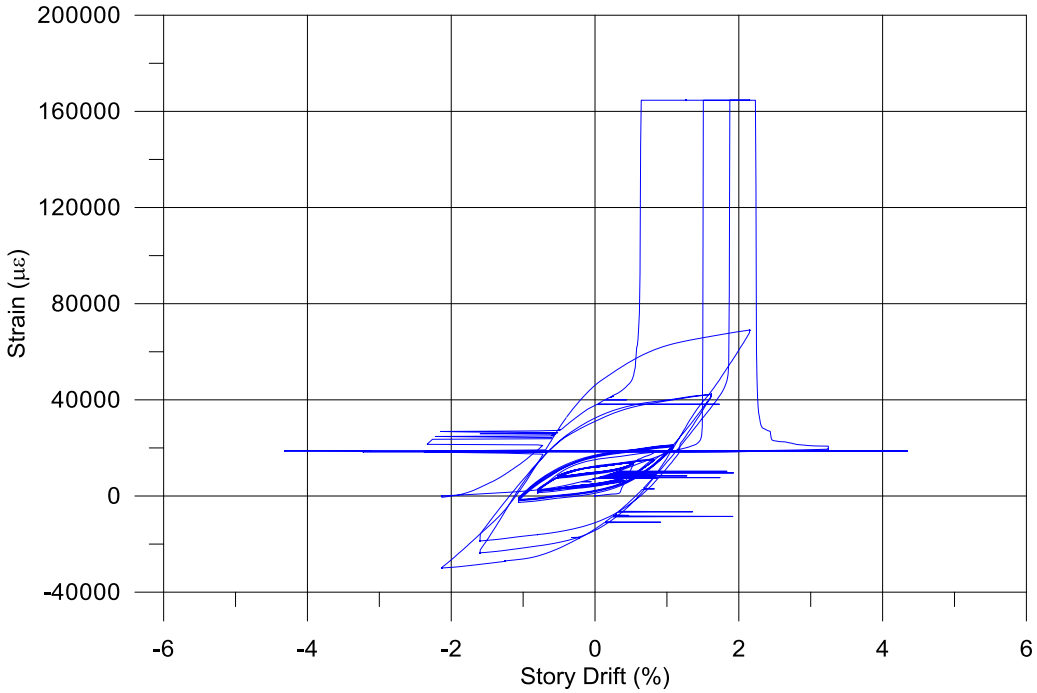
200000
160000
120000
80000
40000
0
-40000
Strain (με)
-6
-4
-2
0
2
4
6
Story Drift (%)

M6-6

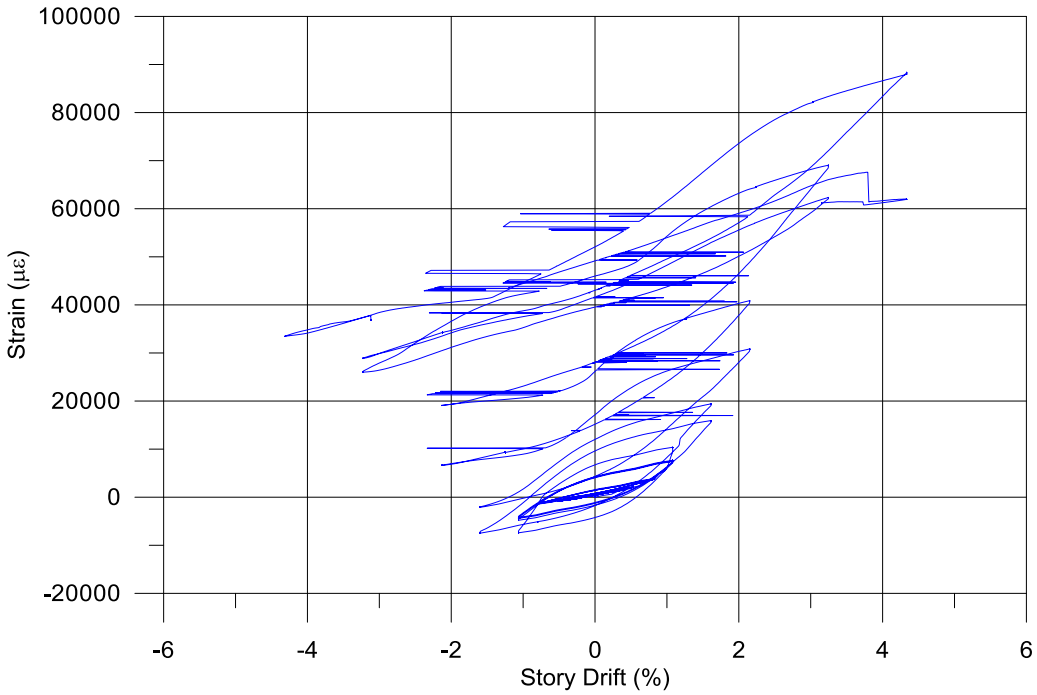
100000
80000
60000
40000
20000
0
-20000
Strain (με)
-6
-4
-2
0
2
4
6
Story Drift (%)

M6-7

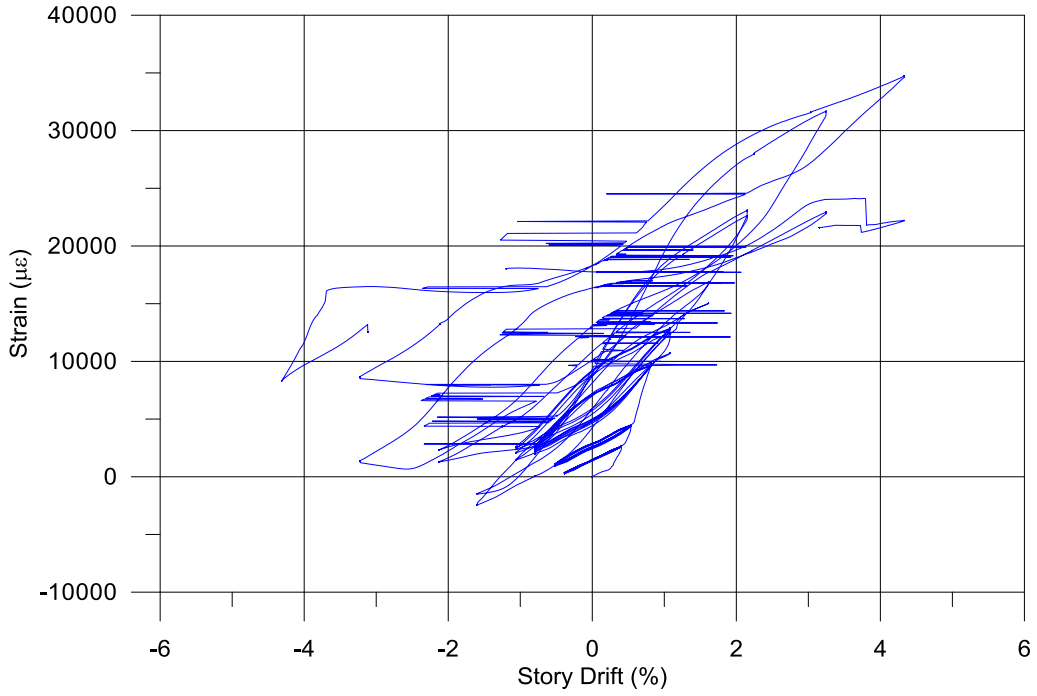
40000
30000
20000
10000
0
-10000
Strain (με)
-6
-4
-2
0
2
4
6
Story Drift (%)

M6-8

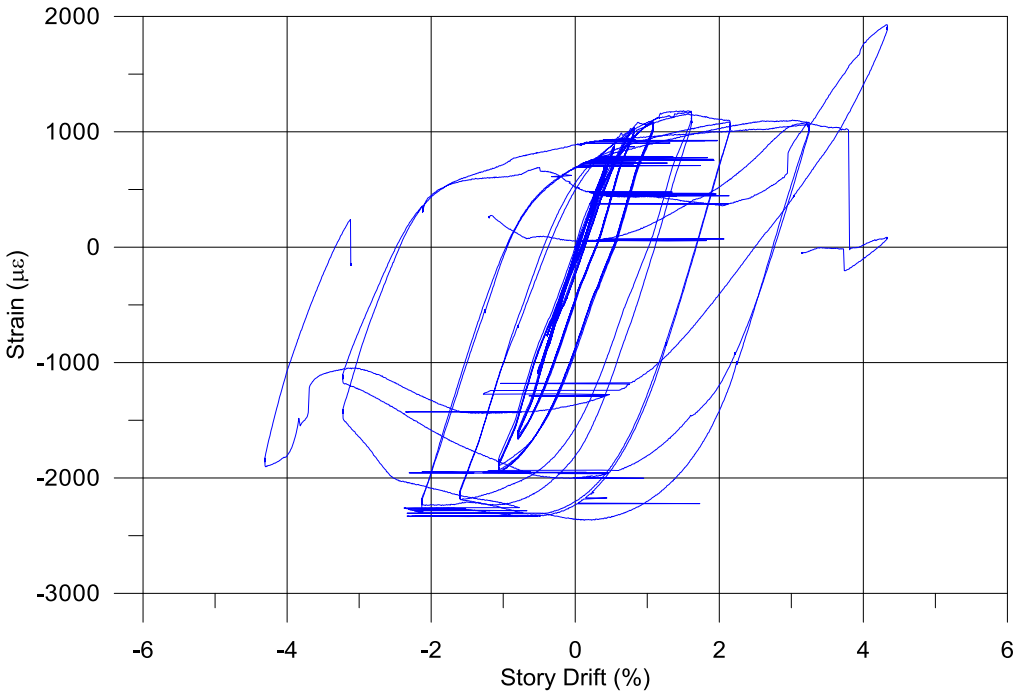
2000
1000
0
-1000
-2000
-3000
Strain (με)
-6
-4
-2
0
2
4
6
Story Drift (%)

M6-9

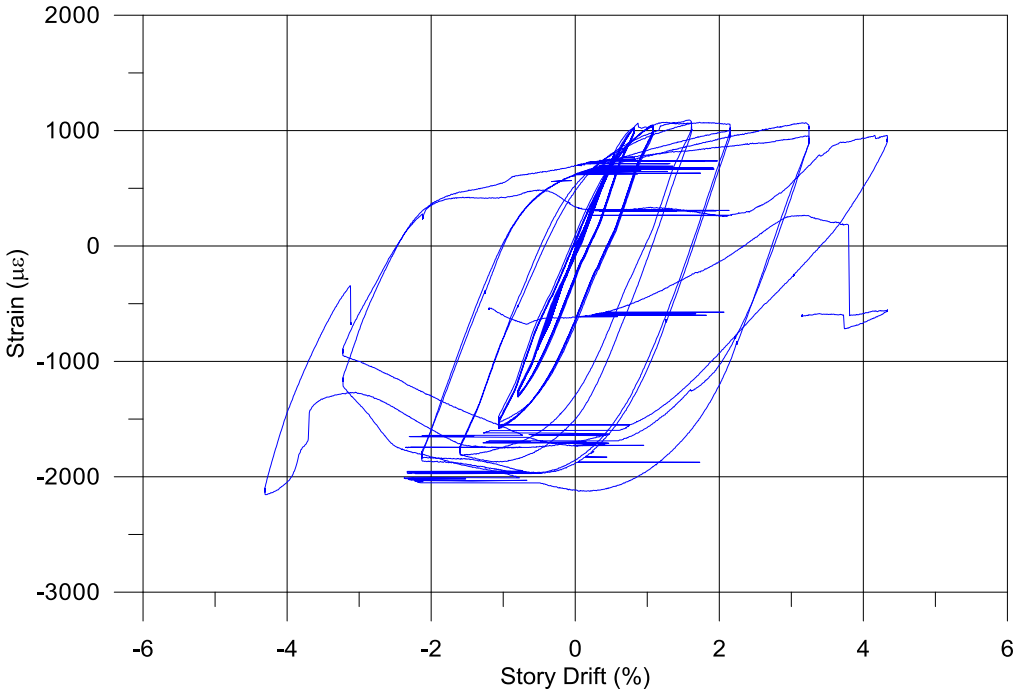
2000
1000
0
-1000
-2000
-3000
Strain (με)
-6
-4
-2
0
2
4
6
Story Drift (%)

M6-10

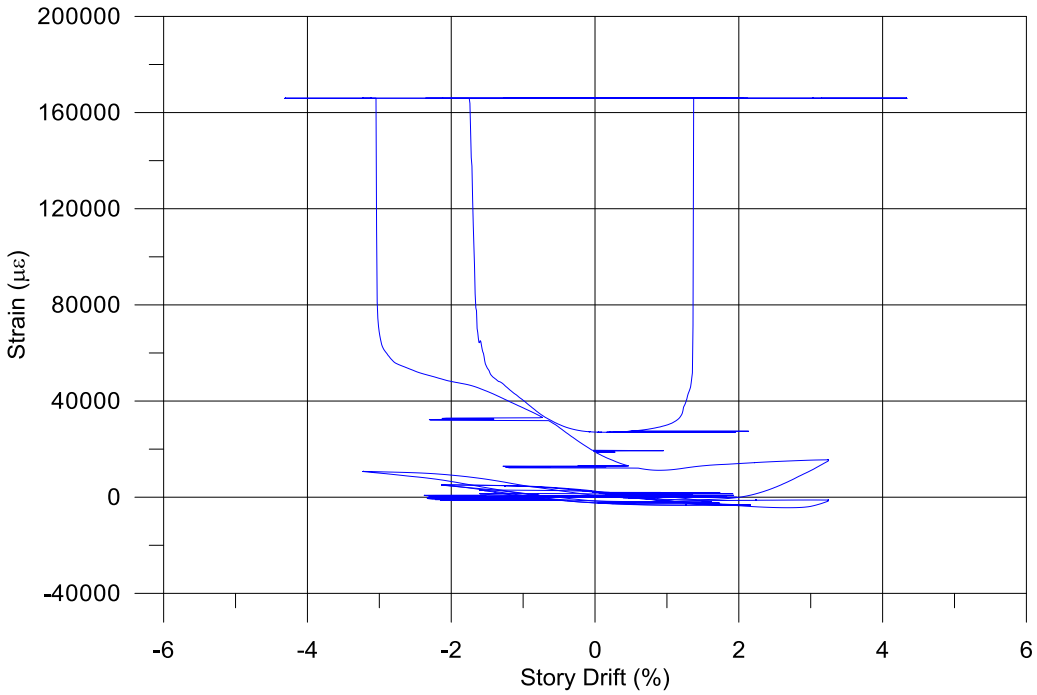

M6-RS1-1

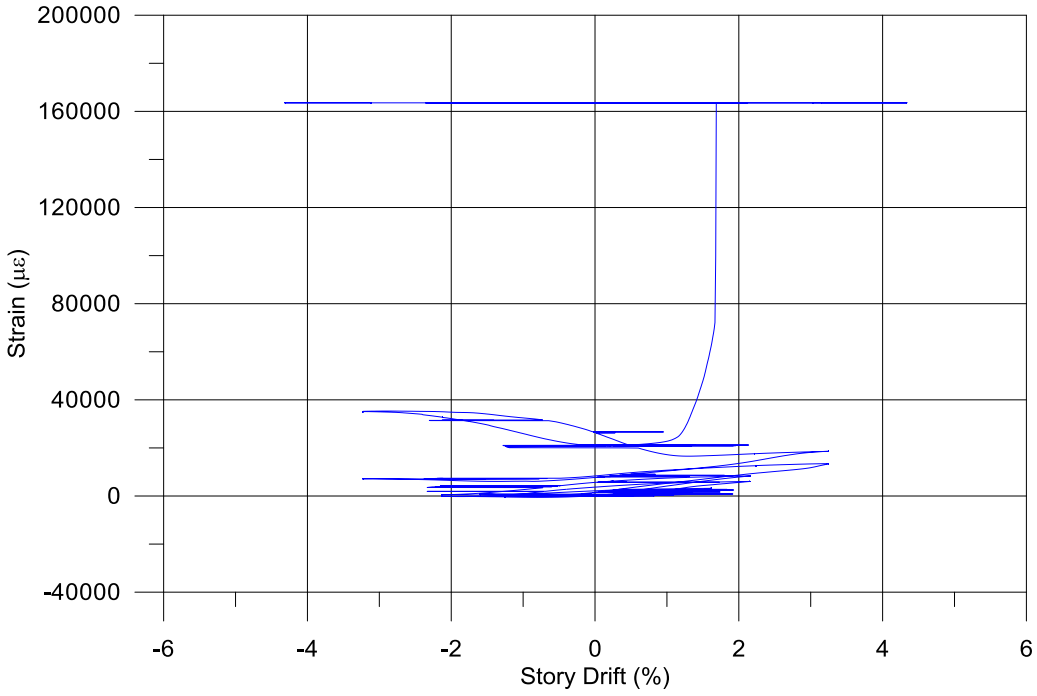

M6-RS1-2

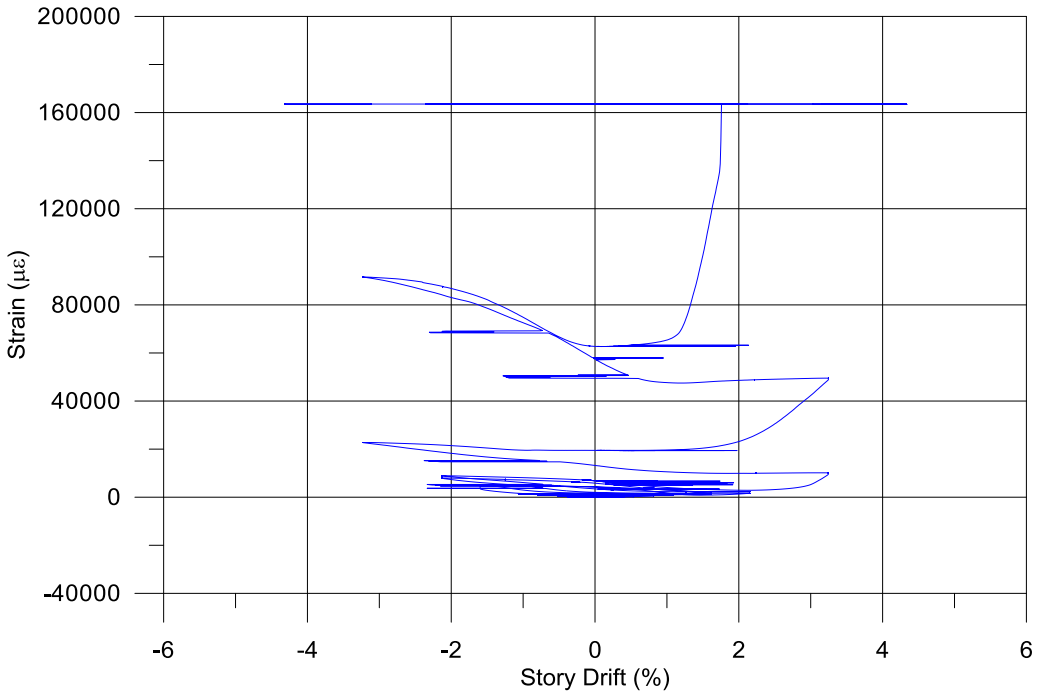

M6-RS1-3

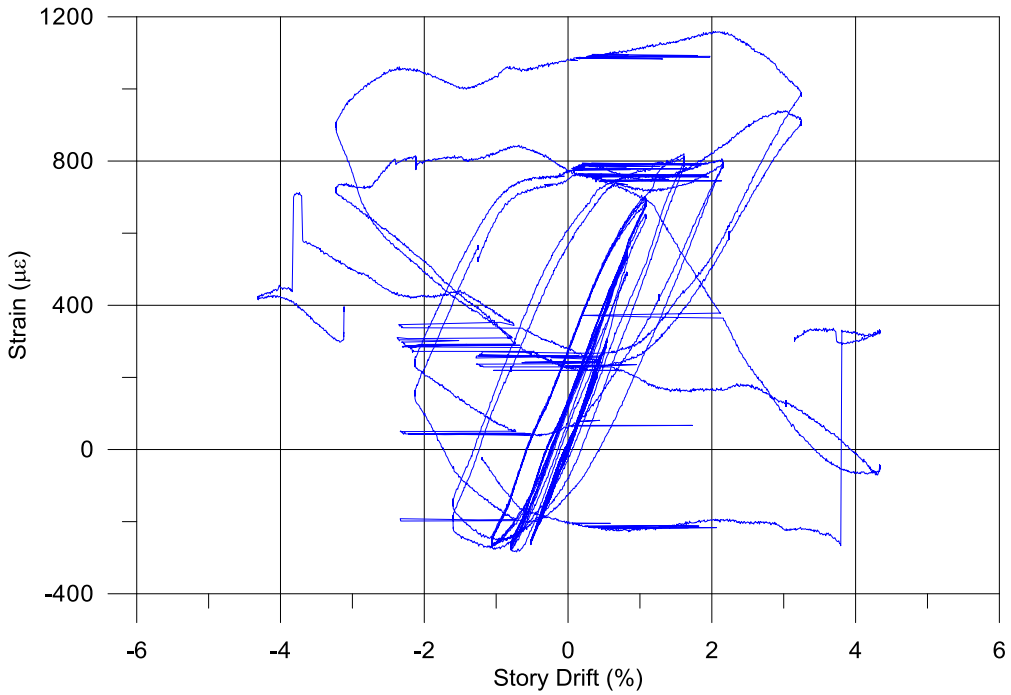

M6-RS2-1

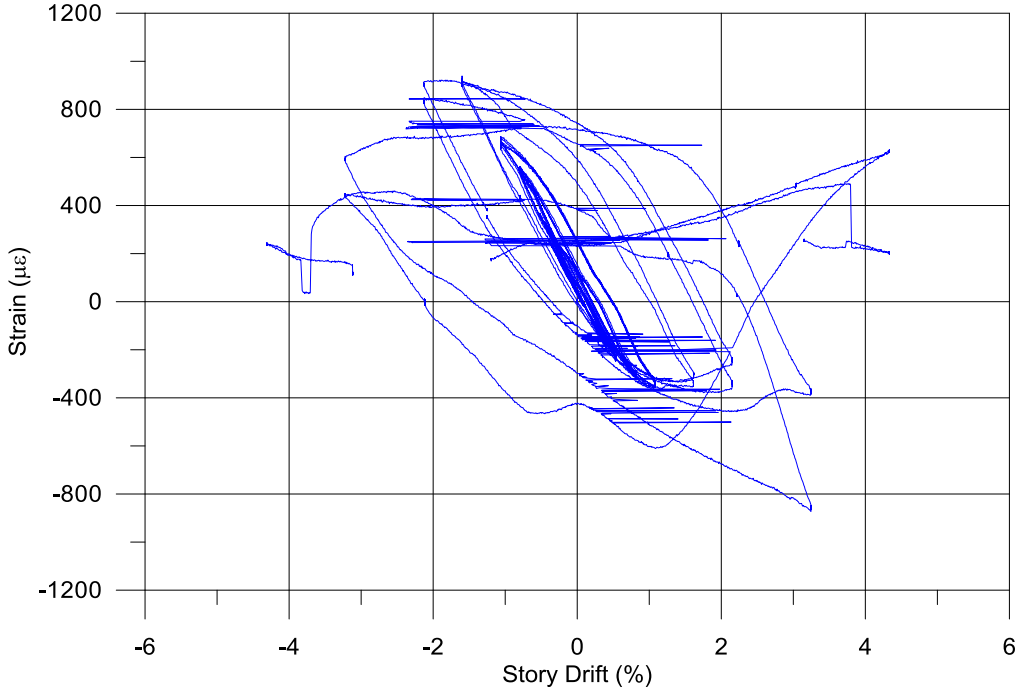

M6-RS2-2

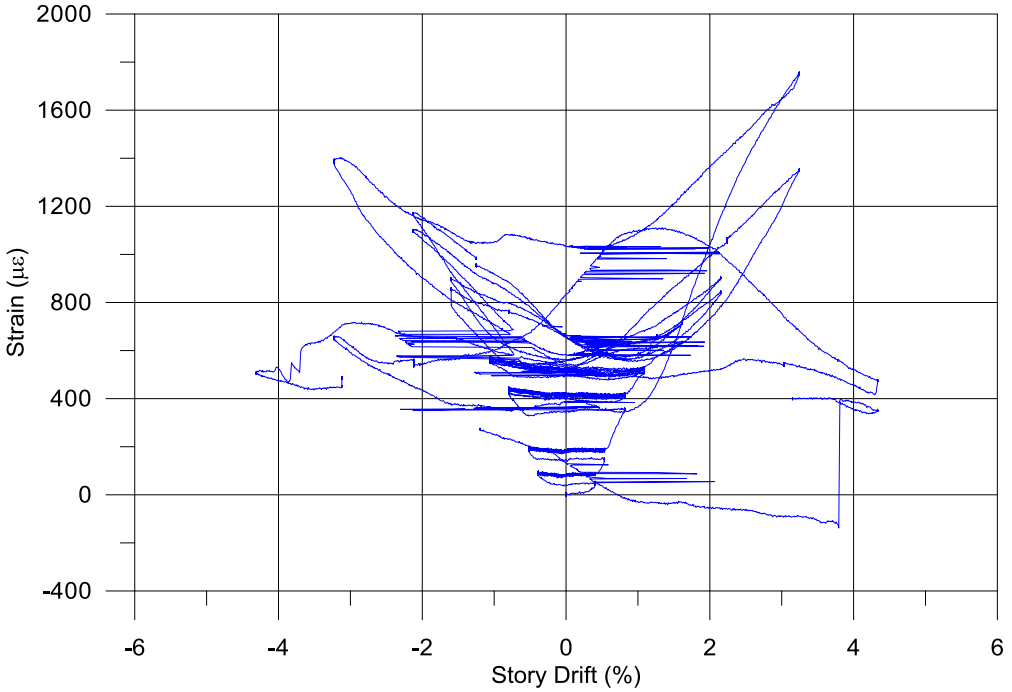

M6-RS2-3

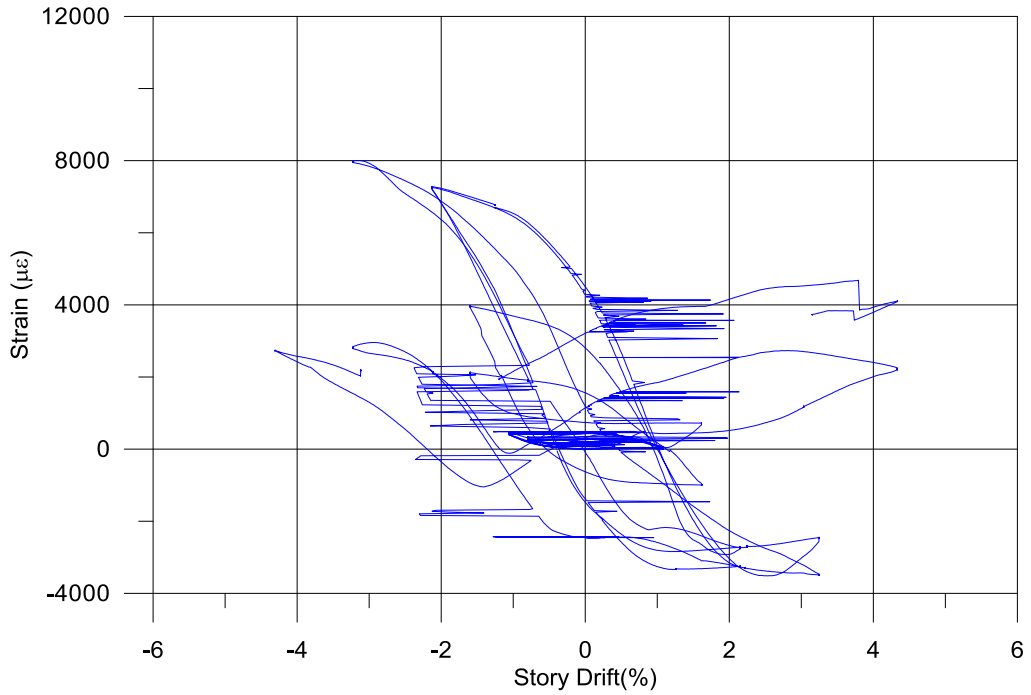

M6-RS3-1

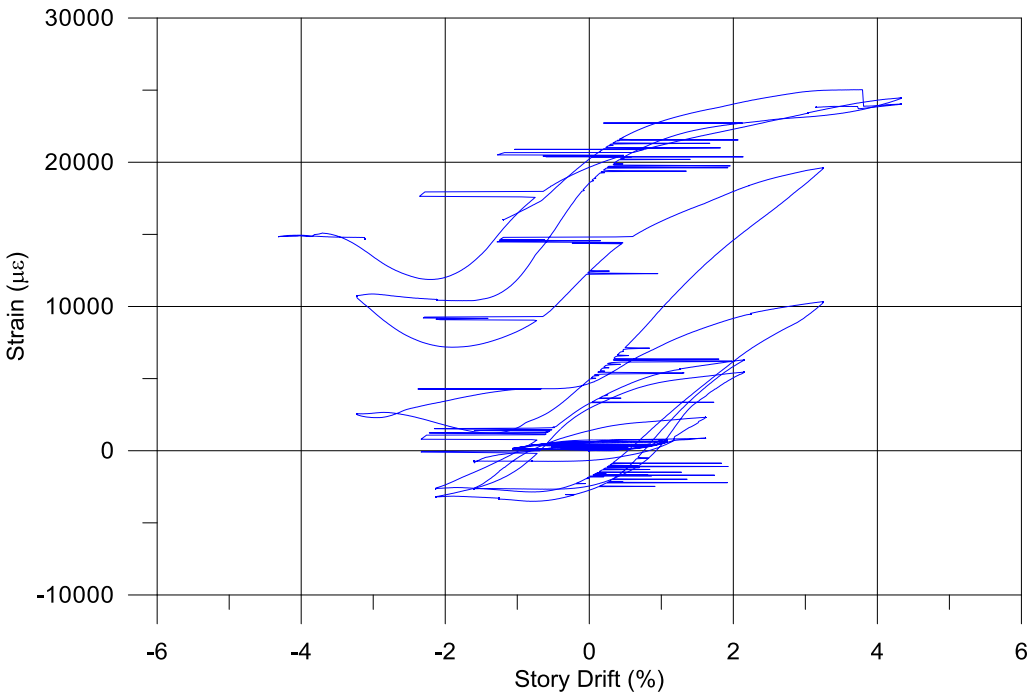

M6-RS3-2

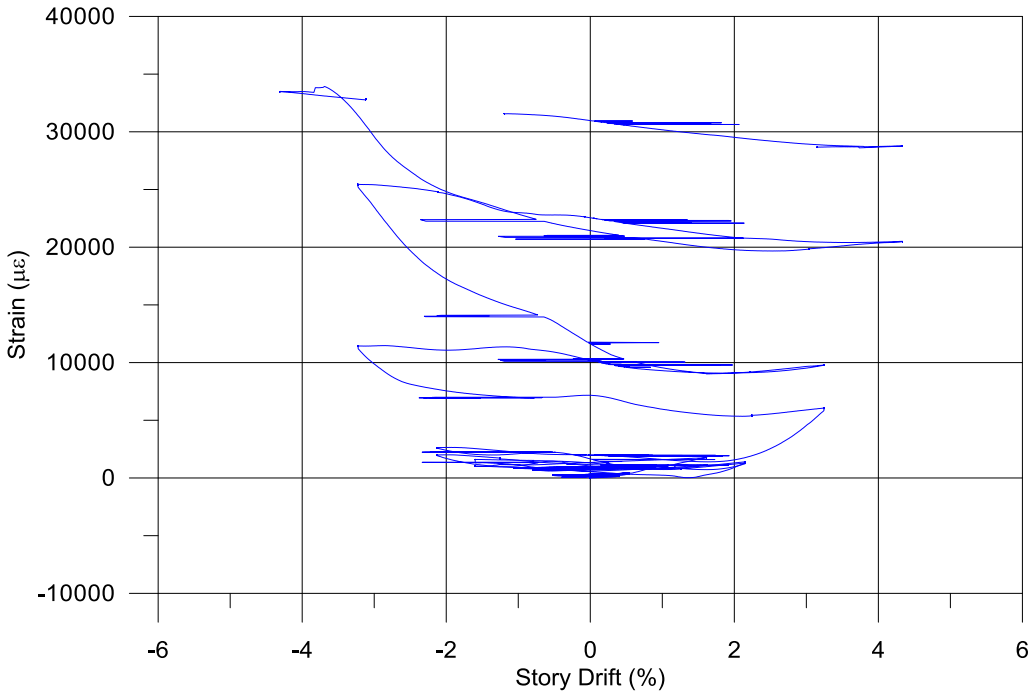
40000
30000
20000
10000
0
-10000
Strain (με)
-6
-4
-2
0
2
4
6
Story Drift (%)

M6-RS3-3

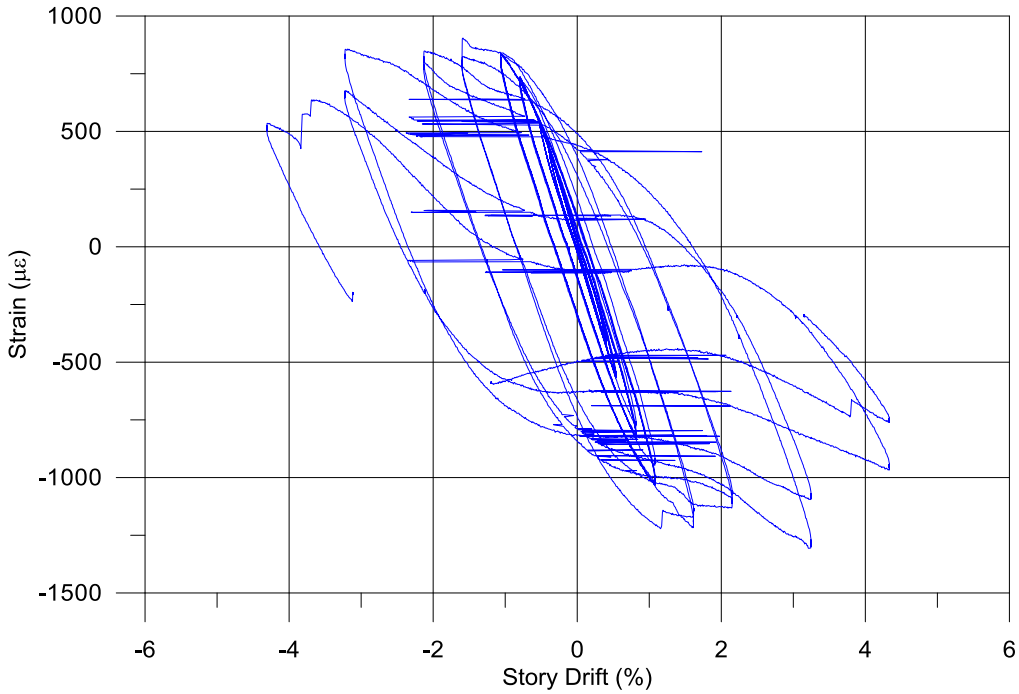
1000
500
0
-500
-1000
-1500
Strain (με)
-6
-4
-2
0
2
4
6
Story Drift (%)

M7-1-1

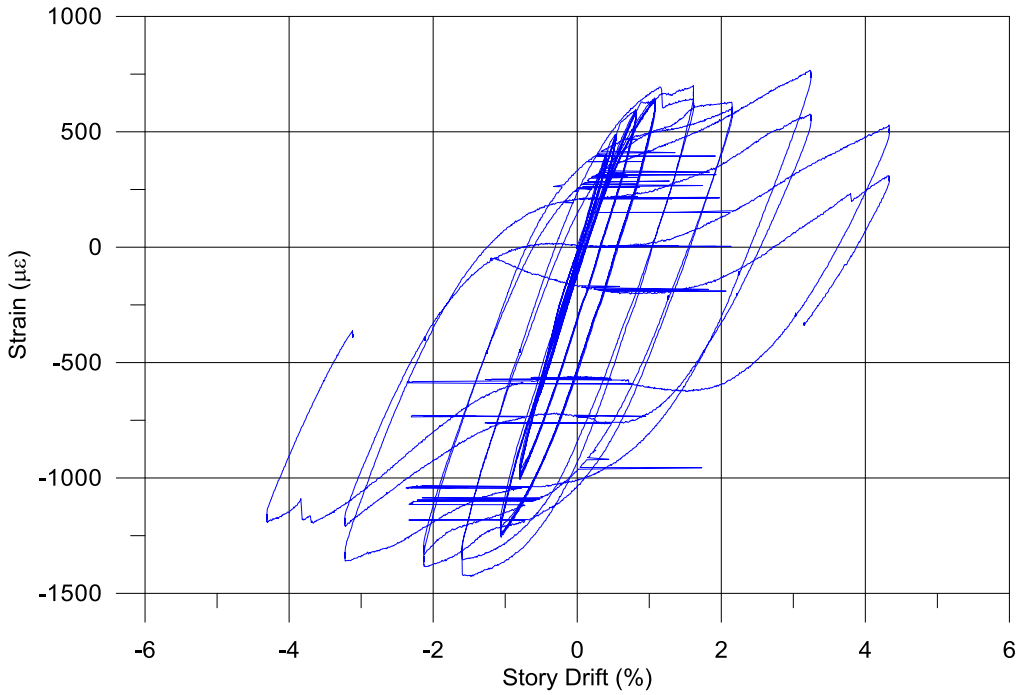
1000
500
0
-500
-1000
-1500
Strain (με)
-6
-4
-2
0
2
4
6
Story Drift (%)

M7-1-2

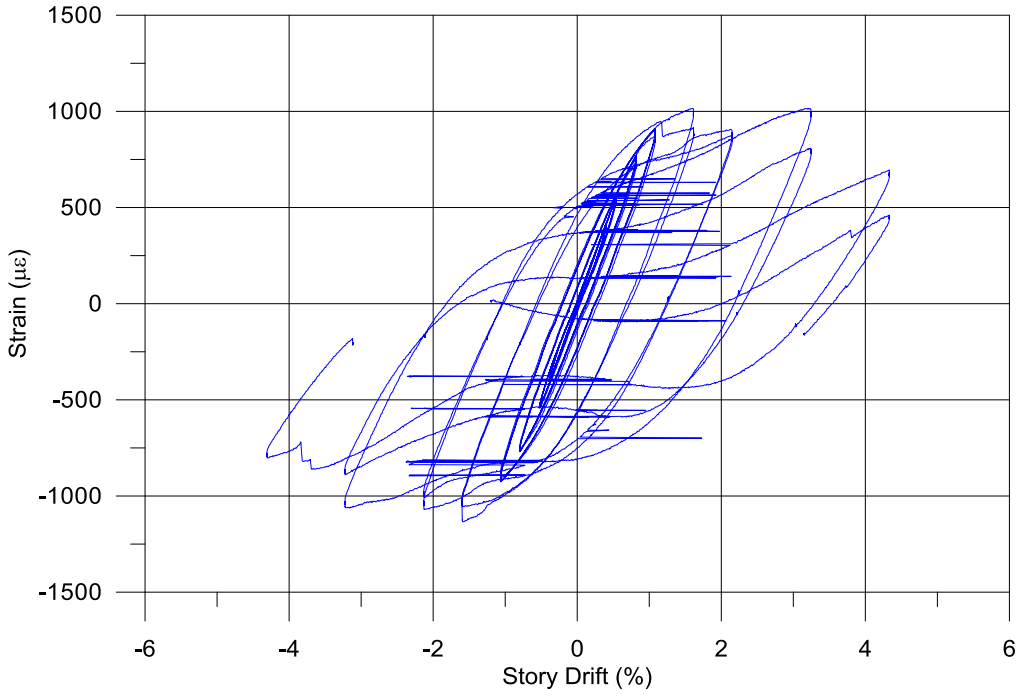
1500
1000
500
0
-500
-1000
-1500
Strain (με)
-6
-4
-2
0
2
4
6
Story Drift (%)

M7-2-1

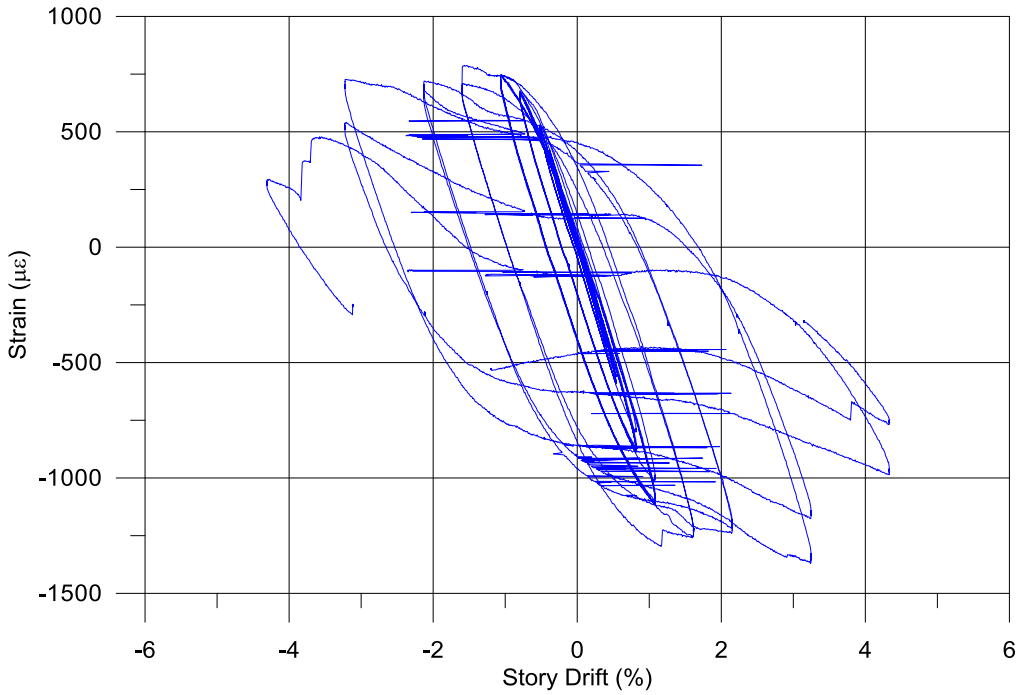
1000
500
0
-500
-1000
-1500
Strain (με)
-6
-4
-2
0
2
4
6
Story Drift (%)

M7-2-2

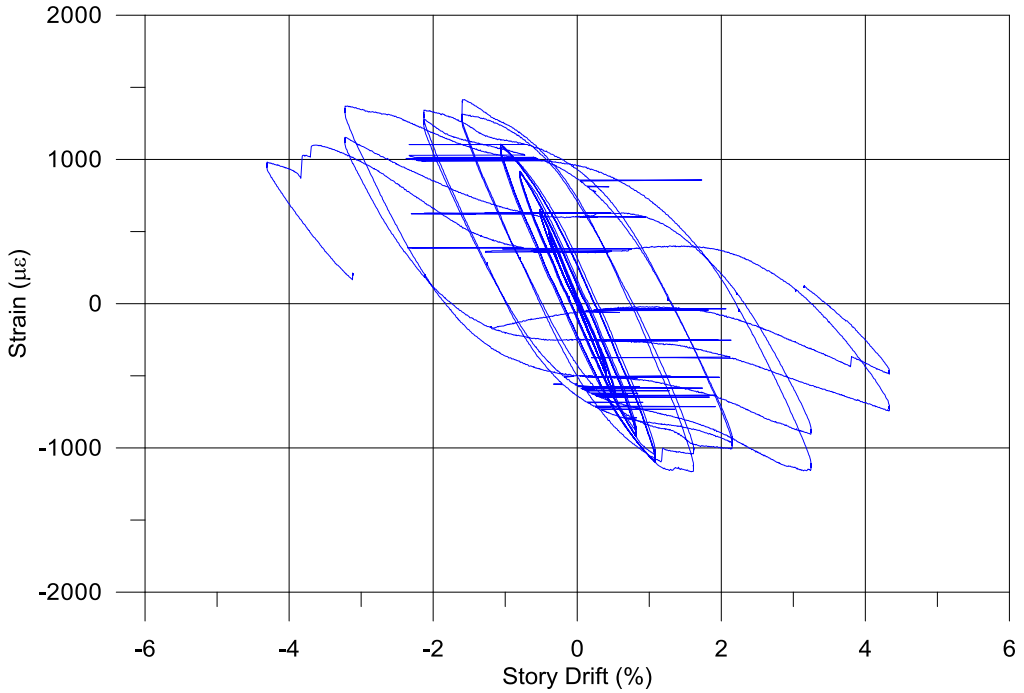
2000
1000
0
-1000
-2000
Strain (με)
-6
-4
-2
0
2
4
6
Story Drift (%)

M7-RS-1

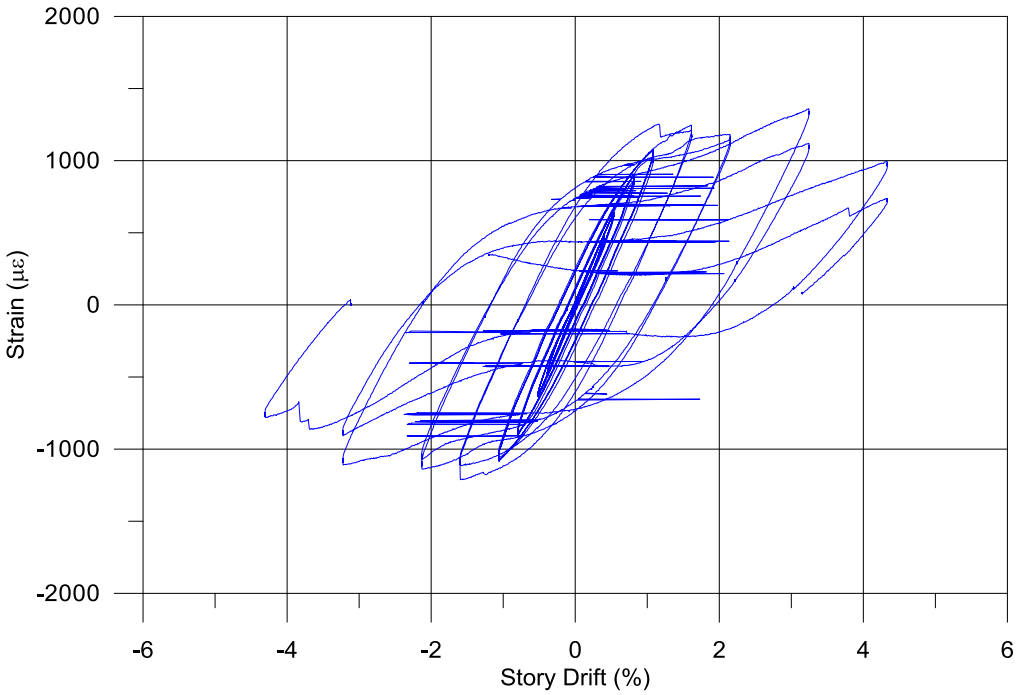
2000
1000
0
-1000
-2000
Strain (με)
-6
-4
-2
0
2
4
6
Story Drift (%)

M7-RS-2

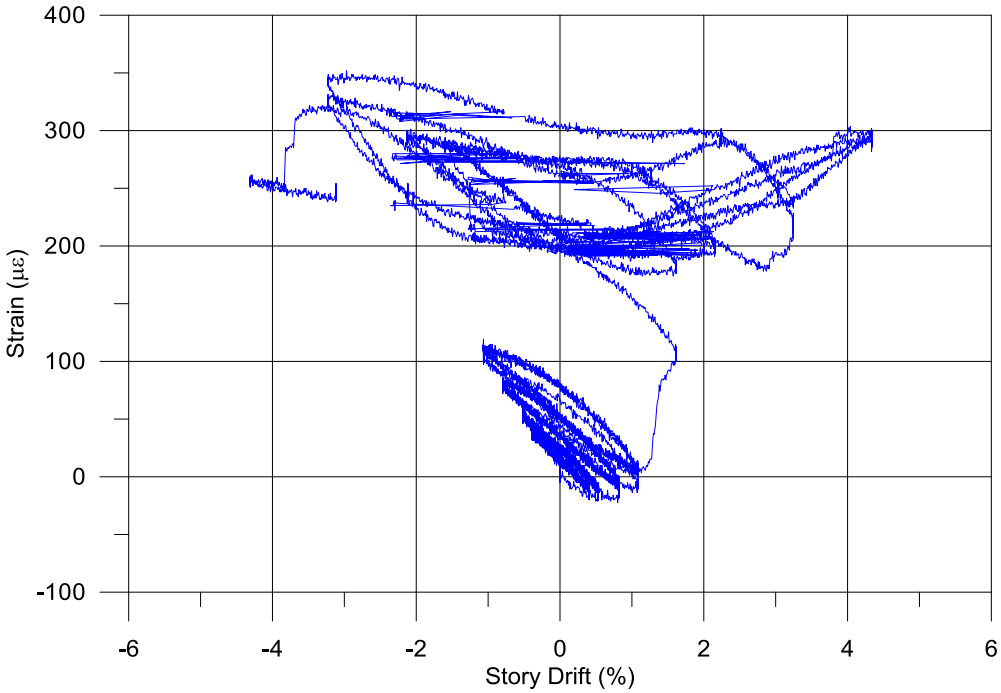
400
300
200
100
0
-100
Strain (με)
-6
-4
-2
0
2
4
6
Story Drift (%)

M7-RS-3

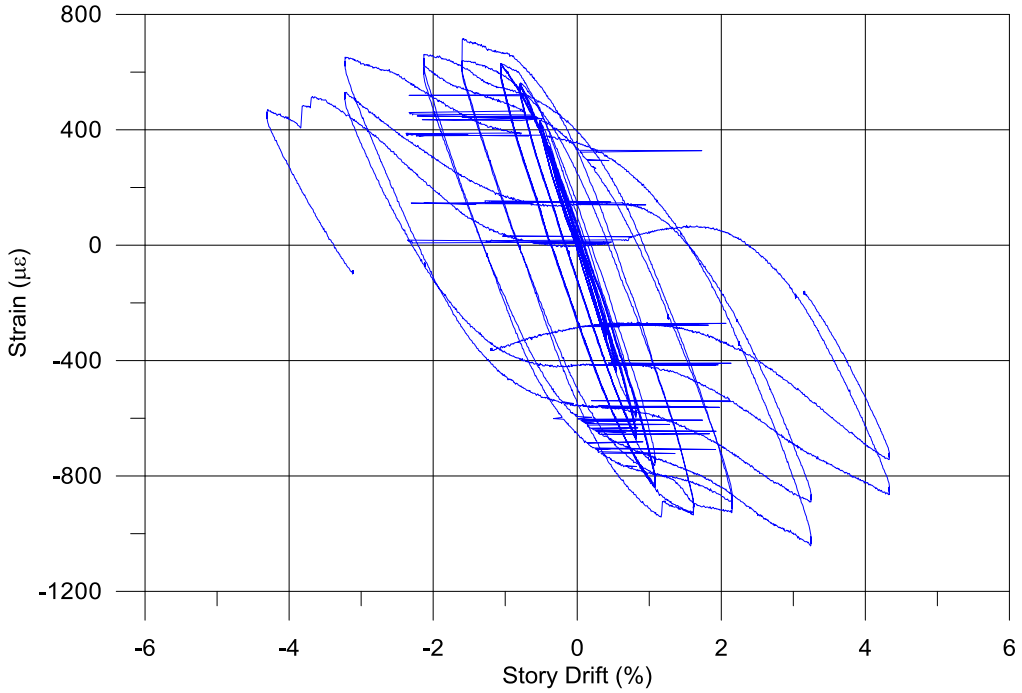
800
400
0
-400
-800
-1200
Strain (με)
-6
-4
-2
0
2
4
6
Story Drift (%)

M7s-1-1

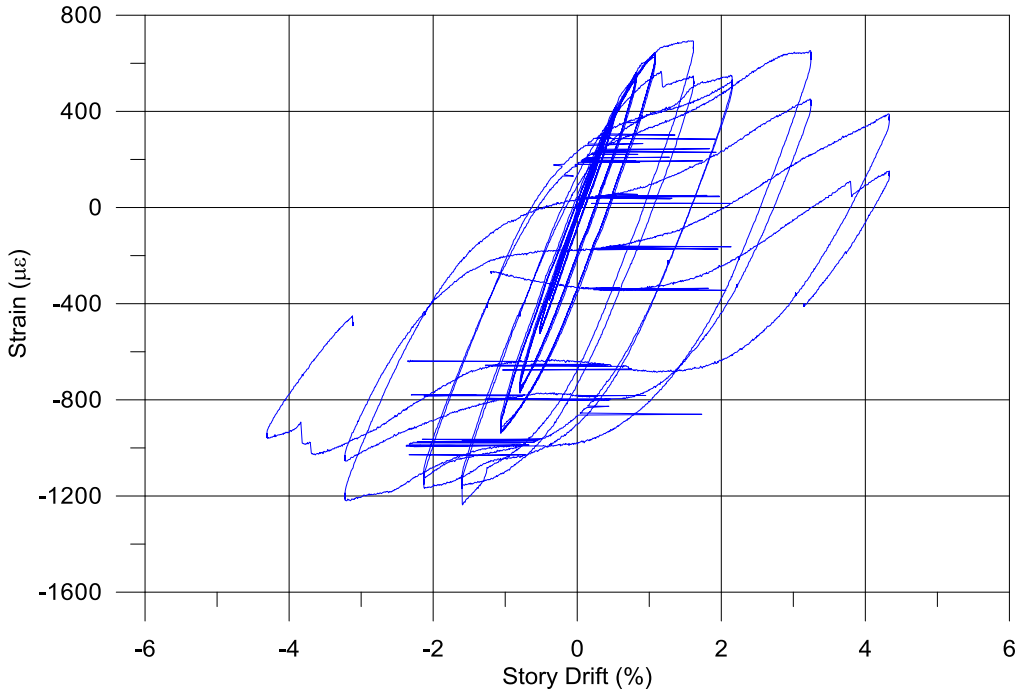
800
400
0
-400
-800
-1200
-1600
Strain (με)
-6
-4
-2
0
2
4
6
Story Drift (%)

M7s-1-2

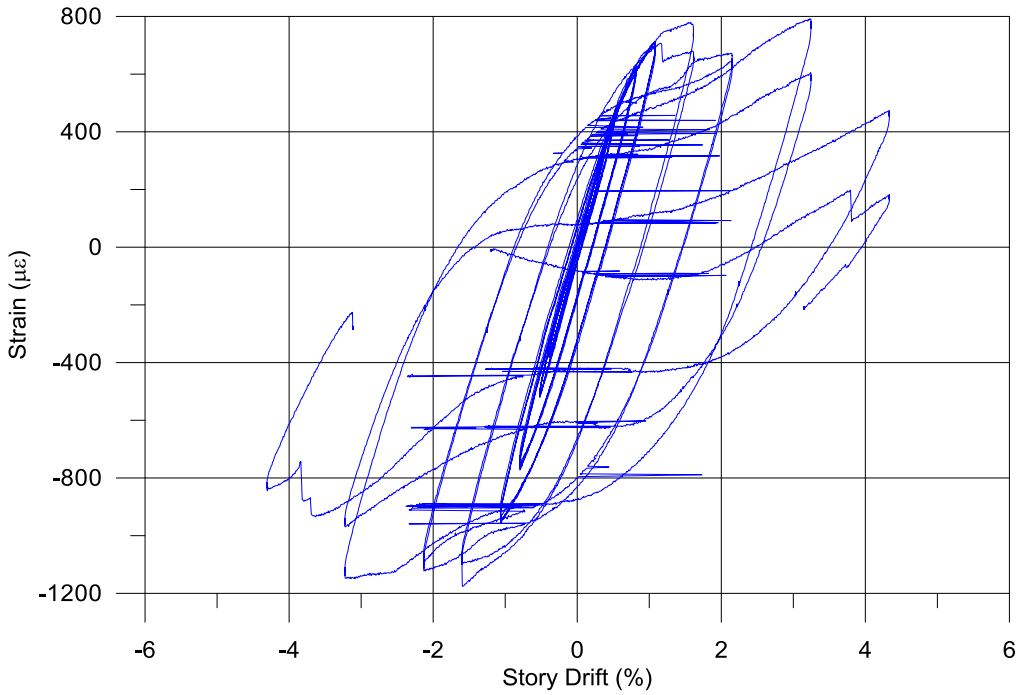
800
400
0
-400
-800
-1200
Strain (με)
-6
-4
-2
0
2
4
6
Story Drift (%)

M7s-2-1

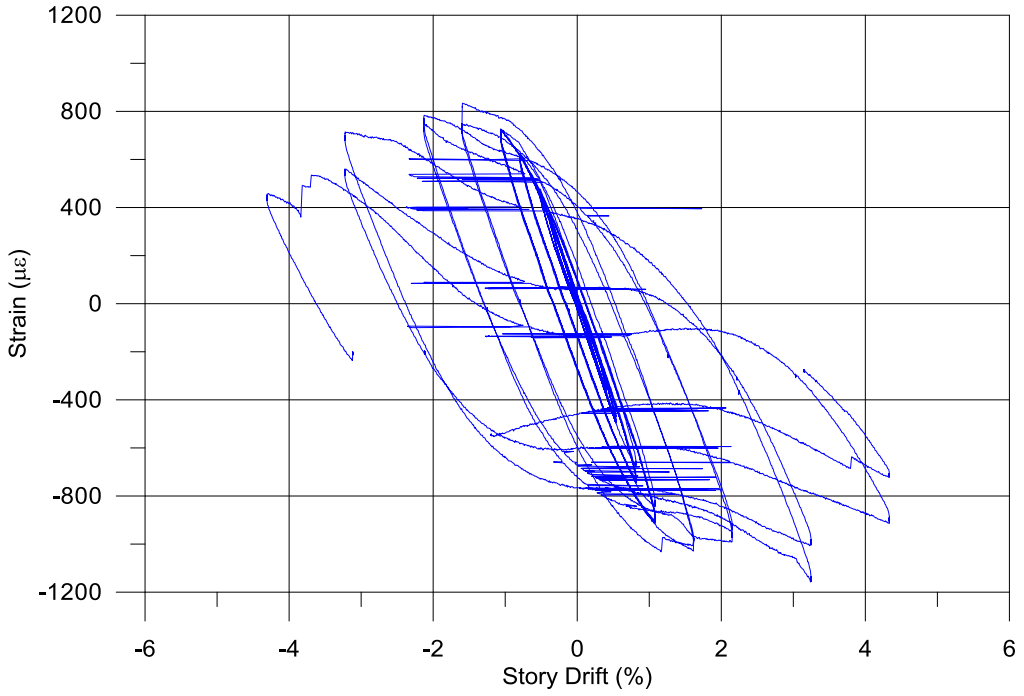
1200
800
400
0
-400
-800
-1200
Strain (με)
-6
-4
-2
0
2
4
6
Story Drift (%)

M7s-2-2

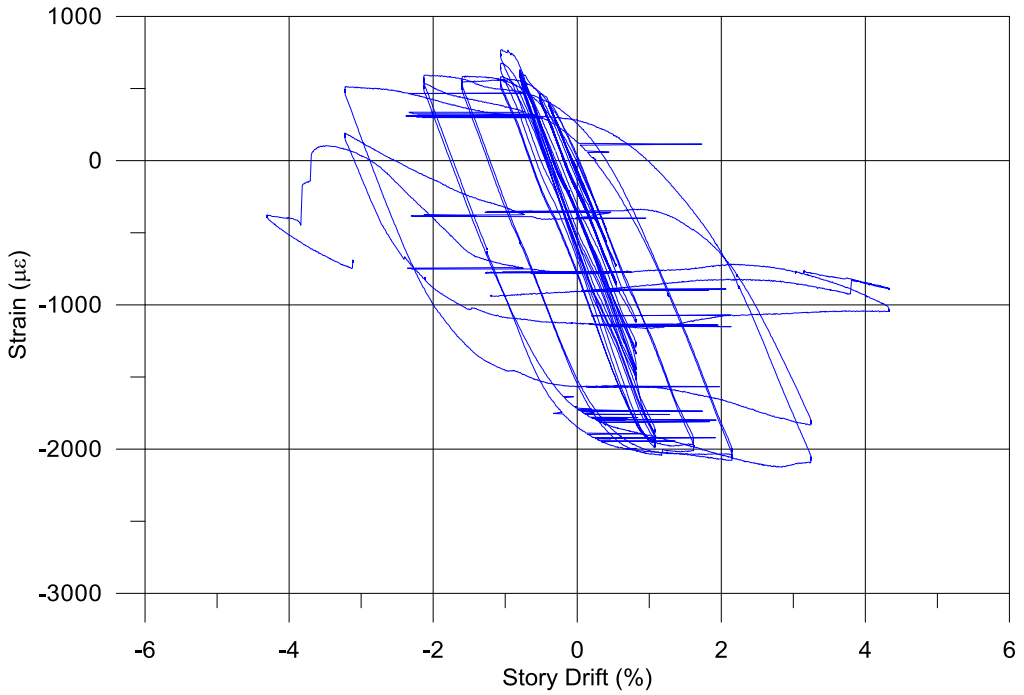
1000
0
-1000
-2000
-3000
Strain (με)
-6
-4
-2
0
2
4
6
Story Drift (%)

M8-1-1

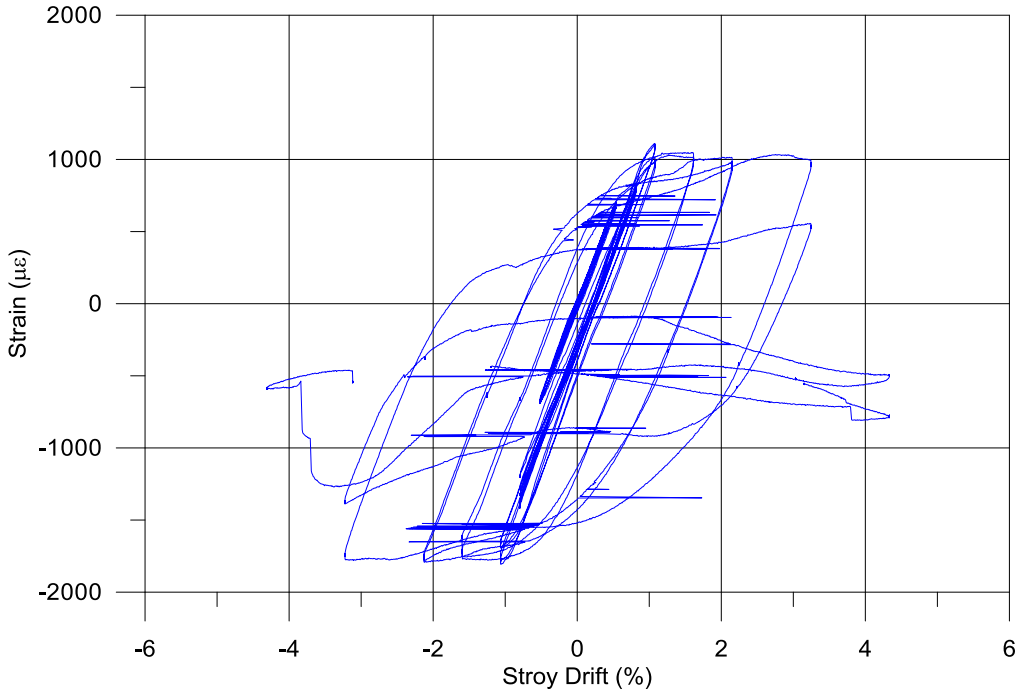
2000
1000
0
-1000
-2000
Strain (με)
-6
-4
-2
0
2
4
6
Stroy Drift (%)

M8-1-2

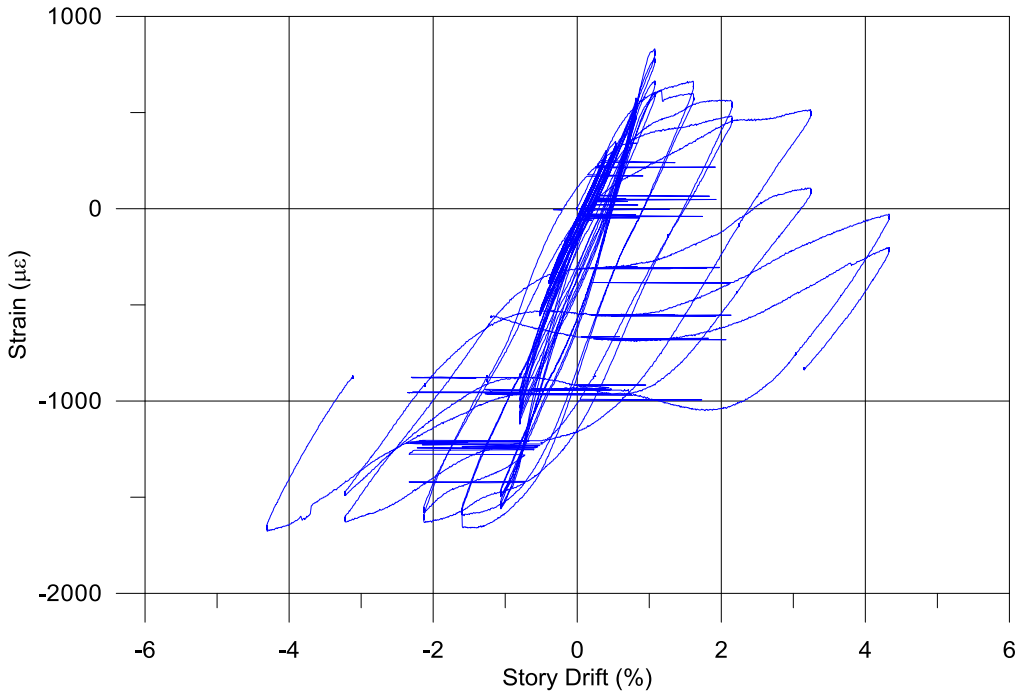
1000
0
-1000
-2000
Strain (με)
-6
-4
-2
0
2
4
6
Story Drift (%)

M8-2-1

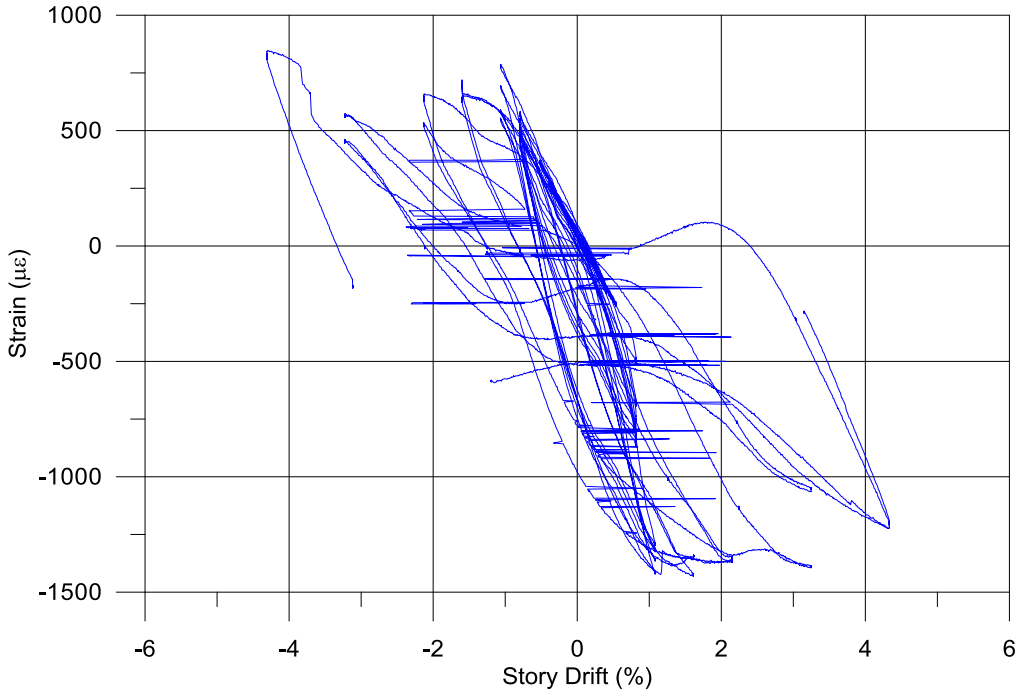
1000
500
0
-500
-1000
-1500
Strain (με)
-6
-4
-2
0
2
4
6
Story Drift (%)

M8-2-2

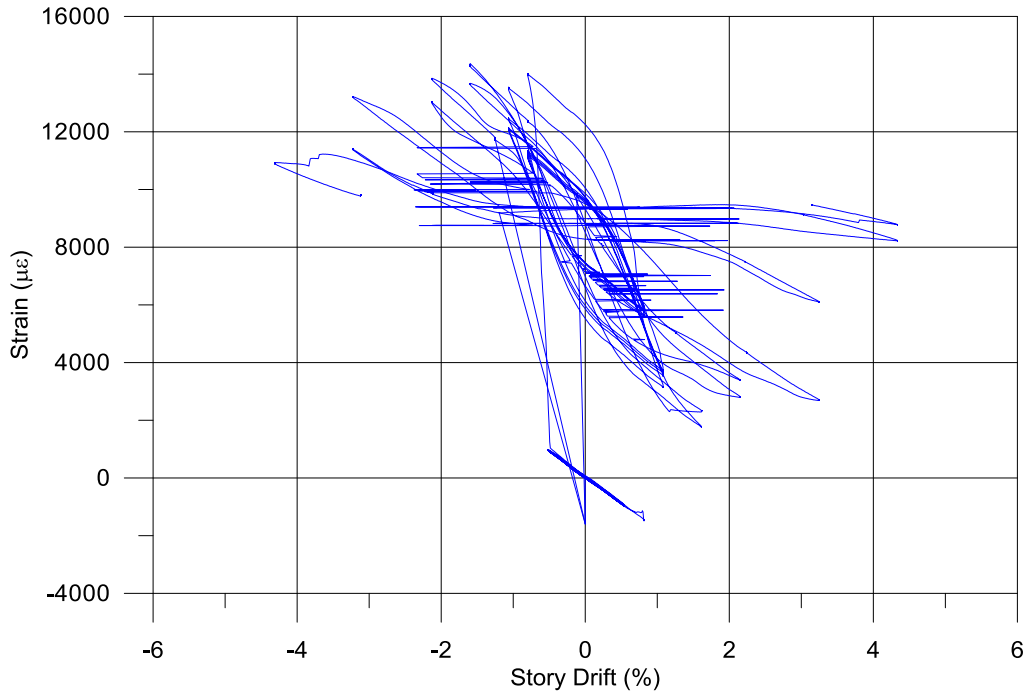
16000
12000
8000
4000
0
-4000
Strain (με)
-6
-4
-2
0
2
4
6
Story Drift (%)

M8-RS-1

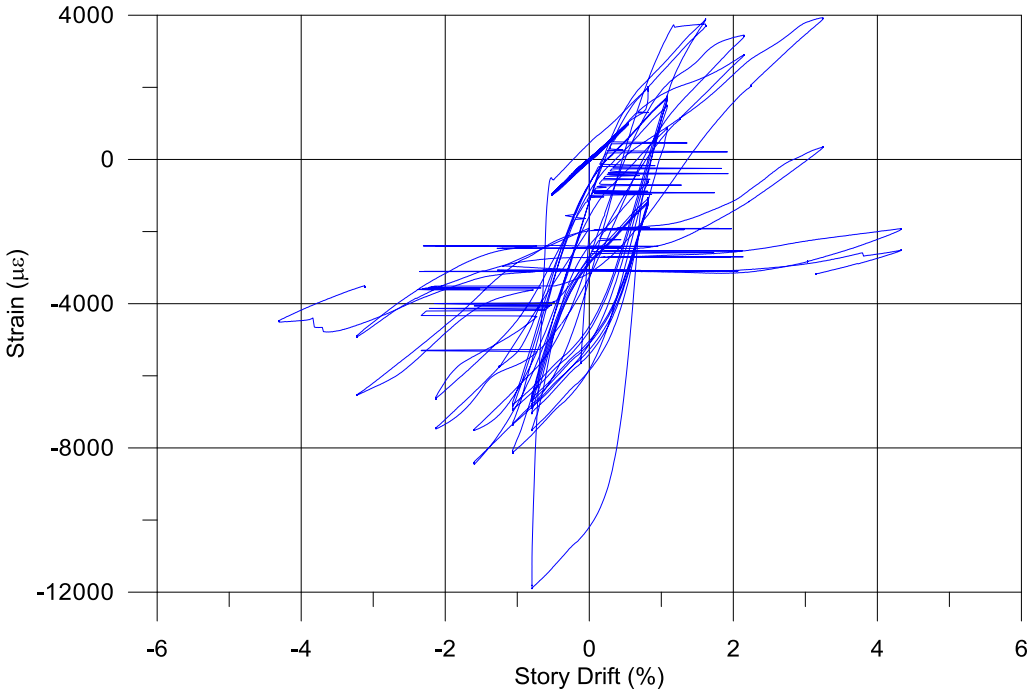
4000
0
-4000
-8000
-12000
Strain (με)
-6
-4
-2
0
2
4
6
Story Drift (%)

M8-RS-2

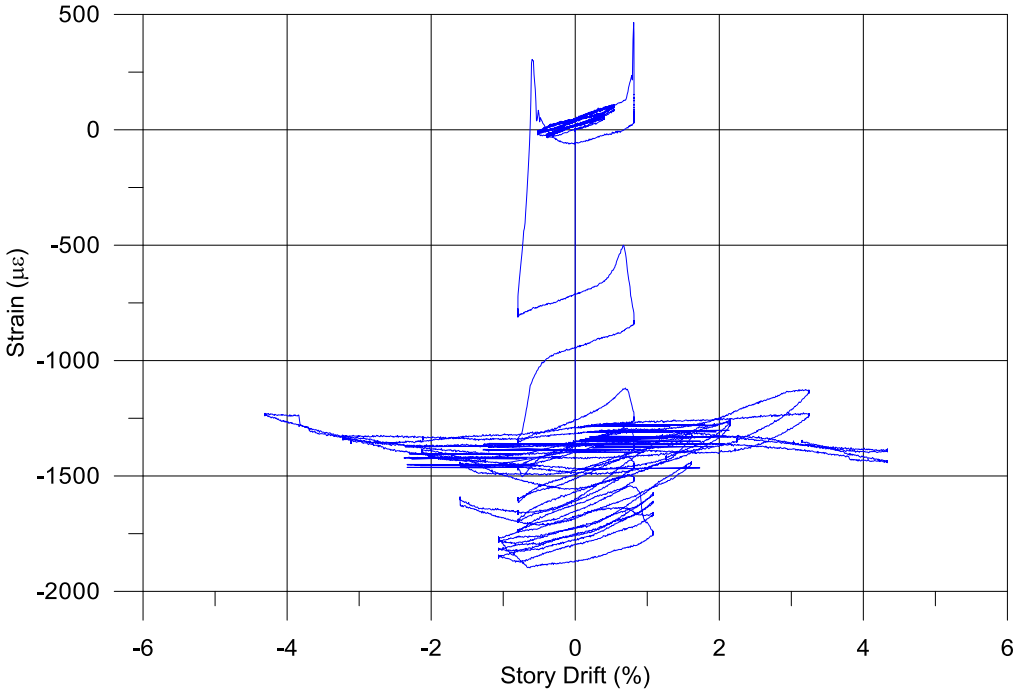
500
0
-500
-1000
-1500
-2000
Strain (με)
-6
-4
-2
0
2
4
6
Story Drift (%)

M8-RS-3

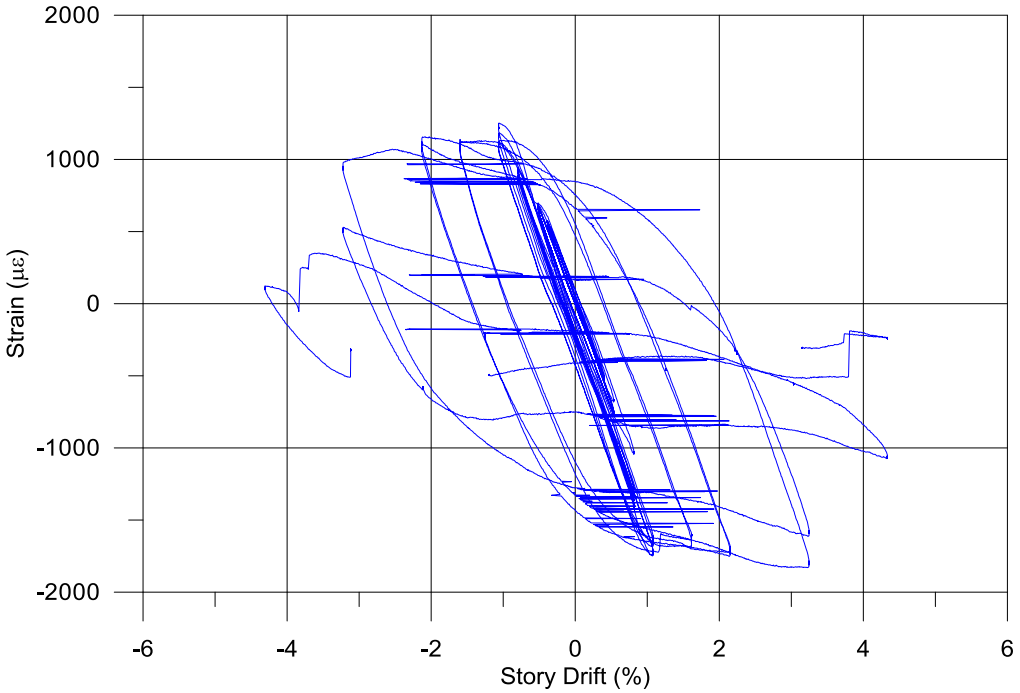
2000
1000
0
-1000
-2000
Strain (με)
-6
-4
-2
0
2
4
6
Story Drift (%)

M8s-1-1

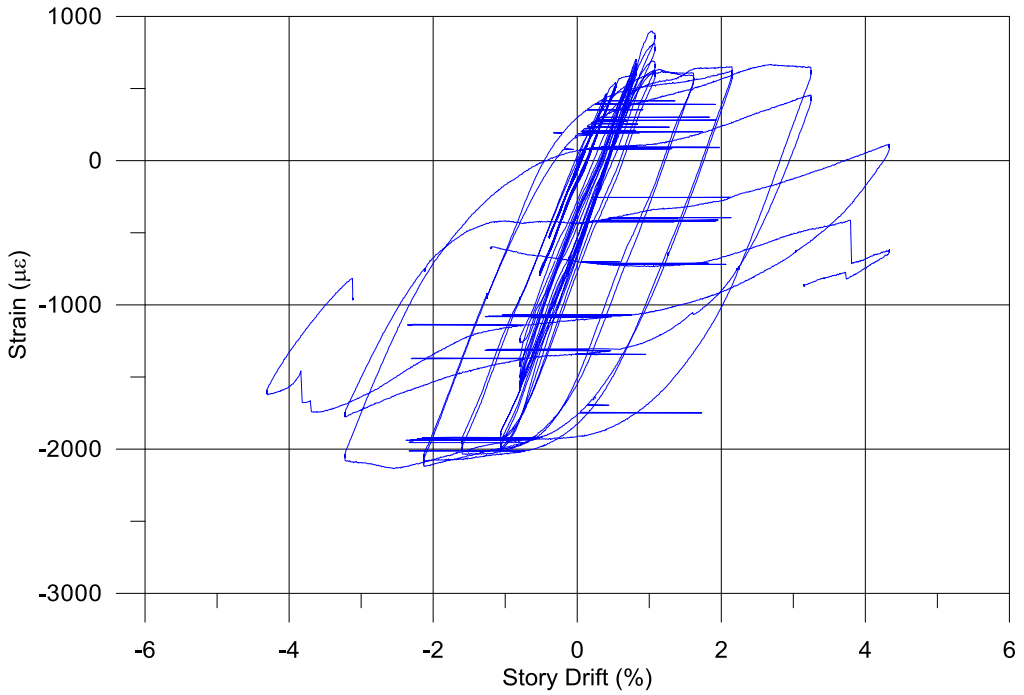
1000
0
-1000
-2000
-3000
Strain (με)
-6
-4
-2
0
2
4
6
Story Drift (%)

M8s-1-2

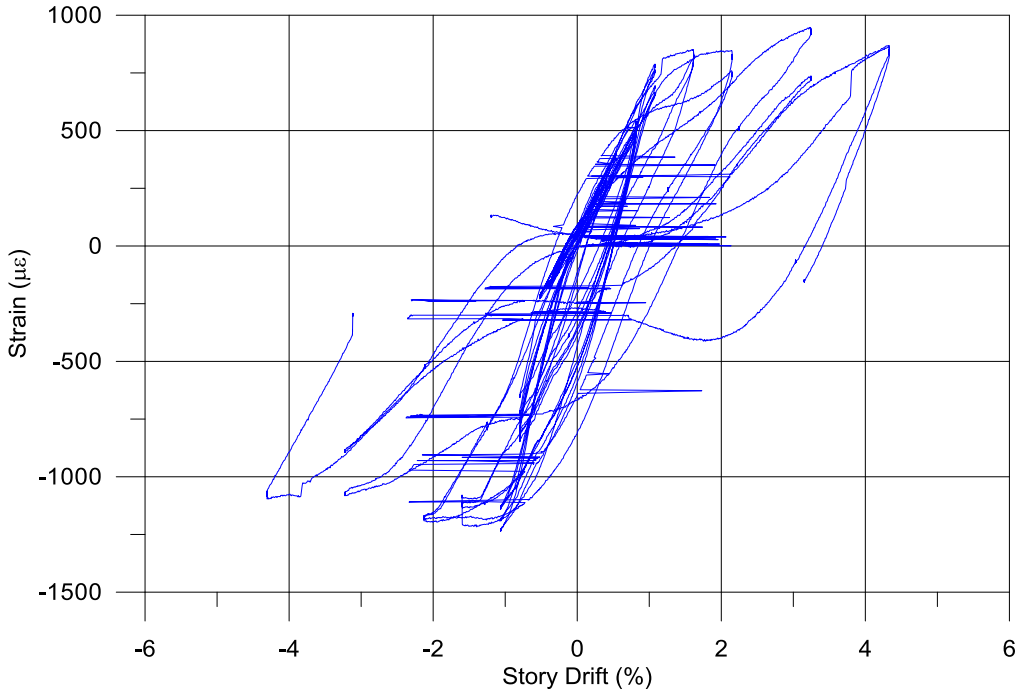
1000
500
0
-500
-1000
-1500
Strain (με)
-6
-4
-2
0
2
4
6
Story Drift (%)

M8s-2-1

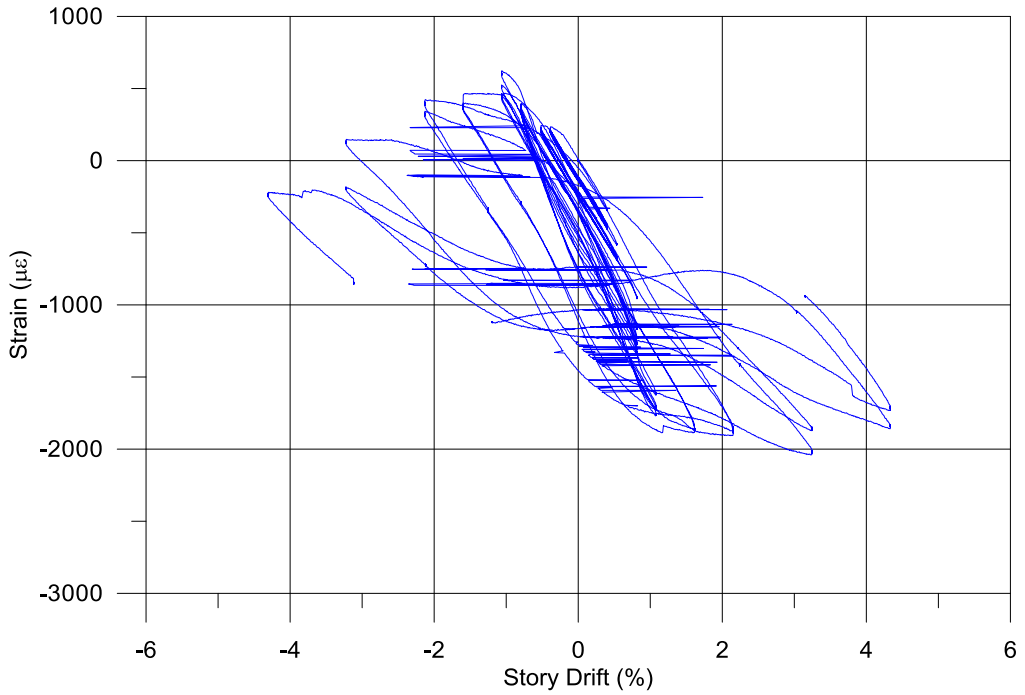

M8s-2-2

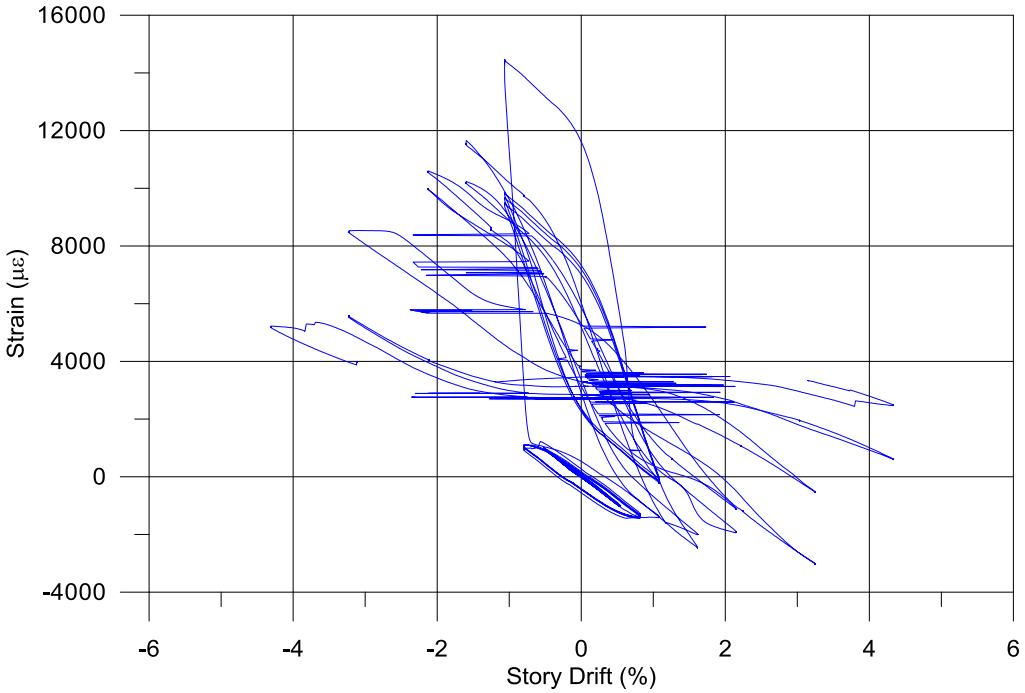

M8s-RS-1

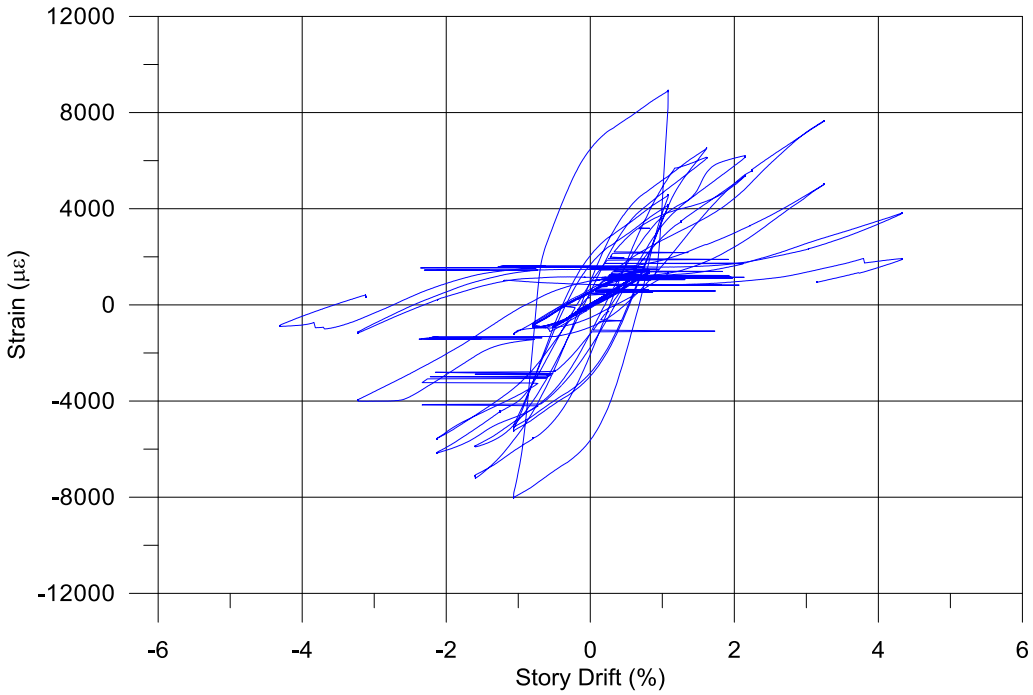

M8s-RS-2

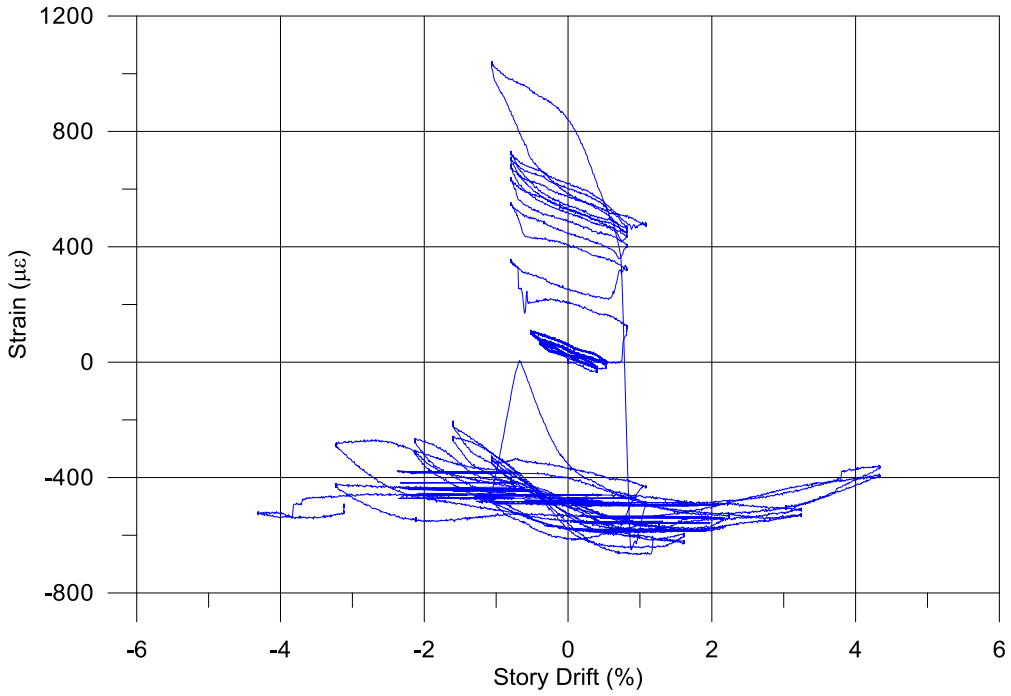

M8s-RS-3

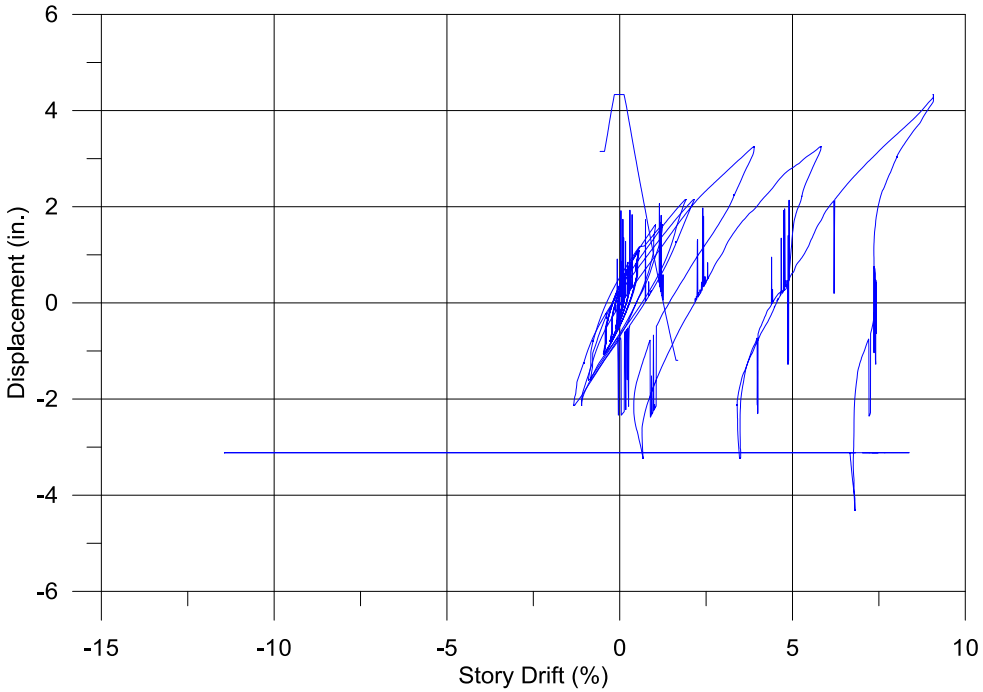

SP-BRB-NE-1

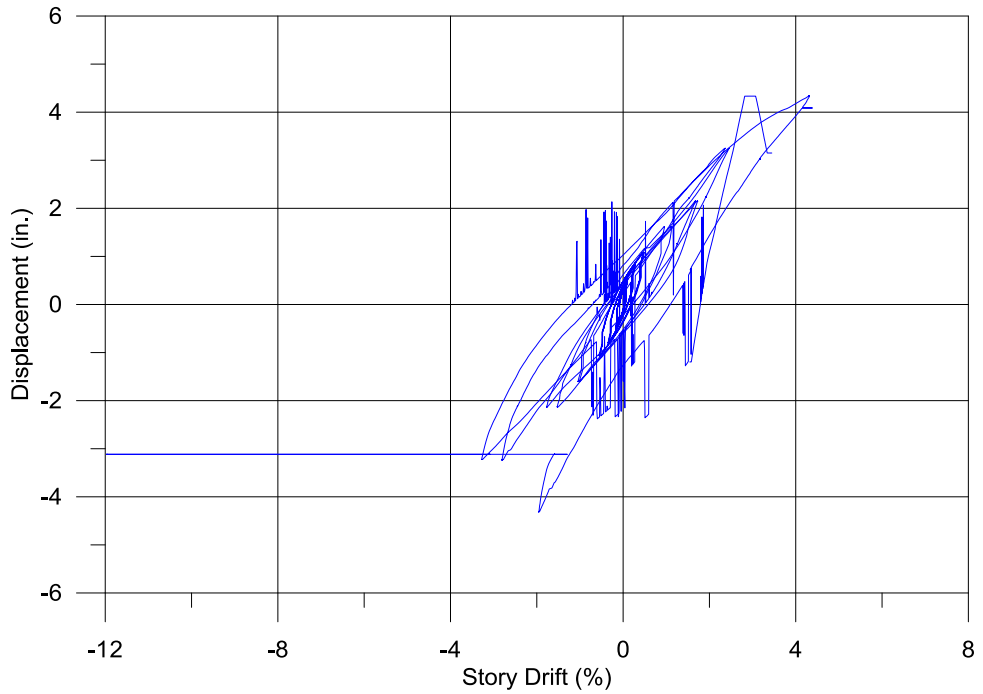

SP-BRB-NE-2

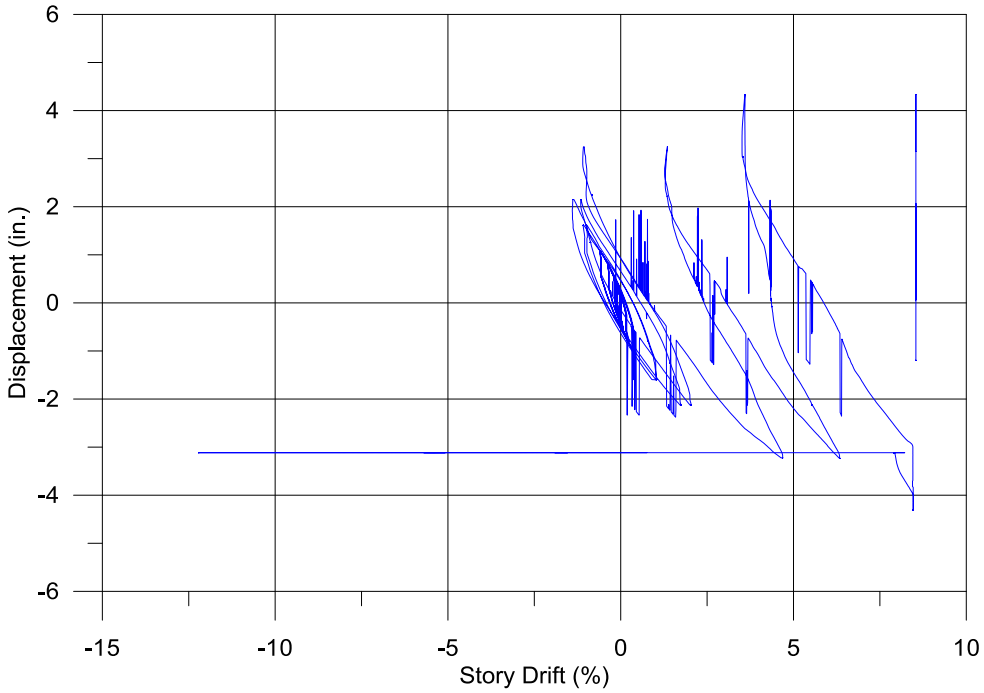

SP-BRB-SW-1

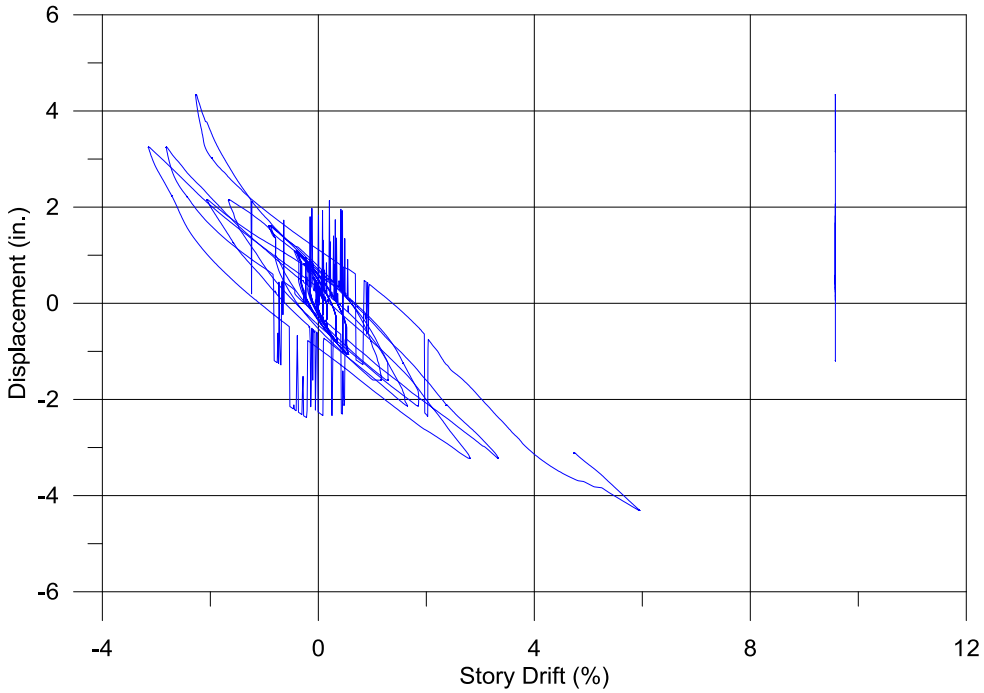

SP-BRB-SW-2

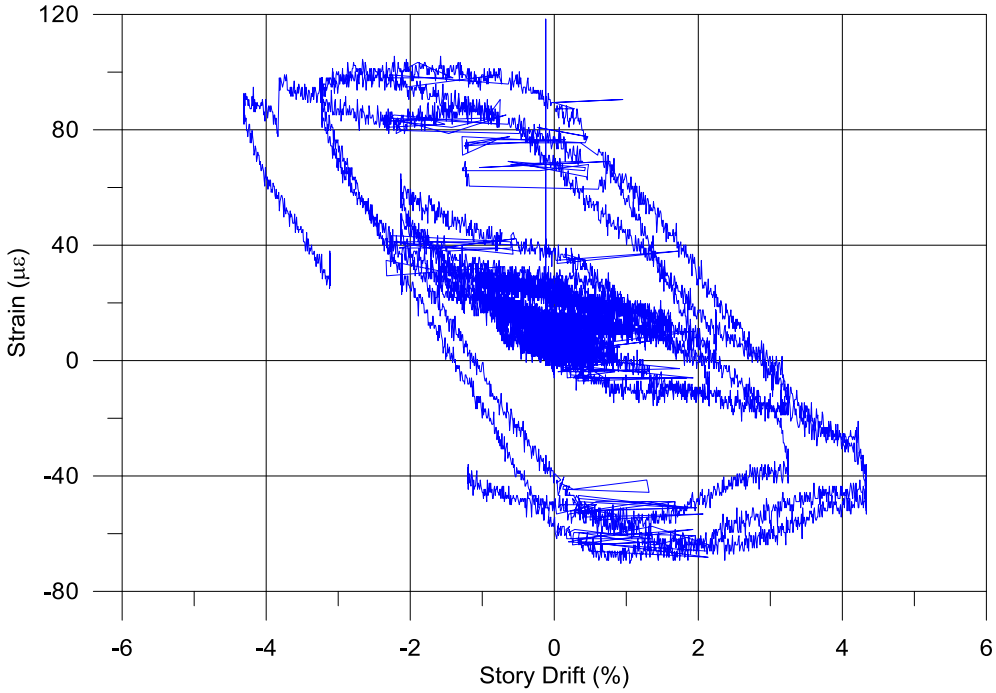
120
80
40
0
-40
-80
Strain (με)
-6
-4
-2
0
2
4
6
Story Drift (%)

TB1-1

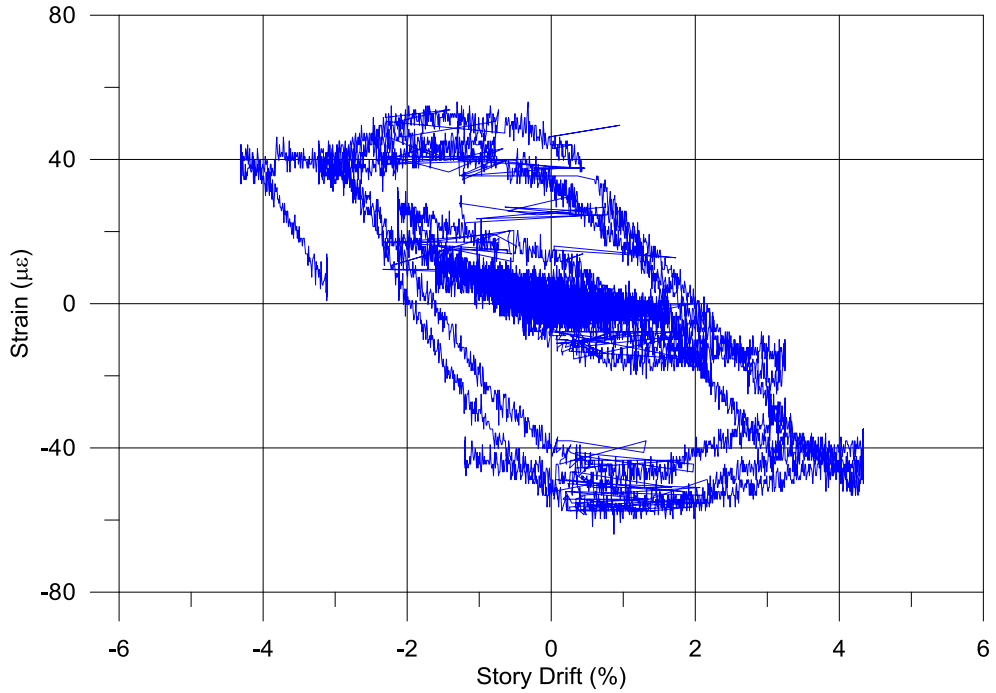
80
40
0
-40
-80
Strain (με)
-6
-4
-2
0
2
4
6
Story Drift (%)

TB1-2

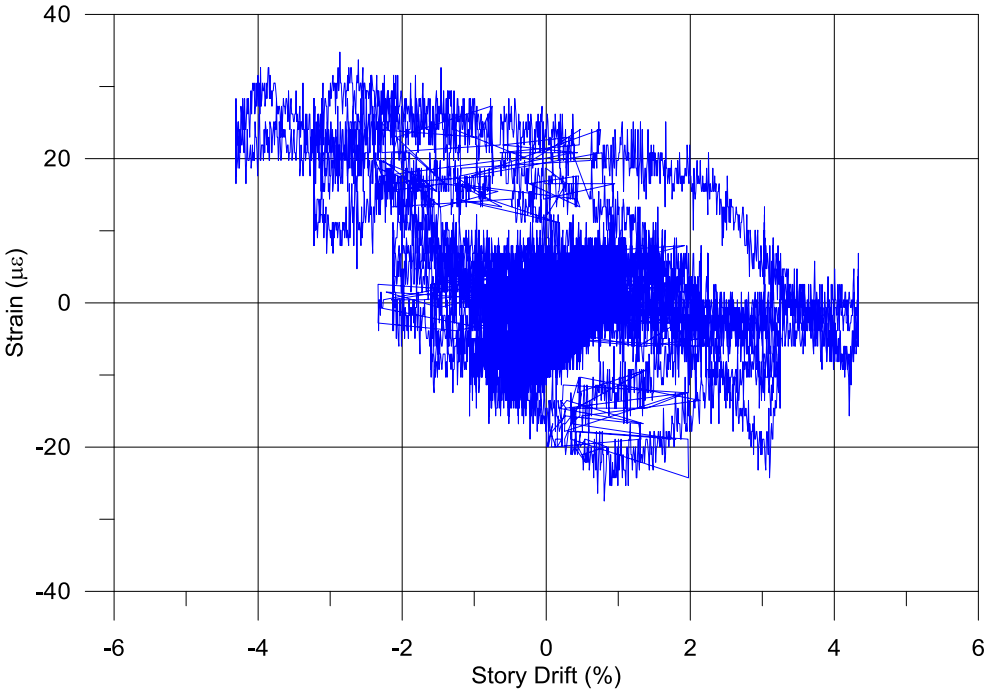
40
20
0
-20
-40
Strain (με)
-6
-4
-2
0
2
4
6
Story Drift (%)

TB2

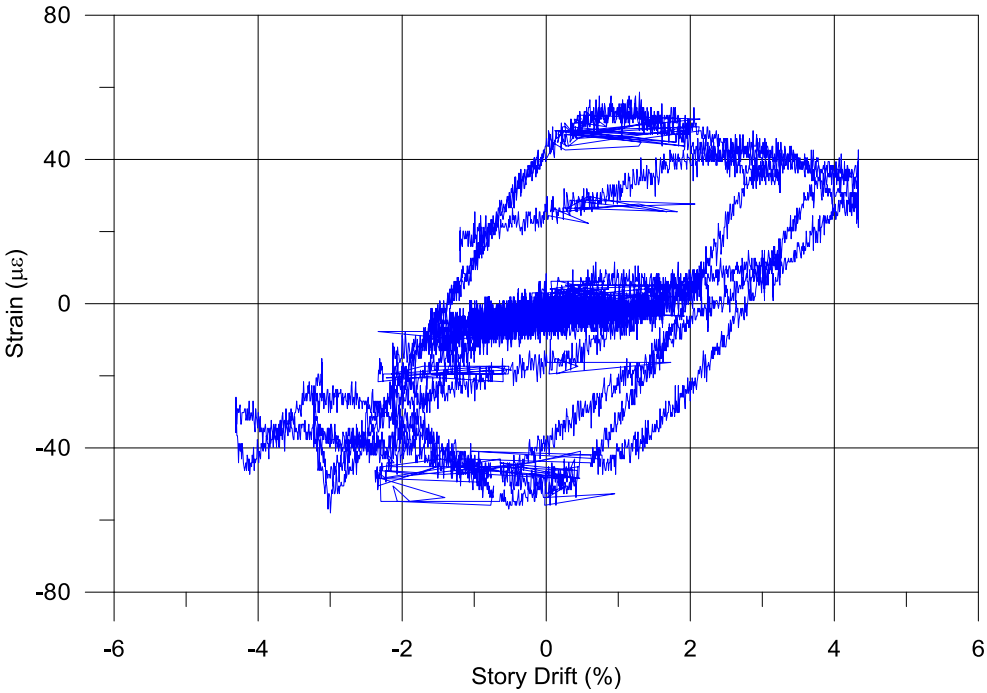
80
40
0
-40
-80
Strain (με)
-6
-4
-2
0
2
4
6
Story Drift (%)

TB3-1

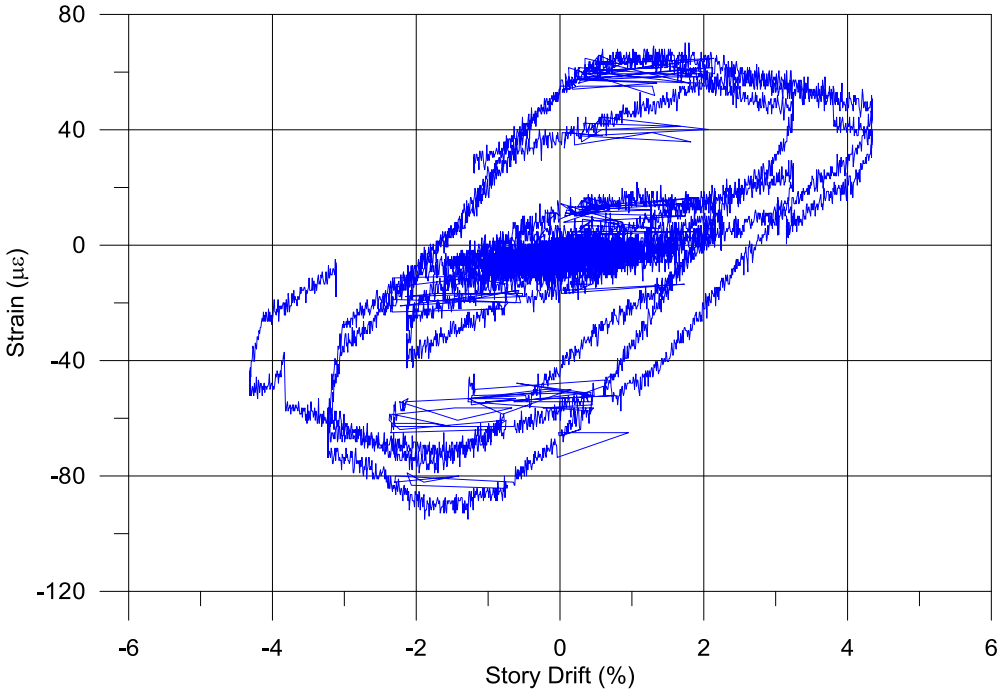
80
40
0
-40
-80
-120
Strain (με)
-6
-4
-2
0
2
4
6
Story Drift (%)

TB3-2

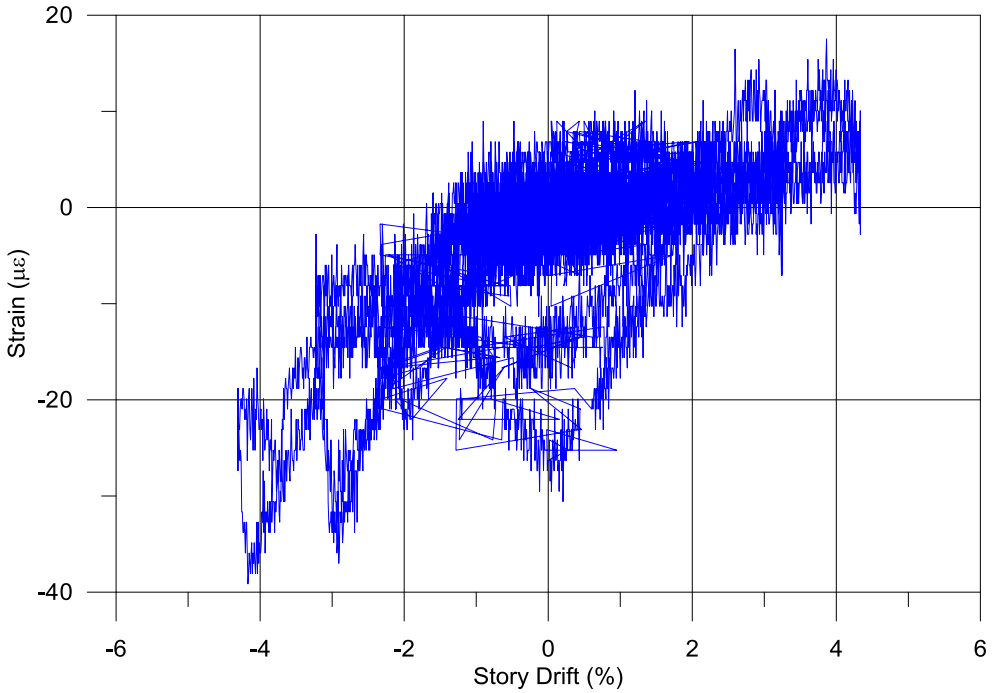
20
0
-20
-40
Strain (με)
-6
-4
-2
0
2
4
6
Story Drift (%)

TB4

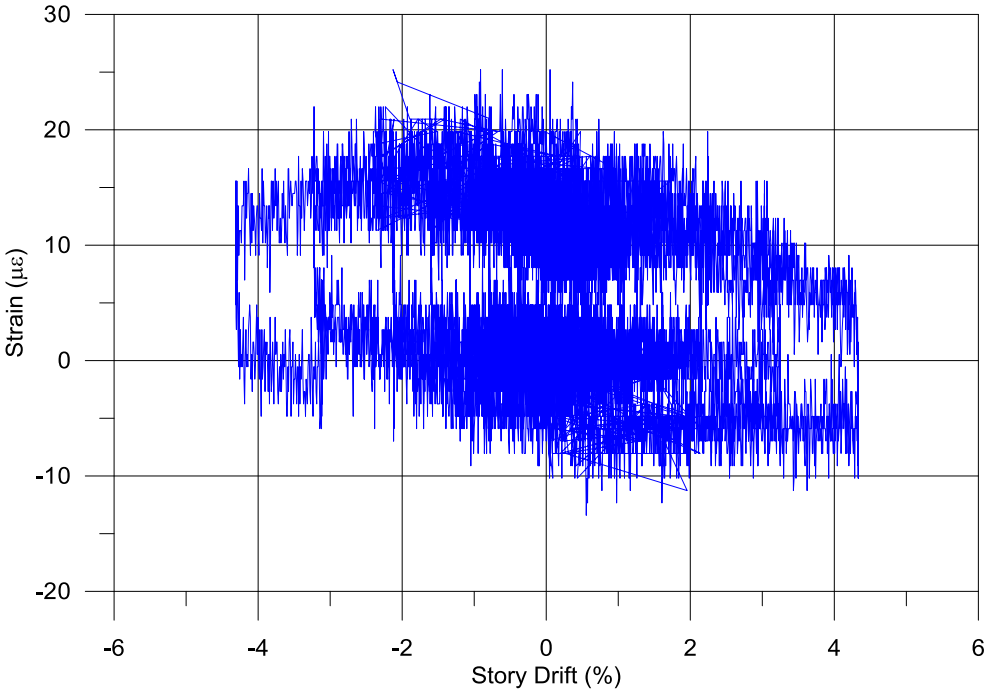
30
20
10
0
-10
-20
Strain (με)
-6
-4
-2
0
2
4
6
Story Drift (%)

TB5

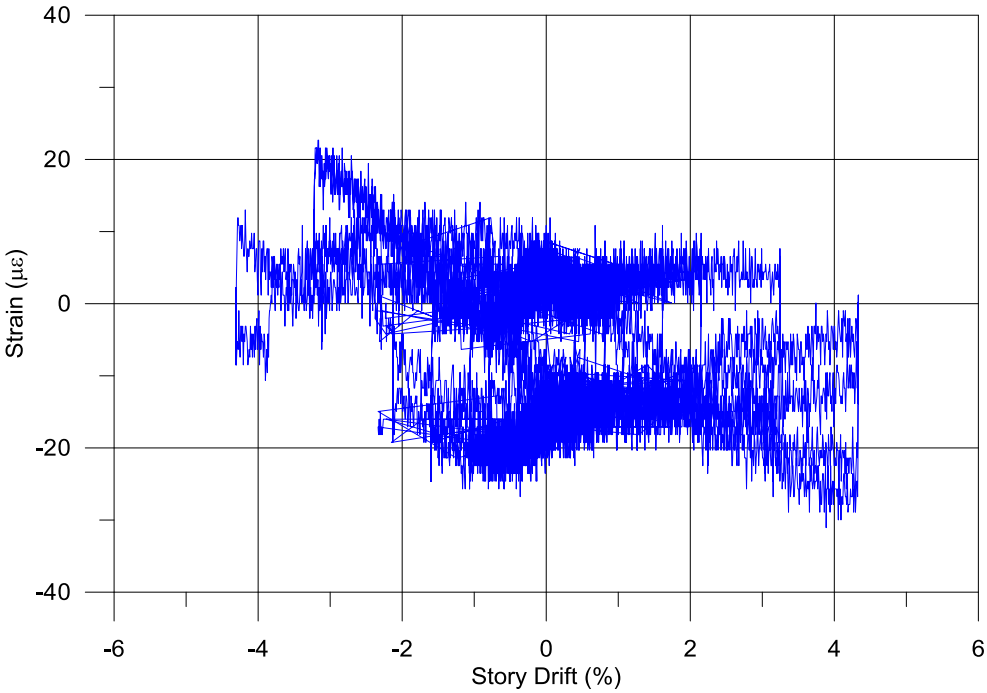
40
20
0
-20
-40
Strain (με)
-6
-4
-2
0
2
4
6
Story Drift (%)

TB6

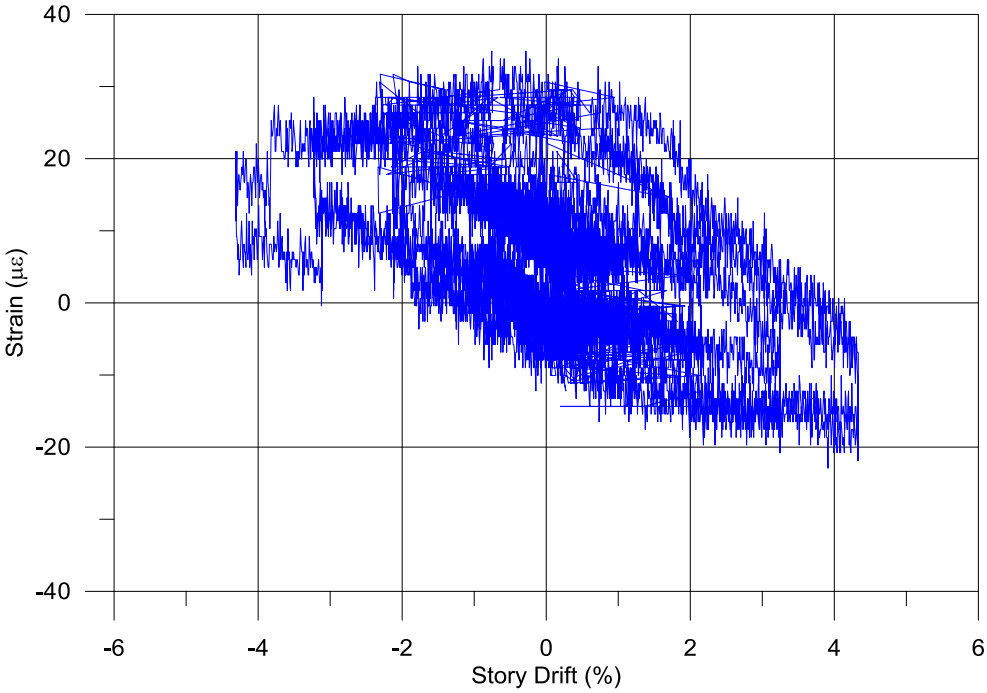
40
20
0
-20
-40
Strain (με)
-6
-4
-2
0
2
4
6
Story Drift (%)

TB7

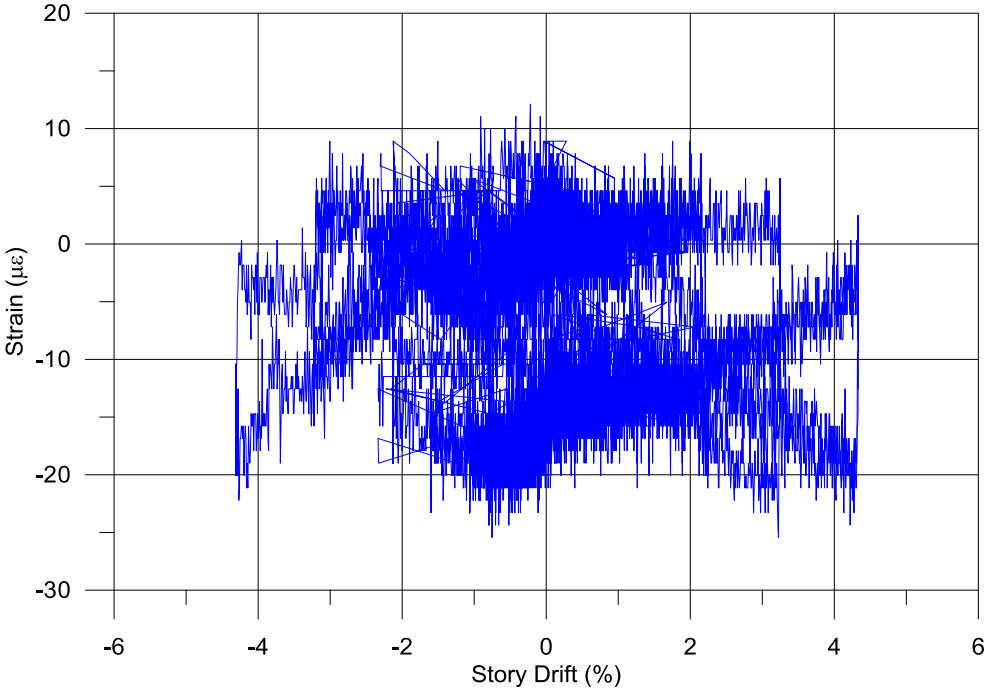
20
10
0
-10
-20
-30
Strain (με)
-6
-4
-2
0
2
4
6
Story Drift (%)

TB8

Appendix G

Test Photographs

Component Test

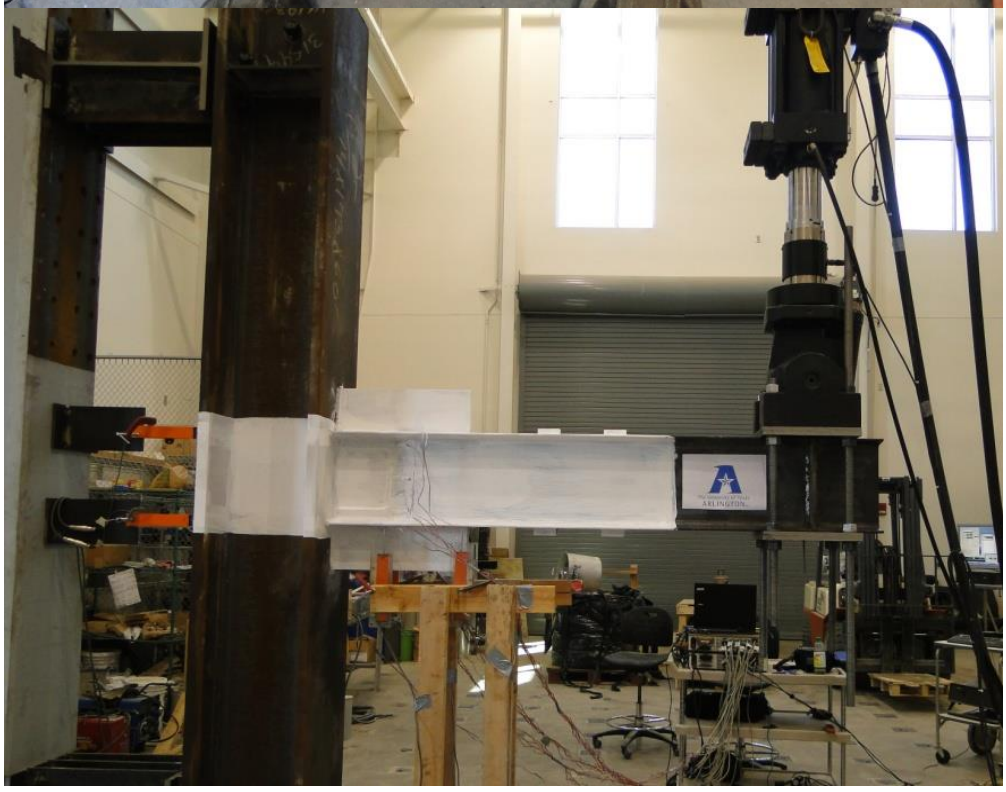

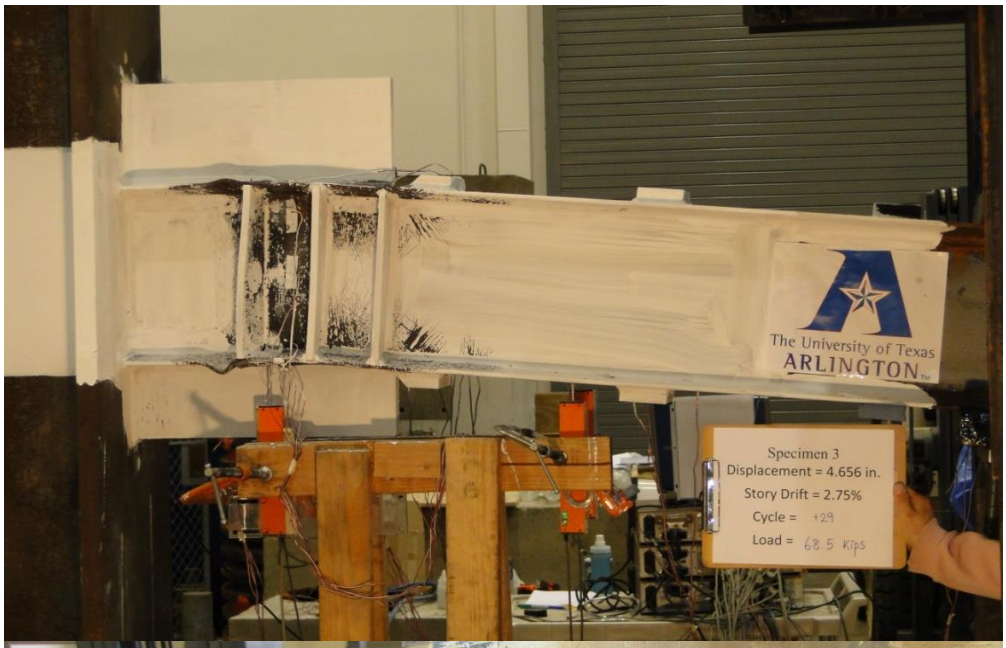
The University of Texas
ARLINGTON
Specimen 3
Displacement = 4.656 in.
Story Drift = 2.75%
Cycle = +29
Load = 68.5 Kips


NISSAN

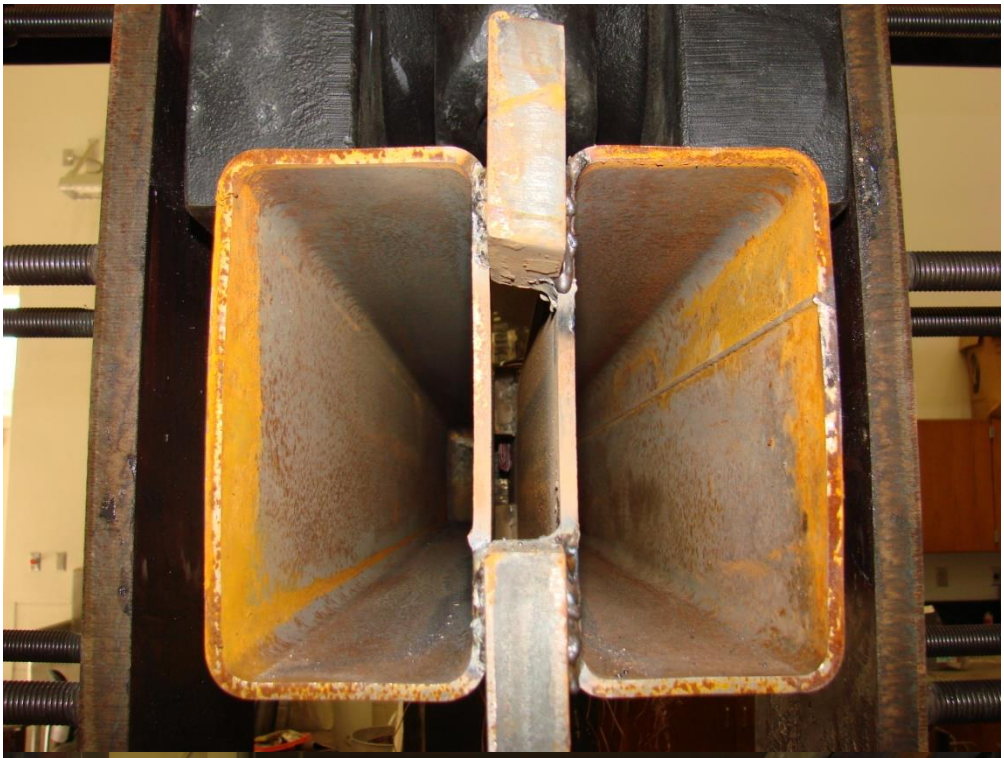

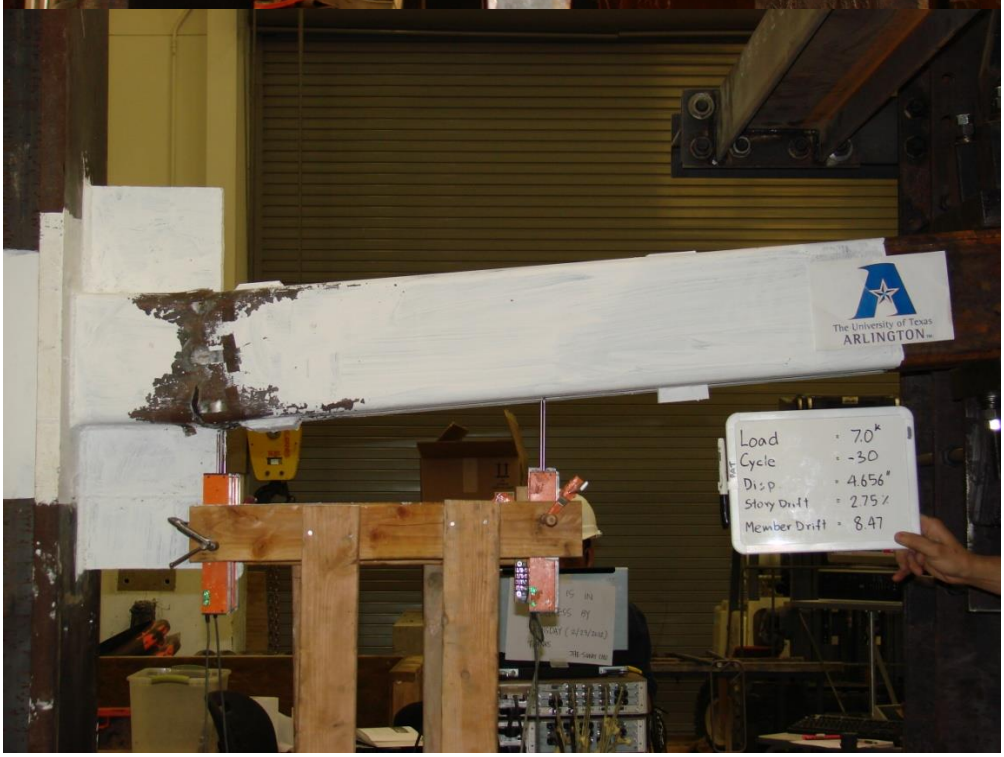
The University of Texas
ARLINGTON
Load = 7.0k
Cycle = -30
Disp = 4.656"
Story Drift = 2.75%
Member Drift = 8.47


The University of Texas
ARLINGTON
Cycle: Final
Story Drift: 2.75%
Load: 26 kips
Displacement: 4.656"

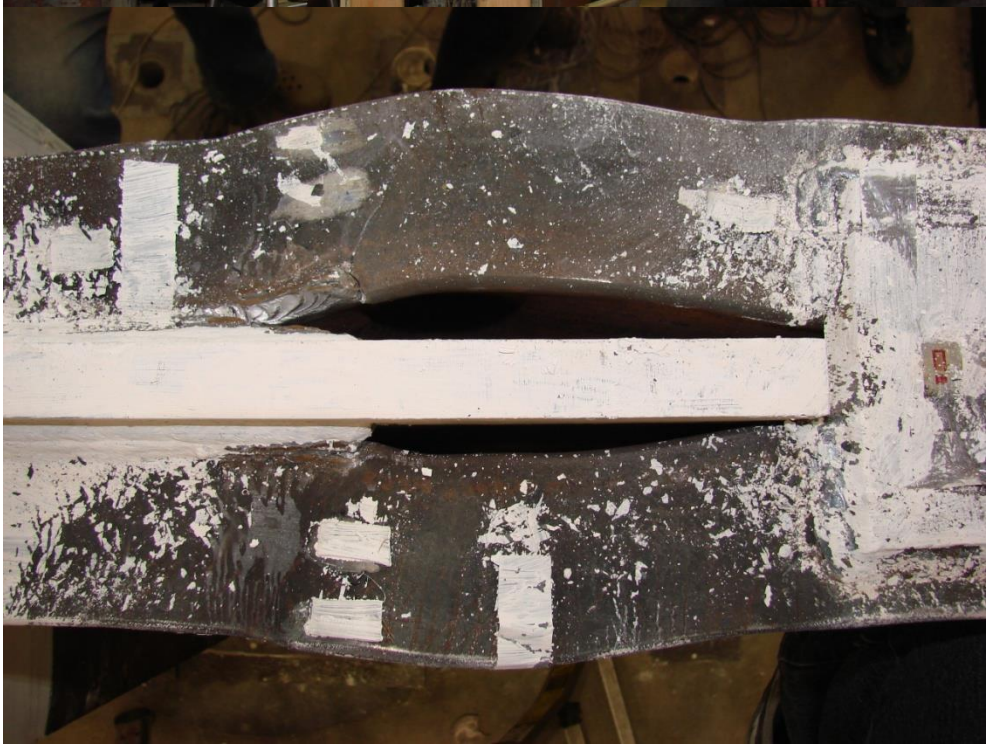

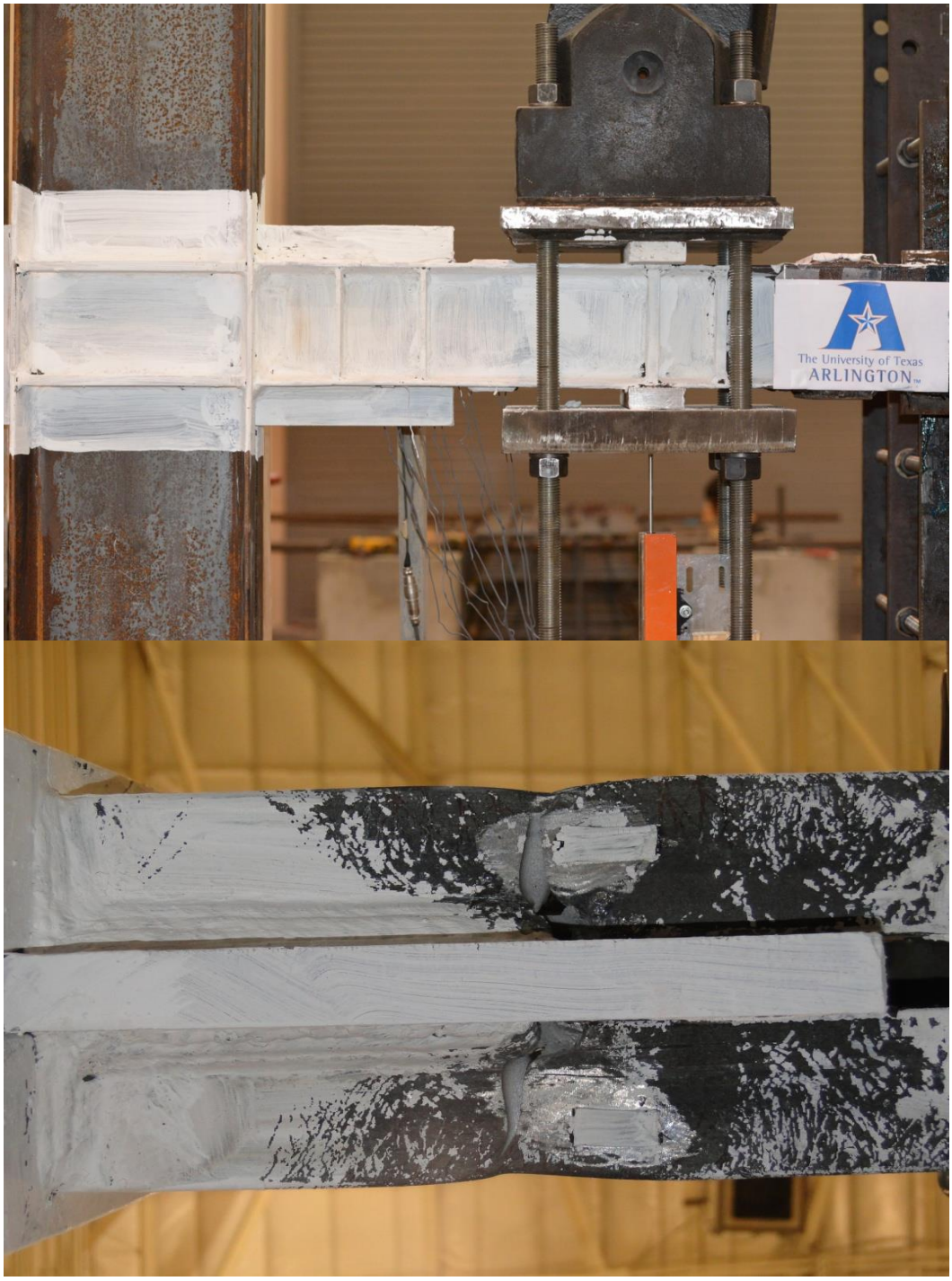
The University of Texas
ARLINGTON


The University of Texas
ARLINGTON
End of Test
Load: 31 k
Story Drift
Member Drift
Displ +0.75in


UBB-1-1

Full Scale Subassemblage Test


UBR-1
4R


ADD
ADD
QC

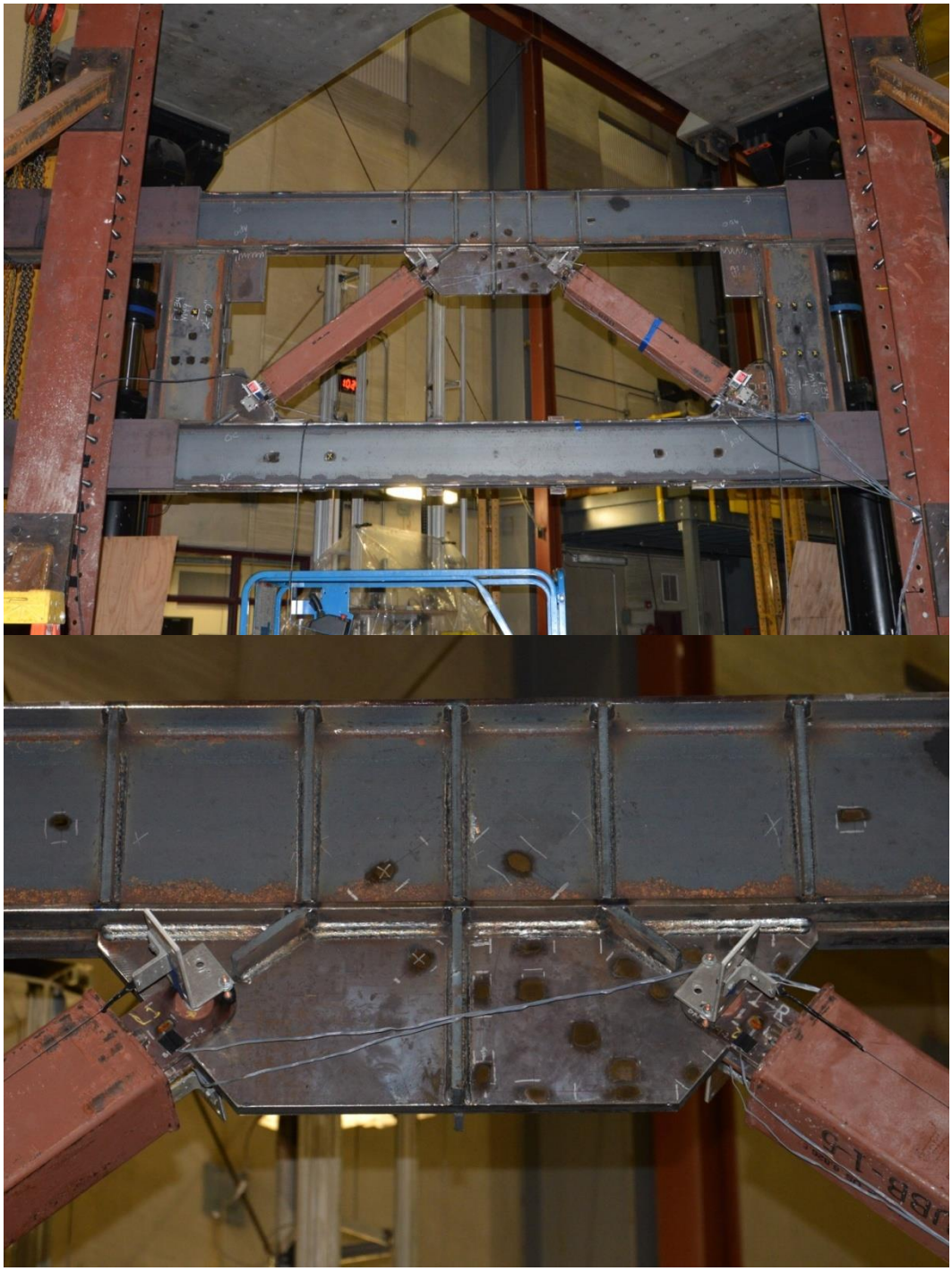

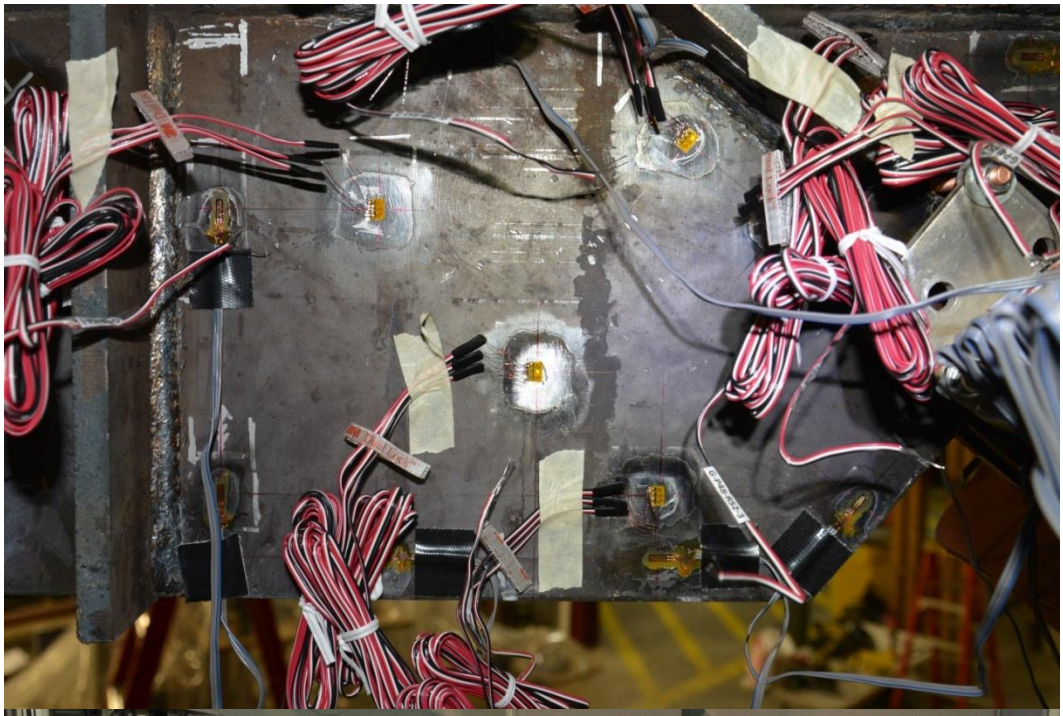

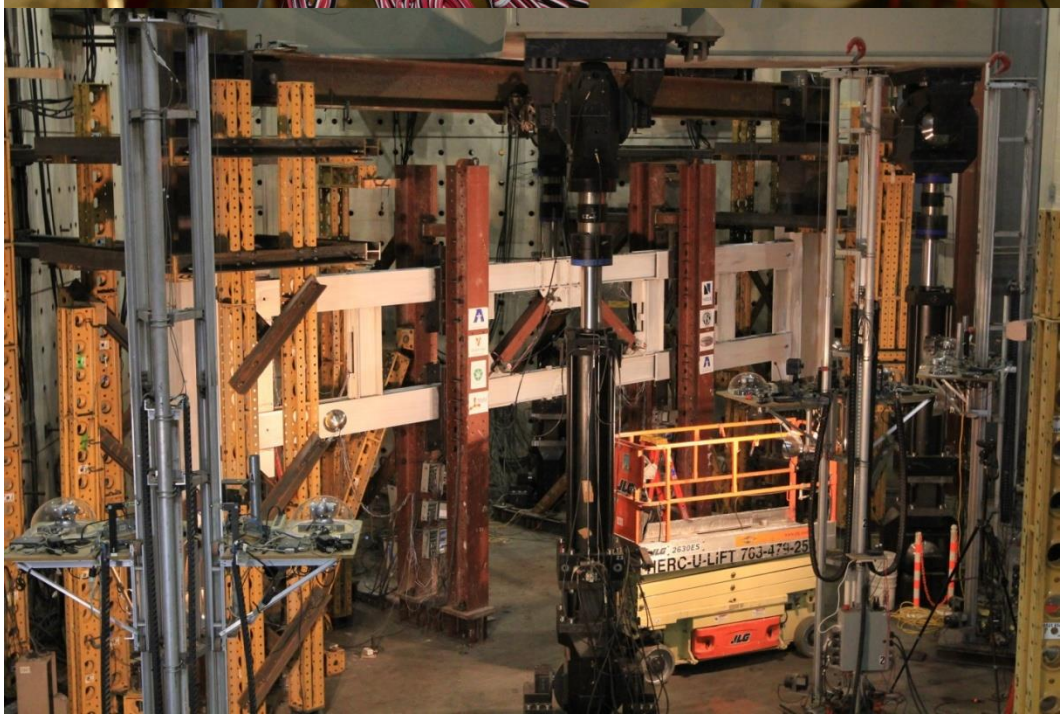
HERC-U-LIFT 763-479-25

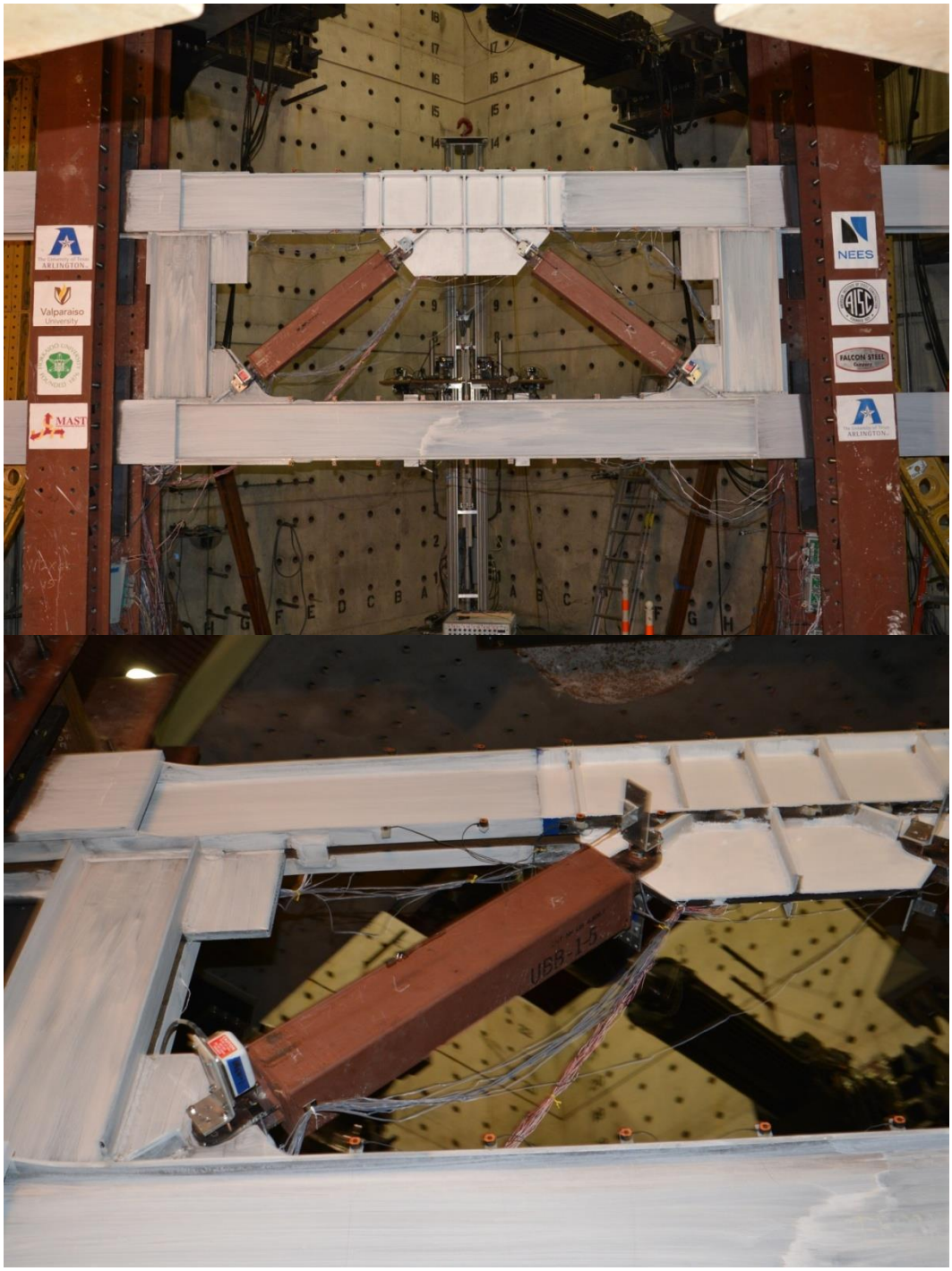
NEES
MAST
Valparaiso
UBB-1-5

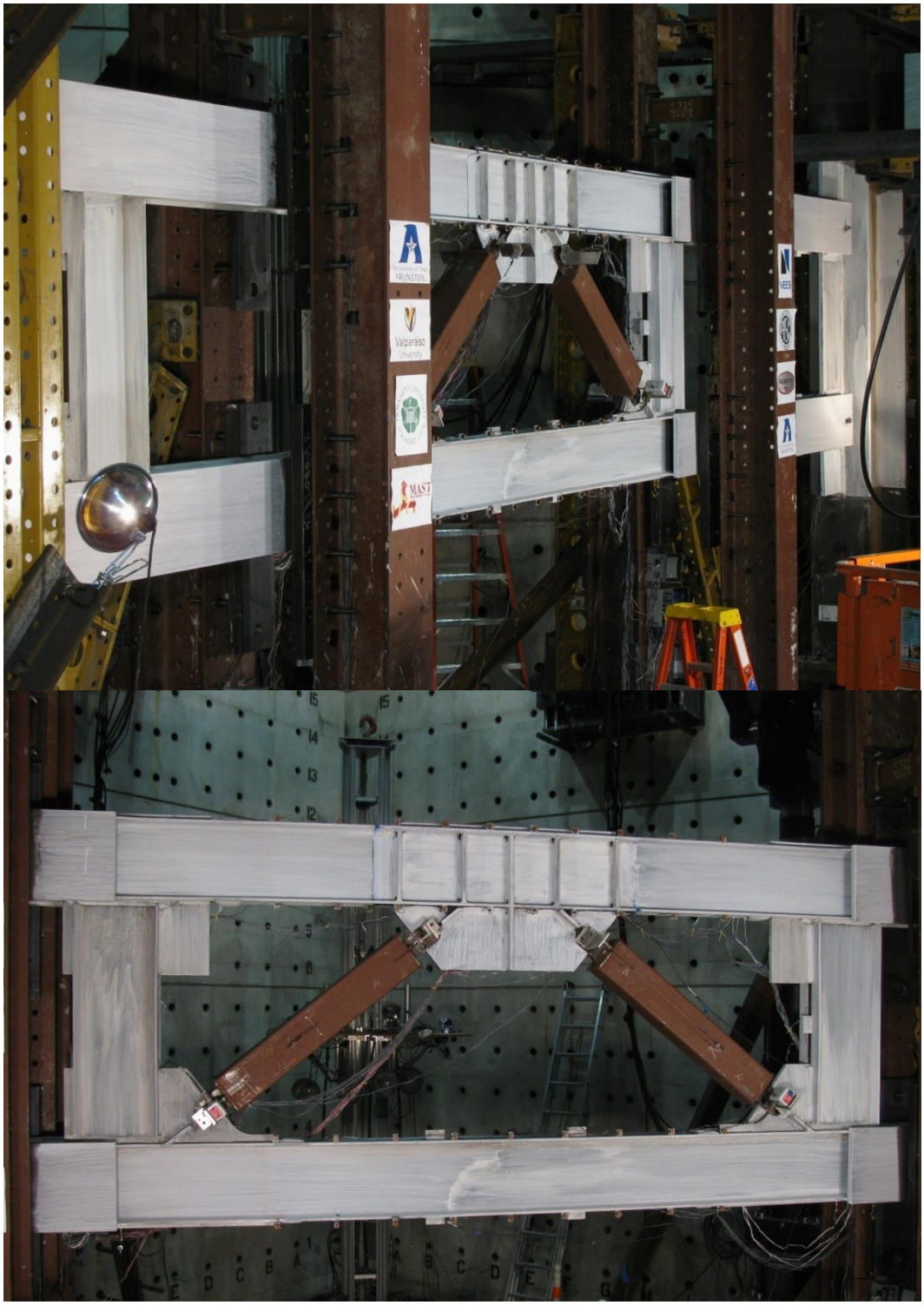
Valparaso
University
MAST


The University of Texas
ARLINGTON
Valparaiso
University
HOKKAIDO UNIVERSITY
FOUNDED 1876
MAST
www.jlg.com
2630ES JLG
HERC-U-LIFT 763-479-2501

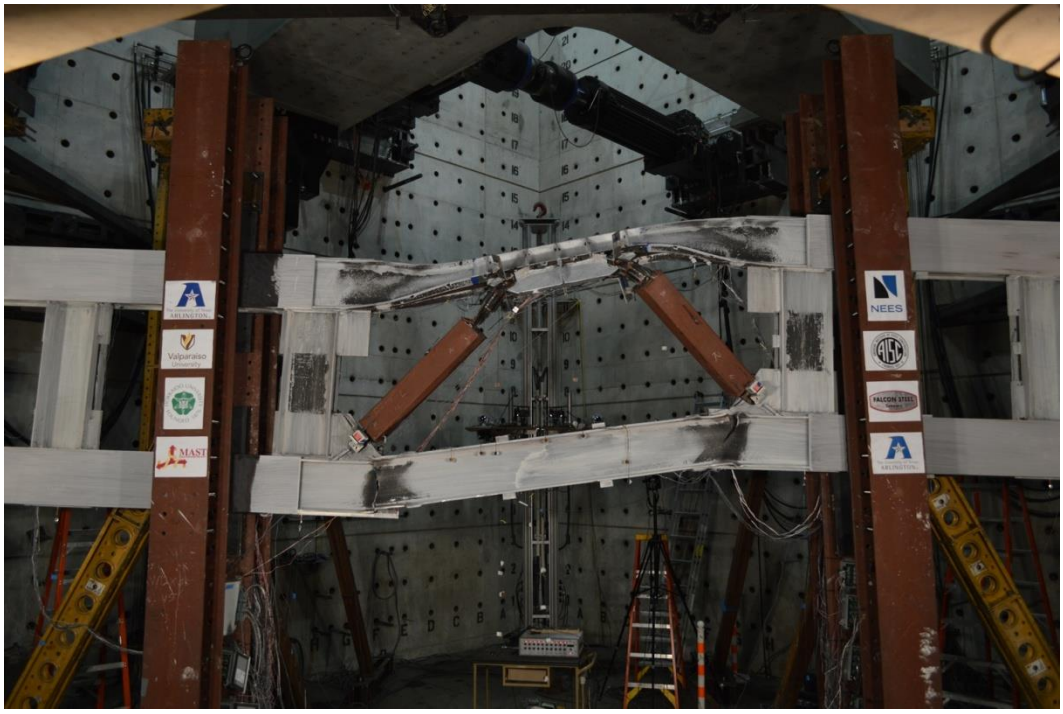
NEES
MAST


2013-10-15 11:48:08.221 CDT

Appendix H

Design of Gusset Plates for BRB Connection

Gusset Plate Design

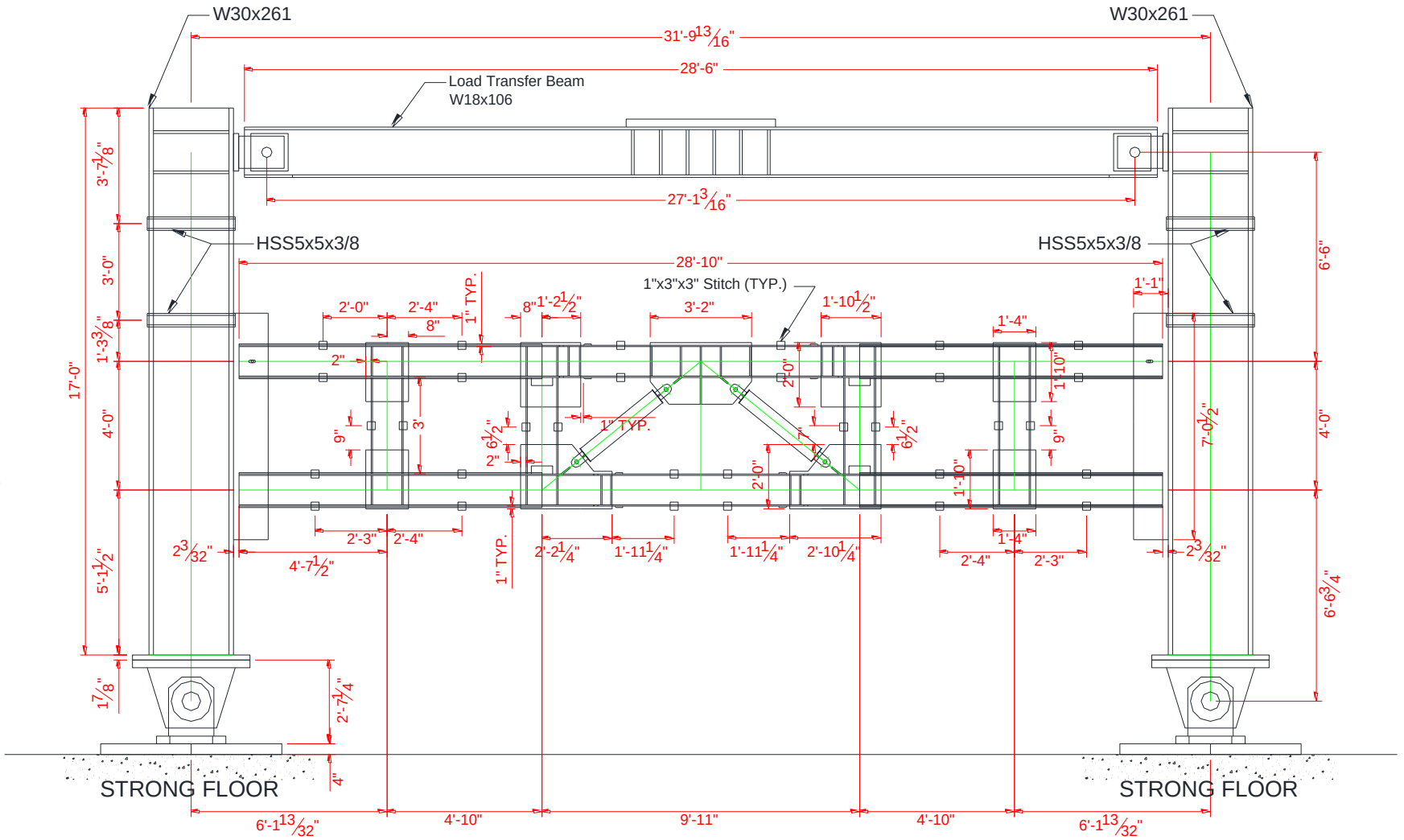

Figure 1. Overall Test Setup of STMF with BRB

Symbols

A_g = Gross area, in.^{2}

A_{pb} = Projected bearing area, in.^{2}

A_{sc} = Cross-sectional area of the yielding segment of steel core, in.^{2}

A_{sf} = Shear area, in.^{2}

C = Ultimate compressive force in brace, kips

F_{cr} = Critical stress, ksi

F_u = Specified minimum tensile strength, ksi

F_y = Specified minimum yield sress of steel, ksi

F_{ysc} = Specified minimum yield stress of the steel core, or actual yield stress of the steel core as determined from a coupon test, ksi

K = Effective length factor

L = Unbraced length, in.

P_{ysc} = Axial yield strength of steel core, kips

R_n = Nominal strength, kips

R_y = Ratio of the expected tensile strength to the specified minimum yield stress, F_y

T = Ultimate tensile force in brace, kips

a = Shortest distance from the pin hole to the end of gusset plate along the brace, in.

b_{eff} = Effective width, in.

d_b = Pin diameter, in.

r = Radius of gyration, in.

t = Thickness, in.

w = Width, in.

β = Compression strength adjustment factor

ϕ = Resistance factor

ω = Strain hardening adjustment factor

Given:

Ultimate tensile force in BRB,

$$T = \omega R_y P_{ysc} \qquad \text{(Seismic Provision F4.2a)}$$
$$= \omega R_y F_{ysc} A_{sc}$$
$$= (1.5)(1)(42.5)(0.5883)$$
$$= 37.5 \ kips$$

Ultimate compressive force in BRB,

$$C = \beta\omega R_y P_{ysc} \qquad \text{(Seismic Provision F4.2a)}$$
$$= \beta\omega R_y F_{ysc} A_{sc}$$
$$= (1.1)(1.5)(1)(42.5)(0.5883)$$
$$= 42.3\ kips$$

Gusset Plate Properties:

$F_y = 50\ ksi$

$F_u = 65\ ksi$

Thickness, $t = 1\ in.$

Design limit states:

- Compression buckling (AISC 327-05)
- Tension yielding (AISC 360-05: D2)
- Tension rupture (AISC 360-05: D5)
- Shear rupture (AISC 360-05: D5)
- Bearing (AISC 360-05: J7)
- Free-edge buckling (Astaneh, 1998)

Solution:

- **Top Joint**

Check compression buckling (AISC 327-05)

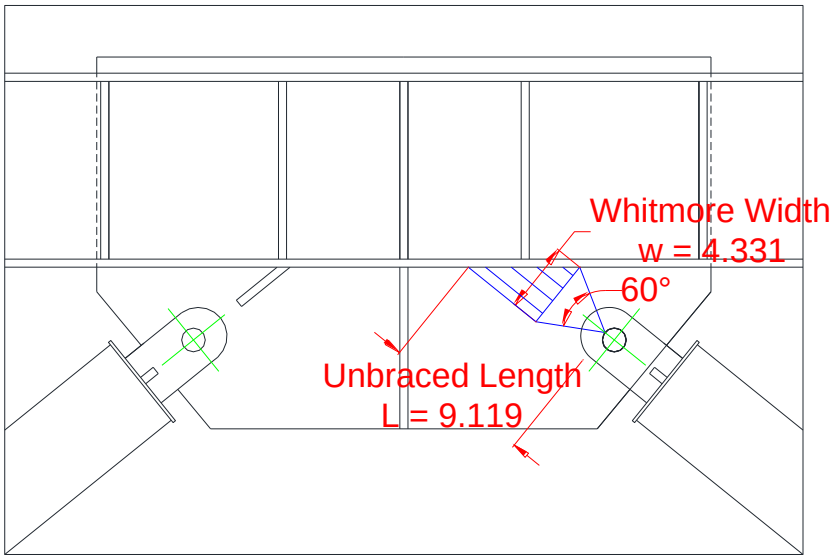

Figure 2. Top Joint and Area of Stress Distribution Treated as Column Strips According to Whitmore's Concept

The Whitmore width is,

$w = 4.331\ in.$

Treat the gusset plate as column strips of 1 in. width according to Whitmore's concept as shown in Figure 2.
To be conservative, use the longest length of the column strip as the unbraced length,

$$L = 9.119 \; in.$$

Since the gusset is attached by one edge only, the buckling mode could be sidesway type as shown in AISC 360-05, Commentary Table C-C2.2. In this case use $K = 1.2$.

$$r = \frac{t}{\sqrt{12}} = \frac{1}{\sqrt{12}} = 0.289 \text{ in.}$$

$$\frac{KL}{r} = \frac{1.2(9.119)}{0.289} = 37.9$$

From AISC 360-05, Table 4-22,

$$\phi F_{cr} = 40.5 \; ksi$$

$$\phi R_n = \phi F_{cr} A_g$$
$$= \phi F_{cr} wt$$
$$= (40.5)(4.331)(1)$$
$$= 175 \; kips > 42.3 \; kips$$

Check tension yielding (AISC 327-05)

$$\phi R_n = \phi F_y A_g \qquad \text{(Specification Eq.D2-1)}$$
$$= \phi F_y wt$$
$$= 0.9(50)(4.331)(1)$$
$$= 195 \; kips > 37.5 \; kips$$

Check tension rupture (AISC 360-05: D5.1)

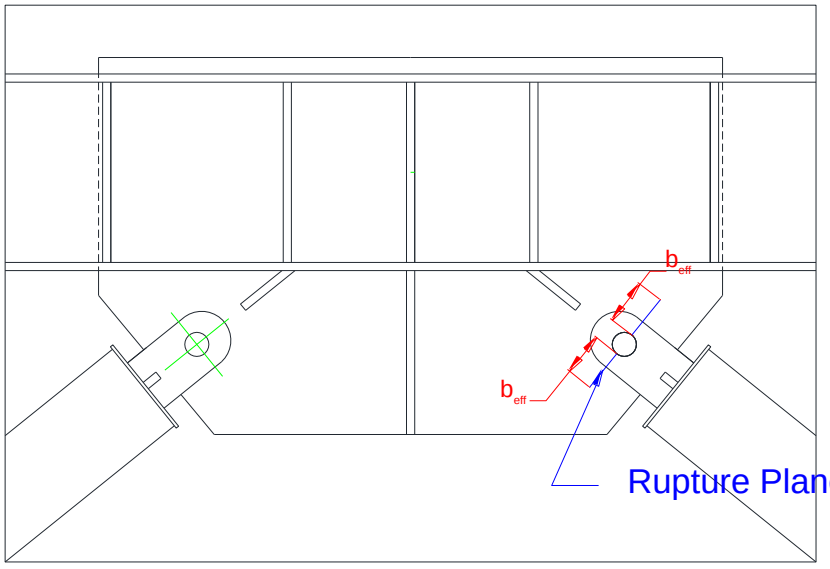

Figure 3. Effective Width in Tensile Rupture Plane of Top Joint

$$b_{eff} = 2t + 0.63 \qquad \text{(Specification D5.1)}$$
$$= 2(1) + 0.63$$
$$= 2.63 \text{ in.}$$
$$\phi R_n = \phi 2 t b_{eff} F_u \qquad \text{(Specification Eq.D5-1)}$$
$$= 0.75(2)(1)(2.63)(65)$$
$$= 256 \; kips > 37.5 \; kips$$

Check shear rupture *(AISC 360-05: D5.1)*

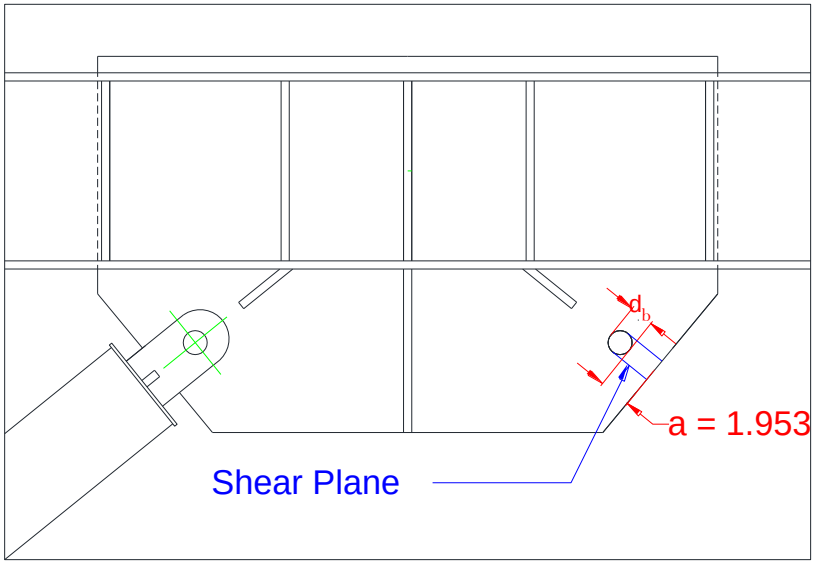

Figure 4. Shear Limit State of Top Joint

$$R_n = 0.6 F_u A_{sf} \qquad \text{(Specification Eq.D5-2)}$$
$$= 0.6 F_u 2t\left(a + \frac{d_b}{2}\right)$$
$$= (0.6)(65)(2)(1)\left(1.953 + \frac{1.46875}{2}\right)$$
$$= 210 \text{ kips}$$
$$\phi R_n = 0.75(210) = 158 \text{ kips} > 37.5 \text{ kips}$$

Check bearing (AISC 360-05: J7)

$$R_n = 1.8 F_y A_{pb} \qquad \text{(Specification Eq.J7-1)}$$
$$= 1.8 F_y d_b t$$
$$= 1.8(50)(1.46875)(1)$$
$$= 132 \; kips$$
$$\phi R_n = 0.75(132)$$
$$= 99 \; kips \; > \; 42.3 \; kips$$

Check Free-edge buckling (Astaneh, 1998)
Since there is no free edge in this join, this limit state does not govern.

- **Bottom Joint**

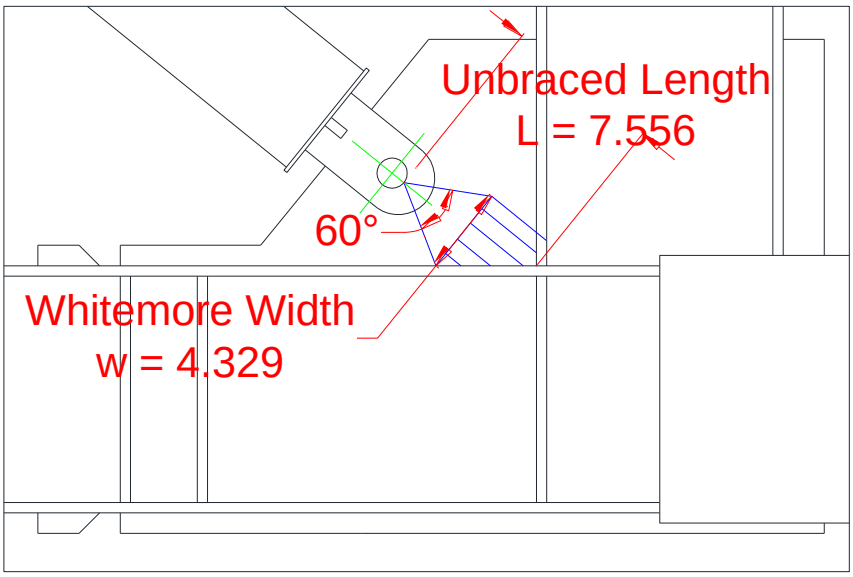

Figure 5. Bottom Joint and Area of Force Distribution Treated as Column Strips

Check compression buckling (AISC 327-05)
The Whitmore width is,

$$w = 4.329 \; in.$$

Treat the gusset plate as column strips of 1 in. width according to Whitmore's concept as shown in Figure 5.
To be conservative, use the longest length of the column strip as the unbraced length,

$$L = 7.556 \; in.$$

Since the gusset is attached by one edge only, the buckling mode could be sidesway type as shown in AISC 360-05, Commentary Table C-C2.2. In this case use $K = 1.2$.

$$r = \frac{t}{\sqrt{12}} = \frac{1}{\sqrt{12}} = 0.289 \text{ in.}$$

$$\frac{KL}{r} = \frac{1.2(7.556)}{0.289} = 31.4$$

From AISC 360-05, Table 4-22,

$$\phi F_{cr} = 41.8 \; ksi$$

$$\phi R_n = \phi F_{cr} A_g$$
$$= \phi F_{cr} wt$$
$$= (41.8)(4.329)(1)$$
$$= 181 \; kips > 42.3 \; kips$$

Check tension yielding (AISC 360-05: D2)

$$\phi R_n = \phi F_y A_g \qquad \text{(Specification Eq.D2-1)}$$
$$= 0.9(50)(4.329)$$
$$= 195 \; kips > 37.5 \; kips$$

Check tension rupture (AISC 360-05: D5.1)

$$b_{eff} = 2t + 0.63 \qquad \text{(Specification D5.1)}$$
$$= 2(1) + 0.63$$
$$= 2.63 \text{ in.}$$

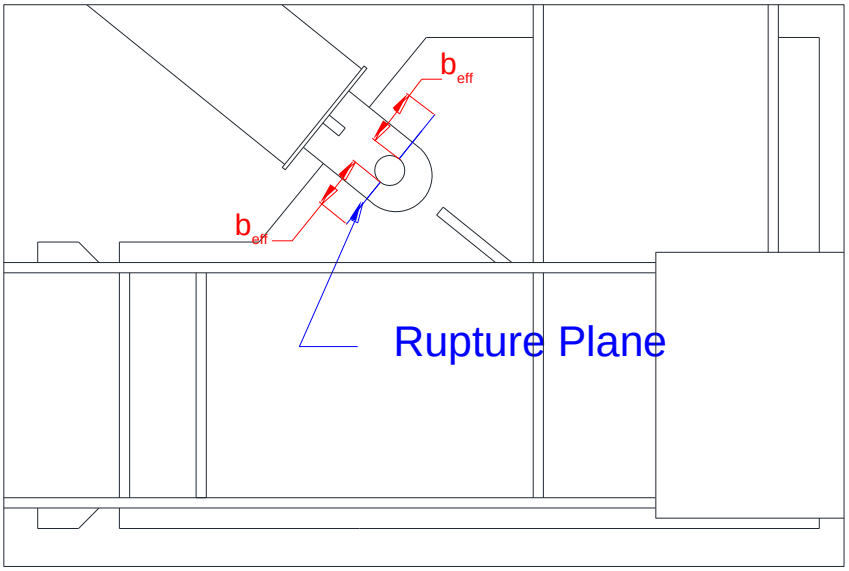

Figure 6. Effective Width in Tensile Rupture Plane of Bottom Joint

$$\phi R_n = \phi 2 t b_{eff} F_u \qquad \text{(Specification Eq.D5-1)}$$
$$= 0.75(2)(1)(2.63)(65)$$
$$= 256 \; kips > 37.5 \; kips$$

Check shear rupture *(AISC 360-05: D5.1)*

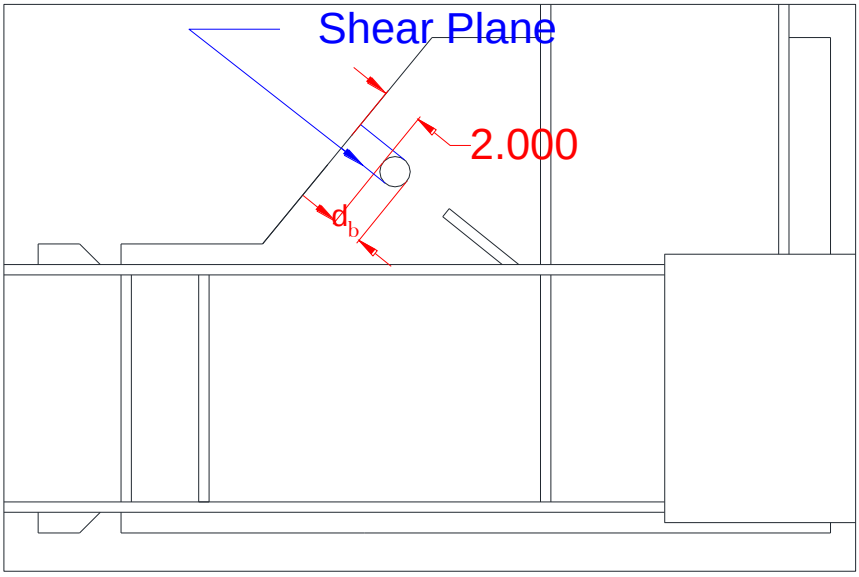

Figure 7. Shear Limit State of Bottom Joint

$$R_n = 0.6F_u A_{sf}$$ (Specification Eq.D5-2)

$$= 0.6F_u 2t\left(a + \frac{d_b}{2}\right)$$

$$= (0.6)(65)(2)(1)\left(2.000 + \frac{1.46875}{2}\right)$$

$$= 213 \text{ kips}$$

$$\phi R_n = 0.75(213) = 160 \text{ kips} > 37.5 \text{ kips}$$

Check bearing (AISC 360-05: J7)

$$R_n = 1.8F_y A_{pb}$$ (Specification Eq.J7-1)

$$= 1.8F_y d_b t$$

$$= 1.8(50)(1.46875)(1)$$

$$= 132 \textit{ kips}$$

$$\phi R_n = 0.75(132)$$

$$= 99 \textit{ kips} > 42.3 \textit{ kips}$$

Check Free-edge buckling (Astaneh, 1998)

Since there is no free edge in this join, this limit state does not govern.

References

AISC (1997), *Seismic Provisions for Structural Steel Buildings*, American Institute of Steel Construction, Chicago, IL.

AISC. (2016). *Prequalified Connections for Special and Intermediate Steel Moment Frames for Seismic Applications*. ANSI/AISC 358-16, American Institute of Steel Construction, Chicago, IL.

AISC (2016), *Seismic Provisions for Structural Steel Buildings*, ANSI/AISC 341-16, American Institute of Steel Construction, Chicago, IL.

AISC (2017), *Specification for Structural Steel Buildings*, ANSI/AISC 360-17, American Institute of Steel Construction, Chicago, IL.

ASCE (2010), *Minimum Design Loads for Buildings and Other Structures*, ASCE 7-10, American Society of Civil Engineers, Reston, VA.

ASCE (2013). *Seismic Evaluation and retrofit of existing buildings*. ASCE/SEI 41-13, Reston, VA.

ASTM International (2015), *E8/E8M-15a Standard Test Methods for Tension Testing of Metallic Materials*, American Society of Testing Material, West Conshohocken, PA.

Basha, H.S., and Goel, S.C. (1994), "Seismic Resistance Truss Moment Frames with Ductile Vierendeel Segment," *Report No. UMCEE 94-29*, Department of Civil and Environmental Engineering, University of Michigan, Ann Arbor, MI.

Basha, H.S., and Goel, S.C. (1995), "Special Truss Moment Frames with Vierendeel Middle Panel," *Engineering Structures*, vol. 17, no. 5, pp. 352-358.

Basha, H.S., and Goel, S.C. (1996), "Seismic Resistant Truss Moment Frames with Ductile Vierendeel Segment," *Paper No. 487, 11th World Conference on Earthquake Engineering*, Acapulco, Mexico.

Barsom, J., and Rolfe, S. T. (1999). Fracture and Fatigue Control in Structures – Applications of Fracture Mechanics. American Society for Testing and Materials, Third Edition. 516 pp.

Bruneau, M., Uang, C. M., and Sabelli, R. (2011). *Ductile Design of Steel Structures*. McGraw-Hill. 905 pp.

Chao, S.-H., and Goel, S.C. (2006), "Performance-Based Plastic Design of Seismic Resistant Special Truss Moment Frames," *Report No. UMCEE 06-03*, Department of Civil and Environmental Engineering, University of Michigan, Ann Arbor, MI.

Chao, S.-H., and Goel, S.C. (2008a), "A Modified Equation for Expected Maximum Shear Strength of the Special Segment for Design of Special Truss Moment Frames," *Engineering Journal*, American Institute of Steel Construction, vol. 45, no. 2, pp.117-125.

Chao, S.-H., and Goel, S.C. (2008b), "Performance-Based Plastic Design of Special Truss Moment Frames," *Engineering Journal*, American Institute of Steel Construction, vol. 45, no. 2, pp.127-150.

Chopra, A.K. (2011), *Dynamics of structures – Theory and Applications to Earthquake Engineering, 4th Ed.*, Pearson Prentice Hall, Upper Saddle River, NJ.

CSi (2011a), *Components and Elements for PERFORM-3D and PERFORM-COLLAPS*, Computers and Structures, Inc., Berkeley, CA.

Dusicka, P., Itani, A.M., and Sahai, R. (2002), "Advances in the Seismic Design of Special Truss Moment Frames," *Proceedings of the 71st Annual Convention of the Structural Engineers of California*, Santa Barbara, CA.

El-Bahey, S. and Bruneau, M. (2010), “Analytical Development and Experimental Validation of a Structureal-Fuse Bridge Pier Concept,” *Report No. MCEER-10-0005*, MCEER, University at Buffalo, Buffalo, NY.

Fadden, M., and McCormick, J. (2012), “Cyclic quasi-static testing of hollow structural section beam members,” *Journal of Structural Engineering*, vol. 135, no. 5, pp.561-570.

Fahnestock, L., Ricles, J., Sause, R. (2007): Experimental evaluation of a large-scale buckling-restrained braced frame. *Journal of Structural Engineering*, vol. 133, no. 9, pp. 1205-1241.

Goel, S.C., and Chao, S.-H. (2008), *Performance-Based Plastic Design: Earthquake-Resistant Steel Structures*, ICC, County Club Hills, IL.

Goel, S.C., and Itani, A.M. (1991), “Seismic resistant special truss moment frames,” *Journal of Structural Engineering*, vol. 120, no. 6, pp.1781-1797.

Goel, S.C., and Itani, A.M. (1994a), “Seismic Behavior of Open-Web Truss-Moment Frames,” *Journal of Structural Engineering*, vol. 120, no. 6, pp.1763-1780.

Goel, S.C., and Itani, A.M. (1994b), “Seismic-Resistant Special Truss-Moment Frames,” *Journal of Structural Engineering*, vol. 120, no. 6, pp.1781-1797.

Goel, S.C., Rai, D.C., and Basha, H.S. (1998), “Special Truss Moment Frames – Design Guide,” *Report No. UMCEE 98-44*, Department of Civil and Environmental Engineering, University of Michigan, Ann Arbor, MI.

Hamburger, R.O. and Malley, J. (2016). “Seismic design of steel special moment frames: a guide for practicing engineers.” *NEHRP seismic design technical brief no.2 Second Edition,* NIST, Gaithersburg, MD.

Hanson, R.D., and Martin, H.W. (1987), “Performance of Steel Structures in the September 19 and 20, 1985 Mexico Earthquakes,” *Earthquake Spectra*, Earthquake Engineering Research Institute, vol. 3, no. 2, pp. 329-346.

Hikino T, Okazaki T, Kajiwara K, Nakashima M. (2012), "Out-of-Plane Stability of Buckling-Restrained Braces Placed in Chevron Arrangement." *Journal of Structural Engineering* 2012; vol. 139, no. 11, pp. 1812-1822.

ICBO (1988), *Uniform Building code*, International Conference of Building Officials, Whittier, CA.

ICBO (1997), *Uniform Building code*, International Conference of Building Officials, Whittier, CA.

Itani, A.M., and Goel, S.C. (1991), “Earthquake Resistance of Open Web Framing Systems,” *Report No. UMCE 91-21*, Department of Civil Engineering, University of Michigan, Ann Arbor, MI.

Kim, T., Whittaker, A.S., Gilani, A.S.J., Bertero, V.V., and Takhirov, S.M. (2000). Cover-Plate and Flange-Plate Reinforced Steel Moment-Resisting Connections. *Report No. PEER 2000/07*, Pacific Earthquake Engineering Research Center.

Kim, T., Whittaker, A.S., Gilani, A.S.J., and Bertero, V.V. (2002). “Experimental Evaluation of Plate-Reinforced Steel Moment-Resisting Connections,” *Journal of Structural Engineering*, V. 28, No. 4, pp. 483-491.

Krawinkler, H., Gupta, A., Medina, R., and Luco, M. (2000). “Development of loading histories for testing of steel beam-to-column assemblies.” *Rep prepared for SAC Steel Project*, Dept. of Civil and Environmental Engineering, Stanford Univ., Palo Alto, CA

Lee, S.-S., and Goel, S.C. (2001), “Performance-Based Design of Steel Moment Frames Using Target Drift and Yield Mechanism,” *Report No. UMCEE 01-17*, Department of Civil and Environmental Engineering, University of Michigan, Ann Arbor, MI.

Maison, B. F. and Speicher, M. S. (2016). “Loading protocols for ASCE 41 backbone curves.” *Earthquake Spectra*, vol. 32, no. 4, pp. 2513-2532.

Nakashima, M., Liu, D., and Kanao, I. (2003). “Lateral-Torsional and Local Instability of Steel Beams Subjected to Large Cyclic Loading,” *International Journal of Steel Structures*, vol. 3, no. 3, pp. 179-189.

Newell, J.D., and Uang, C.-M. (2008), “Cyclic Behavior of Steel Wide-Flange Columns Subjected to Large Drift,” *Journal of Structural Engineering*, vol. 134, no. 8, pp.1334-1342.

Okazaki, T., Liu, D., Nakashima, M., and Engeljardt, M. D. (2006). “Stability Requirements for Beams in Seismic Steel Moment Frames,” *Journal of Structural Engineering*, V. 132, No. 9, pp. 1334-1342.

Ölmez, H.D., and Topkaya, C. (2011), "A Numerical Study on Special Truss Moment Frames with Vierendeel Openings," *Journal of Constructional Steel Research*, vol. 67, no. 4, pp.667-677.

Parra-Montesinos, G.J., Goel, S.C., and Kim, K.-Y. (2006), “Behavior of Steel Double Channel Built-Up Chords of Special Truss Moment Frames under Reversed Cyclic Bending,” *Journal of Structural Engineering*, vol. 132, no. 9, pp.1343-1351.

Pekcan, G., Linke, C., Itani, A.M. (2009), “Damage Avoidance Design of Special Truss Moment Frames with Energy Dissipating Devices,” *Journal of Constructional Steel Research*, vol. 65, no. 6, pp.1374-1384.

Pekcan, G., and Itani, A. (2007), “Seismic Response of Innovative Special Truss Moment Frames with Energy Dissipating Devices,” Department of Civil Engineering, University of Nevada, Reno, NV.

RISA Technology (2011), *RISA-3D User’s Guide*, Foothill Ranch, CA.

Sahoo, D.R., and Chao, S.-H. (2010), “Performance-Based Plastic Design Method for buckling-restrained braced frames,” *Engineering Structures*, vol. 32, no. 9, pp.2950-2958.

Scalzi, J. B. (1971), “The Staggered Truss System-Structural Considerations,” *Engineering Journal*, American Institute of Steel Construction, October, pp.138-143.

SEAOC Seismology Committee (2008), “Special Truss Moment Frames with Vierendeel Segments,” *The SEAOC Blue Book: Seismic Design Recommendations*, Structural Engineers Association of California, Sacramento, CA.

Simasathien, S., Jiansinlapadamrong, C., Okazaki, T., and Chao, S.-H. (2014), “Cyclic Loading Performance of Special Truss Moment Frame with Double-Channel Chord Members,” *Proceedings of the 10th National Conference in Earthquake Engineering*, Earthquake Engineering Research Institute, Anchorage, AK.

Simasathien S. (2016). “Cyclic loading performance of special truss moment frames with innovative details and modified structural layouts for staggered truss framing system for seismically active areas.” Dissertation, University of Texas at Arlington, Arlington, TX.

Somerville, P.G., Smith, N.F., Punyamurthula S., and Sun, J.I. (1997), Development of Ground Motion Time Histories for Phrase 2 of the FEMA/SAC Steel Project,” *Report No. SAC/BD-97/04*, SAC joint Venture, Sacramento, CA.

Takeuchi, T., Ida, M., Yamada, S., and Suzuki, K. (2008), “Estimation of Cumulative Deformation Capacity of Buckling Restrained Braces,” *Journal of Structural Engineering*, vol. 134, no. 5, pp.822-831.

Tremblay, R., Poncet, L.,Bolduc, P., Neville, R., and DeVall, R. "Testing and design of buckling restrained braces for Canadian application," *Proceedings of the 13th World Conference on Earthquake Engineering,* Vancouver, B.C. Canada

Uang, C.-M. and Fan, C.-C. (2001). “Cyclic Stability Criteria for Steel Moment connections with Reduced Beam Section,” *Journal of Structural Engineering*, V. 127, No. 9, pp. 1021-1027

Yu, Q.-S., Gilton, C, and Uang, C.-M. (2000). Cyclic Response of RBS Moment Connections: Loading Sequenceand Lateral Bracing Effects. *Report No. SAC/BD-00/22*, SAC Joint Venture.

Biographical Information

The author obtained a Bachelor of Engineering from Chulalongkorn University in Bangkok, Thailand in 1996. He then joined department of Civil Engineering at King Mongkut's University of Technology North Bangkok (KMUTNB) as a lecturer. In 1997, he came to the U.S. to pursue graduate studies in structural engineering under the Royal Thai Government Scholarship. He obtained a Master of Science in Engineering (Structures) from the University of Michigan in 1999.

Upon resuming his position as a lecturer at KMUTNB, the author was assigned to teach both undergraduate and graduate level classes, supervise undergraduate senior project, and co supervise master thesis. Even though steel structures are not popular in Thailand due to economic reasons, he has always fascinated by them. In 2010, he was grateful to be accepted as Dr. Shih-Ho Chao's Ph.D. student at the University of Texas at Arlington and to work on a National Science Foundation funded steel project. Because of Dr.Shih-Ho Chao variety of interests in structural framing system, he was able to get involved or observed research works in reinforced concrete, fiber reinforced concrete, ultra high performance fiber reinforced concrete, and various structural steel framing systems.

After receiving his PhD, the author plans to gain industry related experiences and a PE and/or SE licenses. However, he plans to stay current with research community and knowledge.